# EFFECTS OF CROSS-SECTIONAL SHAPES ON RESPONSE OF TALL BUILDINGS UNDER WIND LOADS

**Ph.D. THESIS**

**by**

**RITU RAJ**

**DEPARTMENT OF CIVIL ENGINEERING**
**INDIAN INSTITUTE OF TECHNOLOGY ROORKEE**
**ROORKEE – 247667 (INDIA)**
**OCTOBER, 2015**

# EFFECTS OF CROSS-SECTIONAL SHAPES ON RESPONSE OF TALL BUILDINGS UNDER WIND LOADS

**A THESIS**

***Submitted in partial fulfilment of the requirements for the award of the degree***
**of**

**DOCTOR OF PHILOSOPHY**

**in**

**CIVIL ENGINEERING**

**by**

**RITU RAJ**

**DEPARTMENT OF CIVIL ENGINEERING**
**INDIAN INSTITUTE OF TECHNOLOGY ROORKEE**
**ROORKEE – 247667 (INDIA)**
**OCTOBER, 2015**

**©INDIAN INSTITUTE OF TECHNOLOGY ROORKEE, 2015**
**ALL RIGHTS RESERVED**

# INDIAN INSTITUTE OF TECHNOLOGY ROORKEE
# ROORKEE

## CANDIDATE DECLARATION

I hereby certify that the work which is being presented in the thesis entitled "**EFFECTS OF CROSS-SECTIONAL SHAPES ON RESPONSE OF TALL BUILDINGS UNDER WIND LOADS"** in partial fulfilment of the requirements for the award of the degree of Doctor of Philosophy and submitted in the Department of Civil Engineering of the Indian Institute of Technology Roorkee, Roorkee is an authentic record of my own work carried out during the period from December, 2011 to October, 2015 under the supervision of Dr. Ashok K. Ahuja, Professor, Department of Civil Engineering, Indian Institute of Technology Roorkee, Roorkee, India.

The matter presented in this thesis has not been submitted by me for the award of any other degree in this or any other Institution.

(**RITU RAJ)**

This is to certify that the above statement made by the candidate is correct to the best of my knowledge.

(Ashok K. Ahuja)
Supervisor

Date :

# ACKNOWLEDGEMENT

It gives me great pleasure in expressing my gratitude to all those people who have supported me and extended their help in making this thesis possible. Completion of this doctoral dissertation was possible with the support of several people. I would like to express my feeling of gratefulness and submit my acknowledgement for them further in the following lines.

First of all, I wish to express my deep sense of gratitude and indebtedness to Dr. Ashok K. Ahuja, Professor, Department of Civil Engineering, Indian Institute of Technology Roorkee, Roorkee for his expert guidance, valuable suggestion, wholehearted corporation, motivation and help in carrying out this research work. His constant encouragement has immensely contributed to this thesis for which the author wishes to record his profound sense of gratitude to Prof. Ahuja.

I express my special thanks to SRC members Prof. Akhil Upadhyay, Prof. Pramod K. Gupta, Department of Civil Engineering and Prof. R.N. Dubey, Department of Earthquake Engineering, Indian Institute of Technology Roorkee for time to time suggestion and guidance for the right approach of research problem.

The author is extremely thankful to Dr. Deepak Kashyap, Head, Department of Civil Engineering, Indian Institute of Technology Roorkee, Roorkee for providing all assistance required for the completion of this thesis work.

I thank to the Director, IIT Roorkee and the Ministry of Human Resource Development (MHRD), Government of India for providing financial assistance during my Ph.D. Work.

The family atmosphere in the Wind Engineering Laboratory, Hydraulic Engg. Group, Department of Civil Engineering, Indian Institute of Technology Roorkee has been instrumental in the smooth completion of this work. I sincerely acknowledge the association of lab staff of Wind Engineering Laboratory. I am deeply thankful to lab assistant Mr. Ashok Yadav and Mr. Bhairov Singh Bohra for providing me all assistance during my experimental work. Mr. Israr and Mr. Sudhir Kumar also helped me a lot during my experimental work in the laboratory.

I thank all my fellow friends including Dr. Deepak Swami, Assistant Professor, IIT Mandi, Dr. Kunal Jain, Assistant Professor, PEC Chandigarh, Dr. Nikhil Agrawal, Mr. Himanshu Arora, Dr. Nalin Singh Negi, Mr. Himanshu Sharma, Mr. Bhupesh Jain, Mr.

Muftha Ahmed and Ms. Astha Verma for providing their valuable suggestion and help wherever they were approached.

I am thankful from the core of my heart to my reverend parents, Shri Gulab Chand Ahirwar and Smt. Kamla Ahirwar, for their blessing to see this day. My thanks are also due to my sister, Ms. Neetu Ahirwar, and my brother, Mr. Rajeev Ahirwar, for their moral and emotional support. A very special note of thanks to my loving friend, Ms. Sandhya Aherwar. She has been constant source of strength and inspiration during my doctoral work.

At the end, I am thankful and grateful to the almighty for bringing this day in my life.

(RITU RAJ)

# ABSTRACT

Tall buildings are replacing low-rise buildings in almost all the cities. The purpose of construction of high-rise buildings is to accommodate many flats and offices on a small plot area. Wind is one of the important loads considered at the time of analysis while designing both low-rise and high-rise buildings. Although architects generally deign multistoried apartment / office buildings in square or rectangular plan, they design the buildings with irregular cross-sections also at times for aesthetic reasons. For buildings with regular cross-sectional shapes such as square and rectangular shape, wind pressure and force coefficients are available in relevant standards on wind loads. However, the available information is not sufficient to design such type of tall buildings with irregular cross-sectional shapes.

The flow field around tall buildings changes due to the change in cross-sectional shape, thus creating a wind field which is different in comparison to that for uniform plan shape buildings. It results in different wind loads than those which are available in the relevant standards on wind loads of various countries and research publications. Therefore it has become necessary to test the model of such a tall building with irregular plan shape in the wind tunnel to measure the wind loads acting on it every time it is designed.

Further, the information about wind pressure coefficients and force coefficients available in relevant codes of practices on wind loads on tall buildings with regular shapes is for stand-alone or isolated condition only. Pattern and quantum of change in wind loads on a tall building due to the presence of other buildings of same or different cross-sectional shape and height are not reported in standards on wind loads. Wind tunnel tests are the only possible solution as on today to evaluate the wind loads on a tall building under interference condition. Aim of the present study, therefore, is to test the models of tall buildings with varying cross-sectional shapes in the wind tunnel to measure wind loads both under isolated and interference condition.

In present study, eight types of cross-sectional shapes are considered. The cross-sectional shapes are so chosen that floor area remains same in all the cases. The present study is carried out under three major heads namely (i) experimental study-force measurements, (ii) experimental study-pressure measurements and (iii) wind response analysis.

In the experimental study, the rigid models of tall buildings with different cross-sectional shapes are tested in an open circuit boundary layer wind tunnel having test section of length 15m and 2 m x 2 m cross-section. The prototype buildings are considered to be situated in a sub urban terrain with well scattered objects having height between 1.5 m to 10 m, defined as Terrain Category 2, Zone-V in IS: 875 (Part-3) 1987. Vortex generators, barrier

wall and small blocks are used as obstructions to flow to meet the wind tunnel simulation requirements and for the development of turbulent flow for generating the atmospheric surface layer in the wind tunnel.

The prototype buildings are assumed to have ground floor plus 18 storeys with total height of buildings as 60 m and floor area 400 $m^2$. Models for wind tunnel tests are made at a scale of 1:100. Two types of models are fabricated, wooden models for force measurements and Perspex sheet models for pressure measurements. Therefore, 8 no. wooden models and 7 no. Perspex sheet models i.e. 2 models for each 8 cross-sectional shapes except model-E, are made. Many numbers of pressure points are created on the surfaces of Perspex sheet models depending on the requirement.

In first part of the study, base shear, base moments and twisting moments are measured by placing wooden models one by one on force balance under isolated as well as interference conditions. Force measurements are carried out at free stream velocities of 6, 8 and 10 m/sec approximately.

In second part, mean, rms, maximum and minimum wind pressures are obtained at all pressure points on Perspex sheet models at free stream velocity of 10 m/sec. Models are divided into two categories i.e. (i) models having symmetry about both axis and (ii) models having symmetry about one axis. Models having symmetry about both axis are tested in the wind tunnel under 4 wind incidence angles namely $0^0$, $30^0$, $60^0$ and $90^0$. Models having symmetry about only one axis are tested in the wind tunnel under 7 wind incidence angles from $0^0$ to $180^0$ at an interval of $30^0$. Wind pressures measured on the surface of each models are expressed in form of non-dimensional pressure coefficients ($C_p$). Models are tested under isolated as well as interference conditions.

The third part of the work presented in the thesis is to carry out analytical study to obtain response of tall buildings with different plan shapes under wind using wind loads obtained experimentally in part two. Prototype buildings are assumed to be made of R.C.C. beams and columns with gird size as 5 m x 5 m and storey height as 3.75 m for lowest storey and 3.125 m for remaining storeys. The buildings are analyzed using readily available software package STAAD.Pro. Static response including moments about both axis, shear forces, twisting moments and displacements in all columns at every storey are obtained under various wind incidence angles. These values are compared with one another to understand the effects of building cross-sectional shapes and wind incidence angles on the response of tall buildings under wind loads.

At the end, conclusions are drawn as to which of 8 cross-sectional shapes considered in the present study is subjected to minimum wind loads under isolated condition and which

one under interference condition. Similarly the cross-sectional shape which results in optimum response under wind loads is also identified.

Results presented in the thesis can be made used by the architects and structural designers to design tall buildings of same or similar cross-sectional shapes studied and reported in this thesis.

# CONTENTS

**Title** **Page No.**

***Candidate's Declaration*****……i**

***Acknowledgement*****…….....…….ii**

***Abstract*****…….…….iv**

***Contents*****…….vii**

***List of Figures*****……...xiii**

***List of Tables*****…….xxxv**

***List of Photographs*****……...xxxvii**

**1 INTRODUCTION** **1-7**

1.1 GENERAL

1.2 DESIGN LOADS....1

1.3 WIND LOADS....1

1.3.1 Factors Affecting Wind Loads....1

1.3.2 Evaluation Procedure....1

1.4 NEED FOR THE PROPOSED STUDY....4

1.5 OBJECTIVE AND SCOPE....4

1.6 ORGANISATION OF THE THESIS....7

**2 LITERATURE REVIEW** **8-27**

2.1 GENERAL....8

2.2 CODAL INFORMATIONS....8

2.2.1 Australia and New-Zeeland Standard (AS/NZS-1170-2, 2011)....8

2.2.2 American Standard (ASCE-7, 2002)....8

2.2.3 British Standard (BS EN 1991-1-4, 2005)....8

2.2.4 Indian Standard (IS-875, part-3, 1987)....9

2.3 RESEARCH PUBLICATIONS....10

2.3.1 Wind Tunnel Studies - Isolated Condition....10

2.3.2 Wind Tunnel Studies - Interference Condition....18

2.3.3 Wind Response Analysis....23

2.4 LIMITATIONS....27

**3 EXPERIMENTAL PROGRAMME** **28-47**

3.1 GENERAL ..... 28
3.2 WIND TUNNEL USED ..... 28
3.3 WIND FLOW CHARACTERISTICS ..... 28
3.4 EQUIPMENTS USED ..... 33
3.4.1 Velocity Measuring Equipment ..... 33
3.4.2 Force Measuring Equipment ..... 33
3.4.3 Pressure Measuring Equipment ..... 33
3.4.4 Data Acquisition System ..... 33
3.5 PROTOTYPE BUILDINGS ..... 34
3.6 DETAILS OF MODELS ..... 35
3.6.1 Materials ..... 35
3.6.2 Cross-Sectional Shapes ..... 35
3.6.3 Pressure Tappings ..... 38
3.7 EVALUATION OF DRAG FORCE COEFFICIENTS ..... 47
3.8 EVALUATION OF PRESSURE COEFFICIENTS ..... 47

**4 EXPERIMENTAL STUDY - FORCE MEASUREMENT** **48-92**

4.1 GENERAL ..... 48
4.2 ISOLATED CONDITION ..... 49
4.2.1 Model-A (Square Shape) ..... 49
4.2.2 Model-B (Plus shape-1) ..... 51
4.2.3 Model-C (Plus shape-2) ..... 53
4.2.4 Model-D (I-Shape-1) ..... 55
4.2.5 Model-E (I-Shape-2) ..... 57
4.2.6 Model-F (Fish Shape-1) ..... 59
4.2.7 Model-G (Fish Shape-2) ..... 61
4.2.8 Model-H (Fish Shape-3) ..... 63
4.3 INTERFERENCE CONDITION ..... 65
4.3.1 Model-A (Square Shape) ..... 65
4.3.2 Model-B (Plus shape-1) ..... 68
4.3.3 Model-C (Plus shape-2) ..... 70
4.3.4 Model-D (I-shape-1) ..... 72
4.3.5 Model-E (I-Shape-2) ..... 74
4.3.6 Model-F (Fish Shape-1) ..... 76
4.3.7 Model-G (Fish Shape-2) ..... 78
4.3.8 Model-H (Fish Shape-3) ..... 80

4.4 COMPARISON OF DRAG FORCE COEFFICIENTS - ISOLATED CONDITION .....82
4.4.1 Models having symmetry about both axes.....82
4.4.2 Models having symmetry about one axis only .....83
4.5 COMPARISON OF DRAG FORCE COEFFICIENTS - INTERFERENCE CONDITION .....84
4.5.1 Models having symmetry about both axes.....84
4.5.2 Models having symmetry about one axis only .....85
4.6 COMPARISON OF BASE SHEAR, BASE MOMENTS AND TWISTING MOMENT.....87
4.6.1 Models having symmetry about both axes.....87
4.6.2 Models having symmetry about one axis only .....90

**5 EXPERIMENTAL STUDY - PRESSURE MEASUREMENT 93-246**

5.1 GENERAL.....93
5.2 ISOLATED CONDITION.....93
5.2.1 Model-A (Square Shape) .....93
5.2.2 Model-B (Plus Shape-1) .....104
5.2.3 Model-C (Plus Shape-2) .....116
5.2.4 Model-D (I-Shape-1) .....126
5.2.5 Model-F (Fish Shape-1).....136
5.2.6 Model-G (Fish Shape-2) .....152
5.2.7 Model-H (Fish Shape-3) .....168
5.3 INTERFERENCE CONDITION.....184
5.3.1 Model-A (Square Shape) .....184
5.3.2 Model-B (Plus Shape-1) .....192
5.3.3 Model-C (Plus Shape-2) .....200
5.3.4 Model-D (I-Shape-1) .....208
5.3.5 Model-F (Fish Shape-1) .....216
5.3.6 Model-G (Fish Shape-2) .....227
5.3.7 Model-H (Fish Shape-3) .....237

**6 WIND RESPONSE ANALYSIS 247-389**

6.1 GENERAL.....247
6.2 BUILDING DIMENSIONS.....247
6.3 CALCULATION OF WIND LOADS ON PROTOTYPE BUILDINGS .....259
6.4 RESPONSE UNDER ISOLATED CONDITION.....260
6.4.1 Square Shape Building.....260
6.4.1.1 Forces in columns .....260

6.4.1.2 Displacement of columns....261
6.4.2 Plus Shape-1 Building....270
6.4.2.1 Forces in columns....270
6.4.2.2 Displacement of columns....270
6.4.3 Plus Shape-2 Building....279
6.4.3.1 Forces in columns....279
6.4.3.2 Displacement of columns....279
6.4.4 I-Shape-1 Building....289
6.4.4.1 Forces in columns....289
6.4.4.2 Displacement of columns....289
6.4.5 Fish Shape-1 Building....299
6.4.5.1 Forces in columns....299
6.4.5.2 Displacement of columns....299
6.4.6 Fish Shape-2 Building....309
6.4.6.1 Forces in columns....309
6.4.6.2 Deflections of columns....309
6.4.7 Fish Shape-3 Building....319
6.4.7.1 Forces in columns....319
6.4.7.2 Deflections of columns....319
6.5 RESPONSE UNDER INTERFERENCE CONDITION....329
6.5.1 Square Shape Building....329
6.5.1.1 Forces in Columns....329
6.5.1.2 Displacement of columns....330
6.5.2 Plus Shape-1 Building....339
6.5.2.1 Forces in columns....339
6.5.2.2 Displacment of columns....339
6.5.3 Plus Shape-2 Building....348
6.5.3.1 Forces in columns....348
6.5.2.2 Displacment of columns....348
6.5.4 I-Shape-1 Building....357
6.5.4.1 Forces in columns....357
6.5.4.2 Displacement of columns....357
6.5.5 Fish Shape-1 Building....366
6.5.5.1 Forces in columns....366
6.5.5.2 Displacement of columns....366
6.5.6 Fish Shape-2 Building....374

6.5.6.1 Forces in columns .....374
6.5.6.2 Displacement of columns.....374
6.5.7 Fish Shape-3 Building.....382
6.5.7.1 Forces in columns .....382
6.5.7.2 Displacement of columns.....382

**7 CONCLUSIONS** **390-395**

7.1 GENERAL……..……390
7.2 EXPERIMENTAL STUDY – FORCE MEASUREMENTS……..390
7.2.1 Isolated Condition…….390
7.2.1.1 Square Shape building……...390
7.2.1.2 Plus Shape-1 building……390
7.2.1.3 Plus Shape-2 building……390
7.2.1.4 I-Shape-1 building……..391
7.2.1.5 I-Shape-2 building……..391
7.2.1.6 Fish Shape-1 building…….391
7.2.1.7 Fish Shape-2 building…….391
7.2.1.8 Fish Shape-3 building…….391
7.2.1.9 Comparison of forces on buildings with different cross-section shapes…..….392
7.2.2 Interference Condition……...……392
7.2.2.1 Square Shape building……...…….392
7.2.2.2 Plus Shape-1 building…….……....392
7.2.2.3 Plus Shape-2 building……...……..392
7.2.2.4 I-Shape-1 building……..……393
7.2.2.5 I-Shape-2 building……..……393
7.2.2.6 Fish Shape-1 building……..……...393
7.2.2.7 Fish Shape-2 building……..……...393
7.2.2.8 Fish Shape-3 building……..……...393
7.2.2.9 Comparison of $C_d$ on buildings with different cross-section shapes……..…393
7.3 EXPERIMENTAL STUDY – PRESSURE MEASUREMENTS…….…..394
7.3.1 Isolated Condition……394
7.3.1.1 Square Shape building……...……...394
7.3.1.2 Plus Shape-1 building……...……394
7.3.1.3 Plus Shape-2 building……...……394
7.3.1.4 I-Shape-1 building……...……395

7.3.1.5 Fish Shape-1 building……...……395
7.3.1.6 Fish Shape-2 building……...……395
7.3.1.7 Fish Shape-3 building……...……395
7.3.2 Interference Condition……...……..395
7.3.2.1 Square Shape building……...……...395
7.3.2.2 Plus Shape-1 building……...……396
7.3.2.3 Plus Shape-2 building……...……396
7.3.2.4 I-Shape-1 building……...……396
7.3.2.5 Fish Shape-1 building……...……396
7.3.2.6 Fish Shape-2 building……...……397
7.3.2.7 Fish Shape-3 building……...……397
7.4 WIND RESPONSE ANALYSIS……397
7.4.1 Isolated Condition……397
7.4.1.1 Square Shape building……..397
7.4.1.2 Plus Shape-1 building……...……397
7.4.1.3 Plus Shape-2 building……...……398
7.4.1.4 I-Shape-1 building……...……398
7.4.1.5 Fish Shape-1 building……...…….....399
7.4.1.6 Fish Shape-2 building……...……399
7.4.1.7 Fish Shape-3 building……...……399
7.4.2 Interference Condition……...……..400
7.4.2.1 Square Shape building……..……400
7.4.2.2 Plus Shape-1 building……...……400
7.4.2.3 Plus Shape-2 building……...……401
7.4.2.4 I-Shape-1 building……..……..401
7.4.2.5 Fish Shape-1 building……..……402
7.4.2.6 Fish Shape-2 building……..……402
7.4.2.7 Fish Shape-3 building……..……403
7.5 MAJOR CONTRIBUTION / ACHIEVEMENTS……..……403
7.6 RECOMMENDATIONS FOR FUTURE RESEARCH……..…...403

**REFERENCES……..404**

**LIST OF PUBLICATIONS……..413**

# LIST OF FIGURES


| Fig. No. | Description | Page No. |
|---|---|---|
| 1.1 | Isometric view of building models | 6 |
| 2.1 | Force coefficients for rectangular clad buildings in uniform flow [(Clause 6.3.2.1, Fig. 4), IS: 875 (Part-3), 1987] | 10 |
| 3.1 | Longitudinal and plan views of open circuit wind tunnel | 29 |
| 3.2 | Flow roughening devices inside the test section | 30 |
| 3.3 | Measured velocity profile at test section of open circuit wind tunnel | 31 |
| 3.4 | Variation of turbulence intensity with respect to height at the test section | 32 |
| 3.5 | Velocity profile in the open circuit wind tunnel on log-log scale | 32 |
| 3.6 | Plan view of all models used for experimental study | 35 |
| 3.7 | Isometric view of tall building models | 36 |
| 3.8 | Details of pressure points on Model-A (Square Shape) | 39 |
| 3.9 | Details of pressure points on Model-B (Plus Shape-1) | 40 |
| 3.10 | Details of pressure points on Model-C (Plus Shape-2) | 41 |
| 3.11 | Details of pressure points on Model-D (I-Shape-1) | 42 |
| 3.12 | Details of pressure points on Model-F (Fish Shape-1) | 43 |
| 3.13 | Details of pressure points on Model-G (Fish Shape-2) | 44 |
| 3.14 | Details of pressure points on Model-H (Fish Shape-3) | 45 |
| 4.1 | Cross-section of model-A showing different wind incidence angle | 49 |
| 4.2 | Variation of base shear ($F_x$ and $F_y$), base moment ($M_x$ and $M_y$) and twisting moment ($M_z$) on model-A with wind incidence angle | 50 |
| 4.3 | Variation of drag force coefficients on model-A with wind incidence angle | 50 |
| 4.4 | Cross-section of model-B showing different wind incidence angle | 51 |
| 4.5 | Variation of base shear ($F_x$ and $F_y$), base moment ($M_x$ and $M_y$) and twisting moment ($M_z$) on model-B with wind incidence angle | 52 |
| 4.6 | Variation of drag force coefficients on model-B with wind incidence angle | 52 |
| 4.7 | Cross-section of model-C showing different wind incidence angle | 53 |
| 4.8 | Variation of base shear ($F_x$ and $F_y$), base moment ($M_x$ and $M_y$) and twisting moment ($M_z$) on model-C with wind incidence angle | 54 |
| 4.9 | Variation of drag force coefficients on model-C with wind incidence angle | 54 |

| | | |
|---|---|---|
| 4.10 | Cross-section of model-D showing different wind incidence angle | 55 |
| 4.11 | Variation of base shear ($F_x$ and $F_y$), base moment ($M_x$ and $M_y$) and twisting moment ($M_z$) on model-D with wind incidence angle | 56 |
| 4.12 | Variation of drag force coefficients on model-D with wind incidence angle | 56 |
| 4.13 | Cross-section of model-E showing different wind incidence angle | 57 |
| 4.14 | Variation of base shear ($F_x$ and $F_y$), base moment ($M_x$ and $M_y$) and twisting moment ($M_z$) on model-E with wind incidence angle | 58 |
| 4.15 | Variation of drag force coefficients on model-E with wind incidence angle | 58 |
| 4.16 | Cross-section of model-F showing different wind incidence angle | 59 |
| 4.17 | Variation of base shear ($F_x$ and $F_y$), base moment ($M_x$ and $M_y$) and twisting moment ($M_z$) on model-F with wind incidence angle | 60 |
| 4.18 | Variation of drag force coefficients on model-F with wind incidence angle | 60 |
| 4.19 | Cross-section of model-G showing different wind incidence angle | 61 |
| 4.20 | Variation of base shear ($F_x$ and $F_y$), base moment ($M_x$ and $M_y$) and twisting moment ($M_z$) on model-G with wind incidence angle | 62 |
| 4.21 | Variation of drag force coefficients on model-G with wind incidence angle | 62 |
| 4.22 | Cross-section of model-H showing different wind incidence angle | 63 |
| 4.23 | Variation of base shear ($F_x$ and $F_y$), base moment ($M_x$ and $M_y$) and twisting moment ($M_z$) on model-H with wind incidence angle | 64 |
| 4.24 | Variation of drag force coefficients on model-H with wind incidence angle | 64 |
| 4.25 | Cross-section of model-A showing different wind interference conditions | 65 |
| 4.26 | Variation of base shear ($F_x$ and $F_y$), base moment ($M_x$ and $M_y$) and twisting moment ($M_z$) on model-A in wind interference condition | 66 |
| 4.27 | Comparison of drag coefficients on model-A at all three wind interference condition | 67 |
| 4.28 | Cross-section of model-B showing different wind interference conditions | 68 |
| 4.29 | Variation of base shear ($F_x$ and $F_y$), base moment ($M_x$ and $M_y$) and twisting moment ($M_z$) on model-B in wind interference condition | 69 |
| 4.30 | Comparison of drag coefficients on model-B at all three wind interference condition | 69 |
| 4.31 | Cross-section of model-C showing different wind interference conditions | 70 |
| 4.32 | Variation of base shear ($F_x$ and $F_y$), base moment ($M_x$ and $M_y$) and twisting moment ($M_z$) on model-C with wind interference condition | 71 |

| | | |
|---|---|---|
| 4.33 | Comparison of drag coefficients on model-C at all three wind interference condition | 71 |
| 4.34 | Cross-section of model-D showing different wind interference conditions | 72 |
| 4.35 | Variation of base shear ($F_x$ and $F_y$), base moment ($M_x$ and $M_y$) and twisting moment ($M_z$) on model-D with wind interference condition | 73 |
| 4.36 | Comparison of drag coefficients on model-D at all three wind interference condition | 73 |
| 4.37 | Cross-section of model-E showing different wind interference conditions | 74 |
| 4.38 | Variation of base shear ($F_x$ and $F_y$), base moment ($M_x$ and $M_y$) and twisting moment ($M_z$) on model-E with wind interference condition | 75 |
| 4.39 | Comparison of drag coefficients on model-E at all three wind interference condition | 75 |
| 4.40 | Cross-section of model-F showing different wind interference conditions | 76 |
| 4.41 | Variation of base shear ($F_x$ and $F_y$), base moment ($M_x$ and $M_y$) and twisting moment ($M_z$) on model-F with wind interference condition | 77 |
| 4.42 | Comparison of drag coefficients on model-F at all four wind interference condition | 77 |
| 4.43 | Cross-section of model-G showing different wind interference conditions | 78 |
| 4.44 | Variation of base shear ($F_x$ and $F_y$), base moment ($M_x$ and $M_y$) and twisting moment ($M_z$) on model-G with wind interference condition | 79 |
| 4.45 | Comparison of drag coefficients on model-G at all four wind interference condition | 79 |
| 4.46 | Cross-section of model-H showing different wind interference conditions | 80 |
| 4.47 | Variation of base shear ($F_x$ and $F_y$), base moment ($M_x$ and $M_y$) and twisting moment ($M_z$) on model-H with wind interference condition | 81 |
| 4.48 | Comparison of drag coefficients on model-H at all four wind interference condition | 81 |
| 4.49 | Comparison of drag coefficients on building models having symmetry about both axes at various wind incidence angles | 82 |
| 4.50 | Comparison of drag coefficients on building models having symmetry about one axis only at various wind incidence angles | 83 |
| 4.51 | Comparison of drag coefficients on building models having symmetry about both axes in full blockage wind interference condition | 84 |

| | | |
|---|---|---|
| 4.52 | Comparison of drag coefficients on building models having symmetry about both axes in half blockage wind interference condition | 85 |
| 4.53 | Comparison of drag coefficients on building models having symmetry about both axes in no blockage wind interference condition | 85 |
| 4.54 | Comparison of drag coefficients on building models having symmetry about one axis only in back-to-back wind interference condition | 86 |
| 4.55 | Comparison of drag coefficients on building models having symmetry about one axis only in back-to-front wind interference condition | 86 |
| 4.56 | Comparison of drag coefficients on building models having symmetry about one axis only in front-to-back wind interference condition | 87 |
| 4.57 | Comparison of drag coefficients on building models having symmetry about one axis only in front-to-front wind interference condition | 87 |
| 4.58 | Comparison of base shear Fx on building models having symmetry about both axes at various wind incidence angles | 88 |
| 4.59 | Comparison of base shear Fy on building models having symmetry about both axes at various wind incidence angles | 89 |
| 4.60 | Comparison of base moment Mx on building models having symmetry about both axes at various wind incidence angles | 89 |
| 4.61 | Comparison of base moment My on building models having symmetry about both axes at various wind incidence angles | 89 |
| 4.62 | Comparison of twisting moment Mz on building models haing symmetry about both axes at various wind incidence angles | 90 |
| 4.63 | Comparison of base shear Fx on building models having symmetry about one axis only at various wind incidence angles | 91 |
| 4.64 | Comparison of base shear Fy on building models having symmetry about one axis only at various wind incidence angles | 91 |
| 4.65 | Comparison of base moment Mx on building models having symmetry about one axis only at various wind incidence angles | 91 |
| 4.66 | Comparison of base moment My on building models having symmetry about one axis only at various wind incidence angles | 92 |
| 4.67 | Comparison of twisting moment Mz on building models having symmetry about one axis only at various wind incidence angles | 92 |
| 5.1 | Wind incidence angle on Perspex sheet model of model-A in isolated condition | 95 |

| | | |
|---|---|---|
| 5.2 | Distribution of mean wind pressure coefficients ($C_{p,mean}$) on different surfaces of model-A at $0^0$ wind incidence angle | 96 |
| 5.3 | Distribution of mean wind pressure coefficients ($C_{p,mean}$) on different surfaces of model-A at $30^0$ wind incidence angle | 96 |
| 5.4 | Distribution of mean wind pressure coefficients ($C_{p,mean}$) on different surfaces of model-A at $60^0$ wind incidence angle | 97 |
| 5.5 | Distribution of mean wind pressure coefficients ($C_{p,mean}$) on different surfaces of model-A at $90^0$ wind incidence angle | 97 |
| 5.6 | Cross-sectional variation of mean wind pressure coefficients ($C_{p,mean}$) on model-A at $0^0$ wind incidence angle | 99 |
| 5.7 | Cross-sectional variation of mean wind pressure coefficients ($C_{p,mean}$) on model-A at $30^0$ wind incidence angle | 100 |
| 5.8 | Cross-sectional variation of mean wind pressure coefficients ($C_{p,mean}$) on model-A at $60^0$ wind incidence angle | 101 |
| 5.9 | Cross-sectional variation of mean wind pressure coefficients ($C_{p,mean}$) on model-A at $90^0$ wind incidence angle | 102 |
| 5.10 | Wind incidence angles on Perspex sheet model of model-B in isolated condition | 105 |
| 5.11 | Distribution of mean wind pressure coefficients ($C_{p,mean}$) on different surfaces of model-B at $0^0$ wind incidence angle | 106 |
| 5.12 | Distribution of mean wind pressure coefficients ($C_{p,mean}$) on different surfaces of model-B at $30^0$ wind incidence angle | 107 |
| 5.13 | Distribution of mean wind pressure coefficients ($C_{p,mean}$) on different surfaces of model-B at $60^0$ wind incidence angle | 108 |
| 5.14 | Distribution of mean wind pressure coefficients ($C_{p,mean}$) on different surfaces of model-B at $90^0$ wind incidence angle | 109 |
| 5.15 | Cross-sectional variation of mean wind pressure coefficients ($C_{p,mean}$) on model-B at $0^0$ wind incidence angle | 111 |
| 5.16 | Cross-sectional variation of mean wind pressure coefficients ($C_{p,mean}$) on model-B at $0^0$ wind incidence angle | 112 |
| 5.17 | Cross-sectional variation of mean wind pressure coefficients ($C_{p,mean}$) on model-B at $0^0$ wind incidence angle | 113 |
| 5.18 | Cross-sectional variation of mean wind pressure coefficients ($C_{p,mean}$) on model-B at $0^0$ wind incidence angle | 114 |
| 5.19 | Wind incidence angles on Perspex sheet model of model-C in isolated condition | 116 |

| | | |
|---|---|---|
| 5.20 | Distribution of mean wind pressure coefficients ($C_{p,mean}$) on different surfaces of model-C at $0^0$ wind incidence angle | 117 |
| 5.21 | Distribution of mean wind pressure coefficients ($C_{p,mean}$) on different surfaces of model-C at $30^0$ wind incidence angle | 118 |
| 5.22 | Distribution of mean wind pressure coefficients ($C_{p,mean}$) on different surfaces of model-C at $60^0$ wind incidence angle | 119 |
| 5.23 | Distribution of mean wind pressure coefficients ($C_{p,mean}$) on different surfaces of model-C at $90^0$ wind incidence angle | 120 |
| 5.24 | Cross-sectional variation of mean wind pressure coefficients ($C_{p,mean}$) on model-C at $0^0$ wind incidence angle | 121 |
| 5.25 | Cross-sectional variation of mean wind pressure coefficients ($C_{p,mean}$) on model-C at $30^0$ wind incidence angle | 122 |
| 5.26 | Cross-sectional variation of mean wind pressure coefficients ($C_{p,mean}$) on model-C at $60^0$ wind incidence angle | 123 |
| 5.27 | Cross-sectional variation of mean wind pressure coefficients ($C_{p,mean}$) on model-C at $90^0$ wind incidence angle | 124 |
| 5.28 | Wind incidence angles on Perspex sheet model of model-D in isolated condition | 126 |
| 5.29 | Distribution of mean wind pressure coefficients ($C_{p,mean}$) on different surfaces of model-D at $0^0$ wind incidence angle | 127 |
| 5.30 | Distribution of mean wind pressure coefficients ($C_{p,mean}$) on different surfaces of model-D at $30^0$ wind incidence angle | 128 |
| 5.31 | Distribution of mean wind pressure coefficients ($C_{p,mean}$) on different surfaces of model-D at $60^0$ wind incidence angle | 129 |
| 5.32 | Distribution of mean wind pressure coefficients ($C_{p,mean}$) on different surfaces of model-D at $90^0$ wind incidence angle | 130 |
| 5.33 | Cross-sectional variation of mean wind pressure coefficients ($C_{p,mean}$) on model-D at $0^0$ wind incidence angle | 131 |
| 5.34 | Cross-sectional variation of mean wind pressure coefficients ($C_{p,mean}$) on model-D at $30^0$ wind incidence angle | 132 |
| 5.35 | Cross-sectional variation of mean wind pressure coefficients ($C_{p,mean}$) on model-D at $60^0$ wind incidence angle | 133 |
| 5.36 | Cross-sectional variation of mean wind pressure coefficients ($C_{p,mean}$) on model-D at $90^0$ wind incidence angle | 134 |
| 5.37 | Wind incidence angles on Perspex sheet model of model-F in isolated condition | 136 |

| | | |
|---|---|---|
| 5.38 | Distribution of mean wind pressure coefficients ($C_{p,mean}$) on different surfaces of model-F at $0^0$ wind incidence angle | 137 |
| 5.39 | Distribution of mean wind pressure coefficients ($C_{p,mean}$) on different surfaces of model-F at $30^0$ wind incidence angle | 138 |
| 5.40 | Distribution of mean wind pressure coefficients ($C_{p,mean}$) on different surfaces of model-F at $60^0$ wind incidence angle | 139 |
| 5.41 | Distribution of mean wind pressure coefficients ($C_{p,mean}$) on different surfaces of model-F at $90^0$ wind incidence angle | 140 |
| 5.42 | Distribution of mean wind pressure coefficients ($C_{p,mean}$) on different surfaces of model-F at $120^0$ wind incidence angle | 141 |
| 5.43 | Distribution of mean wind pressure coefficients ($C_{p,mean}$) on different surfaces of model-F at $150^0$ wind incidence angle | 142 |
| 5.44 | Distribution of mean wind pressure coefficients ($C_{p,mean}$) on different surfaces of model-F at $150^0$ wind incidence angle | 143 |
| 5.45 | Cross-sectional variation of mean wind pressure coefficients ($C_{p,mean}$) model-F at $0^0$ wind incidence angle | 144 |
| 5.46 | Cross-sectional variation of mean wind pressure coefficients ($C_{p,mean}$) model-F at $30^0$ wind incidence angle | 145 |
| 5.47 | Cross-sectional variation of mean wind pressure coefficients ($C_{p,mean}$) model-F at $60^0$ wind incidence angle | 146 |
| 5.48 | Cross-sectional variation of mean wind pressure coefficients ($C_{p,mean}$) model-F at $90^0$ wind incidence angle | 147 |
| 5.49 | Cross-sectional variation of mean wind pressure coefficients ($C_{p,mean}$) model-F at $120^0$ wind incidence angle | 148 |
| 5.50 | Cross-sectional variation of mean wind pressure coefficients ($C_{p,mean}$) model-F at $150^0$ wind incidence angle | 149 |
| 5.51 | Cross-sectional variation of mean wind pressure coefficients ($C_{p,mean}$) model-F at $180^0$ wind incidence angle | 150 |
| 5.52 | Wind incidence angles on Perspex sheet model of model-G in isolated condition | 152 |
| 5.53 | Distribution of mean wind pressure coefficients ($C_{p,mean}$) on different surfaces of model-G at $0^0$ wind incidence angle | 153 |
| 5.54 | Distribution of mean wind pressure coefficients ($C_{p,mean}$) on different surfaces of model-G at $30^0$ wind incidence angle | 154 |

| | | |
|---|---|---|
| 5.55 | Distribution of mean wind pressure coefficients ($C_{p,mean}$) on different surfaces of model-G at $60^0$ wind incidence angle | 155 |
| 5.56 | Distribution of mean wind pressure coefficients ($C_{p,mean}$) on different surfaces of model-G at $90^0$ wind incidence angle | 156 |
| 5.57 | Distribution of mean wind pressure coefficients ($C_{p,mean}$) on different surfaces of model-G at $120^0$ wind incidence angle | 157 |
| 5.58 | Distribution of mean wind pressure coefficients ($C_{p,mean}$) on different surfaces of model-G at $150^0$ wind incidence angle | 158 |
| 5.59 | Distribution of mean wind pressure coefficients ($C_{p,mean}$) on different surfaces of model-G at $180^0$ wind incidence angle | 159 |
| 5.60 | Cross-sectional variation of mean wind pressure coefficients ($C_{p,mean}$) on model-G at $0^0$ wind incidence angle | 160 |
| 5.61 | Cross-sectional variation of mean wind pressure coefficients ($C_{p,mean}$) on model-G at $30^0$ wind incidence angle | 161 |
| 5.62 | Cross-sectional variation of mean wind pressure coefficients ($C_{p,mean}$) on model-G at $60^0$ wind incidence angle | 162 |
| 5.63 | Cross-sectional variation of mean wind pressure coefficients ($C_{p,mean}$) on model-G at $90^0$ wind incidence angle | 163 |
| 5.64 | Cross-sectional variation of mean wind pressure coefficients ($C_{p,mean}$) on model-G at $120^0$ wind incidence angle | 164 |
| 5.65 | Cross-sectional variation of mean wind pressure coefficients ($C_{p,mean}$) on model-G at $150^0$ wind incidence angle | 165 |
| 5.66 | Cross-sectional variation of mean wind pressure coefficients ($C_{p,mean}$) on model-G at $180^0$ wind incidence angle | 166 |
| 5.67 | Wind incidence angles on Perspex sheet model of model-H in isolated condition | 168 |
| 5.68 | Distribution of mean wind pressure coefficients ($C_{p,mean}$) on different surfaces of model-H at $0^0$ wind incidence angle | 169 |
| 5.69 | Distribution of mean wind pressure coefficients ($C_{p,mean}$) on different surfaces of model-H at $30^0$ wind incidence angle | 170 |
| 5.70 | Distribution of mean wind pressure coefficients ($C_{p,mean}$) on different surfaces of model-H at $60^0$ wind incidence angle | 171 |
| 5.71 | Distribution of mean wind pressure coefficients ($C_{p,mean}$) on different surfaces of model-H at $90^0$ wind incidence angle | 172 |

| | | |
|---|---|---|
| 5.72 | Distribution of mean wind pressure coefficients ($C_{p,mean}$) on different surfaces of model-H at $120^0$ wind incidence angle | 173 |
| 5.73 | Distribution of mean wind pressure coefficients ($C_{p,mean}$) on different surfaces of model-H at $150^0$ wind incidence angle | 174 |
| 5.74 | Distribution of mean wind pressure coefficients ($C_{p,mean}$) on different surfaces of model-H at $180^0$ wind incidence angle | 175 |
| 5.75 | Cross-sectional variation of mean wind pressure coefficients ($C_{p,mean}$) on model-H at $0^0$ wind incidence angle | 176 |
| 5.76 | Cross-sectional variation of mean wind pressure coefficients ($C_{p,mean}$) on model-H at $0^0$ wind incidence angle | 177 |
| 5.77 | Cross-sectional variation of mean wind pressure coefficients ($C_{p,mean}$) on model-H at $0^0$ wind incidence angle | 178 |
| 5.78 | Cross-sectional variation of mean wind pressure coefficients ($C_{p,mean}$) on model-H at $0^0$ wind incidence angle | 179 |
| 5.79 | Cross-sectional variation of mean wind pressure coefficients ($C_{p,mean}$) on model-H at $0^0$ wind incidence angle | 180 |
| 5.80 | Cross-sectional variation of mean wind pressure coefficients ($C_{p,mean}$) on model-H at $0^0$ wind incidence angle | 181 |
| 5.81 | Cross-sectional variation of mean wind pressure coefficients ($C_{p,mean}$) on model-H at $0^0$ wind incidence angle | 182 |
| 5.82 | Details of model-A showing different interference conditions | 185 |
| 5.83 | Distribution of mean wind pressure coefficients ($C_{p,mean}$) on different surfaces of model-A under full blockage interference condition | 186 |
| 5.84 | Distribution of mean wind pressure coefficients ($C_{p,mean}$) on different surfaces of model-A under half blockage interference condition | 186 |
| 5.85 | Distribution of mean wind pressure coefficients ($C_{p,mean}$) on different surfaces of model-A under no blockage interference condition | 187 |
| 5.86 | Cross-sectional variation of mean wind pressure coefficients ($C_{p,mean}$) on model-A in full blockage interference condition | 188 |
| 5.87 | Cross-sectional variation of mean wind pressure coefficients ($C_{p,mean}$) on model-A in half blockage interference condition | 189 |
| 5.88 | Cross-sectional variation of mean wind pressure coefficients ($C_{p,mean}$) on model-A in no blockage interference condition | 190 |
| 5.89 | Details of model-B showing different interference conditions | 192 |

| | | |
|---|---|---|
| 5.90 | Distribution of mean wind pressure coefficients ($C_{p,mean}$) on different surfaces of model-A under full blockage interference condition | 193 |
| 5.91 | Distribution of mean wind pressure coefficients ($C_{p,mean}$) on different surfaces of model-A under half blockage interference condition | 194 |
| 5.92 | Distribution of mean wind pressure coefficients ($C_{p,mean}$) on different surfaces of model-A under no blockage interference condition | 195 |
| 5.93 | Cross-sectional variation of mean wind pressure coefficients ($C_{p,mean}$) on model-B in full blockage interference condition | 196 |
| 5.94 | Cross-sectional variation of mean wind pressure coefficients ($C_{p,mean}$) on model-B in half blockage interference condition | 197 |
| 5.95 | Cross-sectional variation of mean wind pressure coefficients ($C_{p,mean}$) on model-B in no blockage interference condition | 198 |
| 5.96 | Details of model-C showing different interference conditions | 200 |
| 5.97 | Distribution of mean wind pressure coefficients ($C_{p,mean}$) on different surfaces of model-C under full blockage interference condition | 201 |
| 5.98 | Distribution of mean wind pressure coefficients ($C_{p,mean}$) on different surfaces of model-C under half blockage interference condition | 202 |
| 5.99 | Distribution of mean wind pressure coefficients ($C_{p,mean}$) on different surfaces of model-C under no blockage interference condition | 203 |
| 5.100 | Cross-sectional variation of mean wind pressure coefficients ($C_{p,mean}$) on model-C in full blockage interference condition | 204 |
| 5.101 | Cross-sectional variation of mean wind pressure coefficients ($C_{p,mean}$) on model-C in half blockage interference condition | 205 |
| 5.102 | Cross-sectional variation of mean wind pressure coefficients ($C_{p,mean}$) on model-C in no blockage interference condition | 206 |
| 5.103 | Details of model-D showing different wind interference conditions | 208 |
| 5.104 | Distribution of mean wind pressure coefficients ($C_{p,mean}$) on different surfaces of model-D under full blockage interference condition | 209 |
| 5.105 | Distribution of mean wind pressure coefficients ($C_{p,mean}$) on different surfaces of model-D under half blockage interference condition | 210 |
| 5.106 | Distribution of mean wind pressure coefficients ($C_{p,mean}$) on different surfaces of model-D under no blockage interference condition | 211 |
| 5.107 | Cross-sectional variation of mean wind pressure coefficients ($C_{p,mean}$) on model-D in full blockage interference condition | 212 |

| | | |
|---|---|---|
| 5.108 | Cross-sectional variation of mean wind pressure coefficients ($C_{p,mean}$) on model-D in half blockage interference condition | 213 |
| 5.109 | Cross-sectional variation of mean wind pressure coefficients ($C_{p,mean}$) on model-D in no blockage interference condition | 214 |
| 5.110 | Details of model-F showing different interference conditions | 217 |
| 5.111 | Distribution of mean wind pressure coefficients ($C_{p,mean}$) on different surfaces of model-F under back-to-back interference condition | 218 |
| 5.112 | Distribution of mean wind pressure coefficients ($C_{p,mean}$) on different surfaces of model-F under back-to-front interference condition | 219 |
| 5.113 | Distribution of mean wind pressure coefficients ($C_{p,mean}$) on different surfaces of model-F under front-to-back interference condition | 220 |
| 5.114 | Distribution of mean wind pressure coefficients ($C_{p,mean}$) on different surfaces of model-F under front-to-front interference condition | 221 |
| 5.115 | Cross-sectional variation of mean wind pressure coefficients ($C_{p,mean}$) on model-F in back-to-back interference condition | 222 |
| 5.116 | Cross-sectional variation of mean wind pressure coefficients ($C_{p,mean}$) on model-F in back-to-front interference condition | 223 |
| 5.117 | Cross-sectional variation of mean wind pressure coefficients ($C_{p,mean}$) on model-F in front-to-back interference condition | 224 |
| 5.118 | Cross-sectional variation of mean wind pressure coefficients ($C_{p,mean}$) on model-F in front-to-front interference condition | 225 |
| 5.119 | Details of model-G showing different interference conditions | 227 |
| 5.120 | Distribution of mean wind pressure coefficients ($C_{p,mean}$) on different surfaces of model-G under back-to-back interference condition | 228 |
| 5.121 | Distribution of mean wind pressure coefficients ($C_{p,mean}$) on different surfaces of model-G under back-to-front interference condition | 229 |
| 5.122 | Distribution of mean wind pressure coefficients ($C_{p,mean}$) on different surfaces of model-G under front-to-back interference condition | 230 |
| 5.123 | Distribution of mean wind pressure coefficients ($C_{p,mean}$) on different surfaces of model-G under front-to-front interference condition | 231 |
| 5.124 | Cross-sectional variation of mean wind pressure coefficients ($C_{p,mean}$) on model-G in back-to-back interference condition | 232 |

| | | |
|---|---|---|
| 5.125 | Cross-sectional variation of mean wind pressure coefficients ($C_{p,mean}$) on model-G in back-to-front interference condition | 233 |
| 5.126 | Cross-sectional variation of mean wind pressure coefficients ($C_{p,mean}$) on model-G in front-to-back interference condition | 234 |
| 5.127 | Cross-sectional variation of mean wind pressure coefficients ($C_{p,mean}$) on model-G in front-to-front interference condition | 235 |
| 5.128 | Details of model-H showing different interference conditions | 237 |
| 5.129 | Distribution of mean wind pressure coefficients ($C_{p,mean}$) on different surfaces of model-H under back-to-back interference condition | 238 |
| 5.130 | Distribution of mean wind pressure coefficients ($C_{p,mean}$) on different surfaces of model-H under back-to-front interference condition | 239 |
| 5.131 | Distribution of mean wind pressure coefficients ($C_{p,mean}$) on different surfaces of model-H under front-to-back interference condition | 240 |
| 5.132 | Distribution of mean wind pressure coefficients ($C_{p,mean}$) on different surfaces of model-H under front-to-front interference condition | 241 |
| 5.133 | Cross-sectional variation of mean wind pressure coefficients ($C_{p,mean}$) on model-H in back-to-back interference condition | 242 |
| 5.134 | Cross-sectional variation of mean wind pressure coefficients ($C_{p,mean}$) on model-H in back-to-front interference condition | 243 |
| 5.135 | Cross-sectional variation of mean wind pressure coefficients ($C_{p,mean}$) on model-H in front-to-back interference condition | 244 |
| 5.136 | Cross-sectional variation of mean wind pressure coefficients ($C_{p,mean}$) on model-H in front-to-front interference condition | 245 |
| 6.1 | Ground floor plan of Square Shape building | 248 |
| 6.2 | Ground floor plan of Plus Shape-1 building | 249 |
| 6.3 | Ground floor plan of Plus Shape-2 building | 249 |
| 6.4 | Ground floor plan of I-Shape-1 building | 250 |
| 6.5 | Ground floor plan of Fish Shape-1 building | 250 |
| 6.6 | Ground floor plan of Fish Shape-2 building | 251 |
| 6.7 | Ground floor plan of Fish Shape-3 building | 251 |
| 6.8 | Elevation and isometric view of Square Shape building | 252 |
| 6.9 | Elevation and isometric view of Plus Shape-1 building | 253 |
| 6.10 | Elevation and isometric view of Plus Shape-2 building | 254 |
| 6.11 | Elevation and isometric view of I-Shape-1 building | 255 |

| | | |
|---|---|---|
| 6.12 | Elevation and isometric view of Fish Shape-1 building | 256 |
| 6.13 | Elevation and isometric view of Fish Shape-2 building | 257 |
| 6.14 | Elevation and isometric view of Fish Shape-3 building | 258 |
| 6.15 | Effect of wind incidence angle on axial force in column-A of Square Shape building | 262 |
| 6.16 | Effect of wind incidence angle on axial force in column-B of Square Shape building | 262 |
| 6.17 | Effect of wind incidence angle on axial force in column-C of Square Shape building | 263 |
| 6.18 | Effect of wind incidence angle on twisting moment Mz in column-A of Square Shape building | 263 |
| 6.19 | Effect of wind incidence angle on twisting moment Mz in column-B of Square Shape building | 264 |
| 6.20 | Effect of wind incidence angle on twisting moment Mz in column-C of Square Shape building | 264 |
| 6.21 | Effect of wind incidence angle on Mx (global) in column-A of Square Shape building | 265 |
| 6.22 | Effect of wind incidence angle on Mx (global) in column-B of Square Shape building | 265 |
| 6.23 | Effect of wind incidence angle on Mx (global) in column-C of Square Shape building | 266 |
| 6.24 | Effect of wind incidence angle on My (global) in column-A of Square Shape building | 266 |
| 6.25 | Effect of wind incidence angle on My (global) in column-B of Square Shape building | 267 |
| 6.26 | Effect of wind incidence angle on My (global) in column-C of Square Shape building | 267 |
| 6.27 | Effect of wind incidence angle on horizontal displacement of column-A of Square Shape building | 268 |
| 6.28 | Effect of wind incidence angle on horizontal displacement of column-B of Square Shape building | 268 |
| 6.29 | Effect of wind incidence angle on horizontal displacement of column-C of Square Shape building | 269 |
| 6.30 | Effect of wind incidence angle on axial force in column-A of Plus Shape-1 | 271 |

building
6.31 Effect of wind incidence angle on axial force in column-B of Plus Shape-1 building 271
6.32 Effect of wind incidence angle on axial force in column-C of Plus Shape-1 building 272
6.33 Effect of wind incidence angle on twisting moment Mz in column-A of Plus Shape-1 building 272
6.34 Effect of wind incidence angle on twisting moment Mz in column-B of Plus Shape-1 building 273
6.35 Effect of wind incidence angle on twisting moment Mz in column-C of Plus Shape-1 building 273
6.36 Effect of wind incidence angle on Mx (global) in column-A of Plus Shape-1 building 274
6.37 Effect of wind incidence angle on Mx (global) in column-B of Plus Shape-1 building 274
6.38 Effect of wind incidence angle on Mx (global) in column-C of Plus Shape-1 building 275
6.39 Effect of wind incidence angle on My (global) in column-A of Plus Shape-1 building 275
6.40 Effect of wind incidence angle on My (global) in column-B of Plus Shape-1 building 276
6.41 Effect of wind incidence angle on My (global) in column-C of Plus Shape-1 building 276
6.42 Effect of wind incidence angle on horizontal displacement of column-A of Plus Shape-1 building 277
6.43 Effect of wind incidence angle on horizontal displacement of column-B of Plus Shape-1 building 277
6.44 Effect of wind incidence angle on horizontal displacement of column-C of Plus Shape-1 building 278
6.45 Effect of wind incidence angle on axial force in column-A of Plus Shape-2 building 280
6.46 Effect of wind incidence angle on axial force in column-B of Plus Shape-2 building 280

| | | |
|---|---|---|
| 6.47 | Effect of wind incidence angle on axial force in column-C of Plus Shape-2 building | 281 |
| 6.48 | Effect of wind incidence angle on twisting moment Mz in column-A of Plus Shape-2 building | 281 |
| 6.49 | Effect of wind incidence angle on twisting moment Mz in column-B of Plus Shape-2 building | 282 |
| 6.50 | Effect of wind incidence angle on twisting moment Mz in column-C of Plus Shape-2 building | 282 |
| 6.51 | Effect of wind incidence angle on Mx (global) in column-A of Plus Shape-2 building | 283 |
| 6.52 | Effect of wind incidence angle on Mx (global) in column-B of Plus Shape-2 building | 283 |
| 6.53 | Effect of wind incidence angle on Mx (global) in column-C of Plus Shape-2 building | 284 |
| 6.54 | Effect of wind incidence angle on My (global) in column-A of Plus Shape-2 building | 284 |
| 6.55 | Effect of wind incidence angle on My (global) in column-B of Plus Shape-2 building | 285 |
| 6.56 | Effect of wind incidence angle on My (global) in column-C of Plus Shape-2 building | 285 |
| 6.57 | Effect of wind incidence angle on horizontal displacement of column-A of Plus Shape-2 building | 286 |
| 6.58 | Effect of wind incidence angle on horizontal displacement of column-B of Plus Shape-2 building | 287 |
| 6.59 | Effect of wind incidence angle on horizontal displacement of column-C of Plus Shape-2 building | 288 |
| 6.60 | Effect of wind incidence angle on axial force in column-A of I-Shape-1 building | 290 |
| 6.61 | Effect of wind incidence angle on axial force in column-B of I-Shape-1 building | 290 |
| 6.62 | Effect of wind incidence angle on axial force in column-C of I-Shape-1 building | 291 |
| 6.63 | Effect of wind incidence angle on twisting moment Mz in column-A of I-Shape-1 building | 291 |
| 6.64 | Effect of wind incidence angle on twisting moment Mz in column-B of I-Shape-1 building | 292 |

| | | |
|---|---|---|
| 6.65 | Effect of wind incidence angle on twisting moment Mz in column-C of I-Shape-1 building | 292 |
| 6.66 | Effect of wind incidence angle on Mx (global) in column-A of I-Shape-1 building | 293 |
| 6.67 | Effect of wind incidence angle on Mx (global) in column-B of I-Shape-1 building | 293 |
| 6.68 | Effect of wind incidence angle on Mx (global) in column-C of I-Shape-1 building | 294 |
| 6.69 | Effect of wind incidence angle on My (global) in column-A of I-Shape-1 building | 294 |
| 6.70 | Effect of wind incidence angle on My (global) in column-B of I-Shape-1 building | 295 |
| 6.71 | Effect of wind incidence angle on My (global) in column-C of I-Shape-1 building | 295 |
| 6.72 | Effect of wind incidence angle on horizontal displacement of column-A of I-Shape-1 building | 296 |
| 6.73 | Effect of wind incidence angle on horizontal displacement of column-B of I-Shape-1 building | 297 |
| 6.74 | Effect of wind incidence angle on horizontal displacement of column-C of I-Shape building | 298 |
| 6.75 | Effect of wind incidence angle on axial force in column-A of Fish Shape-1 building | 300 |
| 6.76 | Effect of wind incidence angle on axial force in column-B of Fish Shape-1 building | 300 |
| 6.77 | Effect of wind incidence angle on axial force in column-C of Fish Shape-1 building | 301 |
| 6.78 | Effect of wind incidence angle on twisting moment Mz in column-A of Fish Shape-1 building | 301 |
| 6.79 | Effect of wind incidence angle on twisting moment Mz in column-B of Fish Shape-1 building | 302 |
| 6.80 | Effect of wind incidence angle on twisting moment Mz in column-C of Fish Shape-1 building | 302 |
| 6.81 | Effect of wind incidence angle on Mx (global) in column-A of Fish Shape-1 building | 303 |
| 6.82 | Effect of wind incidence angle on Mx (global) in column-B of Fish Shape-1 building | 303 |
| 6.83 | Effect of wind incidence angle on Mx (global) in column-C of Fish Shape-1 building | 304 |

| | | |
|---|---|---|
| 6.84 | Effect of wind incidence angle on My (global) in column-A of Fish Shape-1 building | 304 |
| 6.85 | Effect of wind incidence angle on My (global) in column-B of Fish Shape-1 building | 305 |
| 6.86 | Effect of wind incidence angle on My (global) in column-C of Fish Shape-1 building | 305 |
| 6.87 | Effect of wind incidence angle on horizontal displacement of column-A of Fish Shape-1 building | 306 |
| 6.88 | Effect of wind incidence angle on horizontal displacement of column-B of Fish Shape-1 building | 307 |
| 6.89 | Effect of wind incidence angle on horizontal displacement of column-C of Fish Shape-1 building | 308 |
| 6.90 | Effect of wind incidence angle on axial force in column-A of Fish Shape-2 building | 310 |
| 6.91 | Effect of wind incidence angle on axial force in column-B of Fish Shape-2 building | 310 |
| 6.92 | Effect of wind incidence angle on axial force in column-C of Fish Shape-2 building | 311 |
| 6.93 | Effect of wind incidence angle on twisting moment Mz in column-A of Fish Shape-2 building | 311 |
| 6.94 | Effect of wind incidence angle on twisting moment Mz in column-B of Fish Shape-2 building | 312 |
| 6.95 | Effect of wind incidence angle on twisting moment Mz in column-C of Fish Shape-2 building | 312 |
| 6.96 | Effect of wind incidence angle on Mx (global) in column-A of Fish Shape-2 building | 313 |
| 6.97 | Effect of wind incidence angle on Mx (global) in column-B of Fish Shape-2 building | 313 |
| 6.98 | Effect of wind incidence angle on Mx (global) in column-C of Fish Shape-2 building | 314 |
| 6.99 | Effect of wind incidence angle on My (global) in column-A of Fish Shape-2 building | 314 |
| 6.100 | Effect of wind incidence angle on My (global) in column-B of Fish Shape-2 building | 315 |

| | | |
|---|---|---|
| 6.101 | Effect of wind incidence angle on My (global) in column-C of Fish Shape-2 building | 315 |
| 6.102 | Effect of wind incidence angle on horizontal displacement column-A of Fish Shape-2 building | 316 |
| 6.103 | Effect of wind incidence angle on horizontal displacement column-B of Fish Shape-2 building | 317 |
| 6.104 | Effect of wind incidence angle on horizontal displacement column-C of Fish Shape-2 building | 318 |
| 6.105 | Effect of wind incidence angle on axial force in column-A of Fish shape-3 building | 320 |
| 6.106 | Effect of wind incidence angle on axial force in column-B of Fish shape-3 building | 320 |
| 6.107 | Effect of wind incidence angle on axial force in column-C of Fish shape-3 building | 321 |
| 6.108 | Effect of wind incidence angle on twisting moment Mz in column-A of Fish Shape-3 building | 321 |
| 6.109 | Effect of wind incidence angle on twisting moment Mz in column-B of Fish Shape-3 building | 322 |
| 6.110 | Effect of wind incidence angle on twisting moment Mz in column-C of Fish Shape-3 building | 322 |
| 6.111 | Effect of wind incidence angle on Mx (global) in column-A of Fish Shape-3 building | 323 |
| 6.112 | Effect of wind incidence angle on Mx (global) in column-B of Fish Shape-3 building | 323 |
| 6.113 | Effect of wind incidence angle on Mx (global) in column-C of Fish Shape-3 building | 324 |
| 6.114 | Effect of wind incidence angle on My (global) in column-A of Fish Shape-3 building | 324 |
| 6.115 | Effect of wind incidence angle on My (global) in column-B of Fish Shape-3 building | 325 |
| 6.116 | Effect of wind incidence angle on My (global) in column-C of Fish Shape-3 building | 325 |
| 6.117 | Effect of wind incidence angle on horizontal displacement of column-A of Fish Shape-3 building | 326 |

| | | |
|---|---|---|
| 6.118 | Effect of wind incidence angle on horizontal displacement of column-B of Fish Shape-3 building | 327 |
| 6.119 | Effect of wind incidence angle on horizontal displacement of column-C of Fish Shape-3 building | 328 |
| 6.120 | Relative position of square shape buildings under different interference conditions | 331 |
| 6.121 | Interference effect on axial force in column-A of Square Shape building | 331 |
| 6.122 | Interference effect on axial force in column-B of Square Shape building | 332 |
| 6.123 | Interference effect on axial force in column-C of Square Shape building | 332 |
| 6.124 | Interference effect on twisting moment Mz in column-A of Square Shape building | 333 |
| 6.125 | Interference effect on twisting moment Mz in column-B of Square Shape building | 333 |
| 6.126 | Interference effect on twisting moment Mz in column-C of Square Shape building | 334 |
| 6.127 | Interference effect on Mx (global) in column-A of Square Shape building | 334 |
| 6.128 | Interference effect on Mx (global) in column-B of Square Shape building | 335 |
| 6.129 | Interference effect on Mx (global) in column-C of Square Shape building | 335 |
| 6.130 | Interference effect on My (global) in column-A of Square Shape building | 336 |
| 6.131 | Interference effect on My (global) in column-B of Square Shape building | 336 |
| 6.132 | Interference effect on My (global) in column-C of Square Shape building | 337 |
| 6.133 | Interference effect on horizontal displacement of column-A of Square Shape building | 337 |
| 6.134 | Interference effect on horizontal displacement of column-B of Square Shape building | 338 |
| 6.135 | Interference effect on horizontal displacement of column-C of Square Shape building | 338 |
| 6.136 | Relative position of Plus Shape-1 buildings under different interference conditions | 340 |
| 6.137 | Interference effect on axial force in column-A of Plus Shape-1 building | 340 |
| 6.138 | Interference effect on axial force in column-B of Plus Shape-1 building | 341 |
| 6.139 | Interference effect on axial force in column-C of Plus Shape-1 building | 341 |
| 6.140 | Interference effect on twisting moment Mz in column-A of Plus Shape-1 building | 342 |
| 6.141 | Interference effect on twisting moment Mz in column-B of Plus Shape-1 building | 342 |

| | | |
|---|---|---|
| 6.142 | Interference effect on twisting moment Mz in column-C of Plus Shape-1 building | 343 |
| 6.143 | Interference effect on Mx (global) in column-A of Plus Shape-1 building | 343 |
| 6.144 | Interference effect on Mx (global) in column-B of Plus Shape-1 building | 344 |
| 6.145 | Interference effect on Mx (global) in column-C of Plus Shape-1 building | 344 |
| 6.146 | Interference effect on My (global) in column-A of Plus Shape-1 building | 345 |
| 6.147 | Interference effect on My (global) in column-B of Plus Shape-1 building | 345 |
| 6.148 | Interference effect on My (global) in column-C of Plus Shape-1 building | 346 |
| 6.149 | Interference effect on horizontal displacement of column-A of Plus Shape-1 building | 346 |
| 6.150 | Interference effect on horizontal displacement of column-A of Plus Shape-1 building | 347 |
| 6.151 | Interference effect on horizontal displacement of column-A of Plus Shape-1 building | 347 |
| 6.152 | Relative position of Plus Shape-2 buildings under different interference conditions | 349 |
| 6.153 | Interference effect on axial force in column-A of Plus Shape-2 building | 349 |
| 6.154 | Interference effect on axial force in column-B of Plus Shape-2 building | 350 |
| 6.155 | Interference effect on axial force in column-C of Plus Shape-2 building | 350 |
| 6.156 | Interference effect on twisting moment Mz in column-A of Plus Shape-2 building | 351 |
| 6.157 | Interference effect on twisting moment Mz in column-B of Plus Shape-2 building | 351 |
| 6.158 | Interference effect on twisting moment Mz in column-C of Plus Shape-2 building | 352 |
| 6.159 | Interference effect on Mx (global) in column-A of Plus Shape-2 building | 352 |
| 6.160 | Interference effect on Mx (global) in column-B of Plus Shape-2 building | 353 |
| 6.161 | Interference effect on Mx (global) in column-C of Plus Shape-2 building | 353 |
| 6.162 | Interference effect on My (global) in column-A of Plus Shape-2 building | 354 |
| 6.163 | Interference effect on My (global) in column-B of Plus Shape-2 building | 354 |
| 6.164 | Interference effect on My (global) in column-C of Plus Shape-2 building | 355 |
| 6.165 | Interference effect on horizontal displacement of column-A of Plus Shape-2 building | 355 |
| 6.166 | Interference effect on horizontal displacement of column-B of Plus Shape-2 building | 356 |
| 6.167 | Interference effect on horizontal displacement of column-C of Plus Shape-2 building | 356 |
| 6.168 | Relative position of I-Shape-1 buildings under different interference conditions | 358 |

| | | |
|---|---|---|
| 6.169 | Interference effect on axial force in column-A of I-Shape-1 building | 358 |
| 6.170 | Interference effect on axial force in column-B of I-Shape-1 building | 359 |
| 6.171 | Interference effect on axial force in column-C of I-Shape-1 building | 359 |
| 6.172 | Interference effect on twisting moment Mz in column-A of I-Shape-1 building | 360 |
| 6.173 | Interference effect on twisting moment Mz in column-B of I-Shape-1 building | 360 |
| 6.174 | Interference effect on twisting moment Mz in column-C of I-Shape-1 building | 361 |
| 6.175 | Interference effect on Mx (global) in column-A of I-Shape-1 building | 361 |
| 6.176 | Interference effect on Mx (global) in column-B of I-Shape-1 building | 362 |
| 6.177 | Interference effect on Mx (global) in column-C of I-Shape-1 building | 362 |
| 6.178 | Interference effect on My (global) in column-A of I-Shape-1 building | 363 |
| 6.179 | Interference effect on My (global) in column-B of I-Shape-1 building | 363 |
| 6.180 | Interference effect on My (global) in column-C of I-Shape-1 building | 364 |
| 6.181 | Interference effect on horizonta displacment of column-A of I-Shape-1 building | 364 |
| 6.182 | Interference effect on horizonta displacment of column-B of I-Shape-1 building | 365 |
| 6.183 | Interference effect on horizonta displacment of column-C of I-Shape-1 building | 365 |
| 6.184 | Relative position of Fish Shape-1 buildings under different interference conditions | 367 |
| 6.185 | Interference effect on axial force in column-A of Fish Shape-1 building | 367 |
| 6.186 | Interference effect on axial force in column-B of Fish Shape-1 building | 368 |
| 6.187 | Interference effect on axial force in column-C of Fish Shape-1 building | 368 |
| 6.188 | Interference effect on Mx (global) in column-A of Fish Shape-1 building | 369 |
| 6.189 | Interference effect on Mx (global) in column-B of Fish Shape-1 building | 369 |
| 6.190 | Interference effect on Mx (global) in column-C of Fish Shape-1 building | 370 |
| 6.191 | Interference effect on My (global) in column-A of Fish Shape-1 building | 370 |
| 6.192 | Interference effect on My (global) in column-B of Fish Shape-1 building | 371 |
| 6.193 | Interference effect on My (global) in column-C of Fish Shape-1 building | 371 |
| 6.194 | Interference effect on horizontal displacment of column-A of Fish Shape-1 building | 372 |
| 6.195 | Interference effect on horizontal displacment of column-B of Fish Shape-1 building | 372 |
| 6.196 | Interference effect on horizontal displacment of column-C of Fish Shape-1 building | 373 |
| 6.197 | Relative position of Fish Shape-2 buildings under different interference conditions | 375 |

| | | |
|---|---|---|
| 6.198 | Interference effect on axial force in column-A of Fish Shape-2 building | 375 |
| 6.199 | Interference effect on axial force in column-B of Fish Shape-2 building | 376 |
| 6.200 | Interference effect on axial force in column-C of Fish Shape-2 building | 376 |
| 6.201 | Interference effect on Mx (global) in column-A of Fish Shape-2 building | 377 |
| 6.202 | Interference effect on Mx (global) in column-B of Fish Shape-2 building | 377 |
| 6.203 | Interference effect on Mx (global) in column-C of Fish Shape-2 building | 378 |
| 6.204 | Interference effect on My (global) in column-A of Fish Shape-2 building | 378 |
| 6.205 | Interference effect on My (global) in column-B of Fish Shape-2 building | 379 |
| 6.206 | Interference effect on My (global) in column-C of Fish Shape-2 building | 379 |
| 6.207 | Interference effect on horizontal displacment of column-A of Fish Shape-2 building | 380 |
| 6.208 | Interference effect on horizontal displacment of column-B of Fish Shape-2 building | 380 |
| 6.209 | Interference effect on horizontal displacment of column-C of Fish Shape-2 building | 381 |
| 6.210 | Relative position of Fish Shape-3 buildings under different interference conditions | 383 |
| 6.211 | Interference effect on axial force in column-A of Fish Shape-3 building | 383 |
| 6.212 | Interference effect on axial force in column-B of Fish Shape-3 building | 384 |
| 6.213 | Interference effect on axial force in column-C of Fish Shape-3 building | 384 |
| 6.214 | Interference effect on Mx (global) in column-A of Fish Shape-3 building | 385 |
| 6.215 | Interference effect on Mx (global) in column-B of Fish Shape-3 building | 385 |
| 6.216 | Interference effect on Mx (global) in column-C of Fish Shape-3 building | 386 |
| 6.217 | Interference effect on My (global) in column-A of Fish Shape-3 building | 386 |
| 6.218 | Interference effect on My (global) in column-B of Fish Shape-3 building | 387 |
| 6.219 | Interference effect on My (global) in column-C of Fish Shape-3 building | 387 |
| 6.220 | Interference effect on horizontal displacment of column-A of Fish Shape-3 building | 388 |
| 6.221 | Interference effect on horizontal displacment of column-B of Fish Shape-3 building | 388 |
| 6.222 | Interference effect on horizontal displacment of column-C of Fish Shape-3 building | 389 |

# LIST OF TABLES


| Table No. | Description | Page No. |
|---|---|---|
| 2.1 | Wind pressure coefficients on rectangular clad building [Clause 6.2.2.1, IS: 875 (Part-3), 1987] | 9 |
| 3.1 | Details of pressure points on building models | 46 |
| 4.1 | Drag coefficients for model having symmetry about both axes at various wind incidence angles | 82 |
| 4.2 | Drag coefficients for model having symmetry about one axis at various wind incidence angles | 83 |
| 4.3 | Drag coefficients for model having symmetry about both axes at wind interference condition | 84 |
| 4.4 | Drag coefficients for model having symmetry about one axis at wind interference condition | 86 |
| 5.1 | Typical values of wind pressures and $C_{p,mean}$ on model-A at $0^0$ wind incidence angle under isolated condition | 94 |
| 5.2 | Variation of $C_{p,mean}$ on face-A of model-A with wind incidence angle | 103 |
| 5.3 | Variation of $C_{p,mean}$ on face-A (face A1.A2 and A3) of model-B wind incidence angle | 115 |
| 5.4 | Variation of $C_{p,mean}$ on face-A of model-C with wind incidence angle | 125 |
| 5.5 | Variation of $C_{p,mean}$ on Face-A for Difference wind incidence angle of building model-D | 135 |
| 5.6 | Variation of $C_{p,mean}$ on face-A of model-F with wind incidence angle | 151 |
| 5.7 | Variation of $C_{p,mean}$ on face-A of model-G with wind incidence angle | 167 |
| 5.8 | Variation of $C_{p,mean}$ on face-A of model-H with wind incidence angle | 183 |
| 5.9 | Interference effect on variation of $C_{p,mean}$ on face-A of model-A | 191 |
| 5.10 | Interference effect on variation of $C_{p,mean}$ on face-A of building model-B | 199 |
| 5.11 | Interference effect on variation of $C_{p,mean}$ on face-A of building model-C | 207 |
| 5.12 | Interference effect on variation of $C_{p,mean}$ on face-A of building model-D | 215 |
| 5.13 | Interference effect on variation of $C_{p,mean}$ on face-A of building model-F | 226 |

| | | |
|---|---|---|
| 5.14 | Interference effect on variation of $C_{p,mean}$ on face-A of building model-G | 236 |
| 5.15 | Interference effect on variation of $C_{p,mean}$ on face-A of building model-H | 246 |
| 6.1 | Description of the buildings and frame element | 247 |

# LIST OF PHOTOGRAPHS


| Photo No. | Description | Page No. |
|---|---|---|
| 1.1 | Typical tall buildings | 3 |
| 3.1 | External View of Open Circuit Boundary Layer Wind Tunnel | 29 |
| 3.2 | In-side view of wind tunnel showing flow roughening devices | 31 |
| 3.3 | Velocity measuring devices with Probe | 34 |
| 3.4 | Five component load cell attached to the lower side of the wind tunnel floor | 34 |
| 3.5 | Display unit for five component load cell, Data Acquisition System and Computer | 34 |
| 3.6 | Pressure Transducer: Head and Display unit | 34 |
| 3.7 | Actual image of plywood models | 37 |
| 3.8 | Actual image of Perspex sheet models | 38 |

# Chapter - 1

# INTRODUCTION

## 1.1 GENERAL

There is a gradual increase in number of high-rise buildings in almost all the cities over the world every day. It is either existing low-rise buildings being replaced by tall buildings or new tall buildings are being constructed to meet additional demand of space for office or residential purposes. Apart from satisfying space and functional requirements, architects these days try to give additional aesthetic look to their buildings. Some of the tall buildings with varying appearances are shown in Photo. 1.1.

## 1.2 DESIGN LOADS

Like any other structure, tall buildings are designed for gravity loads and horizontal loads. Wind is equally important horizontal load as earthquake load for design of tall buildings. Whereas gravity loads can be correctly calculated, estimation of horizontal loads specially wind loads to be done very carefully for safe and economical design of tall buildings.

## 1.3 WIND LOADS

### 1.3.1 Factors Affecting Wind Loads

Various parameters which affect wind loads on structures can be classified into two groups as: (i) Flow parameters and (ii) Structural parameters. Flow parameters include wind velocity, direction of wind and ground roughness or turbulence. Structural parameters include aspect ratio, building height, slope of the roof, solidity ratio, shielding effect and opening.

### 1.3.2 Evaluation Procedure

The wind loads on a structure are required to be calculated for (a) individual structural elements such as roofs and wall or on a cladding unit, and (b) the building as a whole. There are two methods generally used for evaluation of wind loads on a structure namely (i) pressure coefficients method, and (ii) force coefficients method.

As per the information given in Indian Standard on Wind Loads [IS: 875 (Part-3) - 1987], design wind force on a member is calculated from the following expression

$F = A \times P$

Where,

$F$ = wind force,

$P$ = wind pressure acting uniformly on area A,

$P = 0.5 \times C_p \times \rho \times V_d^2$,

$\rho$ = density of air,

$C_p$ = pressure coefficient,

$V_d$ = design wind speed.

In case of buildings having openings, $C_p$ is expressed as,

$C_p = C_{pe} - C_{pi}$

Where,

$C_{pe}$ = external pressure coefficient and

$C_{pi}$ = internal pressure coefficient.

Therefore, $P = 0.6 \times (C_{pe} - C_{pi}) \times V_d^2$

As per IS: 875 (Part-3)-1987 design wind speed, $V_d$, is expressed as,

$V_d = V_b \times k_1 \times k_2 \times k_3$

Where, $V_b$ is known as basic wind speed. $k_1$ is risk coefficient or probability factor which depends on the class and design life of the structures, $k_2$ is the terrain, height and structure size factor and $k_3$ is topography factor.

If force coefficient method is employed, design wind force on a member is obtained as,

$F = A \times 0.5 \times C_f \times \rho \times V_d^2$

Where,

$C_f$ = force coefficient.

(a) Burj Khalifa

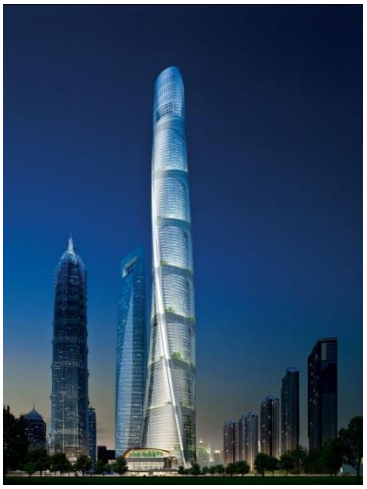

(b) Shanghai Tower

(c) Makkah Royal Clock Tower

(d) One World Trade Center

(e) Taipei 101

(f) Shanghai World Financial Tower

(g) International Commerce Center

(h) Petronas Tower

(i) Zifeng Tower

**Photo. 1.1 Typical tall buildings**

## 1.4 NEED FOR THE PROPOSED STUDY

As explained earlier, it is important to have the information of correct values of wind pressure coefficients ($C_p$) and force coefficients ($C_f$) acting on tall buildings in order to be able to evaluate wind loads correctly for its safe and economical design.

However, as will be seen in Chapter 2 of this thesis, information about $C_p$ and $C_f$ available in relevant codes of practices are primarily for simple cross-sectional shapes only and secondly for isolated or stand-alone condition only. Effects of irregularity in cross-sectional shapes and presence of nearby structures on pressure and force coefficients are not included in standards on wind loads.

An effort has, therefore, been made in the presents study, to generate sufficient data of $C_p$ and $C_f$ on tall buildings with varying cross-sectional shapes firstly under isolated condition and secondly under interference condition through wind tunel tests. After obtaining values of $C_p$ and $C_f$ for many cases, the same has been used to analyze structural frames to obtain the response of the same under wind loads.

## 1.5 OBJECTIVE AND SCOPE

The present study has been carried out with the following objectives and steps.

(i) Eight different types of cross-sectional shapes of tall buildings (Fig. 1.1) are chosen to study the influence of cross-sectional shapes on response of tall buildings under wind loads. All these buildings have same cross-sectional area and height.

(ii) Eight no. wooden models and seven no. Perspex sheet models with pressure points are prepared.

(iii) Wind forces including base shear, base moments and twisting moments acting on all eight models are obtained experimentally by testing wooden models in an open-circuit boundary layer wind tunnel.

(iv) Effect of wind incidence angle on wind forces is studied by allowing the wind to hit the models at many angles.

(v) Effect of interference on wind forces is studied by firstly placing all eight wooden models one by one on load cell and later by placing another model of same cross-section and height in near vicinity at different locations.

(vi) Wind pressure distribution on the surfaces of all building models are obtained by testing all seven Perspex sheet models one after another in the wind tunnel.

(vii) Effect of wind direction on wind pressure distribution is studied by allowing the wind to hit the models at many wind incidence angles.

(viii) Effect of interference on wind pressure distribution is studied by placing wooden model of same cross-section in near vicinity.

(ix) Drag coefficients ($C_D$) or Force coefficients ($C_f$) are calculated from the values of forces measured.

(x) Pressure coefficients ($C_p$) are obtained from the measured values of wind pressures.

(xi) Values of $C_D$ and $C_p$ obtained experimentally are compared with corresponding values available in standards on wind loads and research publications.

(xii) All buildings are assumed to be made of R.C.C. rigid-frames. Out of eight, seven buildings are first designed for gravity loads to arrive at suitable values of cross-sectional dimensions of beams and columns.

(xiii) All seven building frames are analyzed by using experimentally obtained wind loads under isolated condition. Response of the buildings are obtained in the form of column forces, column moments and displacements.

(xiv) Wind response analysis is repeated on all seven buildings for interference conditions.

(xv) Response parameters obtained in isolated condition are compared with those in interference conditions.

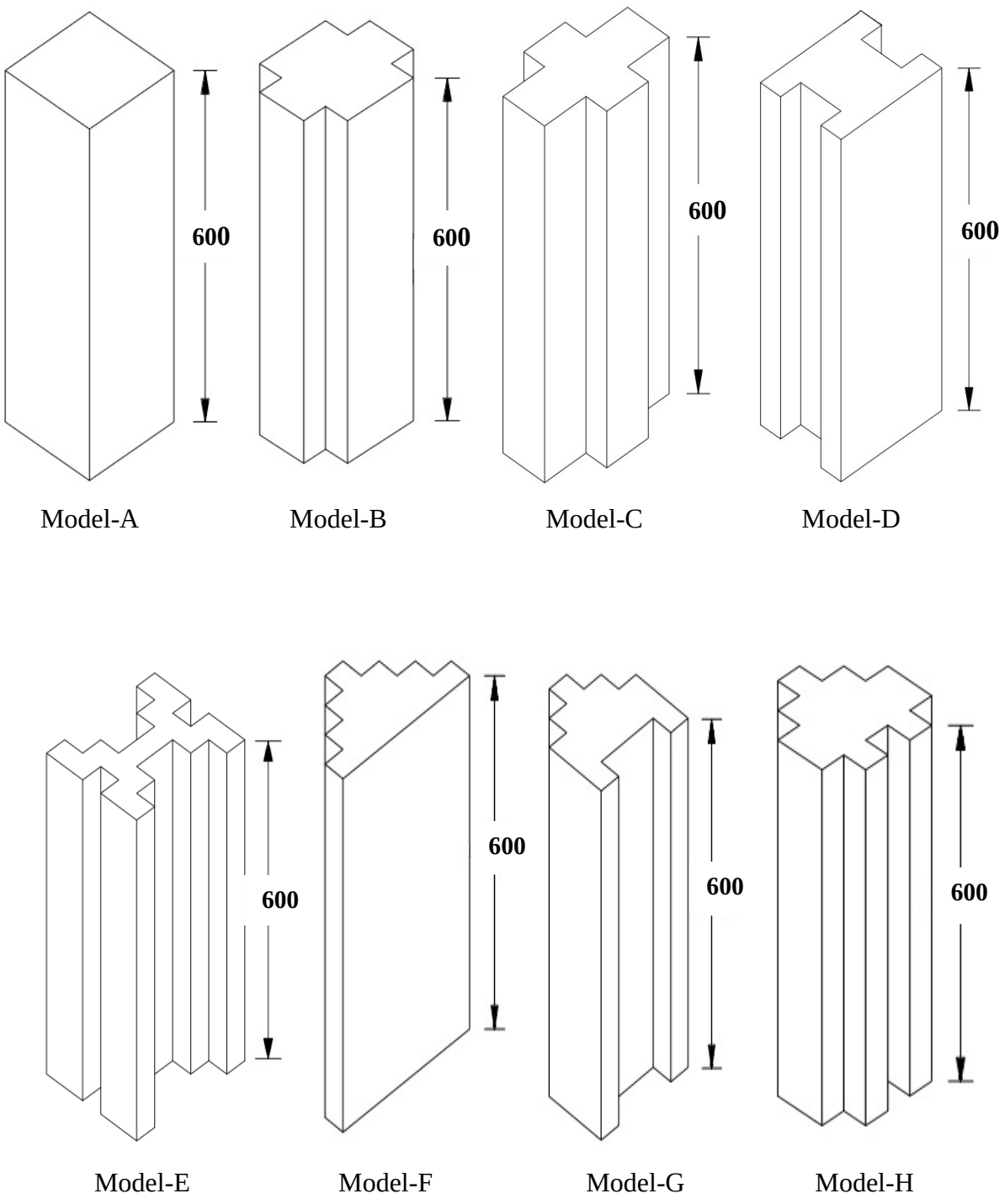


(All dimensions are in mm)

**Fig. 1.1 Isometric view of building models**

## 1.6 ORGANISATION OF THE THESIS

The present research work is described in 7 chapters in this thesis.

Chapter 1 briefly describes method of evaluation of wind loads on tall buildings. It is followed by objective and scope of the present study.

Information available regarding wind pressure coefficients ($C_p$) and wind force coefficients ($C_f$) on tall buildings with varying cross-sectional shapes in standards on wind loads of various countries are enumerated in Chapter 2. This chapter also includes similar information available in research publications.

Chapter 3 gives detailed information about the models prepared and wind tunnel used for experimental study.

Results of the force measurement study are discussed in Chapter 4.

Chapter 5 describes the results of pressure measurement study.

Chapter 6 is devoted for wind response analysis of all the buildings.

Conclusions drawn from the present study are listed in Chapter 7. Utility of present study and scope of further research work are also included in this chapter.

Research publications referred during the present study are listed at the end of the thesis.

# Chapter - 2

# LITERATURE REVIEW

## 2.1 GENERAL

Objectives of the present study is to understand the effects of cross-sectional shapes of tall buildings on (i) wind loads acting on them which includes base shear, base moments and twisting moments, (ii) wind pressure distribution on the surfaces of tall buildings and (iii) response of them under wind loads.

As has been mentioned briefly in Chapter 1, information available in codes of practices of various countries dealing with wind loads, are for limited cross-sectional shapes and limited wind incidence angles only. Detailed descriptions about available codal information are being given in this chapter.

During the last 4 decades, many researchers have carried out wind tunnel as well as analytical studies on the models of tall buildings with different cross-sectional shapes. Findings of some of these researchers are also included in this chapter.

## 2.2 CODAL INFORMATIONS

### 2.2.1 Australia and New-Zeeland Standard (AS/NZS-1170-2, 2011)

This code of practice covers the structures which falls within the criteria such as (i) building less than or equal to 200 m height and (ii) structures with roof span less than 100 m. This code also includes the wind load for structures other than offshore structures, bridges and transmission towers. The information about the cross-sectional shape other than square and rectangular shape is not included in this code of practice. Very little information about the pressure distribution is available when building is attacked by the skew wind angle.

### 2.2.2 American Standard (ASCE-7, 2002)

ASCE-7 gives detailed information about wind loads on low-rise buildings having different types of roof. The information on low-rise buildings with different aspect ratio are also available in this standard. However, there is lack of information about wind loads on high-rise buildings with different cross-sectional shapes. Similarly no information is available in case of skew wind.

### 2.2.3 British Standard (BS EN 1991-1-4, 2005)

This code of practice gives the guidance on the determination of natural wind actions for the structural design of buildings and civil engineering works for each of the load

conditions under consideration. This code of practice is applicable to building and structures with heights up to 200 m and bridge having no span greater than 200 m. This code also intends to predict characteristics wind actions on land based structures and their components. There is no information about the wind pressure distribution for uneven cross-sectional shapes. Information about different skew angle wind is also not included in this code of practice.

### 2.2.4 Indian Standard (IS-875, part-3, 1987)

According to IS: 875 (Part-3), (Clause 6.2.2.1, Table 4), 1987, the external pressure coefficients ($C_p$) for rectangular clad buildings are given only for uniform cross-section along the height. These values are available for different height to width ratios and length to width ratios. However, wind pressure coefficients are given for two different wind incidence angles namely $0^0$ and $90^0$ only. Typical values are shown in Table 2.1. Similarly, force coefficients ($C_f$) are given in the existing code (Clause 6.3.2.1, Fig. 4) for buildings with rectangular cross-section.

**Table 2.1 Wind pressure coefficients on rectangular clad building**

**[Clause 6.2.2.1, IS: 875 (Part-3), 1987]**

| Building plan & height ratio | Elevation | Plan | Wind angle Θ | $C_{pe}$ for surface | | | | Local $C_{pe}$ |
|---|---|---|---|---|---|---|---|---|
| | | | | A | B | C | D | |
| $]< \frac{l}{w} \leq \frac{3}{2}$ and $\frac{3}{2} < \frac{h}{w} < 6$ | 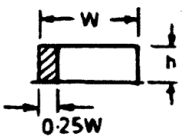  | 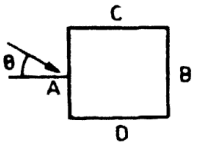  | 0 | +0.8 | -0.25 | -0.8 | -0.8 | -1.2 |
| | | | 90 | -0.8 | -0.80 | +0.8 | -0.25 | |

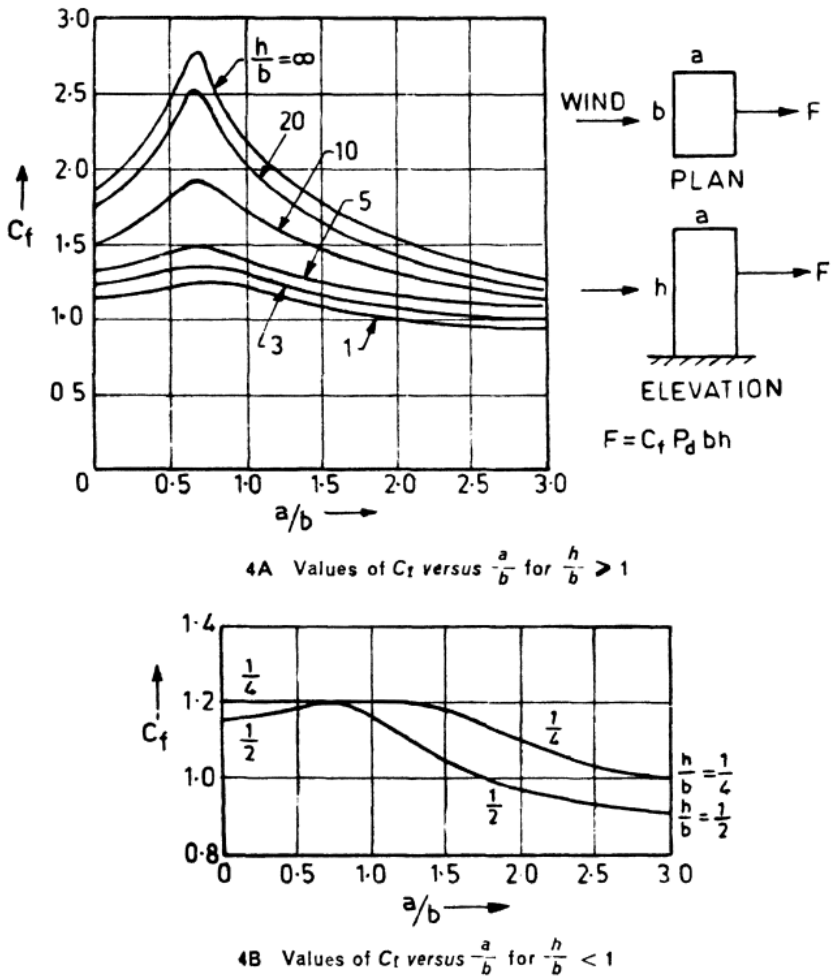


**Fig. 2.1 Force coefficients for rectangular clad buildings in uniform flow [(Clause 6.3.2.1, Fig. 4), IS: 875 (Part-3), 1987]**

## 2.3 RESEARCH PUBLICATIONS

### 2.3.1 Wind Tunnel Studies - Isolated Condition

**Kareem and Cermak (1984)** reported the nature of pressure fluctuations on the side faces of a square building model in boundary-layer flow parallel to these faces. Authors concluded that the effect of increasing the turbulence intensity results in reduction of the lift force coefficient. It was also concluded that the pressure fluctuations on the side faces of a prism are nonhomogeneous, which implies that they are dependent not only on separation distance and time, but also depend on the relative location.

**Stathopoulos (1985)** experimentally investigated the ground-level wind conditions around buildings with chamfered corners. This study included models of both square and chamfered buildings of various heights ranging between 60 m and 180 m which were exposed to a simulated open country terrain. Corners of the building were chamfered at a $45^0$ angle. Effect of chamfered roof was also examined by the author.

**Tanaka and Lawen (1986)** carried out pressure and aeroelastic study of the CAARC standard tall building with the linear scale of 1:1000. Results were compared with other experimental works.

**Balendra and Nathan (1988)** presented the experimental results for longitudinal, lateral and torsional responses of a triangular building model of aspect ratio 1:4.6 in an atmospheric boundary layer, using a linear model with three degree of freedom. Variation of wind incidence angle are used to determine the critical angles for longitudinal, lateral and torsional motions. It was found that the R.M.S displacements of model vary exponentially with reduced velocity.

**Kwok et al. (1987)** conducted wind tunnel model tests to investigate the effect of edge configuration on the wind-induced response of a tall building with rectangular cross-section. Results of wind tunnel model tests showed that modification to the edge of a tall building with a rectangular cross-section has a significant effect on the excitation process and the response characteristics. The authors found that two of the configurations considered are effective in causing significant reductions in both along wind and across wind responses.

**Kwok (1988)** conducted the wind tunnel tests to investigate the effect of building shape on the wind-induced response of a tall building with rectangular cross-section. It was also found that building model with horizontal slots, slotted corner and chamfered corners caused significant reduction in both the along-wind and across-wind responses.

**Stathopoulos and Zhu (1988)** studied the wind pressure on buildings which are affected by various appurtenances such as balconies or general roughness of the building envelope. Influence of the configuration of the building envelope to the wind loads on cladding and structural elements were determined. The authors also investigated the possibility of simplification of wind tunnel building models.

**Szalay (1989)** carried out wind tunnel measurements to determine drag coefficients on 16 sided polygon, 12 sided polygon and circular cylinders. Force and pressure measurements were made Reynolds number dependency was also investigated within limited range.

**Hayashida and Iwasa (1990)** studied the effects of building plan shape on aerodynamic forces and displacement response for high-rise buildings with an assumed height of 600 m in a wind tunnel. Authors carried out experiments using rigid models with 8 different types of building plan shapes of equal floor area (=6400 $m^2$) and equal building height (=600m).

**Lythe and Surry (1990)** examined mean torsional wind loads on tall buildings using data base which is experimentally obtained from wind tunnel tests, and concluded that wind tunnel testing is needed when dynamic properties of a building are unusual, or if the center of stiffness is significantly different from the center of mass or the platform centroid.

**Stathopoulos and Luchian (1990)** carried out experiments which consist of an extensive series of tests in a boundary layer wind tunnel simulating the flow over an open country terrain exposure. The results of the tests for buildings with a two-level flat roof were discussed. The results of the study are compared with the flat roof specifications provided by standards on wind loads.

**Cheong et al. (1992)** presented experimental techniques for determination of wind loads along the height of a tall and slender building. They used an aeroelastic model for conducting the experiment. The dynamic pressures acting on the model were measured simultaneously from two pressure tapping. Then the auto and cross spectral densities were calculated which enabled the calculation of acceleration at a height.

**Isyumov et al. (1992)** studied the performance of a tall building under wind action. Prediction of the wind induced response of a 390 m high office tower have been made using high frequency base balance model and aero elastic model techniques. The authors observed that due to the presence of another building, the aerodynamic interference can also be experienced in a highly built-up terrain.

**Jamieson et al. (1992)** conducted an experimental study for wind tunnel pressure measurement at 2/3 height on a 1:300 scale model of a tall building with various corner configurations based on the CAARC standard tall building. The aim was to investigate the influence of corner configuration on the magnitude and distribution of the peak pressure coefficients. Three different corners such as square, cut corner and beveled corner were included for the wind tunnel pressure measurement study.

**Beneke and Kwok (1993)** tested four different models of buildings in boundary layer wind tunnel to investigate wind induced torsion on tall buildings. Four basic cross-sectional shape namely rectangle, square, triangle and D-shape were considered. Each model was tested at varying reduced velocities and angles of wind induce under wind excitation corresponding to terrain categories 2 and 4. Results indicate that the triangular shape model produced dynamic torsional response in excess of any other model tested. D-shape and diamond shape models yielded significantly lower torsional response.

**Chaudhary and Garg (1993)** conducted experimental study for wind pressure distribution around the high-rise building curved in plan. The aim was to investigate the influence of curved plan on the distribution of the peak pressures.

**Kawai (1993)** studied the bending and torsional vibration of tall buildings in strong wind. Wind tunnel tests were carried out in smooth flow and turbulent boundary layer flow over urban area. It was observed from the experimental studies that the strong vortex induced vibrations in the tall buildings occurred with shallow section both in smooth and turbulent flows. The torsional flutter were also observed by the authors for the model of the side ratio of 4 both in smooth and turbulent flows at the reduced velocity of U/n =6, where U is the flow velocity and n is the natural frequency of the torsional vibration.

**Miyashita et al. (1993)** investigated the characteristics of both the wind force acting on, and the responses of a square building with chamfered corners. The wind forces acting on the building were obtained from the wind tunnel tests. The authors also calculated the response of the building through the employment of modal analysis, which uses the results of the wind tunnel tests. The importance of correlation of the wind forces in along and across direction for the response analysis was addressed in this study.

**Selvam and Konduru (1993)** studied the rood corners pressures on the Texas Tech Building using k-Ɛ turbulence model on a non-staggered grid system. Computed pressures and rms pressures were compared with field and wind tunnel results by authors.

**Surry and Djakovich (1995)** investigated the fluctuating pressures on models of tall buildings. The objective of this study have been to explore the high peak suctions developed on building models and their relationship with building shape and the characteristics of the oncoming simulated atmospheric shear flow. It was concluded that the highest peak suction occurs practically at any location of the model side face and it has reasonable agreement with the current Canadian code requirements for cladding design.

**Cooper et al. (1997)** measured the unsteady wind loads acting on a super-tall building with a tapered cross-section and beveled corners as a functions of reduced velocity and motion amplitude. The damping components of the along-wind and across-wind unsteady aerodynamics forces were also obtained from time histories of fluctuating aerodynamics force.

**Kawai (1998)** investigated the effects of corner cut, recession and roundness on aero elastics instabilities such as vortex induced excitation and galloping oscillation. The author observed that small corner cut and recession were very effective to prevent aero elastic instability for a square prism by increasing the aerodynamics damping, but the large cornet

cut promotes the instability at low velocity even if the damping is small enough. Corner roundness is also effective to increase the aerodynamic damping to suppress the instability. The corner modifications promote the instability at low speed, because the vortex shedding is prevented by the modifications.

**Letchford and Robertson (1999)** studied the full scale mean wind loads on panels within free standing walls and compared with previous and new wind tunnel studies.

**Tamura and Miyagi (1999)** carried out wind tunnel tests for measurements of aerodynamics quantities, like averaged and fluctuating statistics of drag and lift forces which acting on a square sectioned cylinder with sharp, chamfered or rounded corners. Principal results were as follows: (1) side surface with cut corner and round corner promote the reattachment and reduction of drag forces. (2) In case of rounded corner cylinder in turbulent flows, it was found that the spectral peak frequencies are higher than those in uniform flow, due to turbulent flow the shear layer that separate from the windward edges reattached to the side surface even at angle of attack $\alpha = 0^0$. (3) The values of $C_{LRMS}$ for three dimensional cylinders were reduced to about 10% of the values for two dimensional cylinders. This means that effects of Karman vortices and resulting lift force were not so large for three dimensional cylinders.

**Thepmongkorn and Kwok (2002)** carried out a wind tunnel study on the effects of eccentricity between center of mass and center of stiffness of a tall rectangular building on the wind generated response and wind excitation mechanism. The results indicated significant effects of eccentricity on the along-wind, cross-wind, and twisting moment responses for both cases when wind is normal to narrow and wide faces of the building model.

**Balendra et al. (2003)** conducted full scale measurement for wind induced response of some typical tall buildings. Based on these observations they presented an empirical relation for predicting period of vibrations. These also presented the expression relating wind speed to acceleration in buildings.

**Liang et al. (2004)** carried out an experiment to find the wind-induced dynamic torque on rectangular cylinders with various side ratios through a series of model teats in a boundary layer wind tunnel. Based on the experimental investigation, authors presented empirical formulae of torque spectra, RMS torque on rectangular and Strouhal number, as well as coherence functions of torque. An analytical model of wind-induced dynamic torque on rectangular tall building was established accordingly. Comparisons were made between the experimental and analytical study.

**Balendra et al. (2005)** used a new technique of laser positioning measurement system of direct measurement of wind induced tip displacement of tall building. Based on the present study it was recommended that this technique can used for closely spaced structures which can be structurally coupled or uncoupled, to measure the relative displacement. The authors concluded that this method is better than conventional strain gauge method.

**Gomes et al. (2005)** presented the experimental and numerical study of wind pressures on irregular-plan shapes. The experiment were carried out in a closed-circuit wind tunnel and a multi-channel pressure measurement system was used to measure means values of loads on 1:100 scale models. Authors compared the experimental data with the numerical CFD values and found that results were same for normal wind incidence whereas differences have occurred for other directions.

**Lin et al. (2005)** investigated the characteristics of wind loads on tall buildings. Nine models with different rectangular cross section were tested in a wind tunnel. The effects of three parameters namely side ratio, aspect ratio, and elevation were highlighted in analyses of local wind force coefficients. Comparisons were also made with results obtained from high-frequency force balances in two wind tunnels.

**Ahuja et al. (2006)** investigated unpleasant wind condition around tall buildings. Wind velocity near the earth surface is quite close to zero and it increases with increase in height. Authors concluded that the two principal types of flow that adversely affect the pedestrian environment are (i) downwash flow bringing higher energy wind to lower elevation and (ii) horizontally accelerated flow. The comfort criteria for pedestrian within a built environment were also included in this paper.

**Mendis and Ngo (2006)** discussed the changes in tall building design practice after the World Trade Centre (WTC) buildings collapse. These suggestions and the lessons learnt from the collapse are discussed in the paper.

**Garg and Chaudhry (2007)** carried out an experimental study to investigate the wind induced flow-field around the complex shaped buildings.

**Goel et al. (2007)** studied the wind loads on buildings with attached canopies. Six number scaled models of the arch roof building were tested with five types of canopies attached.

**Amin and Ahuja (2008)** presented the experimental results of wind tunnel tests to evaluate wind pressure distributions on different faces of typical plan shape buildings. These models were made from Perspex sheet at geometrical scale of 1:500. Authors focused on the effects of model shapes on the surface pressure distribution. Fluctuating values of wind

pressure were measured at pressure points on all surfaces and mean, maximum, minimum and R.M.S. values of pressure coefficients were evaluated.

**Dalui (2008)** measured wind pressure distribution on building models having square, circular and octagonal cross-section.

**Kim et al. (2008)** conducted an experimental study to investigate the effects of tapering on reducing the RMS across-wind displacement responses of a tall building, using an aeroelastic tapered model of a tall building. Author concluded that the tapering effect appeared when the reduced velocity was high and the structural damping ratio had a moderate value of 2-4% and the less damping ratio causing motion-induced excitation.

**Ngo and Letchford (2008)** studied the topographic effects on gust wind speed. Four major wind-loading codes are reviewed by author in order to make the detailed comparison of topographic effects between codes.

**Goel and Ahuja (2009)** carried out an experimental study in the boundary layer wind tunnel to measure the wind loads on low rise buildings.

**Gu (2009)** carried out wind tunnel tests on 27 typical tall building models by using wind pressure scanning and HFFB techniques. Characteristics of wind pressure and forces acting on these buildings were analyzed by author.

**Merrick and Bitsuamlak (2009)** explored the effect of building shape on the wind induced response of a structure through wind tunnel studies. Load patterns attributed to the cross-sectional shape of the structure were observed in the results. This value of wind load were compared against the values given by NBCC (National Building Code of Canada) and ASCE (American Society of Civil Engineering) standards.

**Verma (2009)** measured wind pressure distribution on the models of structurally coupled tall buildings.

**Amin and Ahuja (2011)** presented the experimental investigation of wind pressure distribution on models of typical plan shape buildings on different wind incidence angel from $0^0$ to $180^0$ at an interval of $15^0$. Two L-shaped and two T-shaped models having same plan area and height but having different dimensions were tested in a closed circuit wind tunnel. It was observed that plan shape and dimensions of models significantly affects the wind pressure distributions on different faces of models.

**Bhatnagar (2011)** carried out an experimental study of five different high-rise buildings with different plan shapes i.e. square, corner cut, corner chamfered, through passage and half through passage in close circuit wind tunnel. The effects of different plan shape on wind pressure distribution were presented by the author.

**Yang et al. (2011)** conducted an experimental study to quantify the characteristics of wall, vortex and flow condition around the high-rise building as well as the resultant wind forces (forces and moments) acting on models in high speed wind. The measurement result clearly revealed that the wake vortex and turbulent around the buildings induced by high speed wind like tornado are totally different from those in conventional straight line winds.

**Ramakant (2012)** conducted wind tunnel test on rigid model of T-shaped building for evaluating pressure coefficients on different face of building model.

**Tanaka et al. (2012)** conducted aerodynamic force measurement and wind pressure measurement for tall building models with various building shapes but with same height and volume. The authors discussed about the mean overturning moment coefficients for all models and their behavior in the along wind direction. It was found that the correlation between maximum mean coefficients and maximum fluctuating coefficients are high for both along-wind and across-wind directions. The power spectral densities of the models, aerodynamics characteristics of the composite models with multiple modifications were also discussed by authors.

**Kumar (2013)** studied wind pressure distribution on tall buildings with steps configuration. It was observed by the author that both base shear and base moments developed due to wind loads are not only influenced by wind direction but these are highly affected by steps configurations also.

**Kushal (2013)** conducted an experimental study on L-shape and T-shape building models with linear scale of 1:200. Author presented the force and pressure coefficients around the tall building models considering isolated and interfering condition.

**Chakraborty et al. (2014)** conducted experimental study to measure the mean wind pressure coefficient on plus shape model. The experiment carried out in an open circuit wind tunnel on a 1:300 scale rigid model.

**Mukherjee et al. (2014)** conducted an experimental study on Y-shape building with linear scale of 1:300. Authors also studied the flow pattern around the model and explained the phenomenon occurring around the model.

**Verma et al. (2014)** presented application of artificial neural networks (ANNs) to estimate pressure coefficients on surface of tall buildings. Authors concluded that the value of $C_p$ (Mean) decreases with increase in wind incidence angle for the same pressure point. Further, suction effect is noticed near the corners of the building.

**Zhang et al. (2014-a)** carried out experimental investigation to quantify the characteristics of the microburst-induced wind loads i.e. both static and dynamic wind loads

acting on a high-rise building model and compared those with the test model placed in conventional atmospheric boundary layer (ABL) winds. Authors performed the experimental study by using an impinging-jet-based microburst simulator available in IOWA State University.

**Zhang et al. (2014-b)** studied the microburst-wind loading effects on low-rise structures. A cubic-shaped building, a grain bin and two gable-roofed buildings were considered and compared by performing laboratory tests on scaled models using a microburst simulator at IOWA State University.

**Verma et al. (2015)** carried out CFD analysis to evaluate wind loads on octagonal tall buildings. Mean area weighted average wind pressures on the faces of the octagonal plan building models are evaluated by the authors with the help of FLUENT-14 (ANSYS 14.0) for CFD analysis.

### 2.3.2 Wind Tunnel Studies - Interference Condition

**Timothy et al. (1977)** tested a single square prism at different wind directions in a wind tunnel in smooth and turbulent flow. A second square prism was placed on upstream side with various separations to provide interference effect. Authors concluded that the presence of buildings and towers in strong winds made situation complicated.

**Shykes (1983)** tested a model of a simple building of rectangular plan form and elevation (CAARC standard model) in a simulated atmospheric shear flow. The model was rigid and mounted on two mutually perpendicular pairs of torsion bars which allowed the model to vibrate with two degrees of freedom with linear mode shapes. Author concluded that the fluctuating lateral displacement was reduced by the presence of the upwind models at reduced wind speed around 10 m/s at which the isolated model experienced peak response. These tests have confirmed the importance of testing particular layouts of the buildings which may give rise to increase in forces when one building lies in or near to the wake of similar size buildings.

**Blessmann and Riera (1985)** conducted the experiment to study the interaction between two square prisms with a height to base length equal to six. Fifteen relative position were studied for wind incidence angle at every $15^0$ under smooth-uniform as well as turbulent shear wind. It was concluded that the buffeting causes an increase in the maximum resultant force coefficient by as much as 30% with respect to the isolated building, in both flow conditions.

**Stathopoulos and Storms (1986)** carried out an experimental measurement in a boundary layer wind tunnel to determine wind velocity and turbulence conditions in passage between two rectangular tall buildings. Experiments were done under simulated open country terrain conditions for a wide range of wind azimuths. The authors also included geometrical parameters such as the height of the buildings and the passage width. Results show that most critical wind velocity conditions occur for buildings of different height at a point near the passage entrance for wind direction skewed by $30^0$ from the center line.

**Chaudhary et al. (1990)** studied the pressure coefficients on tall twin towers of a building complex which was curved plan. Two complex shapes of building were studied for arriving at an optimum configuration of building in respect of wind effects. Pressure coefficients and resulting wind loads on the lattice tower of 63 m developed due the interference of two silos of 40 m height were also evaluated.

**Yahyai et al. (1990)** studied interference effects for tall rectangular buildings which were almost square in plan, with building proportions (1:1.2:6). The authors studied both rigid and aeroelastic models. From the study on rigid models it was concluded that interference effect between two buildings of same size was observed upto 24 times the depth of building located on the upstream of the object building. For mean response in the along-wind direction there was shielding effect. Fluctuating response in along-wind and across-wind directions were observed to have a peak value at 5D-6D spacing for in line positions, in SAB (short afterbody) orientation. In SAB orientation the long side is facing the wind. For LAB (long afterbody) study, the maximum BF for RMS along-wind response was observed at (6D, 2b) position at a reduced velocity of 6.0. In LAB orientation the short side is facing the wind. Maximum BF for RMS across-wind response was observed from (2.5D, 2.5b) position at a reduced velocity of 6.0. Significant increase in the RMS response was reported between 2.5D and 6D spacing and at 1b-4b offsets, D being the dimension of the building along the wind direction. For downstream interference, 2D to 3D spacing, with or without offset was found to be critical. A critical zone of interference was demarcated, which extends between 1b and 3b on either sides of mean wind direction on the face of the model.

**Blessmann (1992)** studied the influence of neighborhood in a large city center on models of two tall buildings by considering the static wind effects. Author concluded that values of the force increase in small extent in case of insolated buildings, but torsional moments due to wind acting on parts of the main facades had an increase of 125% in one case and 54% in the other.

**Taniike (1992)** investigated the proximity effects of tall square building by using neighboring structures of different size in a low turbulence wind environment. It was found that the fluctuating forces on the object building generally increased by the presence of upstream buildings of any size. It was also concluded by the author that, the increase in the fluctuating forces was mainly caused by (i) shed vortices from the upstream building directly hitting the object building (2) transition of the shed vortices into smaller scale vortices through a convection process which increased the fluctuating velocity of the incident flow, (3) the connected flow between the two buildings that strengthened vortices shedding from the object building.

**Tsutsumi et al. (1992)** carried out an experiment to investigate the characteristics of wind pressure on groups of apartment buildings. The main parameter of this study was comparison of staggered grid layout with normal gird layout. The effects of wind incidence angles were also examined. The results were presented as the wind pressure coefficient difference between wind ward and leeward surfaces. The relation between the average wind pressure coefficients in a model with various layouts of buildings was discussed.

**Yahyai et al. (1992)** tested the interference effect of aerolastic model of a typical rectangular multistoreyed building. It was observed that due to the presence of an interfering building, the mean response of the building generally reduced on account of shielding, while the dynamic response usually increased. The effect of interference is much more pronounced when the interfering building is located on the upstream side compared to when it is situated on the downstream side.

**Paterson and Papenfuss (1993)** compared the experimentally obtained wind flows data of two tall buildings with results obtained from a computer simulation. The simulation uses a steady-state solution method with a k-ε model of turbulence. It was concluded that the vortices shed from each building have a strong influence on pressures on and around the other buildings.

**Zhang et al. (1995)** performed wind tunnel model tests to investigate interference effects on torsional response of a tall square cross-section building with structural asymmetry. Two sizes of square cross-section rigid interfering building models were individually located at positions upstream and downstream side of the principal model to generate interference effects. It was concluded that the mean and standard deviation of response of eccentric principal building could be significantly enhanced due to the presence of interfering building.

**Gupta and Krishna (2002)** carried out an experimental study to measure the critical interference around a TV tower.

**Thepmongkorn et al. (2002)** investigated the interference effects on the CAARC standard tall building by an 8:1:1 tall interfering building both upstream and downstream. It was concluded that the along wind and across wind, and twisting moment responses of the principal building were significantly increased when the interfering building was located diagonally upstream.

**Xie and Gu (2004)** studied the mean interference effects between two and among three tall buildings through series of wind tunnel tests. The authors also discussed the shielding and channeling effects to understand the complexity of multiple- building effects. The result shows that the upstream interfering buildings cause certain shielding effect by decreasing the mean wind load on downstream side building. The variation of the shielding effect is found to be significant when the heights of interfering buildings range from 50% to 125% of the height of the principal building.

**Chaudhary and Garg (2006)** investigated the pressure and force coefficients of typical shape building of 24.80 m height made from four rectangular shaped blocks arranged in a cruciform shape. The study was carried out a wind tunnel under simulated Atmospheric Boundary Layers (ABLs) conditions. The pressure coefficients obtained around various faces of the building are used to obtain the design forces. It was concluded that building under consideration was subjected to significantly higher pressure coefficients as compared to the rectangular/square shape buildings.

**Gupta et al. (2007-a & b)** conducted a series of tests in a wind tunnel on four tall residential towers (30 storey/108 m tall and 50 storey/180 m tall) in a simulated boundary layer flow and described the results under stand alone and interference conditions. It was concluded that the wind tunnel study influences the design of window and door sections, the exterior panel walls as well as the thickness of the window glass panels, but there is not a very significant variation in the overall wind design coefficients from IS code when integrated over the whole structure for stand-alone case.

**Lam et al. (2008)** investigated the interference effects on a row of square-plan tall buildings arranged in close proximity with wind tunnel experiments. Forces and moments on each building were measured with base balance under different wind incidence angles and different separation distances between buildings. It was found that the inner buildings inside the row were subjected to reduced wind load components acting along the direction of row at most wind directions. As compared to isolated case, the building surrounded with interfering

building was subjected to less wind loads. The interference effect on fluctuating wind loads was also investigated by the authors. It was also found that across wind load fluctuations are much smaller than the isolated building case with the disappearance of vortex shedding peak in the load spectra.

**Zhang and Gu (2008)** presented the numerical and experimental investigation of wind induced interference effects on the distribution of pressure on a building surround by another building in staggered arrangement. This test was carried out in a low speed boundary layer wind tunnel. Mean and fluctuating pressure measurement on the principal building surrounded by interfering building were obtained.

**Amin and Ahuja (2009)** presented the mean interference effects between a pair of buildings closed to each other in a geometrical configuration of L-shape and T-shape. Experiment was carried out in closed circuit wind tunnel on models of 1:300 scale to measure the mean pressure coefficients on two building models close to each other with different wind incidence angles. Significant changes in wind loads were observed in interference condition as compared to a similar building in an isolated. It was also found that the interference effects mainly depend on the angle of attack and arrangement of the buildings with respect to each other.

**Kim et al. (2009)** performed the experiments to determine interference effects of local peak pressures on an identical pair of tall buildings to establish design cladding pressure. The results show distribution of maximum and minimum pressure coefficients on walls of principal building with critical locations of an interfering building. It was also noticed that the maximum wind pressure coefficients occur on the side walls of the principal building due to interference.

**Gu and Xie (2011)** reported the means and dynamic response interference effect and peak wind pressure interference effects of two and three tall building models. Especially three buildings configuration are investigated through a series of wind tunnel tests on typical tall building models using force balance technique and wind pressure measurements.

**Hui et al. (2013)** investigated the interference effects between two rectangular-section high-rise buildings by wind tunnel experiments, which are focused on local peak pressure coefficients. These experiments were carried out under 72 wind incidence angles for various configurations. In this study two building arrangements were considered namely parallel and perpendicular. Authors presented the evaluation method of interference effects for local peak pressures in detail, and also discussed the interference factor for the largest positive and

smallest negative peak pressures. The result shows that interference effects greatly depend on configuration and directions of wind.

**Menicovich et al. (2014)** studied the integration of active air flow control into the assembly of building envelopes in order to affect the interaction between tall buildings and surrounding air flow.

**Verma (2014)** carried out wind tunnel study on rigid models of rectangular shape high rise buildings coupled through single bridge. Author conducted experimental work for 3 wind incidence angles i.e. $0^0$, $45^0$ and $90^0$ in order to measure the pressure distribution. It is observed by the author that the negative pressure on opposite faces gets increased considerably when the models are close to each other.

**Wang et al. (2014)** conducted wind tunnel experiments to investigate the interference effects of a neighboring building on wind loads on scaffolding with nonporous cladding. Three types of scaffolding were considered. The effects of neighboring building location, neighboring building height ratio and principal building opening ratio were studied. It was concluded that the largest positive and largest negative mean panel pressure coefficient occurs when the neighboring building was located in front of measured scaffolding. The largest positive wind loads on the scaffolding become larger when the neighboring building was located on the left or right side of the measured scaffolding. The building height ratio also had a significant effect on largest mean force coefficients.

### 2.3.3 Wind Response Analysis

**Bailey and Kwok (1985)** presented the effects of interference excitation due to twin tall buildings. Authors studied about the dynamic response of a tall square building under interference excitation from neighboring tall buildings. In a low turbulence wind environment and under normal wind conditions, the dynamic response of pair of twin tall buildings may increase by a factor of up to 4.4. The dynamic loads on the downstream side building of the pair may get increased by a factor of up to 3.2 due to "resonant buffeting".

**Balendra and Nathan (1987, 1988)** conducted the experiments and presented results for longitudinal, lateral and torsional response of square building model and triangular building model. The model was with three degrees of freedom. The critical angles for longitudinal, lateral and torsional response were determined. It was noticed that maximum longitudinal displacement was not for normal wind incidence, whereas the maximum lateral and torsional displacement were for normal wind incidence. It was noticed that root mean square displacements of model vary with the reduced velocity.

**Selvam (1990)** presented the fluid flow around the building using Navier-Stokes equations. Mathematical equations are solved using the finite difference procedure in an iterative form.

**Katagiri et al. (1992)** reported a spectral modal analytical method for the wind-induced lateral-torsional response of high-rise buildings. This method is based on the model forces obtained from a force balance. This method was applied to study the response of under-planning building having a height of 232 meters.

**Chaudhary et al. (1995)** investigated the effect of atmospheric turbulence on the response of the full-scale vertical cantilever structure. It was concluded that the input Gust spectra and the corresponding response spectra are practically identical in shape, for "Background Effects". A sharp peak in the response spectra has been observed at natural frequency of the structure pertaining to the "Resonance Effects".

**Bazeos and Beskos (1996)** presented a numerical method for the determination of wind-induced torsional moments on isolated or a group of rigid buildings of arbitrary cross-section. It was also concluded that the method appeared to be a valuable tool for the rapid determination of wind-induced torsion on building with satisfactory accuracy, especially because there is almost nothing on the subject in wind codes, while experiments are time consuming and costly. The only disadvantage of this method is the difficulty in selecting flow separation points when more than one building is present and their shapes are complicated.

**Selvam (1997)** presented method of computation of pressures on Texas Tech University building using large eddy simulation. Author concluded that the mean pressures computed using Gaussian distribution is much bigger than the field measurement.

**Balendra et al. (1999)** studied the role of TLCD (tuned liquid column damper) in reducing the along-wind response of tall buildings. Building with different mass-stiffness distributions were considered for this study. A continuum formulation which was capable of providing response statistics along height of the building was employed. The performance of TLCD was discussed with respect to mode shapes of the building. A numerical example, illustrating that a second damper could greatly improve the overall response of certain type building was also presented.

**Shankar and Balendra (2002)** investigated the effect of coupling on the vibrations of tall buildings. The buildings under investigation were coupled to rectangular tanks which acted as vibration absorber. Further there was a primary structure coupled to rotary tuned liquid column damper. The behavior was simulated by making use of a beam coupled to many tanks at arbitrary locations the coupling forces and velocities obtained from the

formulations were used in the energy flow analysis. The method balances the input, dissipated and transferred energy of the beam. The energy reduction due to the presence of the energy absorber was noticed. The authors presented a parameter which is indicative of energy reduction due to the presence of energy absorber.

**Rai and Prasad (2005)** carried out non-linear static analysis of a 30 storey framed building by providing shear wall and a new arrangement i.e. diagonal shear wall panels. The authors emphasized the need to carry our non-linear static analysis as the same gives better understanding and more accurate lateral load evaluation of buildings.

**Srinivas et al. (2005)** studied the along wind response of a tall tapered chimney using spectral density approach. The response variance, in the frequency range of interest was worked out using numerical integration. The effect of the taper ratio, mean wind speed and terrain condition on the response of the chimney had been studied and it was concluded that terrain conditions and taper ratio has considerable influence on response.

**Chetia and Talukdar (2006)** discussed the effect of storage water tank on the roof of a ten storied asymmetric building for controlling the vibration during earthquake. The storage water tank is modeled as tuned mass damper (TMD). TMD model consists of an impulsive force on the wall of the tank. Second is due to water in second part is attributed to convective mode of water. The variance of displacement was found for different depths of water. It was concluded that such storage water tank can be an effective TMD device if its optimum location above the roof and water level are maintained.

**Rai et al. (2006-a)** conducted linear static and non-linear static analysis of a 35 storeyed reinforces concrete frame building provided with conventional shear wall (non-staggered) and a new kind of arrangement i.e. frame with staggered shear wall panels to resist the lateral loads. The shear wall panels were bay-wide and storey deep discrete panels. The various arrangements of staggered shear wall panels have been investigated and critically assessed for their feasibility and advantages as compared to the conventional shear wall system. The authors concluded that the performance of staggered shear walls is better with respect to lateral drift, interstorey drift and member forces.

**Rai et al. (2006-b)** presented analysis of bare frame and a frame stiffened with shear wall to keep interstorey and lateral drift within safe limit to prevent excessive damage followed by complete collapse of structure. The lateral and interstorey drift limitations in codes of various countries around world have also been reviewed in this paper. The authors concluded provision of shear walls improves the performance of the building by reducing

lateral displacements and drift. It is also concluded that these are effective against non-structural damages.

**Darla and Talukdar (2007)** studied the fatigue damage analysis of a steel tower using spectral density approach. Power spectral density of axial stress for critical members of the tower were evaluated and then used in Rayleigh's method to obtain the expected damage. It was found that terrain condition and wind speed has considerable influence on the fatigue life of the tower.

**Garg and Goel (2007)** discussed the nonlinear study of residential building tower under cyclonic wind region.

**Mendis et al. (2007)** considered a number of factors which are associated with the design of tall buildings with respect to wind loading. Authors found the importance of structural strength and serviceability in case the tall buildings, as significant dynamic response can result from both buffeting and cross-wind loading excitation mechanism.

**Amin (2008)** studied the effects wind on high-rise buildings namely L-shape and T-shape. The effect of the building shape on the wind induced response of tall buildings was investigated. The expression for the lateral response for different wind angles of incidence was also presented by the author.

**Dalui (2008)** carried out wind response analysis of high-rise buildings of three different building plan shapes namely square, octagonal and circular. Mean wind response such as bending moments, shear force and displacement were obtained under various wind angles in order to study the effects of different combination of shape and wind direction.

**Verma (2009)** carried out analytical study to investigate the influence of the angle of incidence on longitudinal, lateral and torsional oscillation of coupled buildings. To study the effects of structural coupling on the structural response of two high-rise buildings, linear static analysis was carried out using STAAD PRO 2005 software. The expressions for predicting the lateral response for different wind incidence angle were presented by the author.

**Vyavahare et al. (2012)** investigated the importance of wind induced oscillations or excitation around tall buildings in along and across wind directions. The authors found that the curves for values as per IS 875 (part-3) draft and ANN predicted values of various responses for across wind direction are almost overlapping each other which indicate close agreement between ANN predicted values and values as per IS-875 (part -3) draft code.

**Mohotti et al. (2013)** performed the CFD analysis in simulating the wind behavior around tall structures. An isolated rectangular building model considered by the author as the

base model in the analysis. The effect of neighboring buildings onto the nearby tall building also discussed.

**Bairagi and Dalui (2014)** carried out numerical study simulation to obtain optimum spacing in between interfering and principal buildings. Analytical results of rectangular plan shape prismatic bluff bodies in a series of Fluid Flow (CFX) are also investigated by authors.

**Kheyari and Dalui (2015)** presented study of interference effect due to wind over a tall building using CFD package of ANSYS. Authors carried out the analytical study through modeling of the isolated building, interfering building, principal building and domain boundary with different wind incidence angles.

## 2.4 LIMITATIONS

It is observed from the above articles that information available regarding wind pressure and wind force coefficients on tall buildings in different standards on wind loads are primarily for common and regular cross-sections only and secondly for stand-alone conditions only. So far as research publications are concerned, many of them are for interference study between tall buildings of regular cross-sections only. Information about wind pressure and force coefficients on tall buildings with many types of irregular and peculiar cross-sections are neither available for isolated condition nor interference condition.

It is, therefore, proposed in the present study to carry out experimental study to measure wind pressures and wind forces on the models of tall buildings with eight different types of peculiar cross-sections. It is also proposed to carry out response analysis of these tall buildings by applying experimentally obtained wind pressures at many wind incidence angles.

# Chapter - 3

# EXPERIEMENTAL PROGRAMME

## 3.1 GENERAL

As explained in Chapter 1, the objective of the present research work is to carryout wind tunnel testing of tall buildings with different cross-sectional shapes, keeping the plan area and height the same. This chapter deals with the description of the models tested in wind tunnel including material of fabrication and their geometric dimensions. Description about the wind tunnel used along with flow characteristics are also given in this chapter. The instrumentation used and the observations taken are also described in this chapter.

## 3.2 WIND TUNNEL USED

Experimental study is carried out in open circuit boundary layer wind tunnel at the Department of Civil Engineering, Indian Institute of Technology Roorkee, Roorkee, India. The wind tunnel has a single fan to generate uninterrupted flow which is operated by 125 HP motor. The tunnel has 15 m long test section with 2 m X 2 m cross-section. Total length of the tunnel is 38 m (Fig. 3.1). Photograph 3.1 shows the external view of the tunnel. Under normal condition, the flow in the tunnel is uniform. Flow roughening devices including vortex generators, barrier wall and cubical blocks (Fig. 3.2 and Photo. 3.2) are placed on upstream side of the test section in order to generate flow fields of different velocity profiles and turbulence.

## 3.3 WIND FLOW CHARACTERISTICS

The velocity profile measured at the downstream end of the wind tunnel on top of the turn table is shown in Fig. 3.3. The variation of the turbulence intensity of flow in the wind tunnel with height is shown in Fig. 3.4. The turbulence intensity near the floor of the wind tunnel is found to be about 12%.

The theoretical equation of power law is given as:

$$\frac{v}{v_0} = \left(\frac{z}{z_0}\right)^n \qquad \text{.....3.1}$$

Where, $v_0$ is the velocity with reference to height $z_0$. $v$ is the velocity at any height $z$ and $n$ is an index called as power law index.

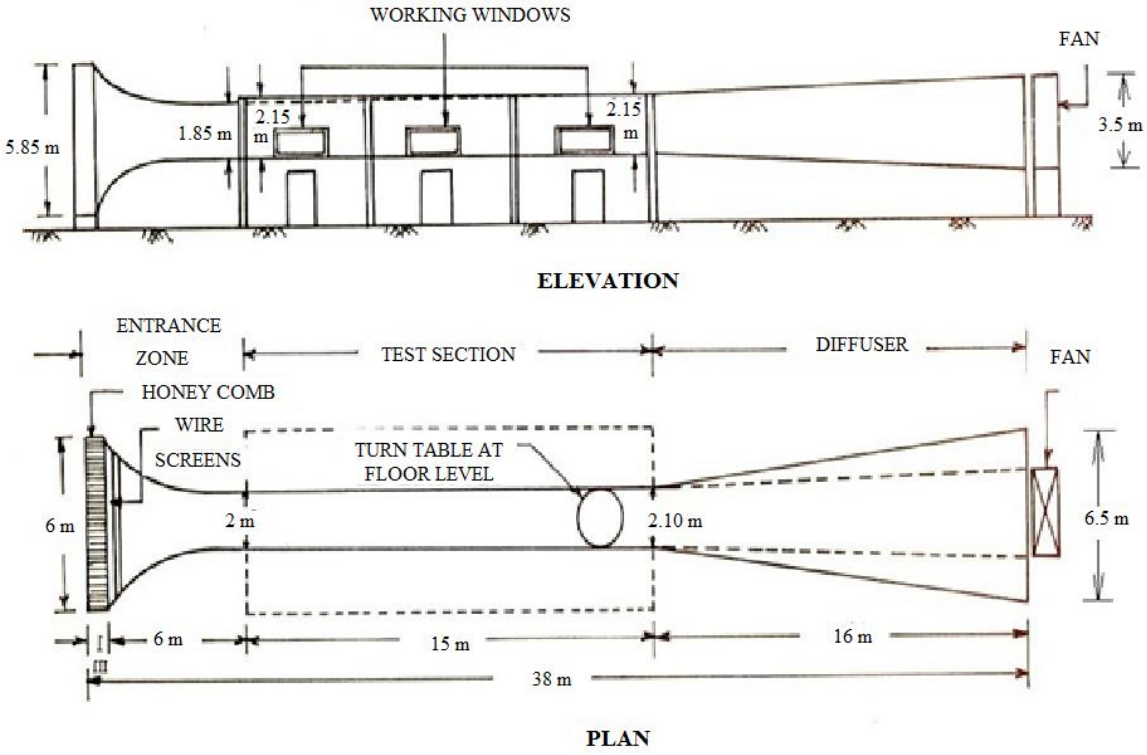


**Fig. 3.1 Longitudinal and plan views of open circuit wind tunnel**

**Photo. 3.1 External view of open circuit boundary layer wind tunnel**

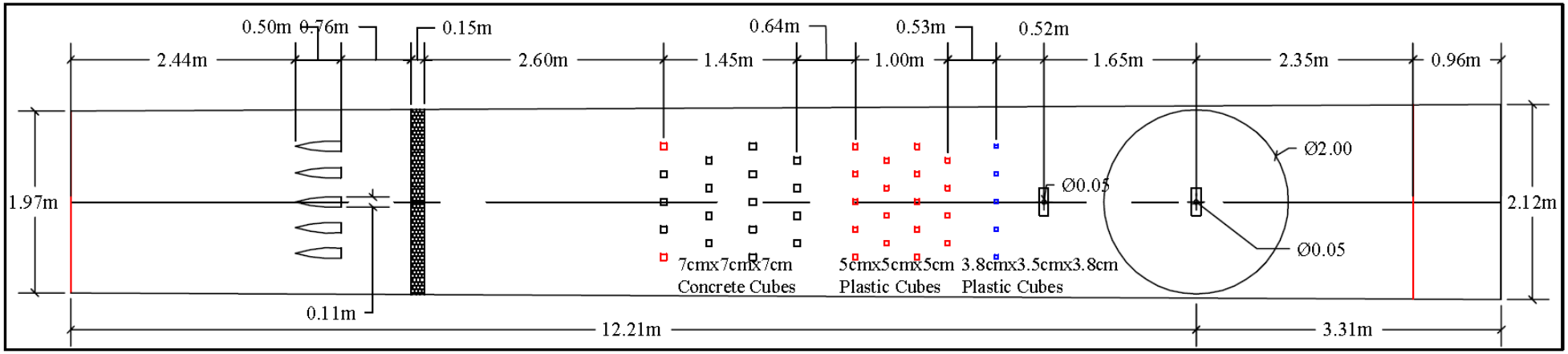


Plan

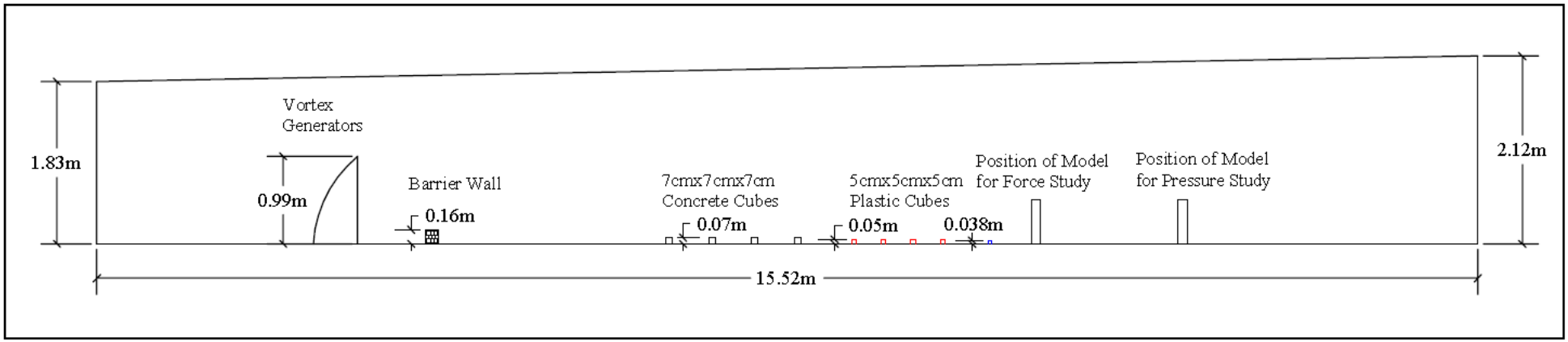


Elevation

**Fig. 3.2 Flow roughening devices inside the test section**

**Photo. 3.2 In-side view of wind tunnel showing flow roughening devices**

In order to find the power law index '$\boldsymbol{n}$', velocity profile is plotted on log-log scale with $\boldsymbol{v/v_0}$ on X-axis and $\boldsymbol{z/z_0}$ on Y-axis. Slope of the straight line gives the value of power law index '$\boldsymbol{n}$' which is found to be 0.22 in the present study (Fig. 3.5).

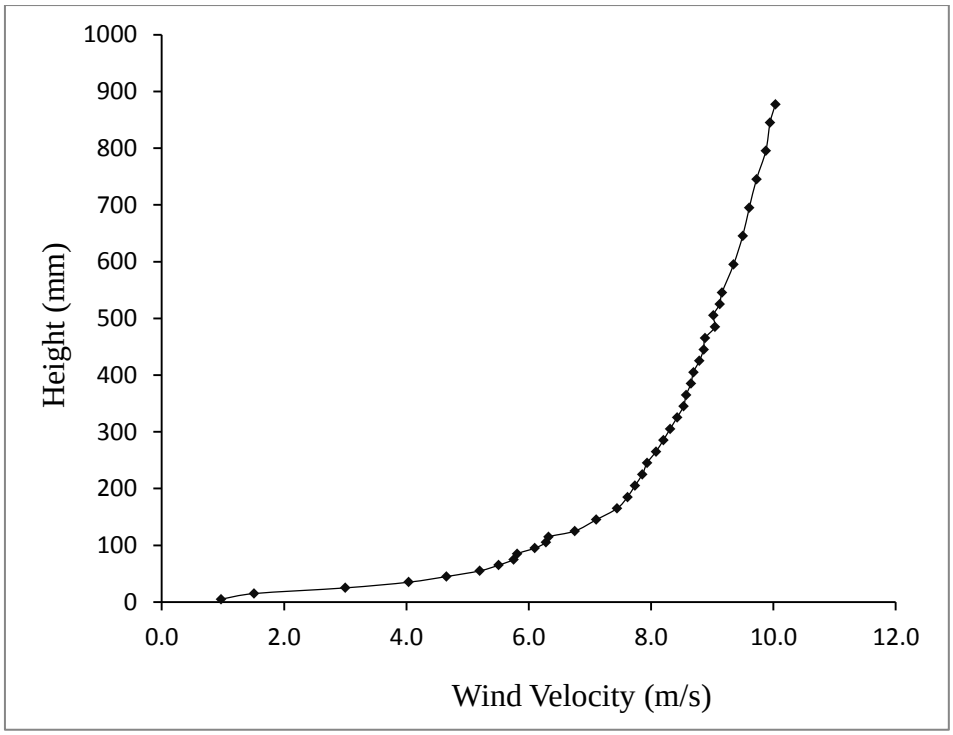


**Fig. 3.3 Measured velocity profile at test section of open circuit wind tunnel**

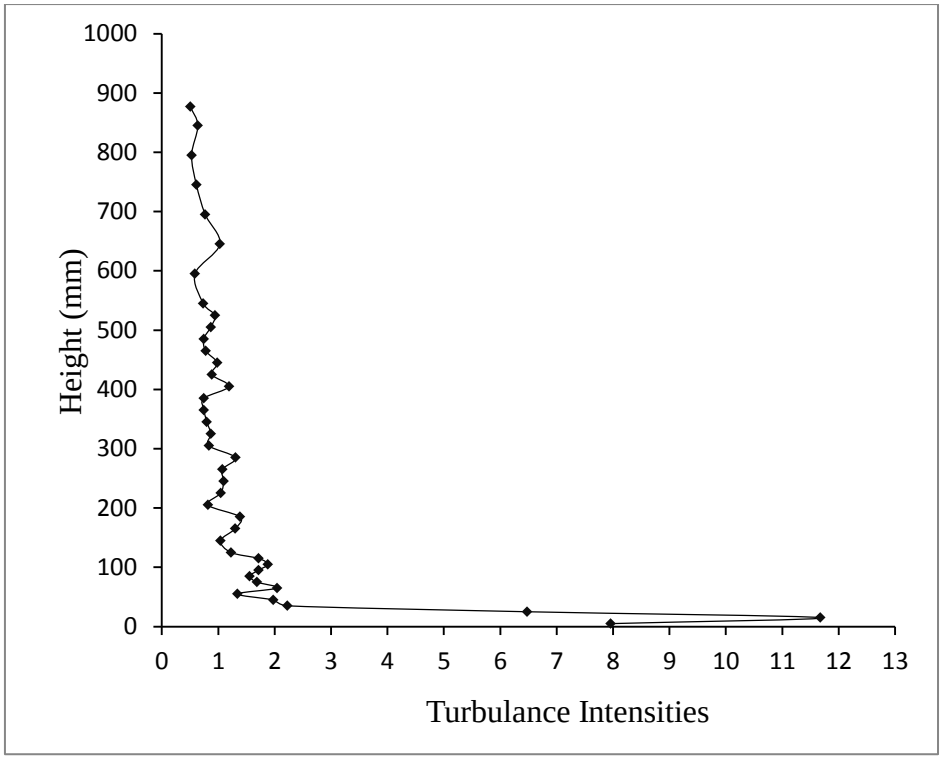


**Fig. 3.4 Variation of turbulence intensity with respect to height at the test section**

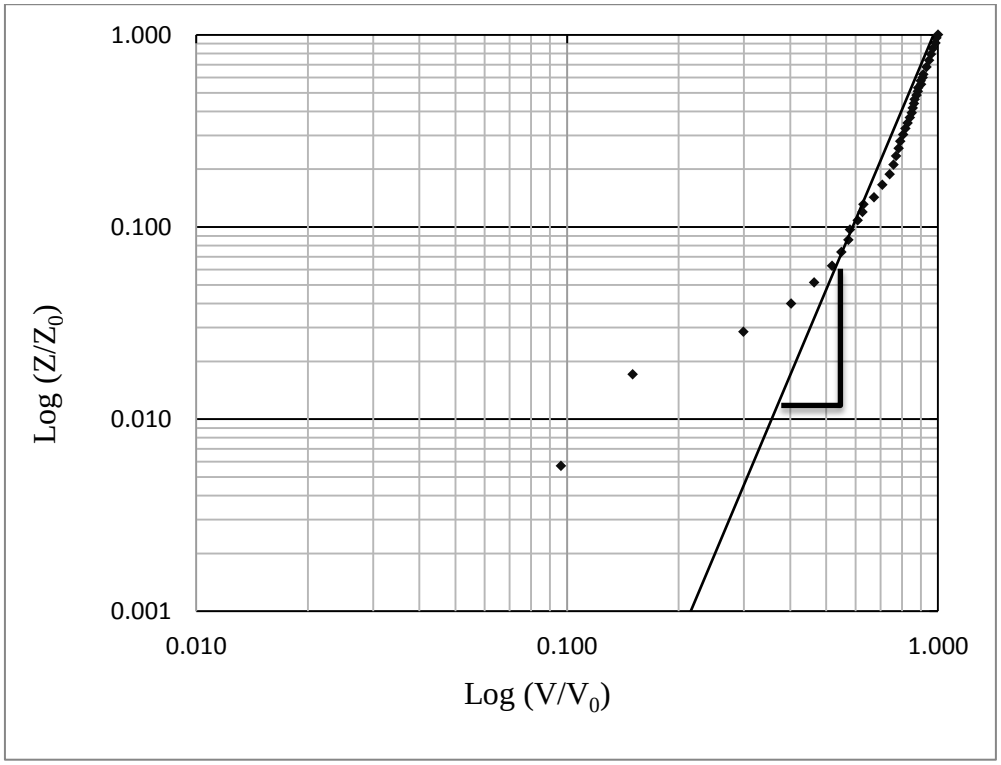


**Fig. 3.5 Velocity profile in the open circuit wind tunnel on log-log scale**

## 3.4 EQUIPMENTS USED

### 3.4.1 Velocity Measuring Equipment

The wind velocity inside the wind tunnel is measured with the help of the instrument "TESTO-480" (Photo. 3.3). A probe is connected to this instrument to measure the wind velocity at different height which has a length of 1 m. This instrument is connected to and operated through a computer.

### 3.4.2 Force Measuring Equipment

Wind loads acting on the plywood models of tall buildings are measured with the help of five component load cell which is attached to the lower side of the wind tunnel floor (Photo. 3.4). It gives five values of forces namely $F_x$, $F_y$, $M_x$, $M_y$ and $M_z$. These values of forces are displayed on display unit and are stored in a computer for further processing through Data Acquisition System (Photo. 3.5).

### 3.4.3 Pressure Measuring Equipment

Wind pressure measurements on the Perspex sheet models of tall buildings are done by using "Baratron Pressure Transducer" (Photo. 3.6). This instrument is capable of measuring extremely low differential heads. It comprises of a pressure head and display unit where the surface pressure measured is directly displayed in terms of mmhg. Later it is converted to $N/m^2$. The output coming from display unit is stored in a computer with the help of Data Acquisition System.

Whereas one end of pressure head is connected to one of the pressure tappings on the model at a time, another end is connected to a reference pressure point on the inner surface of the wall of the test section where velocity of flow is expected to be zero.

### 3.4.4 Data Acquisition System

The instrument receives the electronic signal from the measuring device and transfers it to the computer. It can measure the fluctuating values of force and pressures at every 0.1 sec interval (Photo. 3.5).

Measuring device Probe

**Photo. 3.3 Velocity measuring device with Probe**

**Photo. 3.4 Five component load cell attached to the lower side of the wind tunnel floor**

**Photo. 3.5 Display unit for five components Load Cell, Data Acquisition System and Computer**

**Photo. 3.6 Pressure Transducer: Head and Display unit**

### 3.5 PROTOTYPE BUILDINGS

Eight number tall buildings selected for the study have ground plus eighteen storeys with flat roof. All buildings have different cross sectional shapes but their height and floor area remain same. Height of each building is 60 m and floor area is 400 $m^2$. Other, details of the prototype buildings are discussed in Chapter-6.

## 3.6 DETAILS OF MODELS

### 3.6.1 Materials

Rigid models of tall buildings for force measurements are fabricated using plywood sheets. For the measurement of pressures, the models are fabricated using Perspex sheets. Pressure points are fitted with stainless steel tubes of 2 mm internal diameter and 15-20 mm length flushed on the surface of the model. PVC tubes are connected to free ends of stainless steel tubes. Other ends of PVC tubes are to be connected to the pressure gauge during pressure measurement experiments.

### 3.6.2 Cross-Sectional Shapes

In the present study both plywood and Perspex sheet models are made at a length scale of 1:100. Eight number plywood models (Models A to H) are made, cross-sectional shapes and dimensions of which are shown in Fig. 3.6. Isometric view of all 8 models along with height dimensions are shown in Fig. 3.7.

Only 7 numbers Perspex sheet models namely A, B, C, D, F, G and H, are made. Perspex sheet model of cross-sectional shape-E is not made. Plywood models are shown in Photo. 3.7 and Perspex sheet models in Photo. 3.8.

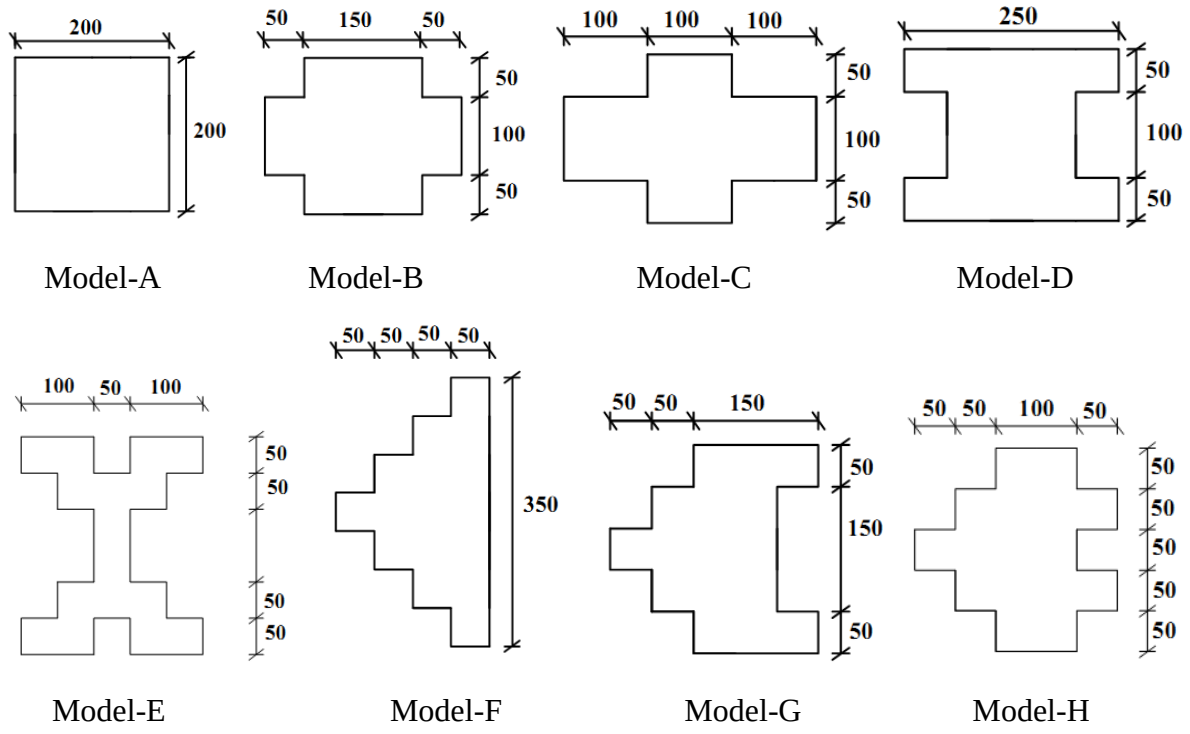


(All dimensions are in mm)

**Fig. 3.6 Plan view of the models used for experimental study**

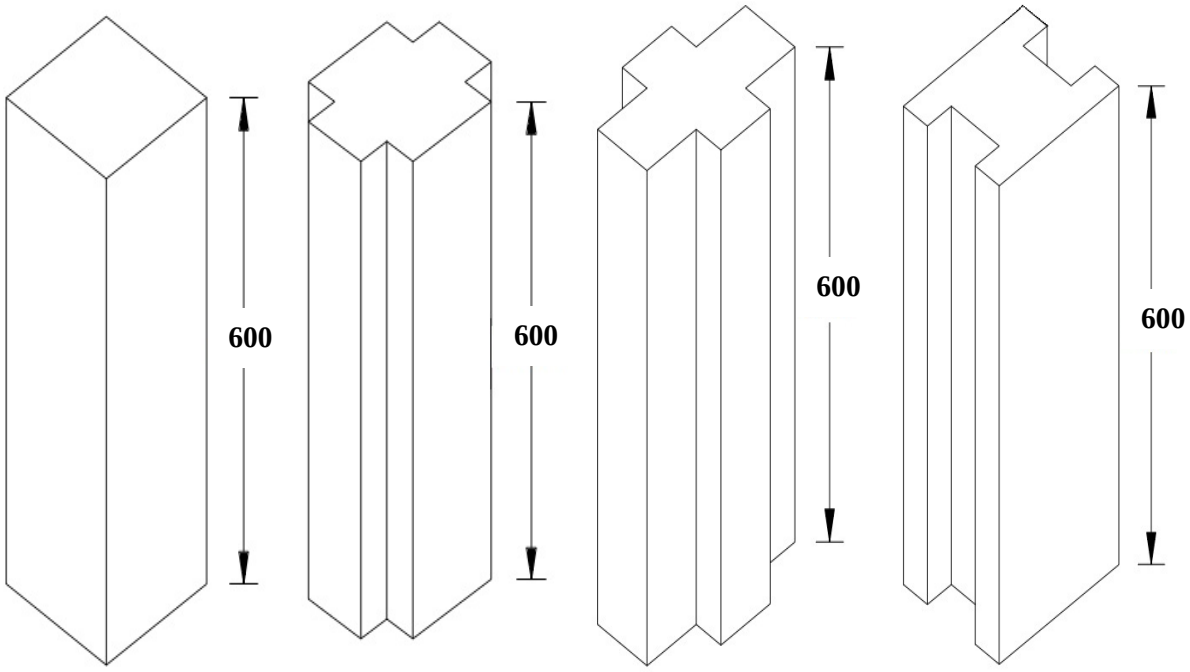


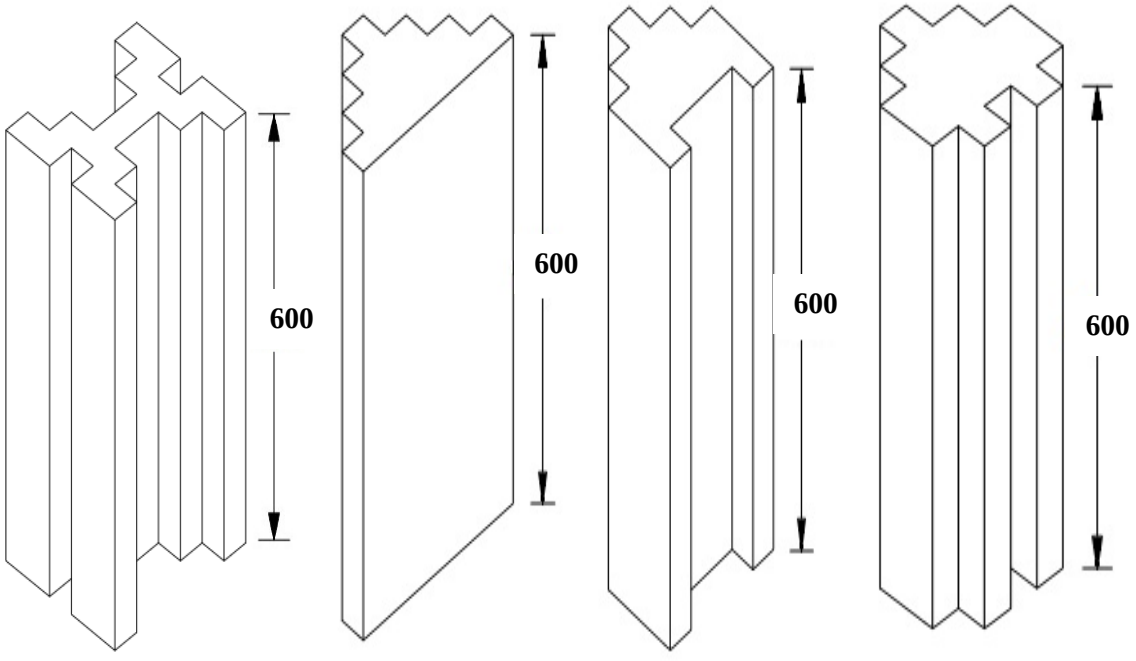


(All dimensions are in mm)

**Fig. 3.7 Isometric view of tall building models**

Model-A Model-B Model-C Model-D

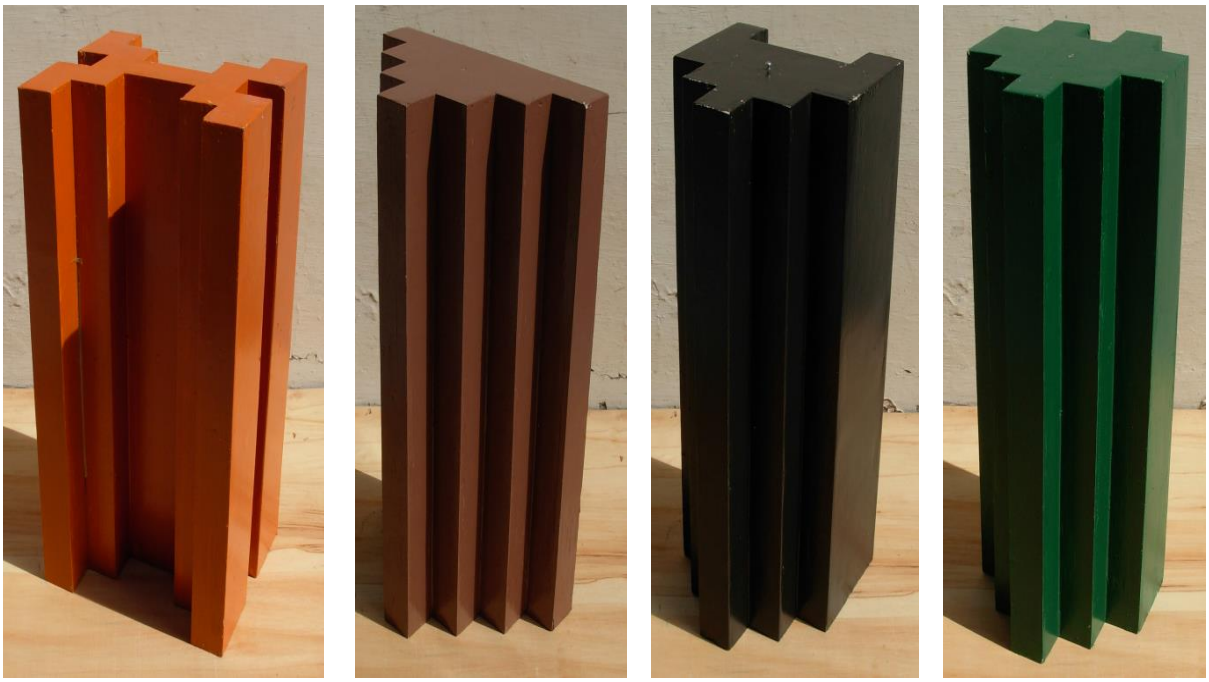

Model-E Model-F Model-G Model-H

**Photo.3.7 Actual images of plywood models**

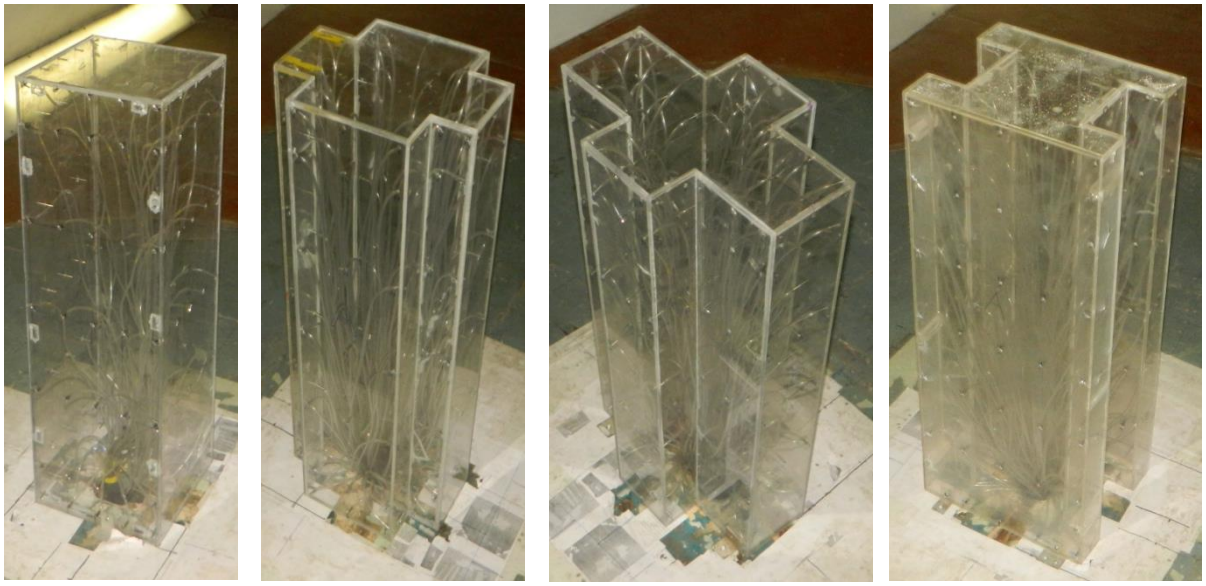

Model-A Model-B Model-C Model-D

Model-F Model-G Model-H

**Photo. 3.8 Actual images of Perspex sheet models**

### 3.6.3 Pressure Tappings

All 7 Perspex sheet models ae provided with many pressure points on its wall surfaces in 7 horizontal sections (Figs. 3.8 to 3.14). Number of pressure points on a section depends upon the cross-sectional shapes (Table 3.1).

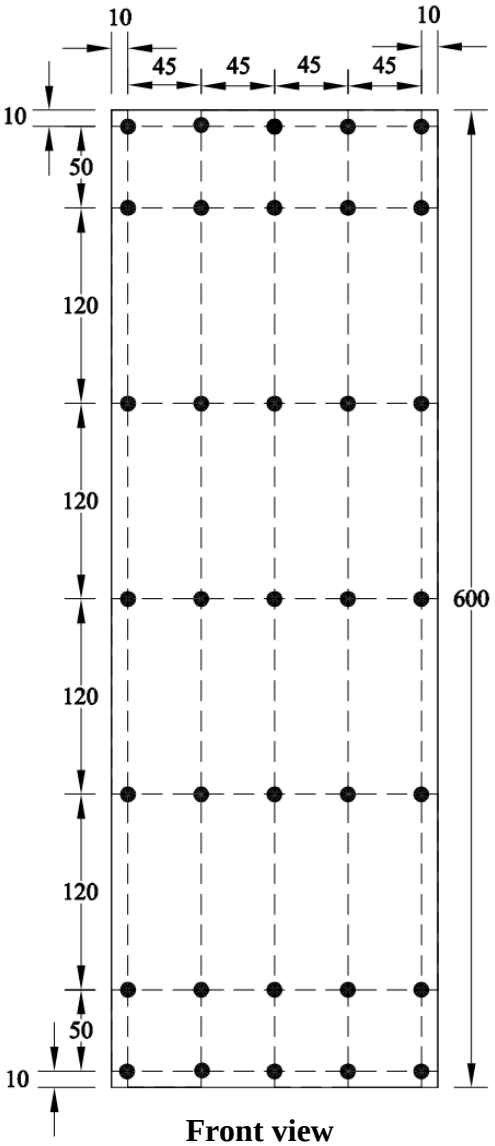


**Front view**

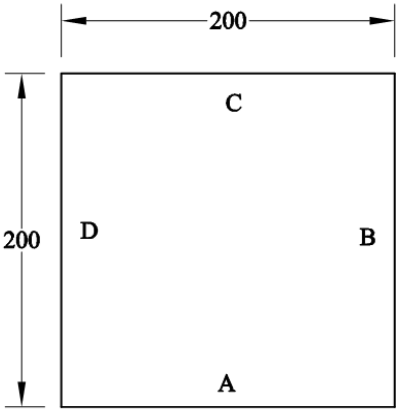


**Plan**

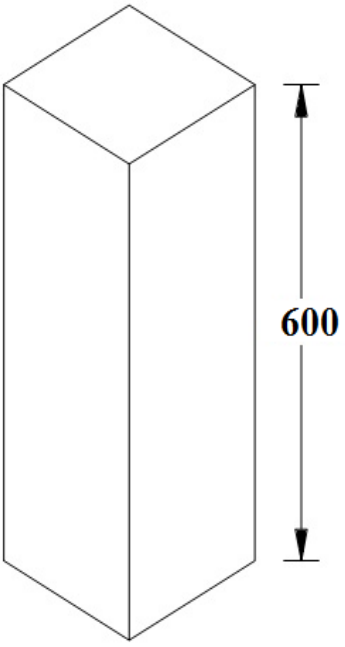


**Isometric**

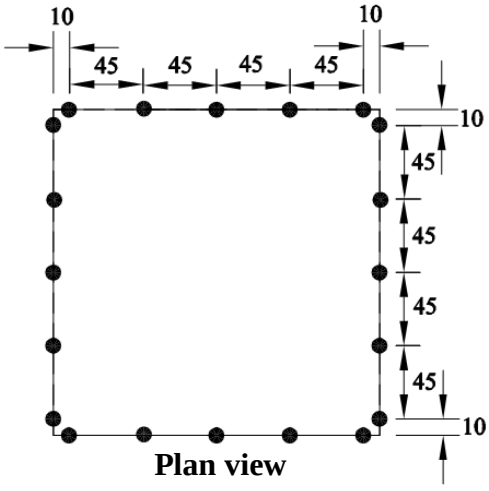


**Plan view**

**Details of pressure tapings on model surface**

**Fig. 3.8 Details of pressure points on Model-A (Square Shape)**

(All dimensions are in mm)

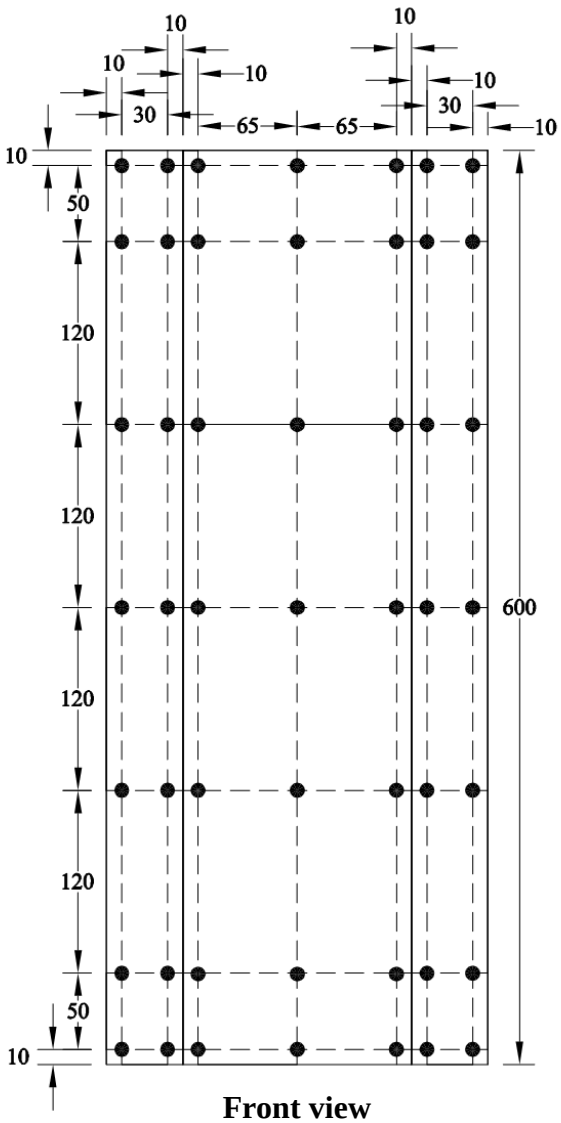


**Front view**

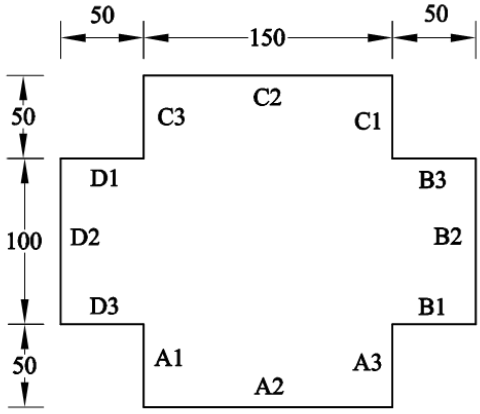


**Plan**

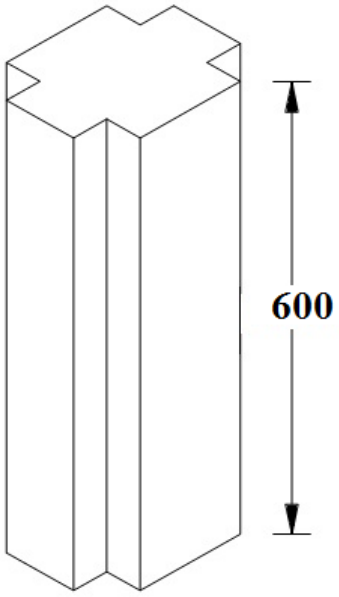


**Isometric**

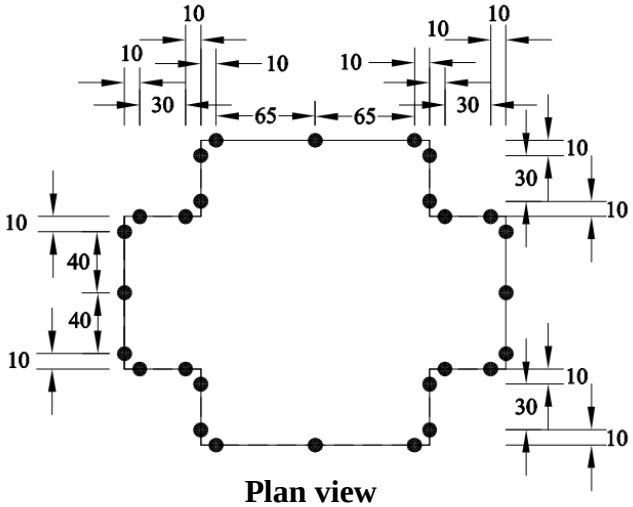


**Plan view**

**Details of pressure tapings on model surface**

**Fig. 3.9 Details of pressure points on Model-B (Plus Shape-1)**

(All dimensions are in mm)

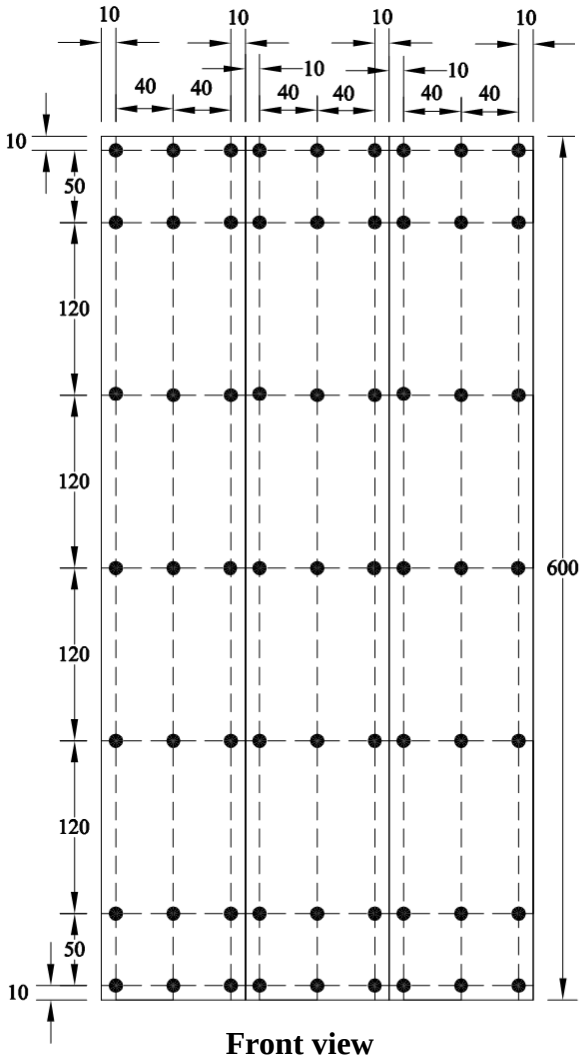


Front view

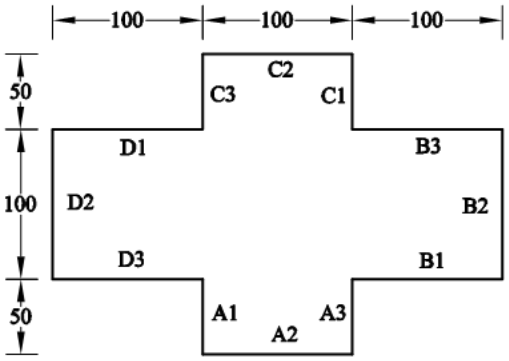


Plan

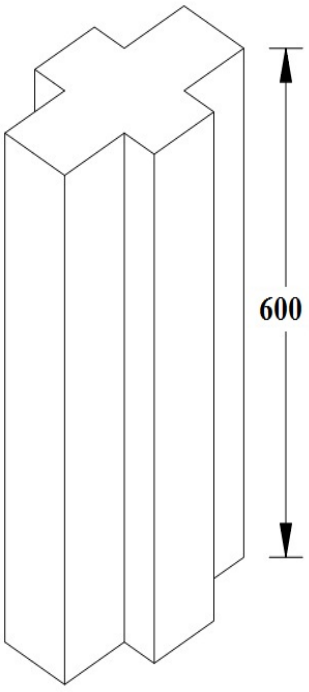


Isometric

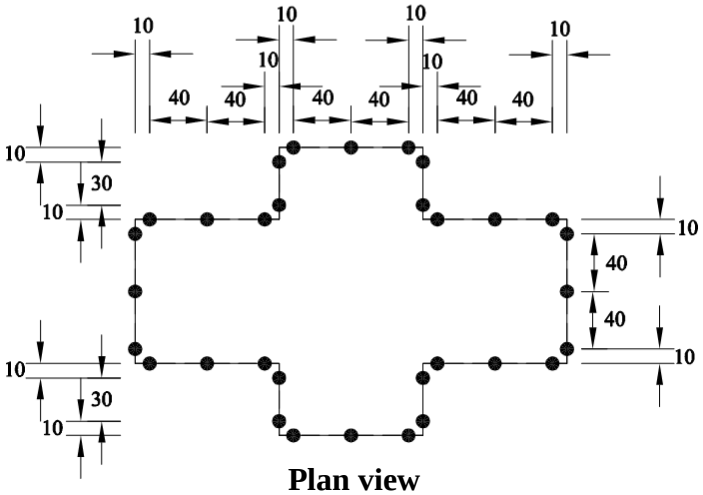


Plan view

Details of pressure tapings on model surface

**Fig. 3.10 Details of pressure points on Model-C (Plus Shape-2)**

(All dimensions are in mm)

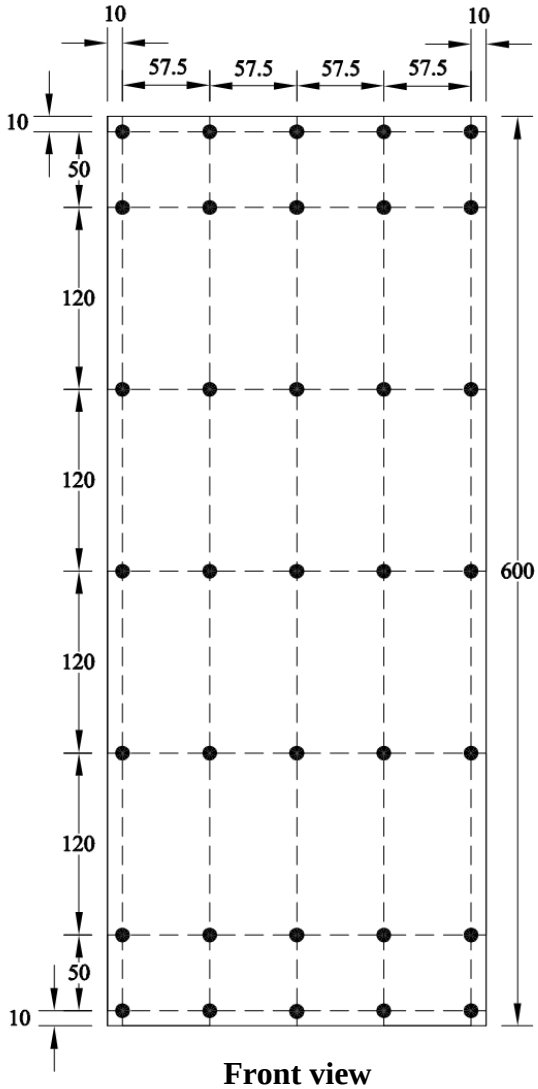


**Front view**

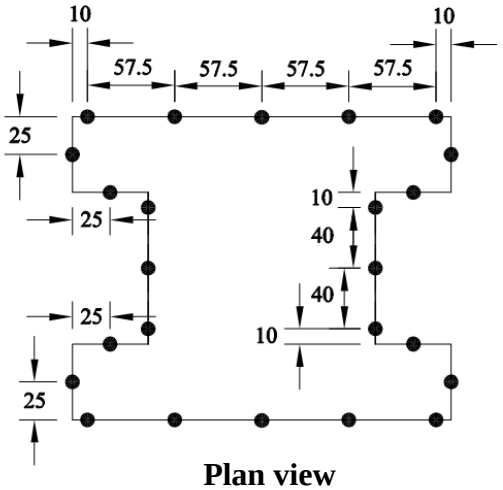


**Plan view**

**Details of pressure tapings on model surface**

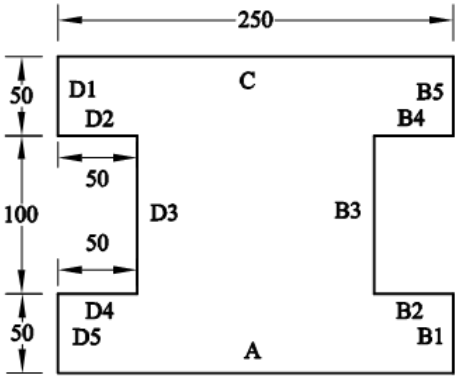


**Plan**

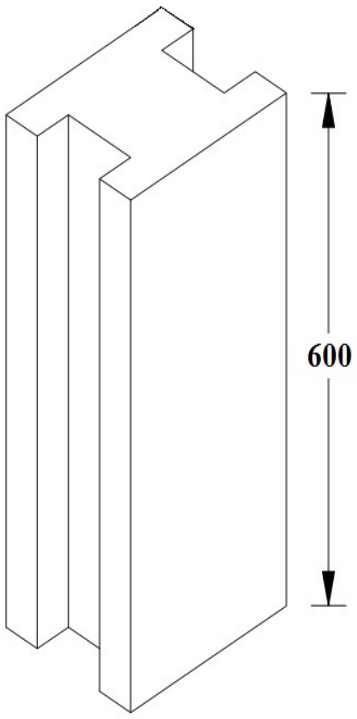


**Isometric**

**Fig. 3.11 Details of pressure points on Model-D (I-Shape-1)**

(All dimensions are in mm)

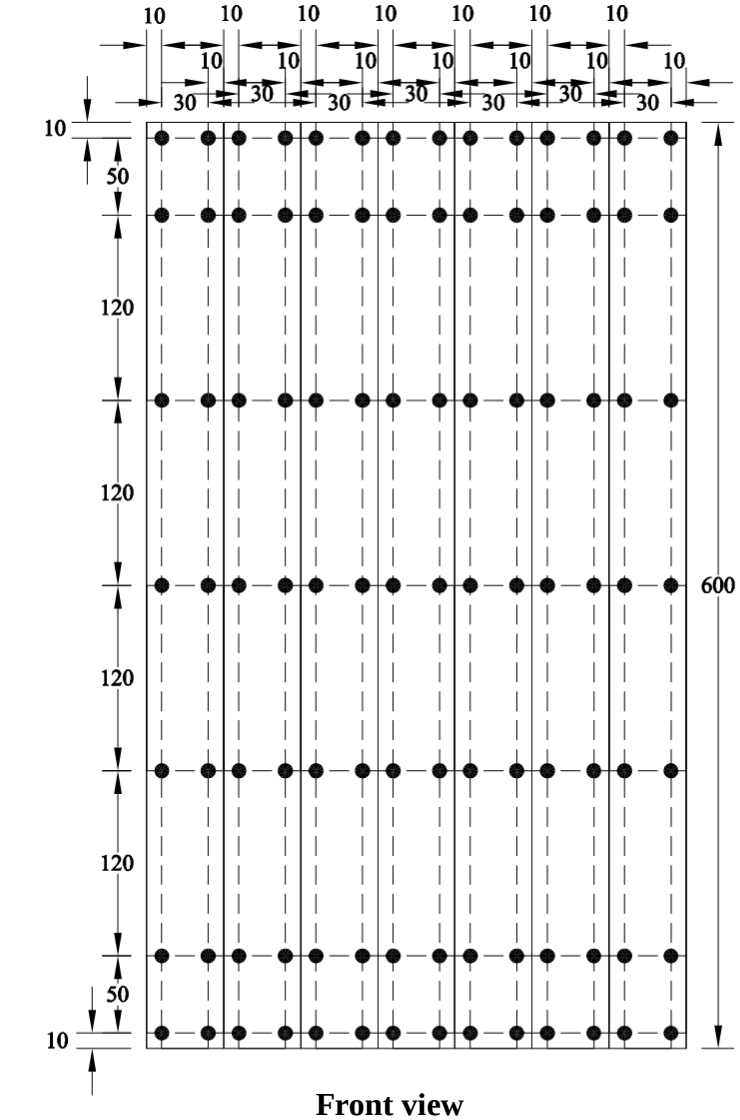


Front view

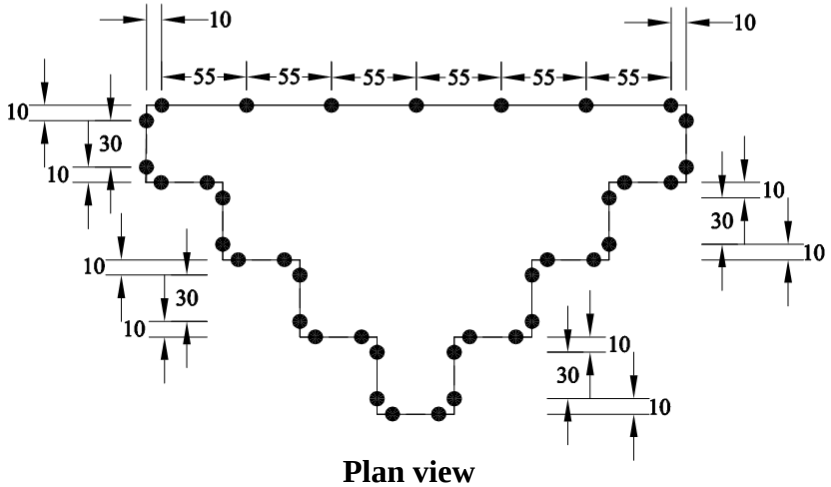


Plan view

Details of pressure tapings on model surface

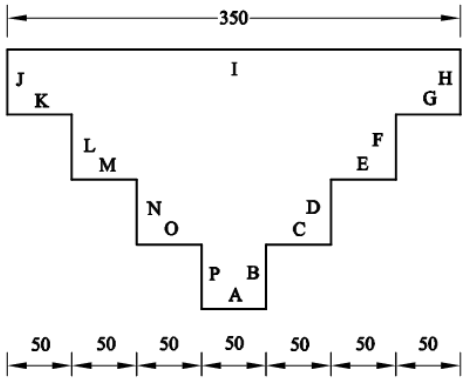


Plan

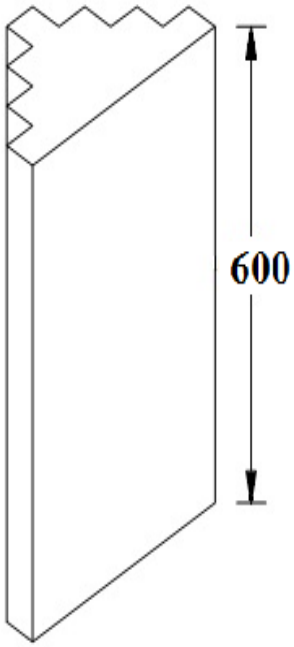


Isometric

**Fig. 3.12 Details of pressure points on Model-F (Fish Shape-1)**

(All dimensions are in mm)

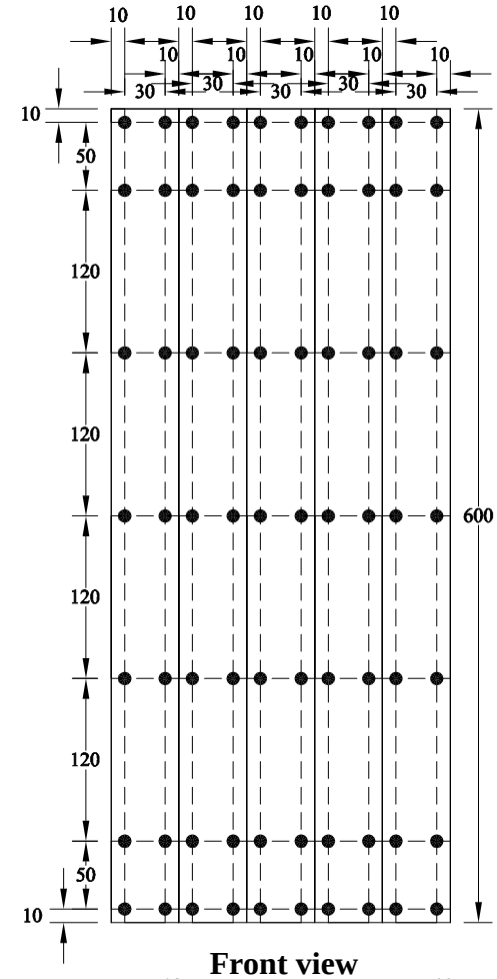


**Front view**

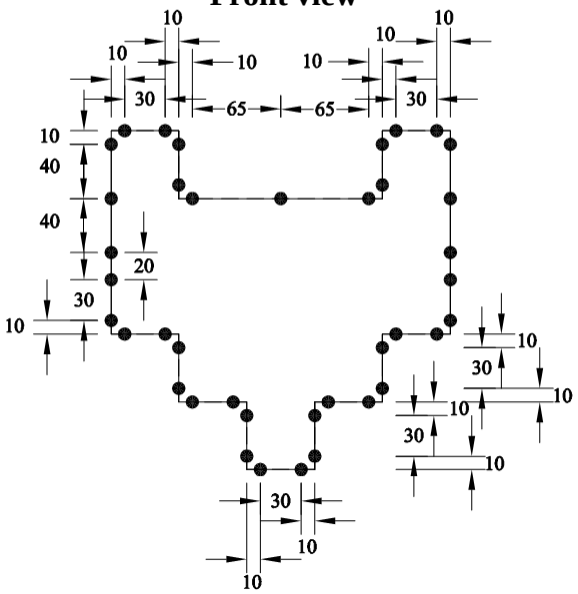


**Plan view**

**Details of pressure tapings on model surface**

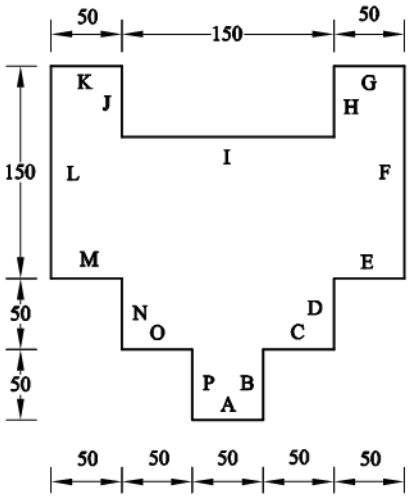


**Plan**

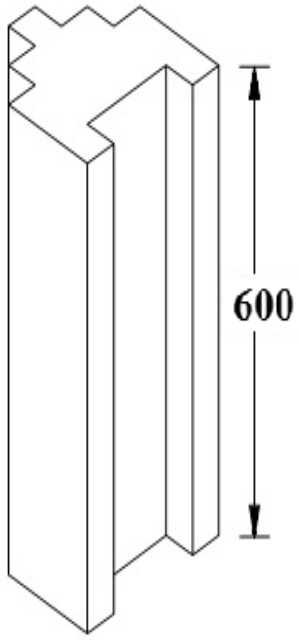


**Isometric**

**Fig. 3.13 Details of pressure points on Model-G (Fish Shape-2)**

(All dimensions are in mm)

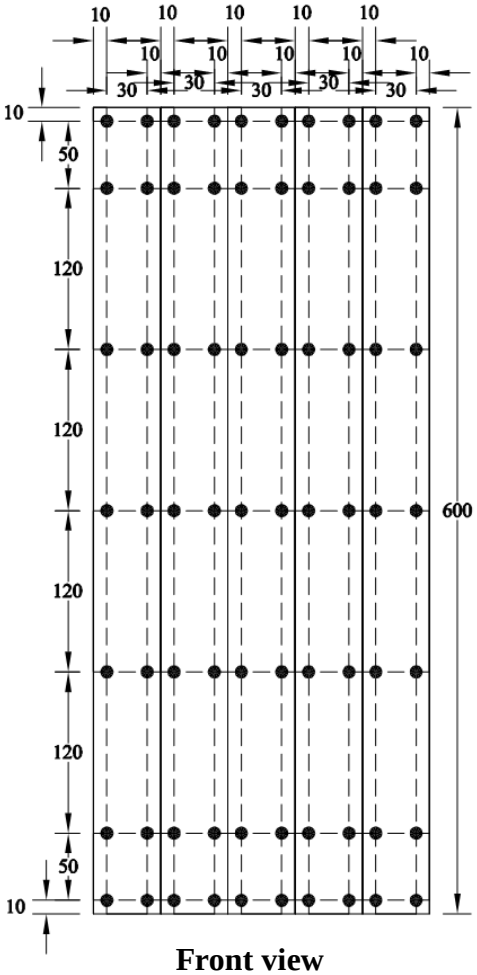


Front view

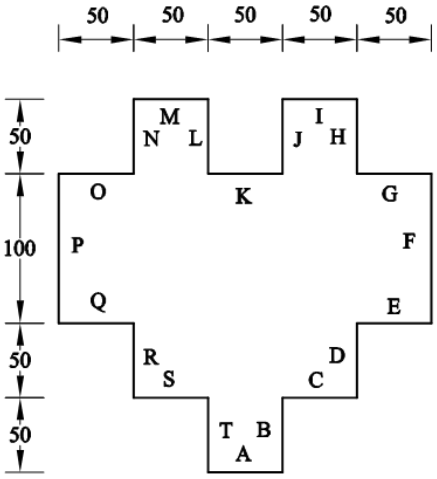


Plan

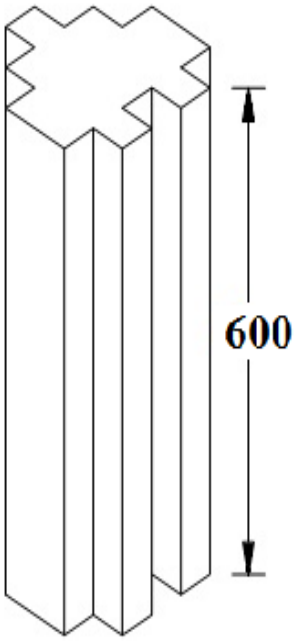


Isometric

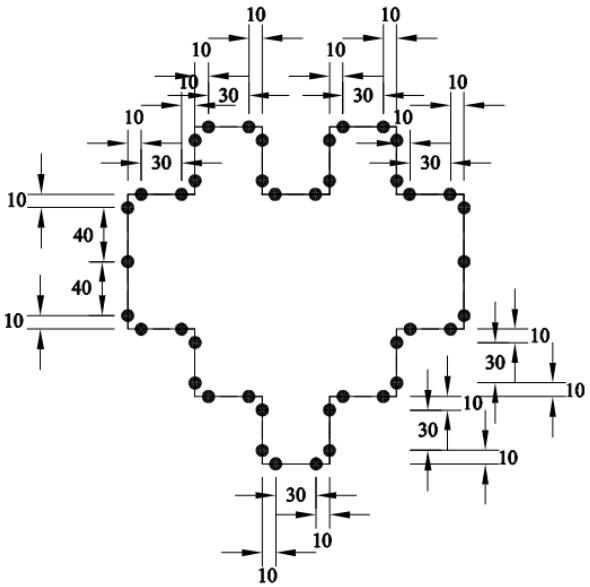


Plan view

**Details of pressure tapings on model surface**

**Fig. 3.14 Details of pressure points on Model-H (Fish Shape-3)**

(All dimensions are in mm)

**Table 3.1 Details of pressure points on building models**

| Building model | Number of pressure points on the model surfaces | | | | | | | | | | | | | | | | No. of pressure points per section | Total no. of pressure points |
|---|---|---|---|---|---|---|---|---|---|---|---|---|---|---|---|---|---|---|
| | A | B | C | D | A1 | A2 | A3 | B1 | B2 | B3 | C1 | C2 | C3 | D1 | D2 | D3 | | |
| Model-A | 35 | 35 | 35 | 35 | - | - | - | - | - | - | - | - | - | - | - | - | 20 | 140 |
| Model-B | - | - | - | - | 14 | 21 | 14 | 14 | 21 | 14 | 14 | 21 | 14 | 14 | 21 | 14 | 28 | 196 |
| Model-C | - | - | - | - | 14 | 21 | 14 | 21 | 21 | 21 | 14 | 21 | 14 | 21 | 21 | 21 | 32 | 224 |

| Building model | Number of pressure points on the model surfaces | | | | | | | | | | | | No. of pressure points per section | Total no. of pressure points |
|---|---|---|---|---|---|---|---|---|---|---|---|---|---|---|
| | A | B1 | B2 | B3 | B4 | B5 | C | D1 | D2 | D3 | D4 | D5 | | |
| Model-D | 35 | 7 | 7 | 21 | 7 | 7 | 35 | 7 | 7 | 21 | 7 | 7 | 24 | 168 |

| Building model | Number of pressure points on the model surfaces | | | | | | | | | | | | | | | | | | | | No. of pressure points per section | Total no. of pressure points |
|---|---|---|---|---|---|---|---|---|---|---|---|---|---|---|---|---|---|---|---|---|---|---|
| | A | B | C | D | E | F | G | H | I | J | K | L | M | N | O | P | Q | R | S | T | | |
| Model-F | 14 | 14 | 14 | 14 | 14 | 14 | 14 | 14 | 49 | 14 | 14 | 14 | 14 | 14 | 14 | 14 | - | - | - | - | 37 | 259 |
| Model-G | 14 | 14 | 14 | 14 | 14 | 35 | 14 | 14 | 21 | 14 | 14 | 35 | 14 | 14 | 14 | 14 | - | - | - | - | 39 | 273 |
| Model-H | 14 | 14 | 14 | 14 | 14 | 21 | 14 | 14 | 14 | 14 | 14 | 14 | 14 | 14 | 14 | 21 | 14 | 14 | 14 | 14 | 42 | 294 |

## 3.7 EVALUATION OF DRAG FORCE COEFFICIENTS

Value of drag force coefficients ($C_d$) on all eight models at all wind incidence angles are calculated from the measured values of along wind loads ($F_x$) using the following relationship.

$$C_d = \frac{F_x}{A\ P_{ref}}$$

Where A is the projected area of the model and $P_{ref}$ is reference wind pressure which is obtained as,

$P_{ref} = 0.6\ V_{ref}^2$ = 0.6 x $(9.78)^2$ = 57.38 N/$m^2$

## 3.8 EVALUATION OF PRESSURE COEFFICIENTS

As mentioned earlier, the fluctuating pressures at each pressure point are measured using Baratron pressure gauge for a duration of 60 seconds. The readings measured at each point are in the form of **mmhg**. All readings recorded from the Baratron pressure gauge are multiplied with some multiplying factor to convert it into the pressure (N/$m^2$).

*Pressure = Multiplying Factor X Baratron Range X Baratron Reading*

The multiplying factor used is constant for the Baratron used and its values is taken as 13.29. The Baratron pressure gauge has different Baratron range like 1, 0.3, 0.1, 0.03, 0.01 and 0.003. Baratron reading is the actual reading recorded from the Baratron pressure gauge using data logger.

Values of pressure measured at all pressure points for duration of 60 seconds are averaged to get mean wind pressure. Mean wind pressure coefficients ($C_{p,mean}$) are then evaluated as

$$C_{p,mean} = \frac{P_{avg}}{0.6V_{ref}^2}$$

Where, $\boldsymbol{P_{avg}}$, = mean wind pressure at a point in N/$m^2$

$\boldsymbol{V_{ref}}$ = free stream wind velocity at 1 m height above the floor in m/sec

# Chapter - 4

# EXPERIMENTAL STUDY - FORCE MEASURMENTS

## 4.1 GENERAL

First phase of the present study is experimental investigation of wind force on base of the model of tall buildings of 8 different cross-sections having same floor area. Wooden models are tested in the wind tunnel by placing them on five component load-cell one by one in isolated condition.

Wind is made to hit the models having symmetry about both axis X-X and Y-Y axis at 7 wind incidence angles from $0^0$ to $90^0$ at an interval of $15^0$. In case of model with symmetry about one axis only, wind forces are measured at 13 wind incidence angles from $0^0$ to $180^0$ at an interval of $15^0$.

After obtaining wind forces such as base shear, base moments and twisting moment in isolated condition under varying wind incidence angles, interference effect on base shear, base moments and twisting moment is studied. For this purpose each wooden model is placed one after another at the center of the load-cell and plywood model of same cross-sections is placed on the upstream side as interfering building model. In this study, base shear, base moments and twisting moment are measured on wooden models for only one wind incidence angle and one value of longitudinal spacing between models. Three transverse spacing namely full blockage, half blockage and no blockage are considered in case of models which are symmetry about both axis. Four interference conditions namely back-to-back, back-to-front, front-to-back and front-to-front are considered for models which have symmetry about one axis only.

## 4.2 ISOLATED CONDITION

### 4.2.1 Model-A (Square Shape)

Wooden model of model-A (Photo. 3.7) is tested in isolated condition under 7 wind incidence angles from $0^0$ to $90^0$ at an interval of $15^0$ (Fig. 4.1). As mentioned earlier, value of force coefficients are obtained originally from five component load-cell in **(mv)** unit which are later converted to kN and N-mm.

Figure 4.2 shows the variation of base shear, base moment and twisting moment with respect to varying wind incidence angle. Base shear Fx is maximum when wind hits the model at $45^0$ wind angle due to large exposed area. Base shear Fy is maximum at $30^0$ and $75^0$ wind incidence angles.

Base moments Mx and My are the function of base shear Fx and Fy respectively. Therefore, variation of base moment is similar to that of base shear. Twisting moment Mz is maximum at $15^0$ and $75^0$ wind angles.

Figure 4.3 shows the variation of drag coefficient ($C_d$) on model-A at different wind incidence angles. It is seen from the figure that drag coefficient is maximum (0.9) at $0^0$ wind incidence angle, which decreases with increase in wind incidence angle, due to the changes in effective frontal area. Drag coefficients is reciprocal to the effective frontal area. Minimum drag coefficients (0.71) is observed at $75^0$ wind incidence angle.

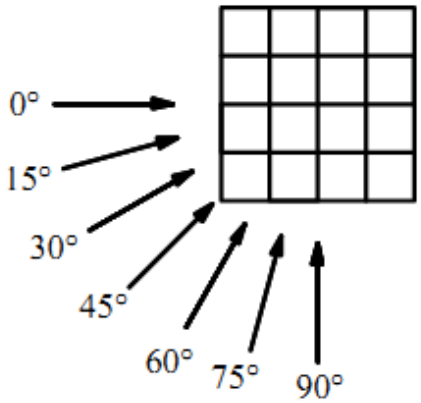


**Fig. 4.1 Cross-section of model-A showing different wind incidence angle**

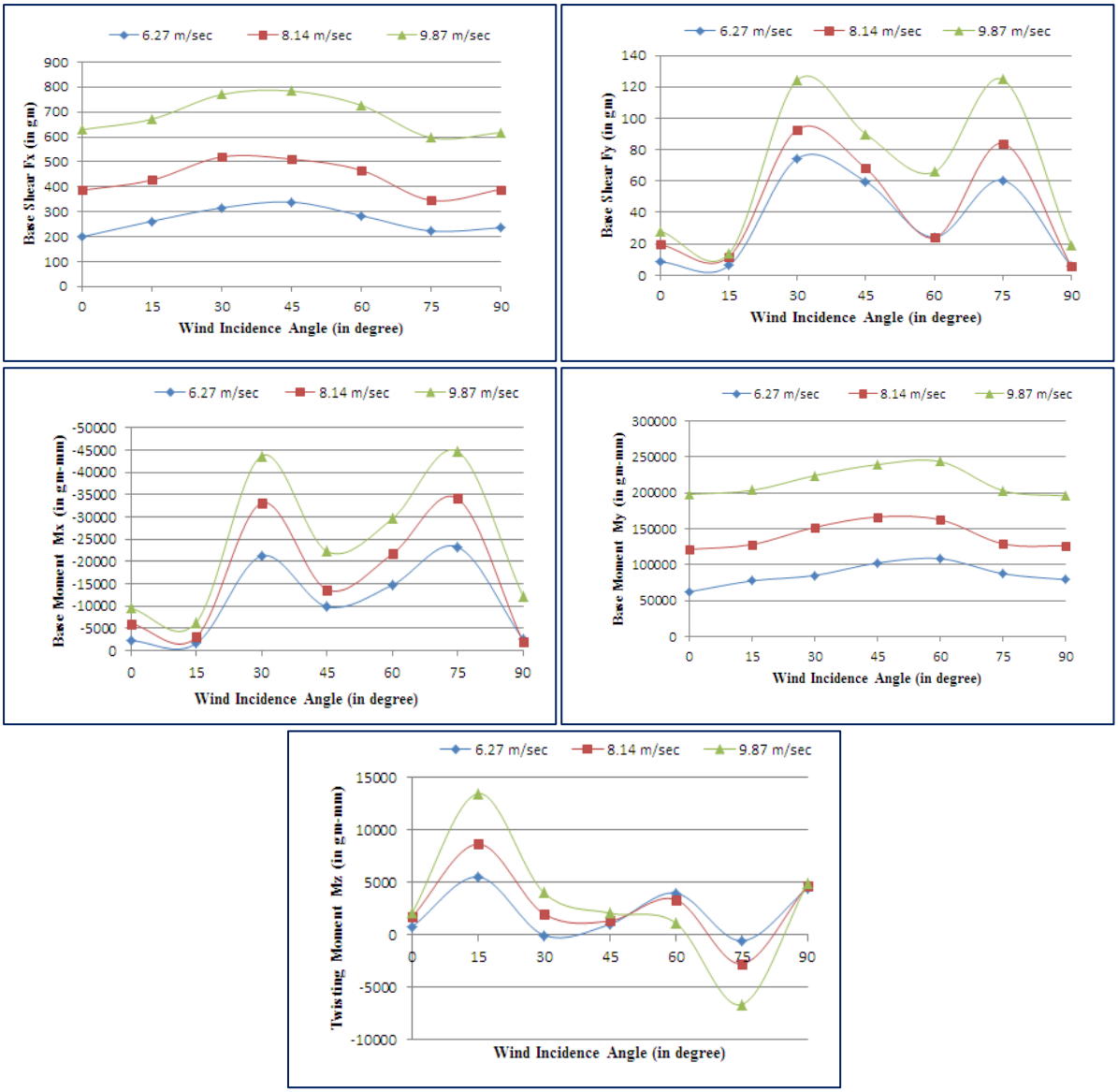


**Fig. 4.2 Variation of base shear ($F_x$ and $F_y$), base moment ($M_x$ and $M_y$) and twisting moment ($M_z$) on model-A with wind incidence angle**

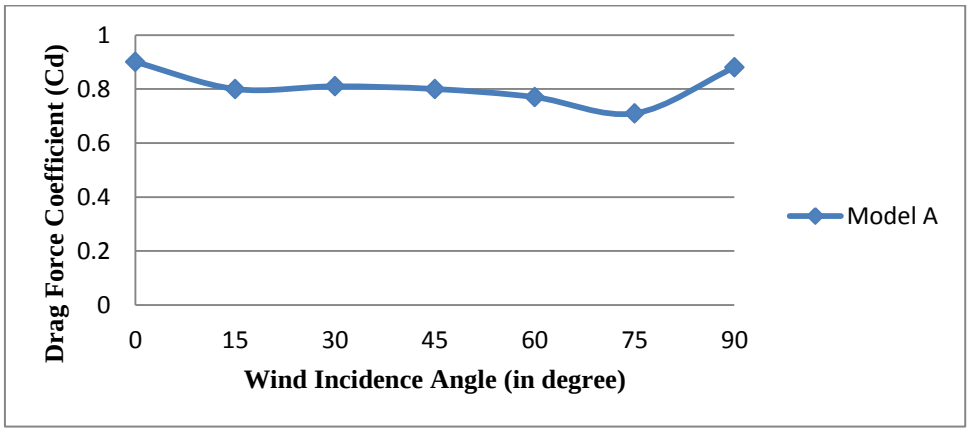


**Fig. 4.3 Variation of drag force coefficient on model-A with wind incidence angle**

### 4.2.2 Model-B (Plus Shape-1)

Wooden model of model-B (Photo. 3.7) is tested in the wind tunnel to measure the base shear, base moments and twisting moment in isolated condition under 7 wind incidence angles namely $0^0$, $15^0$, $30^0$, $45^0$, $60^0$, $75^0$ and $90^0$ (Fig. 4.4).

Base shear, base moment and twisting moment measured on model-B under varying wind incidence angles are shown in Fig. 4.5. It is seen from the figure that maximum base shear Fx occurs at $45^0$ wind angle and minimum at $75^0$ angle. Fy is maximum at $60^0$ wind incidence angle. Twisting moment Mz is maximum at $30^0$ angle.

Figure 4.6 shows the variation of drag coefficient ($C_d$) on model-B at different wind incidence angles. It is seen from the figure that drag coefficient is maximum (0.82) at $45^0$ wind incidence angle and minimum (0.53) at $75^0$ wind incidence angle.

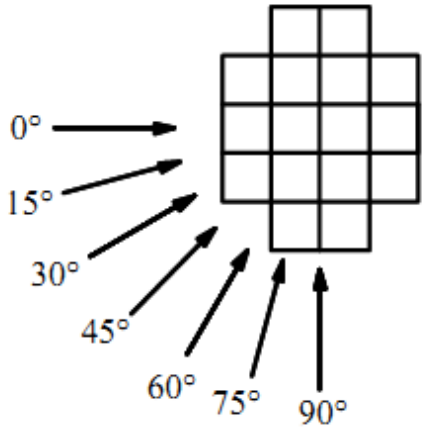


**Fig. 4.4 Cross-section of model-B showing different wind incidence angle**

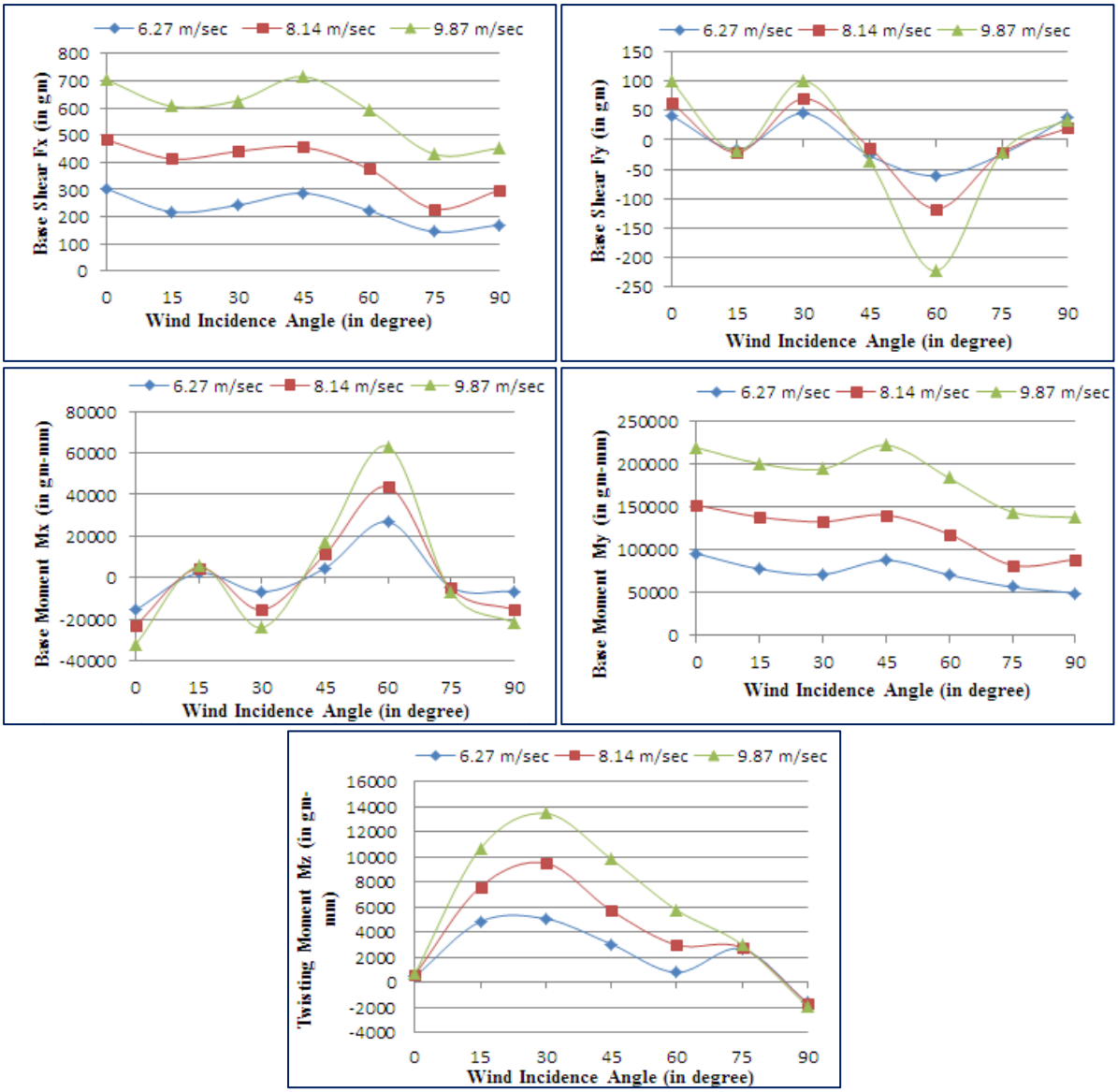


**Fig. 4.5 Variation of base shear ($F_x$ and $F_y$), base moment ($M_x$ and $M_y$) and twisting moment ($M_z$) on model-B with wind incidence angle**

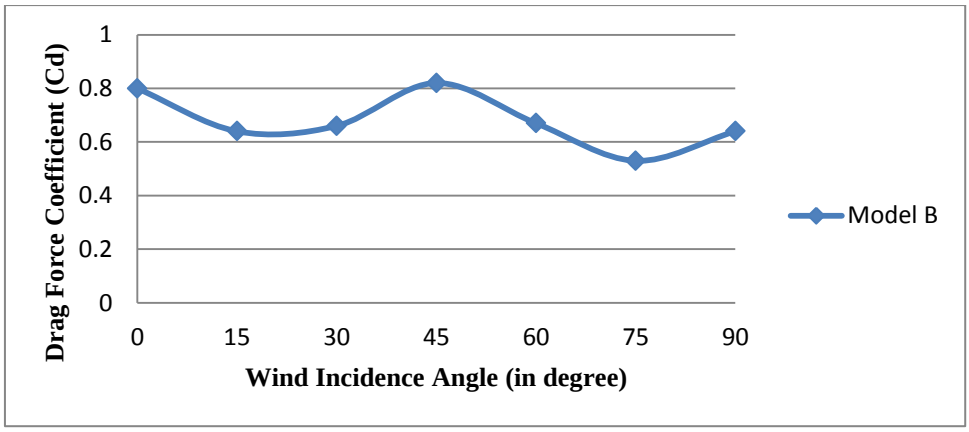


**Fig. 4.6 Variation of drag force coefficient on model-B with wind incidence angle**

### 4.2.3 Model-C (Plus Shape-2)

Wooden model of model-C (Photo. 3.7) is also tested under 7 wind incidence angles (Fig. 4.7) as in the case of model-A and model-B. Base shear, base moments and twisting moment are measured at all wind incidence angles.

Variation of base shear, base moment and twisting moment measured on model-C as a function of wind incidence angle are shown in Fig. 4.8. It is noticed from the figure that base shear Fx, i.e. base shear in direction of the wind varies drastically with respect to wind incidence angle. Maximum base shear occur at $0^0$ wind incidence angle due to its large exposed area.

Variation of Mx and My i.e. base moment, is identical to that of Fx and Fy respectively. Twisting moment Mz is maximum at $60^0$ wind angle and it is almost equal to zero at $0^0$ and $90^0$ wind incidence angles.

Maximum drag coefficient (1.08) is observed at $0^0$ wind incidence angle and minimum (0.49) at $90^0$ wind incidence angle (Fig. 4.9).

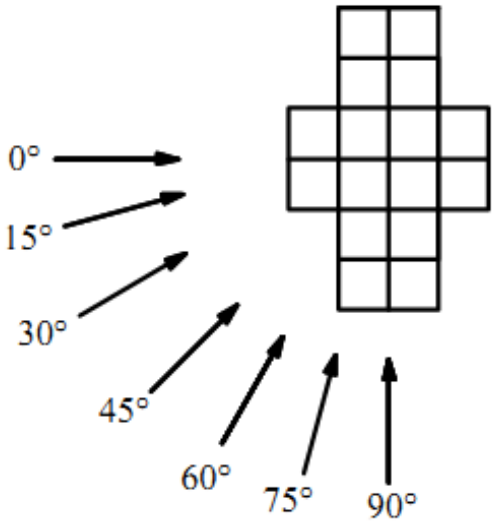


**Fig. 4.7 Cross-section of model-C showing different wind incidence angle**

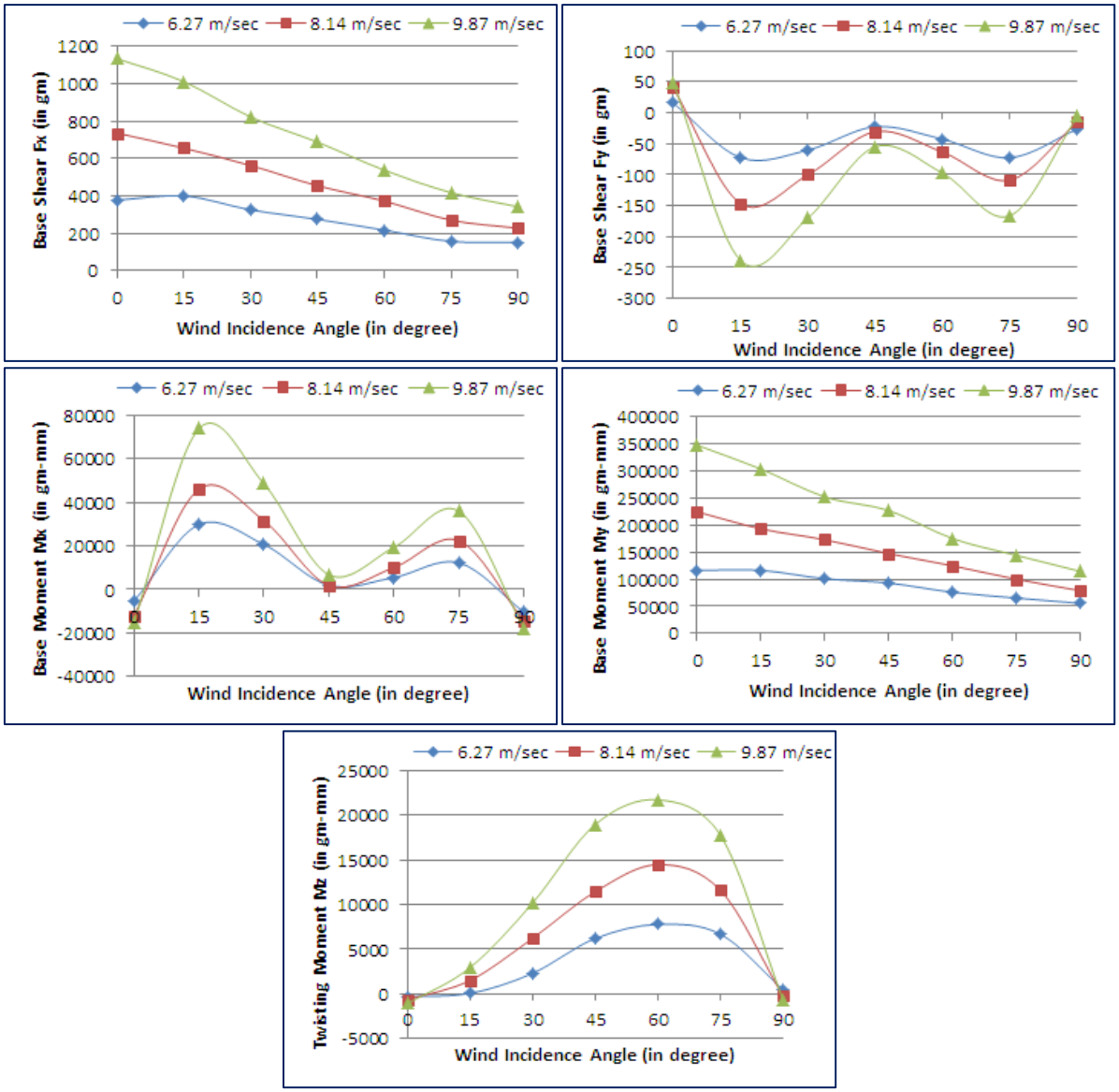


**Fig. 4.8 Variation of base shear ($F_x$ and $F_y$), base moment ($M_x$ and $M_y$) and twisting moment ($M_z$) on model-C with wind incidence angle**

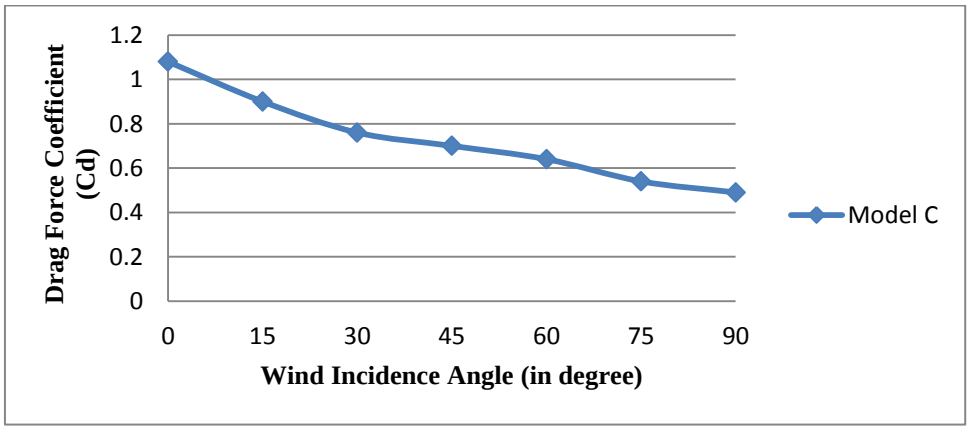


**Fig. 4.9 Variation of drag force coefficient on model-C with wind incidence angle**

### 4.2.4 Model-D (I-Shape-1)

As mentioned earlier, base shear, base moments and twisting moment on I-Shape-1 building model are measured at 7 wind incidence angles (Fig. 4.11). Base shear Fx is maximum at $45^0$ wind angle and it is minimum at $90^0$ angle. Its variation between $0^0$ and $45^0$ is small as compared to the variation between $45^0$ and $90^0$ wind incidence angles. Fy is maximum at $15^0$ wind angle. Twisting moment Mz is maximum at $30^0$ wind incidence angle.

Drag force coefficients on model-D are also plotted and shown in Fig. 4.12. It is clear that drag force is maximum at $0^0$ wind angle due to its large exposed area and minimum at $75^0$ wind angle.

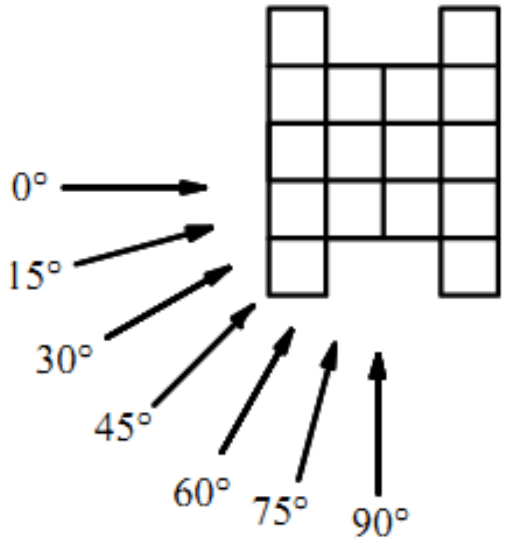


**Fig. 4.10 Cross-section of model-D showing different wind incidence angle**

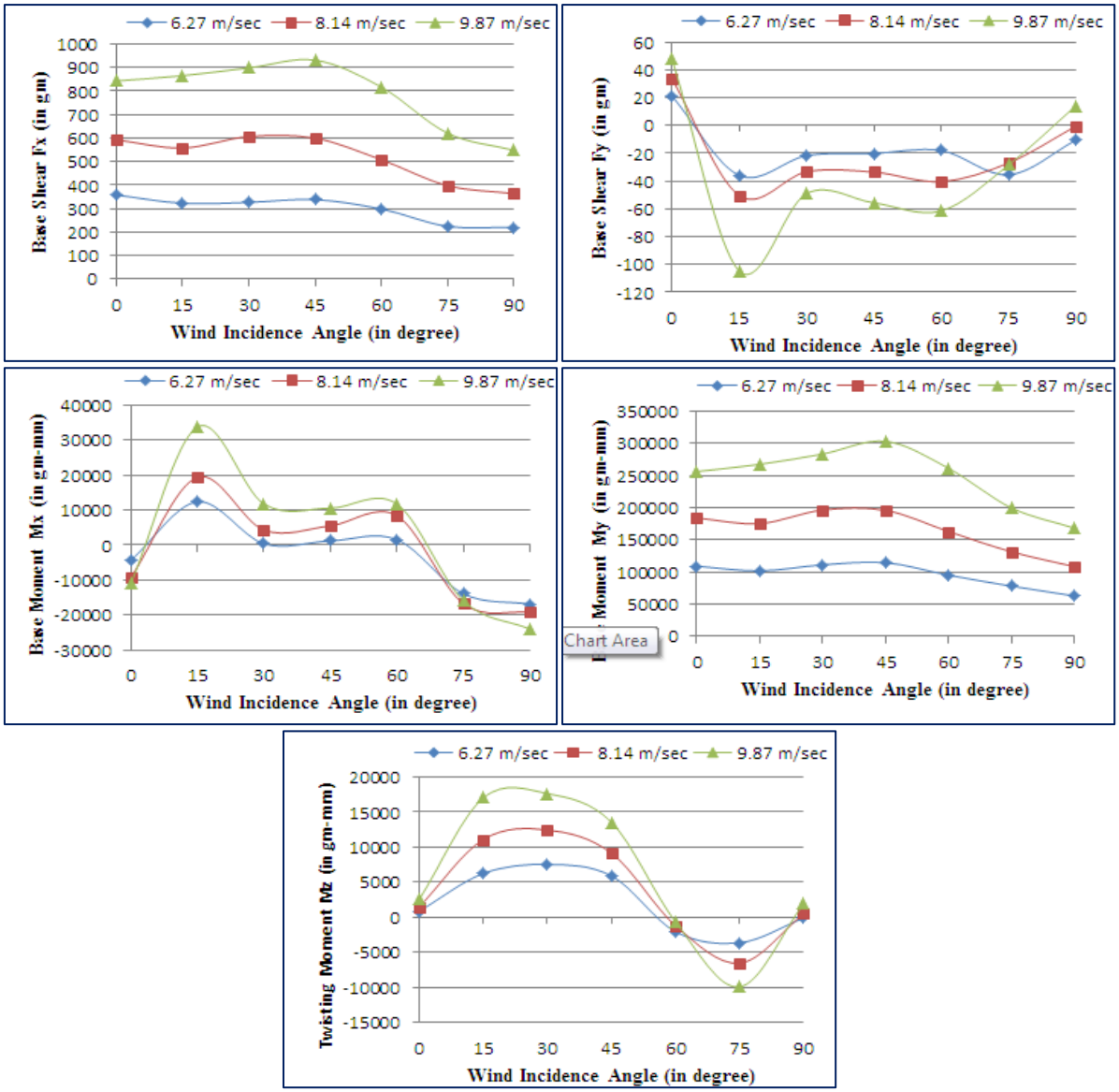


**Fig. 4.11 Variation of base shear ($F_x$ and $F_y$), base moment ($M_x$ and $M_y$) and twisting moment ($M_z$) on model-D with wind incidence angle**

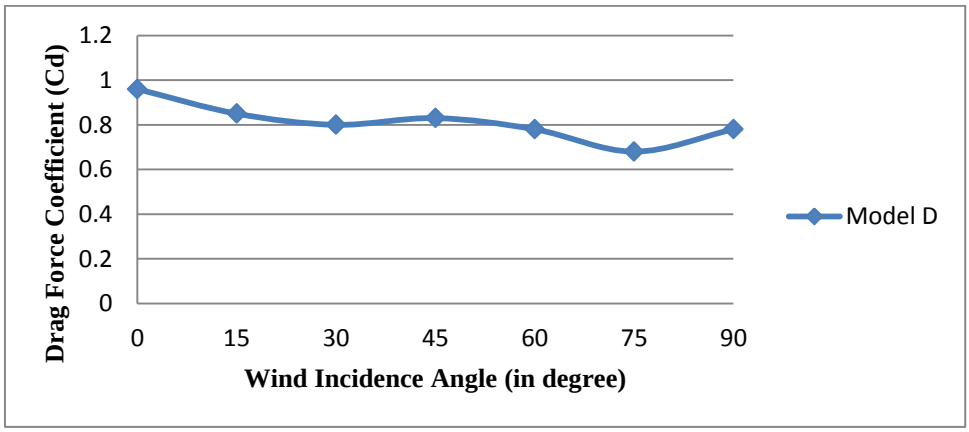


**Fig. 4.12 Variation of drag force coefficient on model-D with wind incidence angle**

### 4.2.5 Model-E (I-Shape-2)

Wooden model of model-E (Phot. 3.7) is tested under 7 wind incidence angles namely $0^0$, $15^0$, $30^0$, $45^0$, $60^0$, $75^0$ and $90^0$ (Fig. 4.13). Base shear, base moment and twisting moment are obtained for model-E (Fig. 4.14). Base shear Fx is maximum when wind angle is $45^0$, while it is minimum in case of $90^0$ angle. Fy is maximum at $75^0$ angle and Mz at $15^0$ and $75^0$ angles.

Drag force coefficients on model-E is plotted with respect to wind incidence angle and it is shown in Fig. 4.15. It is clear that drag force is maximum at $0^0$ wind angle due to its large exposed area and minimum at $75^0$ wind angle. Difference in the values of drag force coeffients at different wind incidence angles are relatively small.

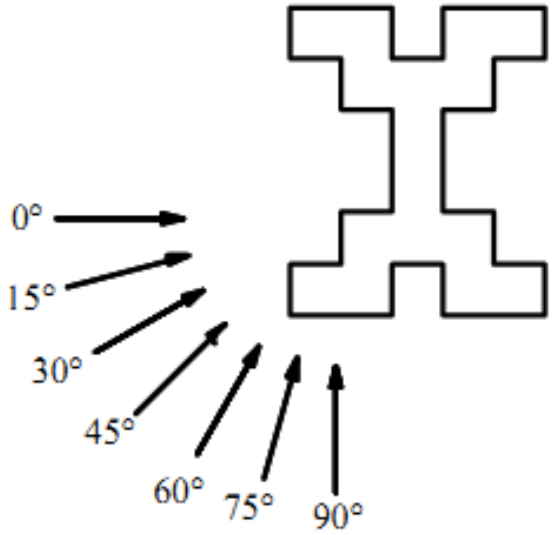


**Fig. 4.13 Cross-section of model-E showing different wind incidence angle**

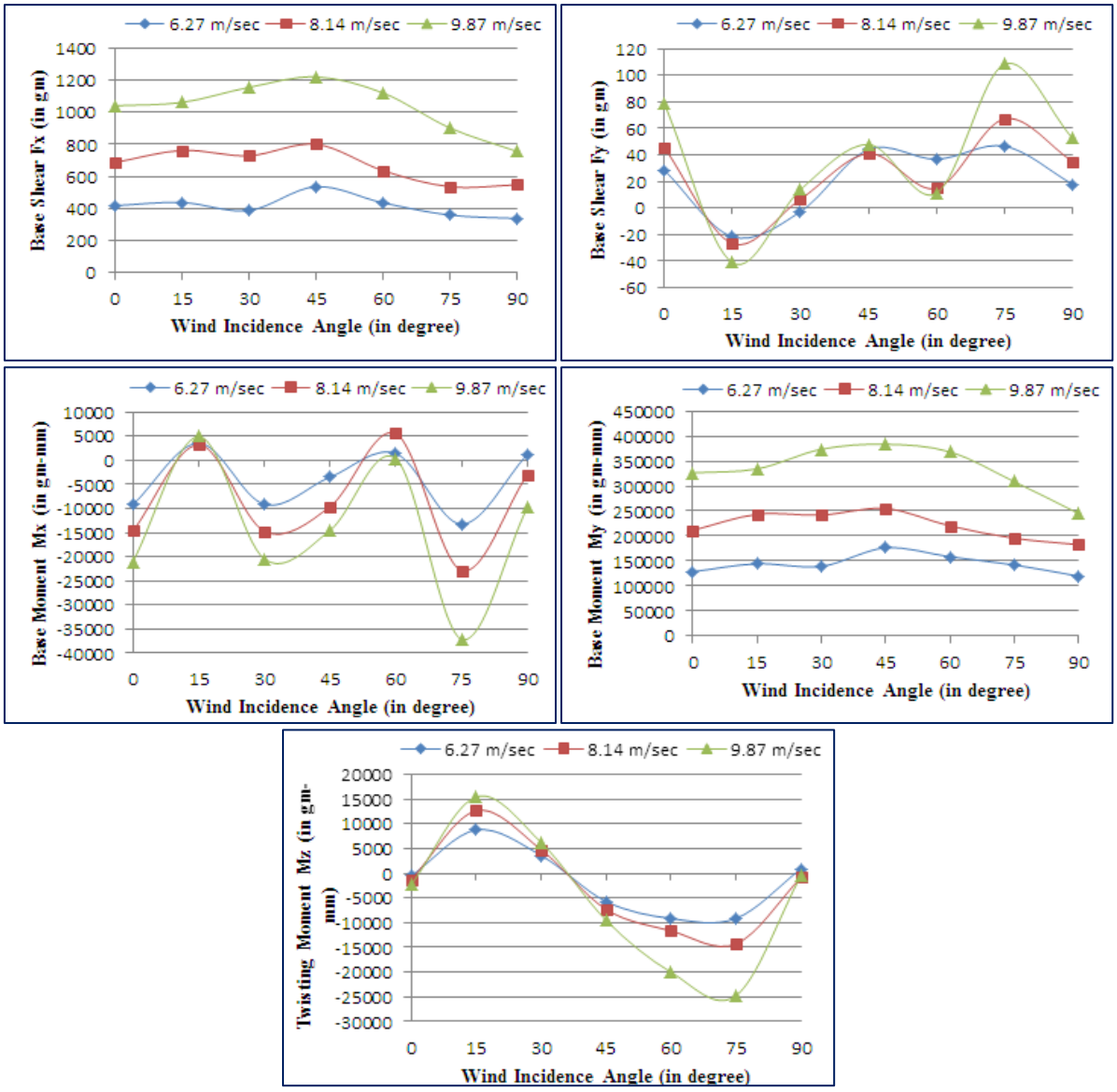


**Fig. 4.14 Variation of base shear ($F_x$ and $F_y$), base moment ($M_x$ and $M_y$) and twisting moment ($M_z$) on model-E with wind incidence angle**

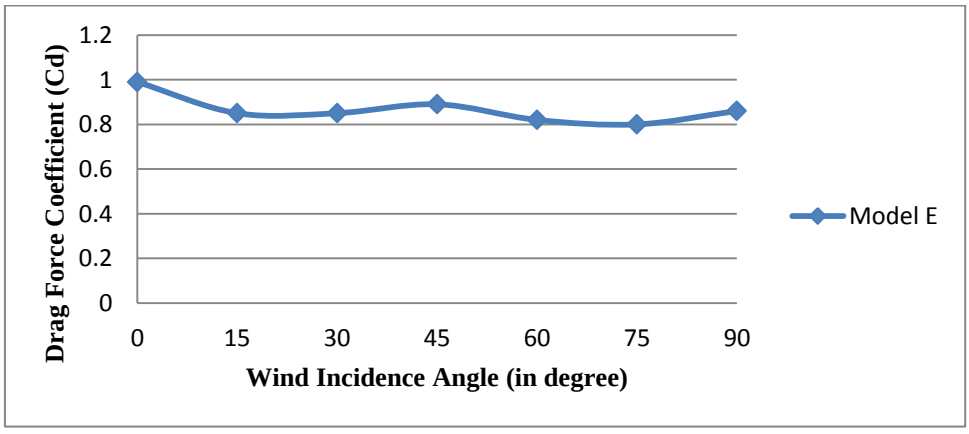


**Fig. 4.15 Variation of drag force coefficient on model-E with wind incidence angle**

### 4.2.6 Model-F (Fish Shape-1)

Wooden model of model-F (Photo. 3.7) is tested under 13 wind incidence angle (Fig. 4.16). Base shear, base moments and twisting moment are measured at all wind incidence angles. Variation of base shear, base moment and twisting moment measured on model-F as a function of wind incidence angle are shown in Fig. 4.17. It is noticed from the figure that base shear Fx, i.e. base shear in direction of the wind varies with respect to wind incidence angle. Maximum base shear occur at $180^0$ wind incidence due to its large exposed area.

Variation of Mx and My i.e. base moment, is identical to that of Fx and Fy respectively. Twisting moment is maximum at $90^0$ wind angle and it is almost equal to zero at $0^0$ and $180^0$ wind incidence angles. Fy is maximum at an angle between $135^0$ and $150^0$. Mz is maximum at $90^0$ angle.

The experimental results for model-F are processed and drag coefficients at all wind incidence angles are calculated. It is seen from Fig. 4.18 that maximum drag coefficient (1.12) and minimum drag coefficient (0.54) are obtained at $180^0$ and $120^0$ wind incidence angles respectively. Large variation of drag coefficients with respect to wind incidence angle is noticed in this model.

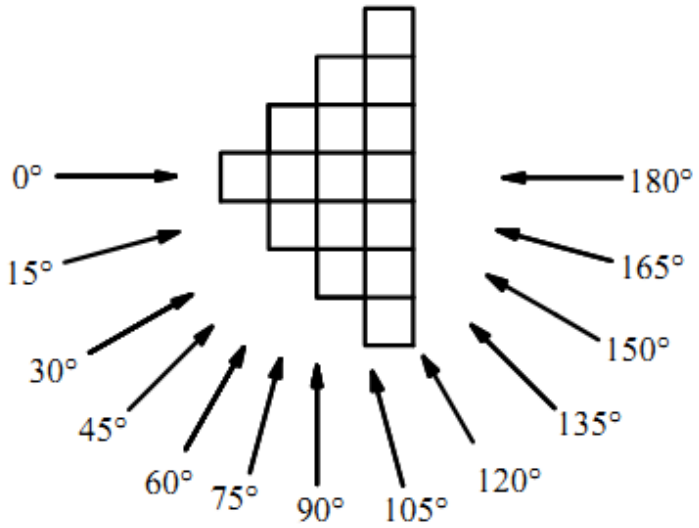


**Fig. 4.16 Cross-section of model-F showing different wind incidence angle**

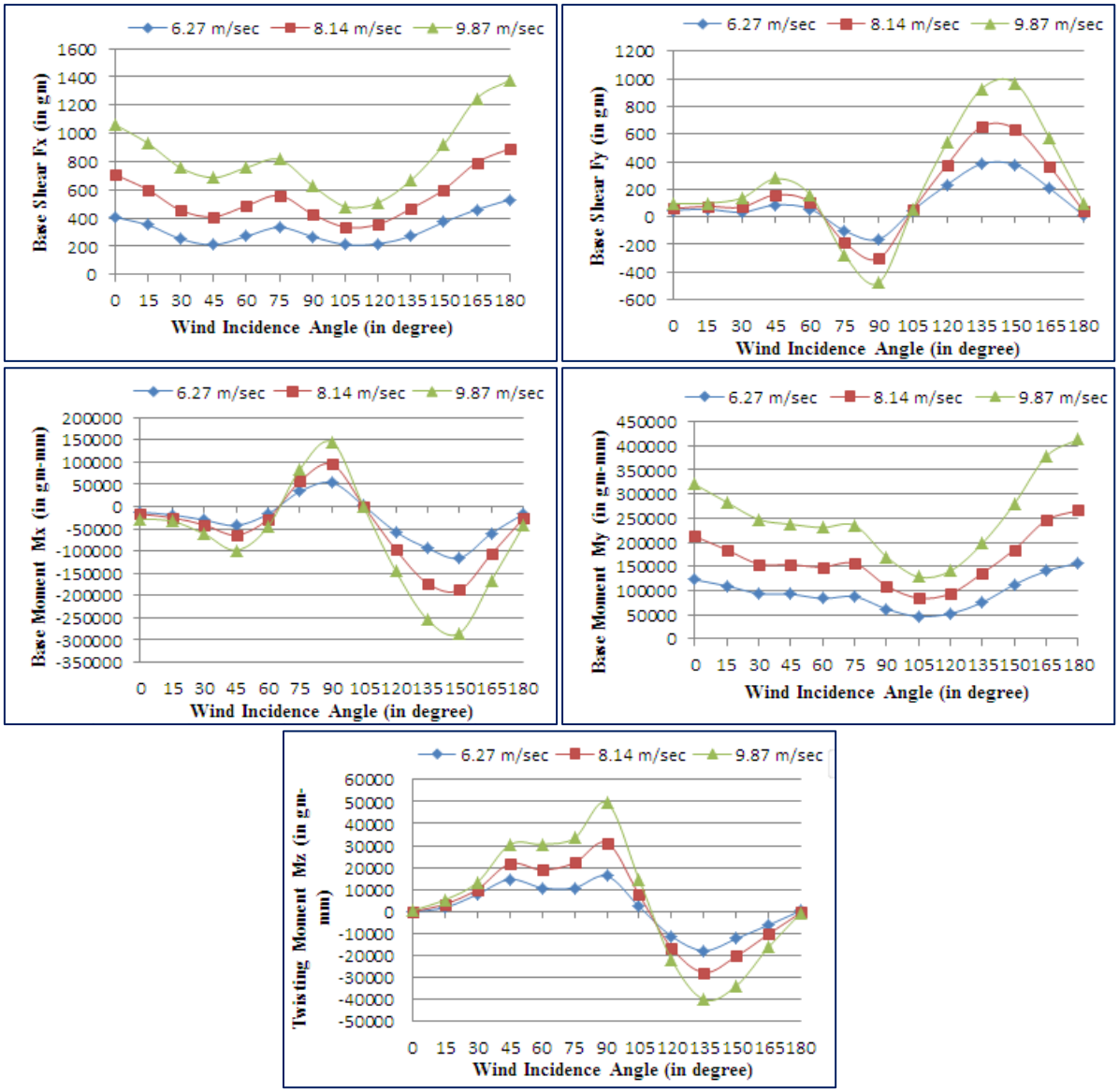


**Fig. 4.17 Variation of base shear ($F_x$ and $F_y$), base moment ($M_x$ and $M_y$) and twisting moment ($M_z$) on model-F with wind incidence angle**

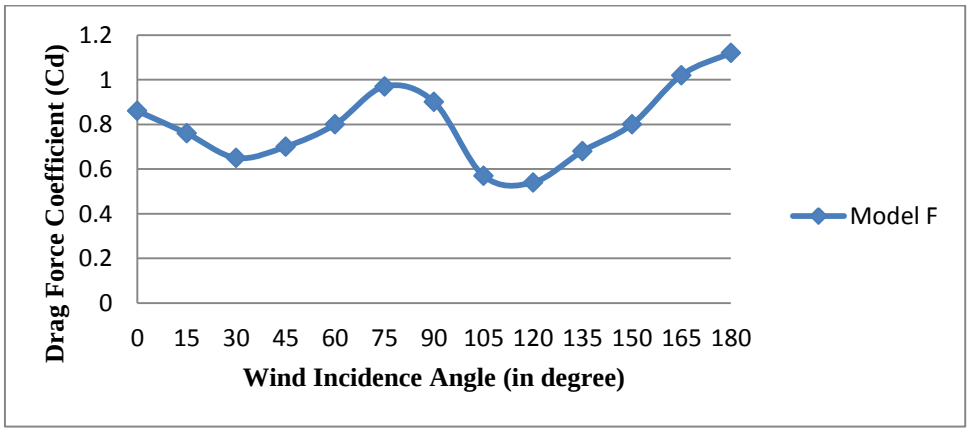


**Fig. 4.18 Variation of drag force coefficient on model-F with wind incidence angle**

### 4.2.7 Model-G (Fish Shape-2)

Wooden model of model-G (Photo. 3.7) is tested in the wind tunnel to measure the base shear, base moments and twisting moment in isolated condition under 13 wind incidence angles from $0^0$ to $180^0$ (Fig. 4.19).

Base shear, base moment and twisting moment measured on model-G under varying wind incidence angles are shown in Fig. 4.20. It is seen from the figure that maximum base shear Fx occurs at $75^0$ wind angle. Fy is maximum at $45^0$, $90^0$ and $135^0$ angles. Twisting moment Mz is maximum at $105^0$ angle.

It is seen from Fig. 4.21 that maximum and minimum drag coefficients on model-G are 0.93 and 0.57 at wind incidence angles $90^0$ and $30^0$ respectively. Effects of wind incidence angle on drag coefficients is large in this model.

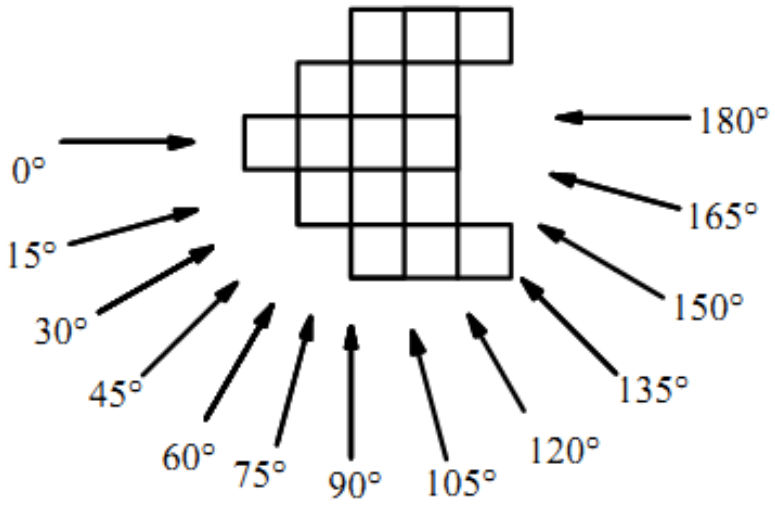


**Fig. 4.19 Cross-section of model-G showing different wind incidence angle**

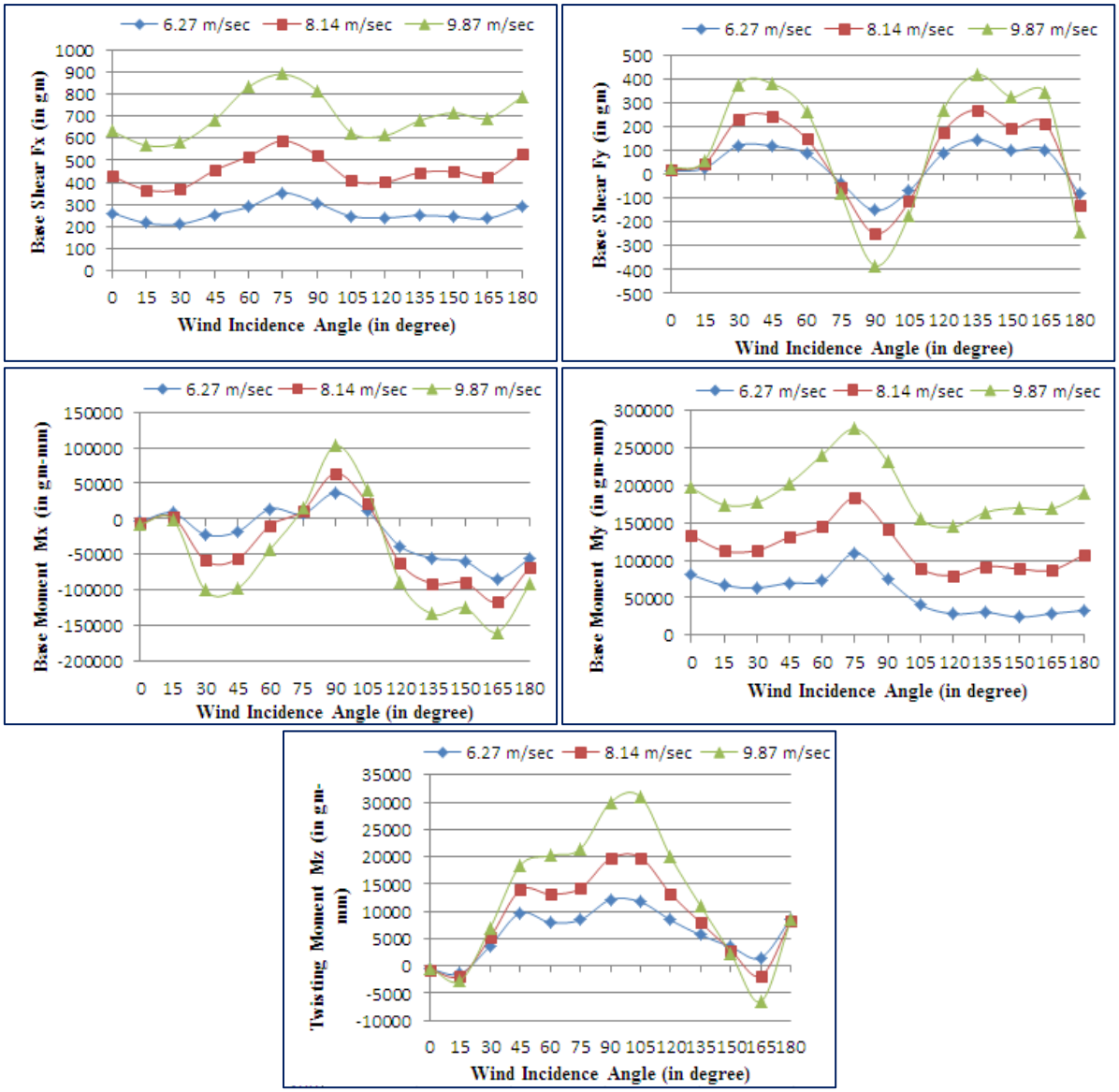


**Fig. 4.20 Variation of base shear ($F_x$ and $F_y$), base moment ($M_x$ and $M_y$) and twisting moment ($M_z$) on model-G with wind incidence angle**

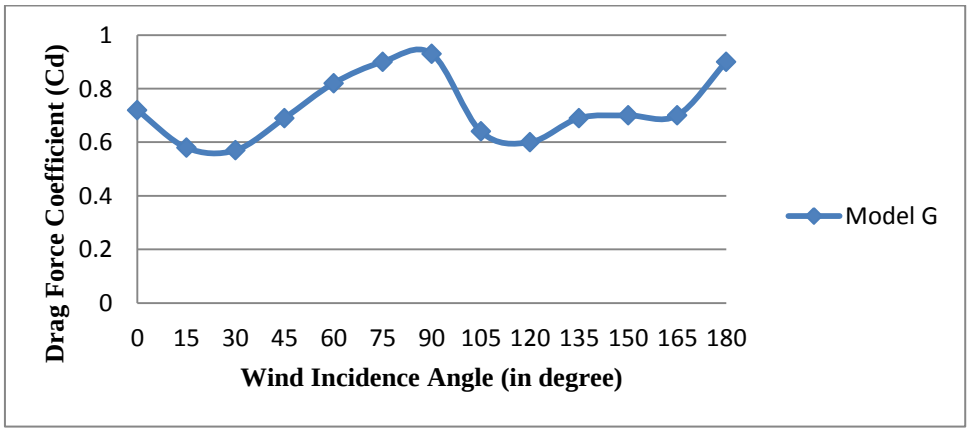


**Fig. 4.21 Variation of drag force coefficient on model-G with wind incidence angle**

### 4.2.8 Model-H (Fish Shape-3)

Figure 4.23 shows the variation of base shear, base moment and twisting moment with respect to varying wind incidence angle. Base shear Fx is maximum when wind hits the model at $90^0$ wind angle due to large exposed area and it is minimum at $30^0$. Base shear Fy is maximum at $135^0$ and this value is approximate similar to that of $45^0$ wind incidence angle.

Base moments Mx and My are the function of base shear Fx and Fy respectively. Therefore, variation of base moment is similar to base shear. Twisting moment Mz is found to be maximum at $90^0$ wind incidence angle.

Maximum and minimum drag coefficients on model-H are 0.91 and 0.58 at $90^0$ and $30^0$ wind incidence angles respectively (Fig. 4.24).

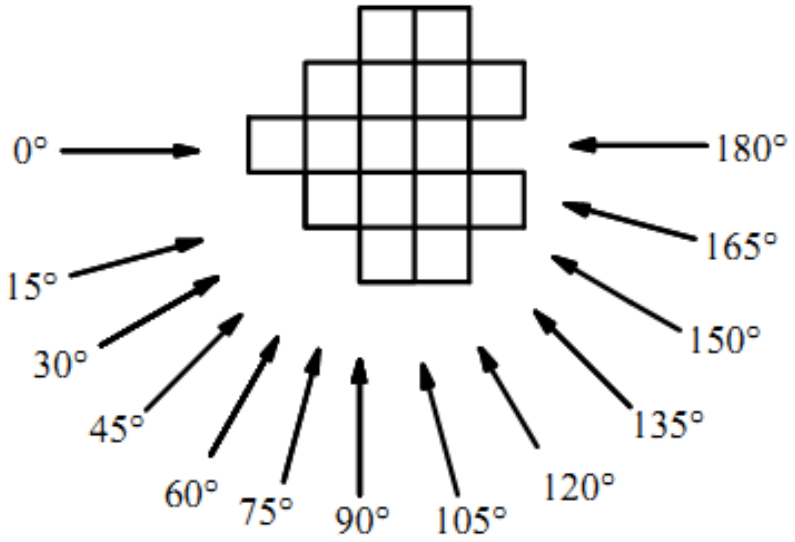


**Fig. 4.22 Cross-section of model-H showing different wind incidence angle**

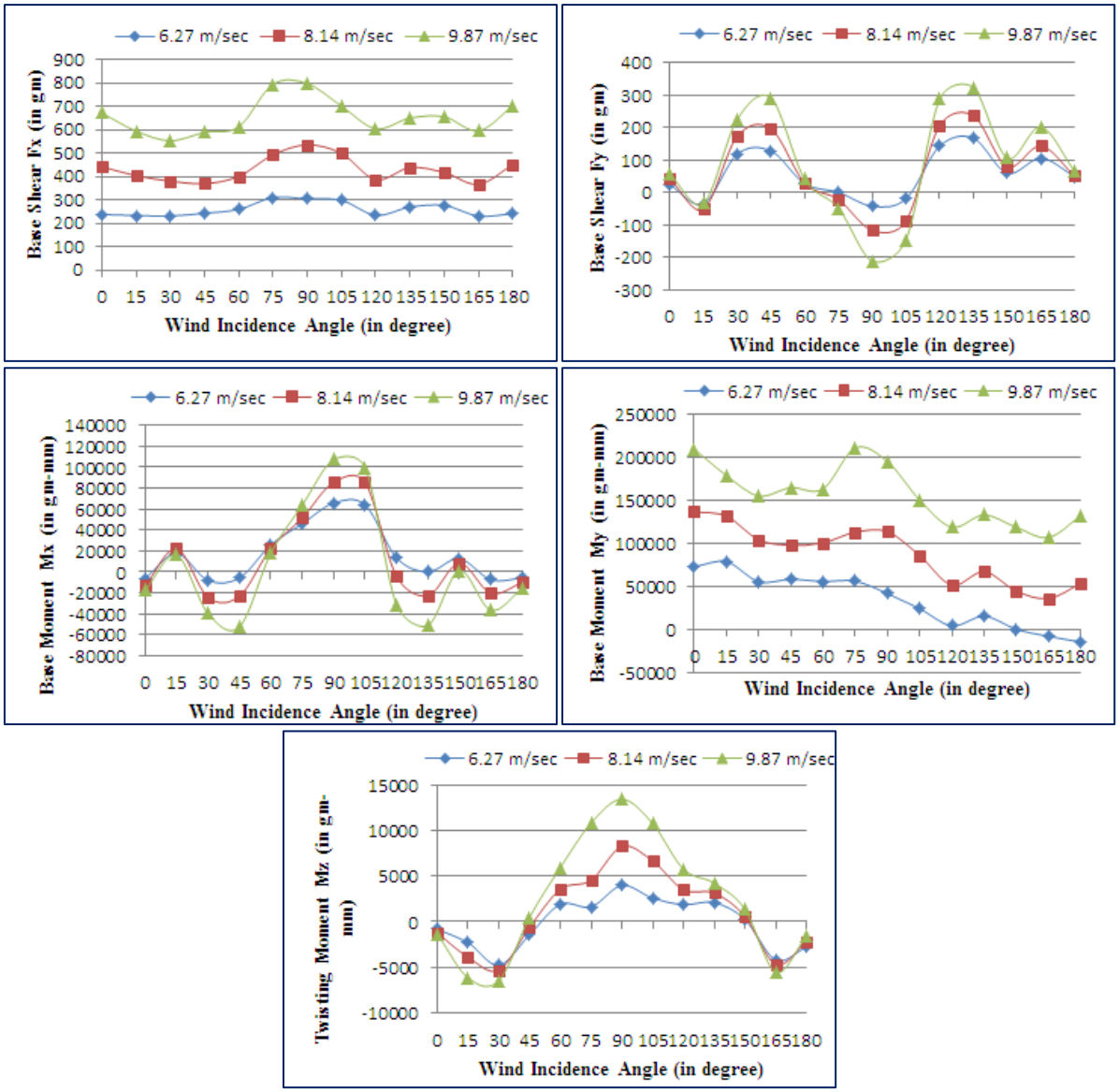


**Fig. 4.23 Variation of base shear ($F_x$ and $F_y$), base moment ($M_x$ and $M_y$) and twisting moment ($M_z$) on model-H with wind incidence angle**

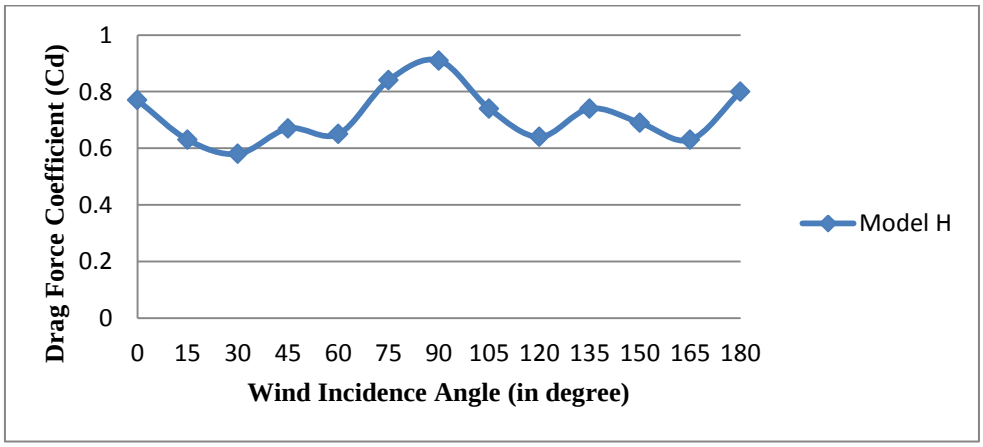


**Fig. 4.24 Variation of drag force coefficient on model-H with wind incidence angle**

## 4.3 INTERFERENCE CONDITION

### 4.3.1 Model-A (Square Shape)

Wind interference effect on base shear, base moments and twisting moments are studied for 3 wind interference conditions namely full blockage, half blockage and no blockage (Fig. 4.26). Wooden model of model-A is placed on five component load-cell with another model of same cross-section as interfering model placed on upstream side. In first condition, interfering building model is placed exactly in front of model placed on load-cell. In second case 50% of front surface of the building model is blocked. In third case, wind is free to hit wind ward surface of the building model.

When tall building are constructed, gap between two buildings vary a lot depending upon the availability of ground space. In the present study, distance between two models in the direction of wind is kept as 60 mm which corresponds to 6 m in case of prototype buildings and is one-tenth of building height.

Base shear, base moment and twisting moment are plotted in the form of histogram, and shown in Fig. 4.26. Fx, Fy, Mx and My are found to be maximum in no blockage condition, whereas Mz is maximum at half blockage condition.

It is seen from Fig. 4.27 that maximum drag coefficient (0.78) is obtained in case of no blockage wind interference condition and minimum drag coefficient (-0.11) in case of full blockage wind interference condition. However, Cd is 0.90 in isolated condition (Fig. 4.3).

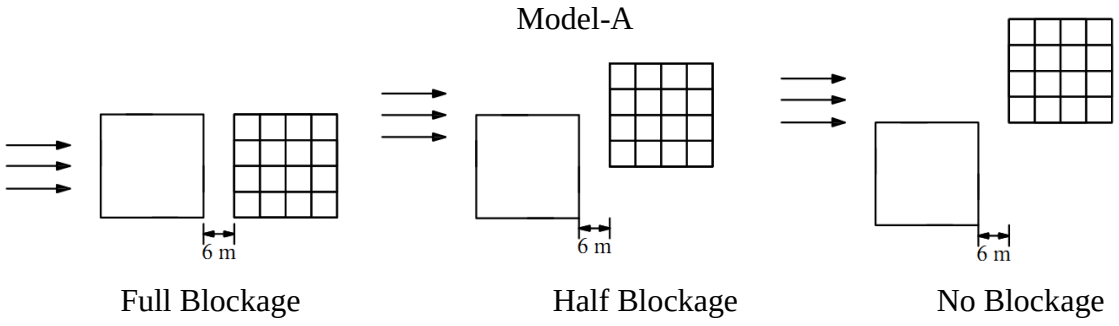


**Fig. 4.25 Cross-section of model-A showing different wind interference conditions**

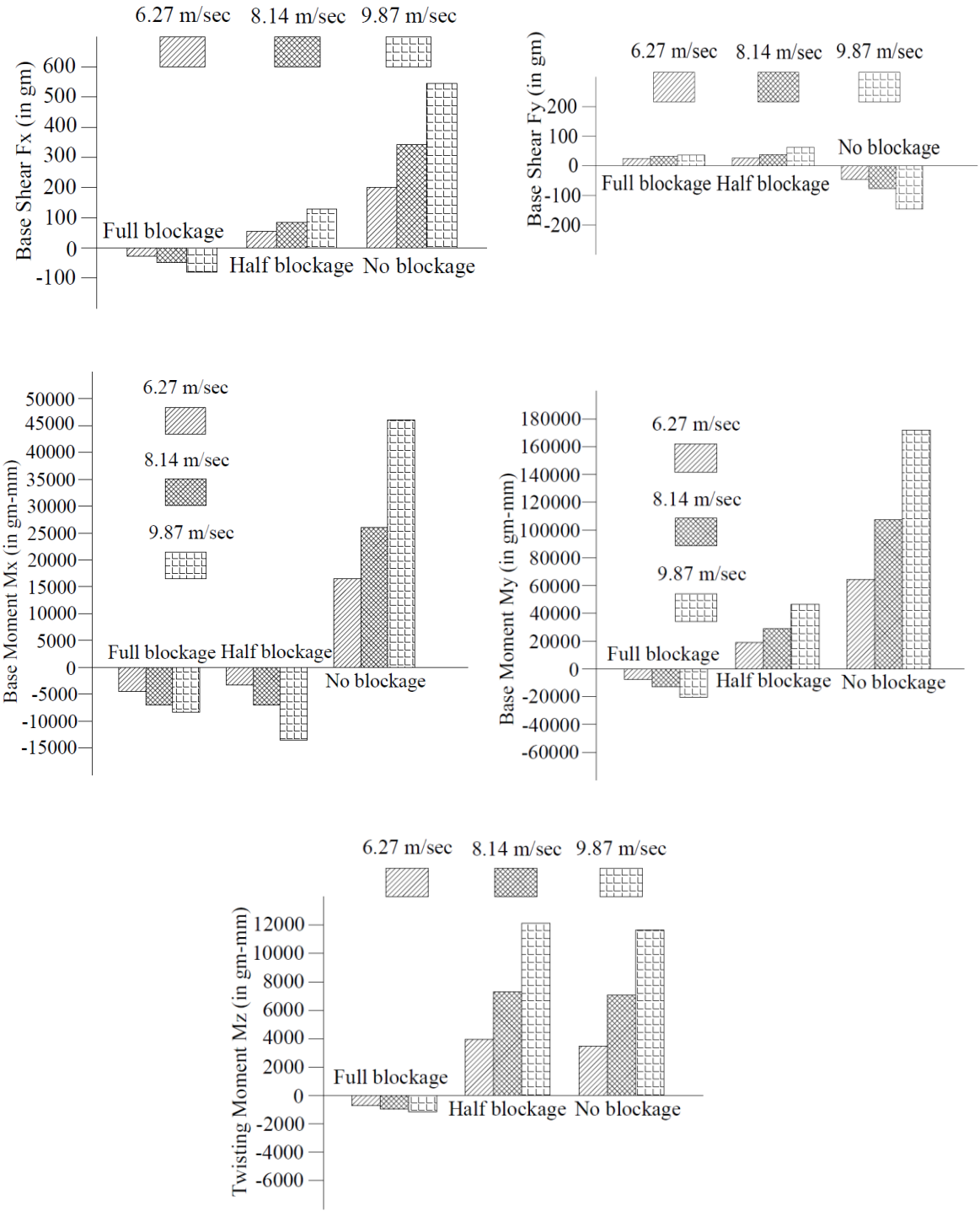


**Fig. 4.26 Variation of base shear ($F_x$ and $F_y$), base moment ($M_x$ and $M_y$) and twisting moment ($M_z$) on model-A in wind interference condition**

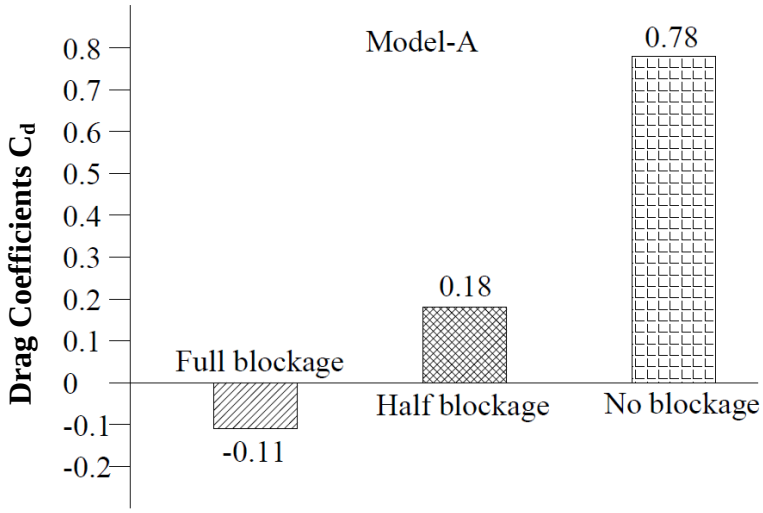


**Fig. 4.27 Comparison of drag coefficients on model-A at all three wind interference condition**

### 4.3.2 Model-B (Plus Shape-1)

Model-B is also tested under 3 interference conditions (Fig. 4.28) as in the case of model-A. Base shear, base moment and twisting moment are plotted in case of full blockage, half blockage and no blockage conditions. Fx, Fy, Mx and My are maximum in case of no blockage condition and minimum in case of full blockage condition. Twisting moment Mz is maximum in case of half blockage wind interference condition (Fig. 4.29).

It is seen from Fig. 4.30 that maximum drag coefficient is 0.59 in case of no blockage wind interference condition and minimum drag coefficients -0.11 is found in case of full blockage wind interference condition. This value is 0.8 in isolated condition (Fig. 4.6)

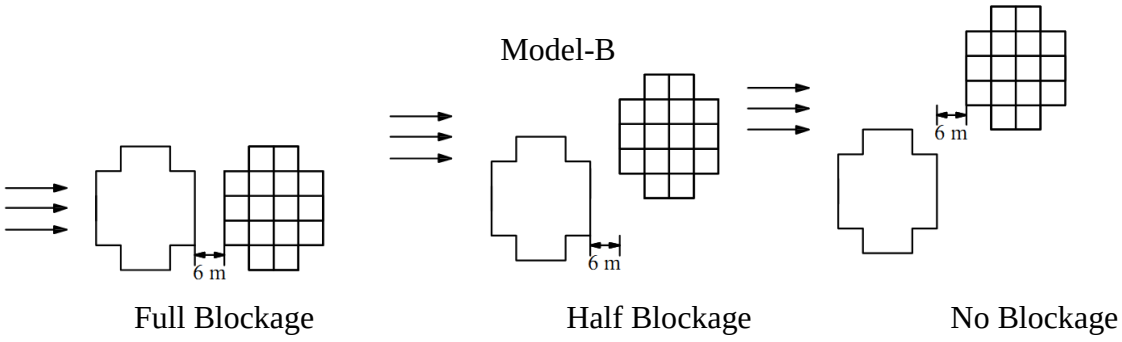


**Fig. 4.28 Cross-section of model-B showing different wind interference conditions**

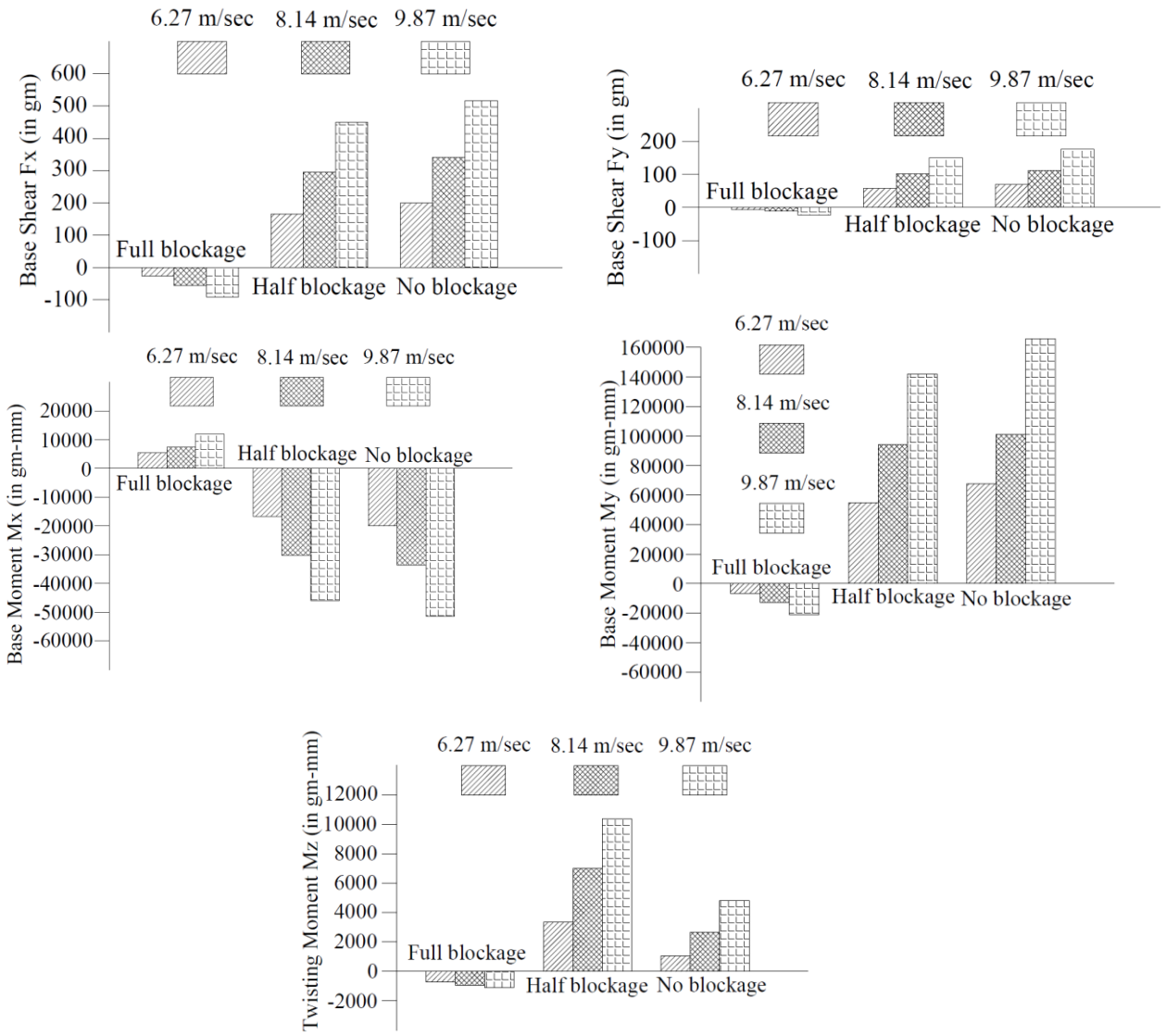


**Fig. 4.29 Variation of base shear ($F_x$ and $F_y$), base moment ($M_x$ and $M_y$) and twisting moment ($M_z$) on model-B in wind interference condition**

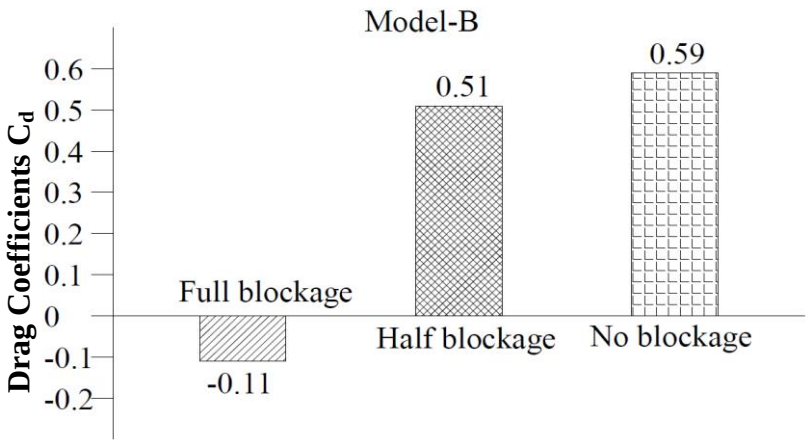


**Fig. 4.30 Comparison of drag coefficient on model-B at all three wind interference conditions**

### 4.3.3 Model-C (Plus Shape-2)

Wooden model of model-C is tested under the 3 wind interference conditions namely full blockage, half blockage and no blockage (Fig. 4.31). Base shear, base moment and twisting moment are also plotted along the wind incidence angle (Fig. 4.32). It is noticed that whereas Fx and My are maximum in no blockage condition, Fy, Mx and Mz are maximum in half blockage condition.

Maximum and minimum drag coefficients can be seen in Fig. 4.33 which is 0.95 and -0.24 in case of no blockage and full blockage wind interference condition respectively.

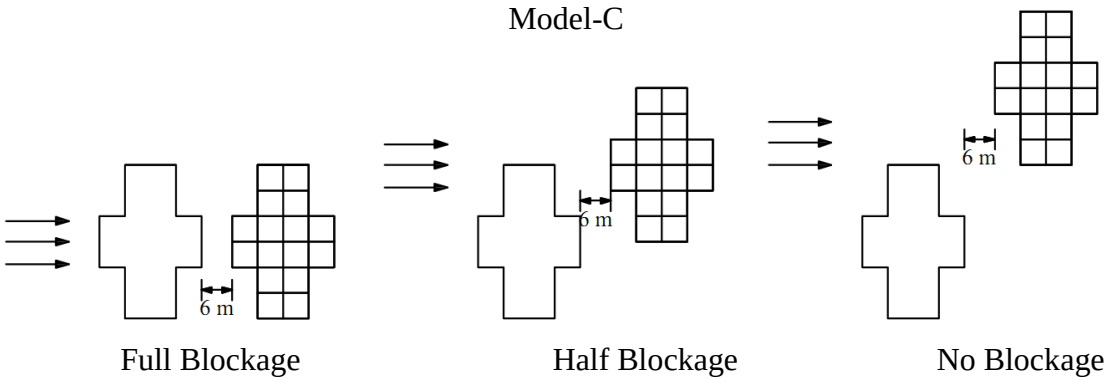


**Fig. 4.31 Cross-section of model-C showing different wind interference conditions**

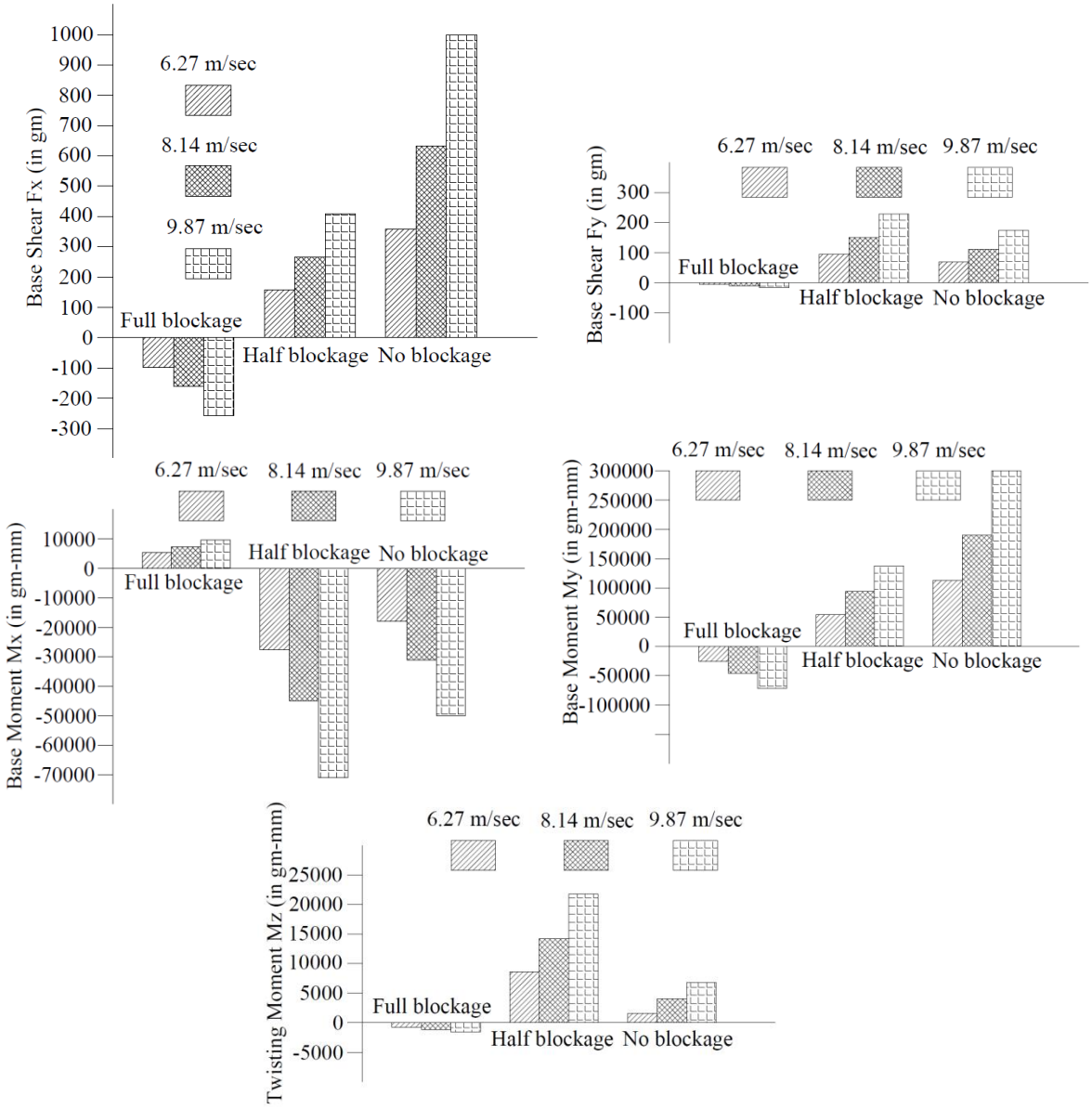


**Fig. 4.32 Variation of base shear ($F_x$ and $F_y$), base moment ($M_x$ and $M_y$) and twisting moment ($M_z$) on model-C with wind interference condition**

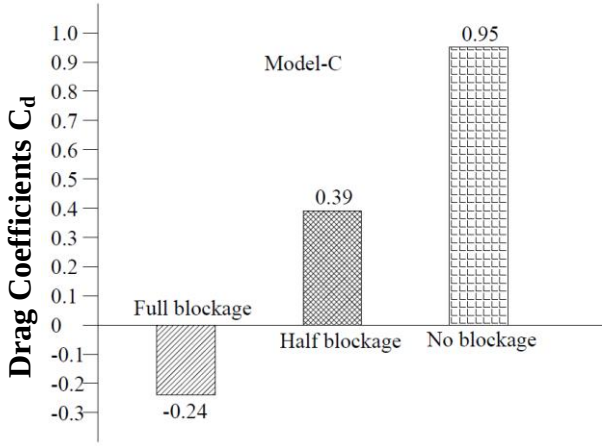


**Fig. 4.33 Comparison of drag coefficients on model-C at all three wind interference conditions**

### 4.3.4 Model-D (I-shape-1)

Wooden model of model-D is also tested under 3 wind interference conditions (Fig. 4.34). Base shear, base moment and twisting moment are also plotted along the wind incidence angle (Fig. 4.35). Fx and My are maximum in no blockage condition. Fy and Mx are maximum at half blockage condition. Twisting moment Mz is also maximum in half blockage condition.

It can be seen from Fig. 4.36 that maximum drag coefficient 0.95 is obtained in case of no blockage wind interference condition and minimum drag coefficient -0.14 evaluated in case of full blockage wind interference condition.

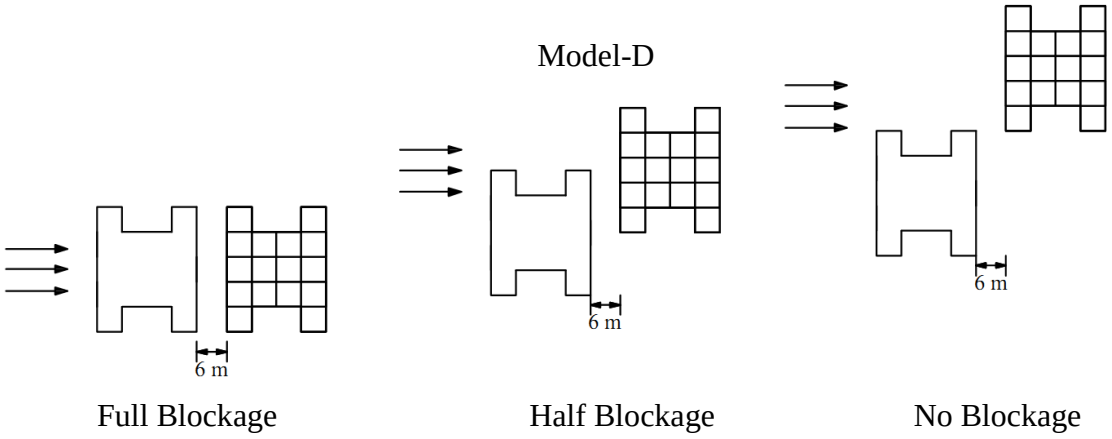


**Fig. 4.34 Cross-section of model-D showing different wind interference conditions**

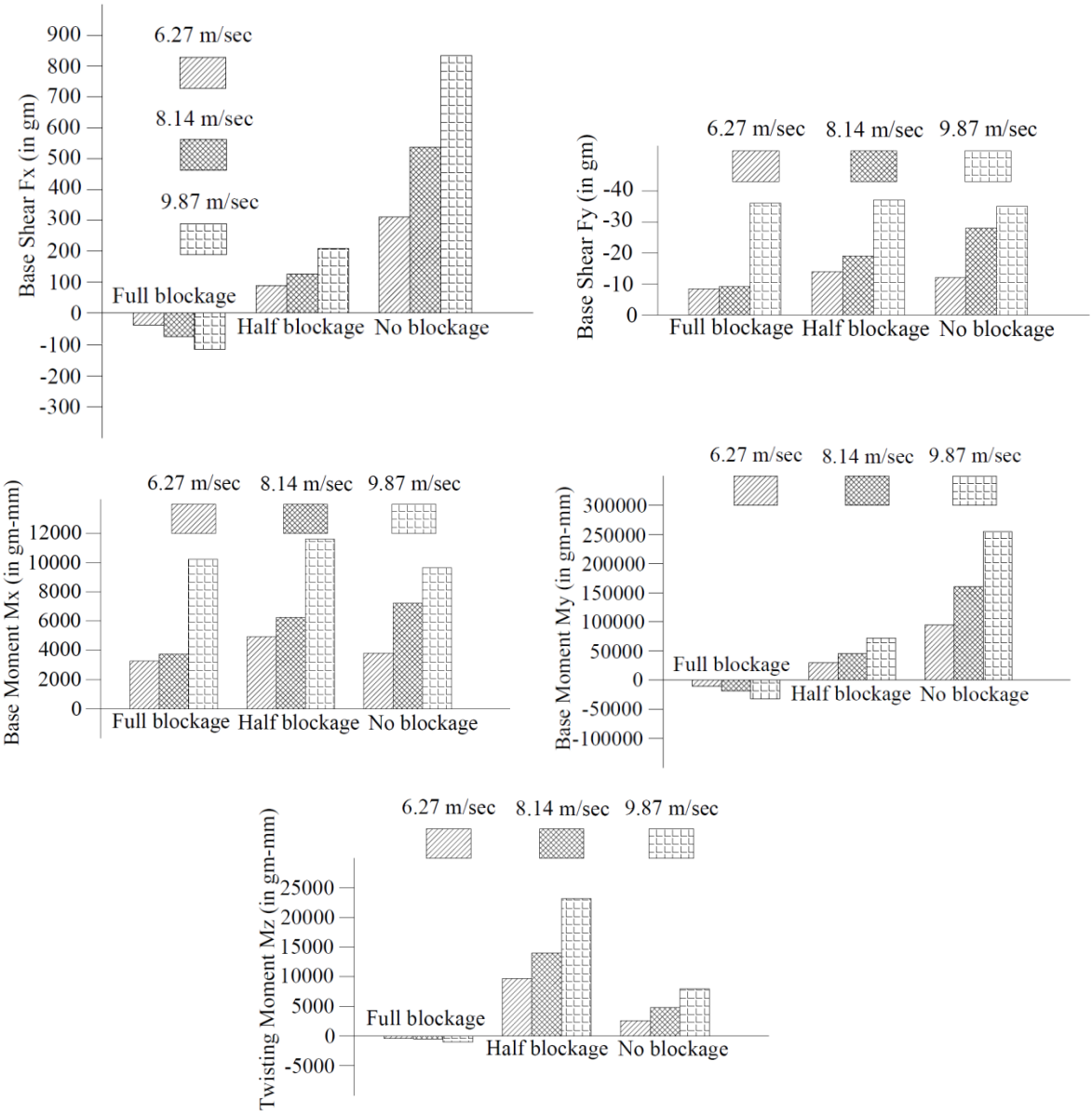


**Fig. 4.35 Variation of base shear ($F_x$ and $F_y$), base moment ($M_x$ and $M_y$) and twisting moment ($M_z$) on model-D with wind interference condition**

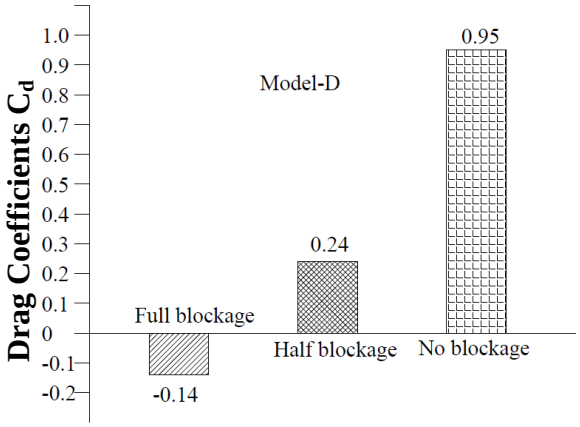


**Fig. 4.36 Comparison of drag coefficients on model-D at all three wind interference conditions**

### 4.3.5 Model-E (I-Shape-2)

Wooden model of model-E is tested under three wind interference conditions namely full blockage, half blockage and no blockage (Fig. 4.37). Base shear, base moment and twisting moment are calculated and plotted (Fig. 4.38). In this case, all parameters namely Fx, Fy, Mx, My and Mz are found to be maximum at no blockage condition.

It is found that maximum drag coefficient is 1.37 in case of no blockage wind interference condition and minimum drag coefficient is -0.28 in case of full blockage wind interference condition (Fig. 4.39).

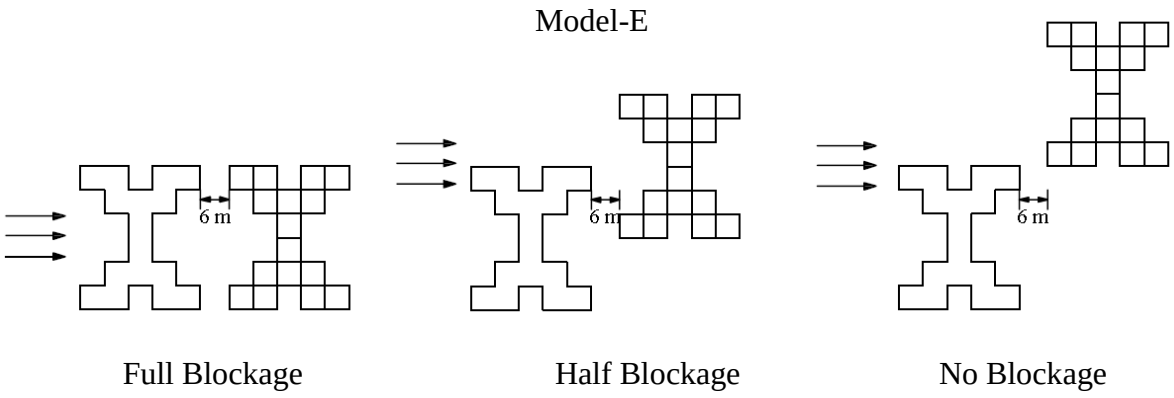


**Fig. 4.37 Cross-section of model-E showing different wind interference conditions**

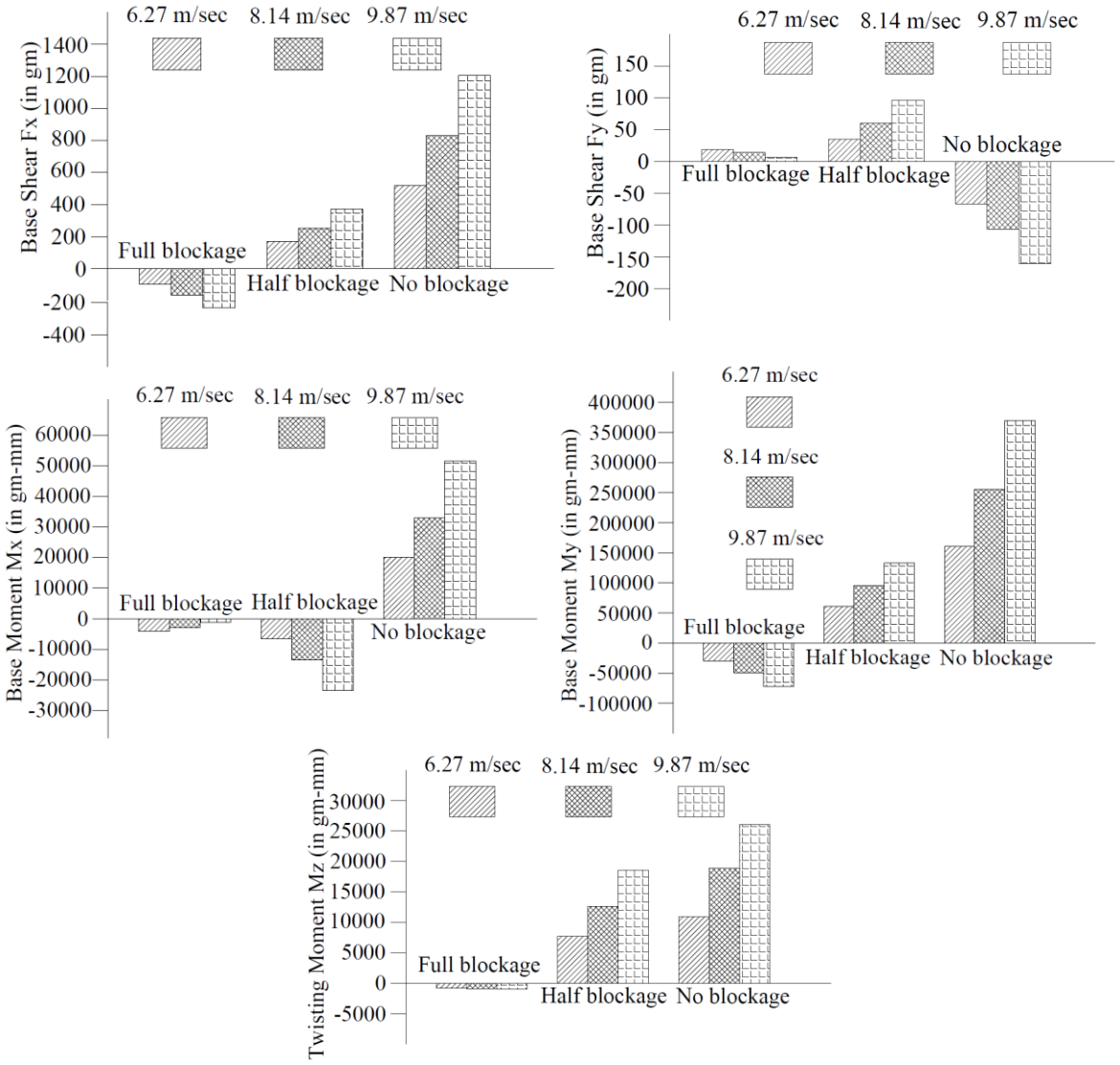


**Fig. 4.38 Variation of base shear ($F_x$ and $F_y$), base moment ($M_x$ and $M_y$) and twisting moment ($M_z$) on model-E with wind interference condition**

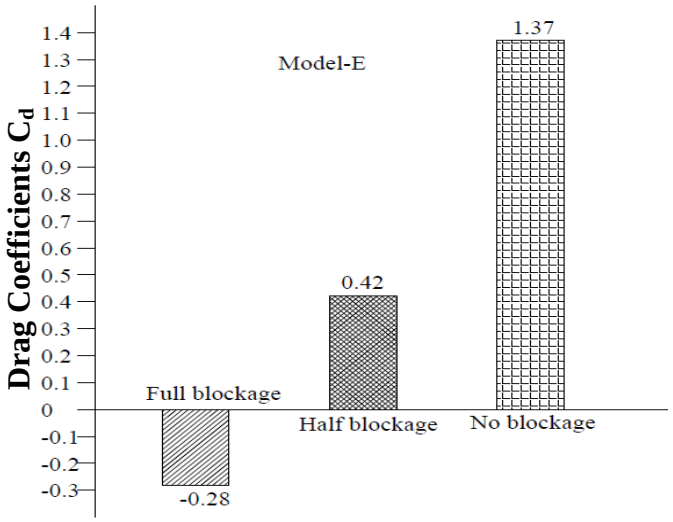


**Fig. 4.39 Comparison of drag coefficients on model-E at all three wind interference conditions**

### 4.3.6 Model-F (Fish Shape-1)

Present article gives detail of force measurements on wooden model of building model-F in four different wind interference conditions namely back-to-back, back-to-front, front-to-back and front-to-front (Fig. 4.40). Results are presented in Fig. 4.41. Fx and My are maximum at front-to-back condition. Fy, Mx and Mz are maximum at front-to-front condition.

Due to the presence of interfering building model on upstream side, negative forces are measured in all four cases experimentally. Therefore, all drag coefficients evaluated are negative. It is noticed that maximum negative drag coefficients is -0.43 in case of front-to-back wind interference condition and minimum negative drag coefficients is -0.14 in case of back-to-back wind interference condition (Fig. 4.42).

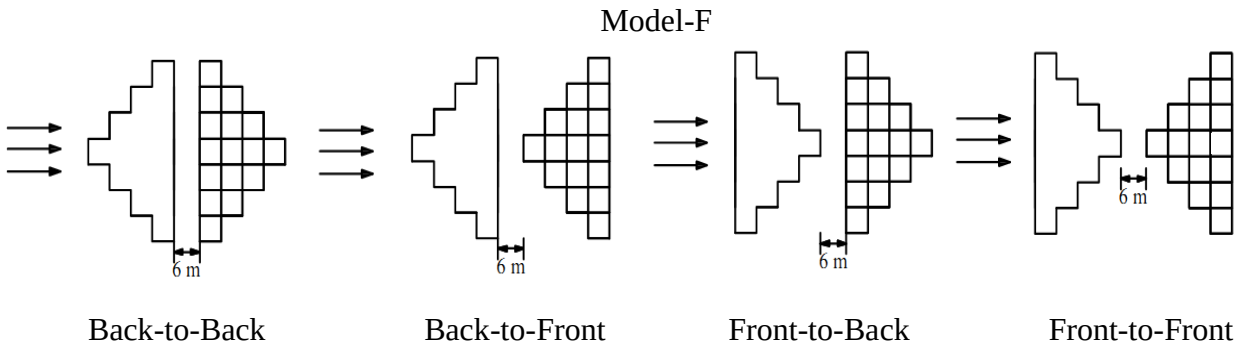


**Fig. 4.40 Cross-section of model-F showing different wind interference conditions**

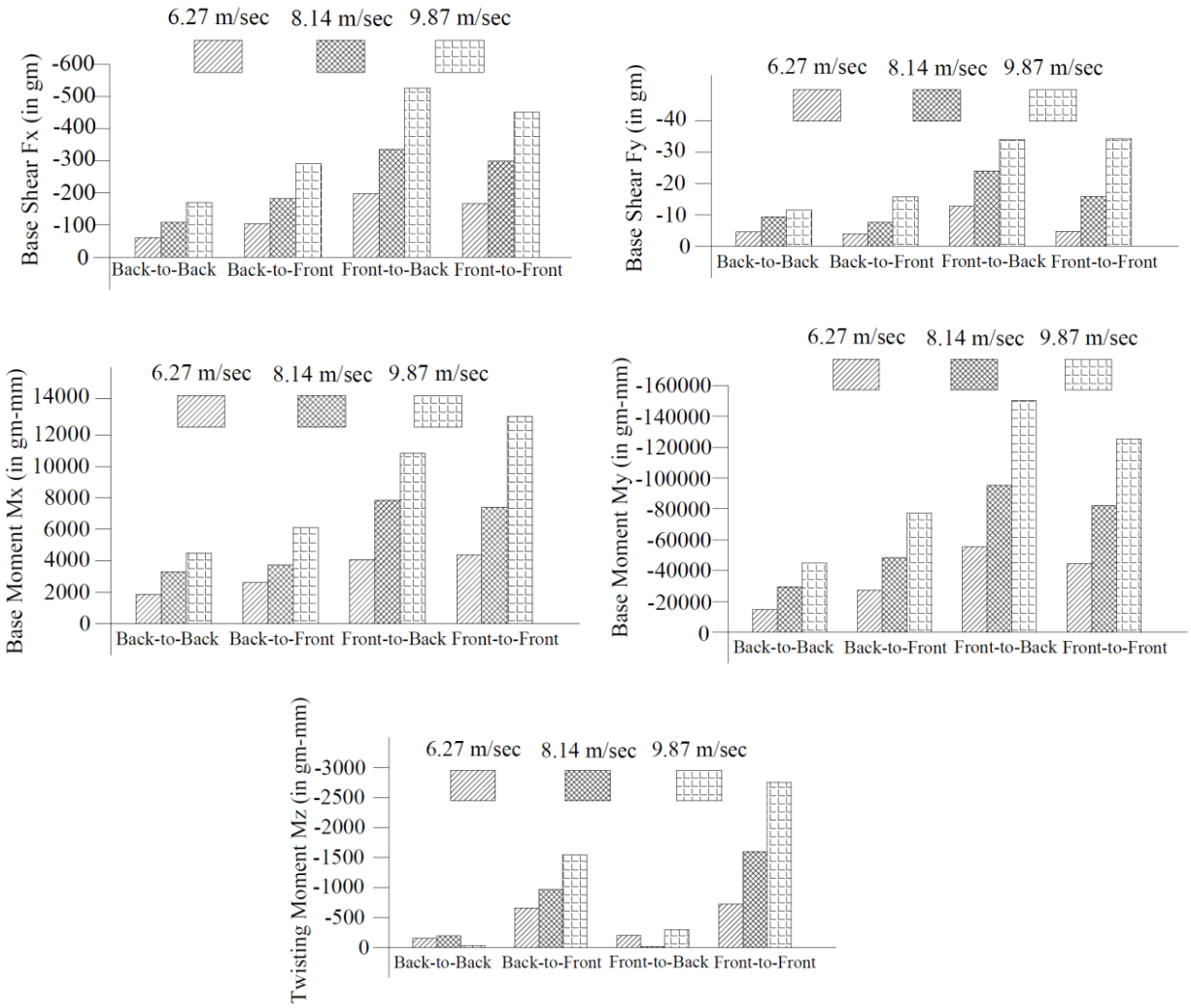


**Fig. 4.41 Variation of base shear ($F_x$ and $F_y$), base moment ($M_x$ and $M_y$) and twisting moment ($M_z$) on model-F with wind interference condition**

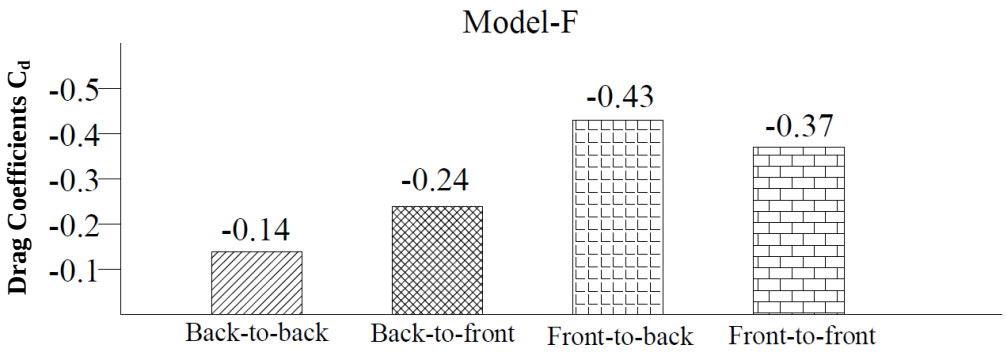


**Fig. 4.42 Comparison of drag coefficients on model-F at all four wind interference conditions**

### 4.3.7 Model-G (Fish Shape-2)

Wooden model of model-G is also tested under four different wind interference conditions (Fig. 4.43). Experimental values of base shear, base moments and twisting moment are evaluated and plotted along the wind incidence angle (Fig. 4.44). Fx and My are maximum in front-to-back condition. Fy and Mx are maximum in front-to-front condition. Mz is maximum in front-to-back condition.

Values of drag coefficients are plotted in form of histogram in Fig. 4.45. Maximum drag coefficients evaluated is -0.17 in case of front-to-back wind interference condition and minimum drag coefficients is -0.11 evaluated in case of back-to-front wind interference condition.

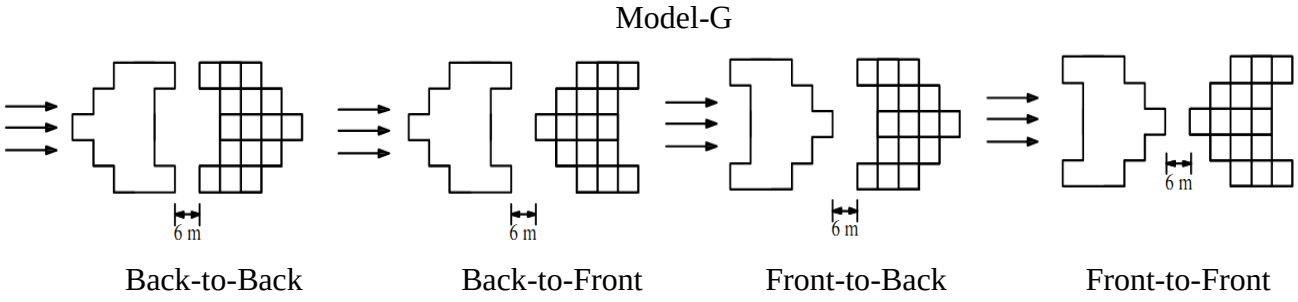


**Fig. 4.43 Cross-section of model-G showing different wind interference conditions**

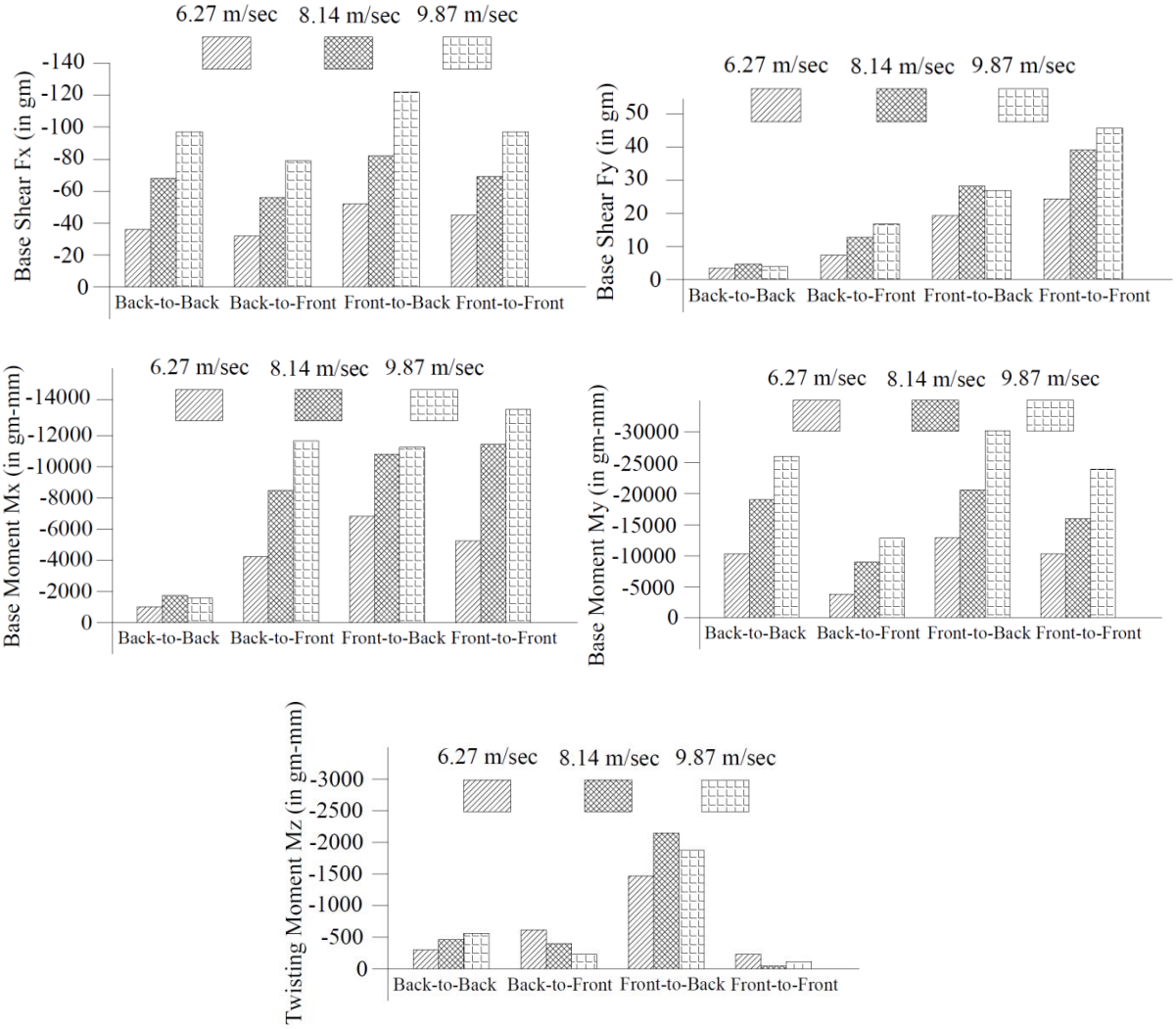


**Fig. 4.44 Variation of base shear ($F_x$ and $F_y$), base moment ($M_x$ and $M_y$) and twisting moment ($M_z$) on model-G with wind interference condition**

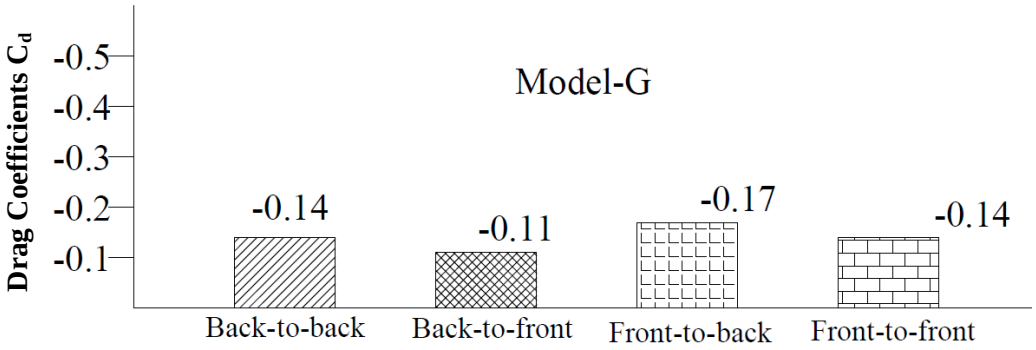


**Fig. 4.45 Comparison of drag coefficients on model-G at all four wind interference conditions**

### 4.3.8 Model-H (Fish Shape-3)

Wooden model of model-H is tested under four different wind interference conditions (Fig. 4.46). Experimental values of base shear, base moments and twisting moment are evaluated and plotted along the wind incidence angle (Fig. 4.47). In this case, Fx, Fy, Mx and My are maximum in back-to-back condition. Mz is maximum in back-to-front condition.

Values of drag coefficients in all four wind interference conditions are evaluated. It is seen in Fig. 4.48 that drag coefficient is maximum in back-to-back condition and minimum in front-to-front condition.

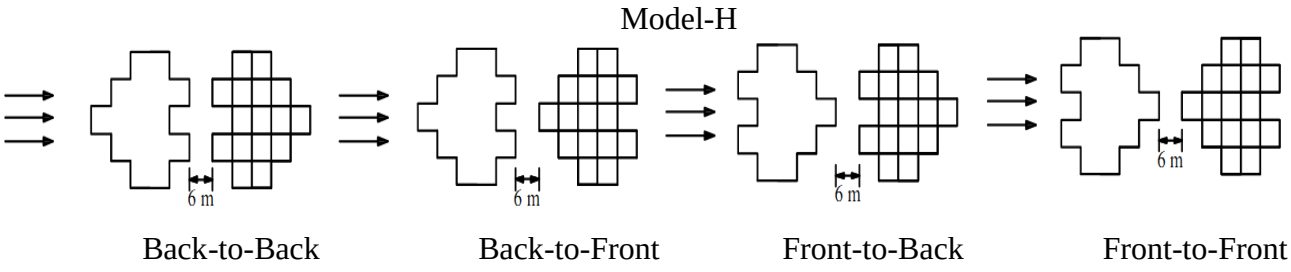


**Fig. 4.46 Cross-section of model-H showing different wind interference conditions**

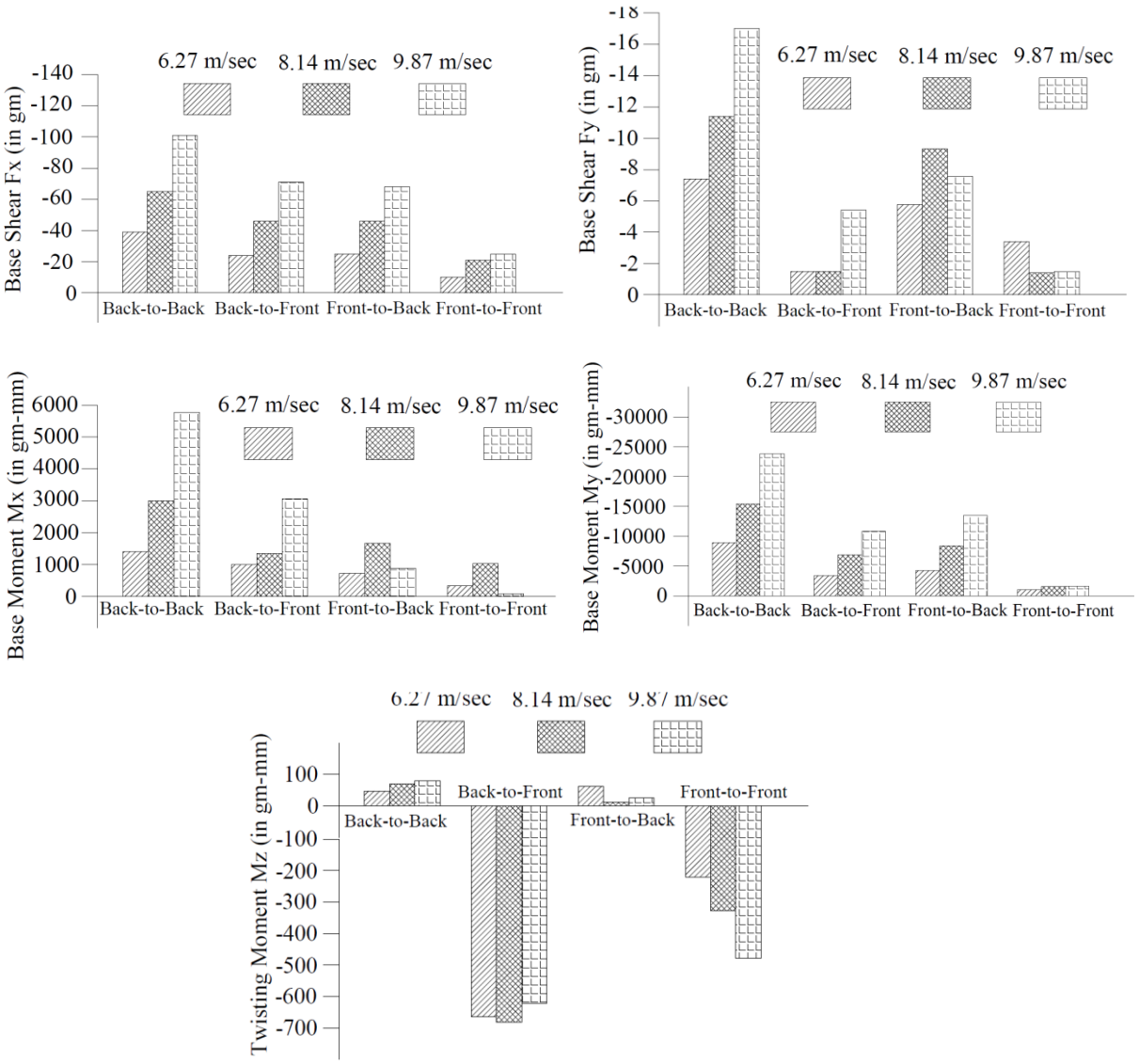


**Fig. 4.47 Variation of base shear ($F_x$ and $F_y$), base moment ($M_x$ and $M_y$) and twisting moment ($M_z$) on model-H with wind interference condition**

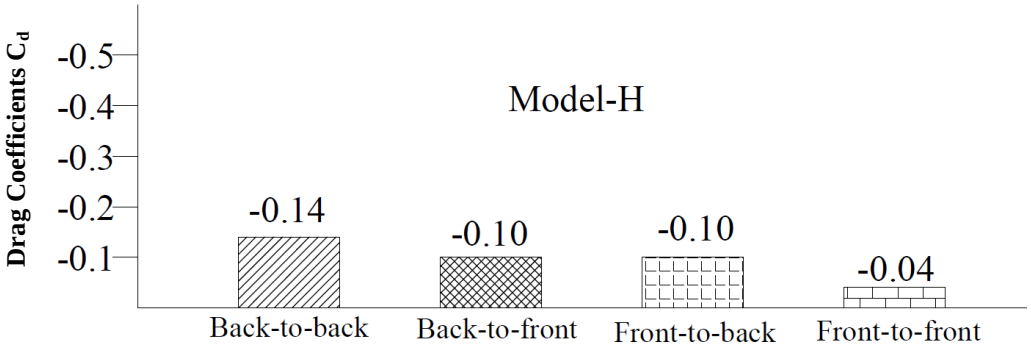


**Fig. 4.48 Comparison of drag coefficients on model-H at all four wind interference conditions**

## 4.4 COMPARISON OF DRAG FORCE COEFFICIENTS - ISOLATED CONDITION

In order to study the influence of plan shape of the building on wind loads, maximum drag coefficients evaluated on all eight building models in isolated condition are compared in this article.

### 4.4.1 Models having symmetry about both axes

Figure 4.49 and Table 4.1 show the comparison of drag coefficients for models having symmetry about both axes. It is seen that maximum drag coefficients (1.08) is observed on model-C at $0^0$ wind incidence angle. This value decrease gradually with increase in wind incidence angle. A comparatively equal maximum drag coefficient occurs on model-A, D and E which varies between 0.90 to 0.99 at $0^0$ wind incidence angle. Minimum drag coefficient also occurs in case of model-C at $90^0$ wind incidence angle.

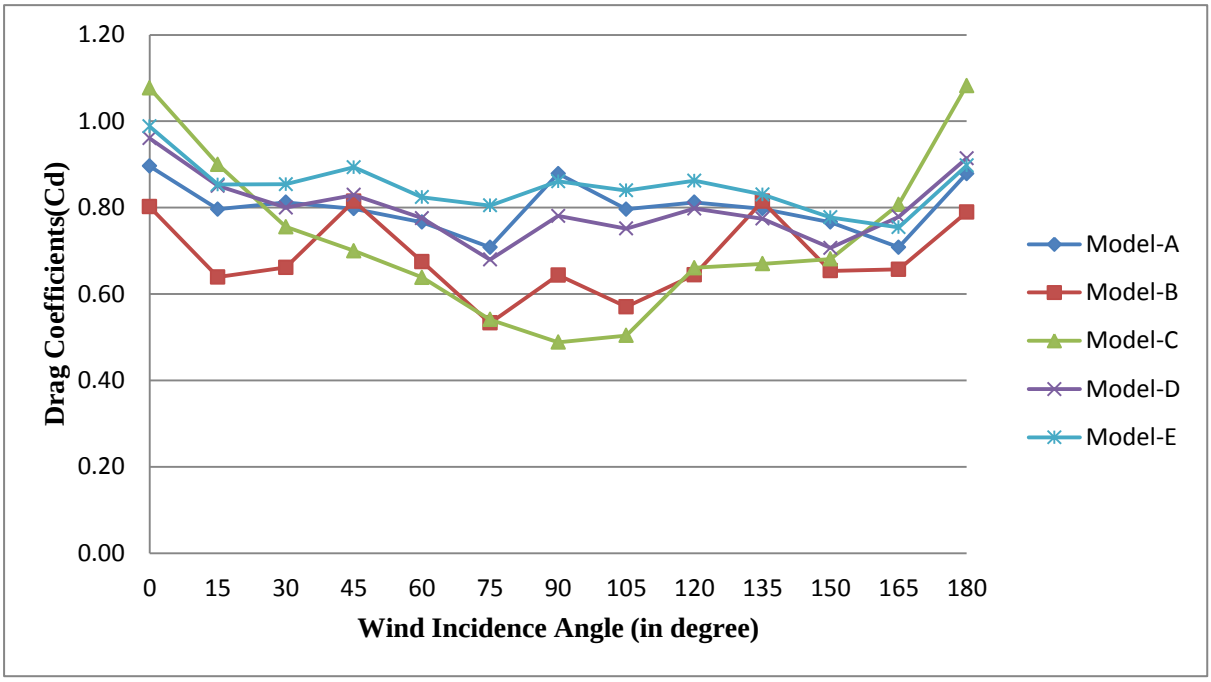


**Fig. 4.49 Comparison of drag coefficients on building models having symmetry about both axes at various wind incidence angles**

**Table 4.1 Drag coefficients for model having symmetry about both axes at various wind incidence angles**

| wind incidence angle (in degree) | Model-A | Model-B | Model-C | Model-D | Model-E |
|---|---|---|---|---|---|
| 0 | 0.90 | 0.80 | 1.08 | 0.96 | 0.99 |
| 15 | 0.80 | 0.64 | 0.90 | 0.85 | 0.85 |
| 30 | 0.81 | 0.66 | 0.76 | 0.80 | 0.85 |
| 45 | 0.80 | 0.82 | 0.70 | 0.83 | 0.89 |
| 60 | 0.77 | 0.67 | 0.64 | 0.78 | 0.82 |
| 75 | 0.71 | 0.53 | 0.54 | 0.68 | 0.80 |
| 90 | 0.88 | 0.64 | 0.49 | 0.78 | 0.86 |

### 4.4.2 Models having symmetry about one axis only

Figure 4.50 and Table 4.2 show the comparison of drag coefficients for models having symmetry about one axes only. It is seen that maximum drag coefficient (1.12) is observed on model-F at $180^0$ wind incidence angle. Minimum drag coefficient occurs on same model-F at an angle of $120^0$ (0.54). Comparatively equal drag coefficients occur on model-G and model-H which varies between 0.72 to 0.90. Maximum drag coefficient (0.93) occurs on model-G at $90^0$ wind incidence angle.

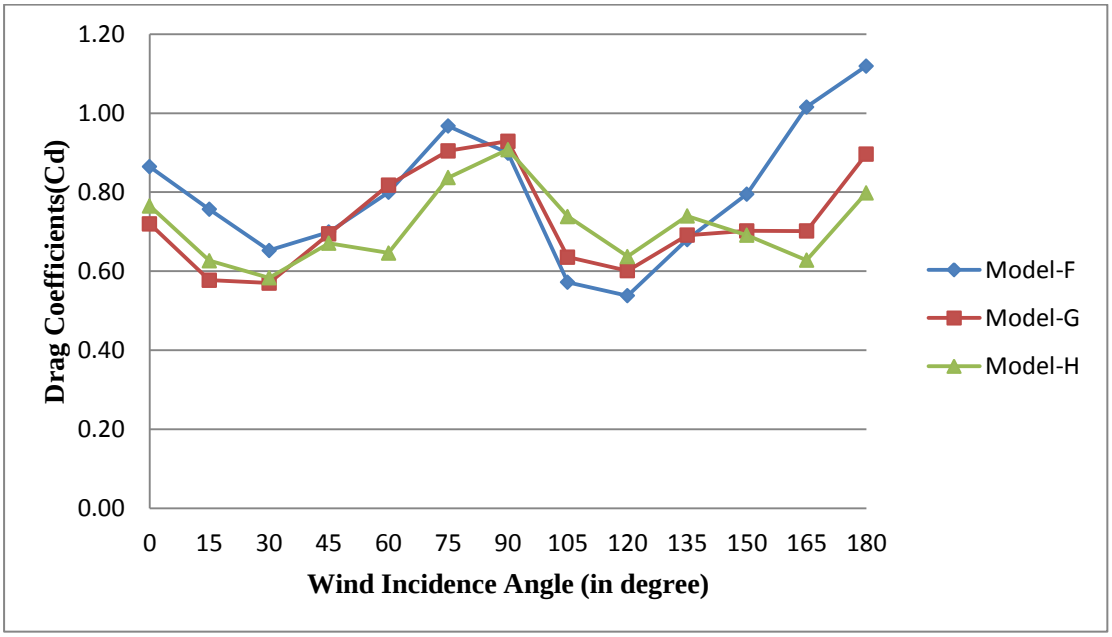


**Fig. 4.50 Comparison of drag coefficients on building models having symmetry about one axis only at various wind incidence angles**

**Table 4.2 Drag coefficients for model having symmetry about one axis only at various wind incidence angles**

| wind incidence angle (in degree) | Model-F | Model-G | Model-H |
|---|---|---|---|
| 0 | 0.86 | 0.72 | 0.77 |
| 15 | 0.76 | 0.58 | 0.63 |
| 30 | 0.65 | 0.57 | 0.58 |
| 45 | 0.70 | 0.69 | 0.67 |
| 60 | 0.80 | 0.82 | 0.65 |
| 75 | 0.97 | 0.90 | 0.84 |
| 90 | 0.90 | 0.93 | 0.91 |
| 105 | 0.57 | 0.64 | 0.74 |
| 120 | 0.54 | 0.60 | 0.64 |
| 135 | 0.68 | 0.69 | 0.74 |
| 150 | 0.80 | 0.70 | 0.69 |
| 165 | 1.02 | 0.70 | 0.63 |
| 180 | 1.12 | 0.90 | 0.80 |

## 4.5 COMPARISON OF DRAG FORCE COEFFICIENTS - INTERFERENCE CONDITION

Comparison of maximum drag coefficients evaluated on all eight building models under interference condition is made herein.

### 4.5.1 Models having symmetry about both axes

Table 4.3 and Figs. 4.51 to 4.53 show the comparison of wind interference effect on drag coefficients on wooden models having symmetry about both axes tested under three different wind interference conditions. In case of full blockage interference condition, maximum drag coefficient -0.28 is evaluated for model-E due to its large exposed area and minimum drag coefficient -0.11 for model-A and model-B. In case of half blockage wind interference condition, maximum drag coefficient is found in model-B as 0.51, and minimum drag coefficient for model-A as 0.18. When wooden models are tested under no blockage wind interference condition, maximum drag coefficient is observed on model-E which is 1.37 and minimum drag coefficient on model-B as 0.59. Equal drag coefficients are evaluated in case of model-C and model-D.

**Table 4.3 Drag coefficients for model having symmetry about both axes at wind interference condition**

| Wind Interference Condition | Model-A | Model-B | Model-C | Model-D | Model-E |
|---|---|---|---|---|---|
| Full Blockage | -0.11 | -0.11 | -0.24 | -0.14 | -0.28 |
| Half Blockage | 0.18 | 0.51 | 0.39 | 0.24 | 0.42 |
| No Blockage | 0.78 | 0.59 | 0.95 | 0.95 | 1.37 |

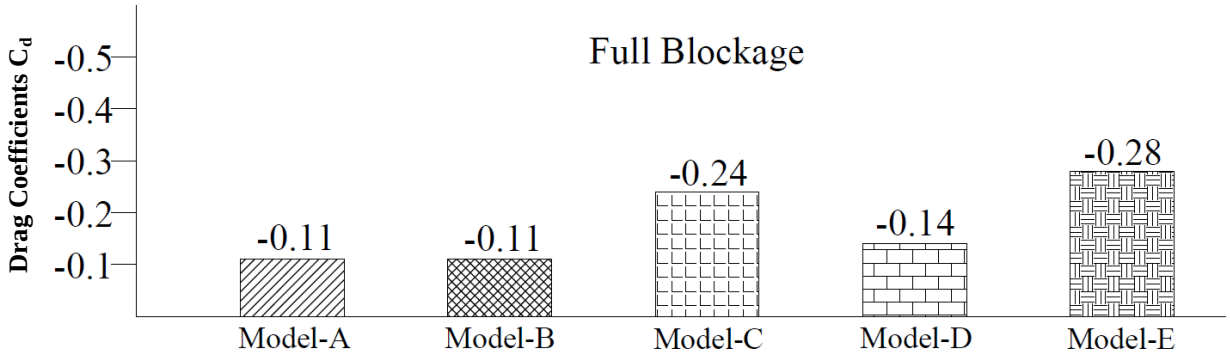


**Fig. 4.51 Comparison of drag coefficients on building models having symmetry about both axes in full blockage wind interference condition**

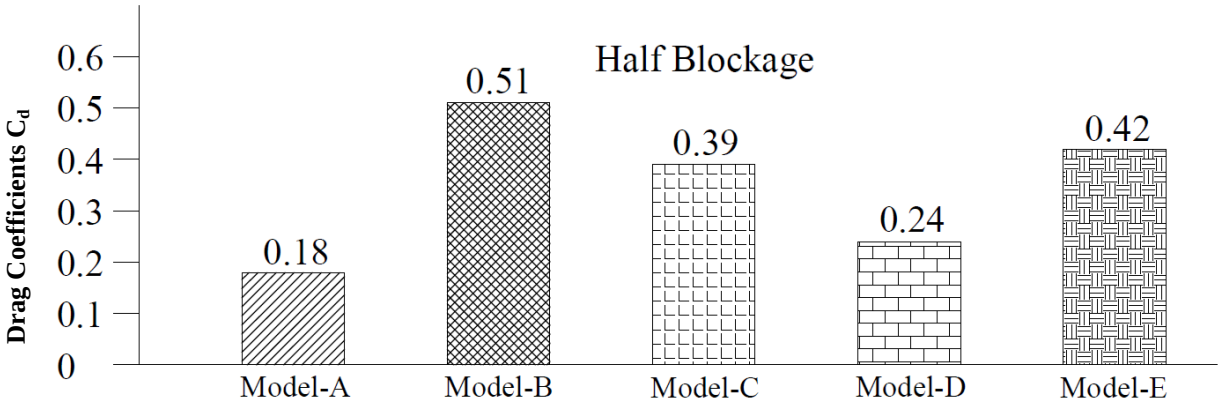


**Fig. 4.52 Comparison of drag coefficients on building models having symmetry about both axes in half blockage wind interference condition**

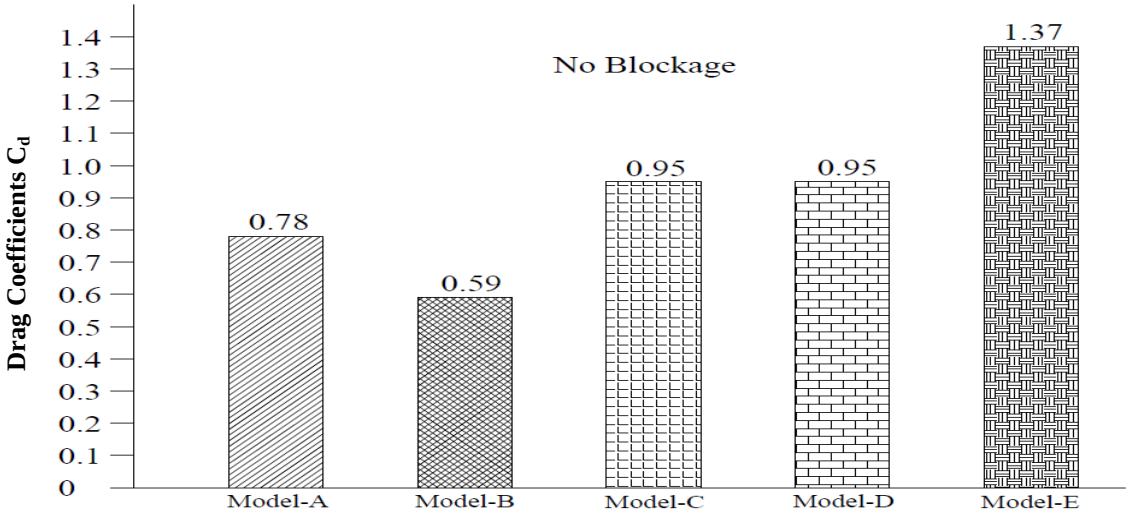


**Fig. 4.53 Comparison of drag coefficients on building models having symmetry about both axes in no blockage wind interference condition**

### 4.5.2 Models having symmetry about one axis only

Models having symmetry about one axes only i.e. model-F, model-G and model-H are tested under four wind interference conditions namely back-to-back, back-to-front, front-to-back and front-to-front (Fig. 4.40, 4.43 and 4.46). Drag coefficients evaluated are compared in Table 4.4. In case of back-to-back wind interference condition (Fig. 4.54), all models have equal drag coefficients (-0.14). When wooden models are tested under back-to-front wind interference condition (Fig, 4.55), maximum drag coefficient -0.24 is evaluated on model-F. Model-G and model-H are subjected to approximately equal drag coefficients. Maximum drag coefficients evaluated on model-F is -0.43 in case of front-to-back wind interference condition (Fig. 4.56). In front-to-front wind interference condition (Fig. 4.57), maximum drag

coefficient is found as -0.37 in case of model-F and minimum drag coefficient is -0.04 evaluated on model-H.

**Table 4.4 Drag coefficients for models having symmetry about one axis only at wind interference condition**

| Wind Interference Condition | Model-F | Model-G | Model-H |
|---|---|---|---|
| Back-to-Back | -0.14 | -0.14 | -0.14 |
| Back-to-Front | -0.24 | -0.11 | -0.10 |
| Front-to-Back | -0.43 | -0.17 | -0.10 |
| Front-to-Front | -0.37 | -0.14 | -0.04 |

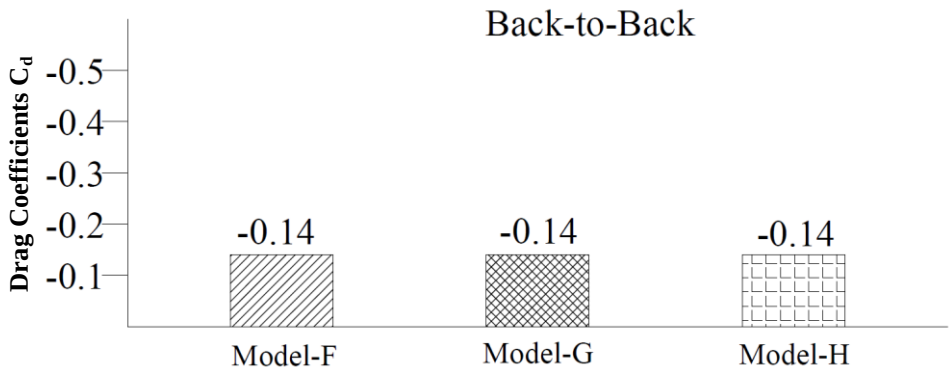


**Fig. 4.54 Comparison of drag coefficients on building models having symmetry about one axis only in back-to-back wind interference condition**

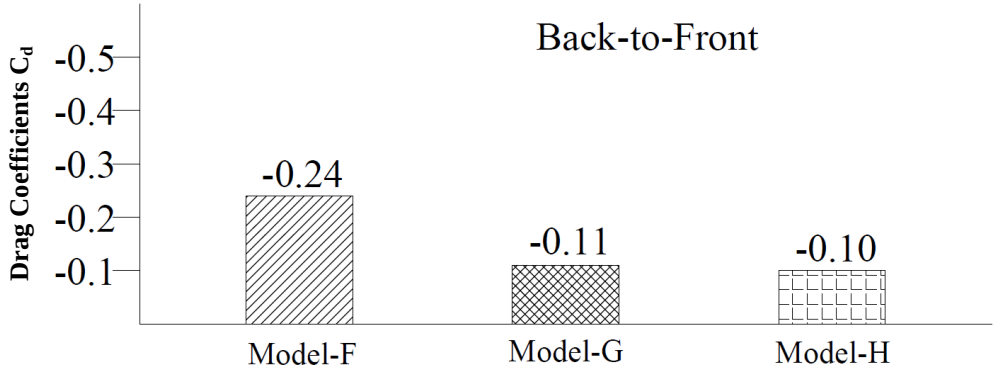


**Fig. 4.55 Comparison of drag coefficients on building models having symmetry about one axis only in back-to-front wind interference condition**

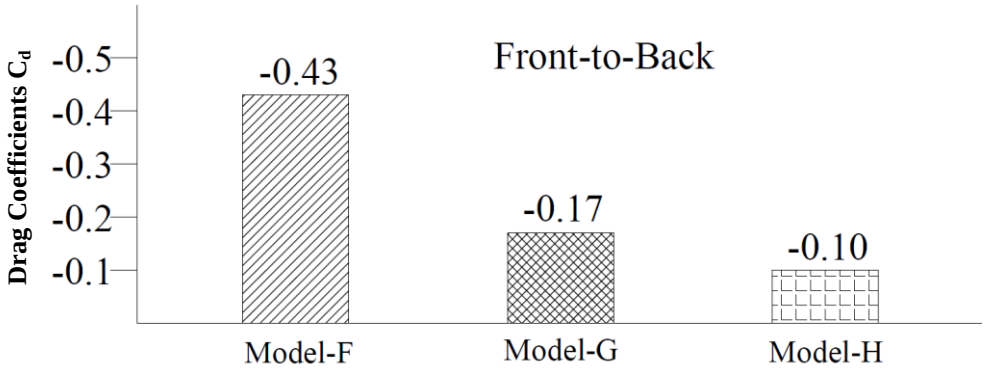


**Fig. 4.56 Comparison of drag coefficients on building models having symmetry about one axis only in front-to-back wind interference condition**

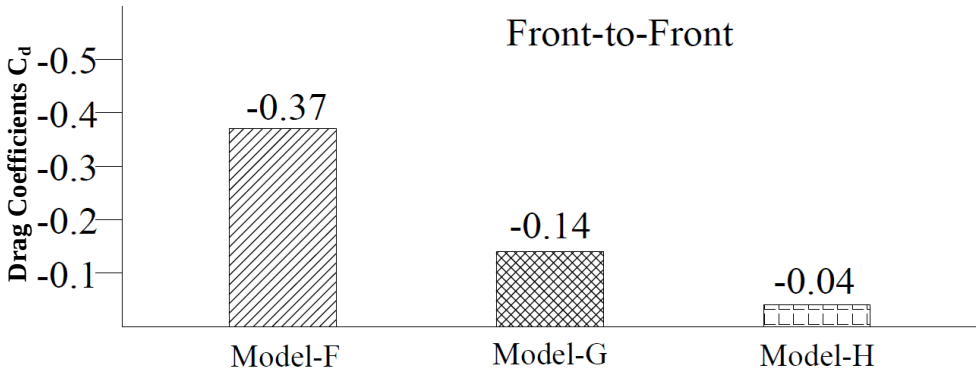


**Fig. 4.57 Comparison of drag coefficients on building models having symmetry about one axis only in front-to-front wind interference condition**

## 4.6 COMPARISON OF BASE SHEAR, BASE MOMENTS AND TWISTING MOMENT

### 4.6.1 Models having symmetry about both axes

Variation of base shear, base moments and twisting moments measured on wooden models namely model-A, B, C, D and E as a function of wind incidence angle are shown in Fig. 4.58 to 4.62 respectively. It is noticed from Fig. 4.58 that force Fx, i.e. base shear varies within a small range in case of model-A, B and D. Further its values are maximum at $45^0$ and $135^0$ wind incidence angles and minimum at $90^0$ wind incidence angles. In case of model-E also, maximum Fx occurs at $45^0$ and $135^0$ wind incidence angles. Maximum value of Fx in case of model-E is approximately equal to maximum value of Fx in case of model-C. Further maximum value of Fx on model-E is almost 1.8 times the maximum value of Fx on model-A and model-B, and 1.5 times the value of model-D. Figure 4.58 thus indicates that the variation in cross-sectional shape causes increase in base shear to a large extent for certain wind incidence angles. Variation of Fx with wind incidence angle is maximum in case of

model-C (Plus Shape-2) where maximum value of Fx is almost 3 times minimum value. Figure 4.59 indicates the variation of base shear Fy with respect to wind incidence angle. It is noticed that difference between maximum and minimum value of Fy is more in case of model-B (Plus Shape-1) and model-C (Plus Shape-2) as compared to other models.

Figure 4.60 shows that variation of Mx i.e. base moment about X-axis is identical to Fy. Maximum Mx is observed at $15^0$ wind incidence angle in case of model-C. Variation of My i.e. base moments is identical to that of Fx (Fig. 4.61). Its maximum value in case of model-E (I-Shape-2) is about two times as compared to the value in case of model-A, model-B and 1.3 times the value in case of model-D (Fig. 4.61). Maximum variation of My is observed in case of model-C.

It is noticed from Fig. 4.62 that variation of twisting moment Mz w.r.t. wind incidence angle is more in case of model-C and E (Plus Shape-2 and I-Shape-2) as compared to other models. Further, Mz is maximum between $60^0$ and $75^0$ wind incidence angle in these models. In case of model-A, twisting moment is maximum at $15^0$ and $105^0$. In case of model-B and D, twisting moment is maximum at $30^0$.

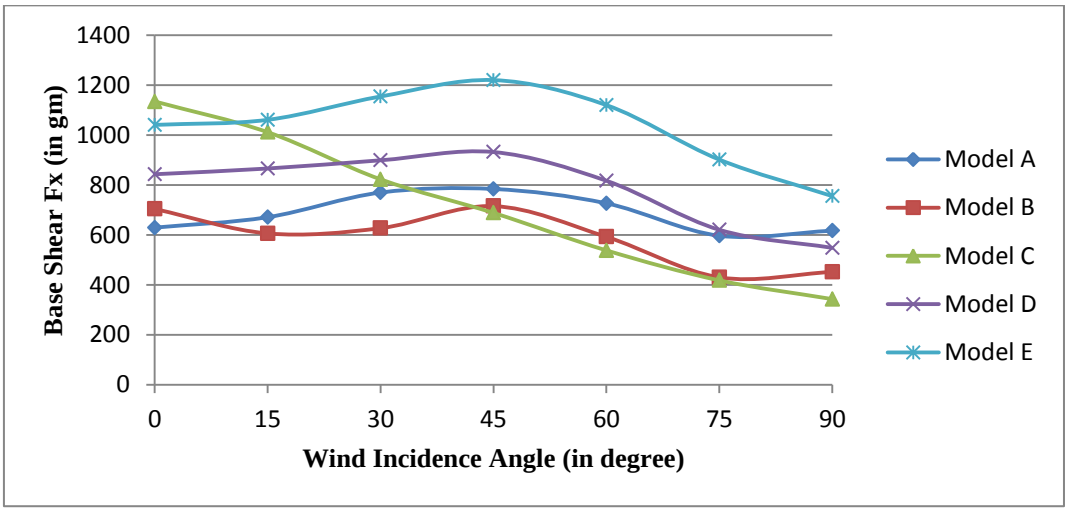


**Fig. 4.58 Comparison of base shear Fx on building models having symmetry about both axes at various wind incidence angles**

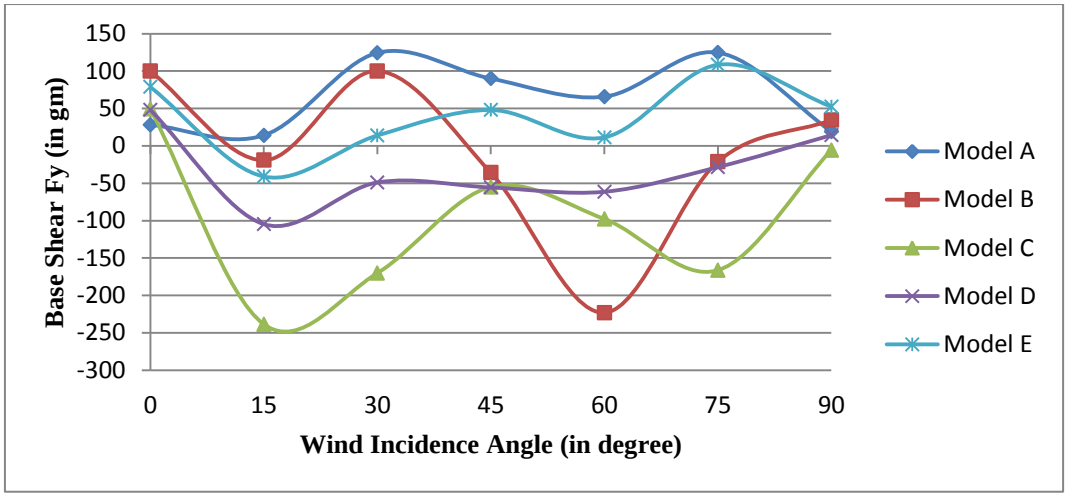


**Fig. 4.59 Comparison of base shear Fy on building models having symmetry about both axes at various wind incidence angles**

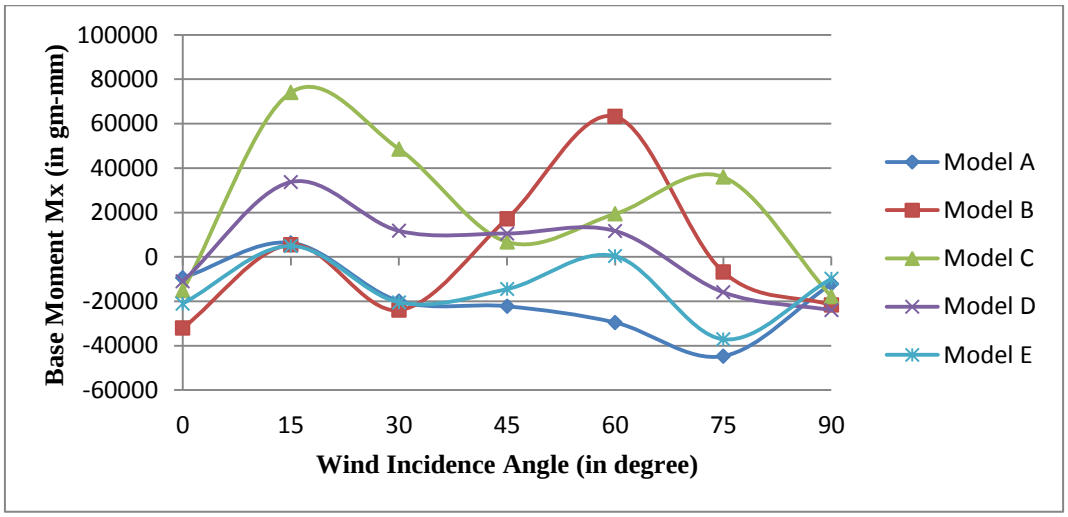


**Fig. 4.60 Comparison of base moment Mx on building models having symmetry about both axes at various wind incidence angles**

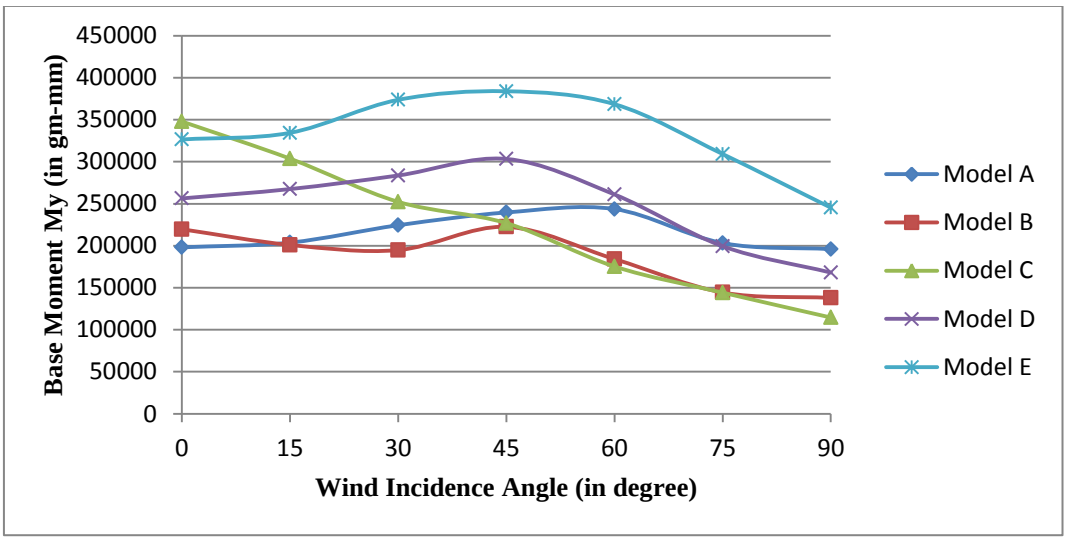


**Fig. 4.61 Comparison of base moment My on building models having symmetry about both axes at various wind incidence angles**

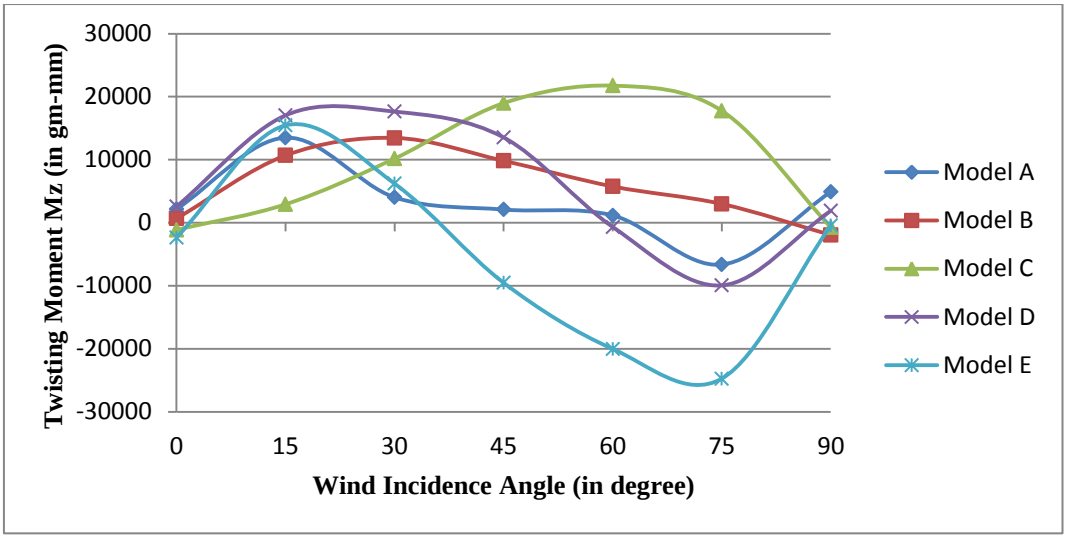


**Fig. 4.62 Comparison of twisting moment Mz on building models haing symmetry about both axes at various wind incidence angles**

### 4.6.2 Models having symmetry about one axis only

Base shear, base moments and twisting moments measured on these wooden models namely Model-F, G and H as a function of wind incidence angle are shown in Figs. 4.63 to 4.67 respectively. It is noticed from Fig. 4.63 that force Fx i.e. base shear in the direction of wind varies within a small range in case of model-G and H. Further, its value is maximum at $75^0$. Maximum Fx is measured on model-F (Fish Shape-1) due to large exposed area at $180^0$ wind incidence angle. Further, this value is 1.8 times the maximum values of Fx in case of model-G and model-H. It is noticed from Fig. 4.64 that force Fy i.e. base shear in the direction perpendicular to wind varies within a small range in case of model-G and H. Maximum value of base shear Fy is observed at $150^0$ in case of model-F, which is 2.5 times the maximum value of model-G (Fish Shape-2) and model-H (Fish Shape-3).

Variation of Mx and My, i.e. base moments is identical to that of Fx and Fy respectively (Figs. 4.65 and 4.66).

It is noticed from Fig. 4.67 that maximum twisting moment Mz is measured on model-F which is about 1.7 times the maximum value of twsinting moment in case of model-G and 4.5 times the maximum value of Mz in case of model-H.

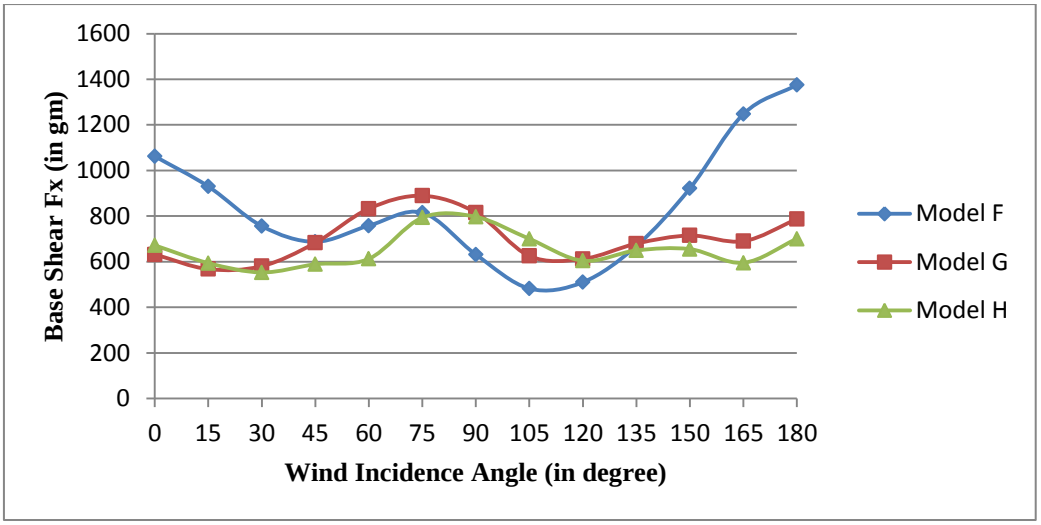


**Fig. 4.63 Comparison of base shear Fx on building models having symmetry about one axis only at various wind incidence angles**

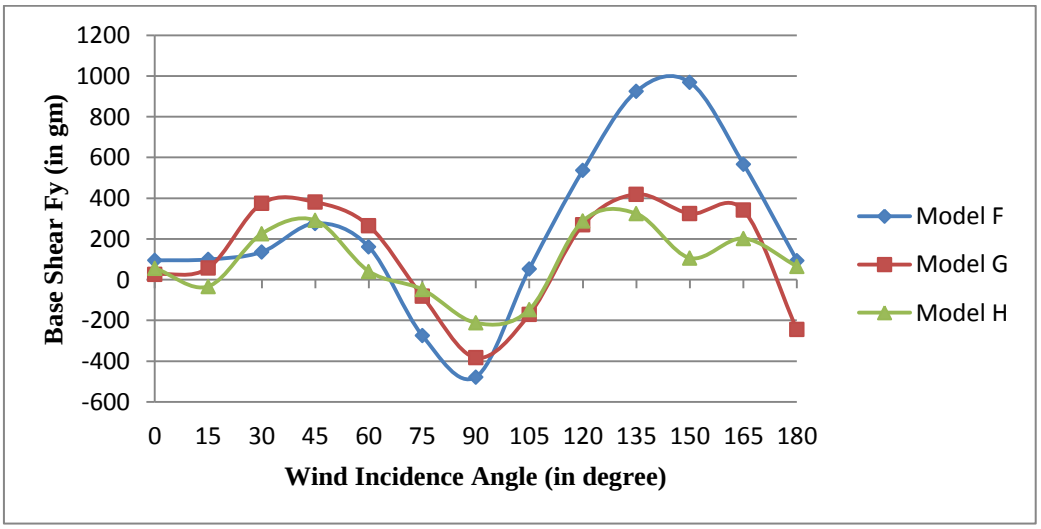


**Fig. 4.64 Comparison of base shear Fy on building models having symmetry about one axis only at various wind incidence angles**

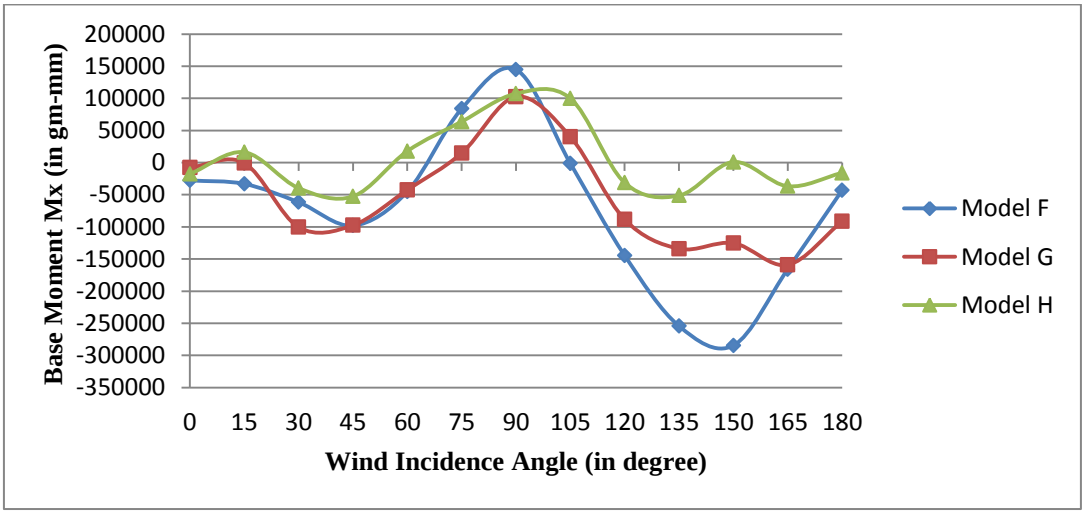


**Fig. 4.65 Comparison of base moment Mx on building models having symmetry about one axis only at various wind incidence angles**

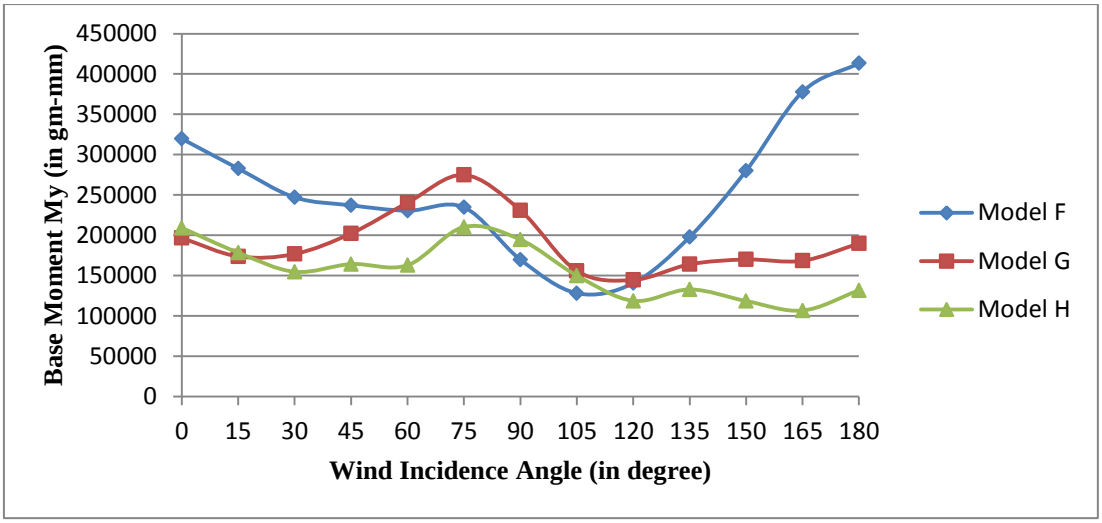


**Fig. 4.66 Comparison of base moment My on building models having symmetry about one axis only at various wind incidence angles**

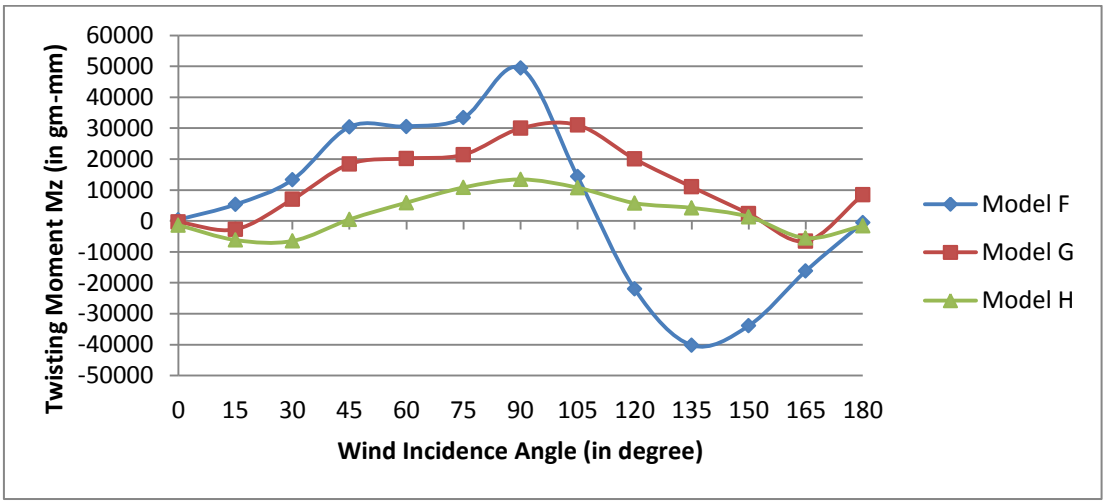


**Fig. 4.67 Comparison of twisting moment Mz on building models having symmetry about one axis only at various wind incidence angles**

# Chapter - 5

# EXPERIMENTAL STUDY - PRESSURE MEASUREMENTS

## 5.1 GENERAL

Second phase of the present study is experimental investigation of wind pressure distribution on the wall surfaces of tall buildings of seven different cross-sections having same floor area. Perspex sheets models provided with pressure points on its wall surfaces (Photo. 3.8) are tested in the wind tunnel by placing them at the center of the turn-table one by one in isolated condition.

Wind is made to hit the models having symmetry about both X-X and Y-Y axis at 4 wind incidence angles from $0^0$ to $90^0$ at an interval of $30^0$. In case of models with symmetry about one axis only, wind pressure distribution is measured at 7 wind incidence angles from $0^0$ to $180^0$ at an interval of $30^0$.

After obtaining wind pressure distribution on 7 Perspex sheet models in isolated condition under varying wind incidence angles, effect of interference on wind pressure distribution is studied. For this purpose, each Perspex sheet model is placed one after another at the center of the turn-table and plywood model of same cross-section is placed on the upstream side as interfering building model. In this study, wind pressure distribution on instrumental model is obtained for only one wind incidence angle and one value of longitudinal spacing between models, but for 3 values of transverse spacing namely full blockage, half blockage and no blockage.

Mean wind pressure coefficients **($C_{p,mean}$)** are calculated from the values of mean wind pressures ($\boldsymbol{P_{avg}}$) obtained experimentally. Results of this study are presented in this chapter in the form of cross-sectional variation and contours of mean wind pressure coefficients.

## 5.2 ISOLATED CONDITION

### 5.2.1 Model-A (Square Shape)

Perspex sheet model of model-A (Photo. 3.8) with a total of 140 pressure points (35 on each face) (Fig. 3.8) is tested in isolated condition under 4 wind incidence angles namely $0^0$, $30^0$, $60^0$ and $90^0$ (Fig. 5.1). As mentioned earlier, values of mean wind pressure obtained originally form pressure transducer are in mmhg unit which are later converted to $N/m^2$. Table 5.1 gives example of such conversion for few pressure points including the values of $C_{p,mean}$.

**Table 5.1 Typical values of wind pressures and $C_{p,mean}$ on model-A at $0^0$ wind incidence angle under isolated condition**

| Pressure Point no. | Baratron Range | Baratron Reading (mmhg) | Pressure ($N/m^2$) | $C_{p,mean}$ |
|---|---|---|---|---|
| 1 | 1 | 0.05 | 9.18 | 0.16 |
| 2 | 1 | 0.09 | 13.13 | 0.23 |
| 3 | 1 | 0.11 | 14.62 | 0.25 |
| 4 | 1 | 0.11 | 13.13 | 0.23 |
| 5 | 1 | 0.09 | 9.18 | 0.16 |
| 6 | 1 | 0.12 | 17.16 | 0.30 |
| 7 | 1 | 0.26 | 34.12 | 0.59 |
| 8 | 1 | 0.28 | 36.69 | 0.64 |
| 9 | 1 | 0.26 | 34.12 | 0.59 |
| 10 | 1 | 0.14 | 17.16 | 0.30 |
| 11 | 1 | 0.11 | 14.92 | 0.26 |
| 12 | 1 | 0.26 | 35.15 | 0.61 |
| 13 | 1 | 0.29 | 39.08 | 0.68 |
| 14 | 1 | 0.27 | 35.15 | 0.61 |
| 15 | 1 | 0.11 | 14.92 | 0.26 |
| 16 | 1 | 0.10 | 13.17 | 0.23 |
| 17 | 1 | 0.25 | 32.19 | 0.56 |
| 18 | 1 | 0.26 | 34.26 | 0.60 |
| 19 | 1 | 0.24 | 32.19 | 0.56 |
| 20 | 1 | 0.10 | 13.17 | 0.23 |
| 21 | 1 | 0.06 | 9.76 | 0.17 |
| 22 | 1 | 0.21 | 28.18 | 0.49 |
| 23 | 1 | 0.23 | 30.23 | 0.53 |
| 24 | 1 | 0.21 | 28.18 | 0.49 |
| 25 | 1 | 0.08 | 9.76 | 0.17 |
| 26 | 1 | 0.02 | 2.40 | 0.04 |
| 27 | 1 | 0.15 | 20.00 | 0.35 |
| 28 | 1 | 0.17 | 23.10 | 0.40 |
| 29 | 1 | 0.15 | 20.00 | 0.35 |
| 30 | 1 | 0.02 | 2.40 | 0.04 |
| 31 | 1 | 0.01 | 1.49 | 0.03 |
| 32 | 1 | 0.18 | 24.40 | 0.43 |
| 33 | 1 | 0.22 | 28.87 | 0.50 |
| 34 | 1 | 0.19 | 24.40 | 0.43 |
| 35 | 1 | 0.02 | 1.49 | 0.03 |

Figure 5.2 shows the variation of mean wind pressure coefficients ($C_{p,mean}$) on all surfaces of model-A at $0^0$ wind incidence angle in the form of contours. It is seen from the figure that pressure occurs on windward face-A which increases from bottom to near the top edge of the face due to increase in wind velocity with height. The values of pressure

coefficients vary from 0.45 to 0.63. It is also observed that maximum positive pressure occurs along the center line of the windward face which decreases towards the edges. Further, wind pressure decreases near the top edge due to the separation of wind flow. Side faces namely face-B and face-D are subjected to suction which decreases from windward edge to leeward edge.

When the building model is attacked by wind at skew angle i.e. $30^0$, pressure on windward face decreases from windward edge to leeward edge (Fig. 5.3). It is also noticed that face-B is now subjected to small value of suction whereas face-C and face-D are still subjected to large suction. At $60^0$ wind incidence angle (Fig. 5.4), wind pressure distribution on face-B becomes similar to that of face-A in case of $30^0$ wind incidence angle. Similarly, pressure distribution on face-C and face-D get interchanged. At $90^0$ wind incidence angle (Fig. 5.5), face-B becomes windward face and face-D becomes leeward face. Therefore, wind pressure distribution, in this case is comparable with that of $0^0$ case. Effect of wind incidence angle on the pressure distribution on Face-A can also be seen from Table 5.2. Maximum value of mean wind pressure on face-A is found to be 0.68 at $0^0$ wind incidence angle, whereas minimum is -0.91 at $90^0$ wind incidence angle.

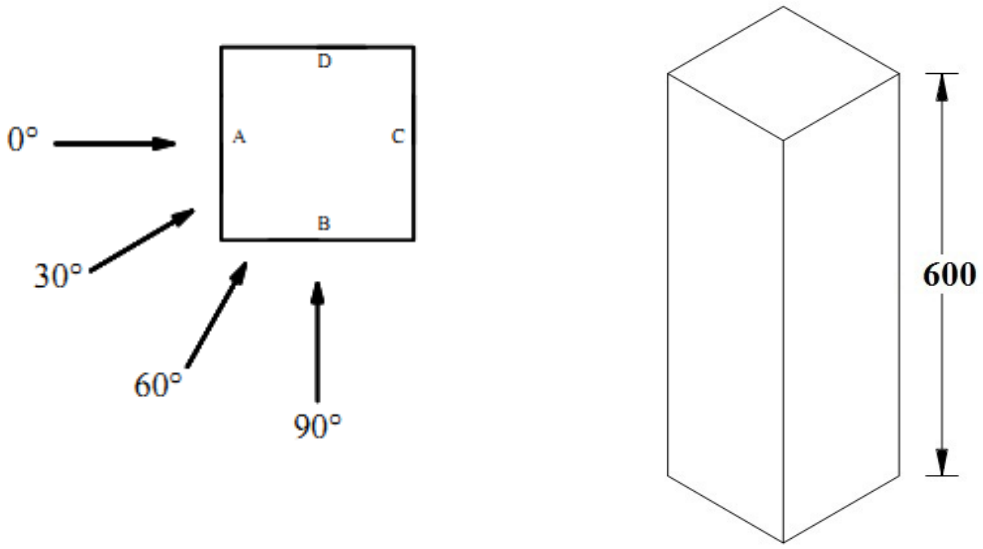


Plan Isometric

**Fig. 5.1 Wind incidence angle on Perspex sheet model of model-A in isolated condition**

(All dimensions are in mm)

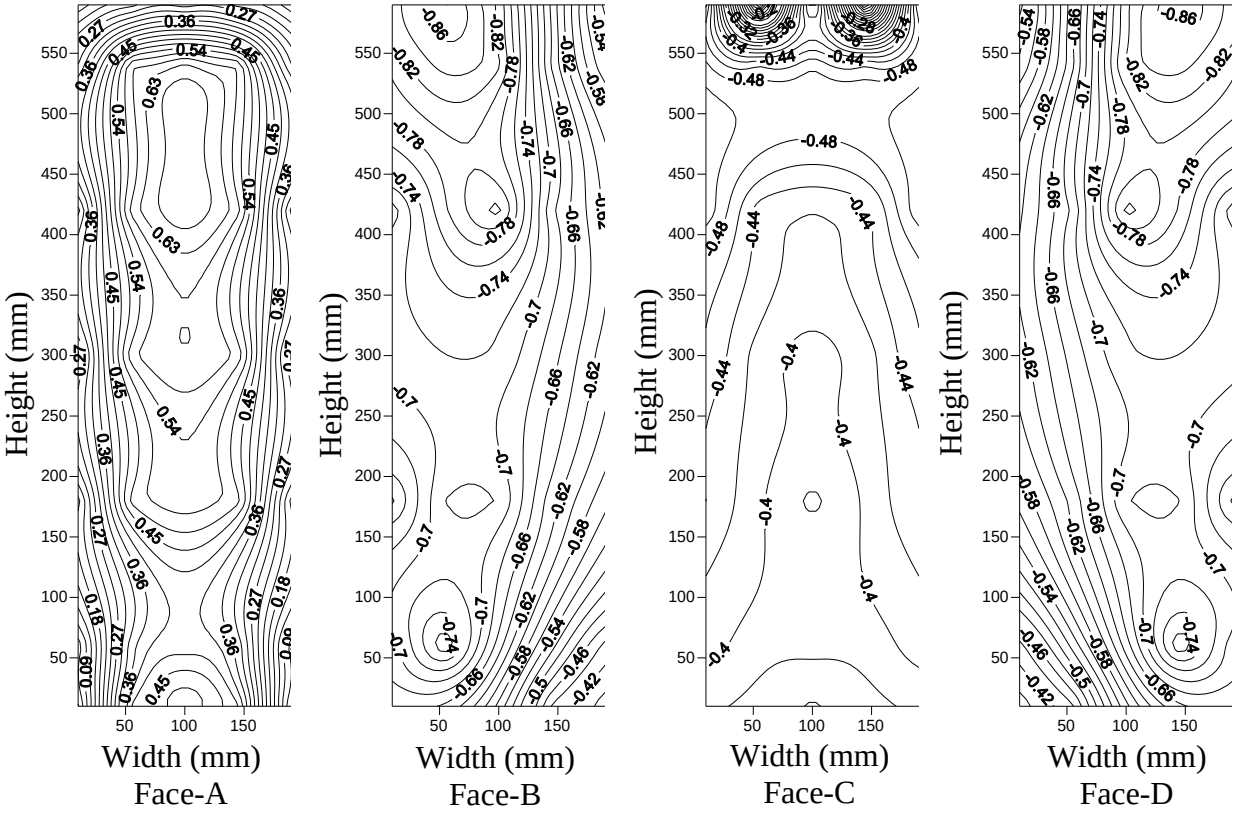


**Fig. 5.2 Distribution of mean wind pressure coefficients ($C_{p,mean}$) on different surfaces of model-A at $0^0$ wind incidence angle**

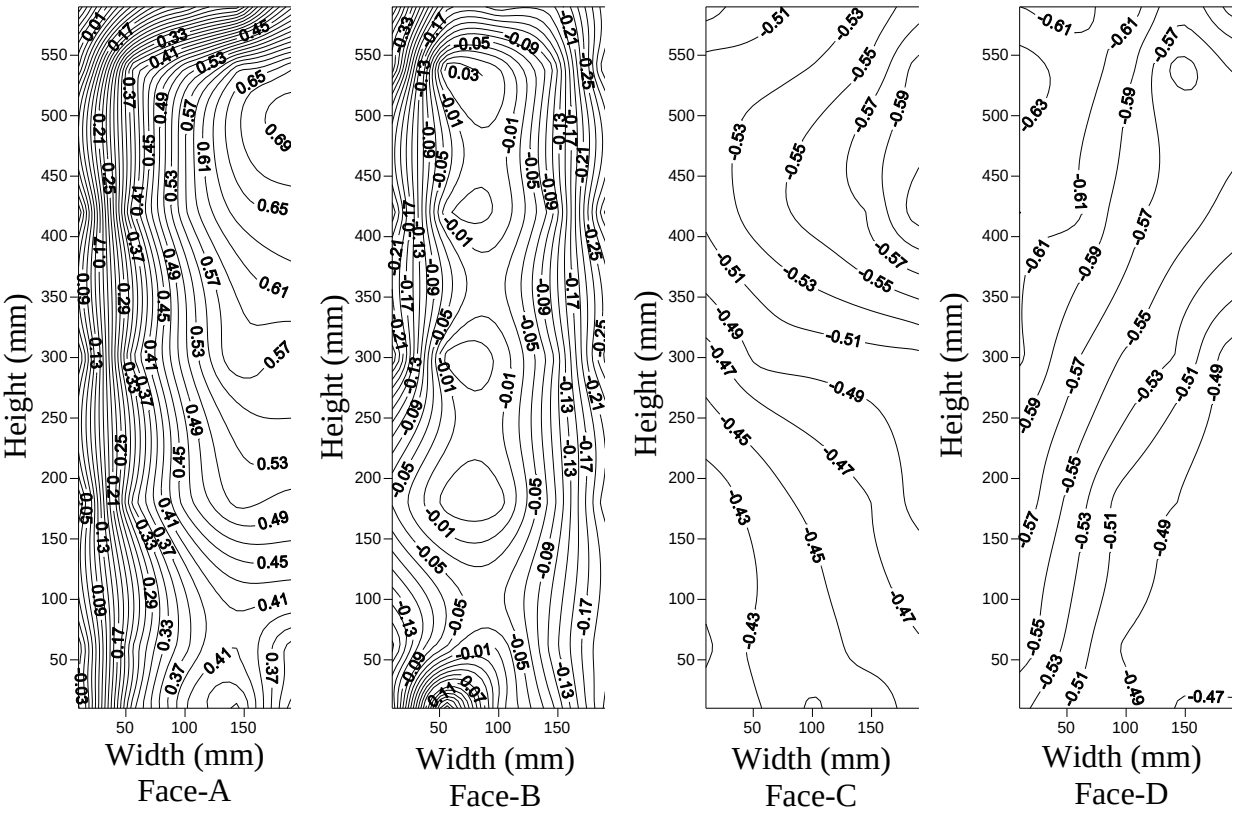


**Fig. 5.3 Distribution of mean wind pressure coefficients ($C_{p,mean}$) on different surfaces of model-A at $30^0$ wind incidence angle**

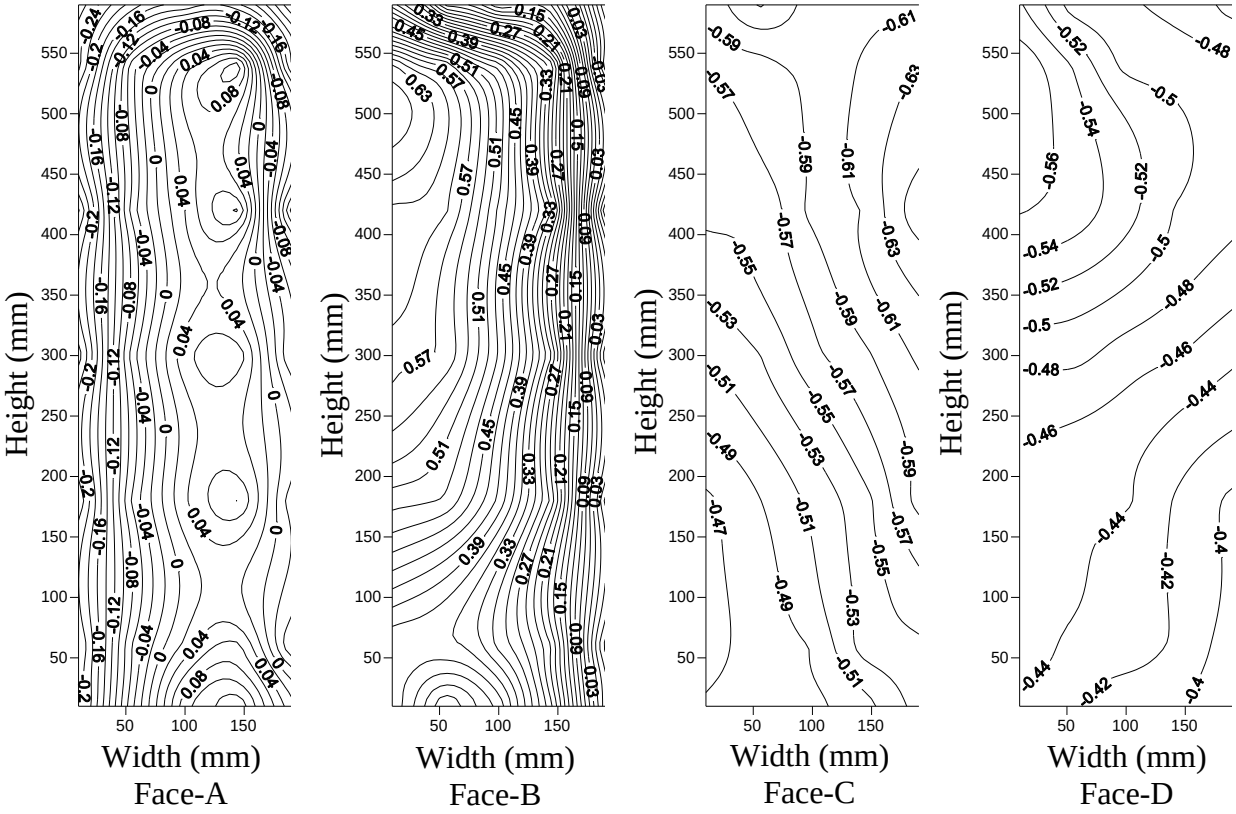


**Fig. 5.4 Distribution of mean wind pressure coefficients ($C_{p,mean}$) on different surfaces of model-A at $60^0$ wind incidence angle**

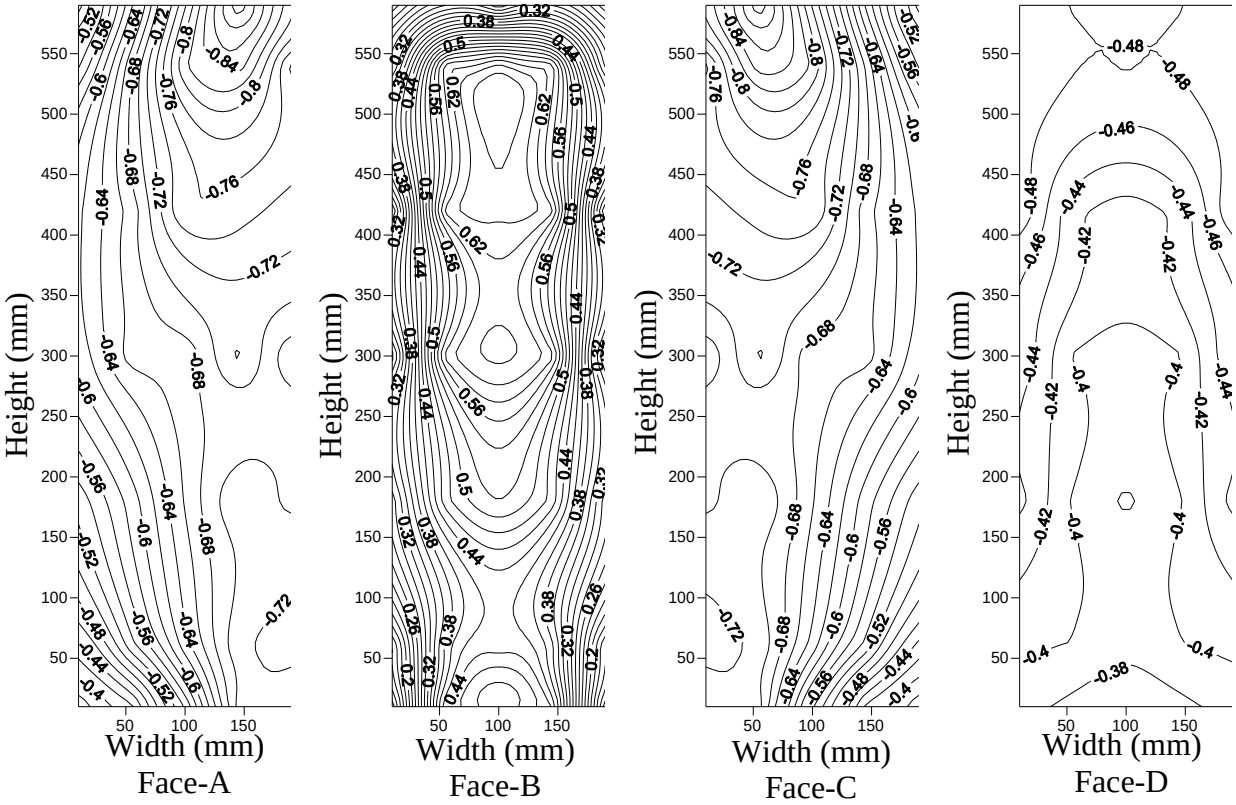


**Fig. 5.5 Distribution of mean wind pressure coefficients ($C_{p,mean}$) on different surfaces of model-A at $90^0$ wind incidence angle**

Cross-sectional variation of mean wind pressure coefficients ($C_{p,mean}$) at seven cross-sections namely A-A, B-B, C-C, D-D, E-E, F-F and G-G (Fig. 5.6), along the height of model-A at $0^0$ wind incidence angle are shown in Fig. 5.6. Location of sections from the top of the model can be seen in Fig. 3.8.

It is observed from Fig. 5.6 that windward face (face-A) is subjected to maximum pressure at section c-c. Suction on side faces (face-B and D) are maximum at top most section (section A-A). Leeward face (face-C) is subject to almost same value of suction at all sections.

Cross-sectional variation of mean wind pressure coefficients ($C_{p,mean}$) at other wind incidence angles namely $30^0$, $60^0$ and $90^0$ are shown in Figs. 5.7 to 5.9 respectively which are self-explanatory. These values of $C_{p,mean}$ available at 7 sections along the height of building model are very useful for analysis of building frame under wind loads at various wind incidence angles. These are also of great advantage in designing the cladding and its connections to main frame.

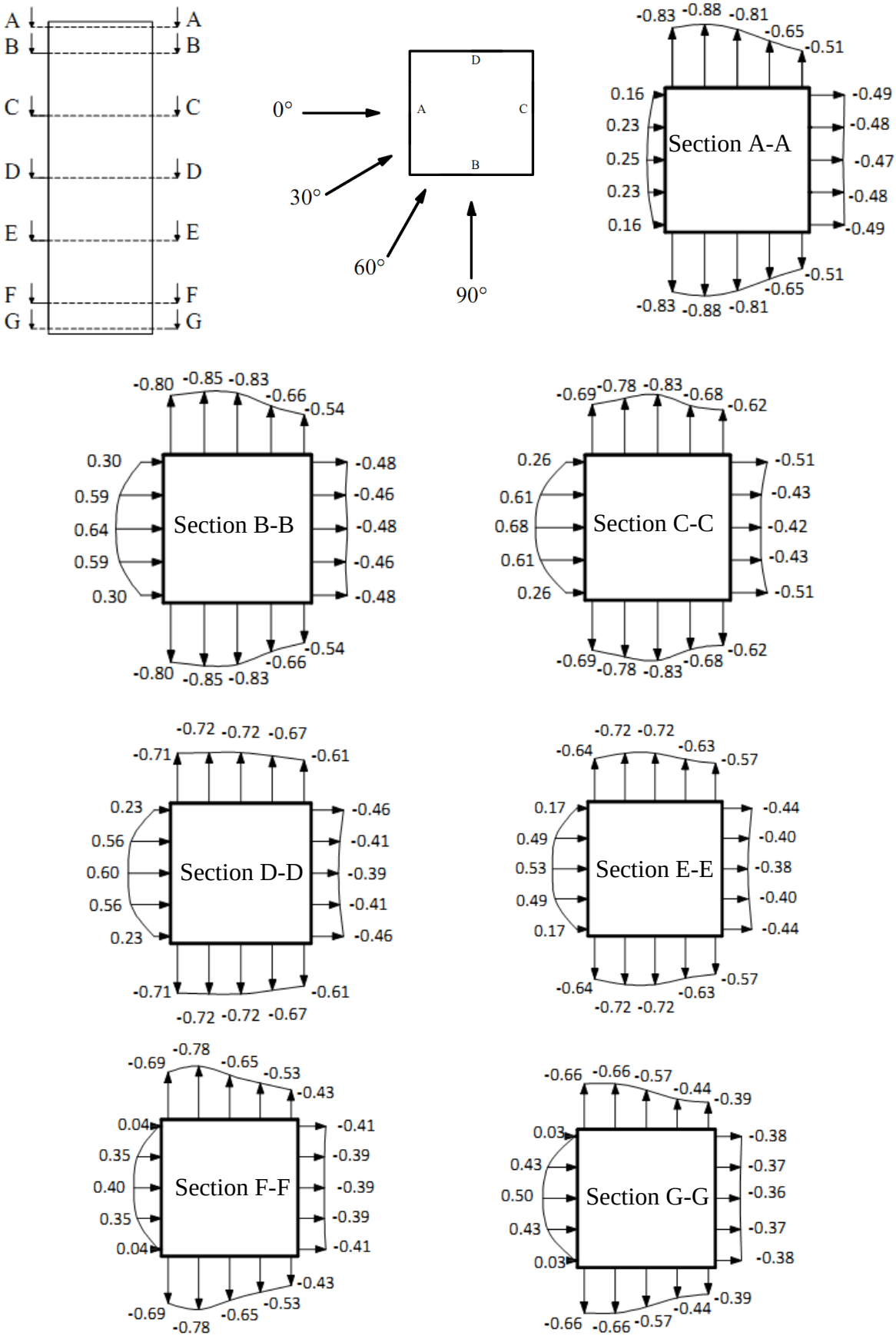


**Fig. 5.6 Cross-sectional variation of mean wind pressure coefficients ($C_{p,mean}$) on model-A at $0^0$ wind incidence angle**

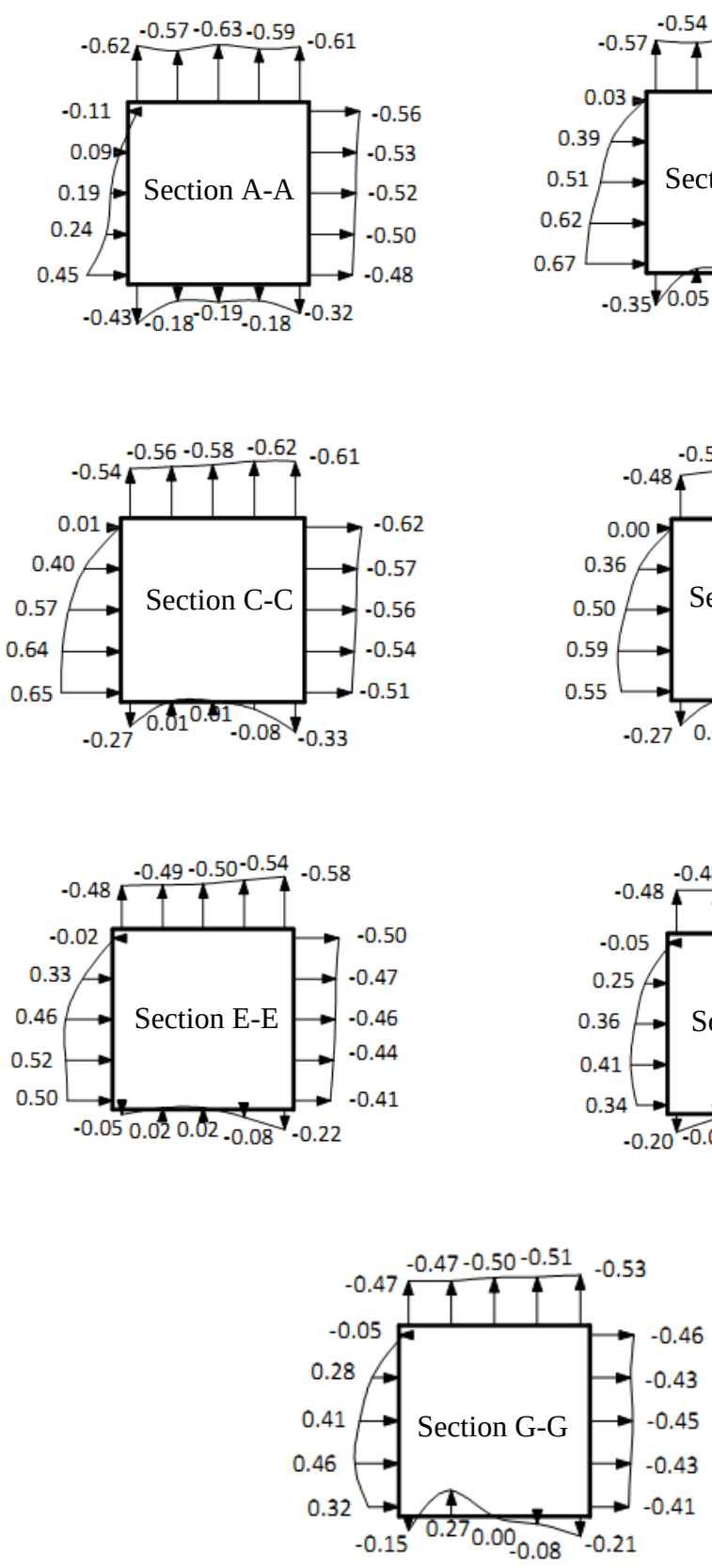


**Fig. 5.7 Cross-sectional variation of mean wind pressure coefficients ($C_{p,mean}$) on model-A at $30^0$ wind incidence angle**

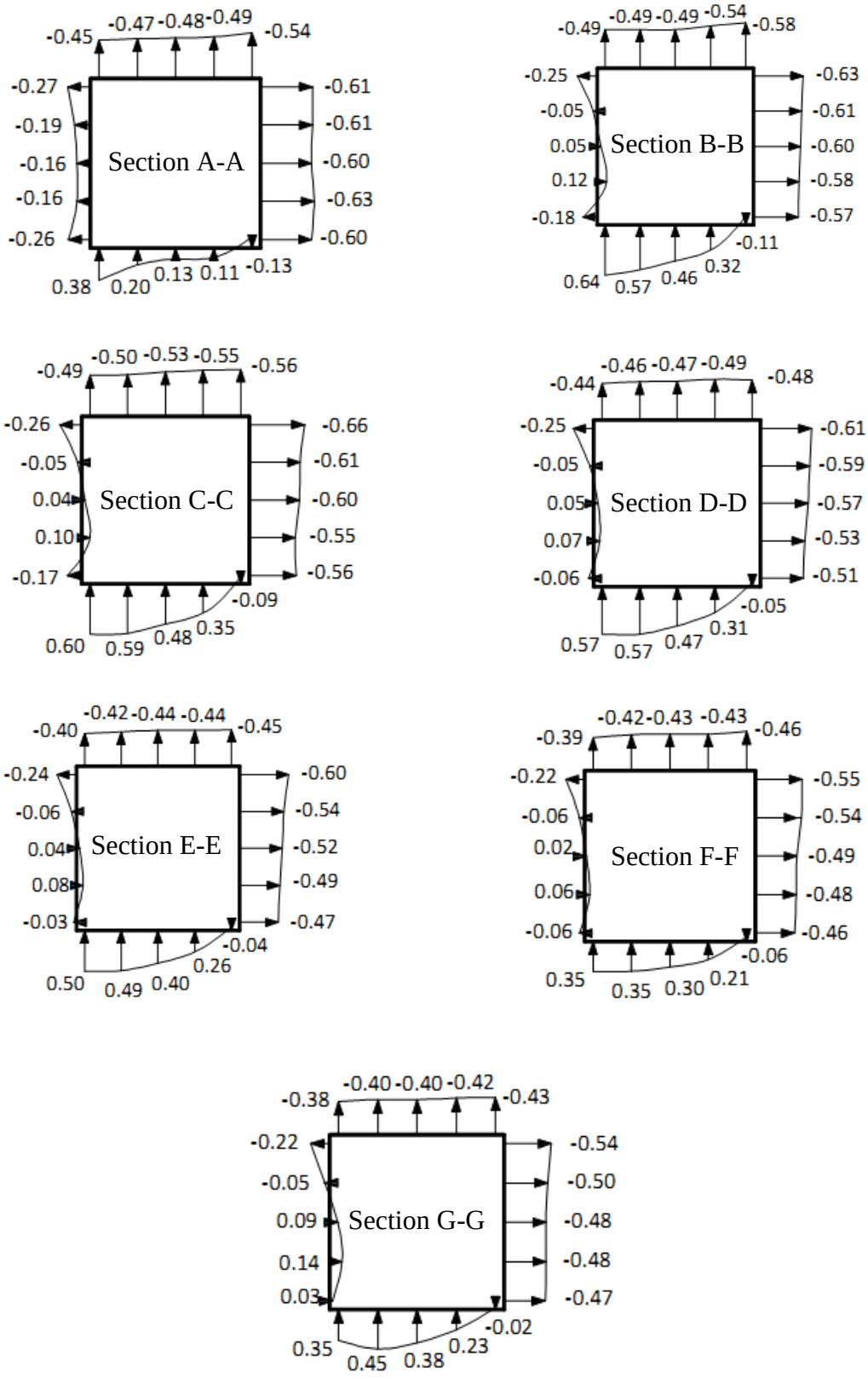


**Fig. 5.8 Cross-sectional variation of mean wind pressure coefficients ($C_{p,mean}$) on model-A at $60^0$ wind incidence angle**

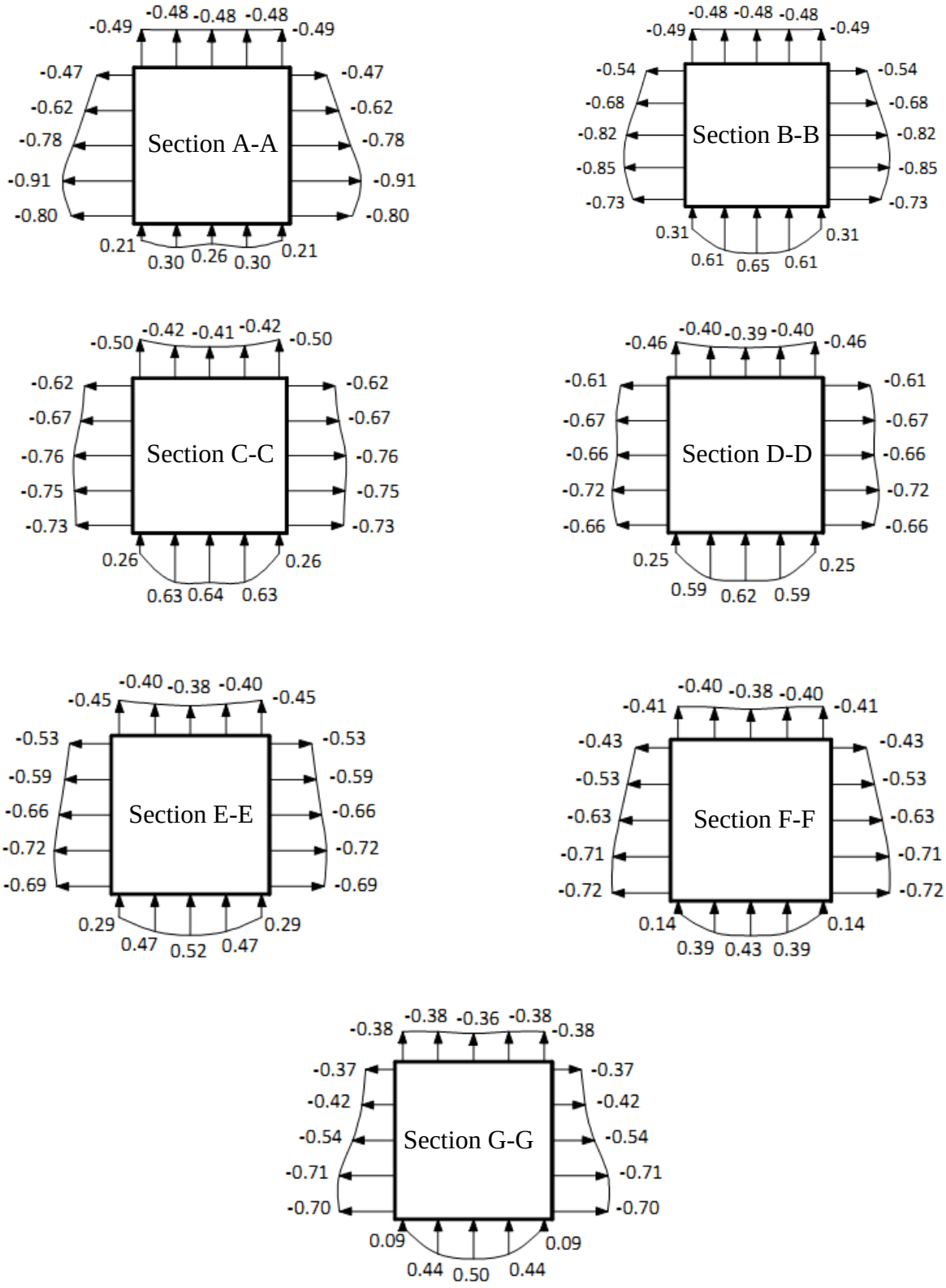


**Fig. 5.9 Cross-sectional variation of mean wind pressure coefficients ($C_{p,mean}$) on model-A at $90^0$ wind incidence angle**

Comparison of $C_{p,mean}$ values at 35 pressure points on face-A of model-A at 7 wind incidence angles are shown in Table 5.2. It is noticed that the face A is subjected to maximum pressure of $C_{p,mean}$ = 0.68 at $0^0$ and minimum pressure of $C_{p,mean}$ = -0.91 at $90^0$.

**Table 5.2 Variation of $C_{p,mean}$ on face-A of model-A with wind incidence angle**

| Pressure point no. | Mean wind pressure coefficients ($C_{p,mean}$) | | | |
|---|---|---|---|---|
| | **0°** | **30°** | **60°** | **90°** |
| 1 | 0.16 | **-0.11** | **-0.27** | -0.47 |
| 2 | 0.23 | 0.09 | -0.19 | -0.62 |
| 3 | 0.25 | 0.19 | -0.16 | -0.78 |
| 4 | 0.23 | 0.24 | -0.16 | **-0.91** |
| 5 | 0.16 | 0.45 | -0.26 | -0.80 |
| 6 | 0.30 | 0.03 | -0.25 | -0.54 |
| 7 | 0.59 | 0.39 | -0.05 | -0.68 |
| 8 | 0.64 | 0.51 | 0.05 | -0.82 |
| 9 | 0.59 | 0.62 | 0.12 | -0.85 |
| 10 | 0.30 | **0.67** | -0.18 | -0.73 |
| 11 | 0.26 | 0.01 | -0.26 | -0.62 |
| 12 | 0.61 | 0.40 | -0.05 | -0.67 |
| 13 | **0.68** | 0.57 | 0.04 | -0.76 |
| 14 | 0.61 | 0.64 | 0.10 | -0.75 |
| 15 | 0.26 | 0.65 | -0.17 | -0.73 |
| 16 | 0.23 | 0.00 | -0.25 | -0.61 |
| 17 | 0.56 | 0.36 | -0.05 | -0.67 |
| 18 | 0.60 | 0.50 | 0.05 | -0.66 |
| 19 | 0.56 | 0.59 | 0.07 | -0.72 |
| 20 | 0.23 | 0.55 | -0.06 | -0.66 |
| 21 | 0.17 | -0.02 | -0.24 | -0.53 |
| 22 | 0.49 | 0.33 | -0.06 | -0.59 |
| 23 | 0.53 | 0.46 | 0.04 | -0.66 |
| 24 | 0.49 | 0.52 | 0.08 | -0.72 |
| 25 | 0.17 | 0.50 | -0.03 | -0.69 |
| 26 | 0.04 | -0.05 | -0.22 | -0.43 |
| 27 | 0.35 | 0.25 | -0.06 | -0.53 |
| 28 | 0.40 | 0.36 | 0.02 | -0.63 |
| 29 | 0.35 | 0.41 | 0.06 | -0.71 |
| 30 | 0.04 | 0.34 | -0.06 | -0.72 |
| 31 | 0.03 | -0.05 | -0.22 | -0.37 |
| 32 | 0.43 | 0.28 | -0.05 | -0.42 |
| 33 | 0.50 | 0.41 | 0.09 | -0.54 |
| 34 | 0.43 | 0.46 | **0.14** | -0.71 |
| 35 | 0.03 | 0.32 | 0.03 | -0.70 |

### 5.2.2 Model-B (Plus Shape-1)

Perspex sheet model of model-B (Photo. 3.8) with a total of 196 pressure points (49 on each face) (Fig. 3.9) is tested in isolated condition under 4 wind incidence angles namely $0^0$, $30^0$, $60^0$ and $90^0$ (Fig. 5.10). The building model-B (plus shape-I) is tested in the wind tunnel to measure the pressure distribution on its all surface under varying wind incidence angle.

Figures 5.11 to 5.14 show the distribution of mean wind pressure coefficients $C_{p,mean}$ on the surfaces of model-B (plus shape-I) in different angles of wind attack. It can be seen from Fig. 5.11 that when wind incidence angle is $0^0$, pressure occurs on frontal surface (i.e. face-A2) of the building model-B. But all other surfaces including cut corners are subjected to suction. Although surfaces B1 and D3 fall on windward side, these are also subjected to suction for almost half of the width as these are recessed surfaces. Values of suction on leeward corners (i.e. faces B3, C1, C3 and D1) are as high as those on leeward flat surface (i.e. face-C2). Suction on side faces (i.e. face B2 and D2) are still higher than leeward face. Frontal corner faces (i.e. faces A1, A3, B1 and D3) experience less suction as compared to the leeward corner faces (i.e. faces B3, C1, C3 and D1).

In case of $30^0$ wind incidence angle the positive pressure zone moves to right side of the model and it occurs on faces A2, A3 and B. All remaining faces experience suction with maximum value on face-D3. Contours of mean wind pressure coefficients ($C_{p,mean}$) at $60^0$ and $90^0$ wind incidence angles are shown in Figs. 5.13 and 5.14 respectively.

As compared to model-A (square shape) (Fig. 5.6), maximum values of pressure on windward surface is small in case of model-B (plus shape-I) (Fig. 5.15) at $0^0$ wind incidence angle. However, suction on side faces is slightly larger.

Comparison of $C_{p,mean}$ at 49 pressure points on face-A of model-B for 4 wind incidence angles can be seen in Table 5.3. This face is subjected to maximum pressure coefficient of 0.62 at $30^0$ wind incidence angle and minimum pressure coefficient of -0.92 both at $30^0$ wind incidence angle.

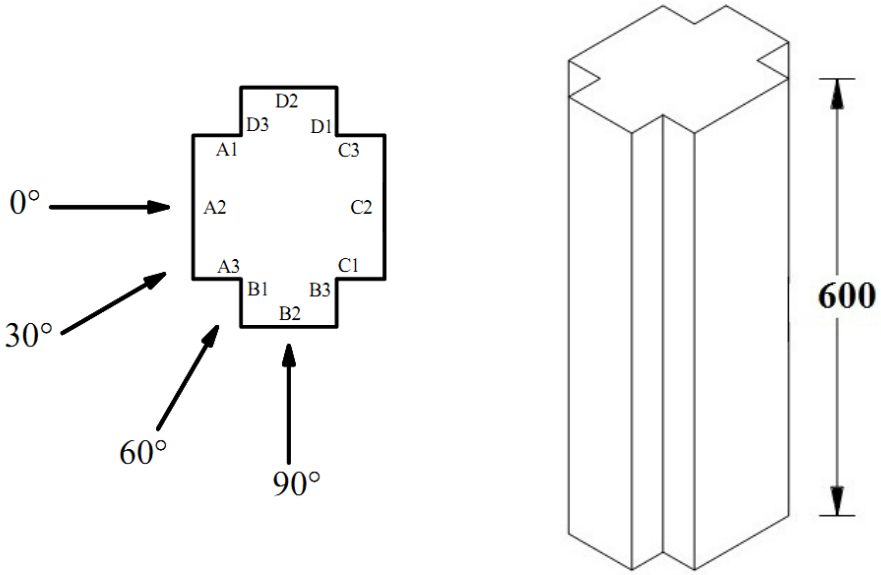


**Fig. 5.10 Wind incidence angles on Perspex sheet model of model-B in isolated condition**

(All dimensions are in mm)

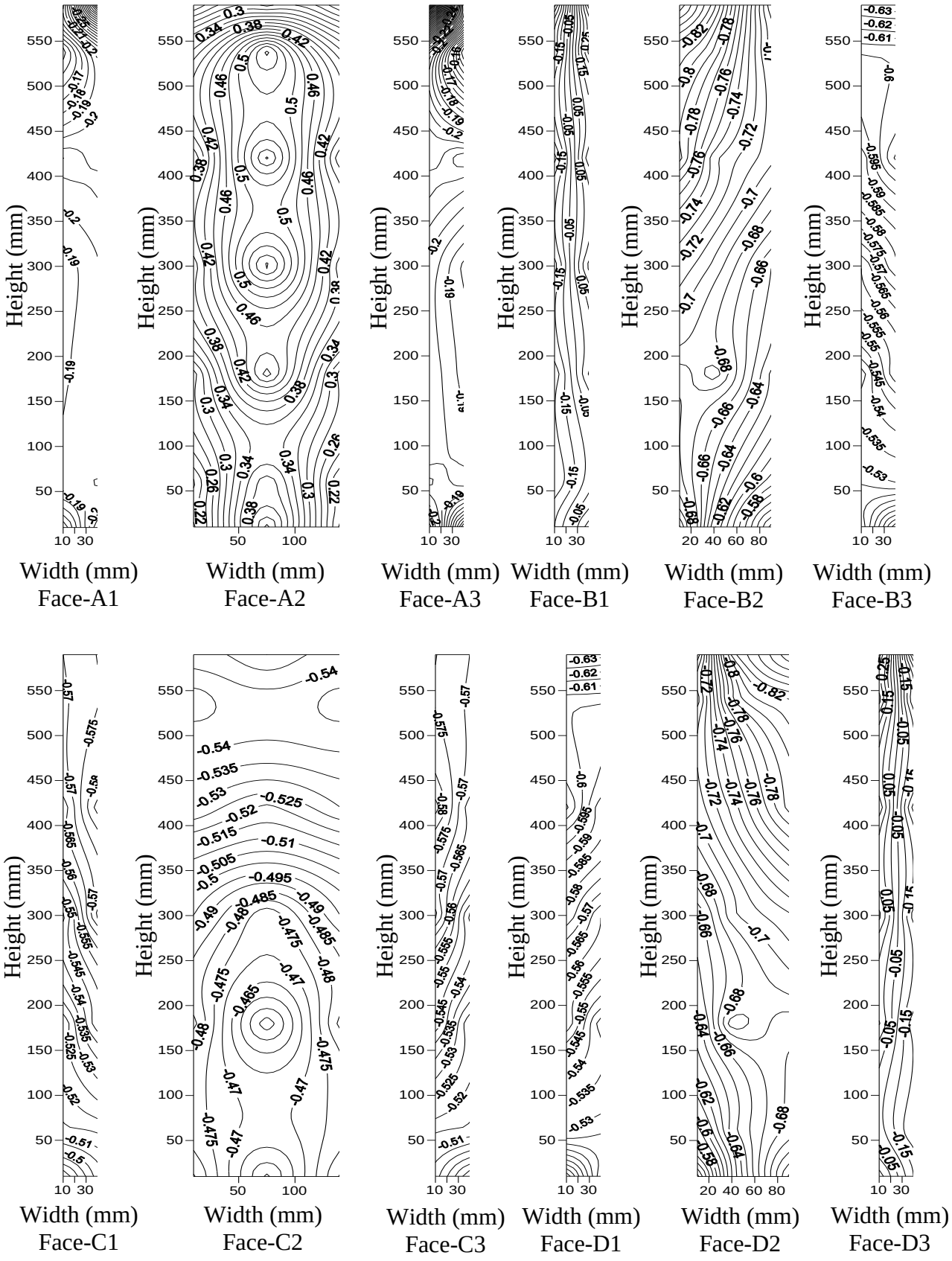


**Fig. 5.11 Distribution of mean wind pressure coefficients ($C_{p,mean}$) on different surfaces of model-B at $0^0$ wind incidence angle**

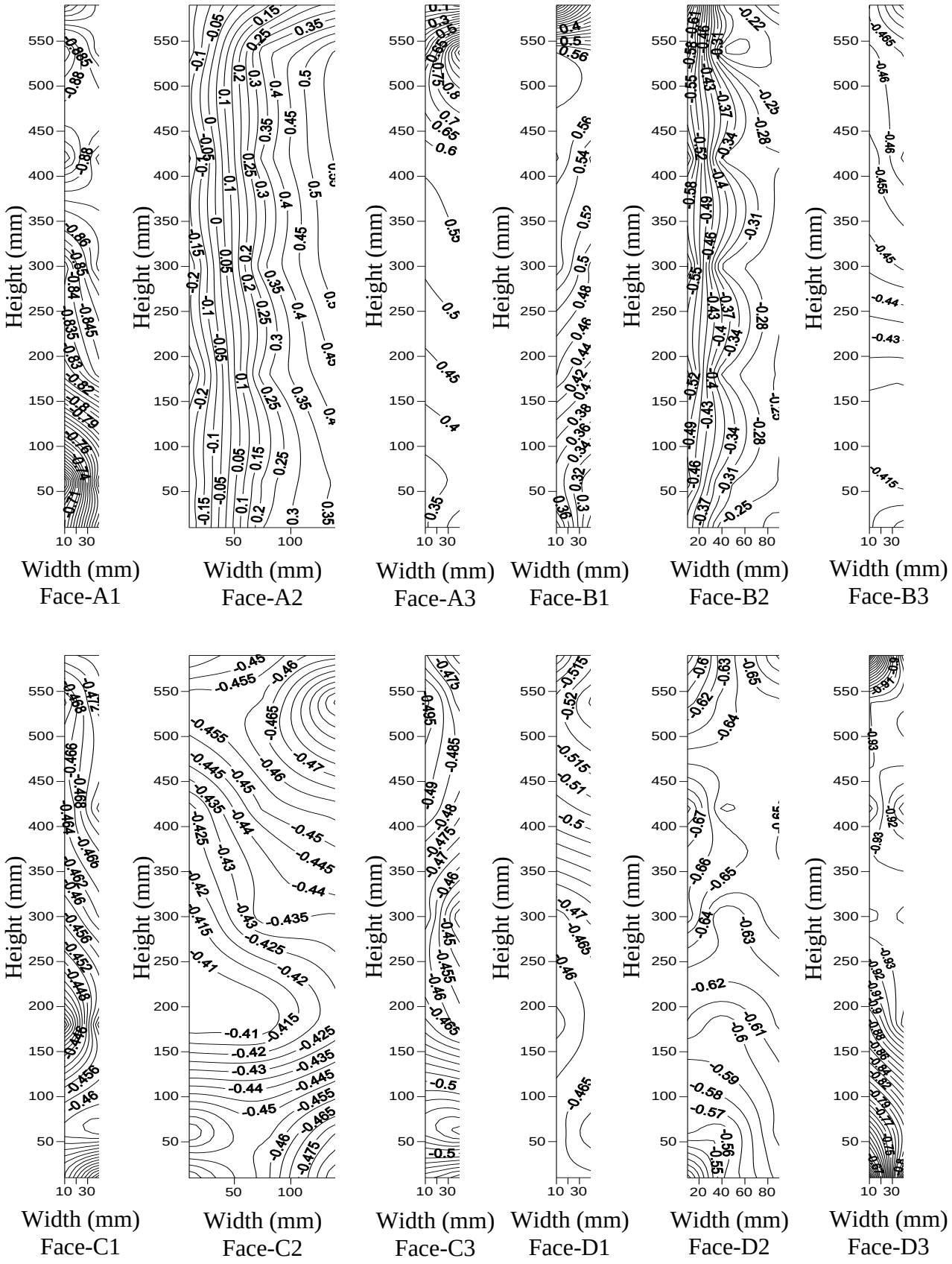


**Fig. 5.12 Distribution of mean wind pressure coefficients ($C_{p,mean}$) on different surfaces of model-B at $30^0$ wind incidence angle**

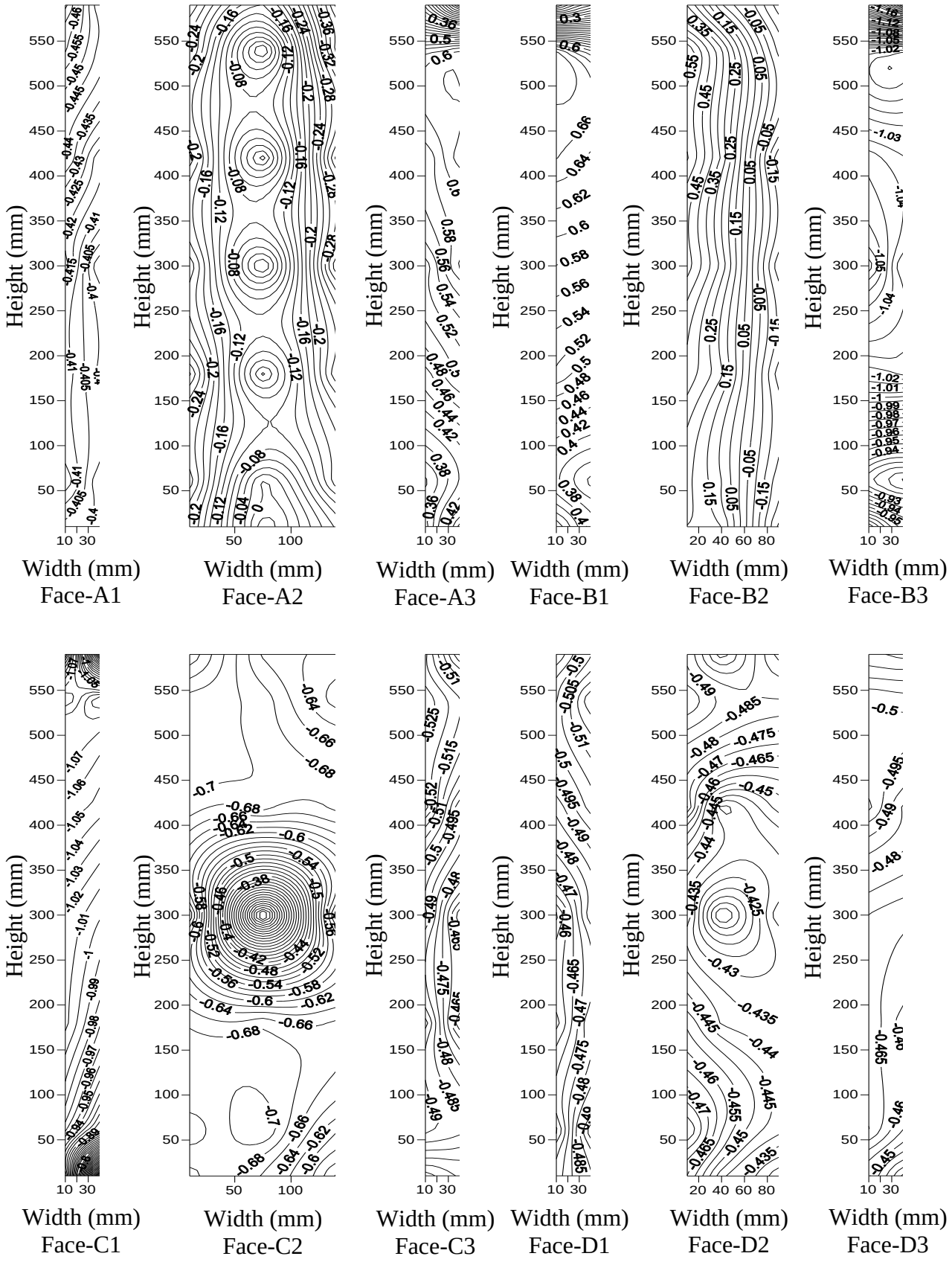


**Fig. 5.13 Distribution of mean wind pressure coefficients ($C_{p,mean}$) on different surfaces of model-B at $60^0$ wind incidence angle**

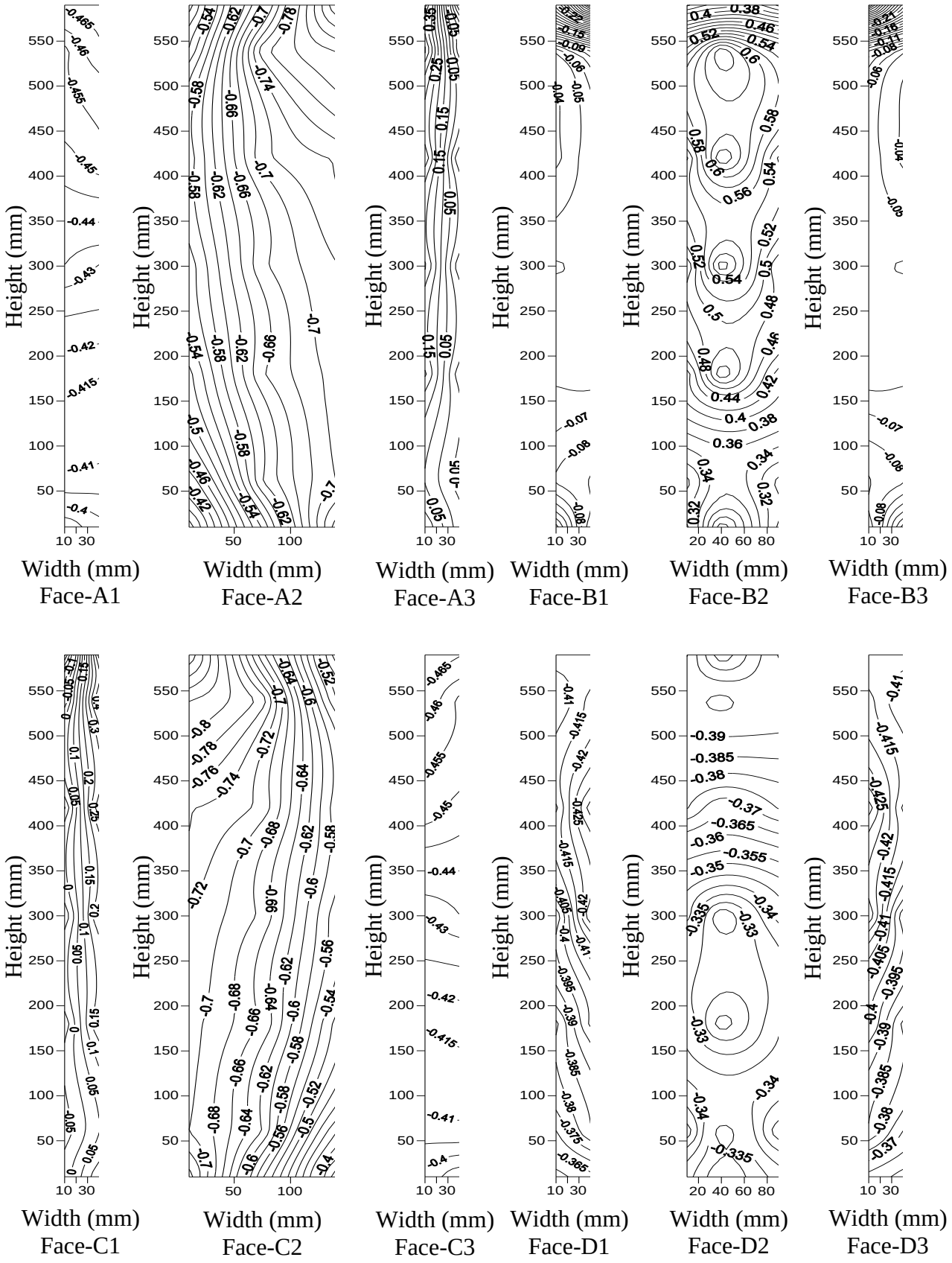


**Fig. 5.14 Distribution of mean wind pressure coefficients ($C_{p,mean}$) on different surfaces of model-B at $90^0$ wind incidence angle**

Figures 5.15 to 5.18 show the cross-sectional variation of mean wind pressure coefficients ($C_{p,mean}$) at 7 different sections along the height in different wind incidence angles of flow. It is noticed from the Fig. 5.15 that the pattern of mean wind pressure distribution is parabolic on face-A2 when wind incidence angle is $0^0$. Figure 5.17 also indicates that maximum suction occurs on face-B3 when wind incidence angle is $60^0$ and corresponding value of $C_{p,mean}$ is -1.21.At other angles namely $0^0$, $30^0$ and $90^0$, suction is smaller than that in case of $60^0$ wind incidence angle.

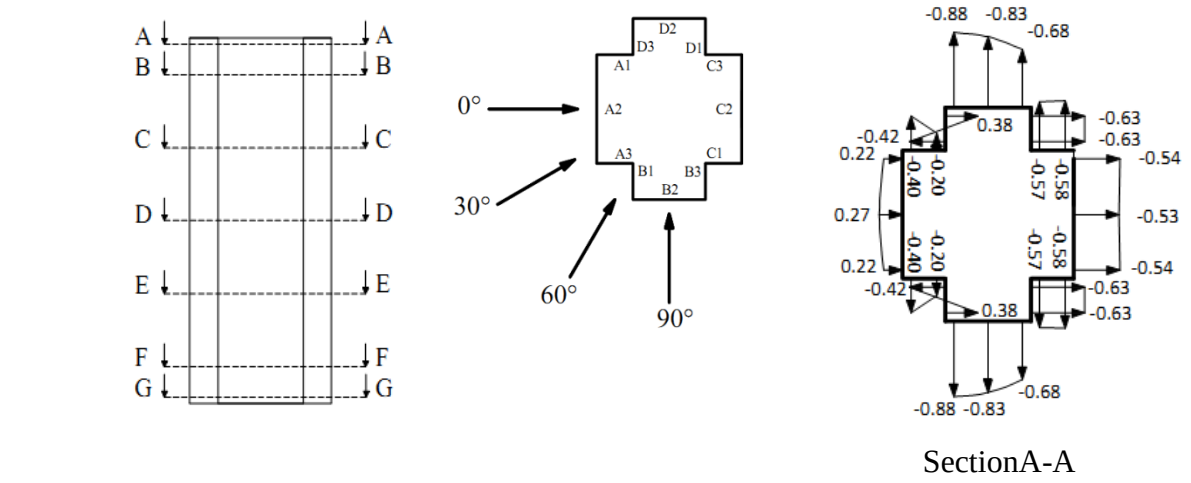


SectionA-A

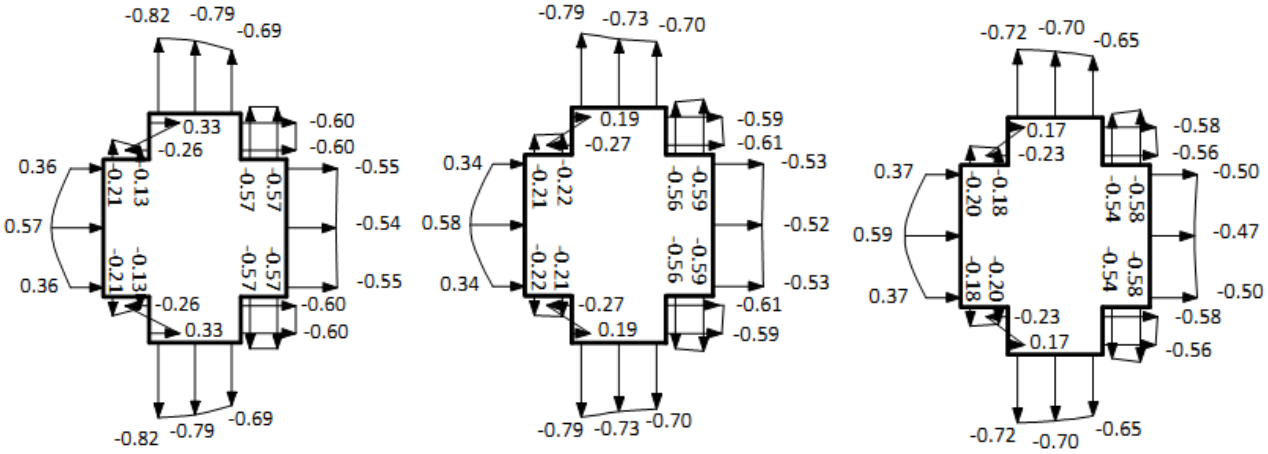

Section B-B Section C-C Section D-D

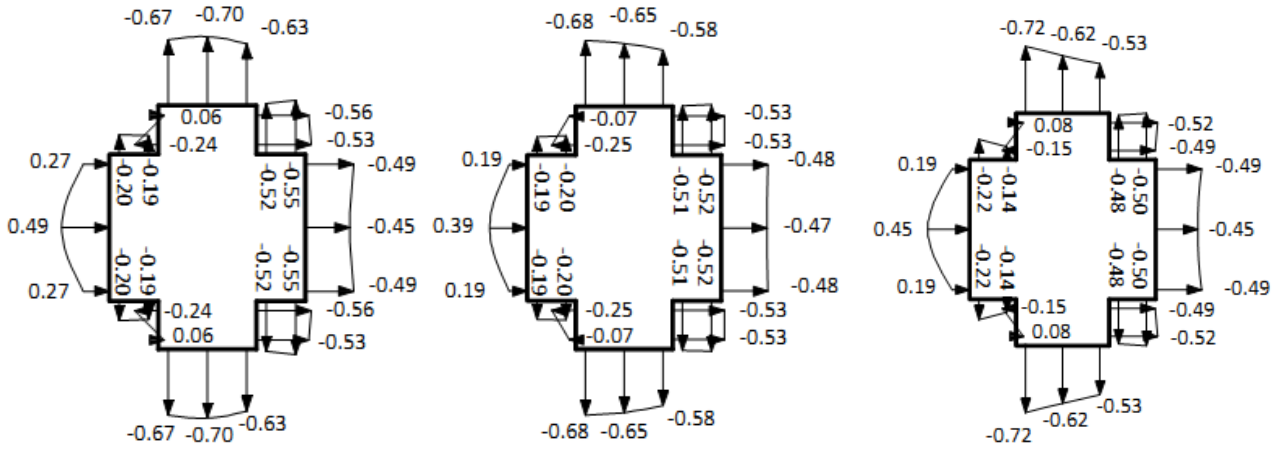

Section E-E Section F-F Section G-G

**Fig. 5.15 Cross-sectional variation of mean wind pressure coefficients ($C_{p,mean}$) on model-B at $0^0$ wind incidence angle**

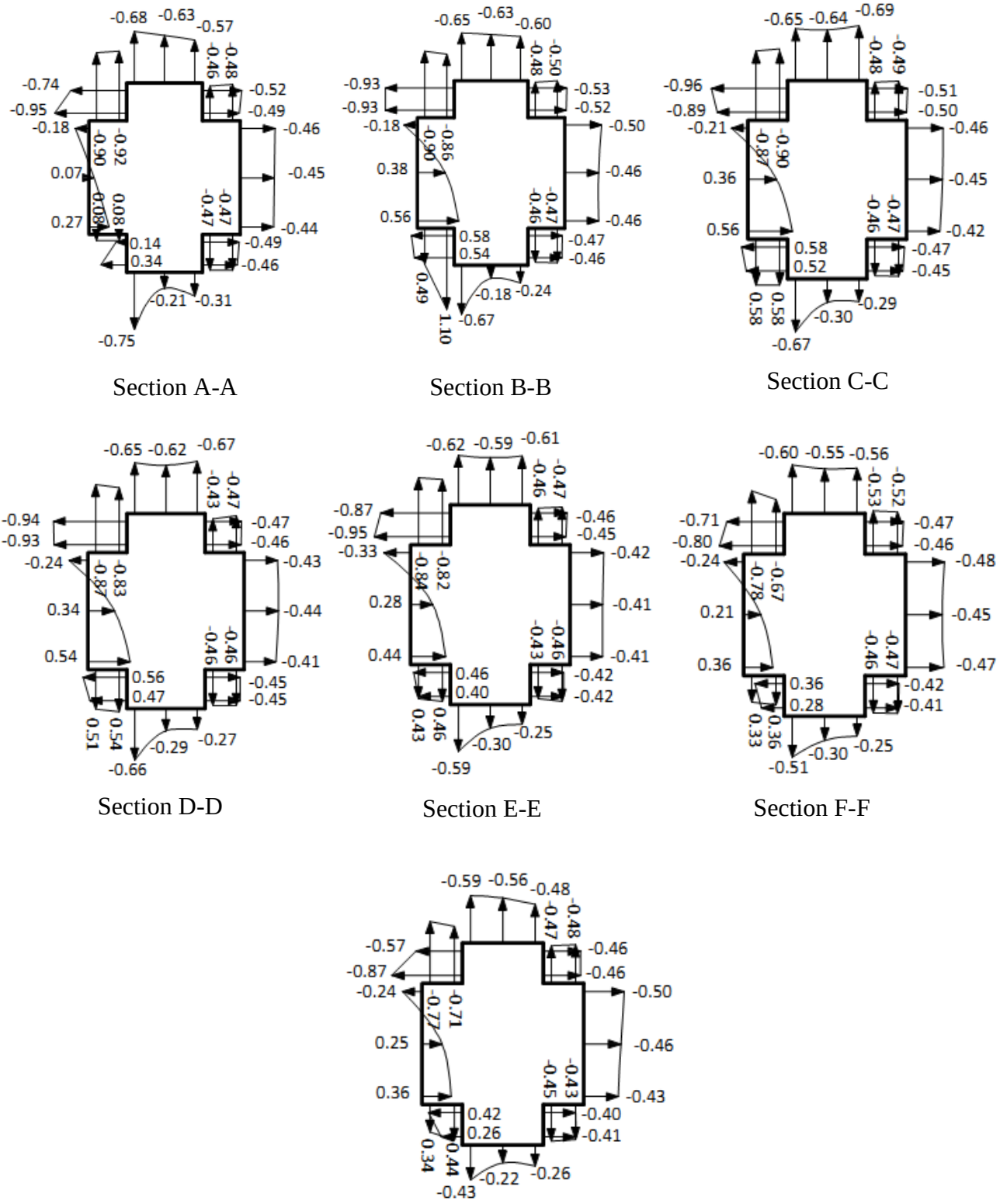


**Fig. 5.16 Cross-sectional variation of mean wind pressure coefficients ($C_{p,mean}$) on model-B at $30^0$ wind incidence angle**

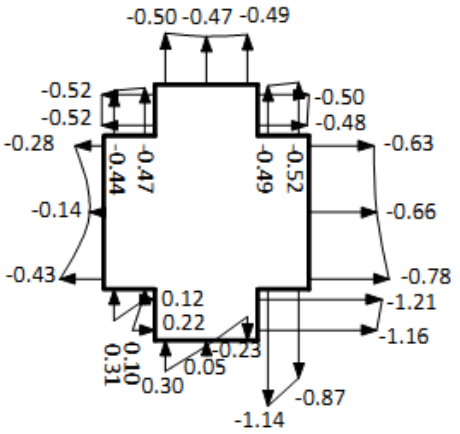


Section A-A

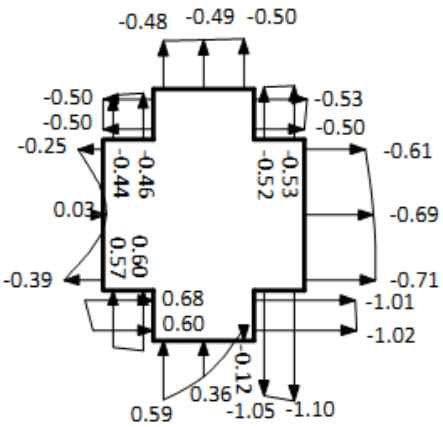


Section B-B

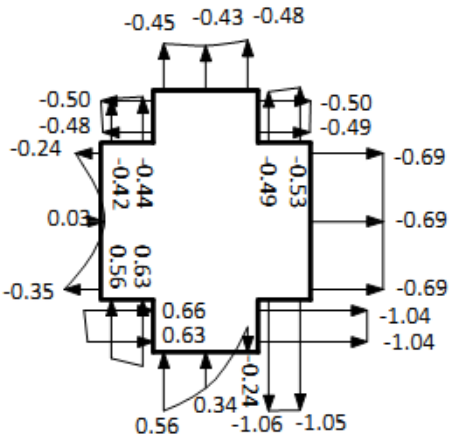


Section C-C

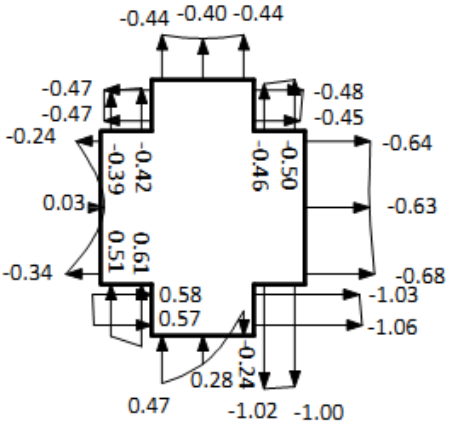


Section D-D

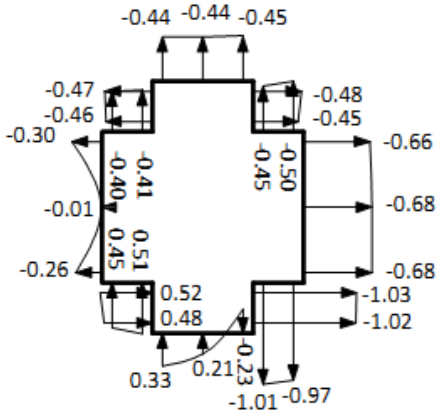


Section E-E

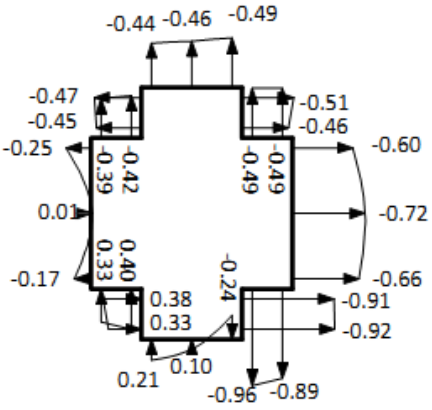


Section F-F

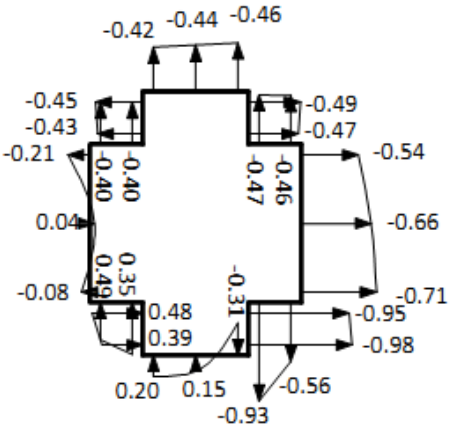


Section G-G

**Fig. 5.17 Cross-sectional variation of mean wind pressure coefficients ($C_{p,mean}$) on model-B at $60^0$ wind incidence angle**

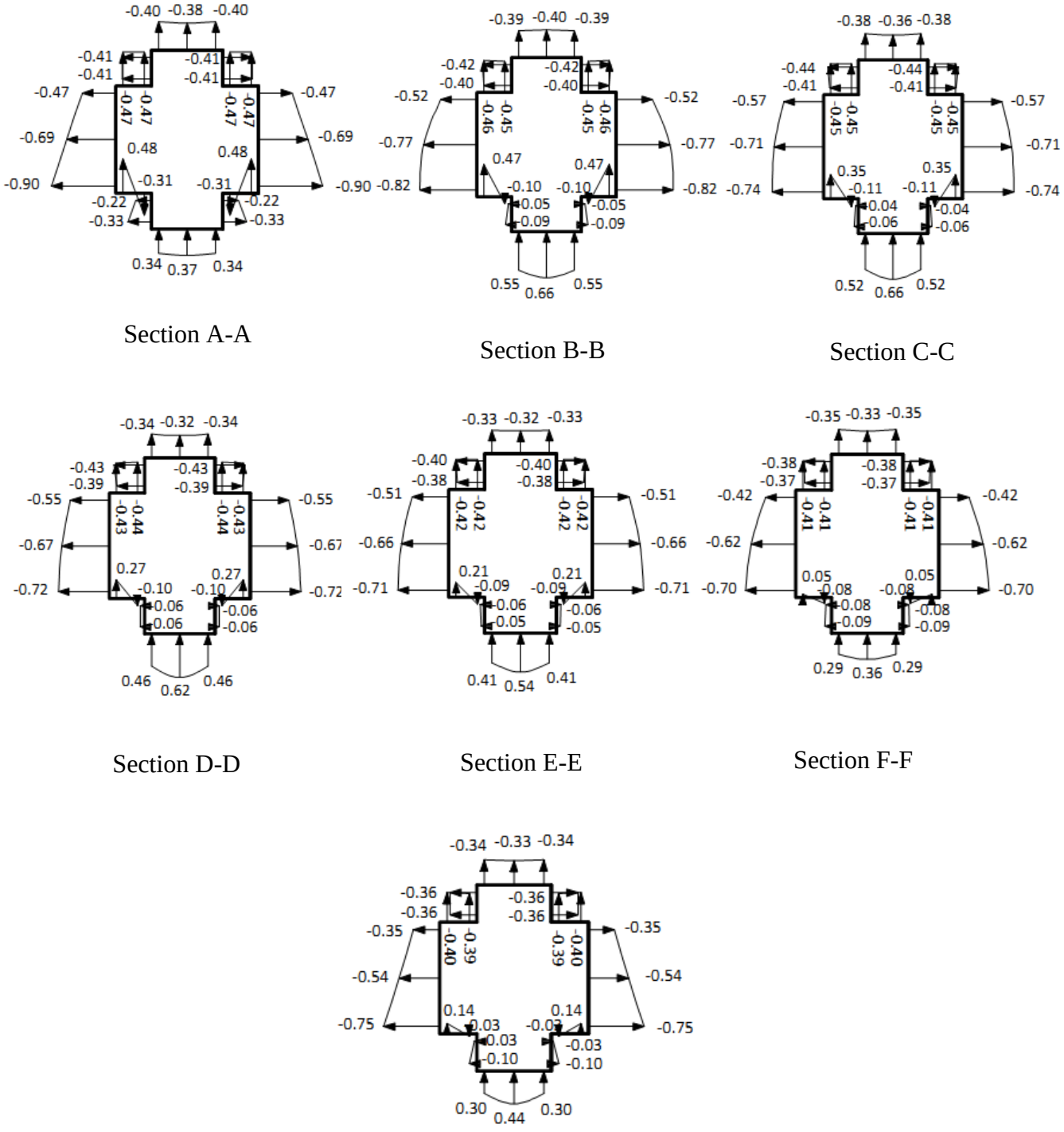


**Fig. 5.18 Cross-sectional variation of mean wind pressure coefficients ($C_{p,mean}$) on model-B at $90^0$ wind incidence angle**

Comparison of $C_{p,mean}$ values at 49 pressure points on face-A of model-B at 7 wind incidence angles are shown in Table 5.3. It is noticed that the face A is subjected to maximum pressure of $C_{p,mean}$ = 0.62 and minimum pressure of $C_{p,mean}$ = -0.92 at $90^0$.

**Table 5.3 Variation of $C_{p,mean}$ on face-A (face A1, A2 and A3) of model-B with wind incidence angle**

| Pressure point no. | Mean wind pressure coefficients ($C_{p,mean}$) | | | |
|---|---|---|---|---|
| | $0^0$ | $30^0$ | $60^0$ | $90^0$ |
| 1 | **-0.20** | **-0.92** | **-0.47** | **-0.47** |
| 2 | -0.40 | -0.90 | -0.44 | -0.47 |
| 3 | 0.22 | -0.18 | -0.28 | -0.47 |
| 4 | 0.27 | 0.07 | -0.14 | -0.69 |
| 5 | 0.22 | 0.27 | -0.43 | -0.90 |
| 6 | -0.40 | 0.08 | 0.31 | **0.48** |
| 7 | -0.20 | 0.08 | 0.10 | -0.31 |
| 8 | -0.13 | -0.86 | -0.46 | -0.45 |
| 9 | -0.21 | -0.90 | -0.44 | -0.46 |
| 10 | 0.36 | -0.18 | -0.25 | -0.52 |
| 11 | 0.57 | 0.38 | 0.03 | -0.77 |
| 12 | 0.36 | 0.56 | -0.39 | -0.82 |
| 13 | -0.21 | 0.49 | 0.57 | 0.47 |
| 14 | -0.13 | **0.62** | 0.60 | -0.10 |
| 15 | -0.22 | -0.90 | -0.44 | -0.45 |
| 16 | -0.21 | -0.87 | -0.42 | -0.45 |
| 17 | 0.34 | -0.21 | -0.24 | -0.57 |
| 18 | 0.58 | 0.36 | 0.03 | -0.71 |
| 19 | 0.34 | 0.56 | -0.35 | -0.74 |
| 20 | -0.21 | 0.58 | 0.56 | 0.35 |
| 21 | -0.22 | 0.58 | **0.63** | -0.11 |
| 22 | -0.18 | -0.83 | -0.42 | -0.44 |
| 23 | -0.20 | -0.87 | -0.39 | -0.43 |
| 24 | 0.37 | -0.24 | -0.24 | -0.55 |
| 25 | **0.59** | 0.34 | 0.03 | -0.67 |
| 26 | 0.37 | 0.54 | -0.34 | -0.72 |
| 27 | -0.20 | 0.51 | 0.51 | 0.27 |
| 28 | -0.18 | 0.54 | 0.61 | -0.10 |
| 29 | -0.19 | -0.82 | -0.41 | -0.42 |
| 30 | -0.20 | -0.84 | -0.40 | -0.42 |
| 31 | 0.27 | -0.33 | -0.30 | -0.51 |
| 32 | 0.49 | 0.28 | -0.01 | -0.66 |
| 33 | 0.27 | 0.44 | -0.26 | -0.71 |
| 34 | -0.20 | 0.43 | 0.45 | 0.21 |
| 35 | -0.19 | 0.46 | 0.51 | -0.09 |
| 36 | -0.20 | -0.67 | -0.42 | -0.41 |
| 37 | -0.19 | -0.78 | -0.39 | -0.41 |
| 38 | 0.19 | -0.24 | -0.25 | -0.42 |
| 39 | 0.39 | 0.21 | 0.01 | -0.62 |
| 40 | 0.19 | 0.36 | -0.17 | -0.70 |
| 41 | -0.19 | 0.33 | 0.33 | 0.05 |
| 42 | -0.20 | 0.36 | 0.40 | -0.08 |
| 43 | -0.14 | -0.71 | -0.40 | -0.39 |
| 44 | -0.22 | -0.77 | -0.40 | -0.40 |
| 45 | 0.19 | -0.24 | -0.21 | -0.35 |
| 46 | 0.45 | 0.25 | 0.04 | -0.54 |
| 47 | 0.19 | 0.36 | -0.08 | -0.75 |
| 48 | -0.22 | 0.34 | 0.35 | 0.14 |
| 49 | -0.14 | 0.44 | 0.49 | -0.03 |

### 5.2.3 Model-C (Plus Shape-2)

Perspex sheet model of model-C (Photo. 3.8) is also tested under 4 wind incidence angles (Fig. 5.19) as in the case of model-A and model-B. Mean wind pressure distribution contours are plotted on all surfaces of the model (Figs. 5.20 to 5.23).

Figure 5.20 indicates that maximum pressure ($C_{p,mean}$ = 0.7) occurs at almost ¾ height of the model on face-A2 at $0^0$ degree wind incidence angle. Comparatively less pressure is observed in upper and lower parts of the model on windward faces. In this model, all windward faces namely A1, A2 and A3 are subjected to pressures of almost equal magnitude. This difference w.r.t. model-B is observed due to long length of cut corners in model-C as compared to model-B. Suction is noticed on parallel side faces and leeward faces. Maximum suction occurs on side face-B2 and face-D2 ($C_{p,mean}$ = -0.7). The figure also indicates that less pressure variation occurs on leeward side of building model-C.

At $30^0$ wind incidence angle (Fig. 5.21), positive pressure zone move from windward face to leeward face. Face-B2 experiences maximum suction ($C_{p,mean}$ = -0.8) near the top of the building model.

At $90^0$ wind incidence angle (Fig. 5.23), wind direction is perpendicular to its small faces. Maximum positive pressure occurs on face-B2 with $C_{p,mean}$ = 0.64. Suction occurs on face-A2 and face-C2 with $C_{p,mean}$ = -0.75.

Table 5.4 compares the values of $C_{p,mean}$ on face-A of model-C at 4 different wind incidence angles. Maximum value of $C_{p,mean}$ on this face is 0.78 at $60^0$ wind incidence angle and minimum value is -0.88 at $90^0$ wind incidence angle.

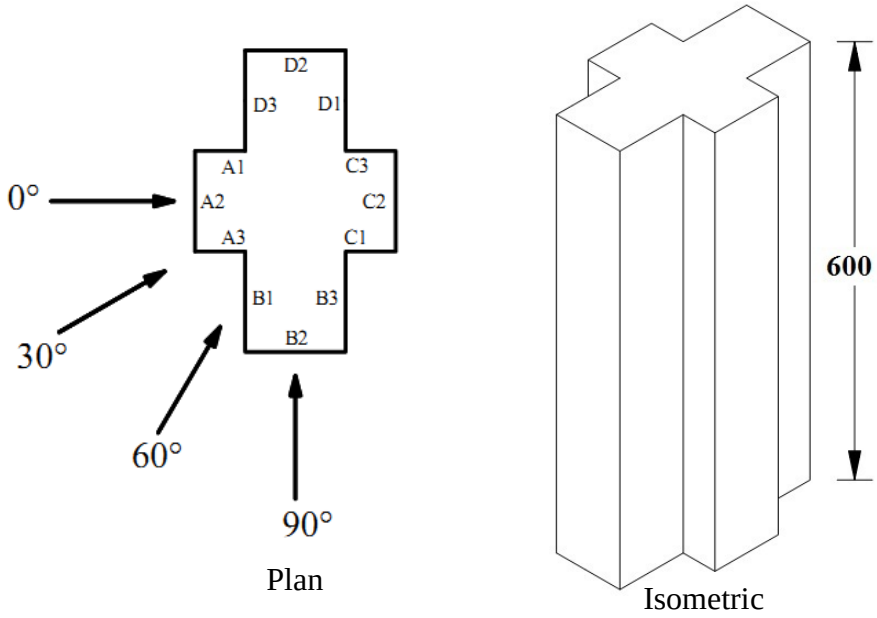


**Fig. 5.19 Wind incidence angles on Perspex sheet model of model-C in isolated condition**
(All dimensions are in mm)

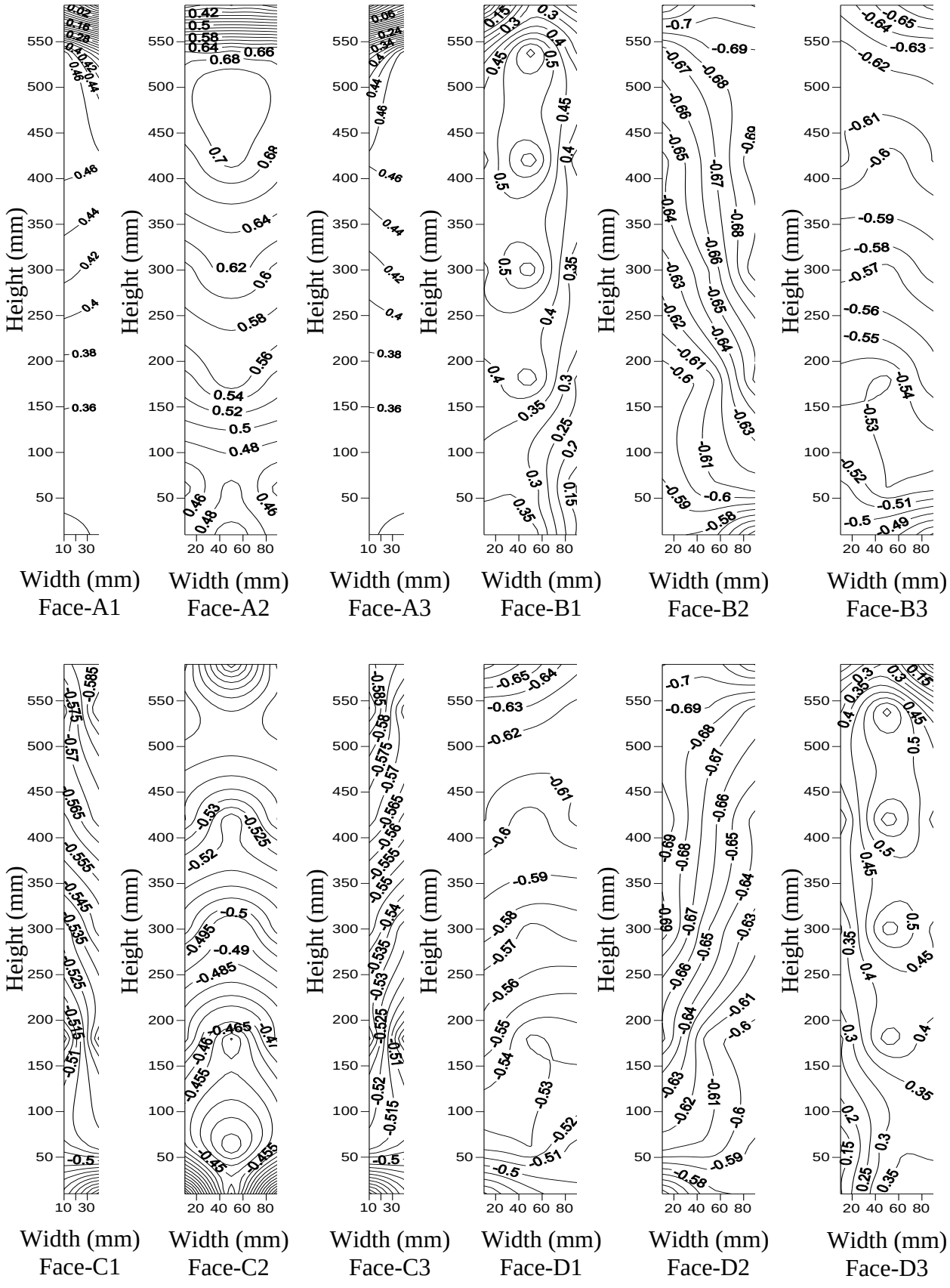


**Fig. 5.20 Distribution of mean wind pressure coefficients ($C_{p,mean}$) on different surfaces of model-C at $0^0$ wind incidence angle**

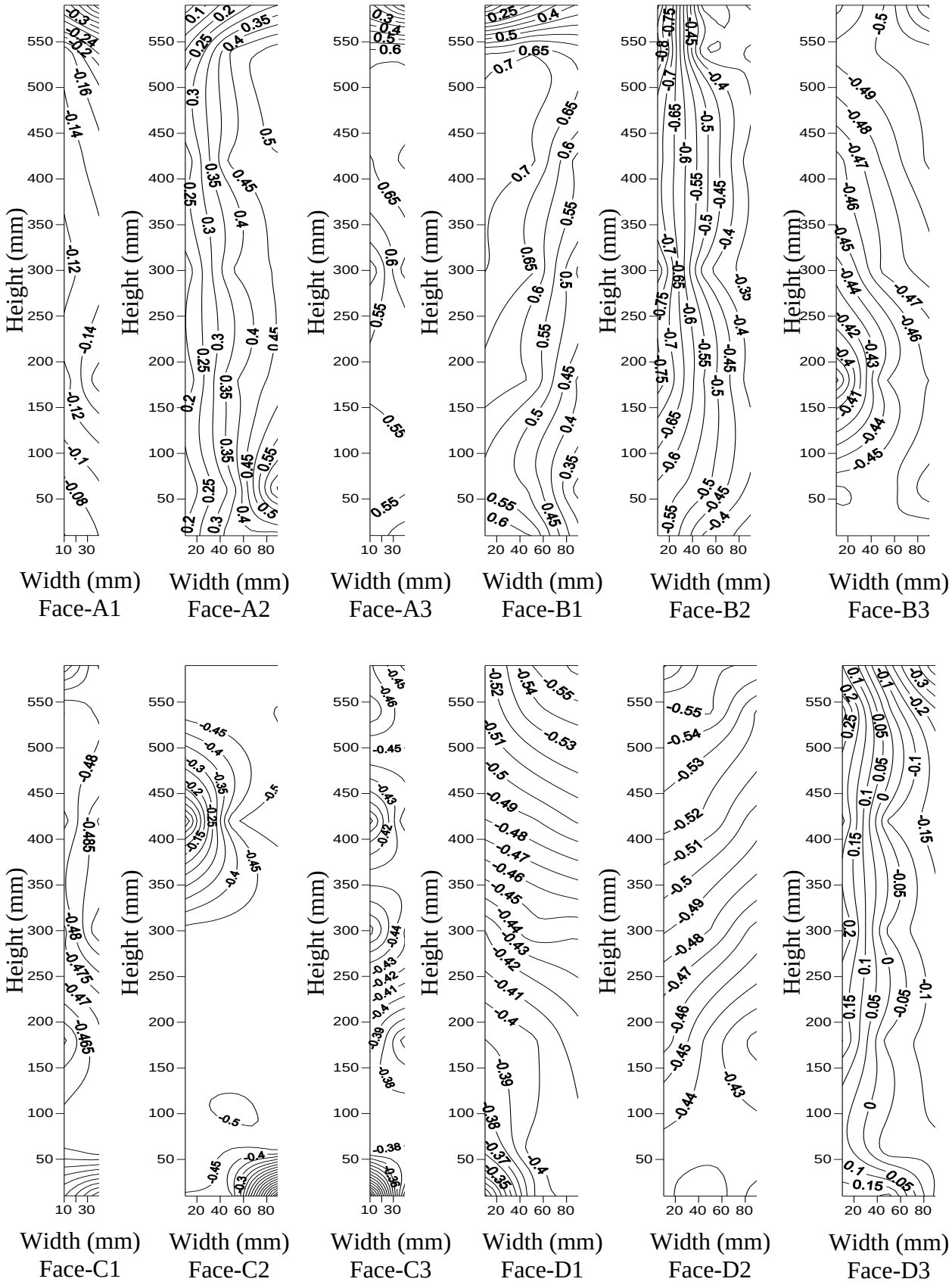


**Fig. 5.21 Distribution of mean wind pressure coefficients ($C_{p,mean}$) on different surfaces of model-C at $30^0$ wind incidence angle**

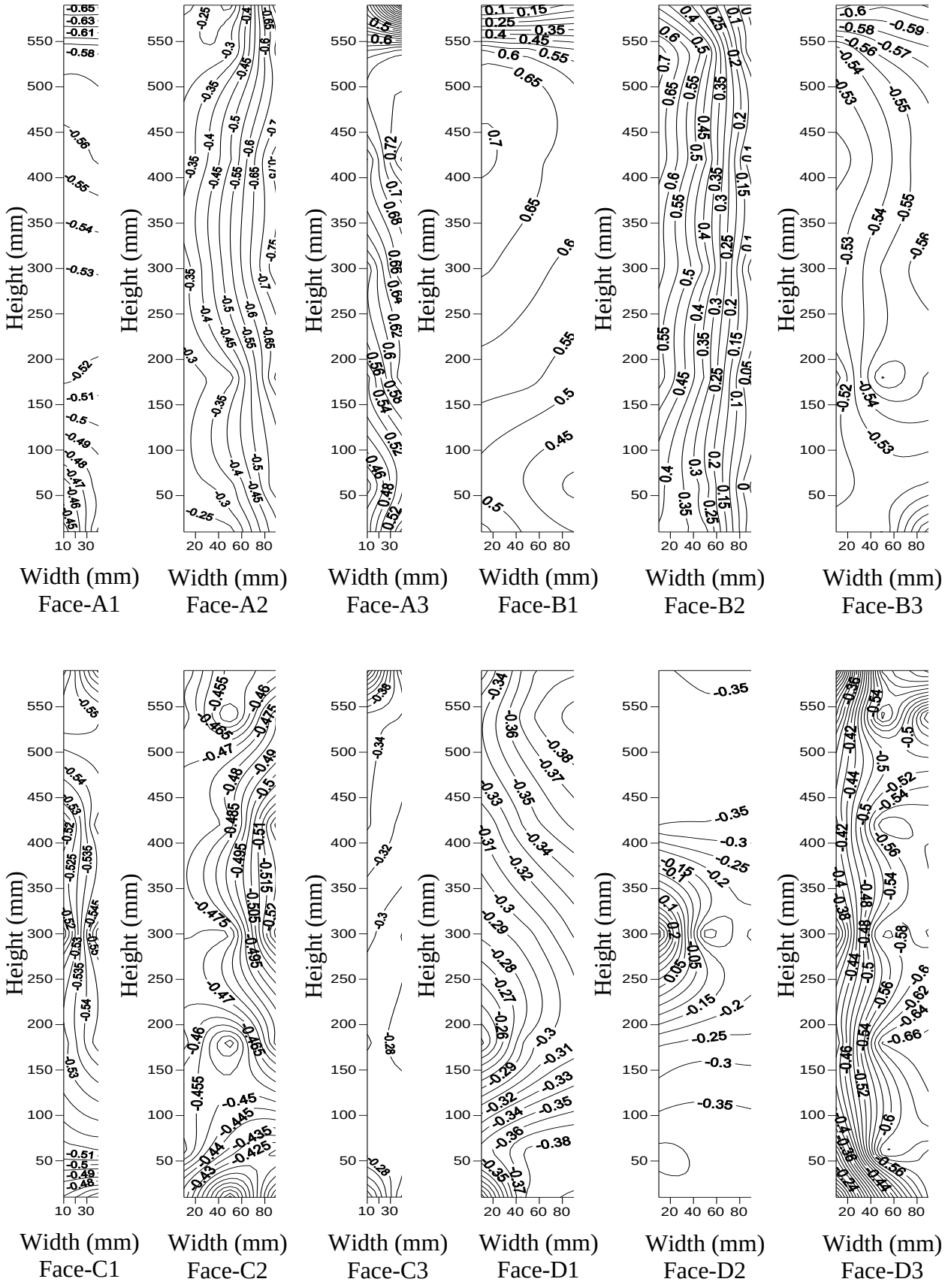


**Fig. 5.22 Distribution of mean wind pressure coefficients ($C_{p,mean}$) on different surfaces of model-C at $60^0$ wind incidence angle**

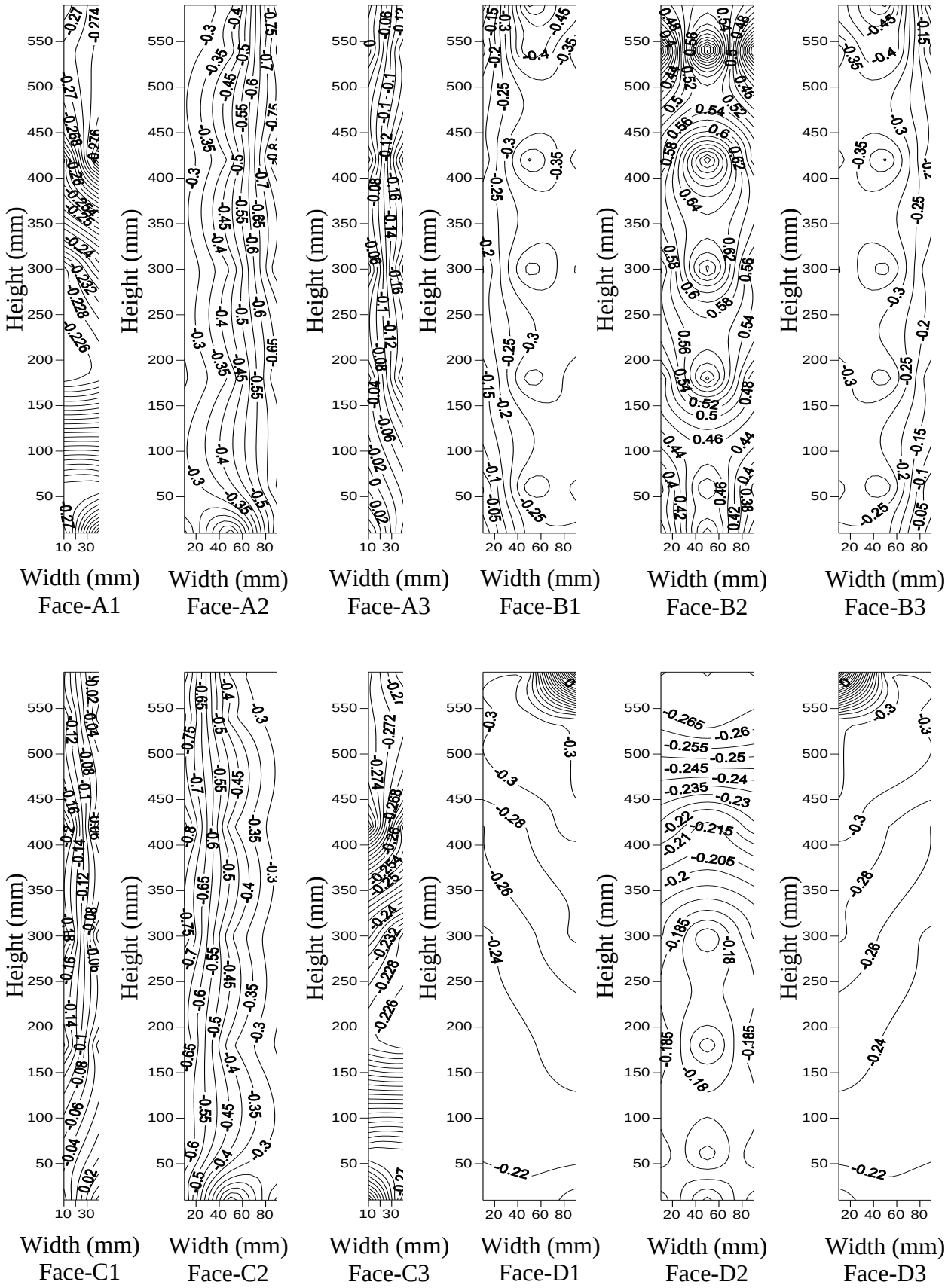


**Fig. 5.23 Distribution of mean wind pressure coefficients ($C_{p,mean}$) on different surfaces of model-C at $90^0$ wind incidence angle**

Cross-sectional variation of $C_{p,mean}$ at 7 sections along the height of model-C can be seen in Figs. 5.24 to 5.27 for 4 different wind incidence angles.

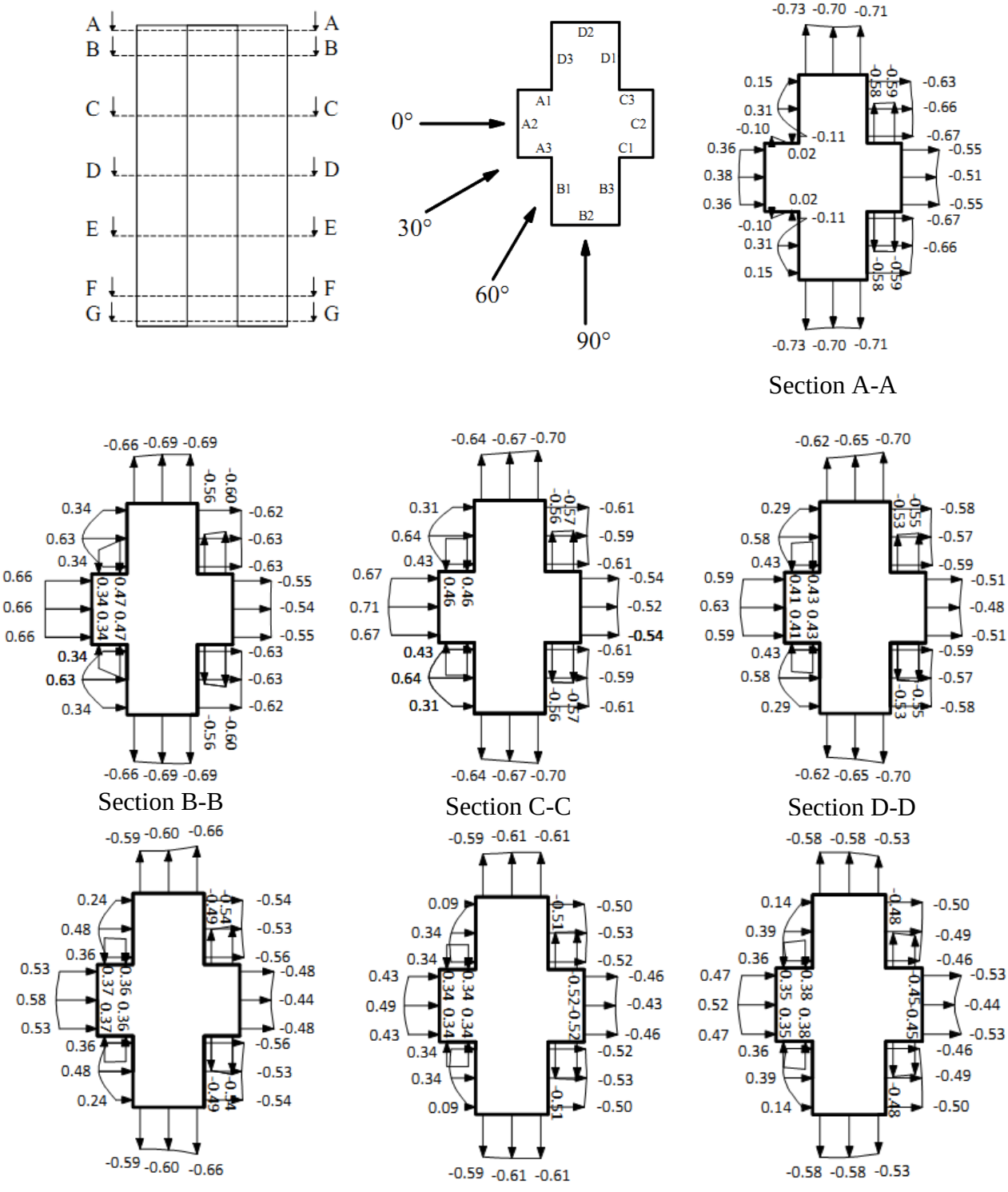


**Fig. 5.24 Cross-sectional variation of mean wind pressure coefficients ($C_{p,mean}$) on model-C at $0^0$ wind incidence angle**

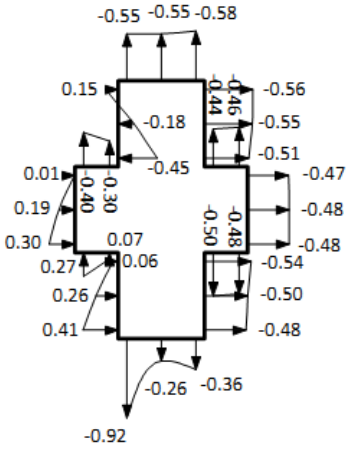


Section A-A

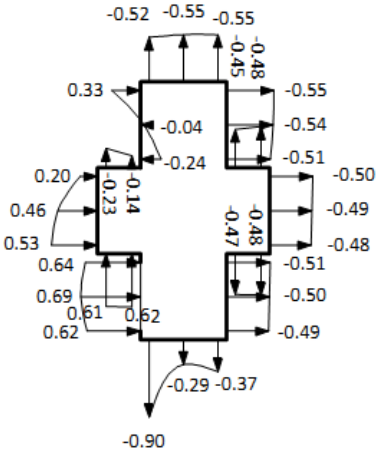


Section B-B

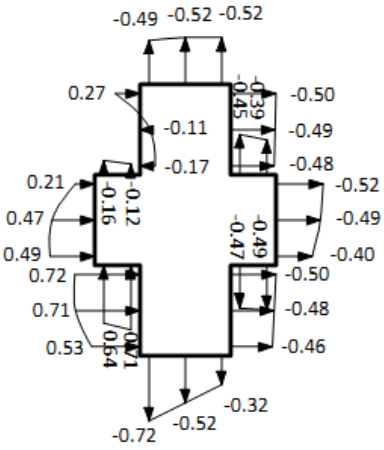


Section C-C

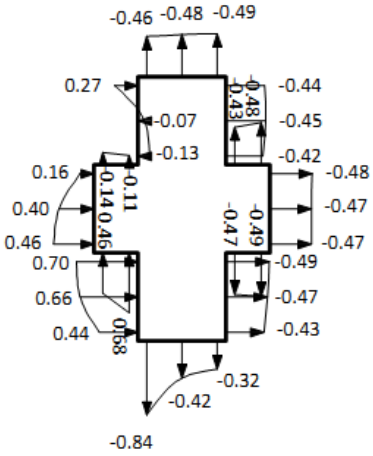


Section D-D

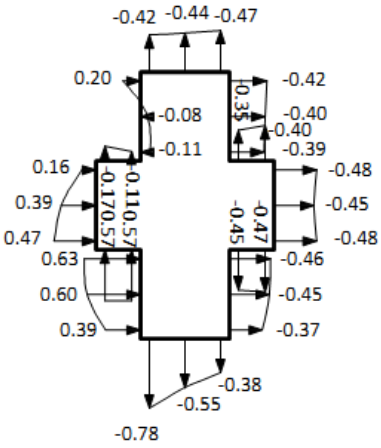


Section E-E

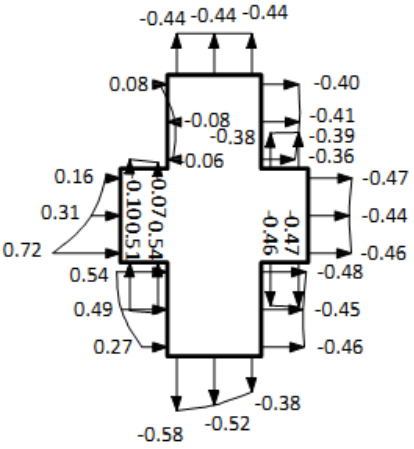


Section F-F

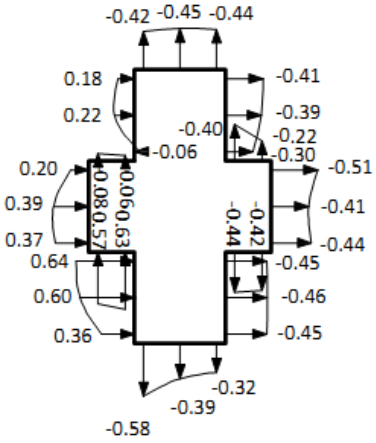


Section G-G

**Fig. 5.25 Cross-sectional variation of mean wind pressure coefficients ($C_{p,mean}$) on model-C at $30^0$ wind incidence angle**

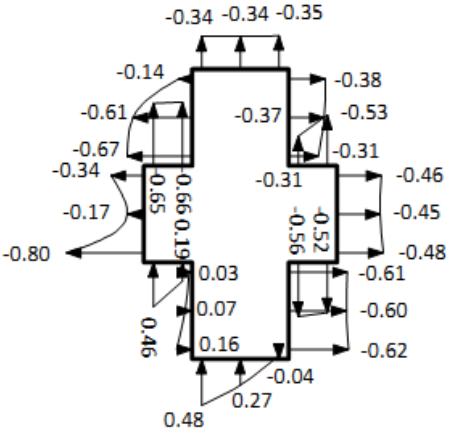


Section A-A

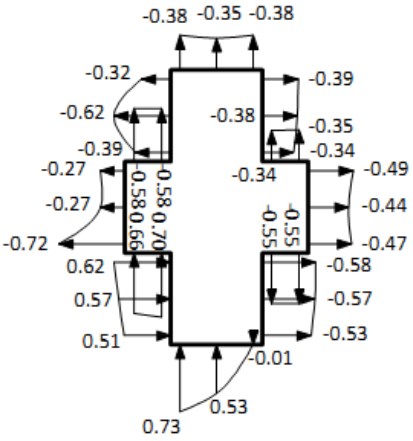


Section B-B

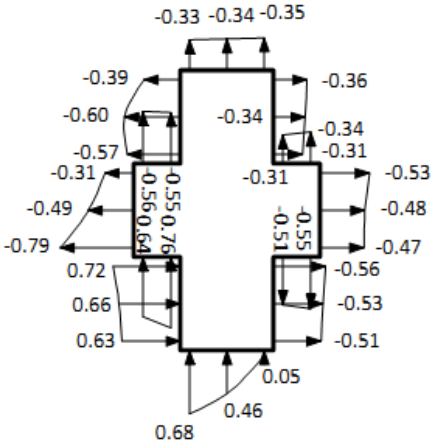


Section C-C

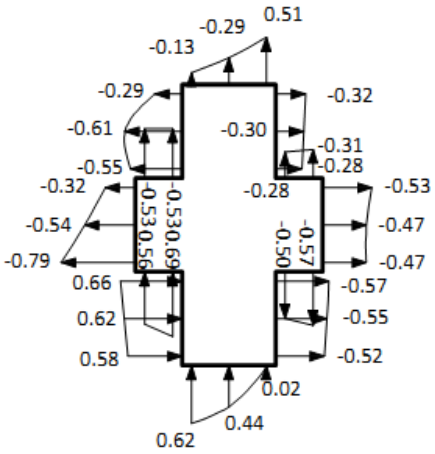


Section D-D

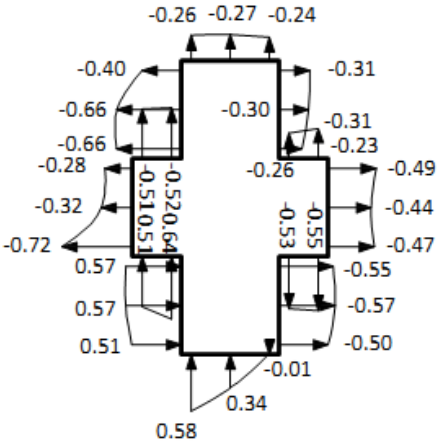


Section E-E

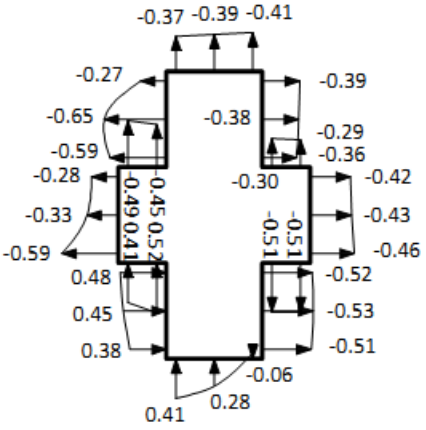


Section F-F

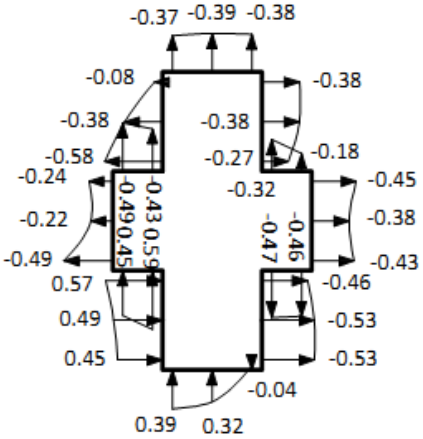


Section G-G

**Fig. 5.26 Cross-sectional variation of mean wind pressure coefficients ($C_{p,mean}$) on model-C at $60^0$ wind incidence angle**

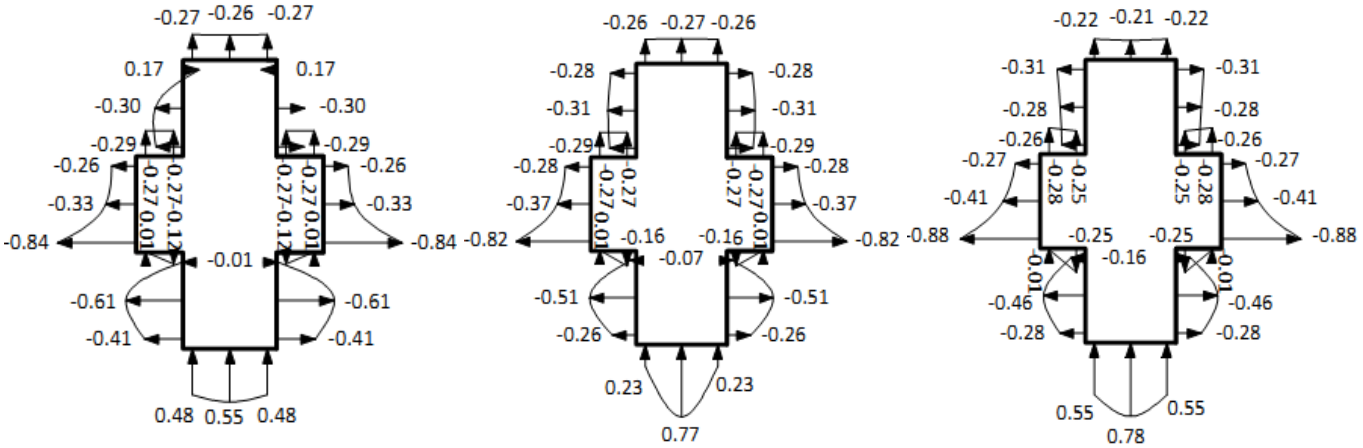


Section A-A Section B-B Section C-C

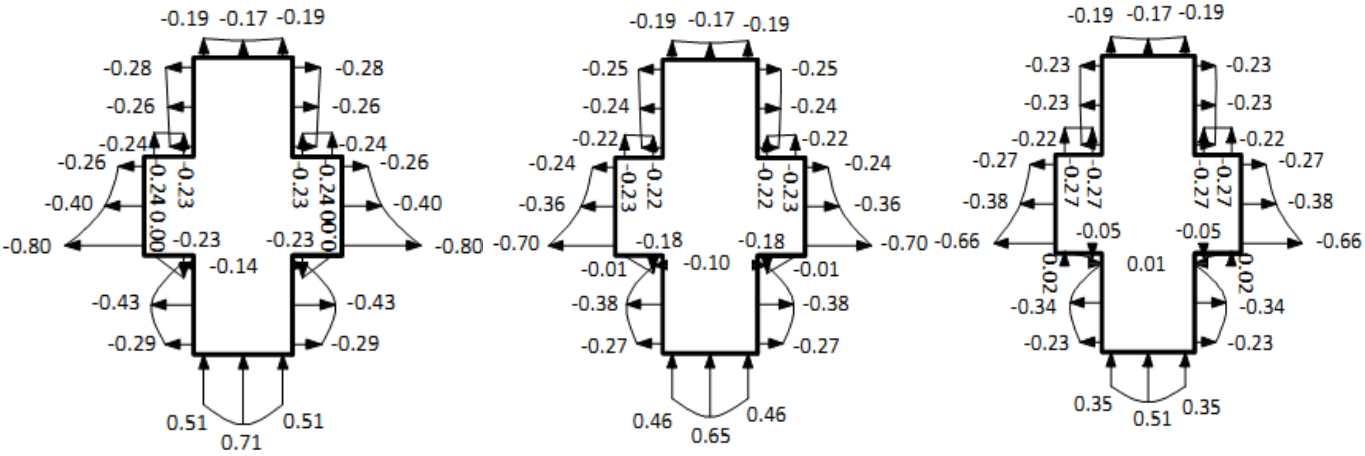


SectionD-D Section E-E Section F-F

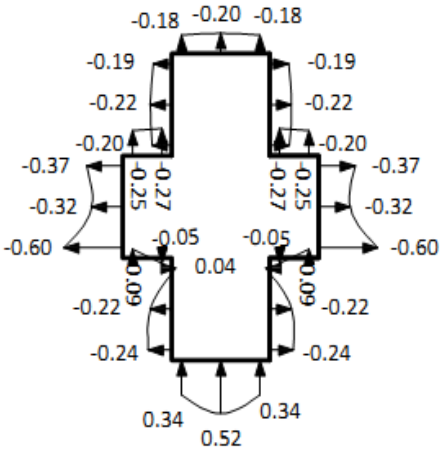


Section G-G

**Fig. 5.27 Cross-sectional variation of mean wind pressure coefficients ($C_{p,mean}$) on model-C at $90^0$ wind incidence angle**

Comparison of $C_{p,mean}$ values at 49 pressure points on face-A of model-C at 7 wind incidence angles are shown in Table 5.4. It is noticed that the face A is subjected to maximum pressure of $C_{p,mean}$ = 0.76 at $60^0$ and minimum pressure of $C_{p,mean}$ = -0.88 at $90^0$.

**Table 5.4 Variation of $C_{p,mean}$ on face-A of model-C with wind incidence angle**

| Pressure point no. | Mean wind pressure coefficients ($C_{p,mean}$) | | | |
|---|---|---|---|---|
| | $0^0$ | $30^0$ | $60^0$ | $90^0$ |
| 1 | 0.02 | -0.30 | -0.66 | -0.27 |
| 2 | **-0.10** | **-0.40** | -0.65 | -0.27 |
| 3 | 0.36 | 0.01 | -0.34 | -0.26 |
| 4 | 0.38 | 0.19 | -0.17 | -0.33 |
| 5 | 0.36 | 0.30 | **-0.80** | -0.84 |
| 6 | -0.10 | 0.27 | 0.46 | 0.01 |
| 7 | 0.02 | 0.07 | 0.19 | -0.12 |
| 8 | 0.47 | -0.14 | -0.58 | -0.27 |
| 9 | 0.34 | -0.23 | -0.58 | -0.27 |
| 10 | 0.66 | 0.20 | -0.27 | -0.28 |
| 11 | 0.66 | 0.46 | -0.27 | -0.37 |
| 12 | 0.66 | 0.53 | -0.72 | -0.82 |
| 13 | 0.34 | 0.61 | 0.66 | 0.01 |
| 14 | 0.47 | 0.62 | 0.70 | -0.16 |
| 15 | 0.46 | -0.12 | -0.55 | -0.25 |
| 16 | 0.46 | -0.16 | -0.56 | -0.28 |
| 17 | 0.67 | 0.21 | -0.31 | -0.27 |
| 18 | **0.71** | 0.47 | -0.49 | -0.41 |
| 19 | 0.67 | 0.49 | -0.79 | **-0.88** |
| 20 | 0.46 | 0.64 | 0.64 | -0.01 |
| 21 | 0.46 | 0.71 | **0.76** | -0.25 |
| 22 | 0.43 | -0.11 | -0.53 | -0.23 |
| 23 | 0.41 | -0.14 | -0.53 | -0.24 |
| 24 | 0.59 | 0.16 | -0.32 | -0.26 |
| 25 | 0.63 | 0.40 | -0.54 | -0.40 |
| 26 | 0.59 | 0.46 | -0.79 | -0.80 |
| 27 | 0.41 | 0.68 | 0.56 | 0.00 |
| 28 | 0.43 | 0.67 | 0.69 | -0.23 |
| 29 | 0.36 | -0.11 | -0.52 | -0.22 |
| 30 | 0.37 | -0.17 | -0.51 | -0.23 |
| 31 | 0.53 | 0.16 | -0.28 | -0.24 |
| 32 | 0.58 | 0.39 | -0.32 | -0.36 |
| 33 | 0.53 | 0.47 | -0.72 | -0.70 |
| 34 | 0.37 | 0.57 | 0.51 | -0.01 |
| 35 | 0.36 | 0.57 | 0.64 | -0.18 |
| 36 | 0.34 | -0.07 | -0.45 | -0.27 |
| 37 | 0.34 | -0.10 | -0.49 | -0.27 |
| 38 | 0.43 | 0.16 | -0.28 | -0.27 |
| 39 | 0.49 | 0.31 | -0.33 | -0.38 |
| 40 | 0.43 | **0.72** | -0.59 | -0.66 |
| 41 | 0.34 | 0.51 | 0.41 | 0.02 |
| 42 | 0.34 | 0.54 | 0.52 | -0.05 |
| 43 | 0.38 | -0.06 | -0.43 | -0.27 |
| 44 | 0.35 | -0.08 | -0.49 | -0.25 |
| 45 | 0.47 | 0.20 | -0.24 | -0.37 |
| 46 | 0.52 | 0.39 | -0.22 | 0.00 |
| 47 | 0.47 | 0.37 | -0.49 | -0.60 |
| 48 | 0.35 | 0.57 | 0.45 | **0.09** |
| 49 | 0.38 | 0.63 | 0.59 | -0.05 |

### 5.2.4 Model-D (I-Shape-1)

Present article gives details of the experimental results on I-shape-1 building model. As mentioned earlier, mean wind pressure on the all surfaces of building model-D are measured in four wind incidence angles (Fig. 5.28) in order to see its effects on different faces of building model.

Figures 5.29 to 5.32 show the distribution of mean wind pressure coefficients ($C_{p,mean}$) on surface of building model at $0^0$, $30^0$, $60^0$ and $90^0$ angle of wind attack. It is seen from Fig. 5.29 that when wind incidence angle is $0^0$, front surface of building model (face-A) is subjected to pressure whereas suction occurs on leeward faces and side faces.

Cross-sectional variation of $C_{p,mean}$ on model-D can be seen in Figs. 5.33 to 5.36. It is noticed from the figures that maximum value of $C_{p,mean}$ on any surface is 0.96 and minimum value is -0.80. These values for 35 pressure points on face-A (Fig. 3.11) are compared in Table 5.5 for 4 wind incidence angles. It is noticed from the table that face-A is subjected to maximum pressure of $C_{p,mean}$ = 0.76 and minimum pressure of $C_{p,mean}$ = -0.81.

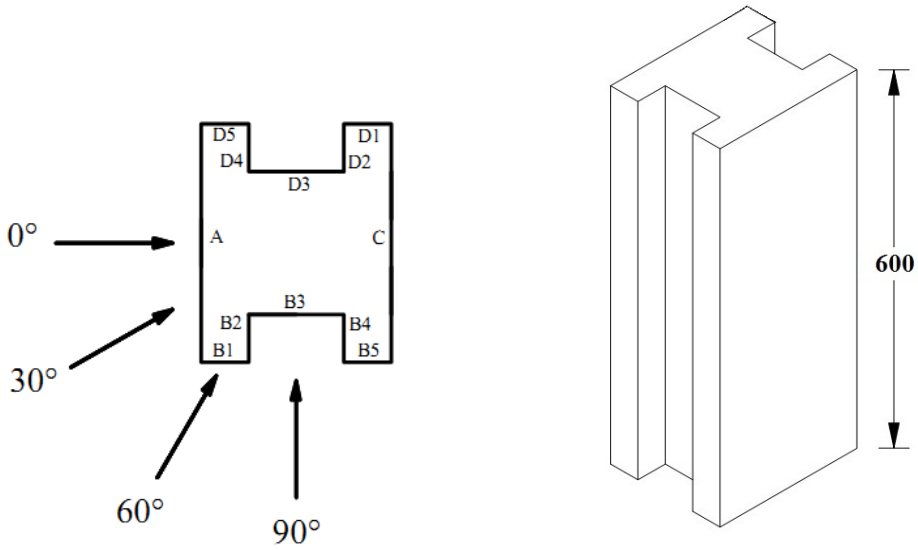


Plan Isometric

**Fig. 5.28 Wind incidence angles on Perspex sheet model of model-D in isolated condition**

(All dimensions are in mm)

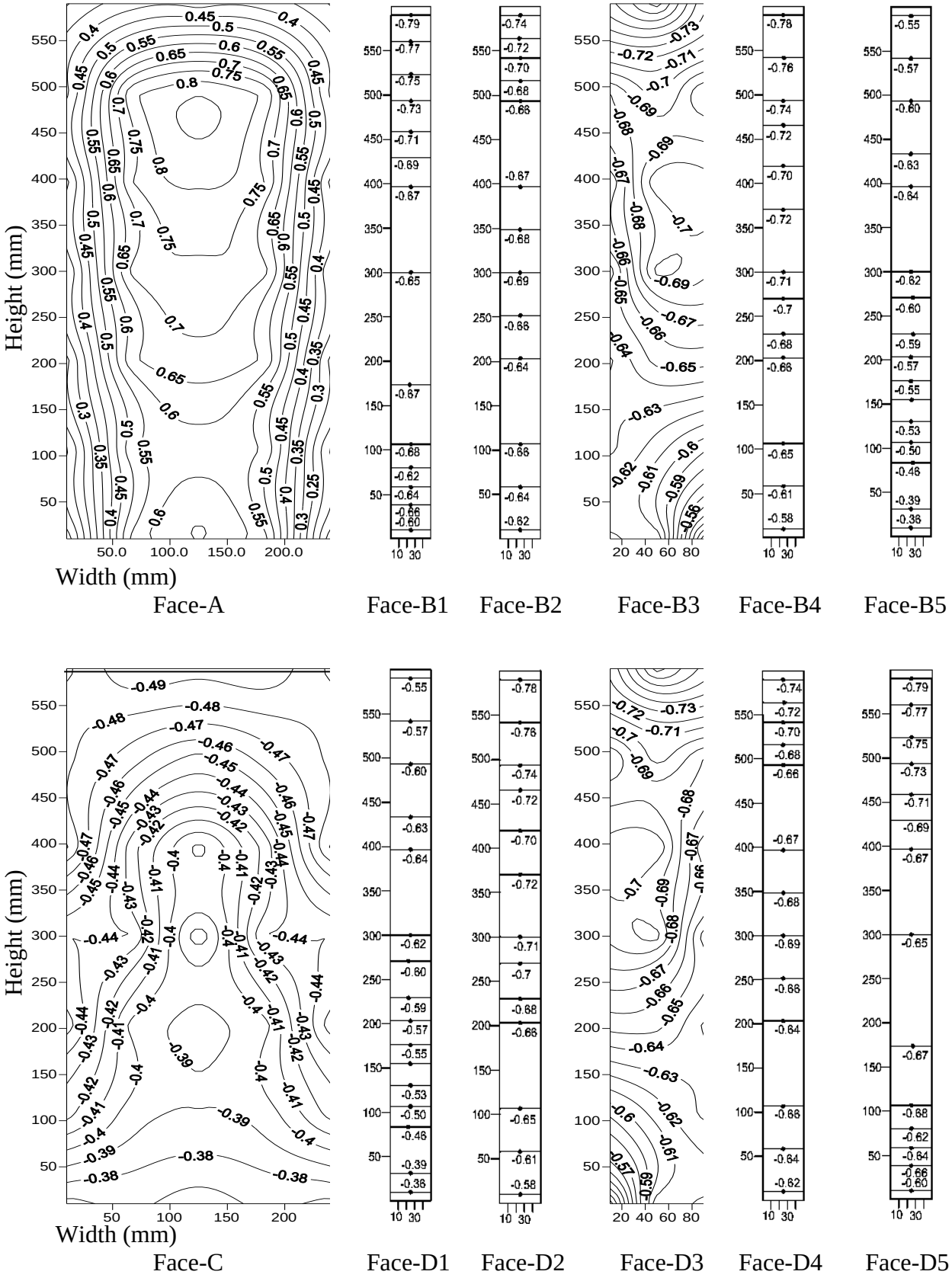


**Fig. 5.29 Distribution of mean wind pressure coefficients ($C_{p,mean}$) on different surfaces of model-D at $0^0$ wind incidence angle**

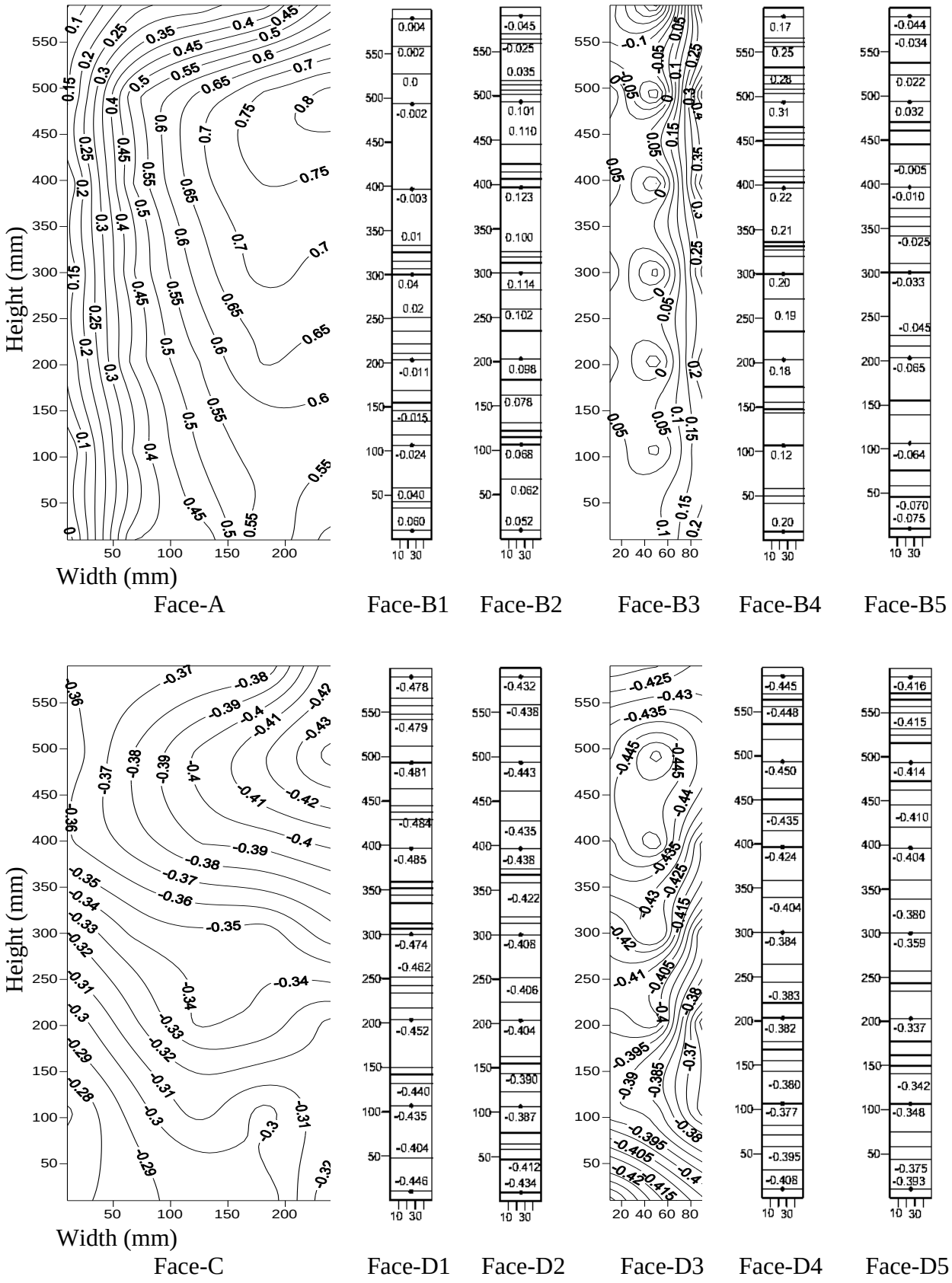


**Fig. 5.30 Distribution of mean wind pressure coefficients ($C_{p,mean}$) on different surfaces of model-D at $30^0$ wind incidence angle**

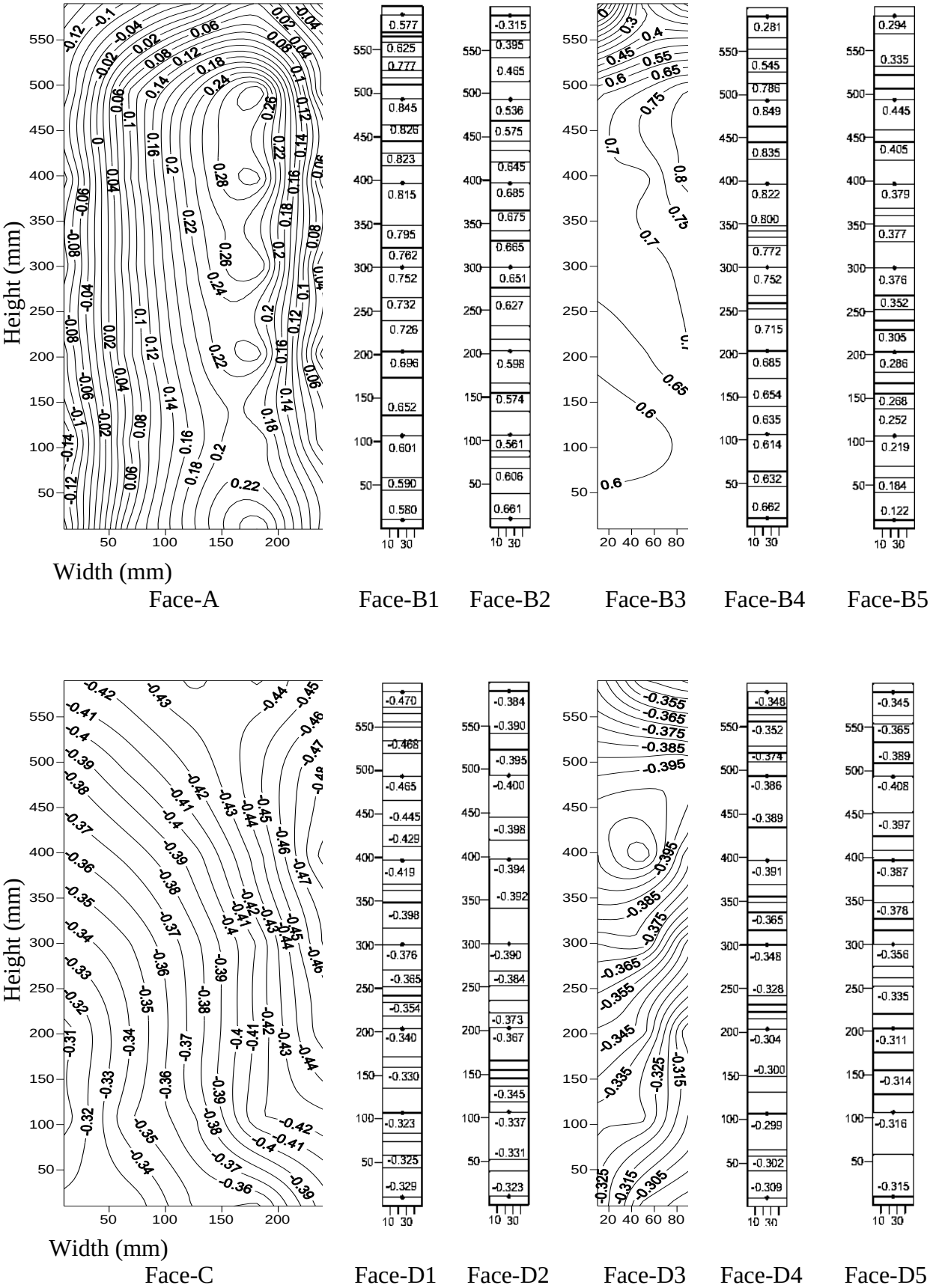


**Fig. 5.31Distribution of mean wind pressure coefficients ($C_{p,mean}$) on different surfaces of model-D at $60^0$ wind incidence angle**

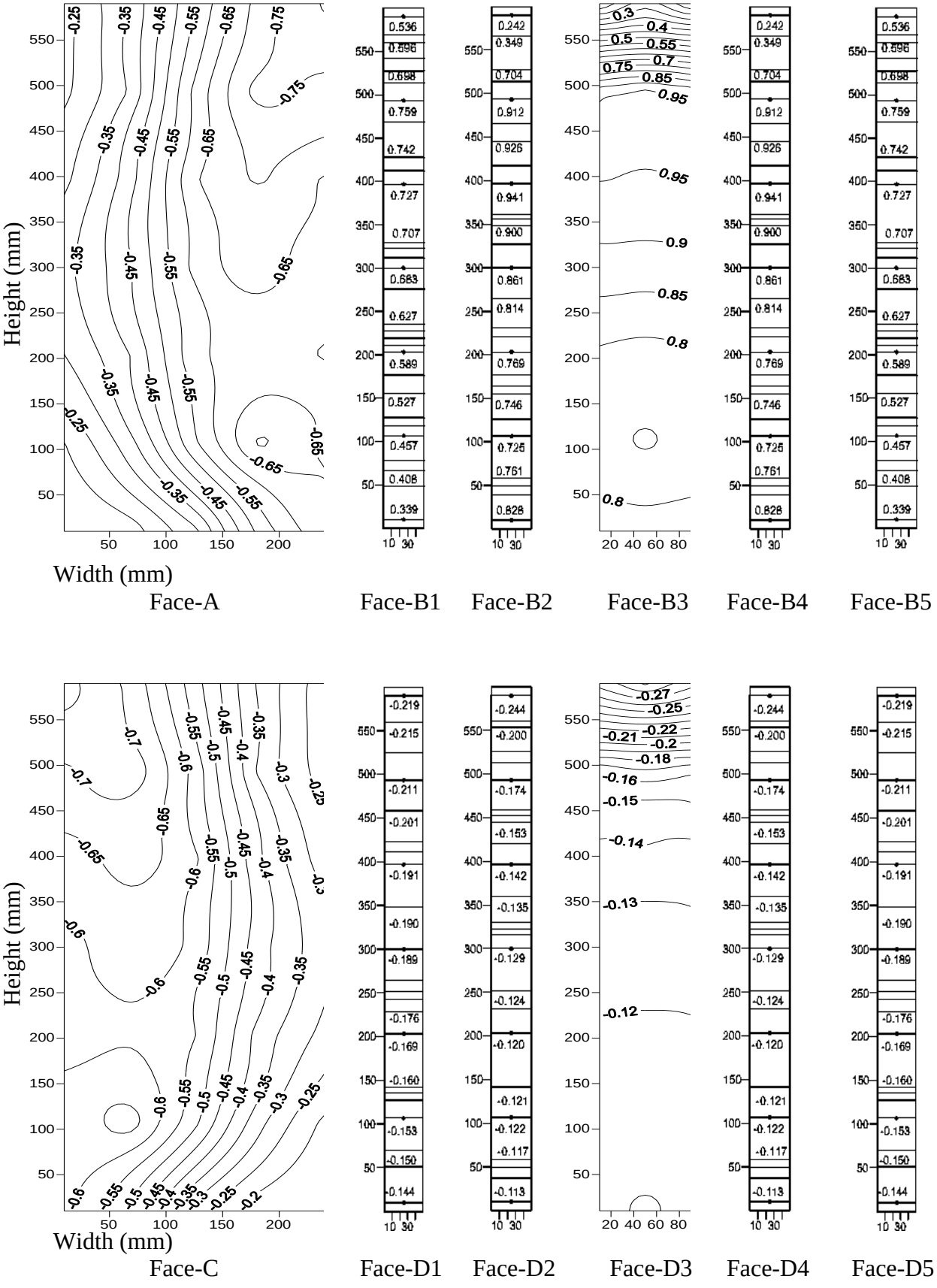


**Fig. 5.32 Distribution of mean wind pressure coefficients ($C_{p,mean}$) on different surfaces of model-D at $90^0$ wind incidence angle**

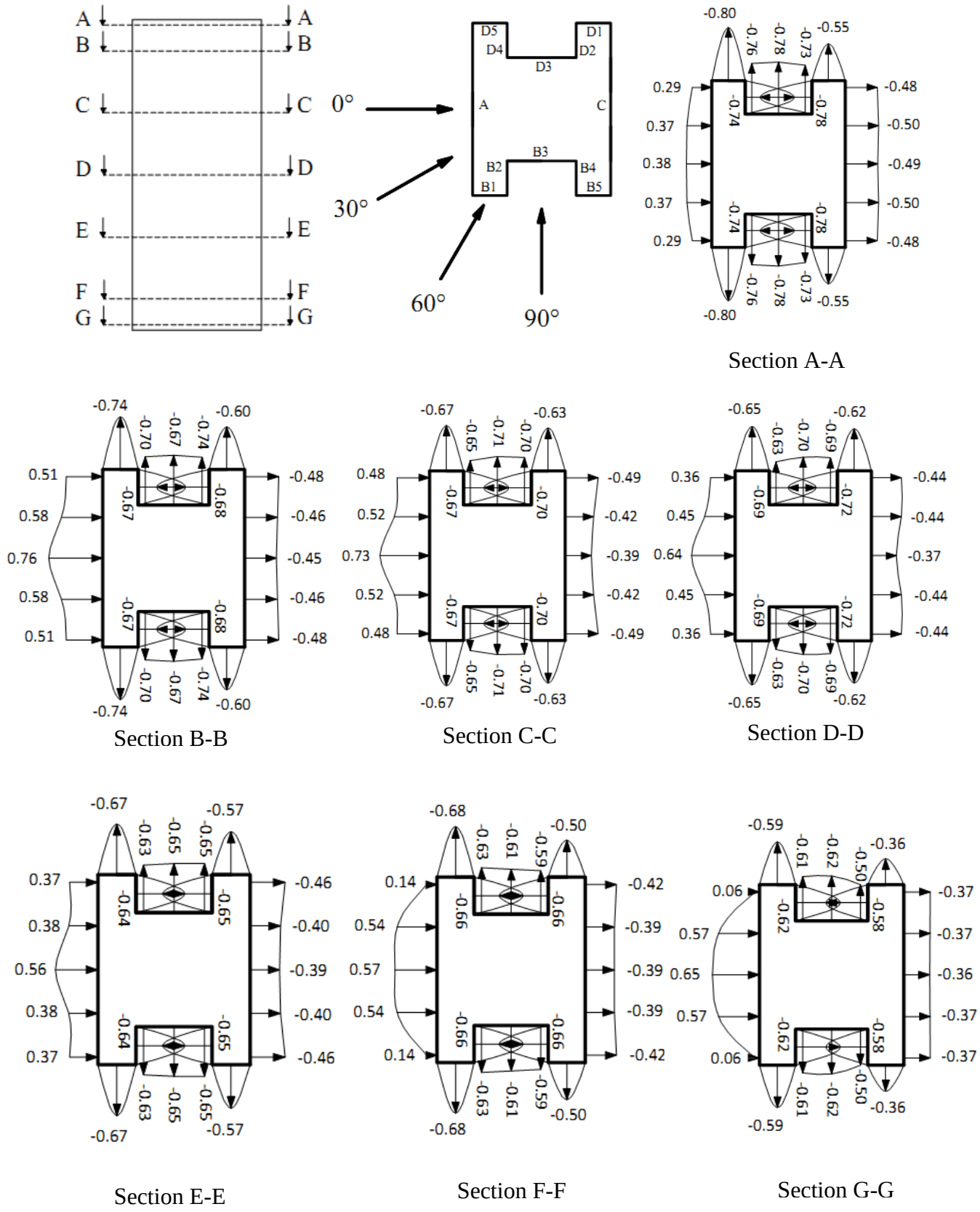


**Fig. 5.33 Cross-sectional variation of mean wind pressure coefficients ($C_{p,mean}$) on model-D at $0^0$ wind incidence angle**

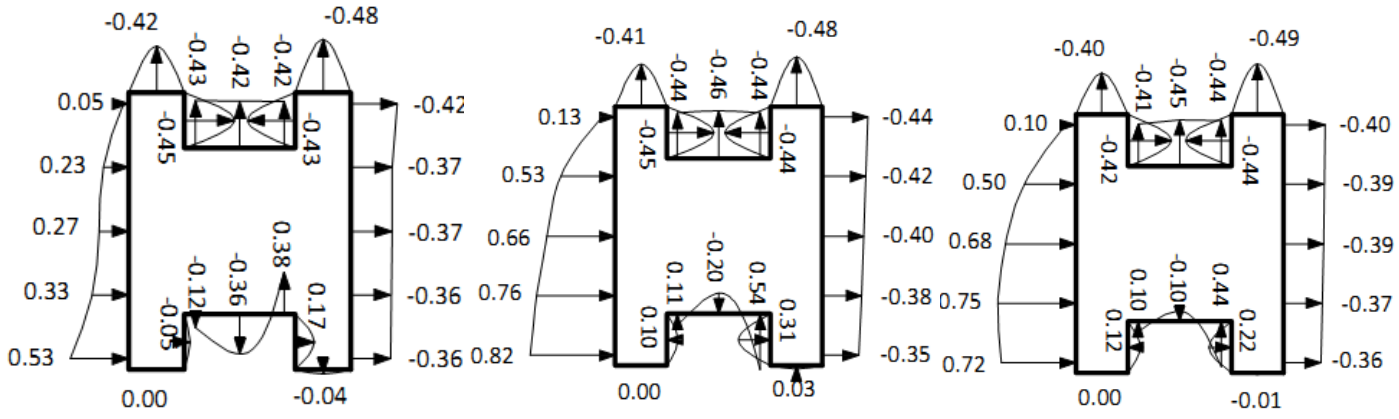


Section A-A Section B-B Section C-C

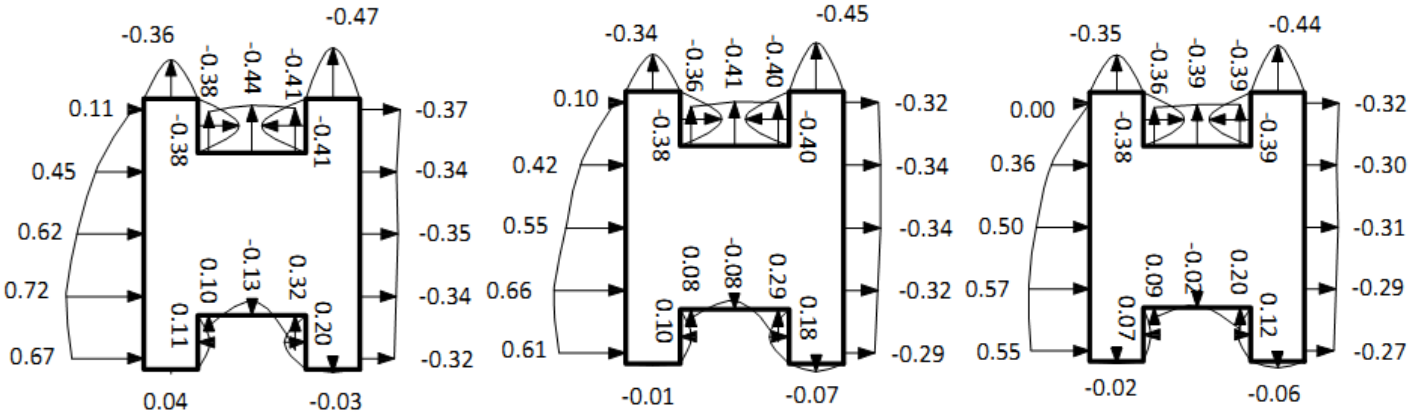


Section D-D Section E-E Section F-F

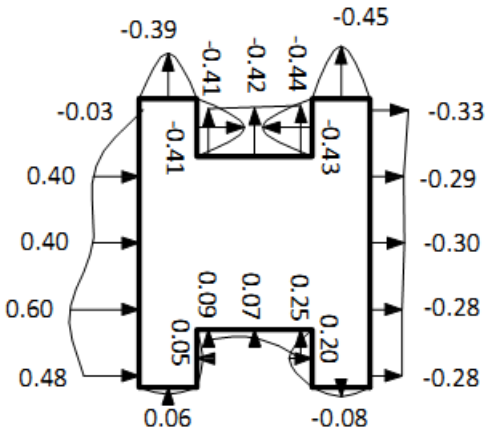


Section G-G

**Fig. 5.34 Cross-sectional variation of mean wind pressure coefficients ($C_{p,mean}$) on model-D at $30^0$ wind incidence angle**

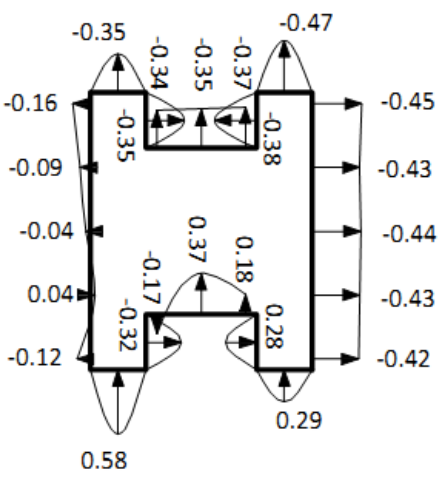


Section A-A

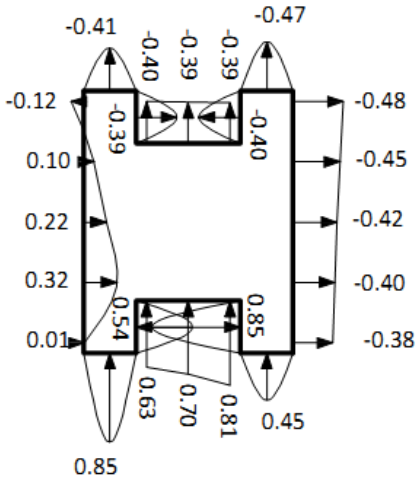


Section B-B

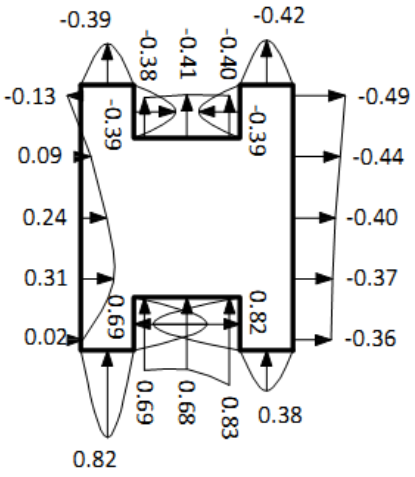


Section C-C

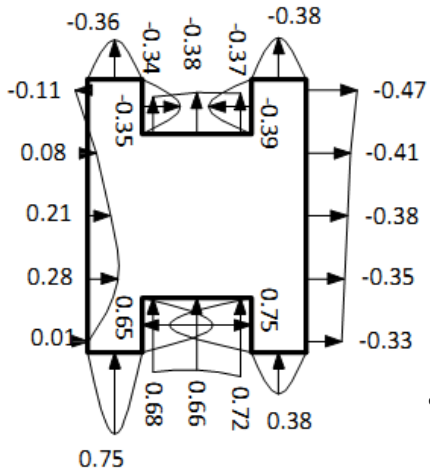


Section D-D

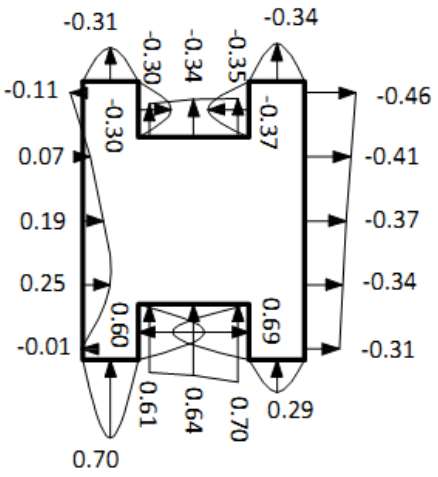


Section E-E

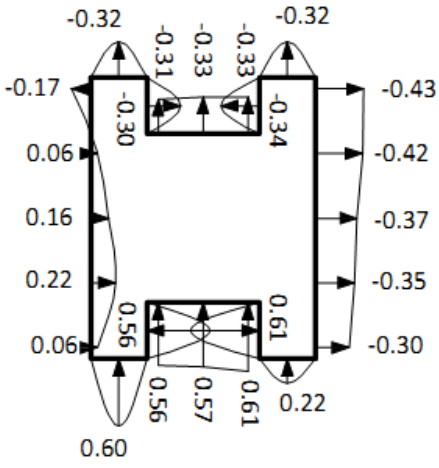


Section F-F

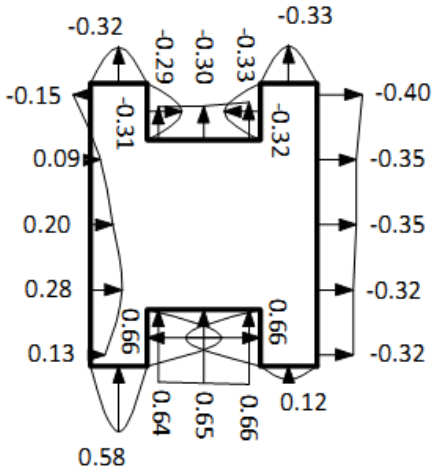


Section G-G

**Fig. 5.35 Cross-sectional variation of mean wind pressure coefficients ($C_{p,mean}$) on model-D at $60^0$ wind incidence angle**

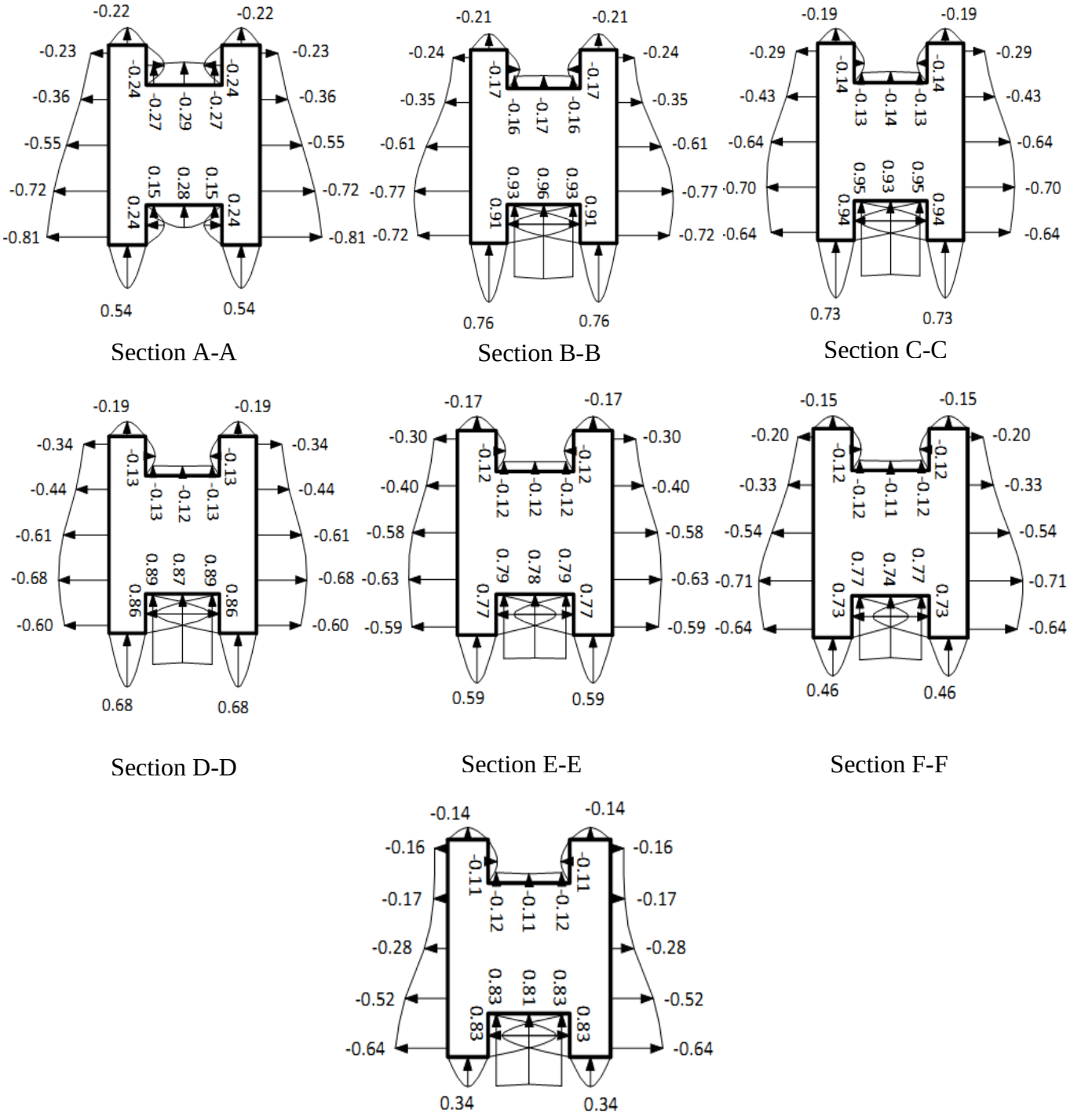


**Fig. 5.36 Cross-sectional variation of mean wind pressure coefficients ($C_{p,mean}$) on model-D at $90^0$ wind incidence angle**

Comparison of $C_{p,mean}$ values at 35 pressure points on face-A of model-D at 7 wind incidence angles are shown in Table 5.5. It is noticed that the face A is subjected to maximum pressure of $C_{p,mean}$ = 0.82 at $30^0$ and minimum pressure of $C_{p,mean}$ = -0.81 at $90^0$.

**Table 5.5 Variation of $C_{p,mean}$ on Face-A for Difference wind incidence angle of building model-D**

| Pressure points | Mean Pressure Coefficients ($C_{p,mean}$) | | | |
|---|---|---|---|---|
| | $0^0$ | $30^0$ | $60^0$ | $90^0$ |
| 1 | 0.29 | 0.05 | -0.16 | -0.23 |
| 2 | 0.37 | 0.23 | -0.09 | -0.36 |
| 3 | 0.38 | 0.27 | -0.04 | -0.55 |
| 4 | 0.37 | 0.33 | 0.04 | -0.72 |
| 5 | 0.29 | 0.53 | -0.12 | **-0.81** |
| 6 | 0.51 | 0.13 | -0.12 | -0.24 |
| 7 | 0.58 | 0.53 | 0.10 | -0.35 |
| 8 | **0.76** | 0.66 | 0.22 | -0.61 |
| 9 | 0.58 | 0.76 | **0.32** | -0.77 |
| 10 | 0.51 | **0.82** | 0.01 | -0.72 |
| 11 | 0.48 | 0.10 | -0.13 | -0.29 |
| 12 | 0.52 | 0.50 | 0.09 | -0.43 |
| 13 | 0.73 | 0.68 | 0.24 | -0.64 |
| 14 | 0.52 | 0.75 | 0.31 | -0.70 |
| 15 | 0.48 | 0.72 | 0.02 | -0.64 |
| 16 | 0.36 | 0.11 | -0.11 | -0.34 |
| 17 | 0.45 | 0.45 | 0.08 | -0.44 |
| 18 | 0.64 | 0.62 | 0.21 | -0.61 |
| 19 | 0.45 | 0.72 | 0.28 | -0.68 |
| 20 | 0.36 | 0.67 | 0.01 | -0.60 |
| 21 | 0.37 | 0.10 | -0.11 | -0.30 |
| 22 | 0.38 | 0.42 | 0.07 | -0.40 |
| 23 | 0.56 | 0.55 | 0.19 | -0.58 |
| 24 | 0.38 | 0.66 | 0.25 | -0.63 |
| 25 | 0.37 | 0.61 | -0.01 | -0.59 |
| 26 | 0.14 | 0.00 | **-0.17** | -0.20 |
| 27 | 0.54 | 0.36 | 0.06 | -0.33 |
| 28 | 0.57 | 0.50 | 0.16 | -0.54 |
| 29 | 0.54 | 0.57 | 0.22 | -0.71 |
| 30 | 0.14 | 0.55 | 0.06 | -0.64 |
| 31 | **0.06** | **-0.03** | -0.15 | **-0.16** |
| 32 | 0.57 | 0.40 | 0.09 | -0.17 |
| 33 | 0.65 | 0.40 | 0.20 | -0.28 |
| 34 | 0.57 | 0.60 | 0.28 | -0.52 |
| 35 | 0.06 | 0.48 | 0.13 | -0.64 |

### 5.2.5 Model-F (Fish Shape-1)

The experimental results for the building model-F for 7 wind incidence angle (Fig. 5.37) are presented in this article. Mean wind pressure distribution on building model surfaces are shown in Fig. 5.38 to 5.44 at seven wind incidence angles from $0^0$ to $180^0$ at the interval of $30^0$.

Cross-sectional variation of $C_{p,mean}$ on model-F is shown in Figs. 5.45 to 5.51. It is noticed that at $0^0$ wind incidence angle, on windward side all surfaces perpendicular to wind are subjected to pressure, whereas surfaces parallel to wind are subjected to suction. As wind incidence angle increases, pressure on many surfaces becomes suction. Largest face (face-I) is subjected to suction from $0^0$ to $90^0$ angles beyond which it is subjected to pressure with maximum value of pressure ($C_{p,mean}$ = 0.67) at $180^0$ angle. At this angle, all other surfaces of the model are subjected to suction.

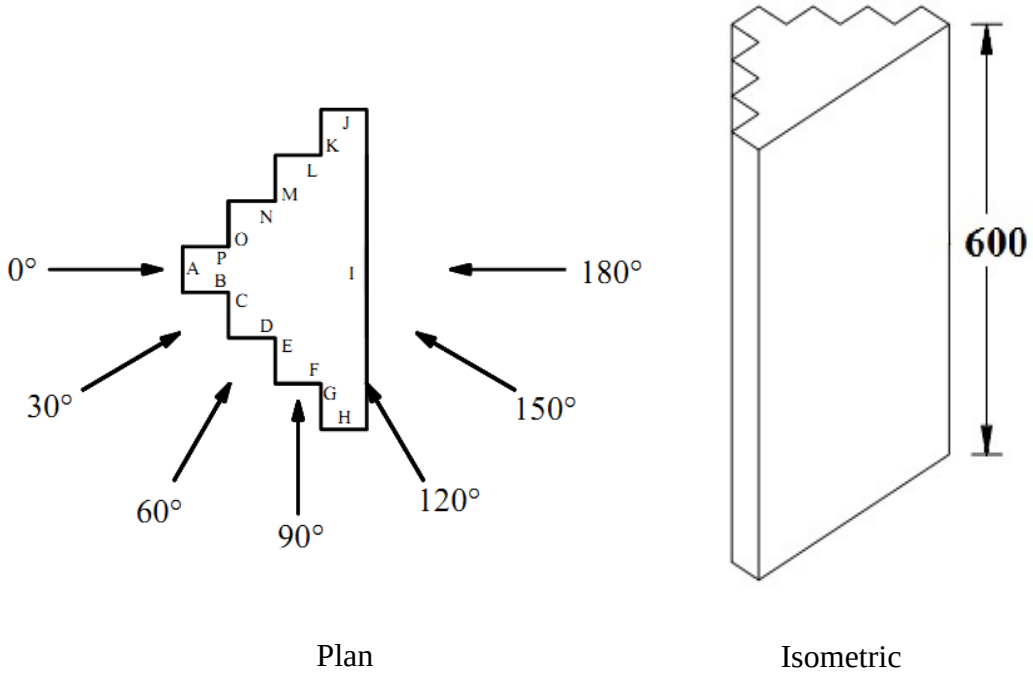


Plan Isometric

**Fig. 5.37 Wind incidence angles on Perspex sheet model of model-F in isolated condition**

(All dimensions are in mm)

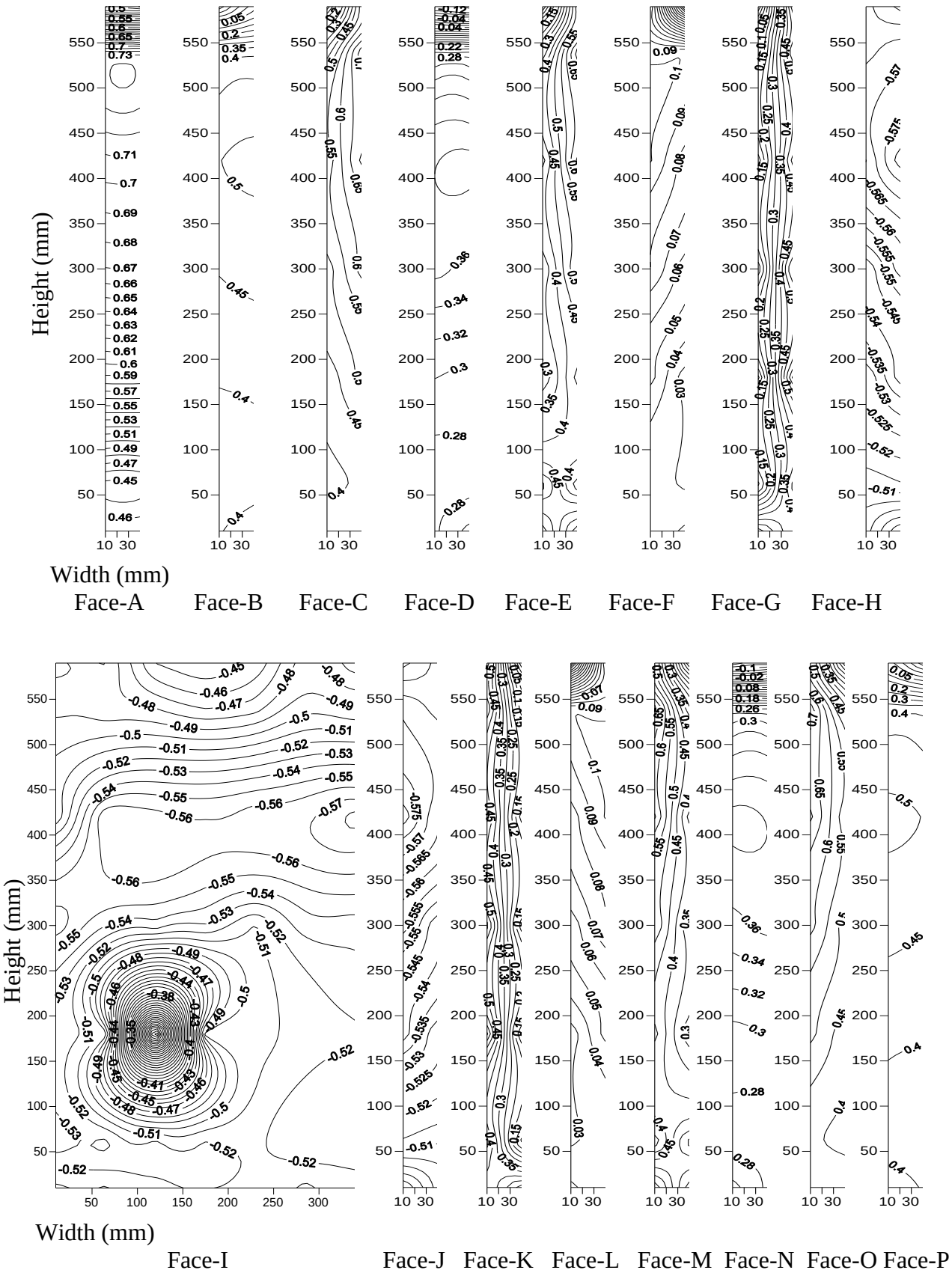


**Fig. 5.38 Distribution of mean wind pressure coefficients ($C_{p,mean}$) on different surfaces of model-F at $0^0$ wind incidence angle**

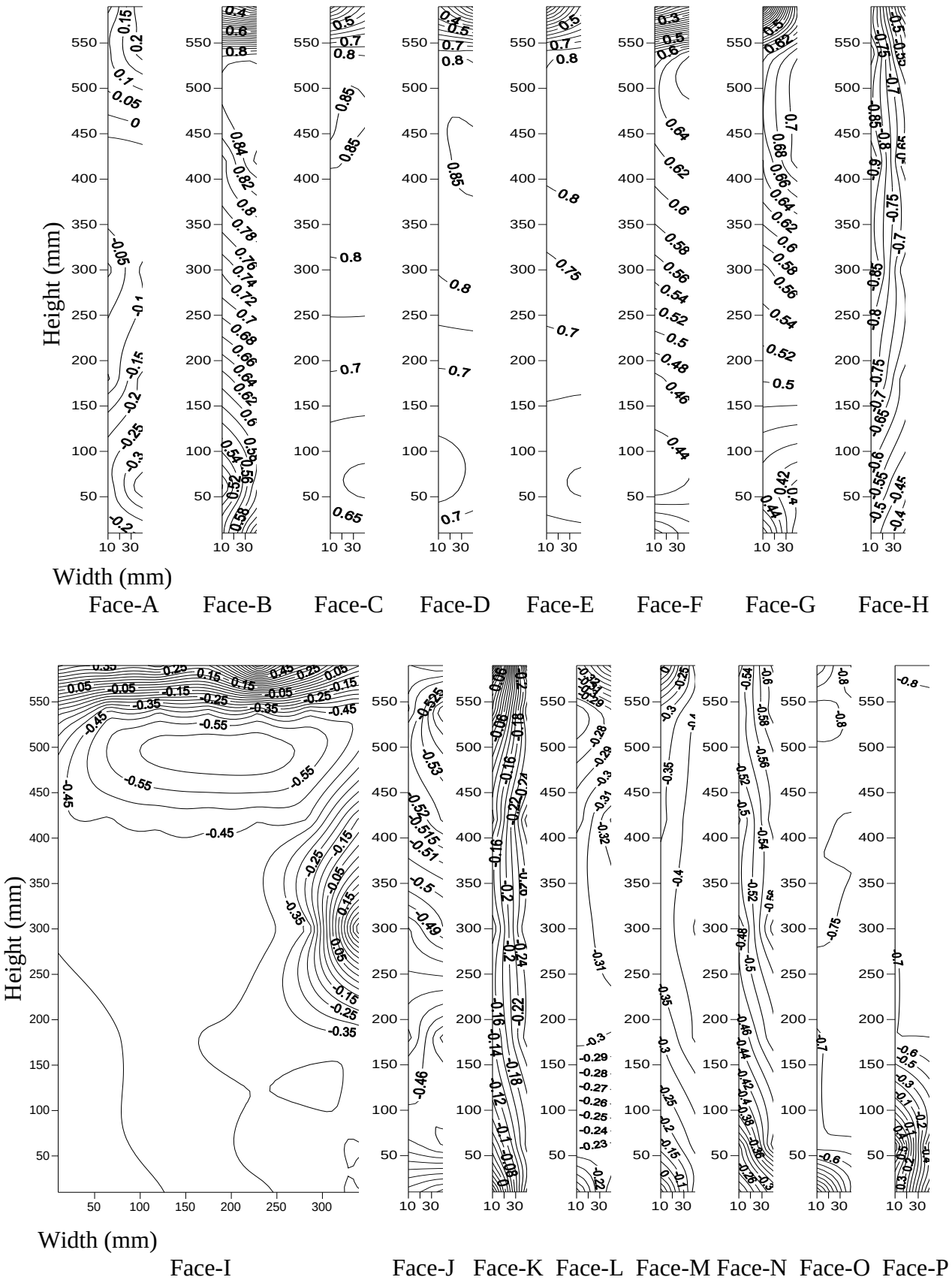


**Fig. 5.39 Distribution of mean wind pressure coefficients ($C_{p,mean}$) on different surfaces of model-F at $30^0$ wind incidence angle**

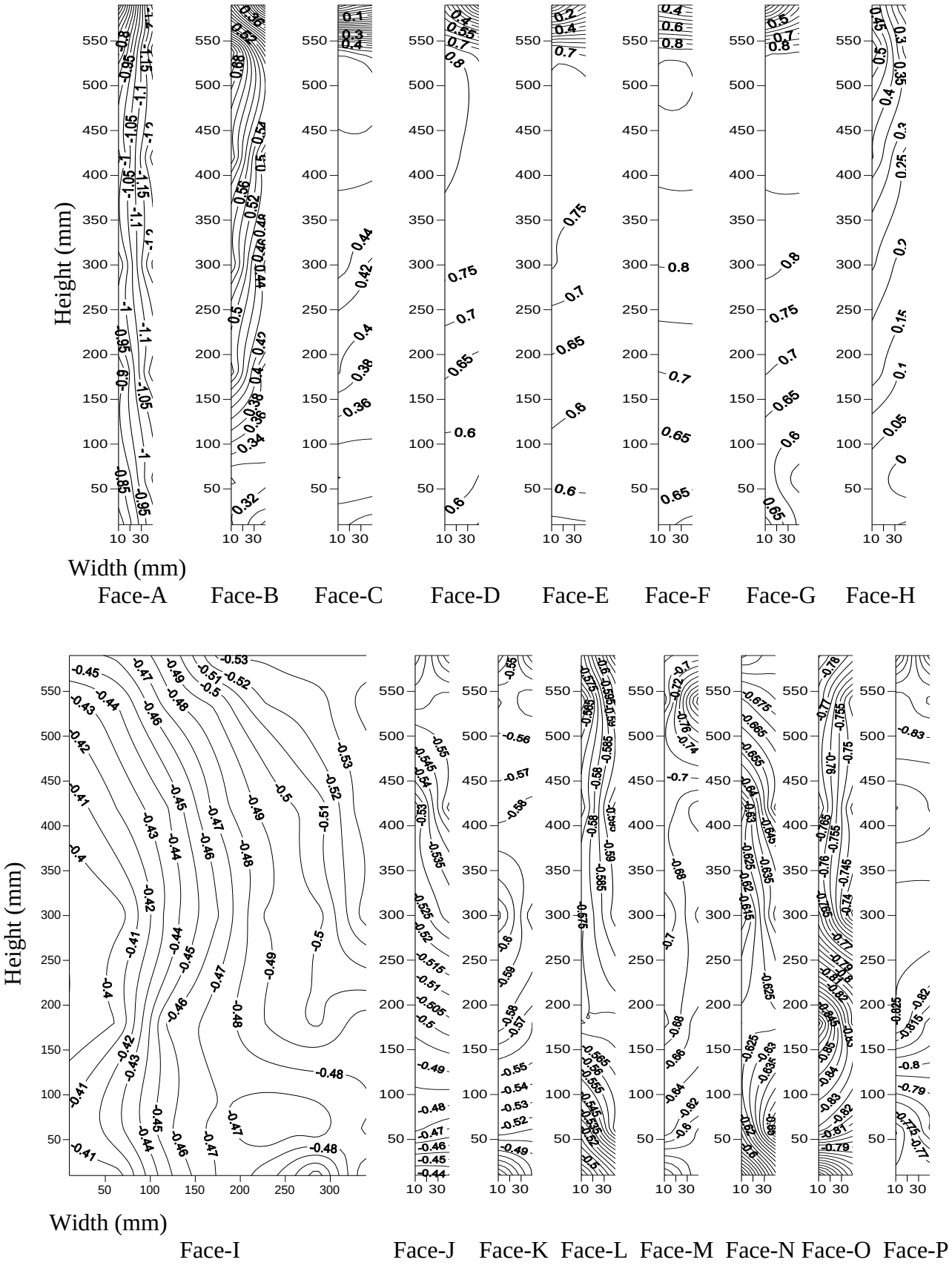


**Fig. 5.40 Distribution of mean wind pressure coefficients ($C_{p,mean}$) on different surfaces of model-F at $60^0$ wind incidence angle**

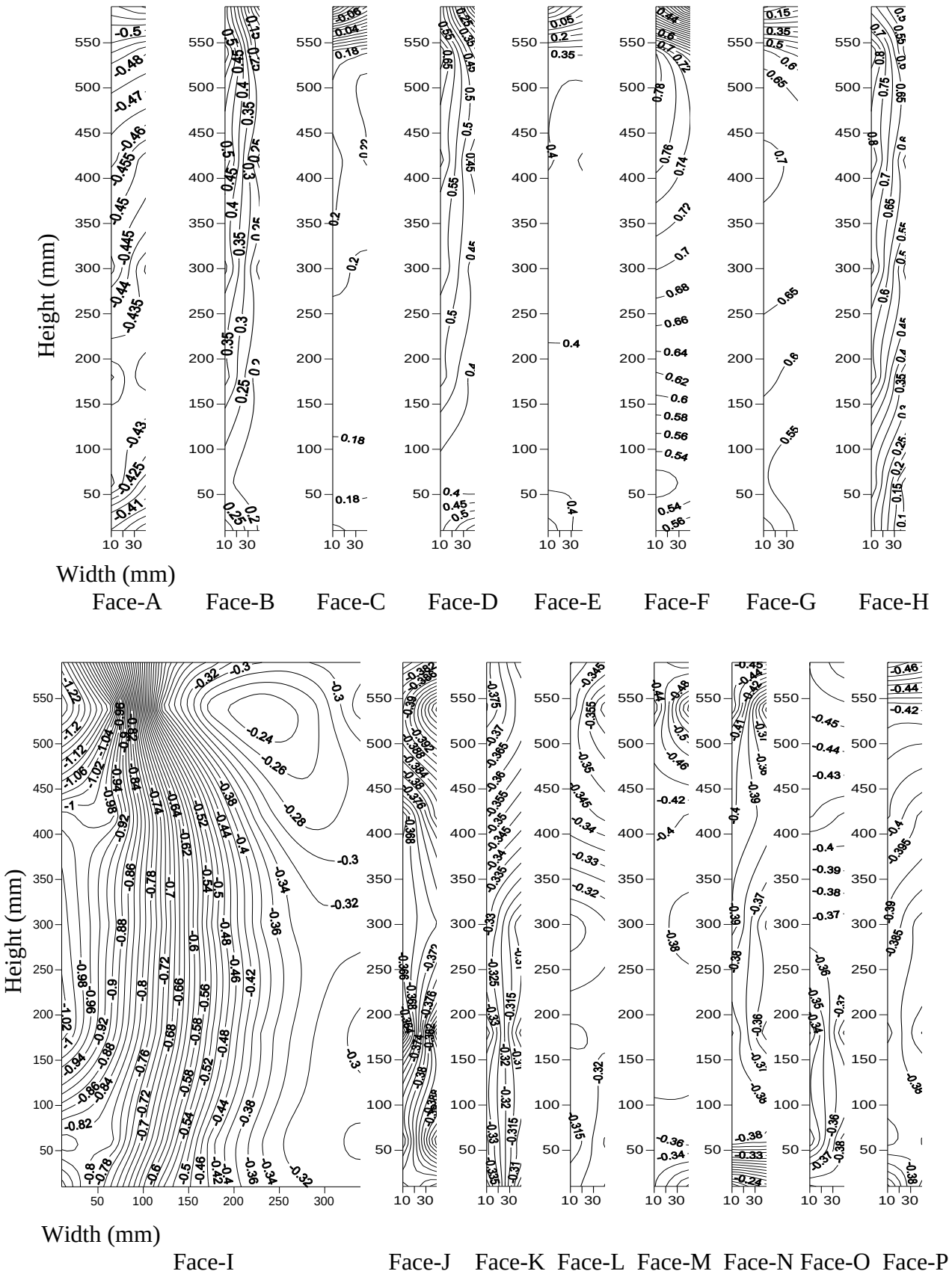


**Fig. 5.41 Distribution of mean wind pressure coefficients ($C_{p,mean}$) on different surfaces of model-F at $90^0$ wind incidence angle**

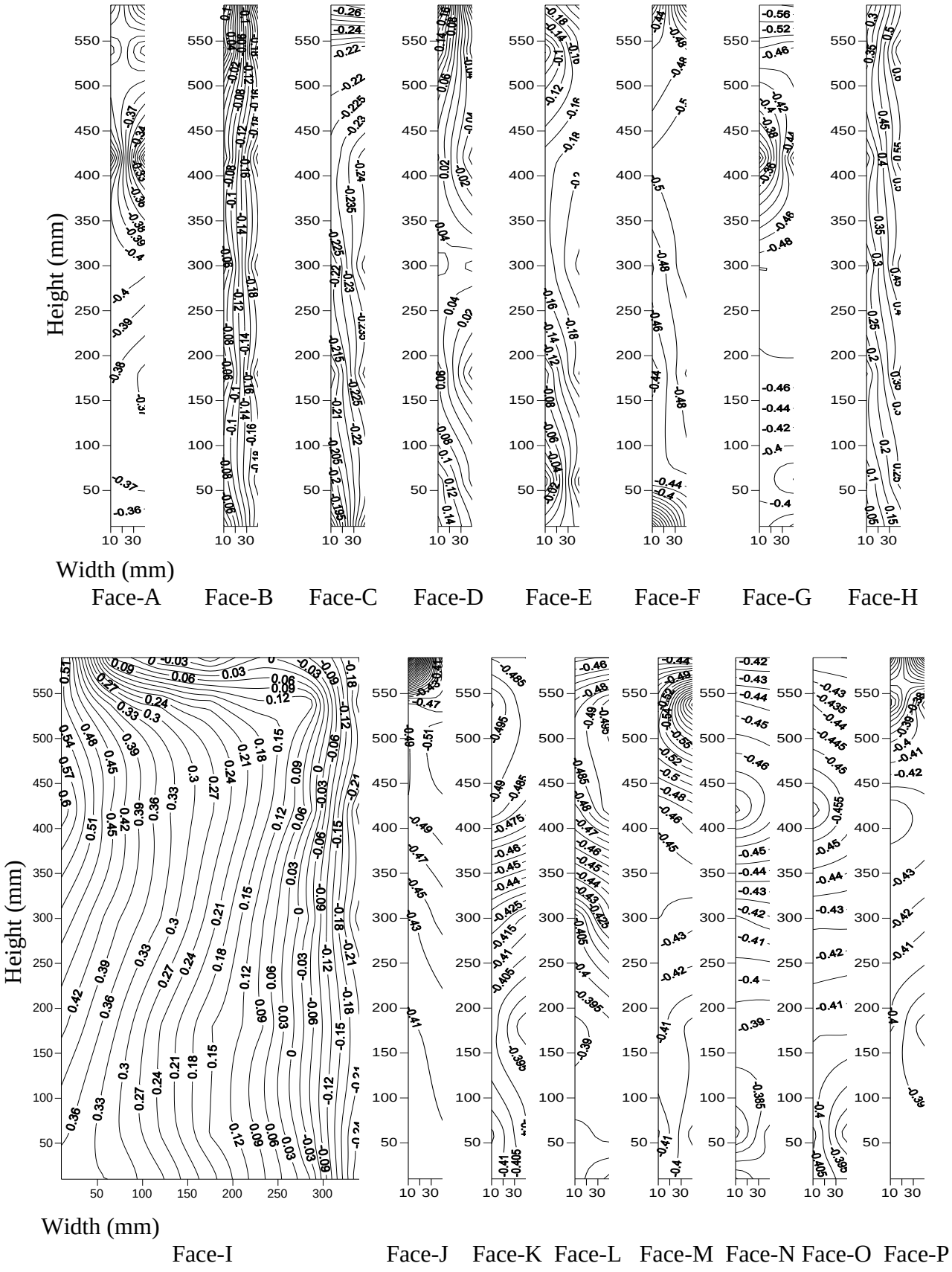


**Fig. 5.42 Distribution of mean wind pressure coefficients ($C_{p,mean}$) on different surfaces of model-F at $120^0$ wind incidence angle**

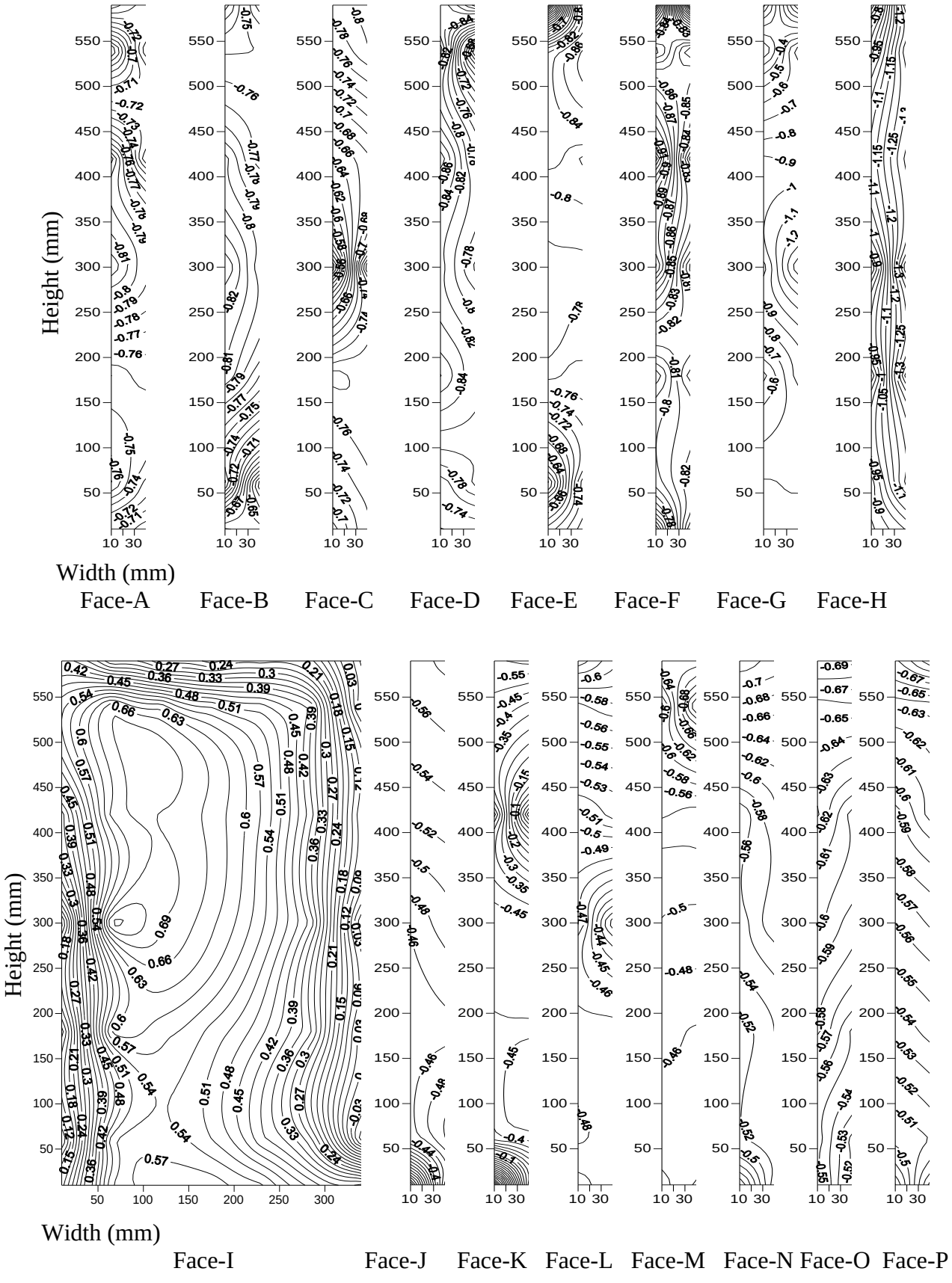


**Fig. 5.43 Distribution of mean wind pressure coefficients ($C_{p,mean}$) on different surfaces of model-F at $150^0$ wind incidence angle**

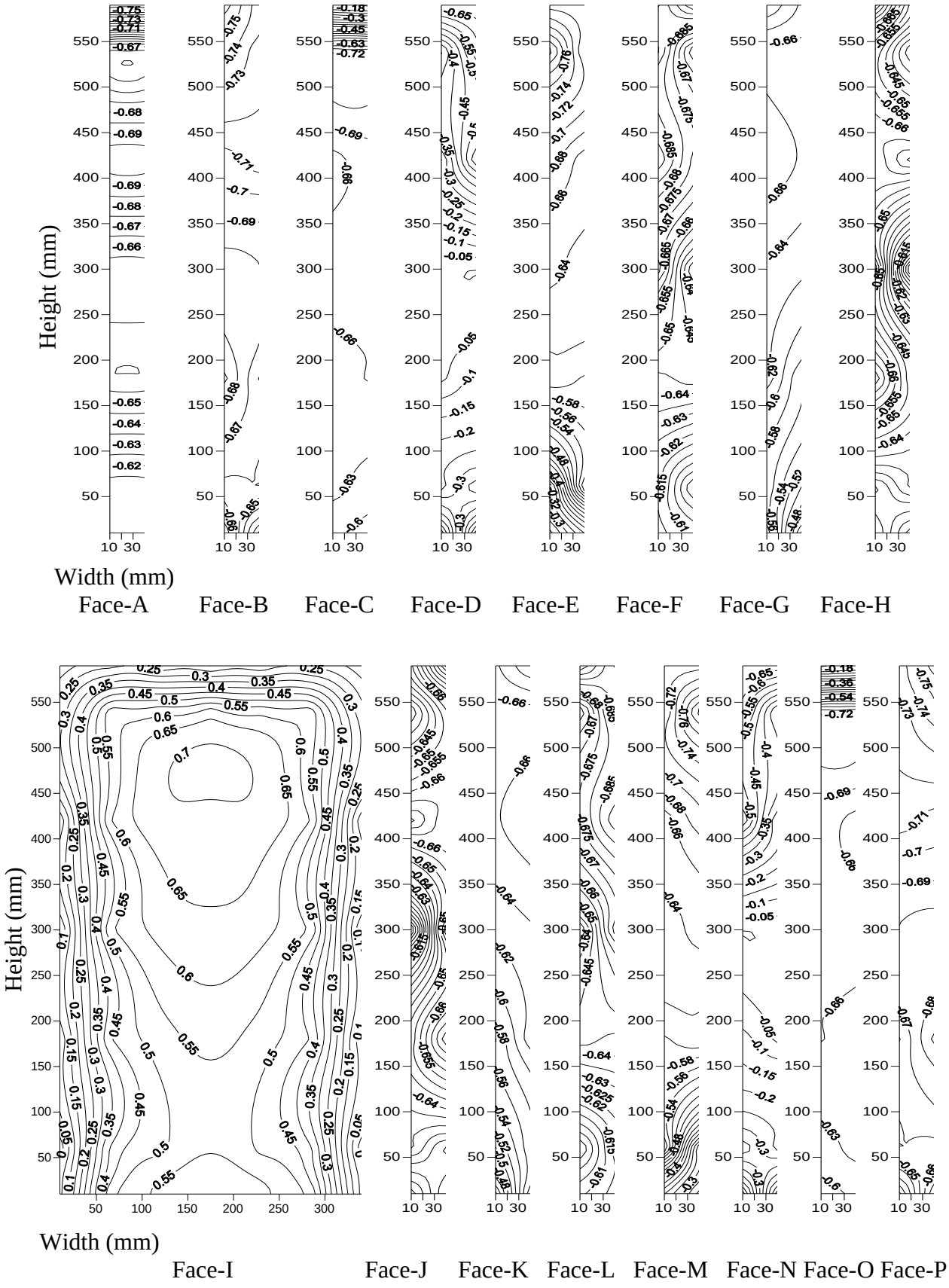


**Fig. 5.44 Distribution of mean wind pressure coefficients ($C_{p,mean}$) on different surfaces of model-F at $180^0$ wind incidence angle**

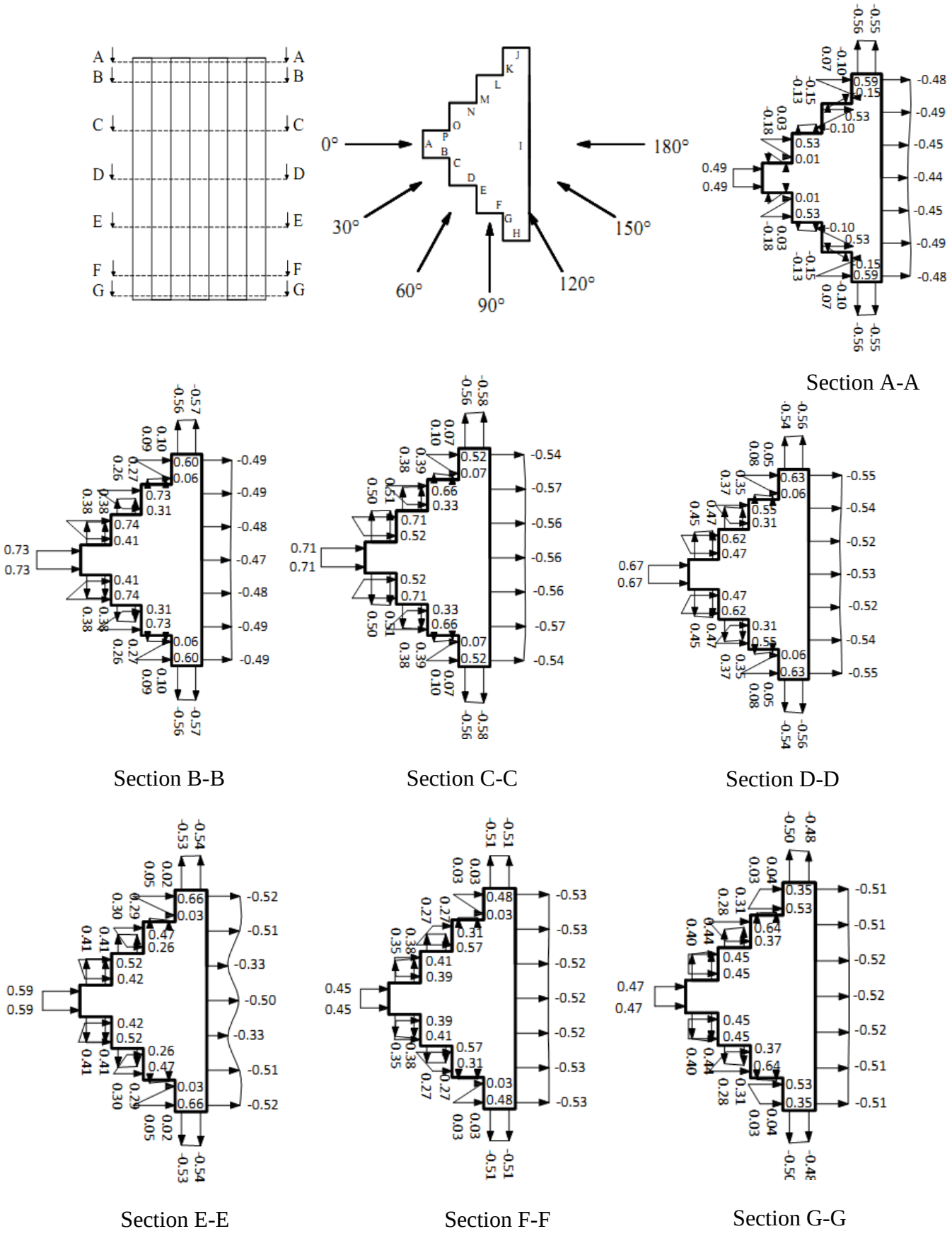


**Fig. 5.45 Cross-sectional variation of mean wind pressure coefficients ($C_{p,mean}$) model-F at $0^0$ wind incidence angle**

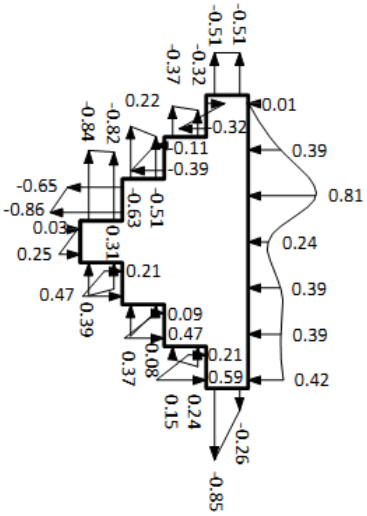


Section A-A

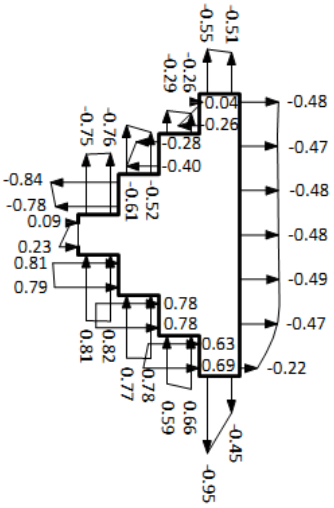


Section B-B

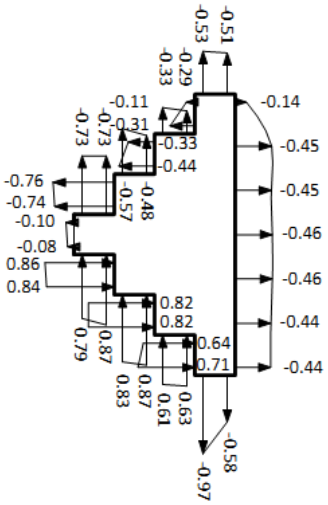


Section C-C

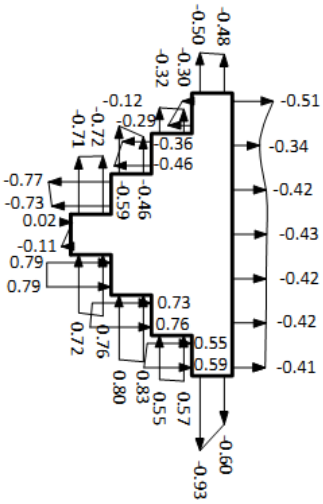


Section D-D

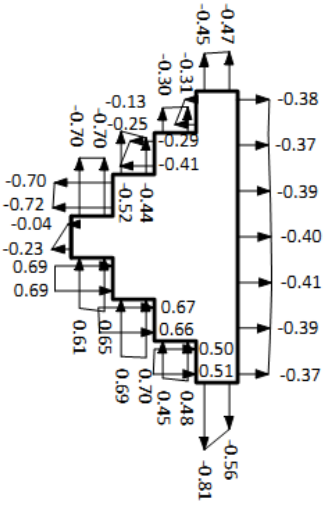


Section E-E

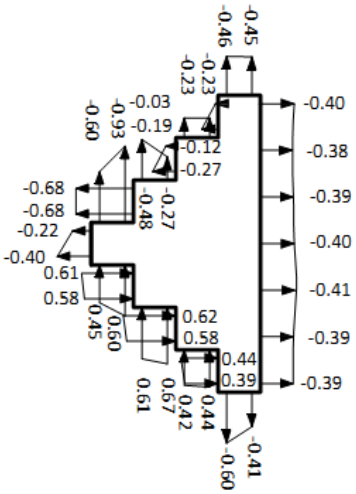


Section F-F

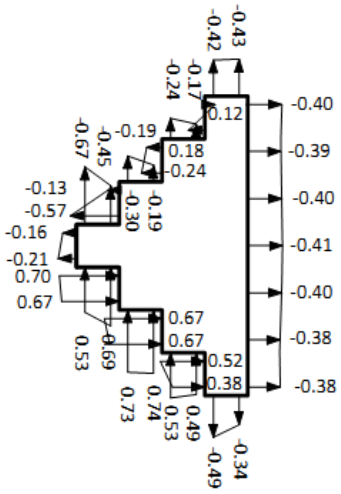


Section G-G

**Fig. 5.46 Cross-sectional variation of mean wind pressure coefficients ($C_{p,mean}$) model-F at $30^0$ wind incidence angle**

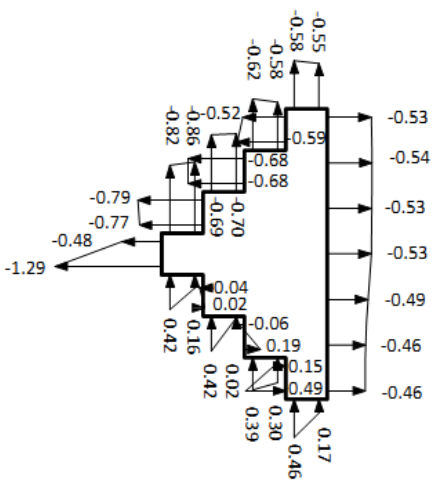

Section A-A

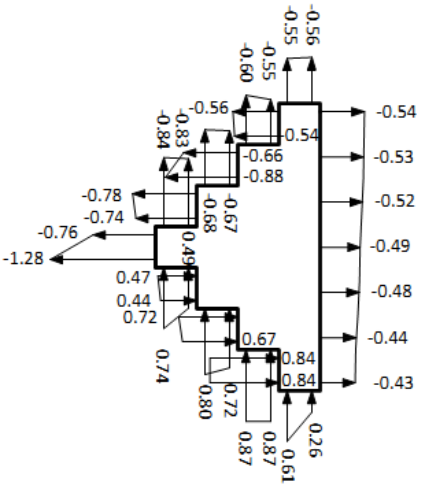

Section B-B

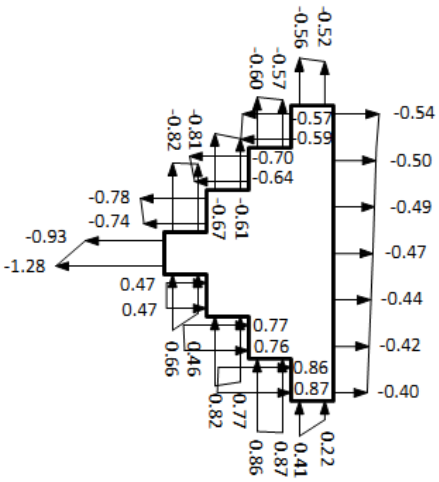

Section C-C

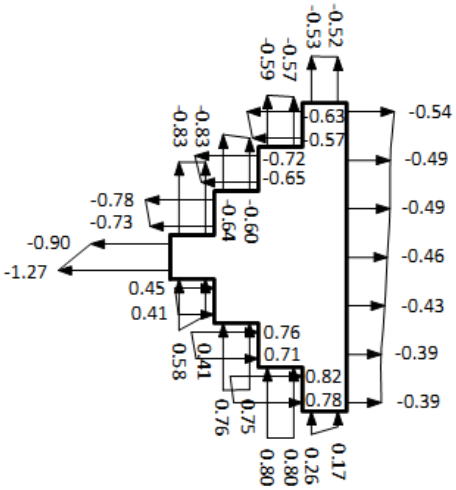

Section D-D

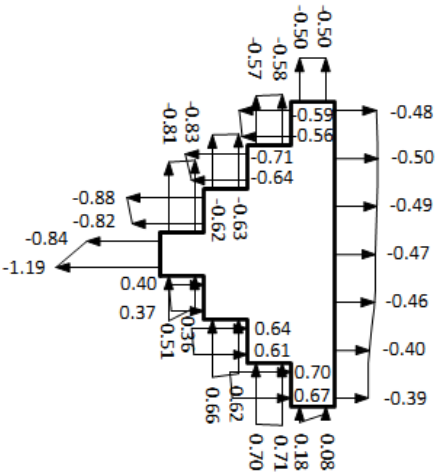

Section E-E

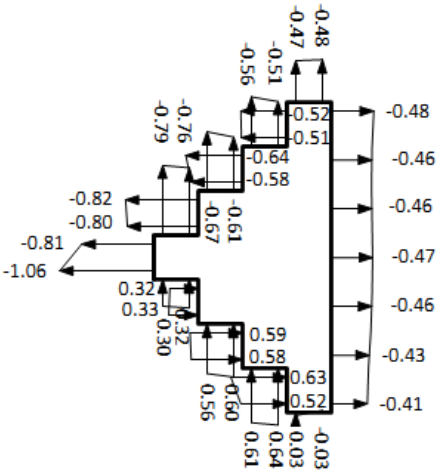

Section F-F

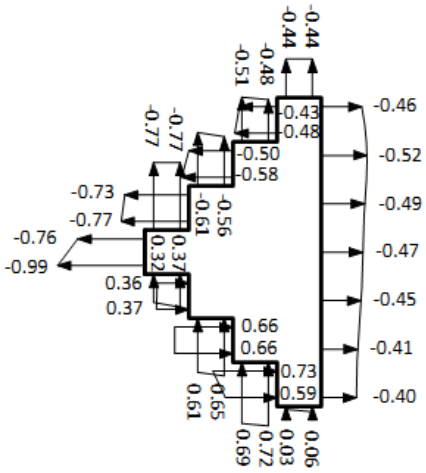

Section G-G

**Fig. 5.47 Cross-sectional variation of mean wind pressure coefficients ($C_{p,mean}$) model-F at $60^0$ wind incidence angle**

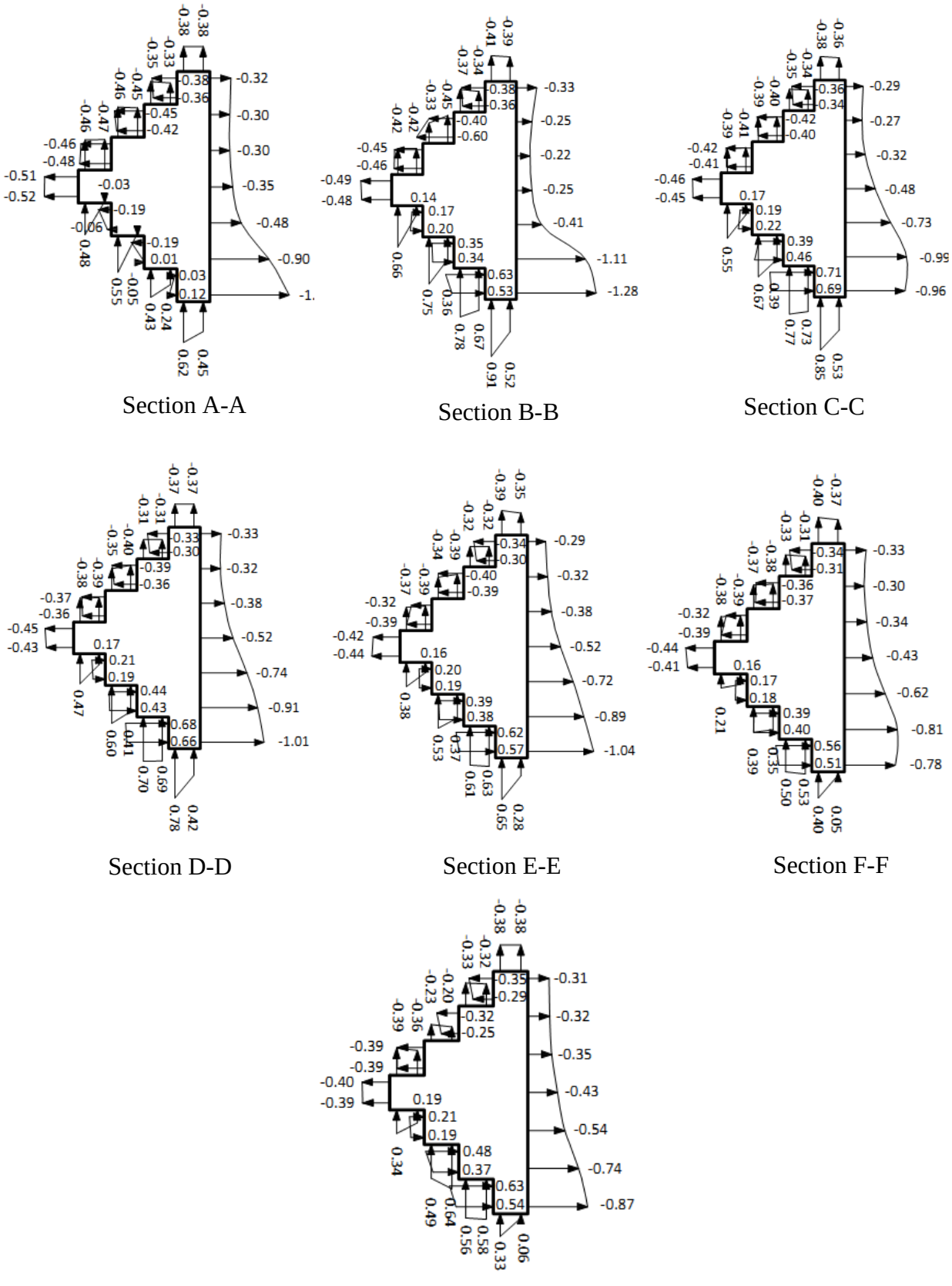


**Fig. 5.48 Cross-sectional variation of mean wind pressure coefficients ($C_{p,mean}$) model-F at $90^0$ wind incidence angle**

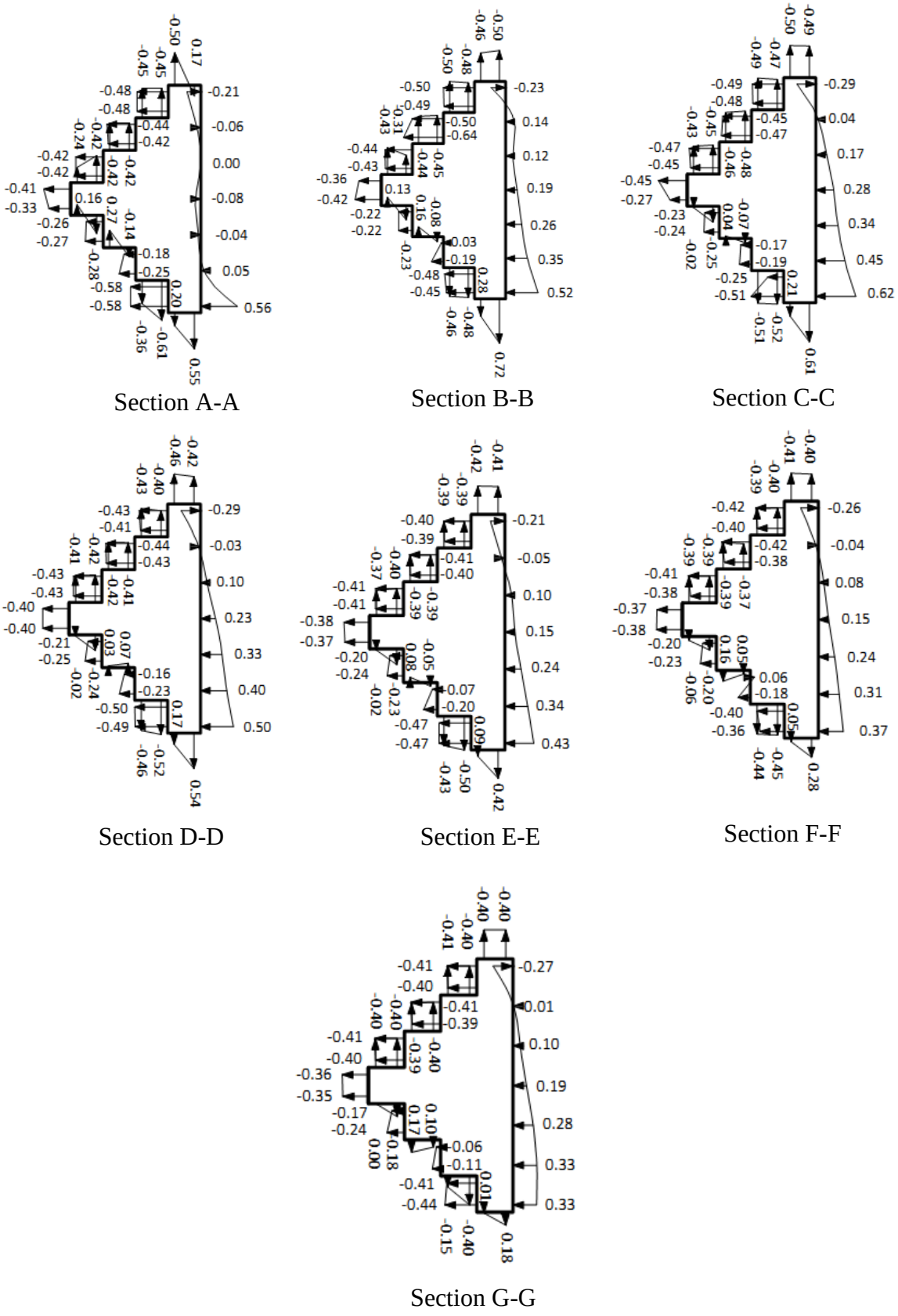


**Fig. 5.49 Cross-sectional variation of mean wind pressure coefficients ($C_{p,mean}$) model-F at $120^0$ wind incidence angle**

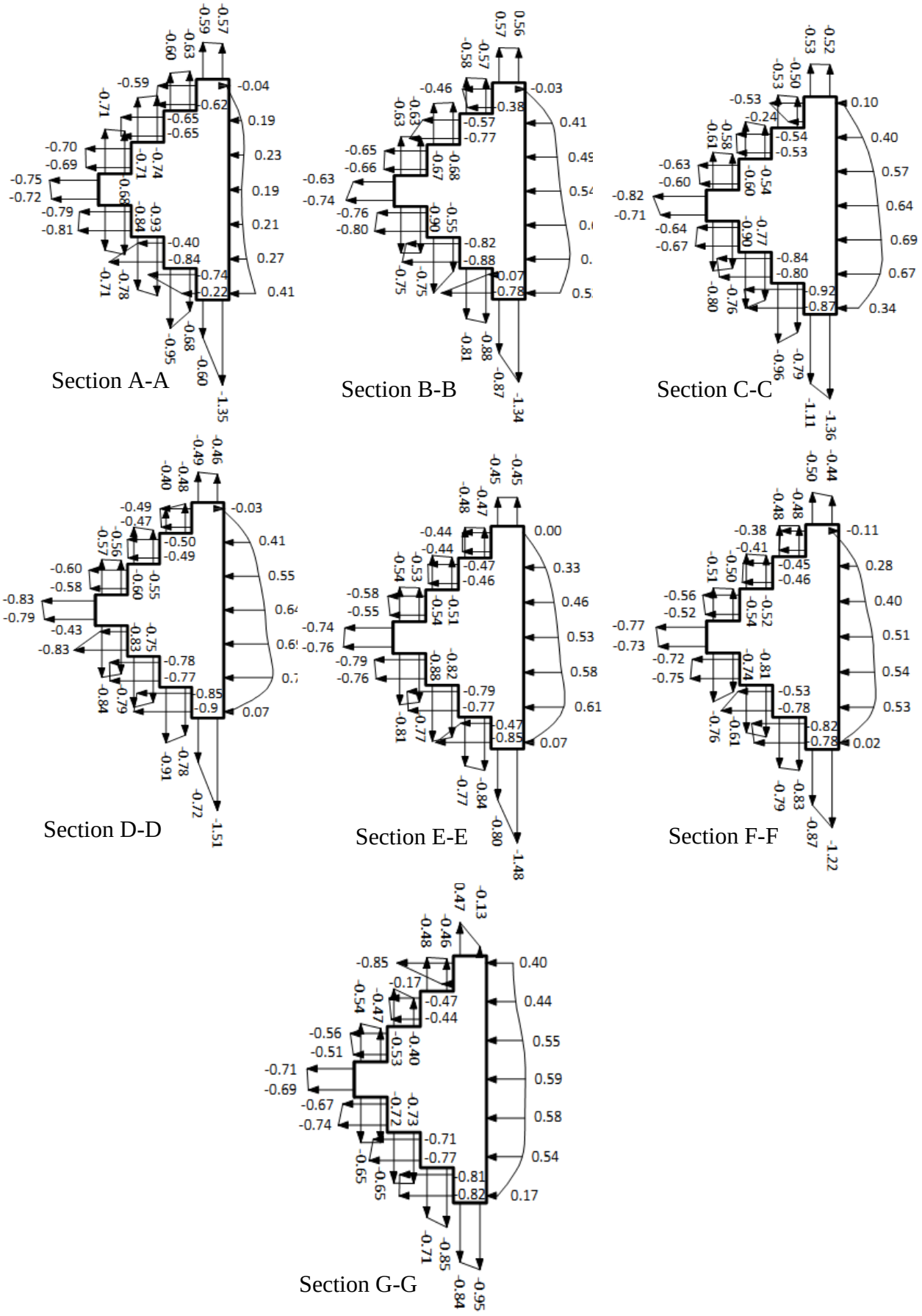


**Fig. 5.50 Cross-sectional variation of mean wind pressure coefficients ($C_{p,mean}$) model-F at $150^0$ wind incidence angle**

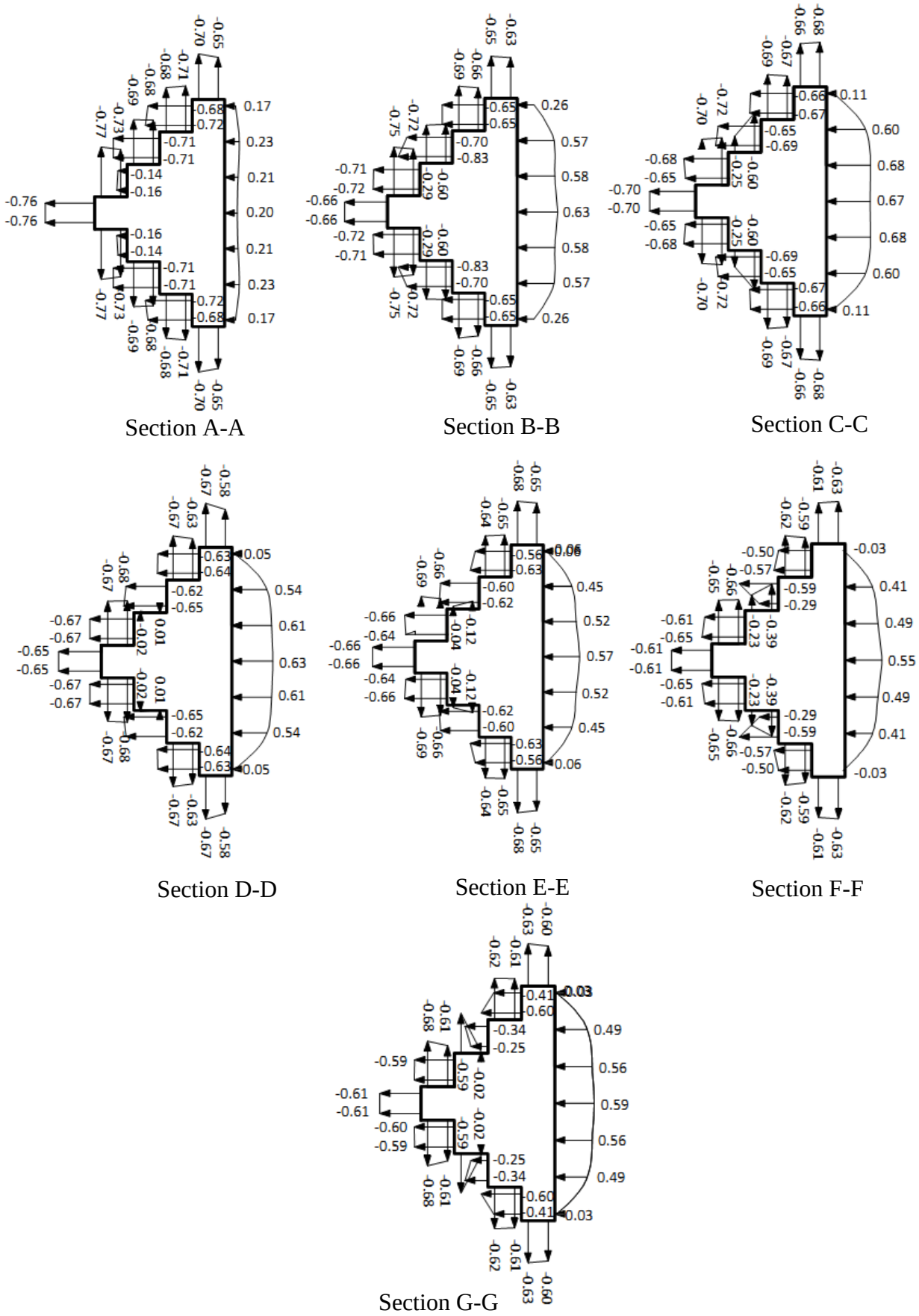


**Fig. 5.51 Cross-sectional variation of mean wind pressure coefficients ($C_{p,mean}$) model-F at $180^0$ wind incidence angle**

Comparison of $C_{p,mean}$ values at 14 pressure points on face-A of model-F at 7 wind incidence angles are shown in Table 5.6. it is noticed that the face A is subjected to maximum pressure of $C_{p,mean}$ = 0.73 at $0^0$ and minimum pressure of $C_{p,mean}$ = -1.29.

**Table 5.6 Variation of $C_{p,mean}$ on face-A of model-F with wind incidence angle**

| **Pressure points** | **Mean wind pressure coefficients ($C_{p,mean}$)** | | | | | | |
|---|---|---|---|---|---|---|---|
| | **$0^0$** | **$30^0$** | **$60^0$** | **$90^0$** | **$120^0$** | **$150^0$** | **$180^0$** |
| 1 | 0.49 | 0.03 | -0.48 | -0.51 | -0.41 | -0.75 | **-0.77** |
| 2 | 0.49 | **0.25** | **-1.29** | **-0.52** | -0.33 | -0.72 | -0.75 |
| 3 | **0.73** | 0.09 | -0.76 | -0.49 | -0.36 | -0.63 | -0.60 |
| 4 | **0.73** | 0.23 | -1.28 | -0.48 | -0.42 | -0.74 | -0.72 |
| 5 | 0.71 | -0.10 | -0.93 | -0.46 | **-0.45** | -0.82 | -0.70 |
| 6 | 0.71 | -0.08 | -1.28 | -0.45 | -0.27 | -0.71 | -0.70 |
| 7 | 0.67 | 0.02 | -0.90 | -0.45 | -0.40 | **-0.83** | -0.65 |
| 8 | 0.67 | -0.11 | -1.27 | -0.43 | -0.40 | -0.79 | -0.65 |
| 9 | 0.59 | -0.04 | -0.84 | -0.42 | -0.38 | -0.74 | -0.66 |
| 10 | 0.59 | -0.23 | -1.19 | -0.44 | -0.37 | -0.76 | -0.66 |
| 11 | 0.45 | -0.22 | -0.81 | -0.44 | -0.37 | -0.77 | -0.59 |
| 12 | 0.45 | **-0.40** | -1.06 | -0.41 | -0.38 | -0.73 | -0.63 |
| 13 | 0.47 | -0.16 | -0.76 | -0.40 | -0.36 | -0.71 | -0.65 |
| 14 | 0.47 | -0.21 | -0.99 | -0.39 | -0.35 | -0.69 | 0.00 |

### 5.2.6 Model-G (Fish Shape-2)

The experimental results for the building model-G for 7 wind direction are given in the present article. Distribution of mean wind pressure coefficients on various surfaces of building model are shown in Figs. 5.53 to 5.59 at various angle of wind attack.

Cross-sectional variations of pressures are shown in Figs 5.60 to 5.66. Except face-I, wind pressure distribution on model-G is similar to that of model-F. Face-I is subjected to slightly larger pressure at $180^0$ wind incidence angle in case of model-G as compared to model-F due to the fact that air is entrapped between the fins in model-G.

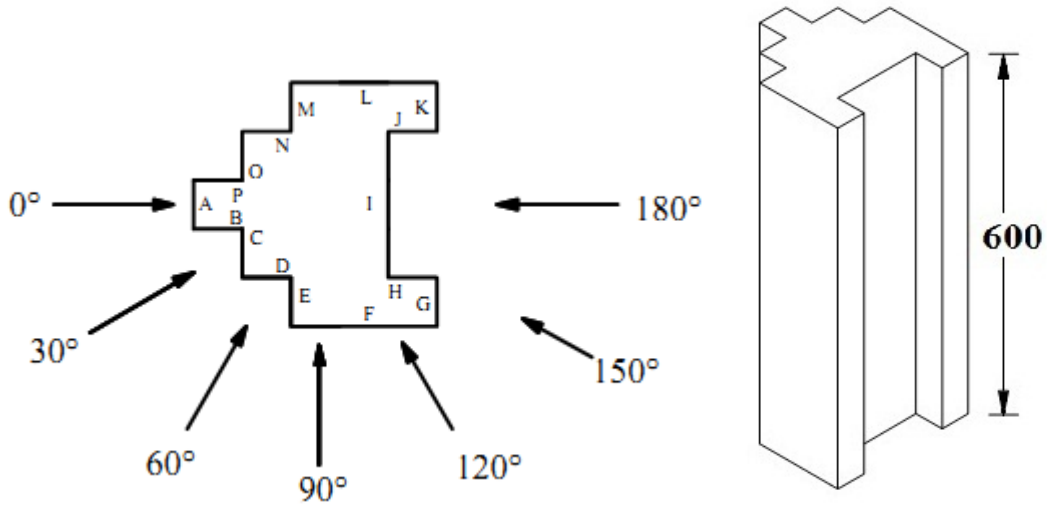


Plan Isometric

**Fig. 5.52 Wind incidence angles on Perspex sheet model of model-G in isolated condition**

(All dimensions are in mm)

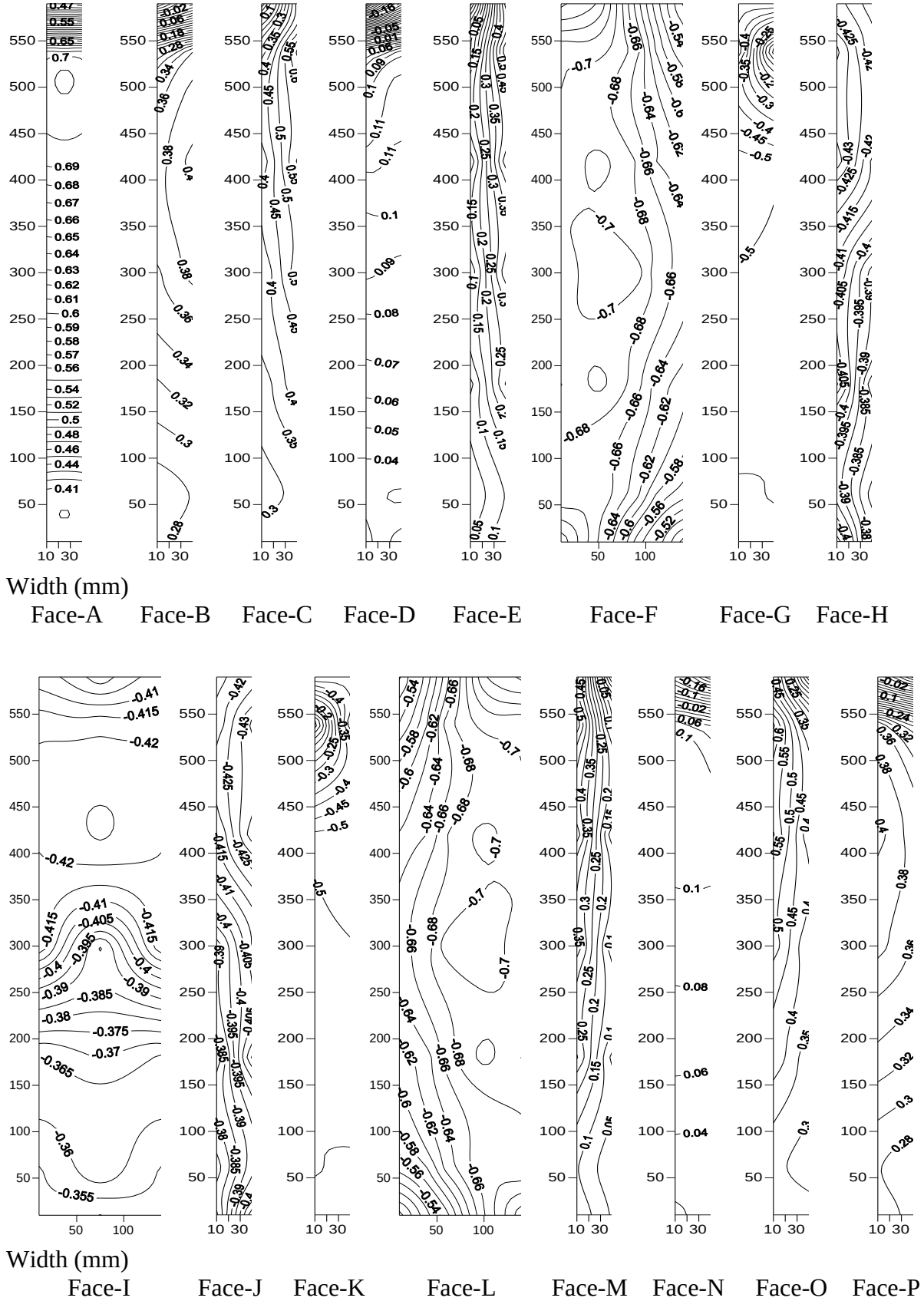


**Fig. 5.53 Distribution of mean wind pressure coefficients ($C_{p,mean}$) on different surfaces of model-G at $0^0$ wind incidence angle**

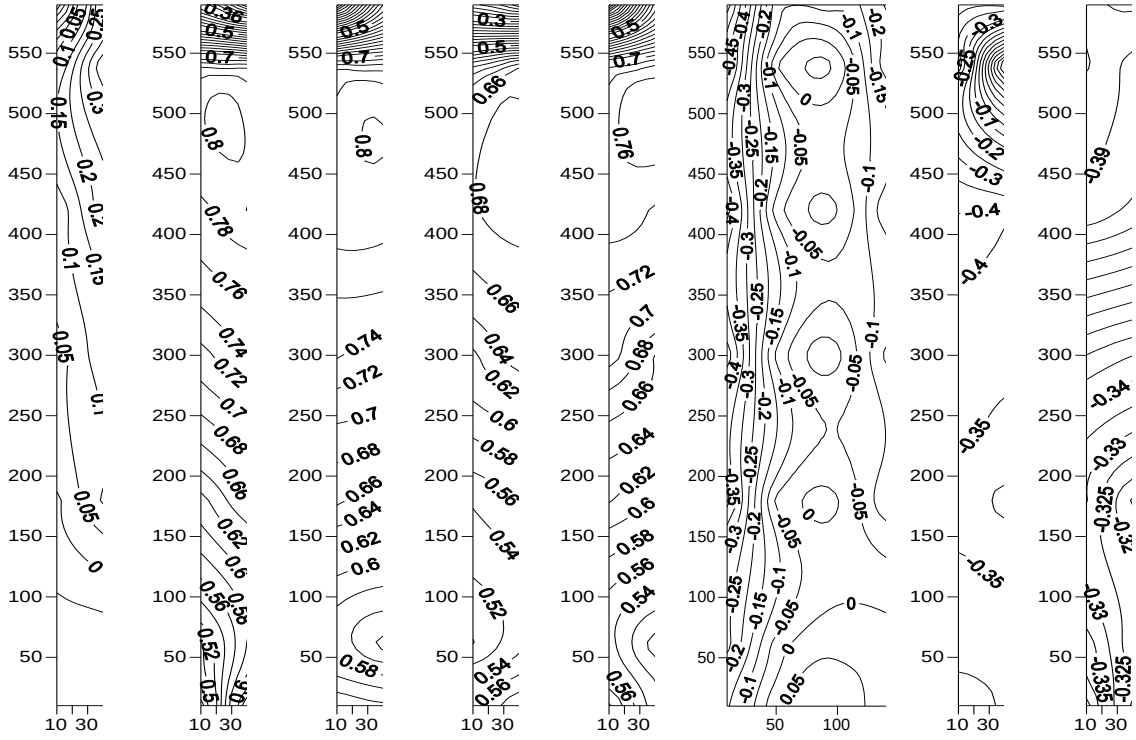


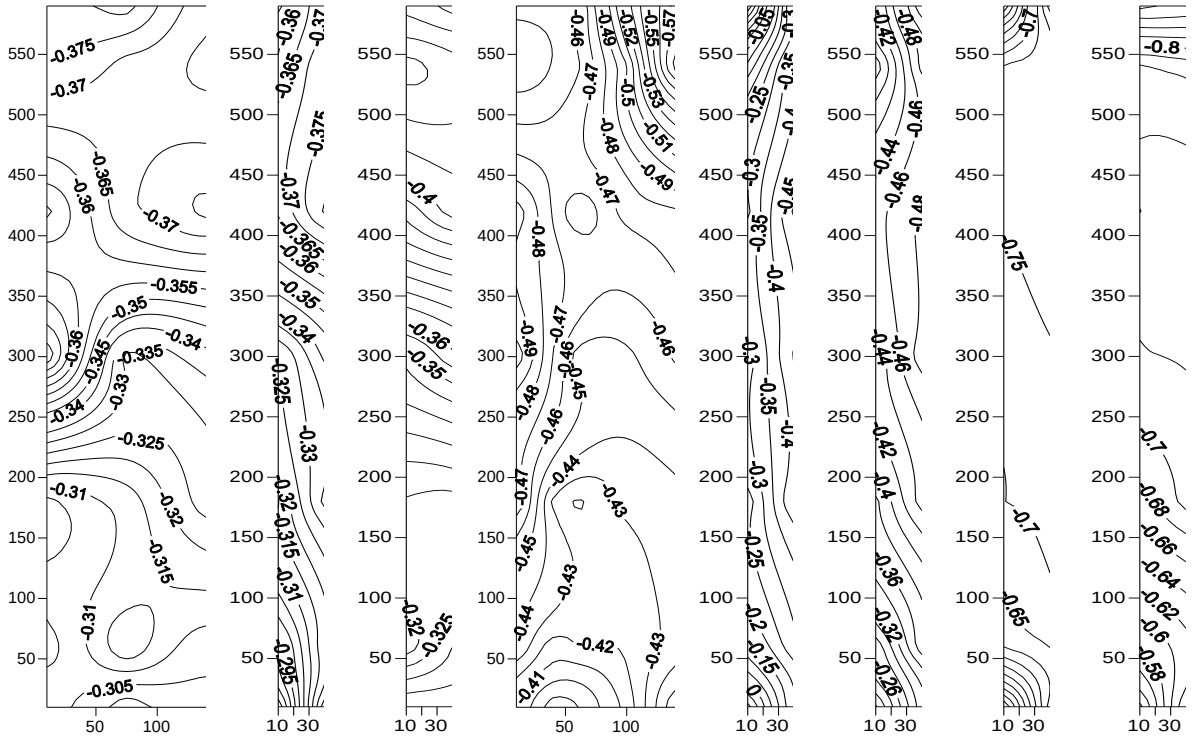


**Fig. 5.54 Distribution of mean wind pressure coefficients ($C_{p,mean}$) on different surfaces of model-G at $30^0$ wind incidence angle**

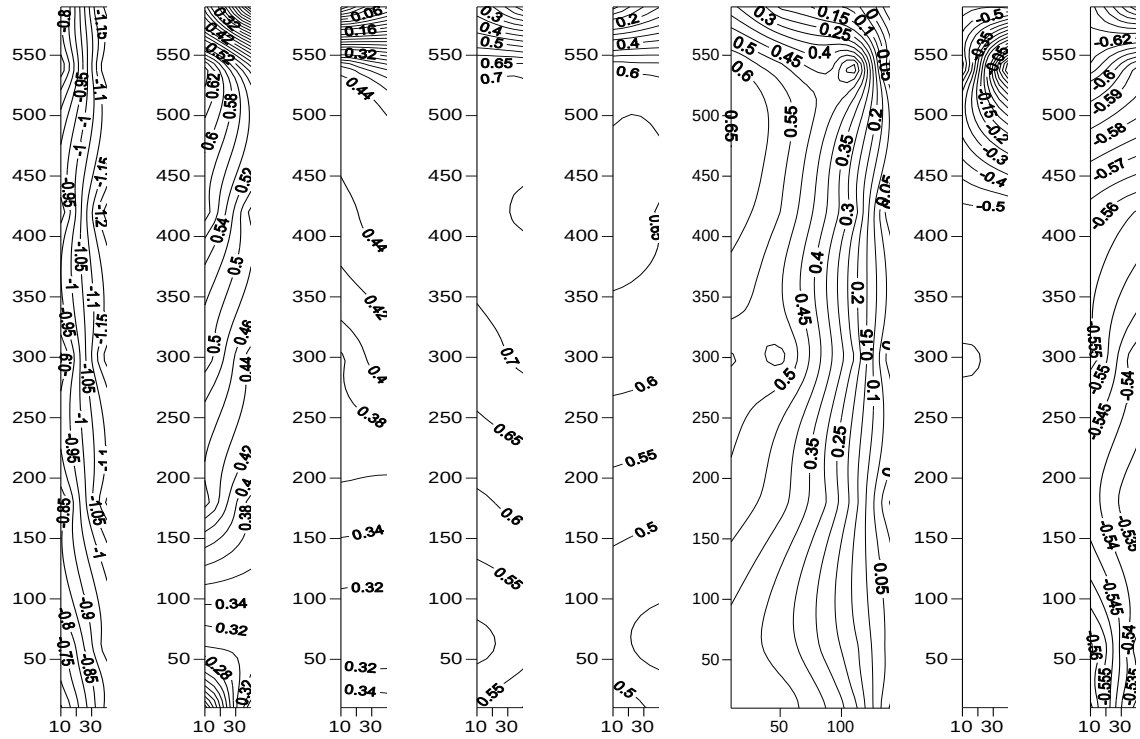


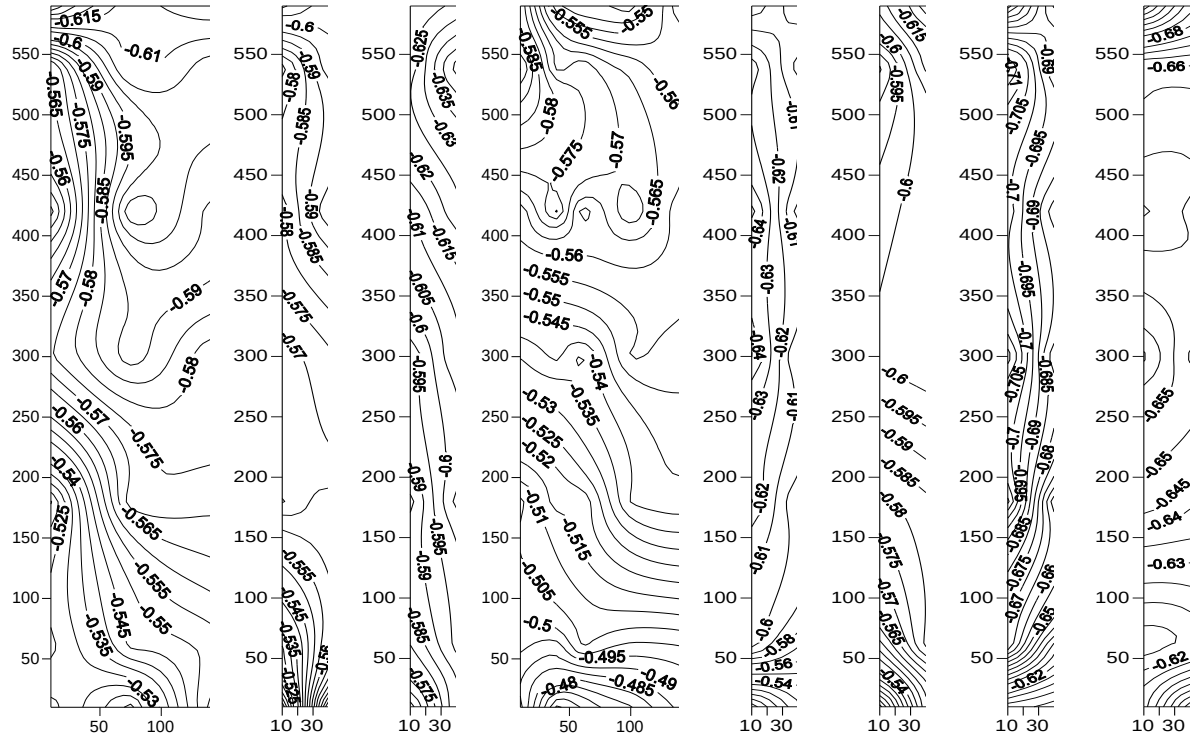


**Fig. 5.55 Distribution of mean wind pressure coefficients ($C_{p,mean}$) on different surfaces of model-G at $60^0$ wind incidence angle**

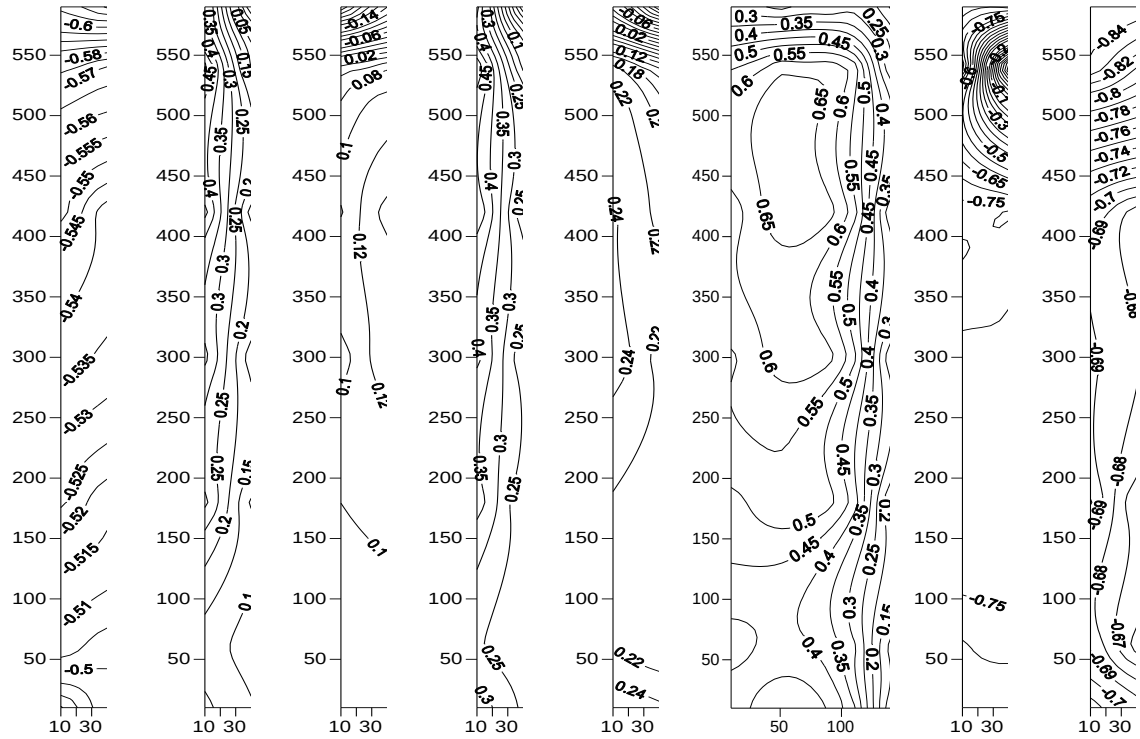


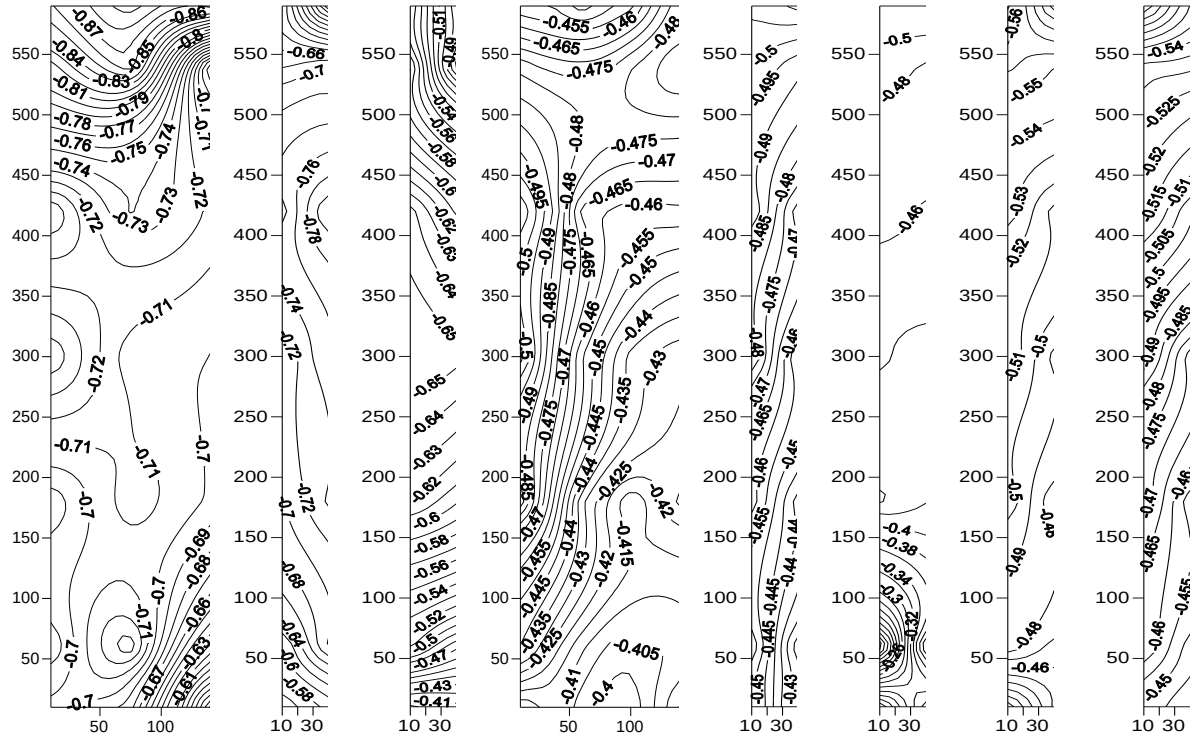


**Fig. 5.56 Distribution of mean wind pressure coefficients ($C_{p,mean}$) on different surfaces of model-G at $90^0$ wind incidence angle**

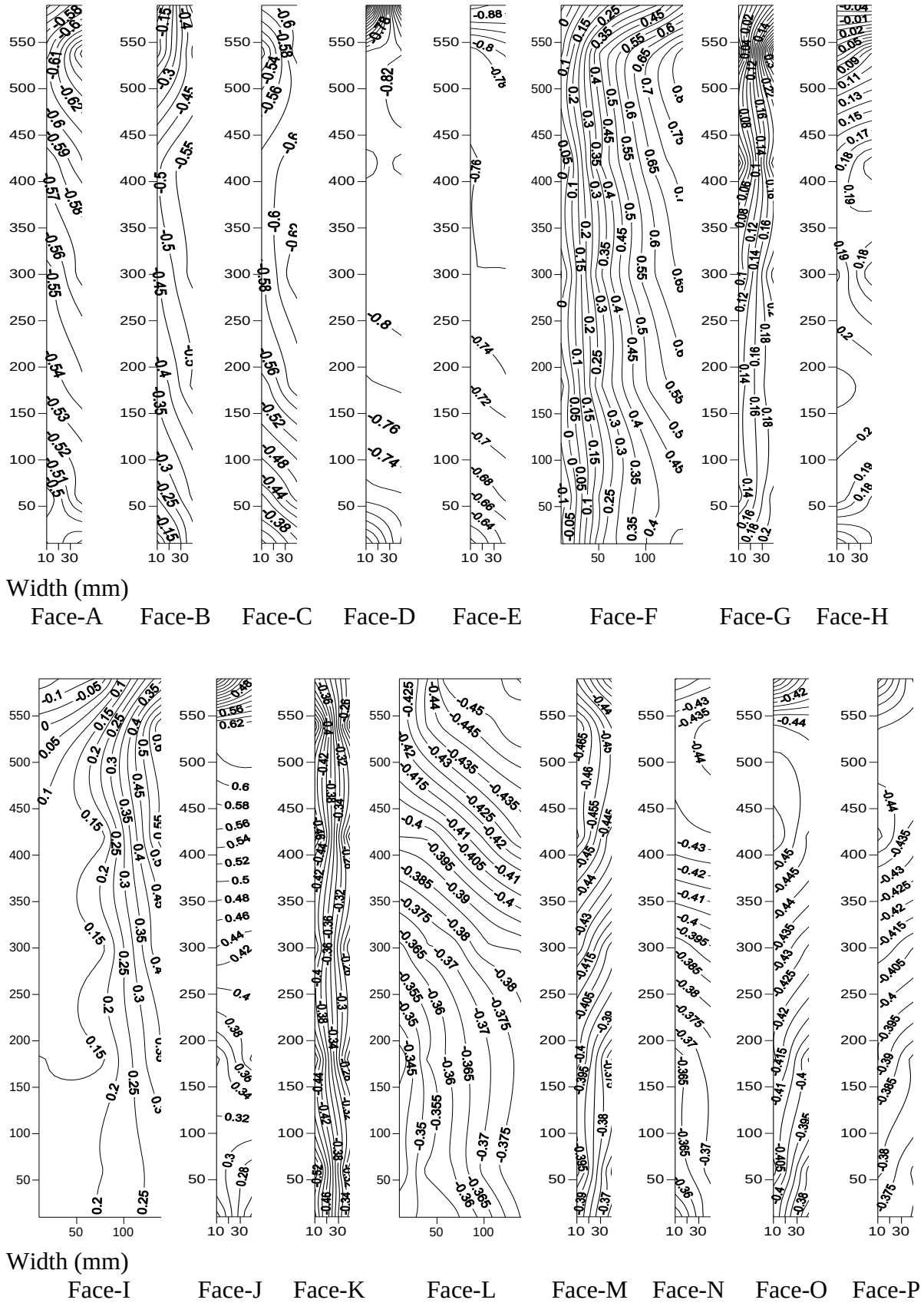


**Fig. 5.57 Distribution of mean wind pressure coefficients ($C_{p,mean}$) on different surfaces of model-G at $120^0$ wind incidence angle**

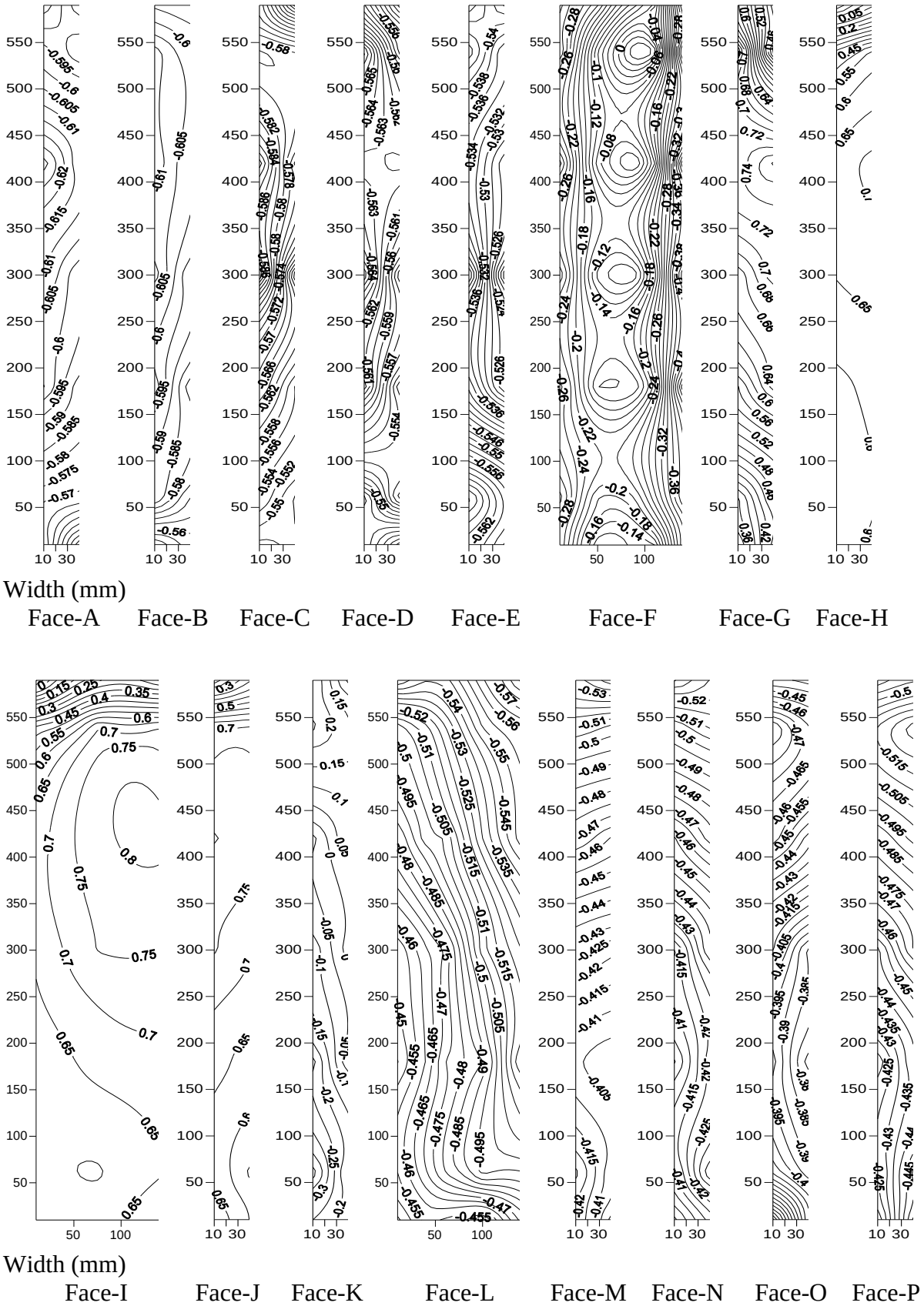


**Fig. 5.58 Distribution of mean wind pressure coefficients ($C_{p,mean}$) on different surfaces of model-G at $150^0$ wind incidence angle**

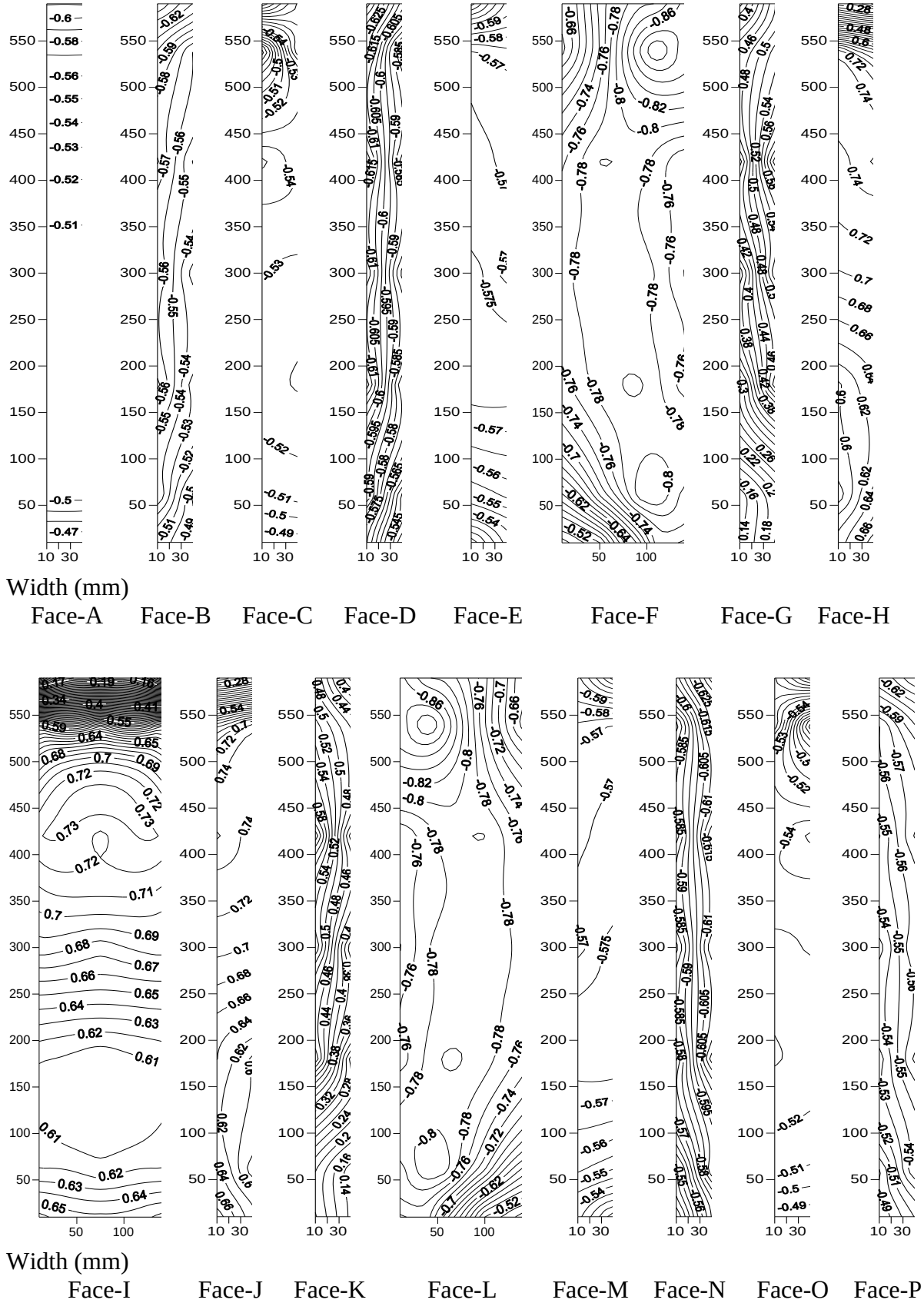


**Fig. 5.59 Distribution of mean wind pressure coefficients ($C_{p,mean}$) on different surfaces of model-G at $180^0$ wind incidence angle**

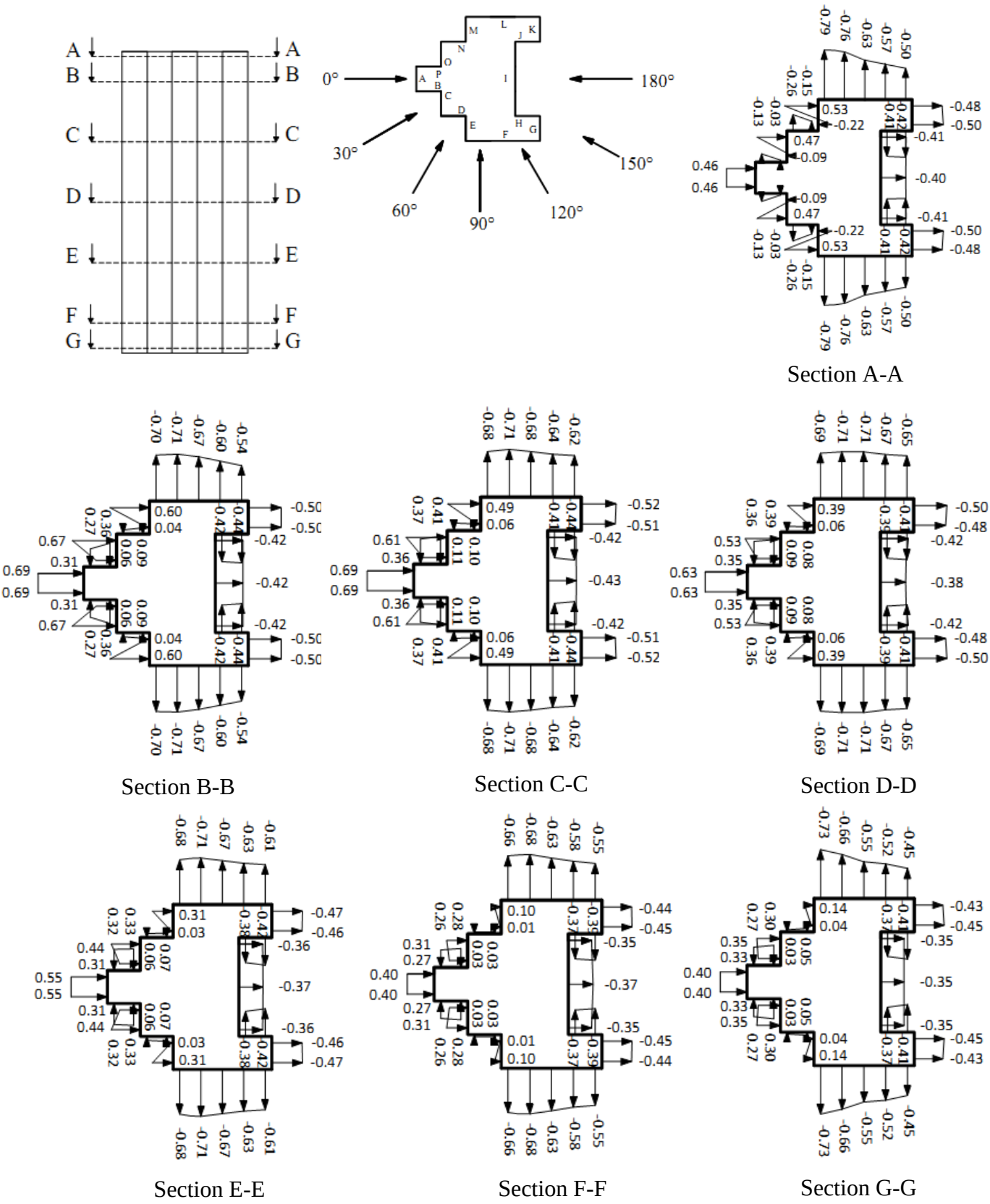


**Fig. 5.60 Cross-sectional variation of mean wind pressure coefficients ($C_{p,mean}$) on model-G at $0^0$ wind incidence angle**

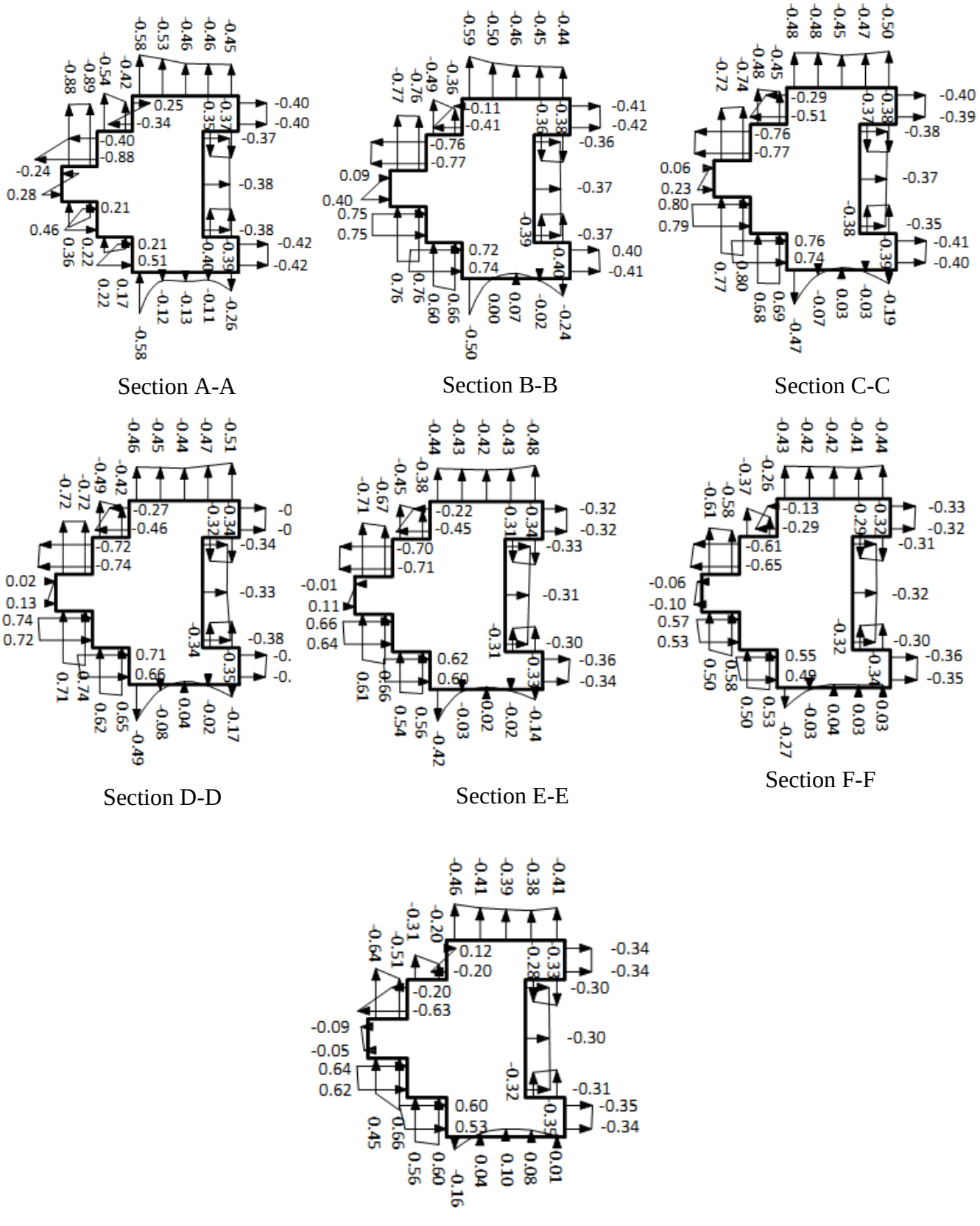


**Fig. 5.61 Cross-sectional variation of mean wind pressure coefficients ($C_{p,mean}$) on model-G at $30^0$ wind incidence angle**

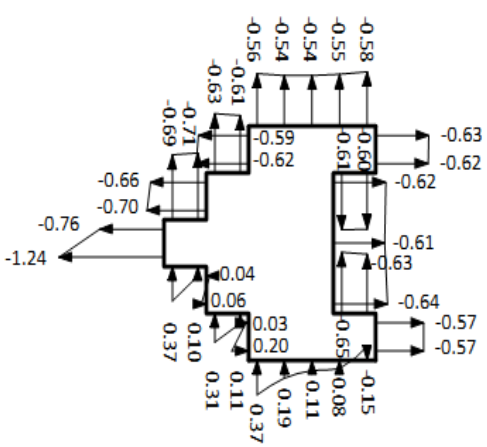

Section A-A

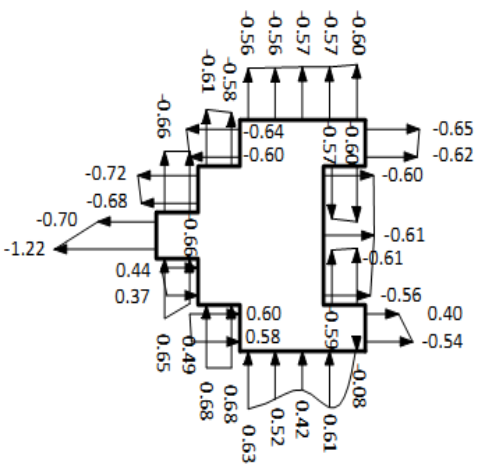

Section B-B

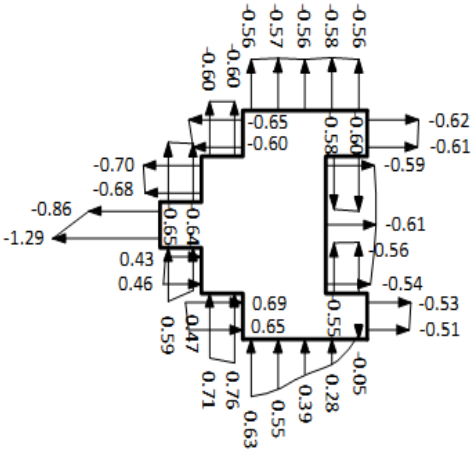

Section C-C

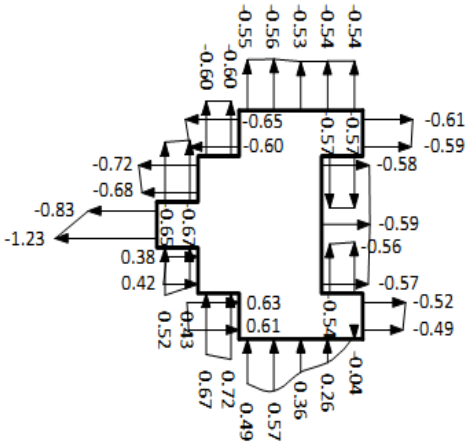

Section D-D

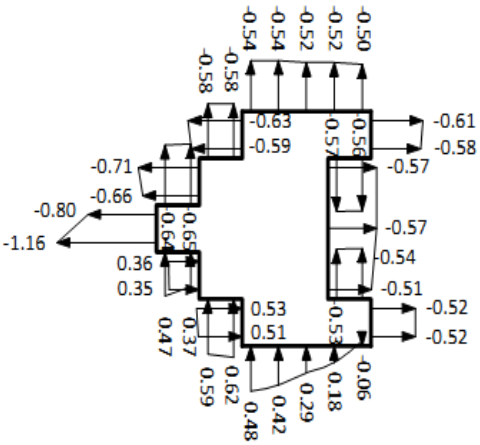

Section E-E

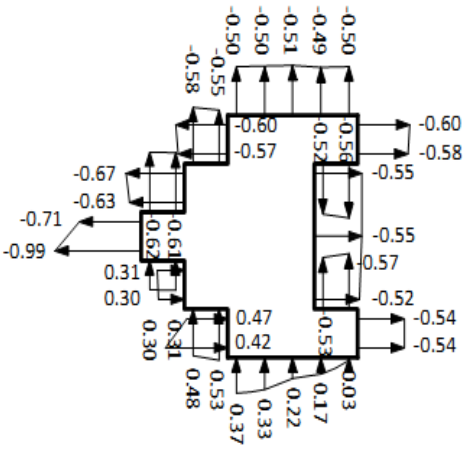

Section F-F

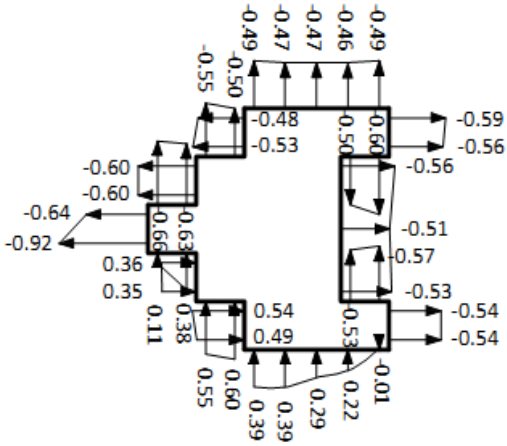

Section G-G

**Fig. 5.62 Cross-sectional variation of mean wind pressure coefficients ($C_{p,mean}$) on model-G at $60^0$ wind incidence angle**

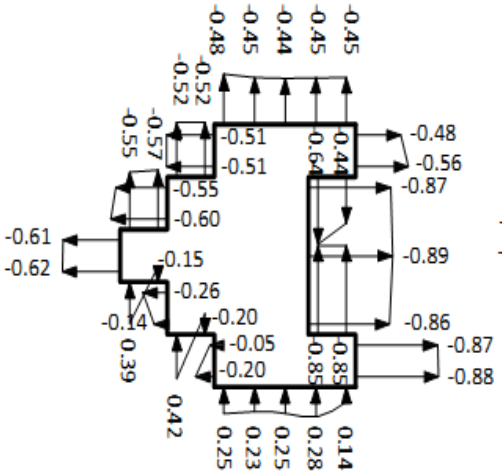


Section A-A

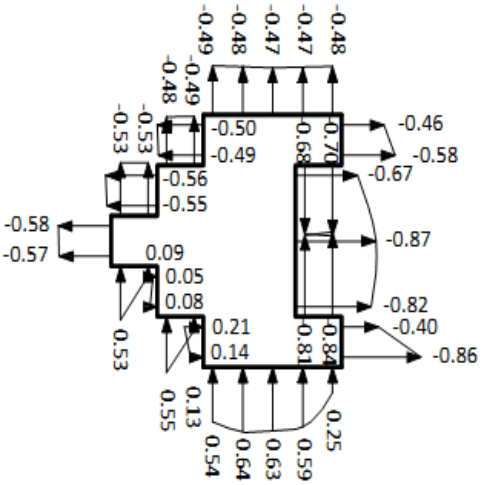


Section B-B

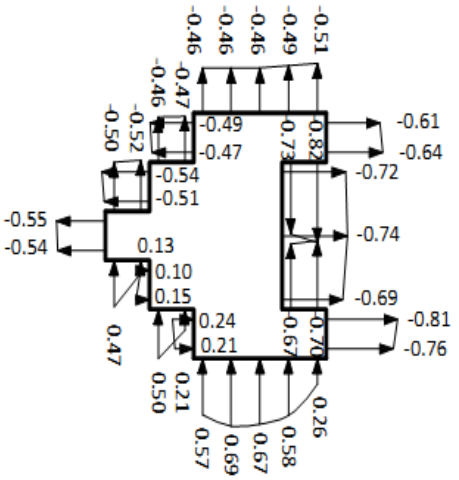


Section C-C

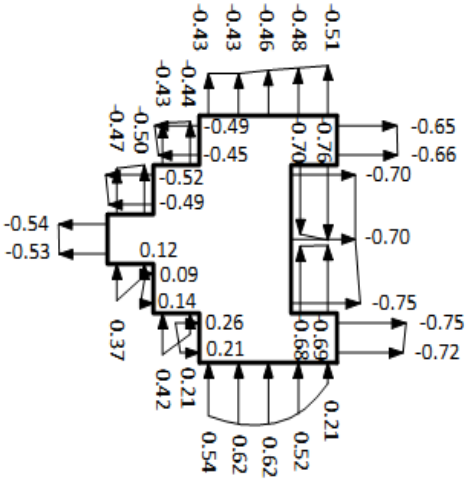


Section D-D

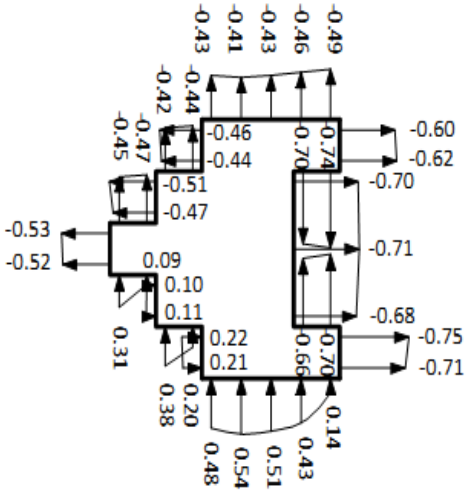


Section E-E

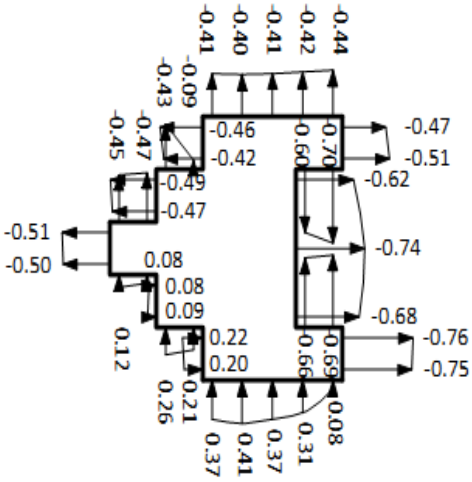


Section F-F

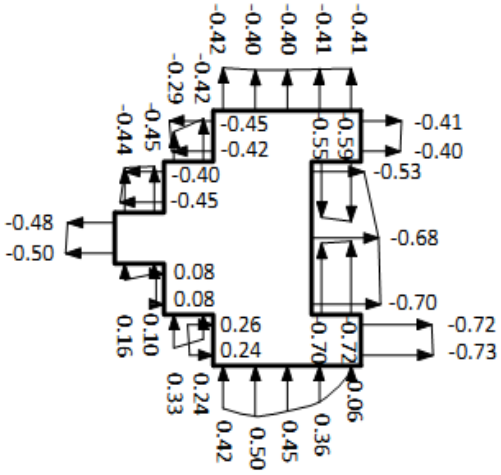


Section G-G

**Fig. 5.63 Cross-sectional variation of mean wind pressure coefficients ($C_{p,mean}$) on model-G at $90^0$ wind incidence angle**

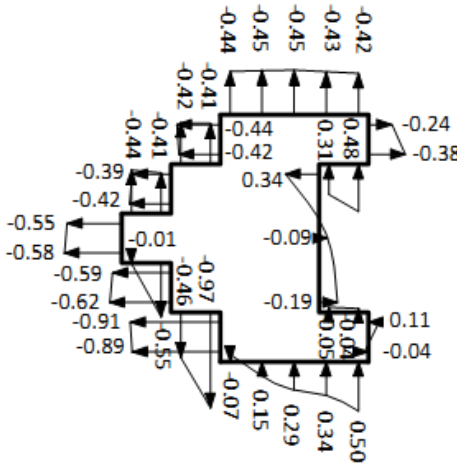


Section A-A

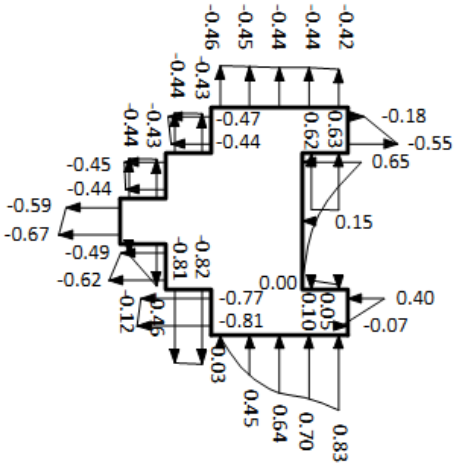


Section B-B

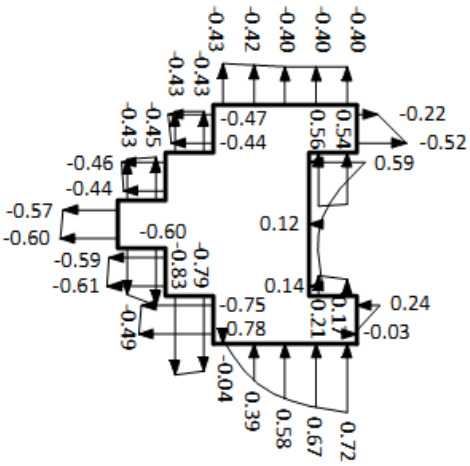


Section C-C

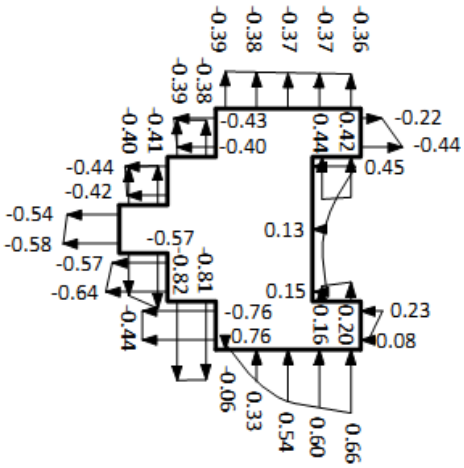


Section D-D

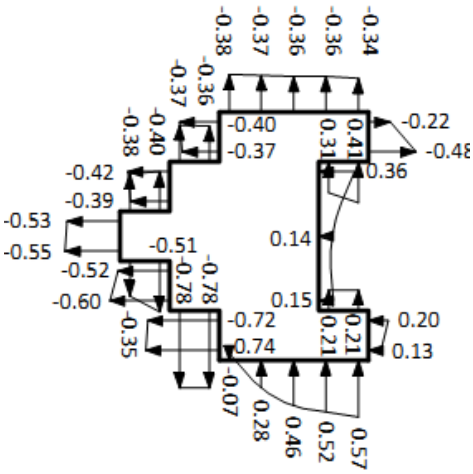


Section E-E

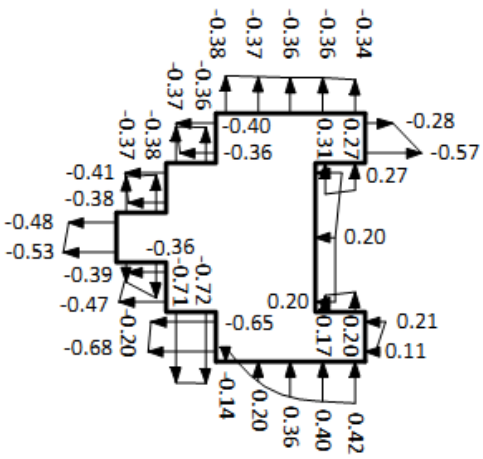


Section F-F

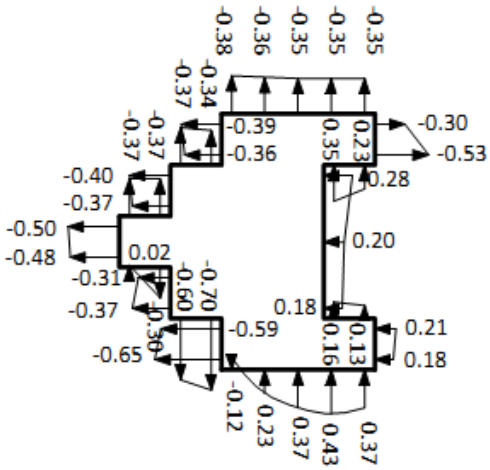


Section G-G

**Fig. 5.64 Cross-sectional variation of mean wind pressure coefficients ($C_{p,mean}$) on model-G at $120^0$ wind incidence angle**

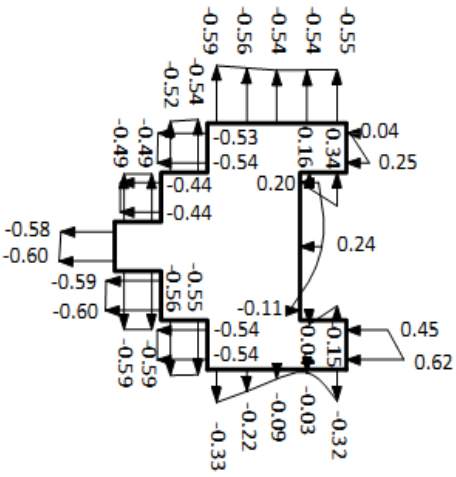


Section A-A

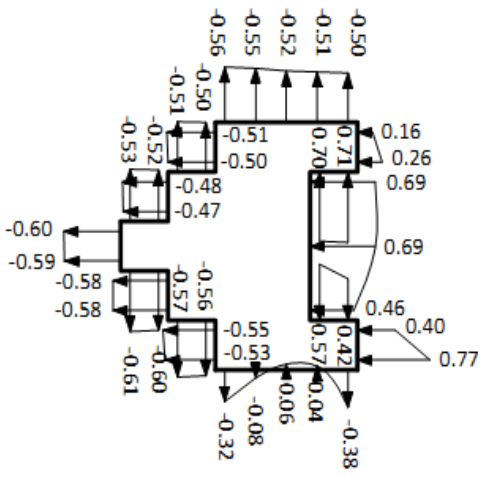


Section B-B

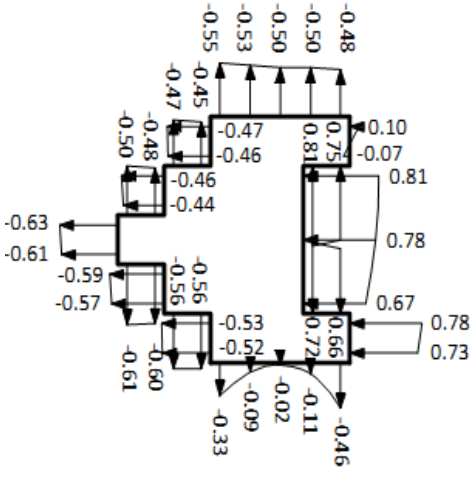


Section C-C

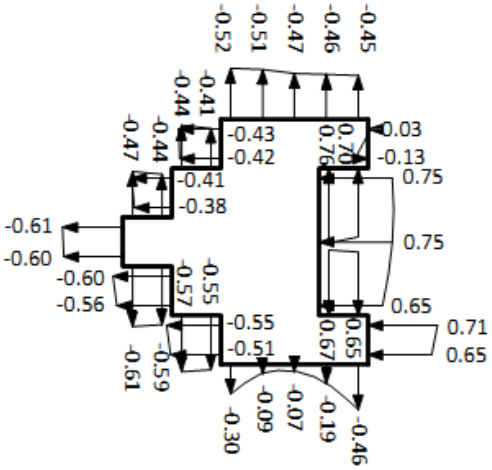


Section D-D

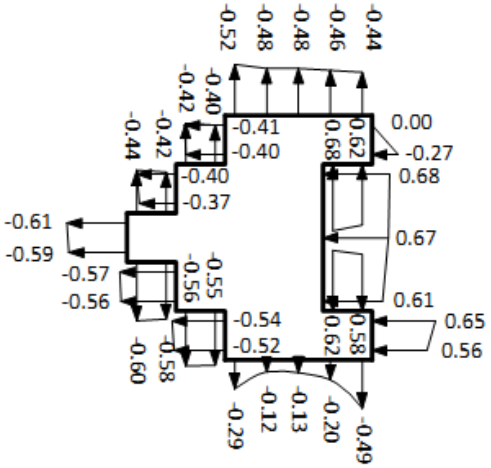


Section E-E

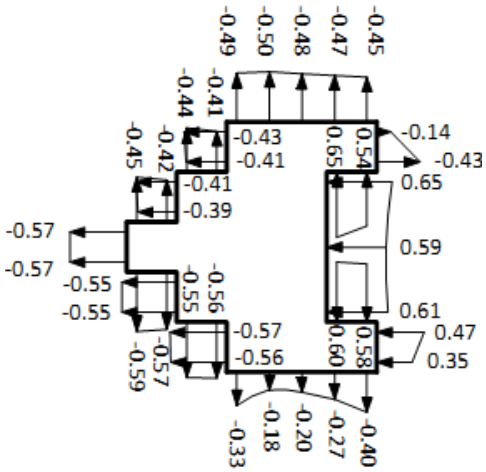


Section F-F

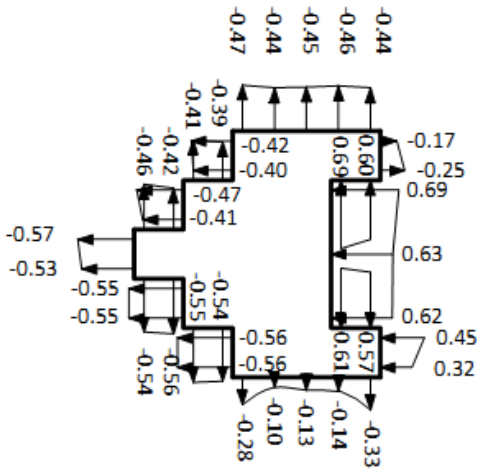


Section G-G

**Fig. 5.65 Cross-sectional variation of mean wind pressure coefficients ($C_{p,mean}$) on model-G at $150^0$ wind incidence angle**

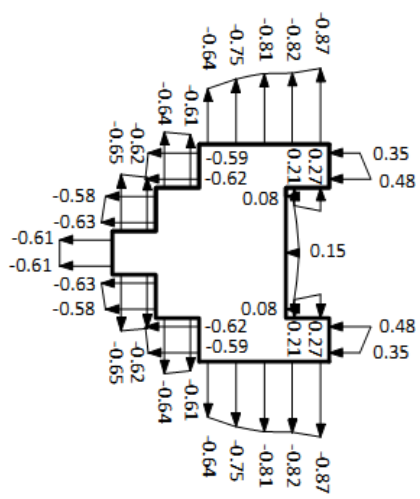


Section A-A

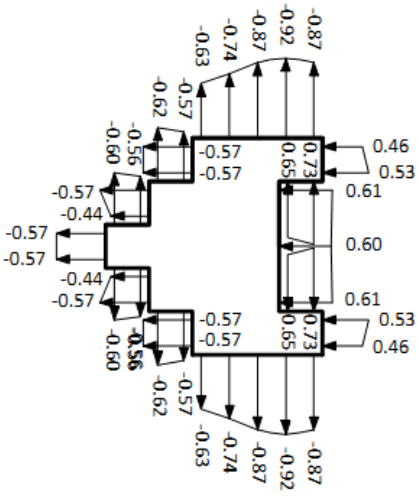


Section B-B

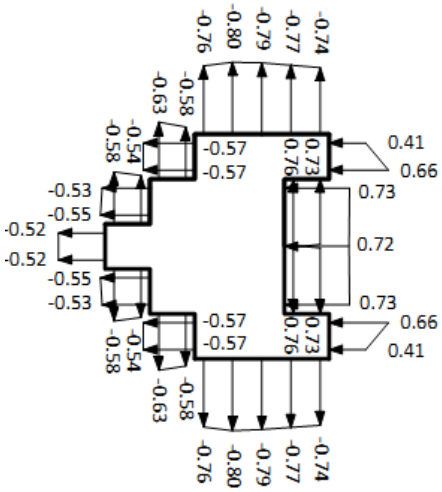


Section C-C

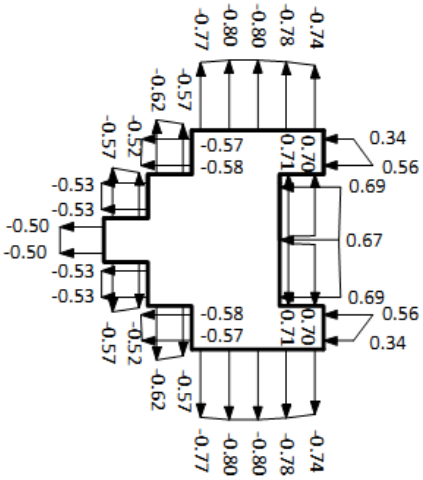


Section D-D

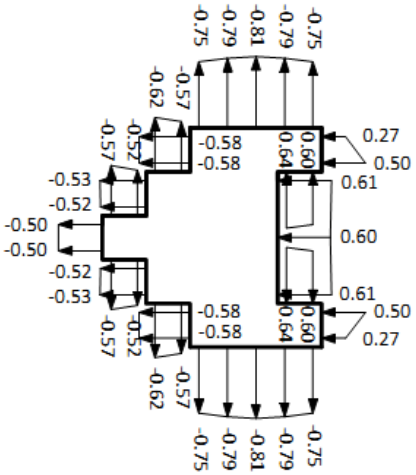


Section E-E

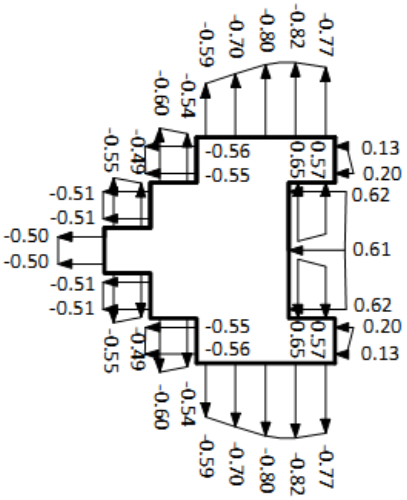


Section F-F

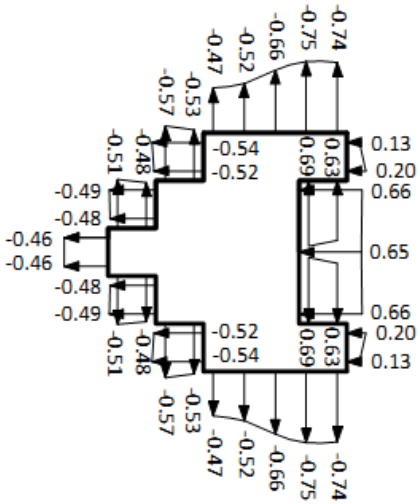


Section G-G

**Fig. 5.66 Cross-sectional variation of mean wind pressure coefficients ($C_{p,mean}$) on model-G at $180^0$ wind incidence angle**

Value of $C_{p,mean}$ on Face-A of models-G for 7 wind direction are compared in Table 5.7. Maximum value of $C_p$ is 0.69 and minimum is -1.29 which occur at $0^0$ and $60^0$ wind angles respectively.

**Table 5.7 Variation of $C_{p,mean}$ on face-A of model-G with wind incidence angle**

| **Pressure point no.** | **Mean wind pressure coefficients ($C_{p,mean}$)** | | | | | | |
|---|---|---|---|---|---|---|---|
| | **$0^0$** | **$30^0$** | **$60^0$** | **$90^0$** | **$120^0$** | **$150^0$** | **$180^0$** |
| 1 | 0.46 | **-0.24** | -0.76 | -0.61 | -0.55 | -0.58 | **-0.62** |
| 2 | 0.46 | 0.28 | -1.24 | **-0.62** | -0.58 | -0.60 | -0.60 |
| 3 | **0.69** | 0.09 | -0.70 | -0.58 | -0.59 | -0.60 | -0.57 |
| 4 | **0.69** | **0.40** | -1.22 | -0.57 | **-0.67** | -0.59 | -0.58 |
| 5 | **0.69** | 0.06 | -0.86 | -0.55 | -0.57 | **-0.63** | -0.52 |
| 6 | **0.69** | 0.23 | **-1.29** | -0.54 | -0.60 | -0.61 | -0.53 |
| 7 | 0.63 | 0.02 | -0.83 | -0.54 | -0.54 | -0.61 | -0.50 |
| 8 | 0.63 | 0.13 | -1.23 | -0.53 | -0.58 | -0.60 | -0.50 |
| 9 | 0.55 | -0.01 | -0.80 | -0.53 | -0.53 | -0.61 | -0.51 |
| 10 | 0.55 | 0.11 | -1.16 | -0.52 | -0.55 | -0.59 | -0.49 |
| 11 | 0.40 | -0.06 | -0.71 | -0.51 | **-0.48** | -0.57 | -0.51 |
| 12 | 0.40 | -0.10 | -0.99 | -0.50 | -0.53 | -0.57 | -0.50 |
| 13 | 0.40 | -0.09 | **-0.64** | **-0.48** | -0.50 | -0.57 | -0.48 |
| 14 | 0.40 | -0.05 | -0.92 | -0.50 | **-0.48** | **-0.53** | **-0.44** |

### 5.2.7 Model-H (Fish Shape-3)

Mean pressure contours plotted in on various surfaces of model-H at different wind incidence angles are shown in Figs. 5.68 to 5.74.

Rear face in this model is subjected to different pressure distribution at $180^0$ wind incidence angle as compared to model-F and model-G (Figs. 5.51, 5.66 and 5.81).

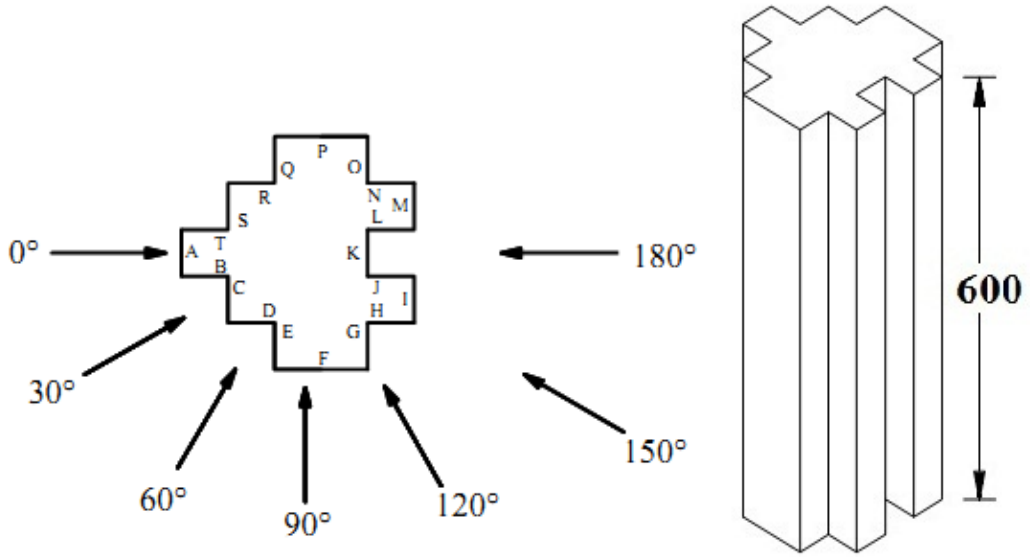


Plan Isometric

**Fig. 5.67 Wind incidence angles on Perspex sheet model of model-H in isolated condition**

(All dimensions are in mm)

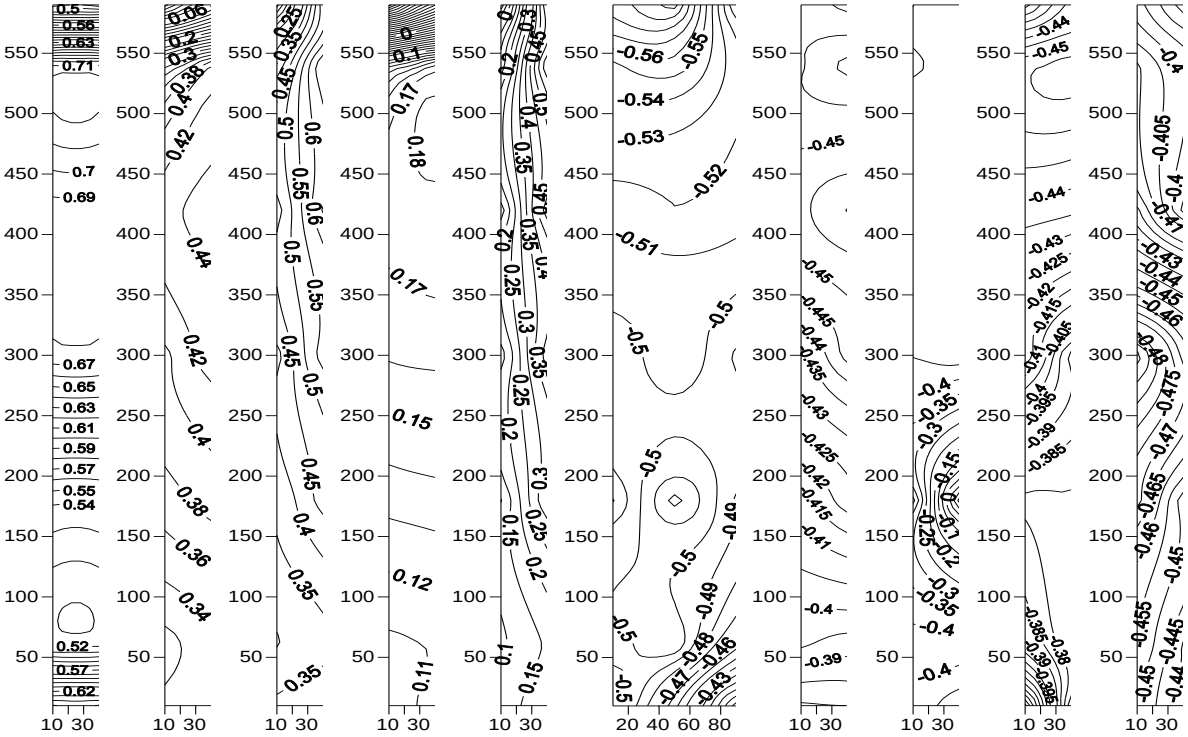

Width (mm)

Face-A Face-B Face-C Face-D Face-E Face-F Face-G Face-H Face-I Face-J

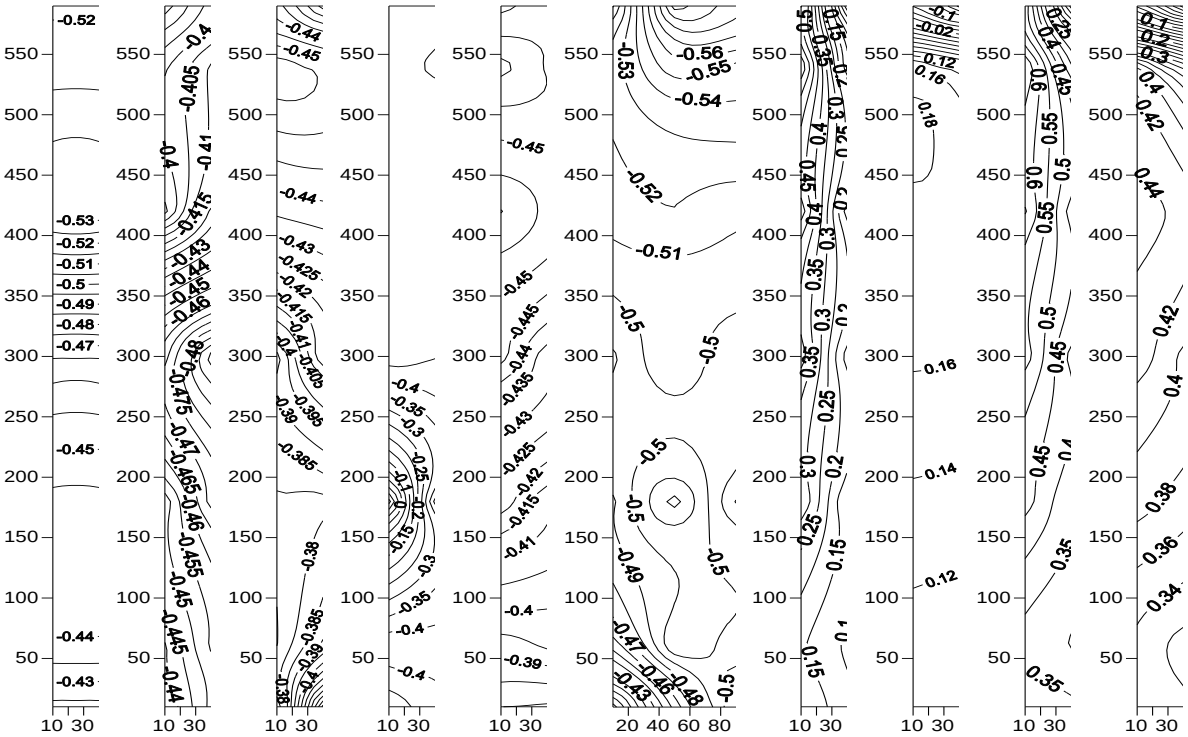

Width (mm)

Face-K Face-L Face-M Face-N Face-O Face-P Face-Q Face-R Face-S Face-T

**Fig. 5.68 Distribution of mean wind pressure coefficients ($C_{p,mean}$) on different surfaces of model-H at $0^0$ wind incidence angle**

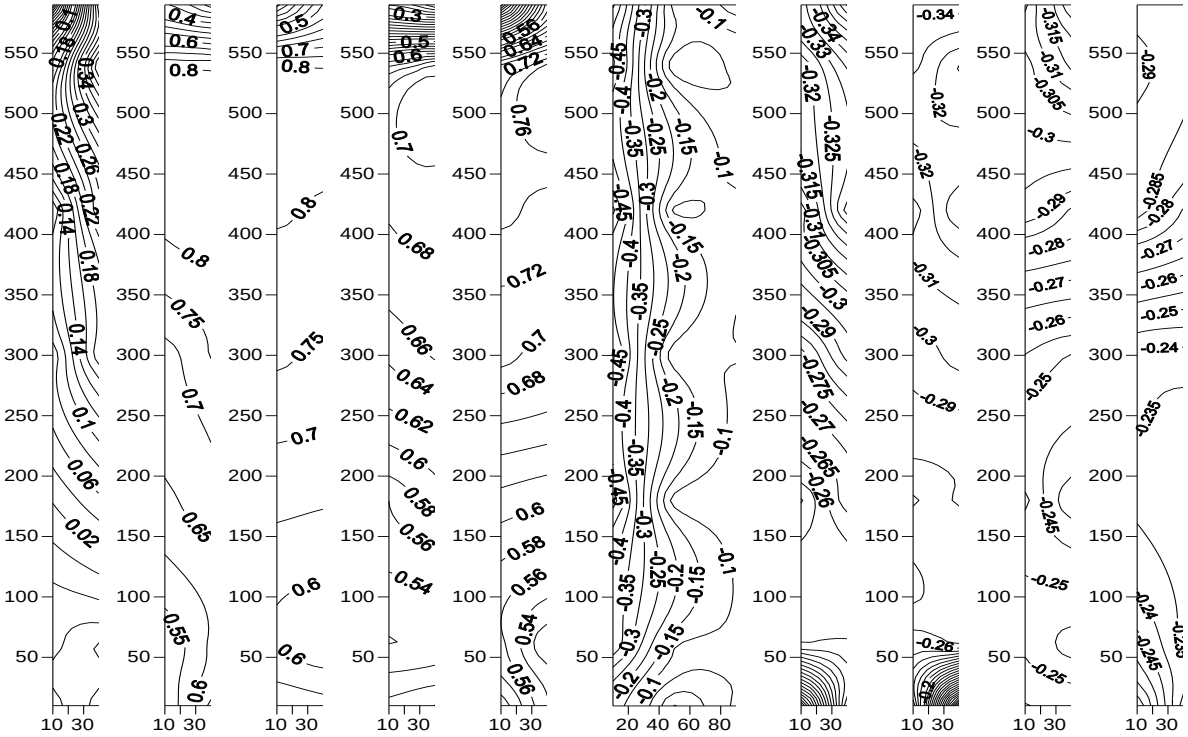

Width (mm)

Face-A Face-B Face-C Face-D Face-E Face-F Face-G Face-H Face-I Face-J

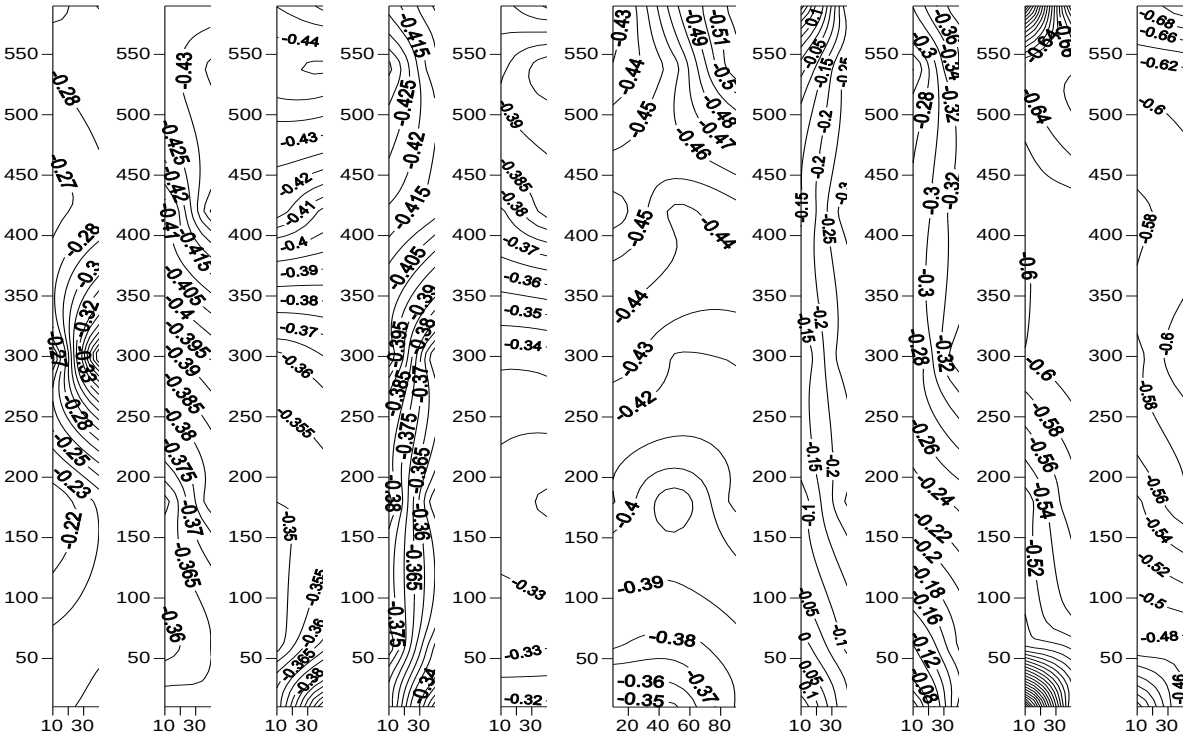

Width (mm)

Face-K Face-L Face-M Face-N Face-O Face-P Face-Q Face-R Face-S Face-T

**Fig. 5.69 Distribution of mean wind pressure coefficients ($C_{p,mean}$) on different surfaces of model-H at $30^0$ wind incidence angle**

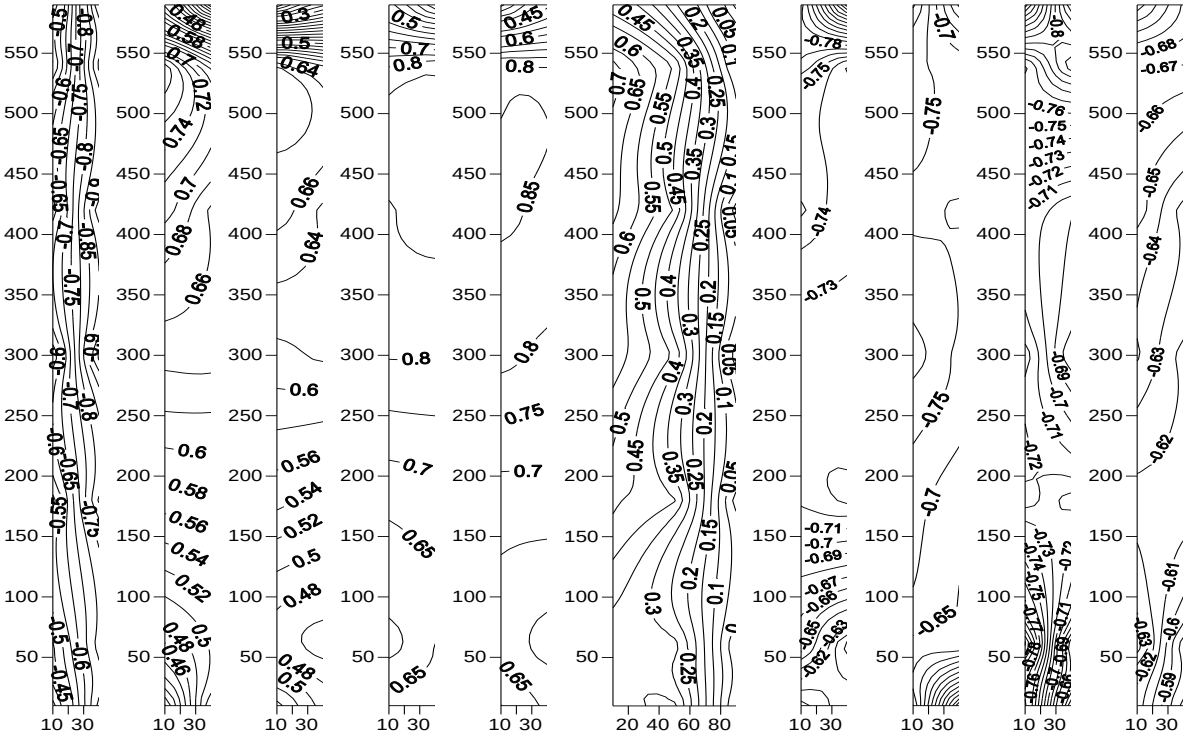

Width (mm)

Face-A Face-B Face-C Face-D Face-E Face-F Face-G Face-H Face-I Face-J

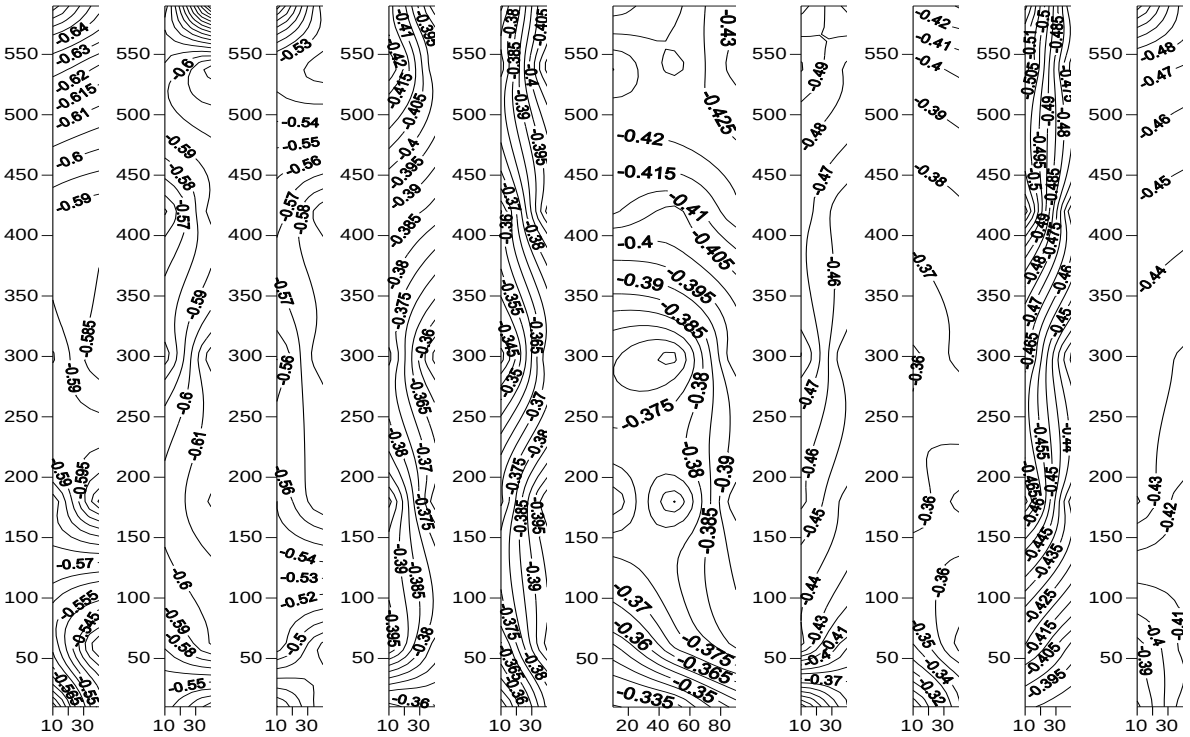

Width (mm)

Face-K Face-L Face-M Face-N Face-O Face-P Face-Q Face-R Face-S Face-T

**Fig. 5.70 Distribution of mean wind pressure coefficients ($C_{p,mean}$) on different surfaces of model-H at $60^0$ wind incidence angle**

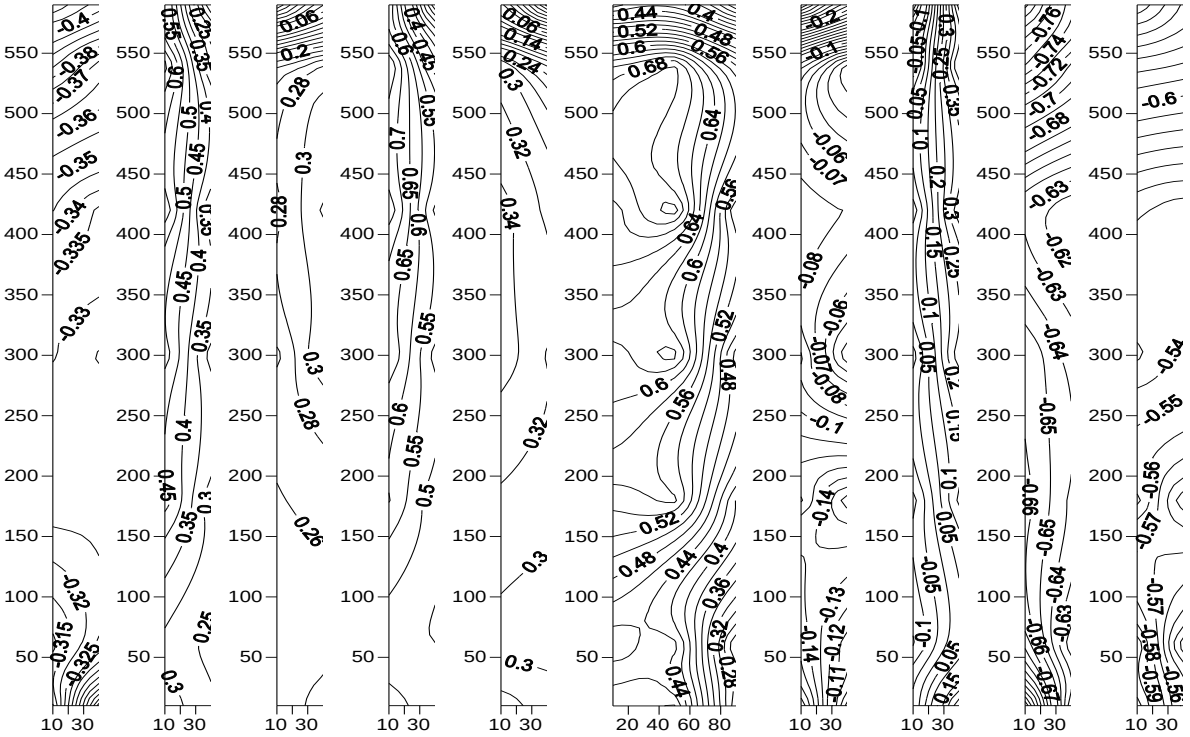


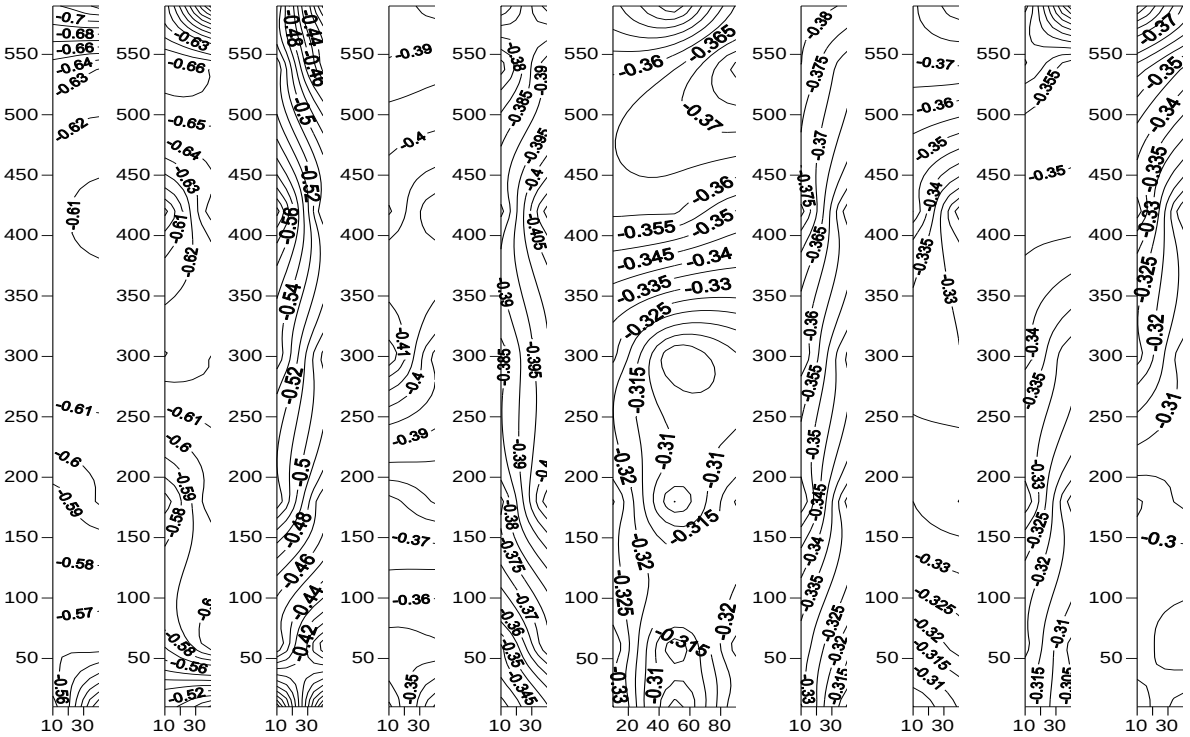


**Fig. 5.71 Distribution of mean wind pressure coefficients ($C_{p,mean}$) on different surfaces of model-H at $90^0$ wind incidence angle**

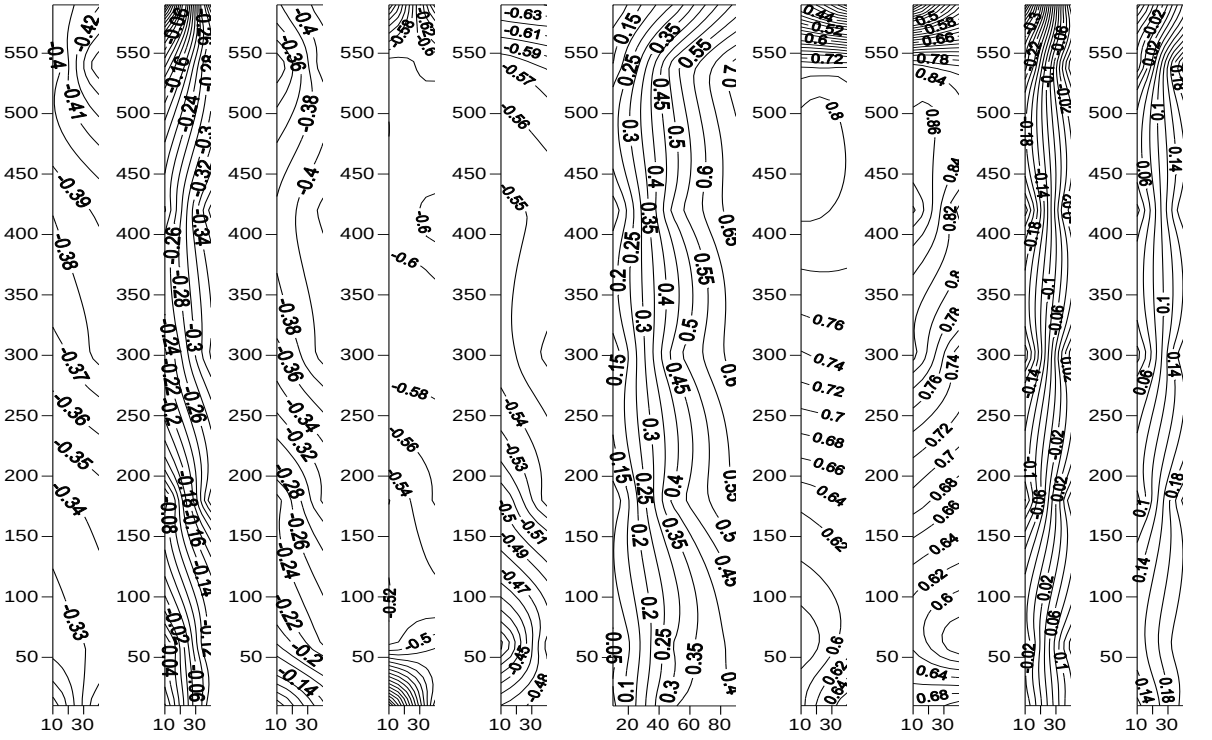

Width (mm)

Face-A Face-B Face-C Face-D Face-E Face-F Face-G Face-H Face-I Face-J

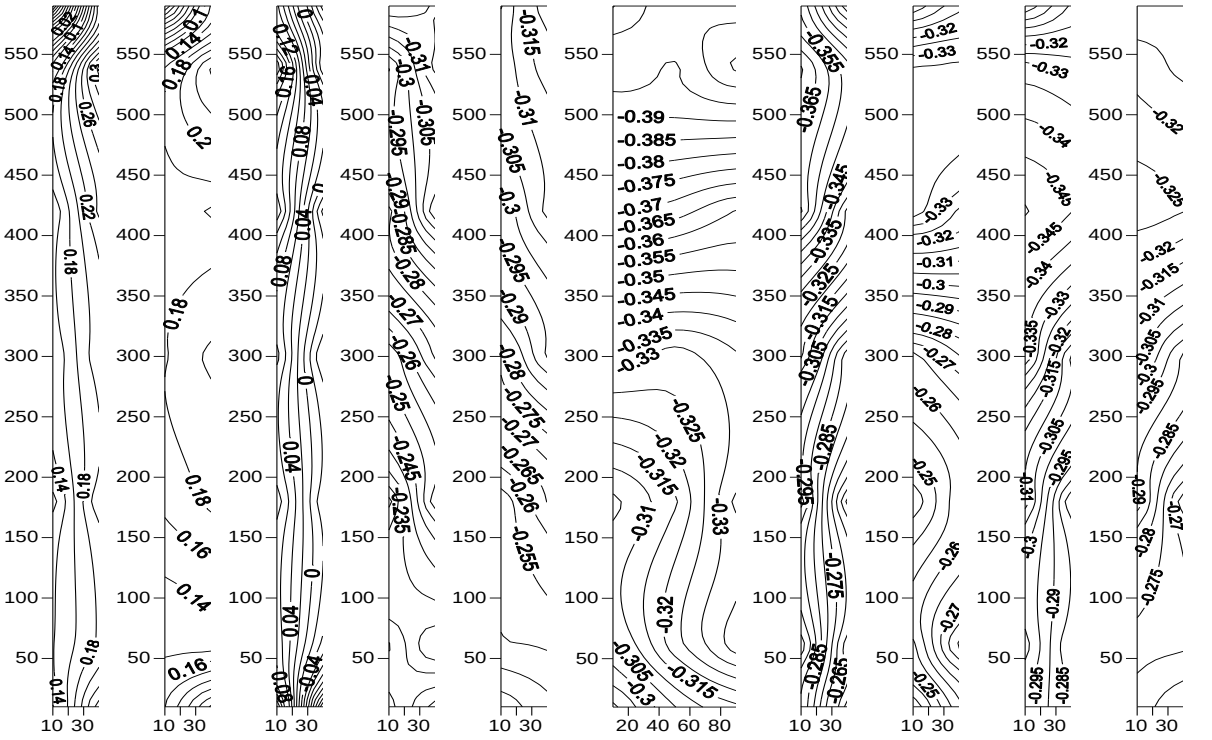

Width (mm)

Face-K Face-L Face-M Face-N Face-O Face-P Face-Q Face-R Face-S Face-T

**Fig. 5.72 Distribution of mean wind pressure coefficients ($C_{p,mean}$) on different surfaces of model-H at $120^0$ wind incidence angle**

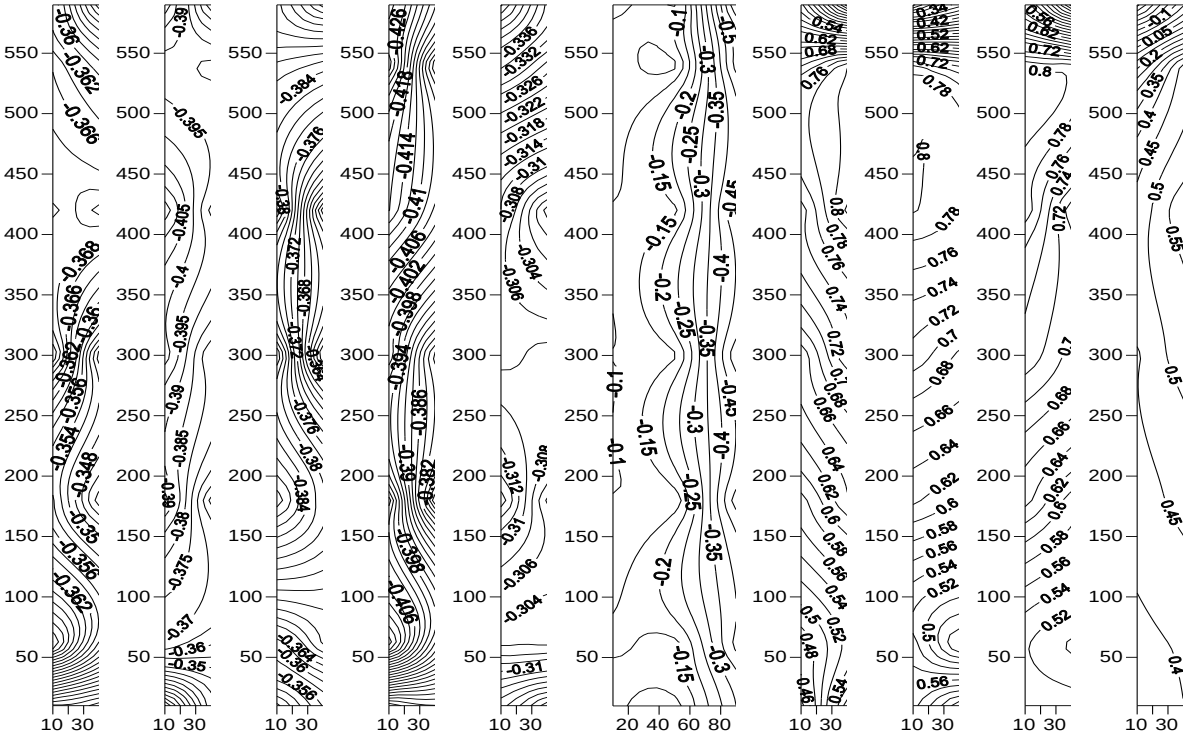


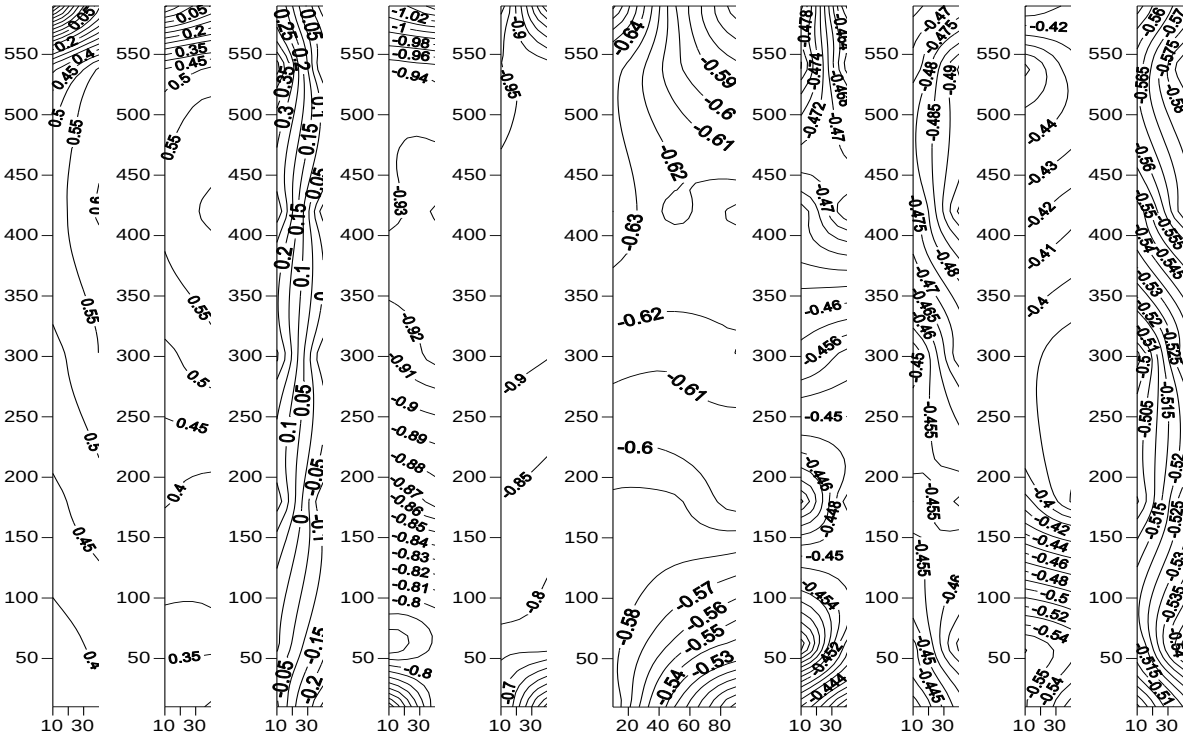


**Fig. 5.73 Distribution of mean wind pressure coefficients ($C_{p,mean}$) on different surfaces of model-H at $150^0$ wind incidence angle**

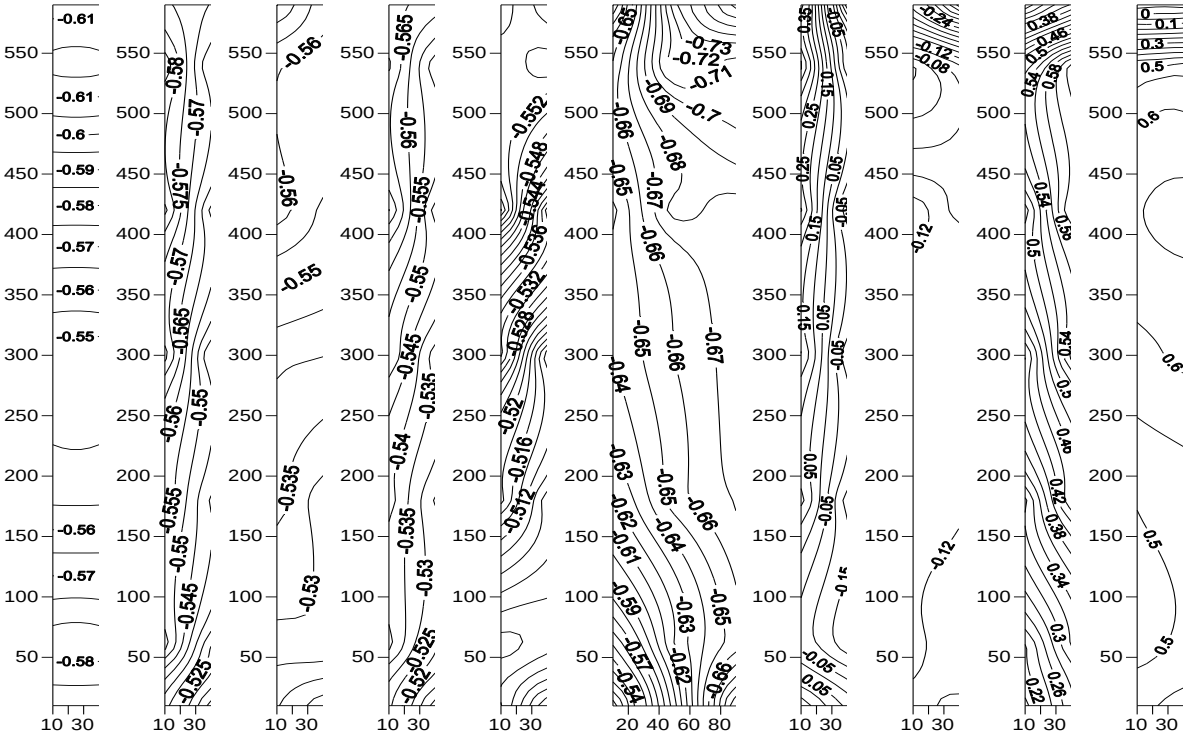

Width (mm)

Face-A Face-B Face-C Face-D Face-E Face-F Face-G Face-H Face-I Face-J

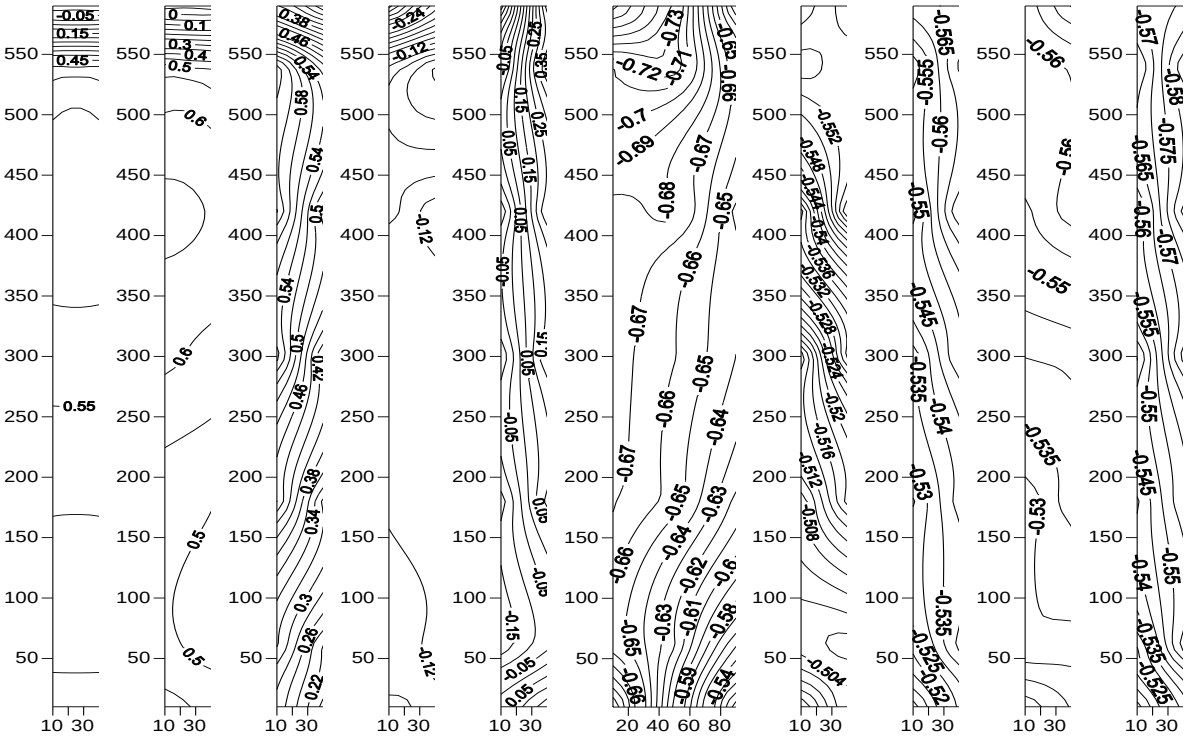

Width (mm)

Face-K Face-L Face-M Face-N Face-O Face-P Face-Q Face-R Face-S Face-T

**Fig. 5.74 Distribution of mean wind pressure coefficients ($C_{p,mean}$) on different surfaces of model-H at $180^0$ wind incidence angle**

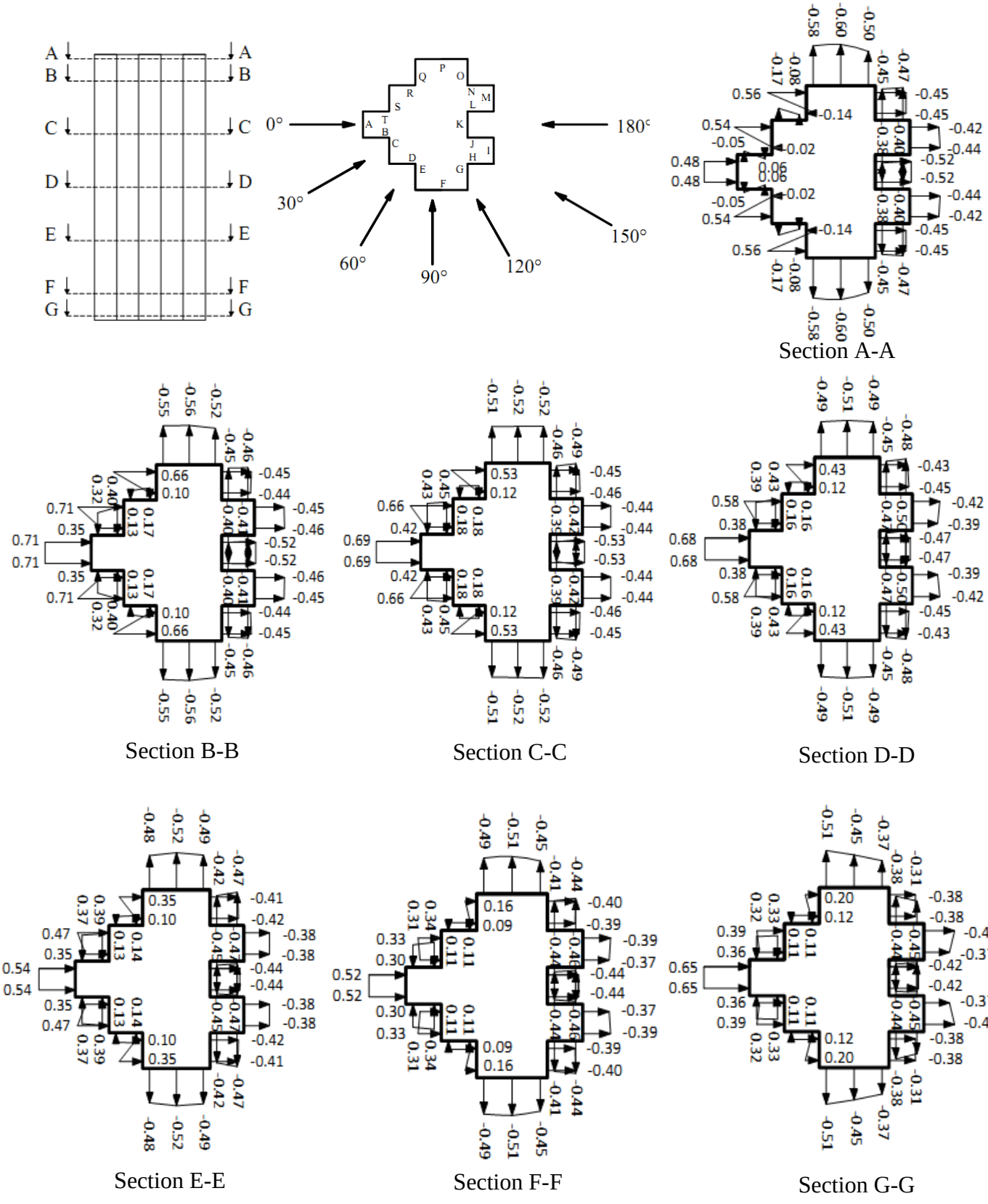


**Fig. 5.75 Cross-sectional variation of mean wind pressure coefficients ($C_{p,mean}$) on model-H at $0^0$ wind incidence angle**

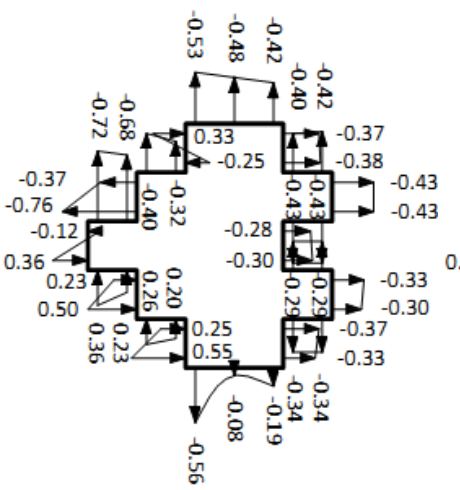


Section A-A

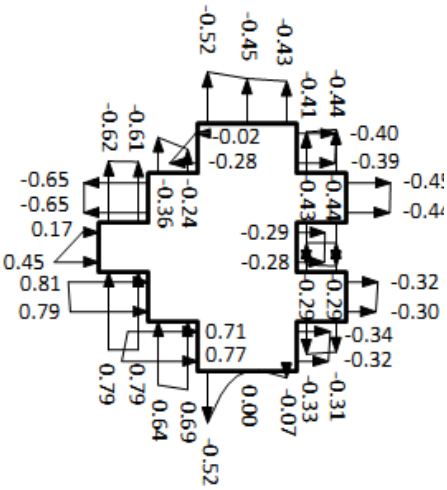


Section B-B

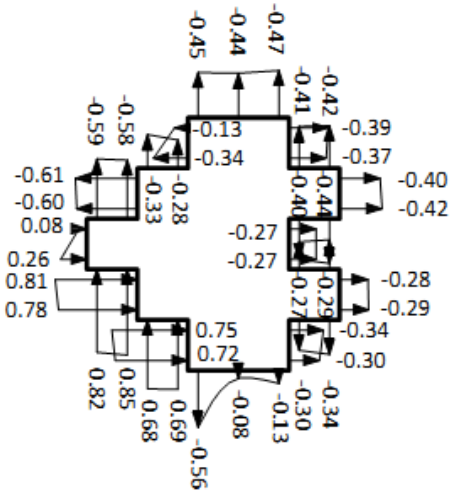


Section C-C

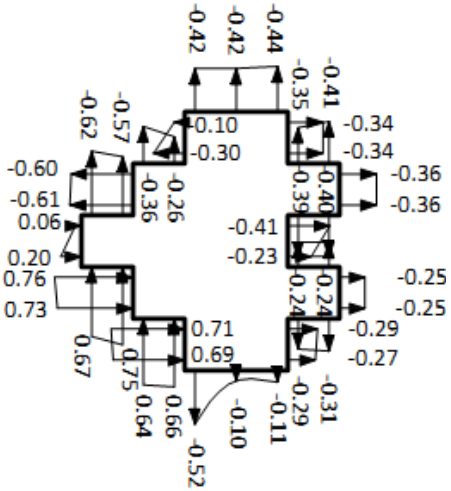


Section D-D

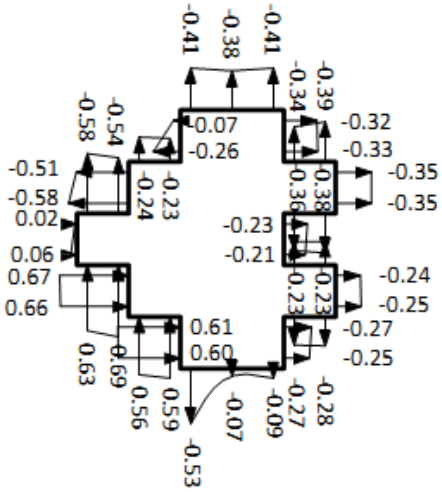


Section E-E

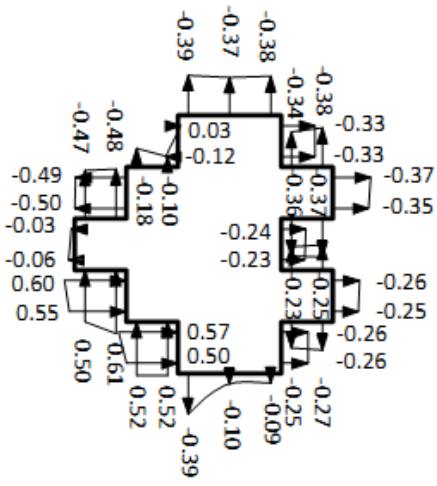


Section F-F

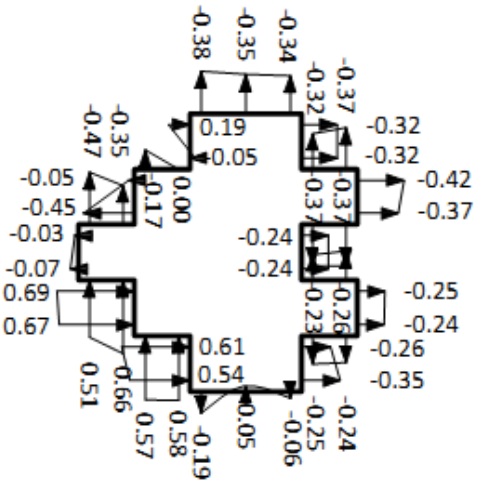


Section G-G

**Fig. 5.76 Cross-sectional variation of mean wind pressure coefficients ($C_{p,mean}$) on model-H at $30^0$ wind incidence angle**

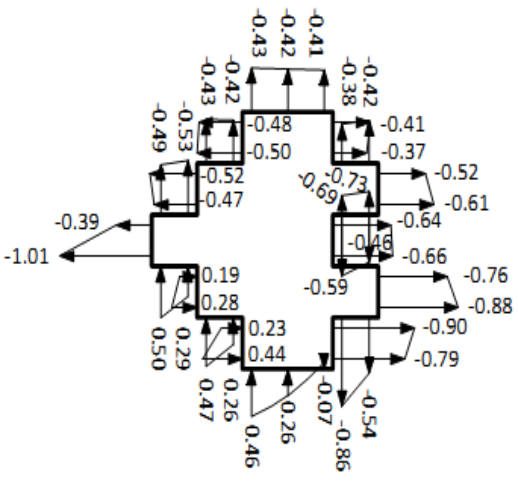

Section-AA

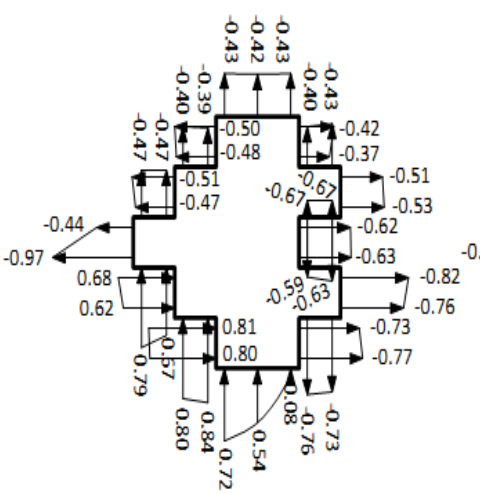

Section-BB

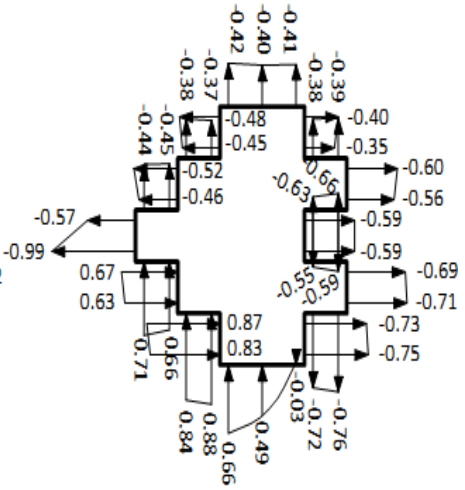

Section-CC

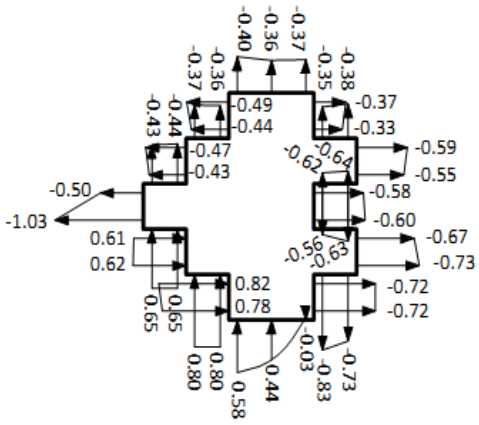

Section D-D

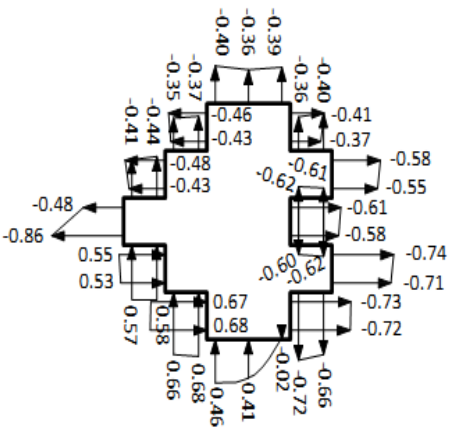

Section E-E

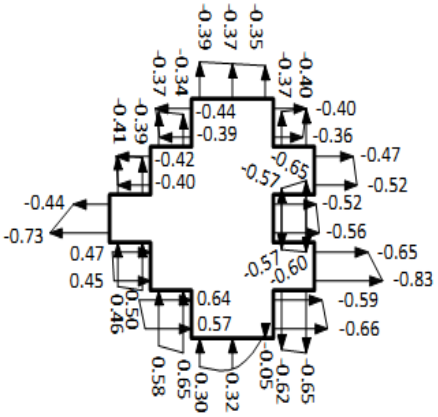

Section F-F

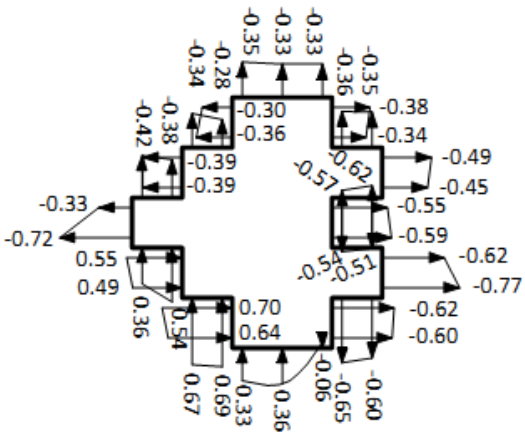

Section G-G

**Fig. 5.77 Cross-sectional variation of mean wind pressure coefficients ($C_{p,mean}$) on model-H at $60^0$ wind incidence angle**

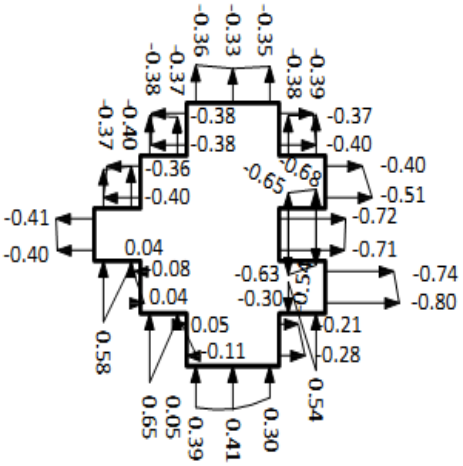

Section A-A

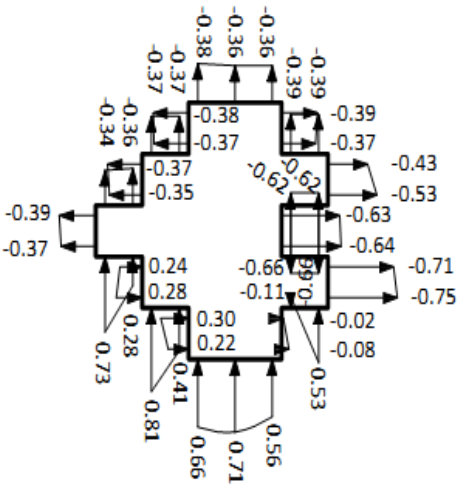

Section B-B

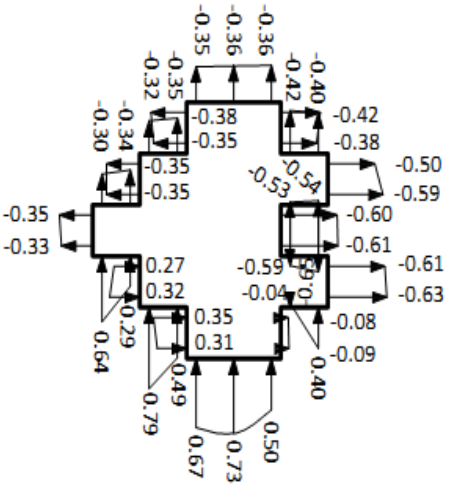

Section C-C

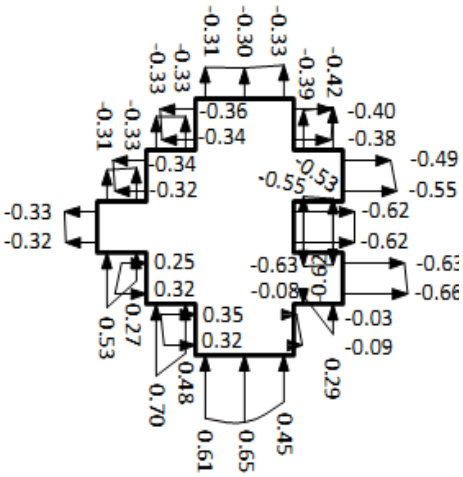

Section D-D

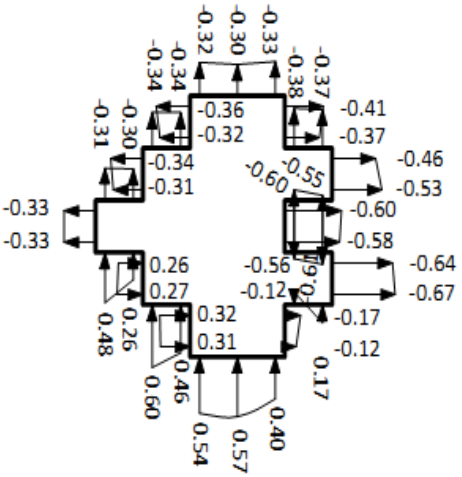

Section E-E

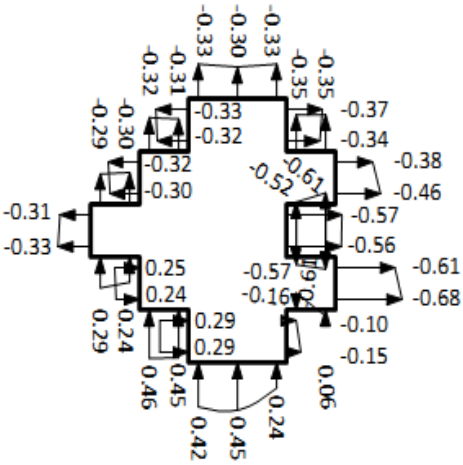

Section F-F

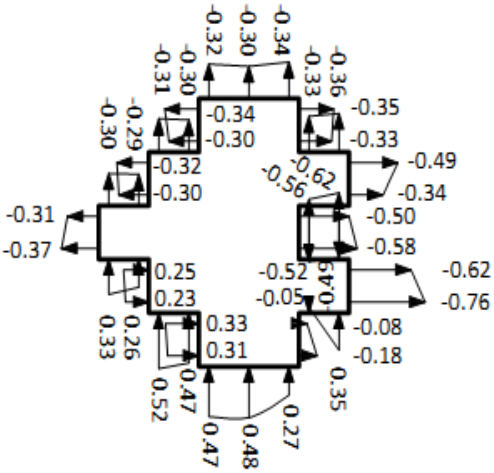

Section G-G

**Fig. 5.78 Cross-sectional variation of mean wind pressure coefficients ($C_{p,mean}$) on model-H at $90^0$ wind incidence angle**

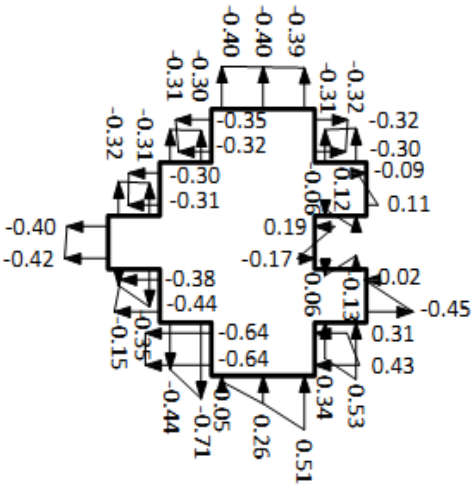


Section A-A

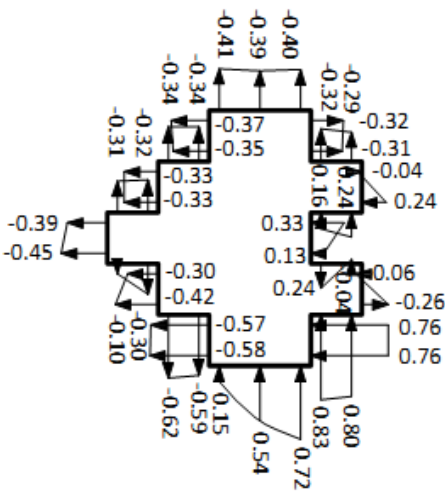


Section B-B

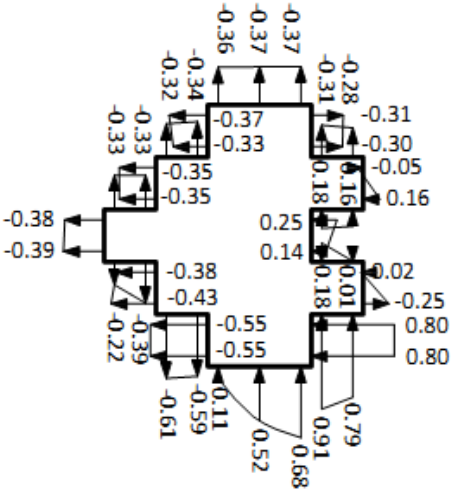


Section C-C

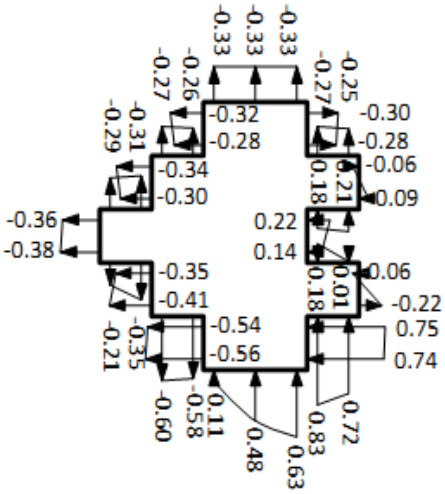


Section D-D

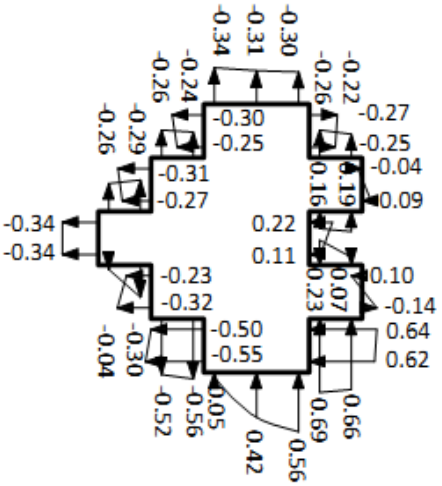


Section E-E

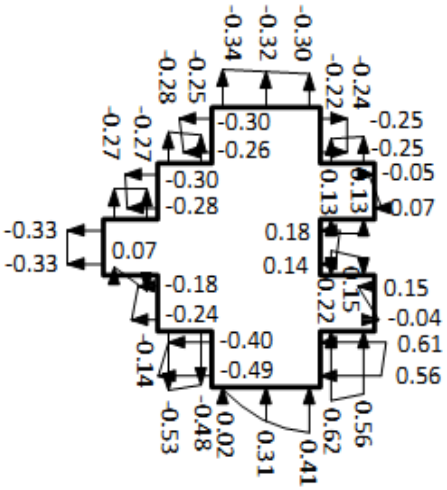


Section F-F

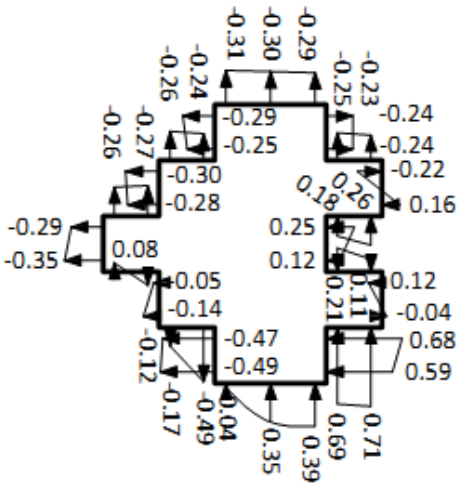


Section G-G

**Fig. 5.79 Cross-sectional variation of mean wind pressure coefficients ($C_{p,mean}$) on model-H at $120^0$ wind incidence angle**

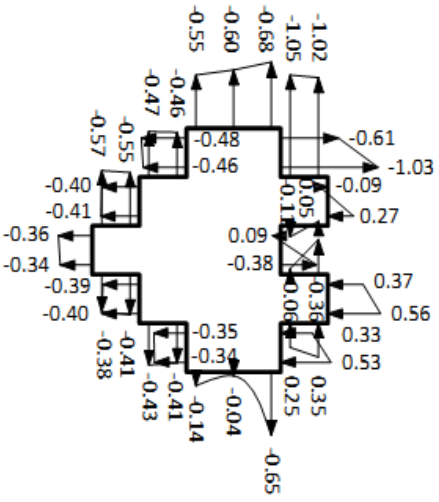

Section A-A

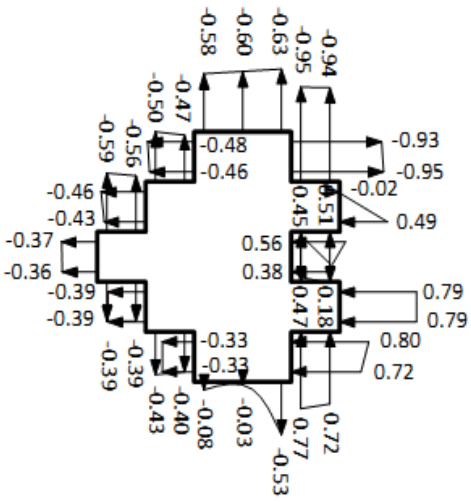

Section B-B

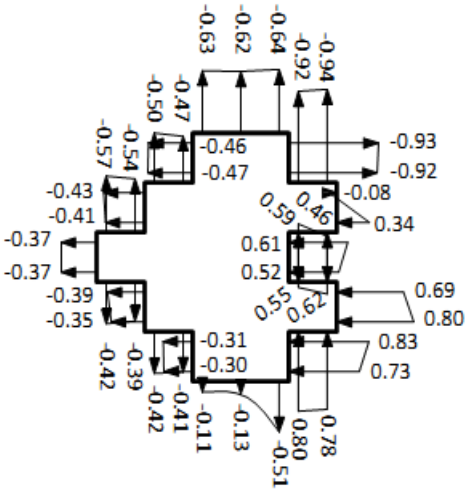

Section C-C

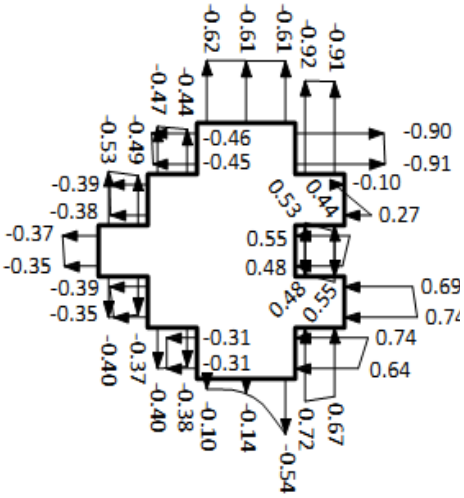

Section D-D

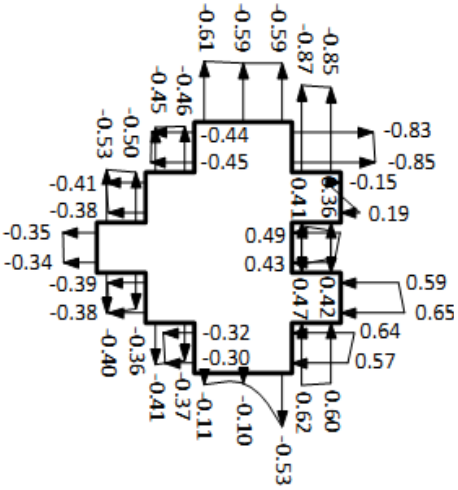

Section E-E

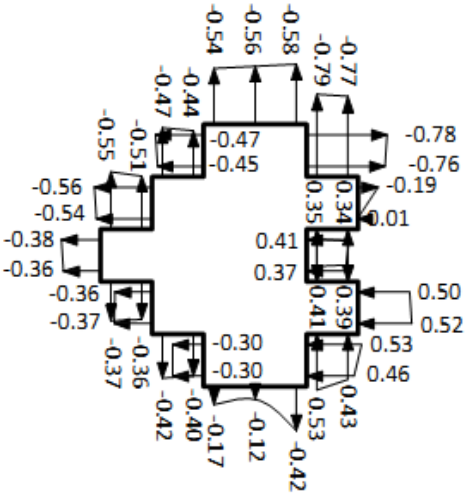

Section F-F

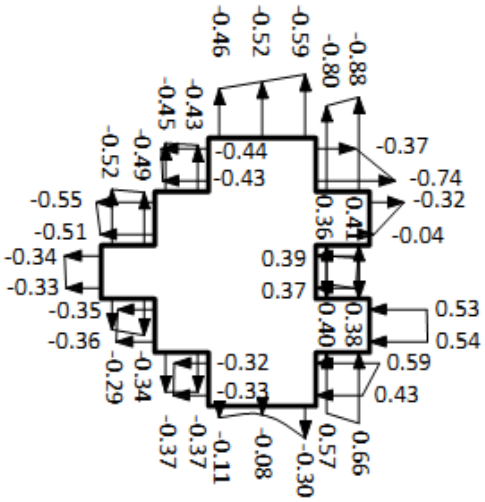

Section G-G

**Fig. 5.80 Cross-sectional variation of mean wind pressure coefficients ($C_{p,mean}$) on model-H at $150^0$ wind incidence angle**

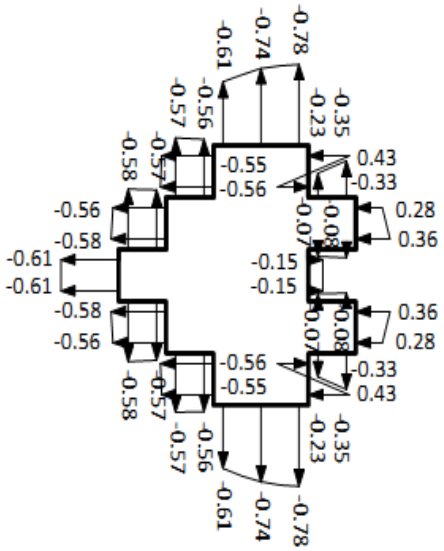


Section A-A

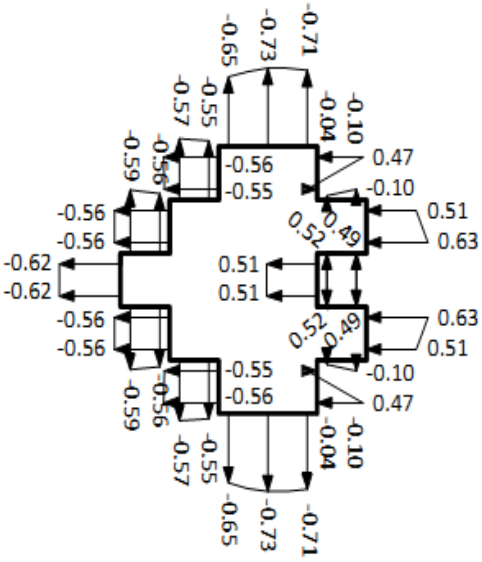


Section B-B

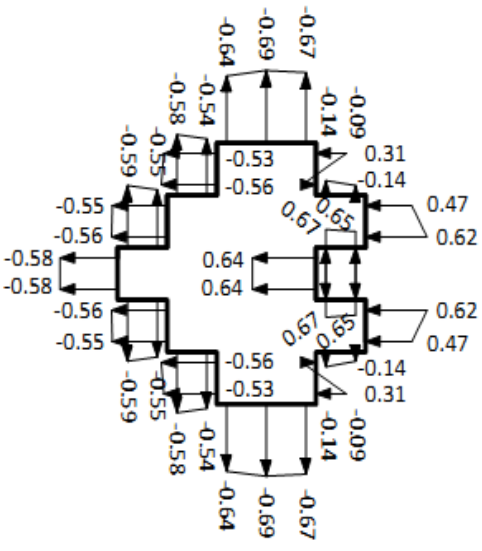


Section C-C

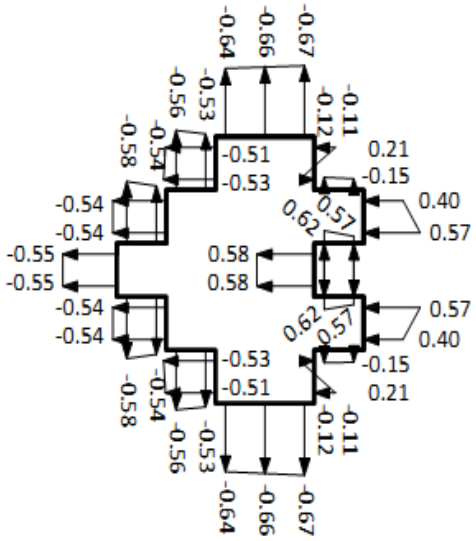


Section D-D

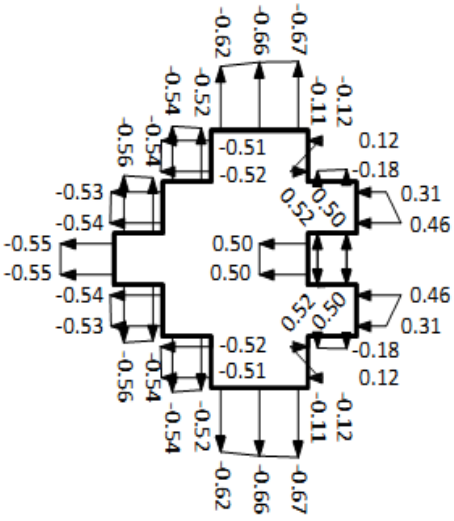


Section E-E

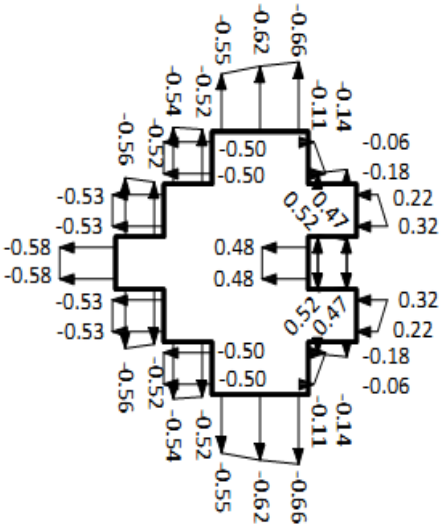


Section F-F

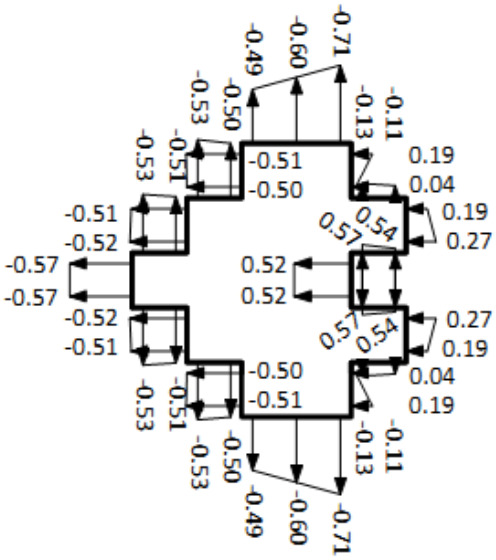


Section G-G

**Fig. 5.81 Cross-sectional variation of mean wind pressure coefficients ($C_{p,mean}$) on model-H at $180^0$ wind incidence angle**

Value of $C_{p,mean}$ on Face-A of models-H for 7 wind direction are compared in Table 5.8. Maximum value of $C_p$ is 0.71 and minimum is -1.03 which occur at $0^0$ and $60^0$ wind angles respectively.

**Table 5.8 Variation of $C_{p,mean}$ on face-A of model-H with wind incidence angle**

| **Pressure points** | **Mean wind pressure coefficients ($C_{p,mean}$)** | | | | | | |
|---|---|---|---|---|---|---|---|
| | **$0^0$** | **$30^0$** | **$60^0$** | **$90^0$** | **$120^0$** | **$150^0$** | **$180^0$** |
| 1 | 0.48 | **-0.12** | -0.39 | **-0.41** | -0.40 | -0.36 | -0.61 |
| 2 | 0.48 | 0.36 | -1.01 | -0.40 | -0.42 | -0.34 | -0.60 |
| 3 | **0.71** | 0.17 | -0.44 | -0.39 | -0.39 | -0.37 | -0.61 |
| 4 | **0.71** | **0.45** | -0.97 | -0.37 | **-0.45** | -0.36 | **-0.62** |
| 5 | 0.69 | 0.08 | -0.57 | -0.35 | -0.38 | -0.37 | -0.59 |
| 6 | 0.69 | 0.26 | -0.99 | -0.33 | -0.39 | -0.37 | -0.57 |
| 7 | 0.68 | 0.06 | -0.50 | -0.33 | -0.36 | -0.37 | **-0.54** |
| 8 | 0.68 | 0.20 | **-1.03** | -0.32 | -0.38 | -0.35 | -0.55 |
| 9 | 0.54 | 0.02 | -0.48 | -0.33 | -0.34 | -0.35 | -0.56 |
| 10 | 0.54 | 0.06 | -0.86 | -0.33 | -0.34 | -0.34 | -0.55 |
| 11 | 0.52 | -0.03 | -0.44 | **-0.31** | -0.33 | **-0.38** | -0.59 |
| 12 | 0.52 | -0.06 | -0.73 | -0.33 | -0.33 | -0.36 | -0.58 |
| 13 | 0.65 | -0.03 | **-0.33** | **-0.31** | **-0.29** | -0.34 | -0.57 |
| 14 | 0.65 | -0.07 | -0.72 | -0.37 | -0.35 | **-0.33** | -0.57 |

## 5.3 INTERFERENCE CONDITION

### 5.3.1 Model-A (Square Shape)

Wind interference effects on distribution of mean wind pressure coefficients on different surfaces of model-A are studied for 3 interference conditions namely full blockage, half blockage and no blockage (Fig. 5.82). Instrumented model i.e. Perspex sheet model of model-A is placed at the center of the turn-table with plywood model as interfering model placed in front of it on windward side. In first situation, plywood model is placed exactly in front of Perspex sheet model causing full blockage to stream of wind. In second case, 50% of front surface of instrumented building is blocked. In third case, wind is free to hit windward surface of instrumented building. Gap between two models in the direction of wind is kept as 60 mm, i.e. 0.1 times depth of the model.

In full blockage interference condition, all faces are subjected to suction (Fig. 5.83) due to the presence of interfering building model. Windward face i.e. face-A, is subjected to maximum suction and leeward face i.e. face-C, is subjected to minimum suction. Face-B and face-D which are parallel to the direction of wind flow are subjected to intermediate values of suction. It is also noticed that suction on these faces reduces from windward edges to leeward edges.

In half blockage wind interference condition, 50% area of the front face is subjected to wind. It is observed that some part of face-A subjected to pressure and remaining is subjected to suction. Maximum pressure occurs near the edge of face-A and the value is 0.7. Remaining faces are subjected to suction. Maximum suction (-0.44) occurs on face-D.

It is seen from Fig. 5.82 that 100% area of face-A is open to wind in no blockage interference condition. Although entire face-A is subjected to pressure (Fig. 5.85), one edge of the face is subjected to very small pressure as compared to another edge. Further, maximum pressure does not occur along centerline, but along a line towards one edge. All remaining faces are subjected to suction. Face-B is subjected to minimum suction in full blockage condition and maximum suction in no blockage condition.

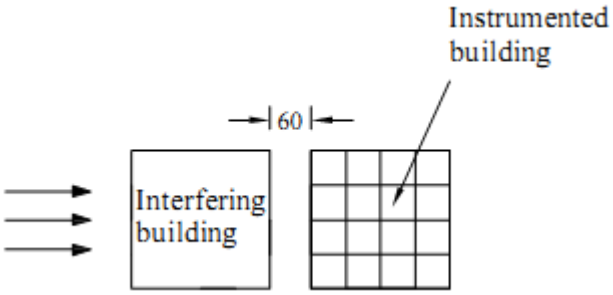


Full blockage interference condition

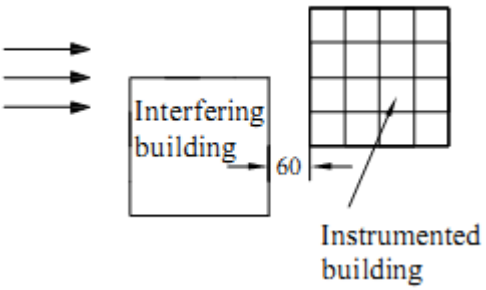


Half blockage interference condition

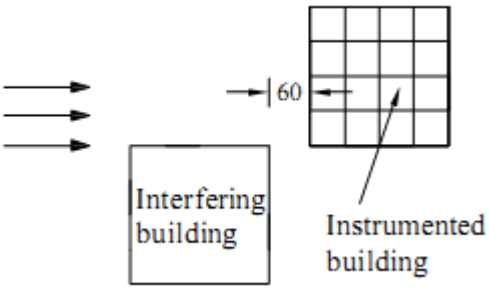


No blockage interference condition

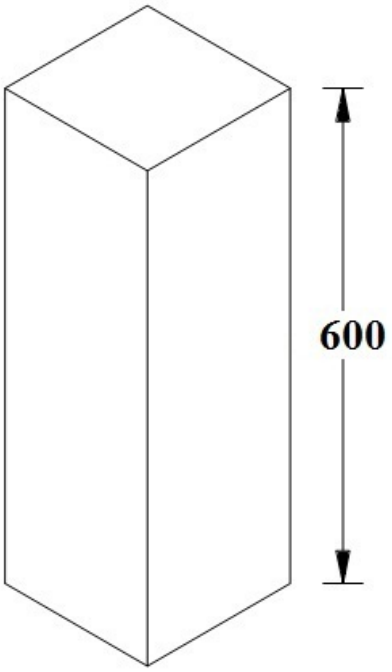


Isometric

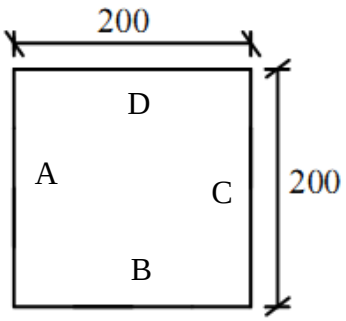


Plan

All dimensions are in mm

**Fig. 5.82 Details of model-A showing different interference conditions**

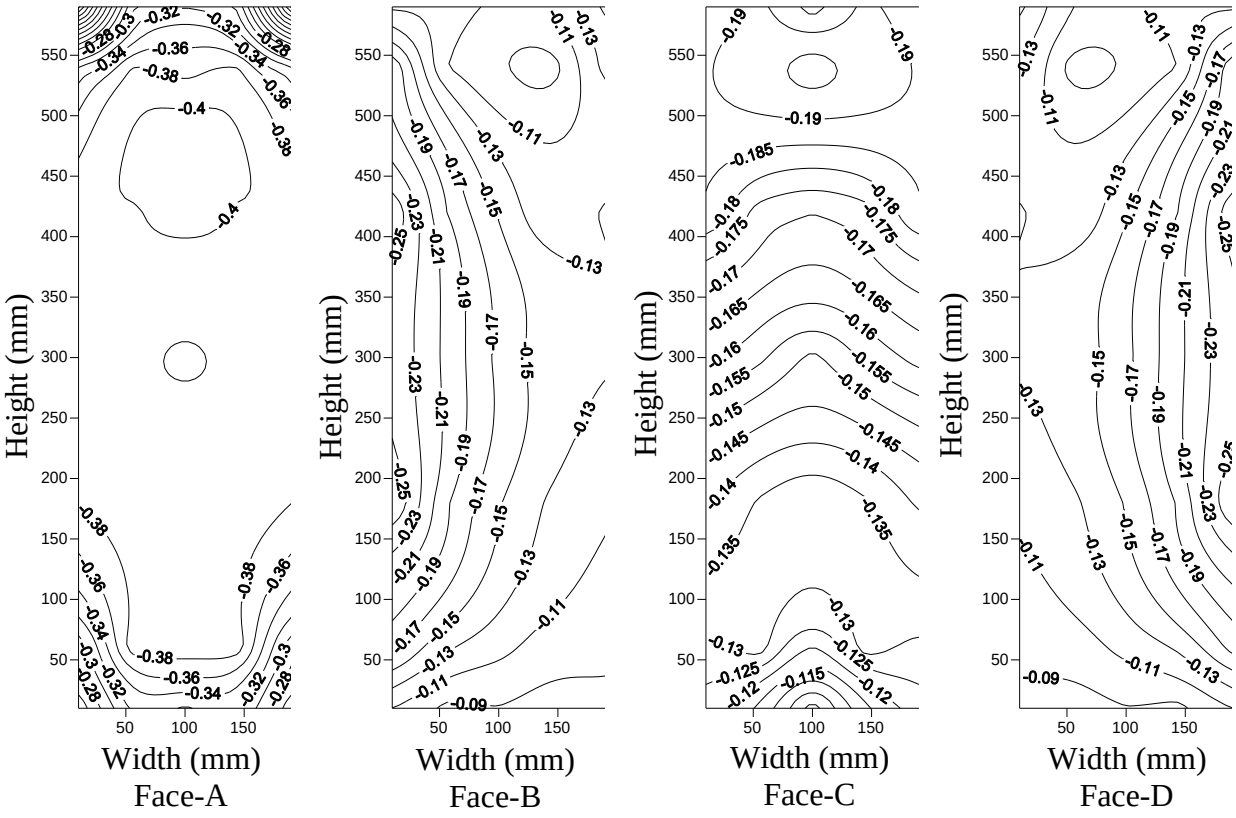


**Fig. 5.83 Distribution of mean wind pressure coefficients ($C_{p,mean}$) on different surfaces of model-A under full blockage interference condition**

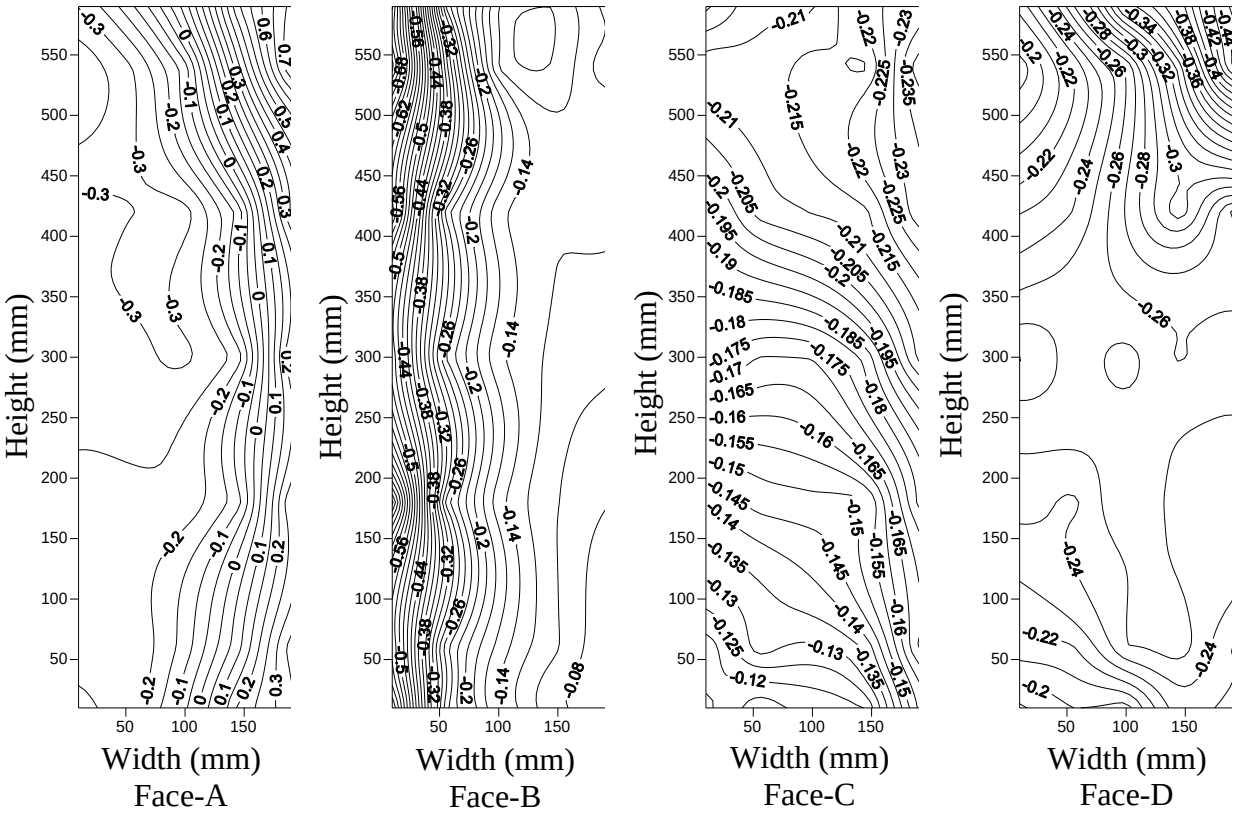


**Fig. 5.84 Distribution of mean wind pressure coefficients ($C_{p,mean}$) on different surfaces of model-A under half blockage interference condition**

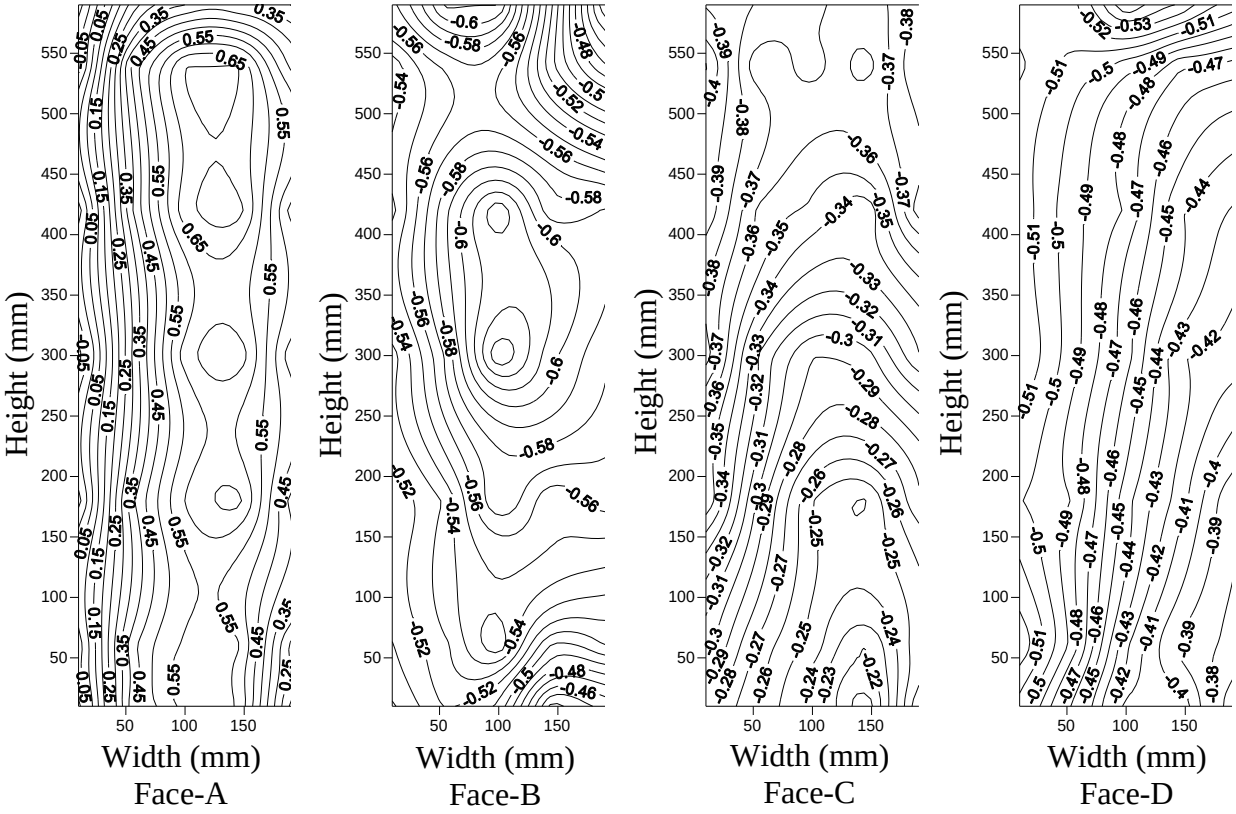


**Fig. 5.85 Distribution of mean wind pressure coefficients ($C_{p,mean}$) on different surfaces of model-A under no blockage interference condition**

Figures 5.86 to 5.88 show the detailed variation of mean wind pressure coefficients at different sections along the height in various interference conditions of wind flow. It is observed from Fig.5.86 that variation of mean wind pressure coefficients is parabolic at section A-A in full blockage interference condition. Maximum suction occurs on face-A at section C-C of building model-A and value of suction is -0.40.

It can be seen from the Fig. 5.87 that some portion of face-A is subjected to pressure and rest is subjected to suction. The maximum pressure occurs at section B-B of face-A and its value is 0.75. Maximum suction occurs on face-B due to the presence of interfering building and value of the suction is -0.77.

In case of no blockage interference condition (Fig. 5.88), most of the portion of face-A is subjected to pressure while some of its portion is subjected to suction. Rest all faces are subjected to suction and the value of the suction varies between -0.3 to -0.6.

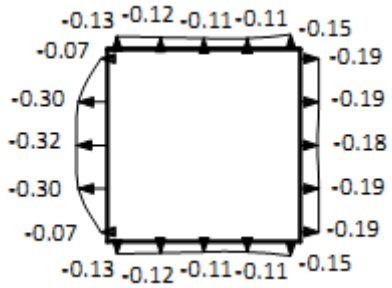


Section A-A

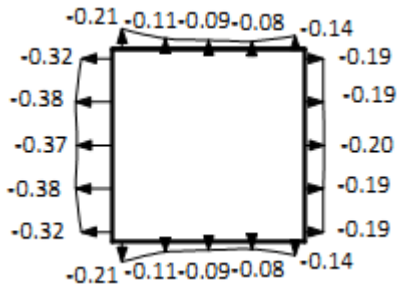


Section B-B

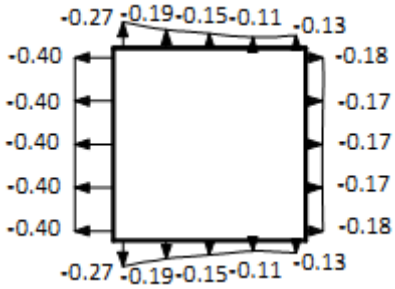


Section C-C

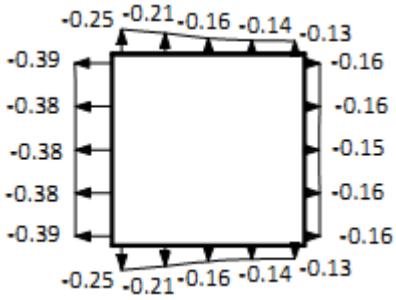


Section D-D

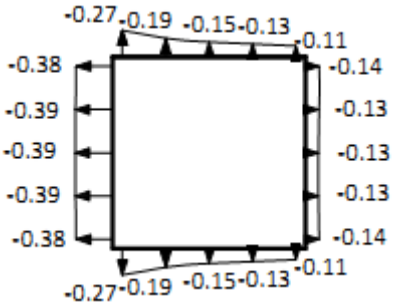


Section E-E

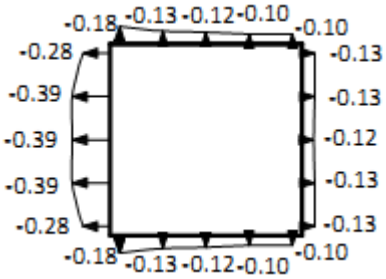


Section F-F

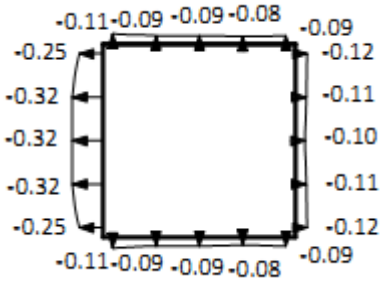


Section G-G

**Fig. 5.86 Cross-sectional variation of mean wind pressure coefficients ($C_{p,mean}$) on model-A in full blockage interference condition**

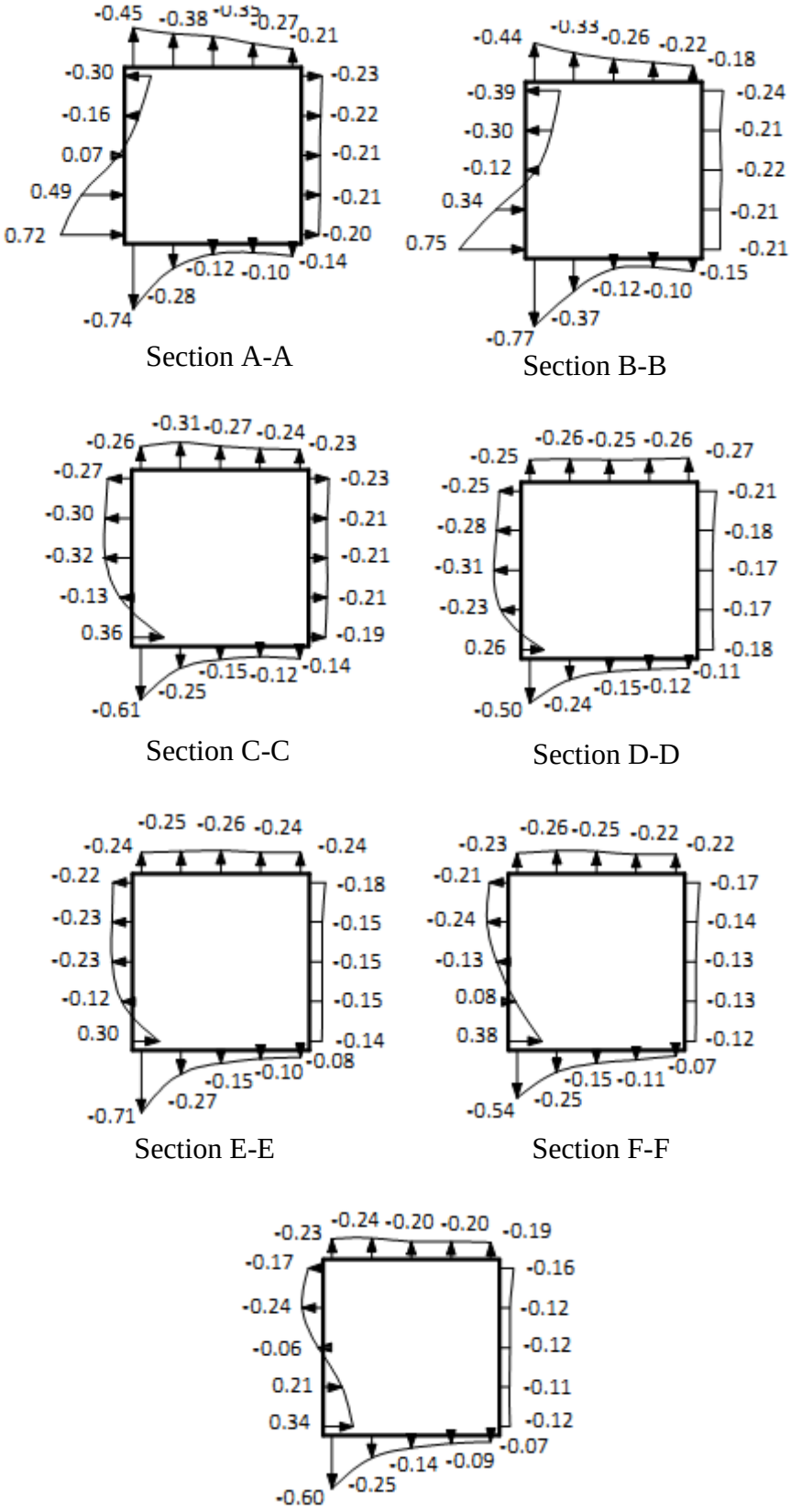


**Fig. 5.87 Cross-sectional variation of mean wind pressure coefficients ($C_{p,mean}$) on model-A in half blockage interference condition**

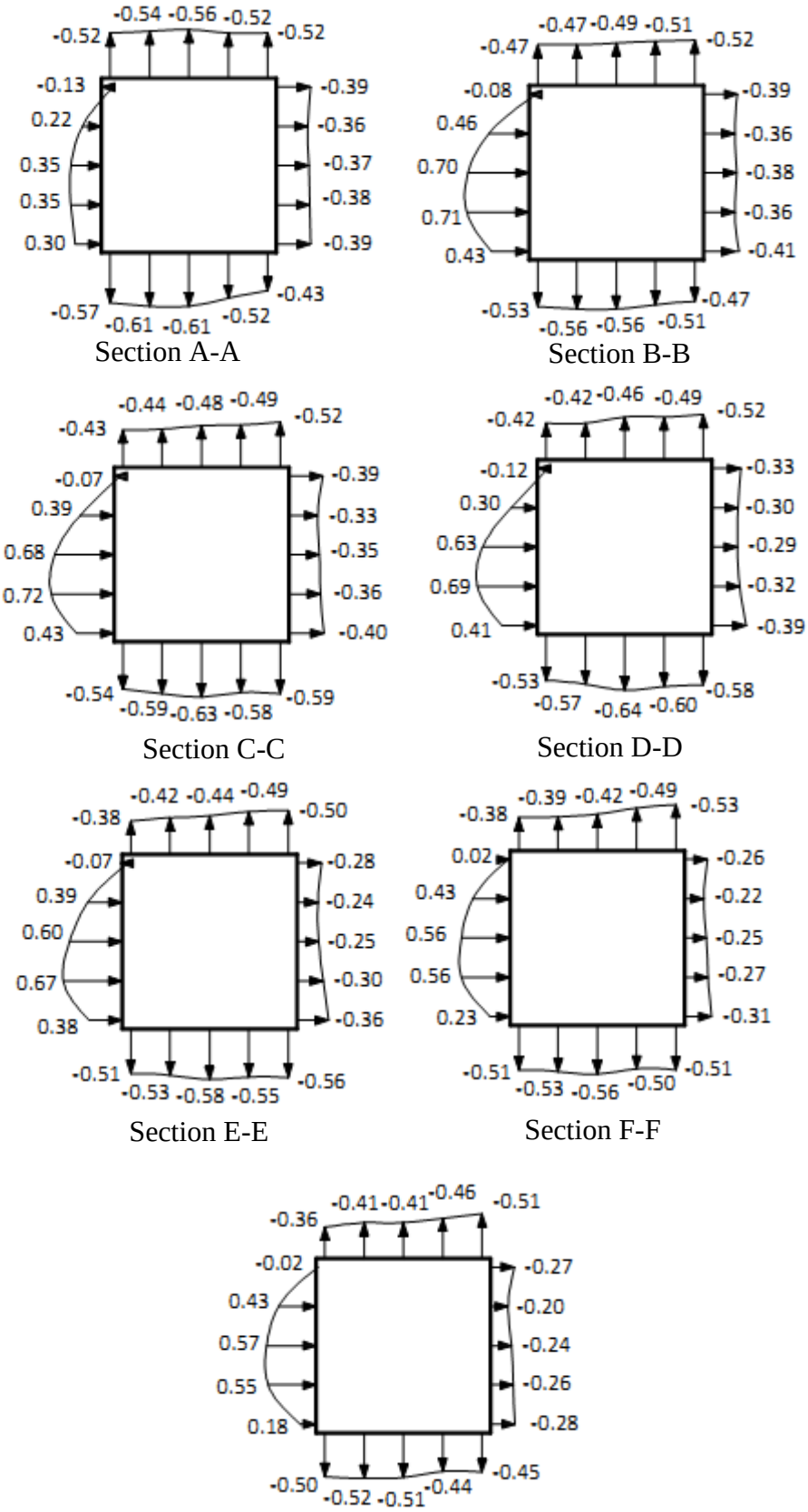


**Fig. 5.88 Cross-sectional variation of mean wind pressure coefficients ($C_{p,mean}$) on model-A in no blockage interference condition**

Table 5.9 compares the values of $C_{p,mean}$ at 35 pressure points on face-A under different interference conditions with isolated condition.

**Table 5.9 Interference effect on variation of $C_{p,mean}$ on face-A of model-A**

| Pressure points | Mean wind pressure coefficients ($C_{p,mean}$) | | | |
|---|---|---|---|---|
| | Full blockage | Half blockage | No blockage | Isolated ($0^0$ wind incidence angle) |
| 1 | -0.07 | -0.30 | **-0.13** | 0.16 |
| 2 | -0.30 | -0.16 | 0.22 | 0.23 |
| 3 | -0.32 | 0.07 | 0.35 | 0.25 |
| 4 | -0.30 | 0.49 | 0.35 | 0.23 |
| 5 | -0.07 | 0.72 | 0.30 | 0.16 |
| 6 | -0.32 | **-0.39** | -0.08 | 0.30 |
| 7 | -0.38 | -0.30 | 0.46 | 0.59 |
| 8 | -0.37 | -0.12 | 0.70 | 0.64 |
| 9 | -0.38 | 0.34 | 0.71 | 0.59 |
| 10 | -0.32 | **0.75** | 0.43 | 0.30 |
| 11 | **-0.40** | -0.27 | -0.07 | 0.26 |
| 12 | **-0.40** | -0.30 | 0.39 | 0.61 |
| 13 | **-0.40** | -0.32 | 0.68 | **0.68** |
| 14 | **-0.40** | -0.13 | **0.72** | 0.61 |
| 15 | **-0.40** | 0.36 | 0.43 | 0.26 |
| 16 | -0.39 | -0.25 | -0.12 | 0.23 |
| 17 | -0.38 | -0.28 | 0.30 | 0.56 |
| 18 | -0.38 | -0.31 | 0.63 | 0.60 |
| 19 | -0.38 | -0.23 | 0.69 | 0.56 |
| 20 | -0.39 | 0.26 | 0.41 | 0.23 |
| 21 | -0.38 | -0.22 | -0.07 | 0.17 |
| 22 | -0.39 | -0.23 | 0.39 | 0.49 |
| 23 | -0.39 | -0.23 | 0.60 | 0.53 |
| 24 | -0.39 | -0.12 | 0.67 | 0.49 |
| 25 | -0.38 | 0.30 | 0.38 | 0.17 |
| 26 | -0.28 | -0.21 | 0.02 | 0.04 |
| 27 | -0.39 | -0.24 | 0.43 | 0.35 |
| 28 | -0.39 | -0.13 | 0.56 | 0.40 |
| 29 | -0.39 | 0.08 | 0.56 | 0.35 |
| 30 | -0.28 | 0.38 | 0.23 | 0.04 |
| 31 | -0.25 | -0.17 | -0.02 | 0.03 |
| 32 | -0.32 | -0.24 | 0.43 | 0.43 |
| 33 | -0.32 | -0.06 | 0.57 | 0.50 |
| 34 | -0.32 | 0.21 | 0.55 | 0.43 |
| 35 | -0.25 | 0.34 | 0.18 | 0.03 |

### 5.3.2 Model-B (Plus Shape-1)

Model-B is also tested under 3 interference conditions (Fig. 5.89) as in the case of model-A. Wind pressure distribution in the form of contours of $C_{p,mean}$ on various surfaces are shown in Figs. 5.90 to 5.92. Cross-sectional variation of $C_{p,mean}$ at 7 sections along the height of the model are plotted in Figs. 5.93 to 5.95 for full blockage, half blockage and no blockage condition respectively. Windward face of model-B is subjected to suction in full blockage case. It is subjected to partly pressure and partly suction in half blockage case. In no blockage case, entire surface is subjected to pressure.

Table 5.10 compares the values of $C_{p,mean}$ at 49 pressure points on face-A under different interference conditions with isolated condition.

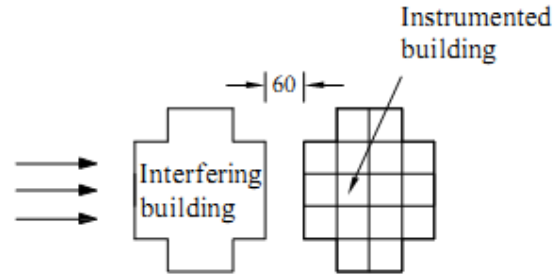


Full blockage interference condition

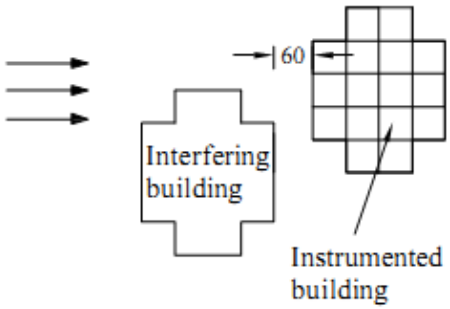


Half blockage interference condition

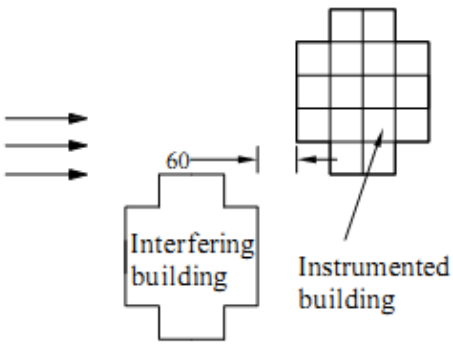


No blockage interference condition

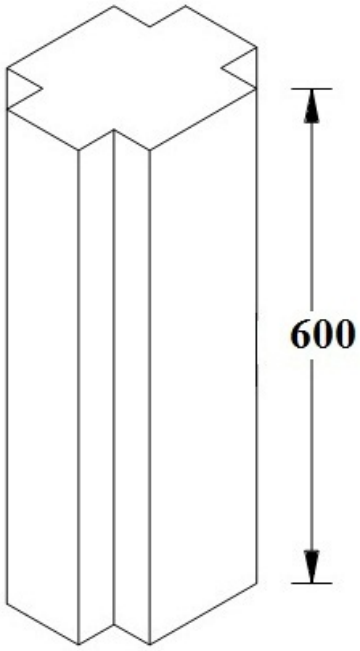


Isometric

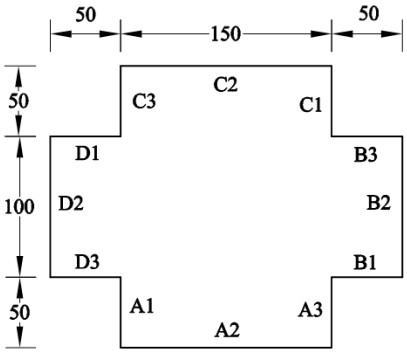


Plan

All dimensions are in mm

**Fig. 5.89 Details of model-B showing different interference conditions**

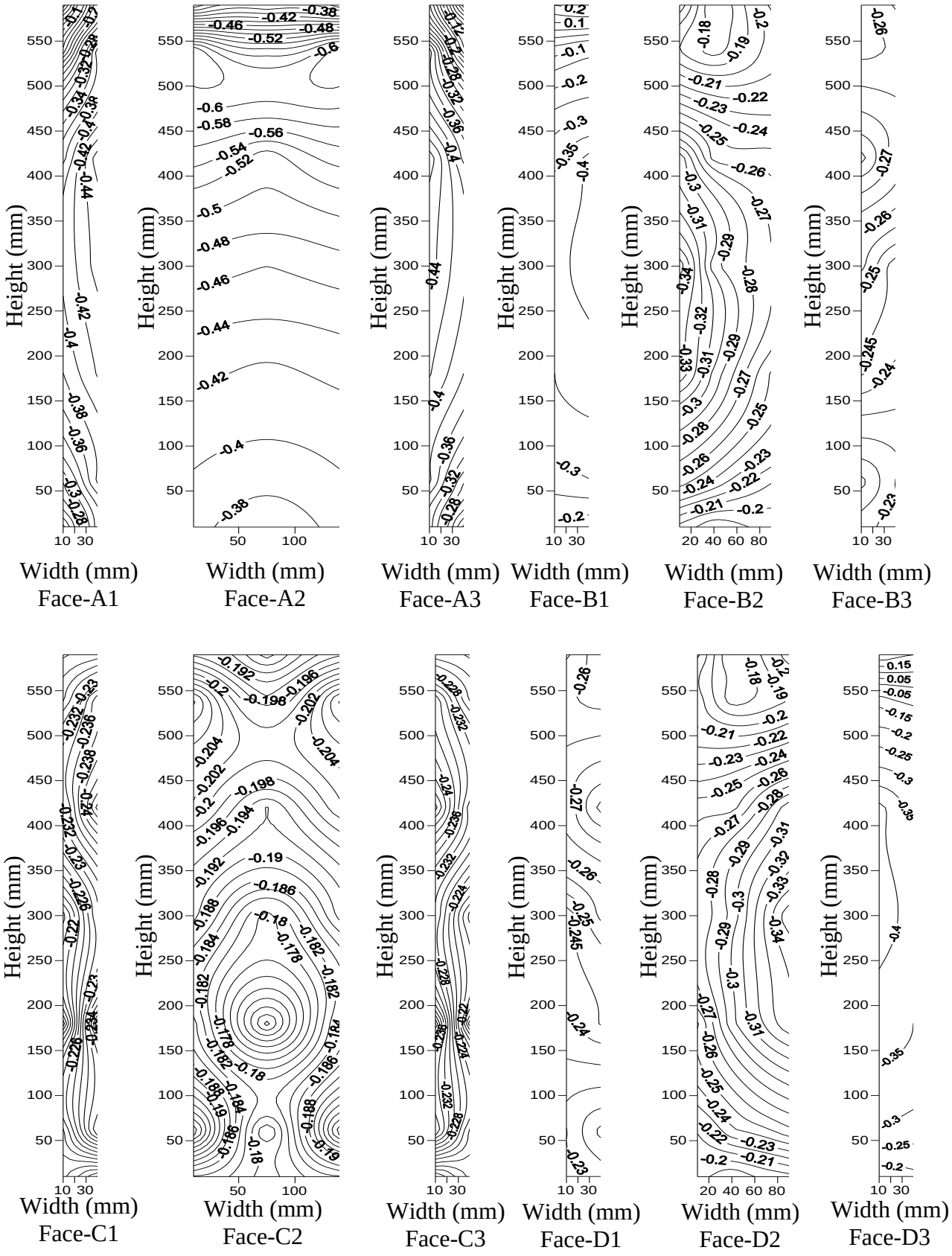


**Fig. 5.90 Distribution of mean wind pressure coefficients ($C_{p,mean}$) on different surfaces of model-A under full blockage interference condition**

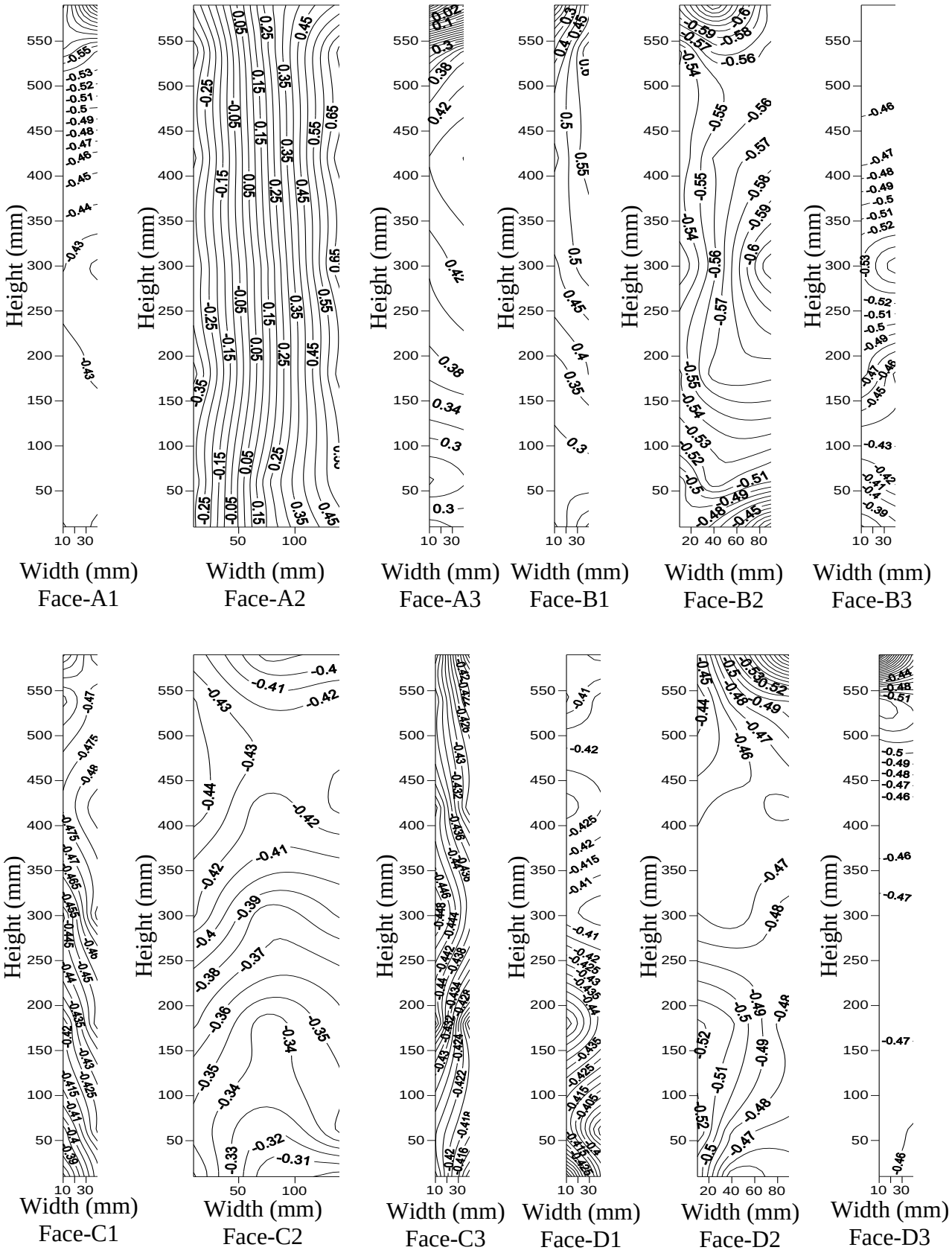


**Fig. 5.91 Distribution of mean wind pressure coefficients ($C_{p,mean}$) on different surfaces of model-A under half blockage interference condition**

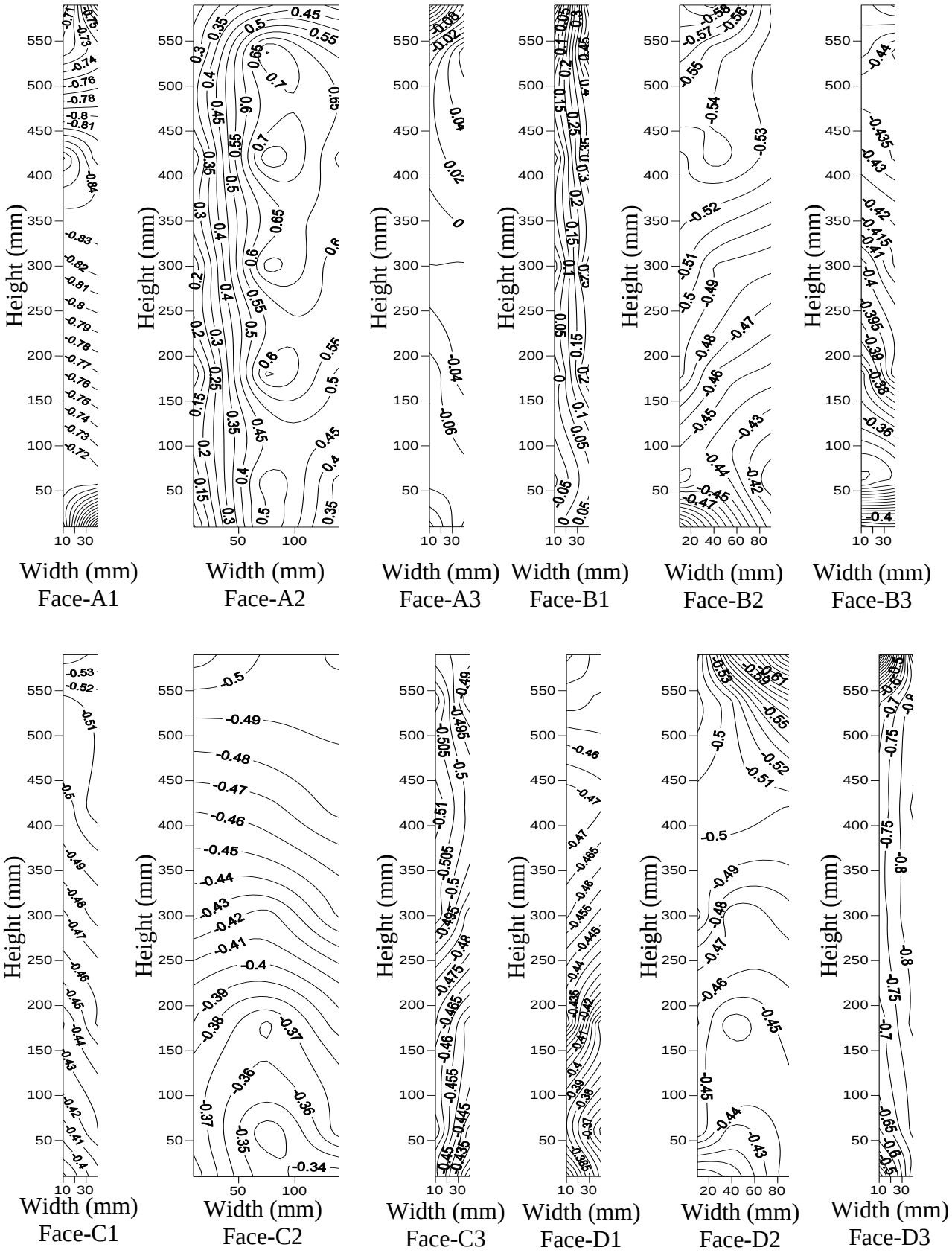


**Fig. 5.92 Distribution of mean wind pressure coefficients ($C_{p,mean}$) on different surfaces of model-A under no blockage interference condition**

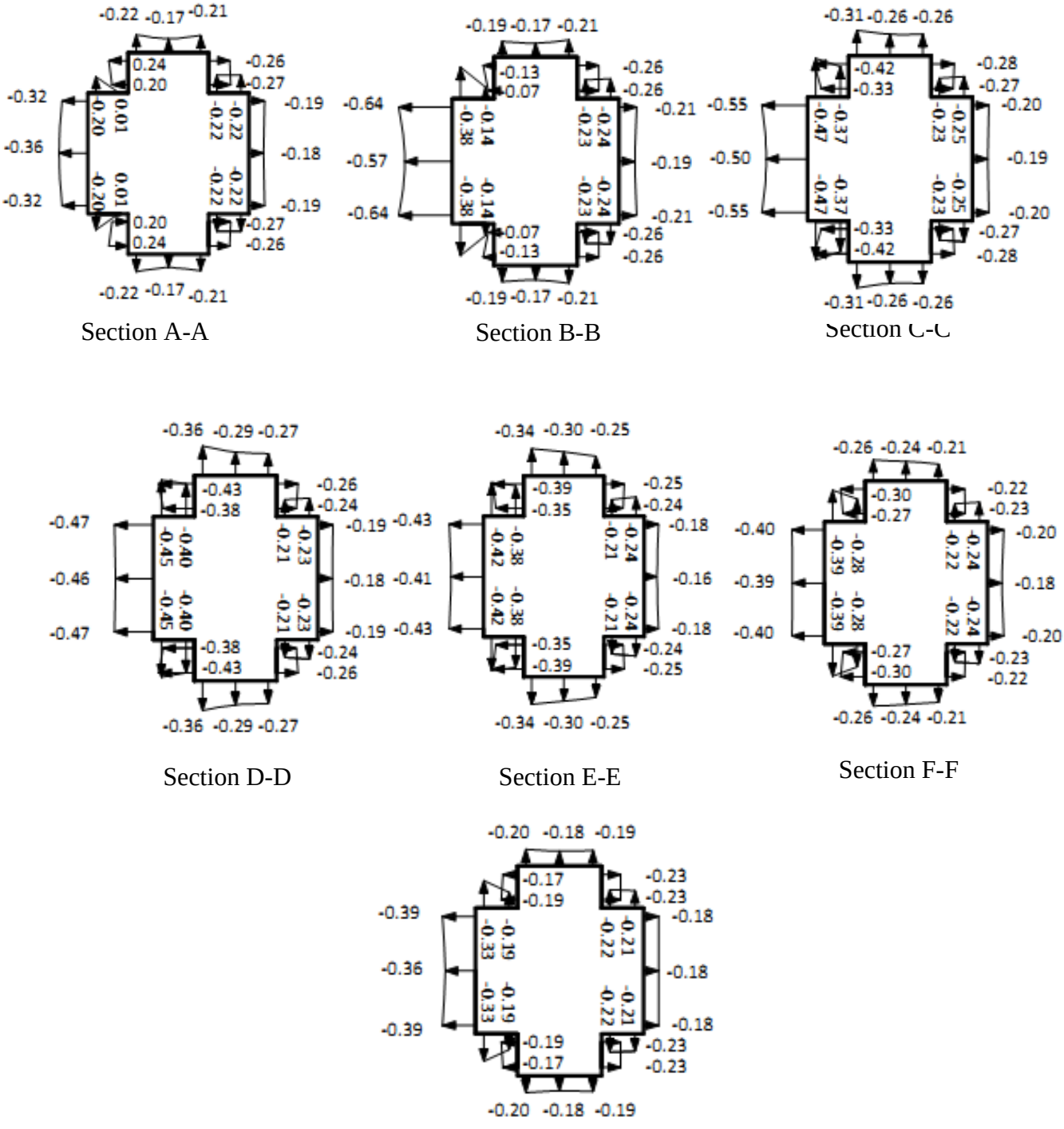


**Fig. 5.93 Cross-sectional variation of mean wind pressure coefficients ($C_{p,mean}$) on model-B in full blockage interference condition**

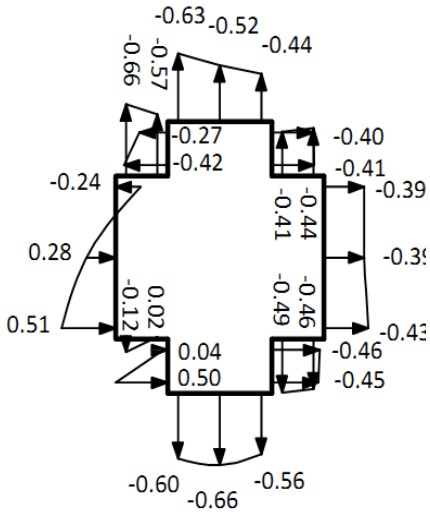


Section A-A

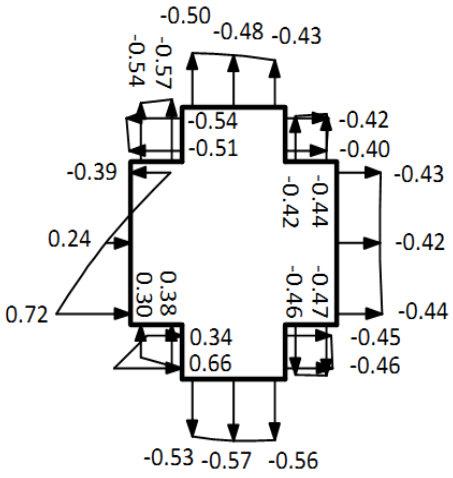


Section B-B

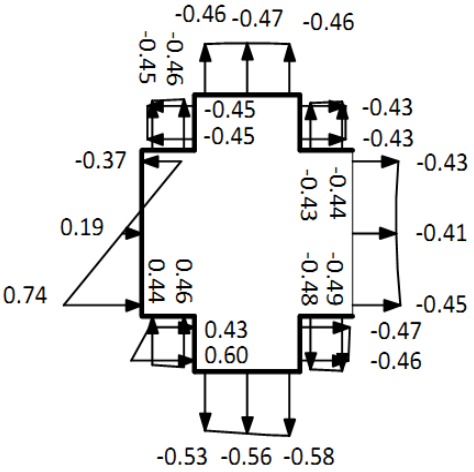


Section C-C

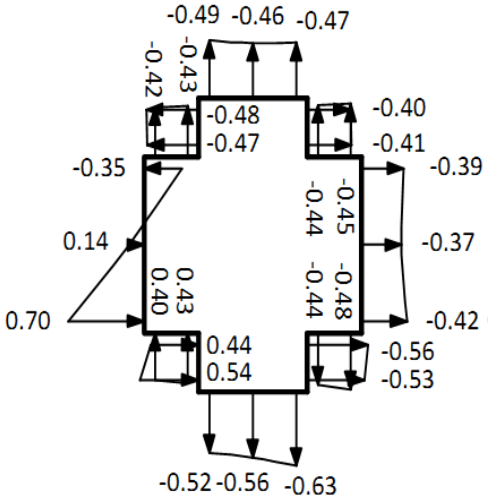


Section D-D

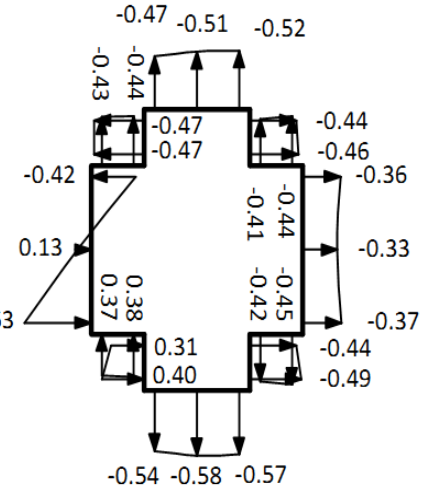


Section E-E

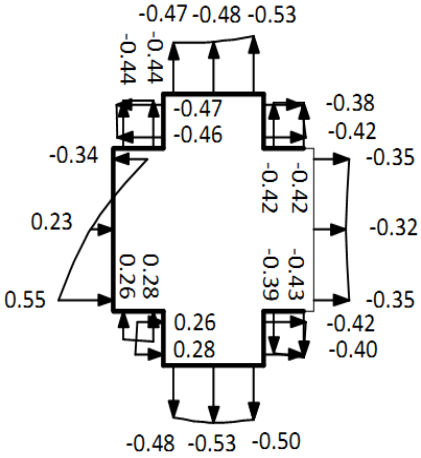


Section F-F

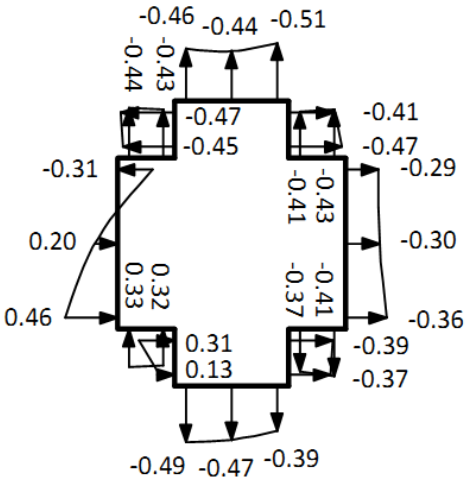


Section G-G

**Fig. 5.94 Cross-sectional variation of mean wind pressure coefficients ($C_{p,mean}$) on model-B in half blockage interference condition**

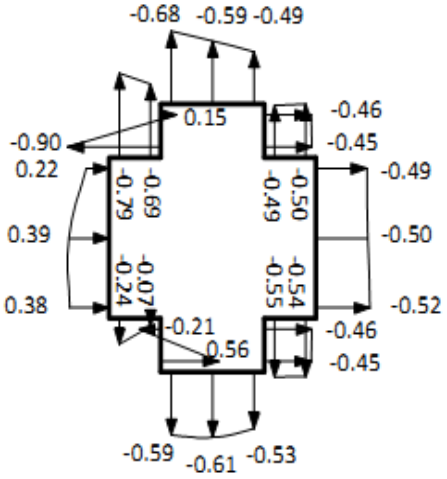


Section A-A

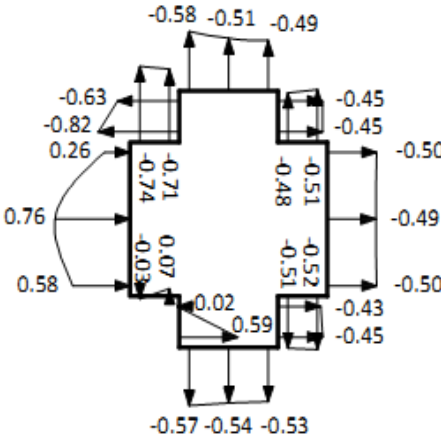


Section B-B

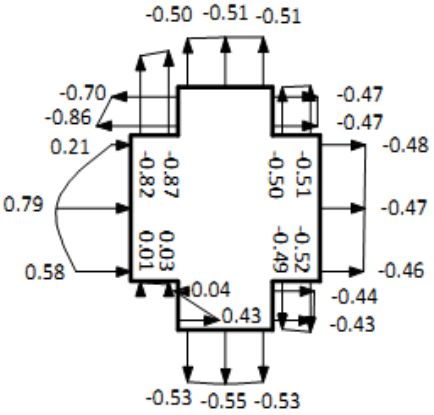


Section C-C

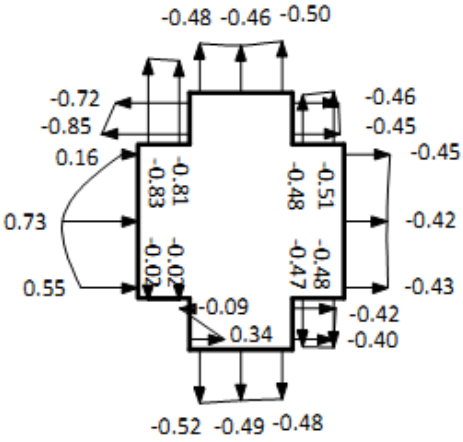


Section D-D

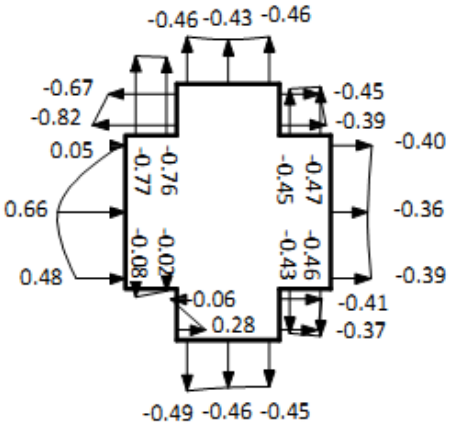


Section E-E

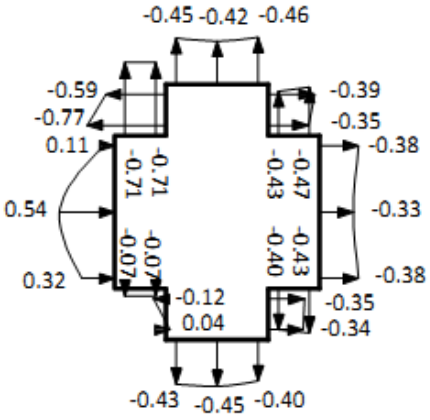


Section F-F

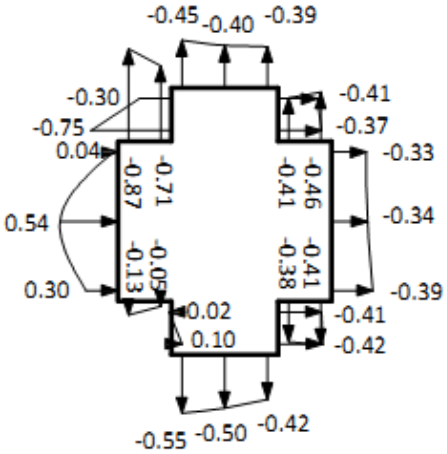


Section G-G

**Fig. 5.95 Cross-sectional variation of mean wind pressure coefficients ($C_{p,mean}$) on model-B in no blockage interference condition**

**Table 5.10 Interference effect on variation of $C_{p,mean}$ on face-A of building model-B**

| Pressure points | Mean wind pressure coefficients ($C_{p,mean}$) | | | |
|---|---|---|---|---|
| | Full blockage | Half blockage | No blockage | Isolated ($0^0$ wind incidence angle) |
| 1 | 0.01 | -0.57 | -0.69 | -0.2 |
| 2 | -0.2 | **-0.66** | -0.79 | **-0.4** |
| 3 | -0.32 | -0.24 | 0.22 | 0.22 |
| 4 | -0.36 | 0.28 | 0.39 | 0.27 |
| 5 | -0.32 | 0.51 | 0.38 | 0.22 |
| 6 | -0.2 | -0.12 | -0.24 | -0.4 |
| 7 | 0.01 | 0.02 | -0.07 | -0.2 |
| 8 | -0.14 | -0.57 | -0.71 | -0.13 |
| 9 | -0.38 | -0.54 | -0.74 | -0.21 |
| 10 | **-0.64** | -0.39 | 0.26 | 0.36 |
| 11 | -0.57 | 0.24 | 0.76 | 0.57 |
| 12 | -0.64 | 0.72 | 0.58 | 0.36 |
| 13 | -0.38 | 0.3 | -0.03 | -0.21 |
| 14 | -0.14 | 0.38 | 0.07 | -0.13 |
| 15 | -0.37 | -0.46 | -0.87 | -0.22 |
| 16 | -0.47 | -0.45 | -0.82 | -0.21 |
| 17 | -0.55 | -0.37 | 0.21 | 0.34 |
| 18 | -0.5 | 0.19 | **0.79** | 0.58 |
| 19 | -0.55 | **0.74** | 0.58 | 0.34 |
| 20 | -0.47 | 0.44 | 0.01 | -0.21 |
| 21 | -0.37 | 0.46 | 0.03 | -0.22 |
| 22 | -0.4 | -0.43 | -0.81 | -0.18 |
| 23 | -0.45 | -0.42 | -0.83 | -0.2 |
| 24 | -0.47 | -0.35 | 0.16 | 0.37 |
| 25 | -0.46 | 0.14 | 0.73 | **0.59** |
| 26 | -0.47 | 0.7 | 0.55 | 0.37 |
| 27 | -0.45 | 0.4 | -0.02 | -0.2 |
| 28 | -0.4 | 0.43 | -0.02 | -0.18 |
| 29 | -0.38 | -0.44 | -0.76 | -0.19 |
| 30 | -0.42 | -0.43 | -0.77 | -0.2 |
| 31 | -0.43 | -0.42 | 0.05 | 0.27 |
| 32 | -0.41 | 0.13 | 0.66 | 0.49 |
| 33 | -0.43 | 0.63 | 0.48 | 0.27 |
| 34 | -0.42 | 0.37 | -0.08 | -0.2 |
| 35 | -0.38 | 0.38 | -0.02 | -0.19 |
| 36 | -0.28 | -0.44 | -0.71 | -0.2 |
| 37 | -0.39 | -0.44 | -0.71 | -0.19 |
| 38 | -0.4 | -0.34 | 0.11 | 0.19 |
| 39 | -0.39 | 0.23 | 0.54 | 0.39 |
| 40 | -0.4 | 0.55 | 0.32 | 0.19 |
| 41 | -0.39 | 0.26 | -0.07 | -0.19 |
| 42 | -0.28 | 0.28 | -0.07 | -0.2 |
| 43 | -0.19 | -0.43 | -0.71 | -0.14 |
| 44 | -0.33 | -0.44 | **-0.87** | -0.22 |
| 45 | -0.39 | -0.31 | 0.04 | 0.19 |
| 46 | -0.36 | 0.2 | 0.54 | 0.45 |
| 47 | -0.39 | 0.46 | 0.3 | 0.19 |
| 48 | -0.33 | 0.33 | -0.13 | -0.22 |
| 49 | -0.19 | 0.32 | -0.05 | -0.14 |

### 5.3.3 Model-C (Plus Shape-2)

Model-C is also tested under 3 interference conditions (Fig. 5.96) like model-A and model-B. Figures 5.97 to 5.99 show wind pressure distribution on various surfaces in the form of contours of $C_{p,mean}$. Cross-sectional variation of $C_{p,mean}$ are shown in Figs. 5.100 to 5.102. Pattern of wind pressure distribution is similar to those of model-A and model-B.

Comparison of the values of $C_{p,mean}$ under different interference conditions with isolated condition can be seen in Table 5.11.

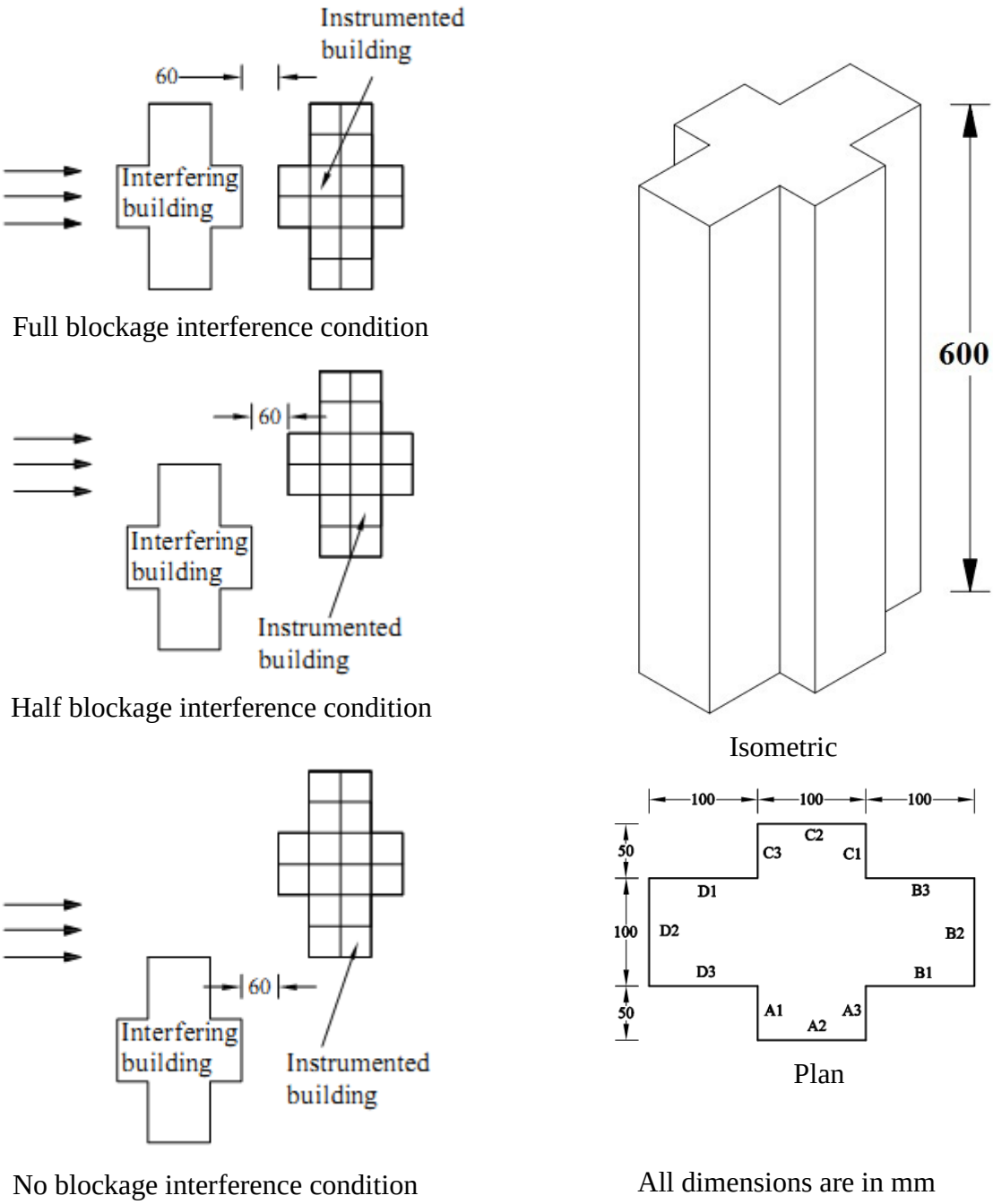


**Fig. 5.96 Details of model-C showing different interference conditions**

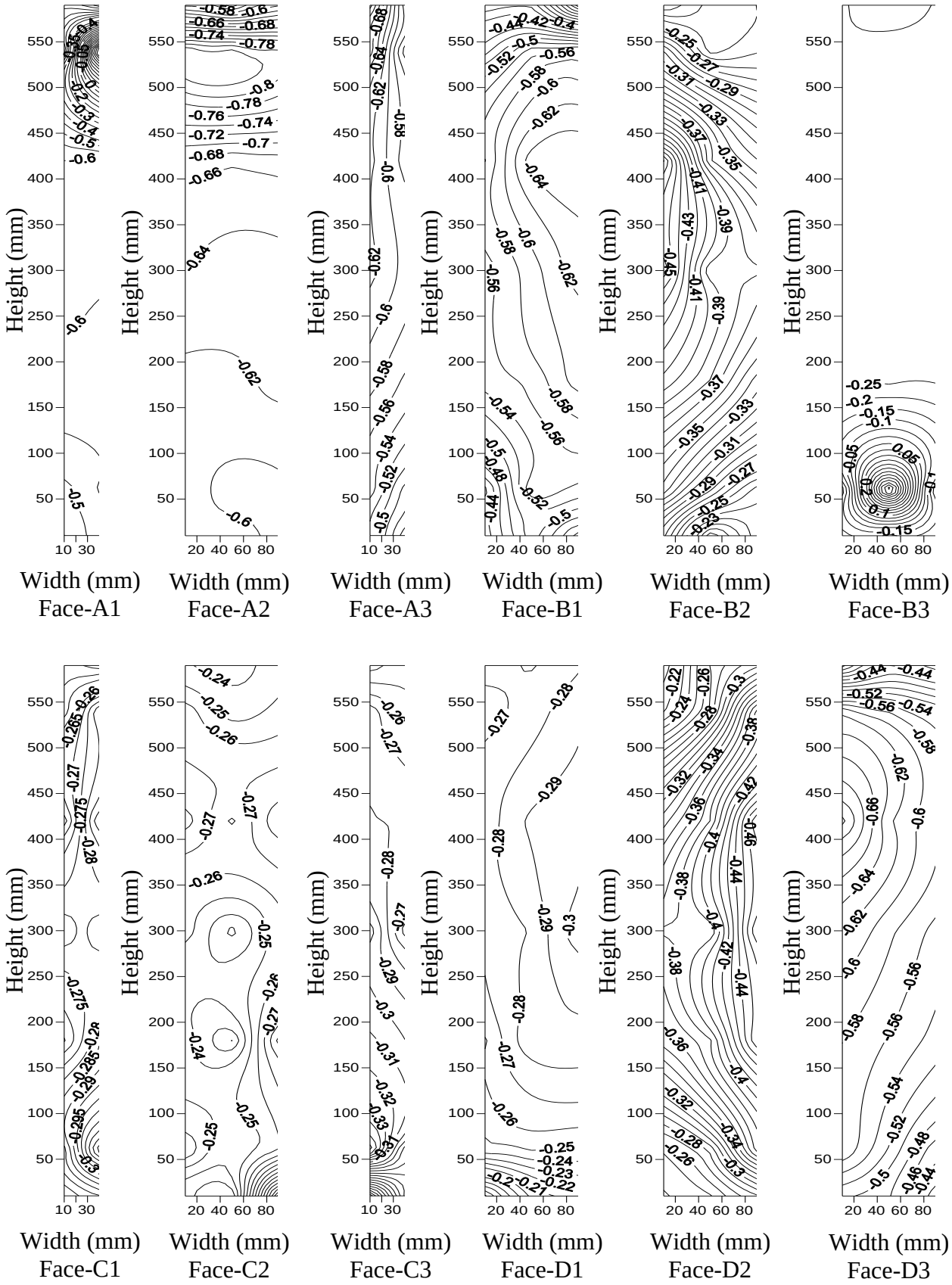


**Fig. 5.97 Distribution of mean wind pressure coefficients ($C_{p,mean}$) on different surfaces of model-C under full blockage interference condition**

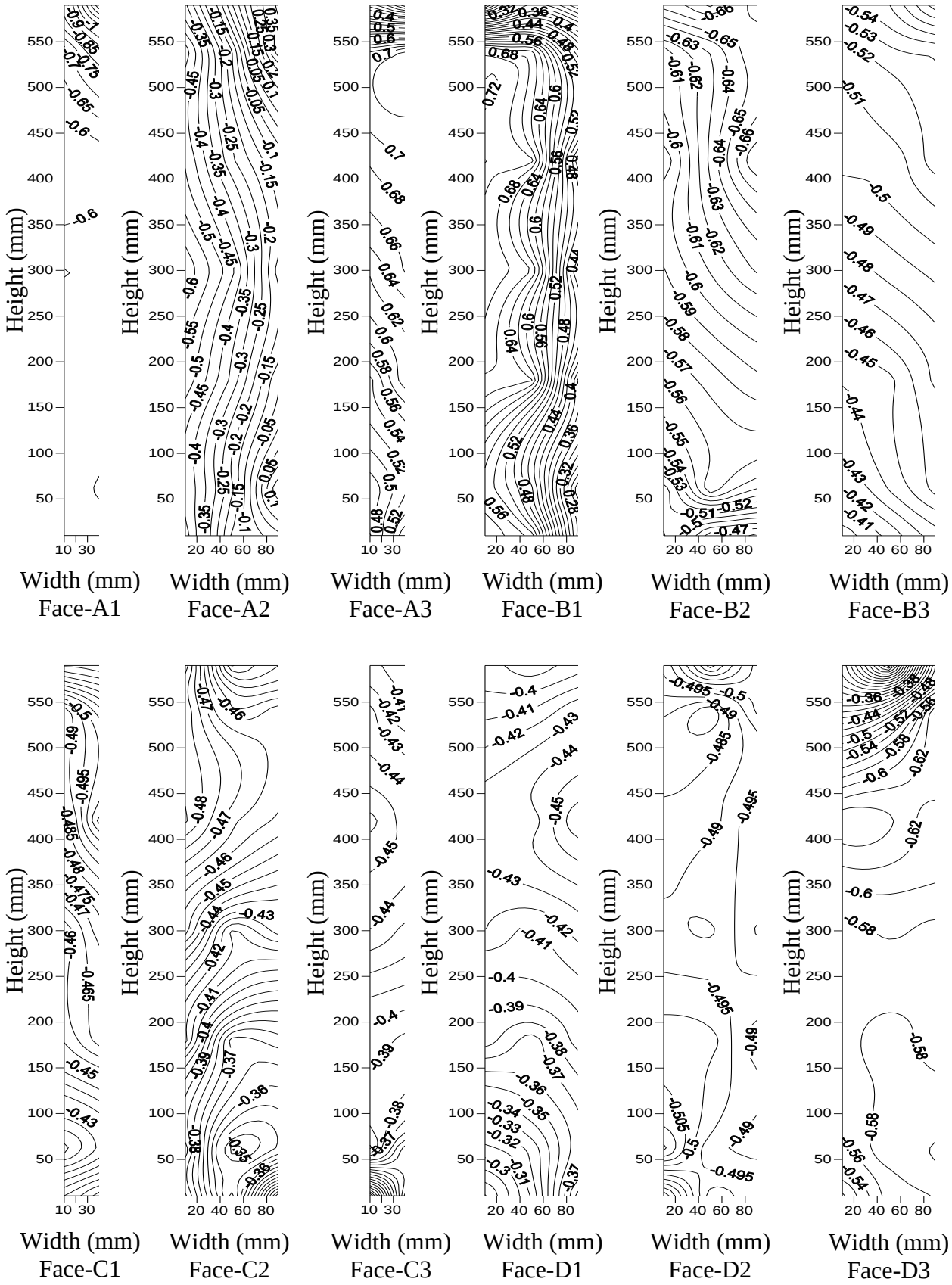


**Fig. 5.98 Distribution of mean wind pressure coefficients ($C_{p,mean}$) on different surfaces of model-C under half blockage interference condition**

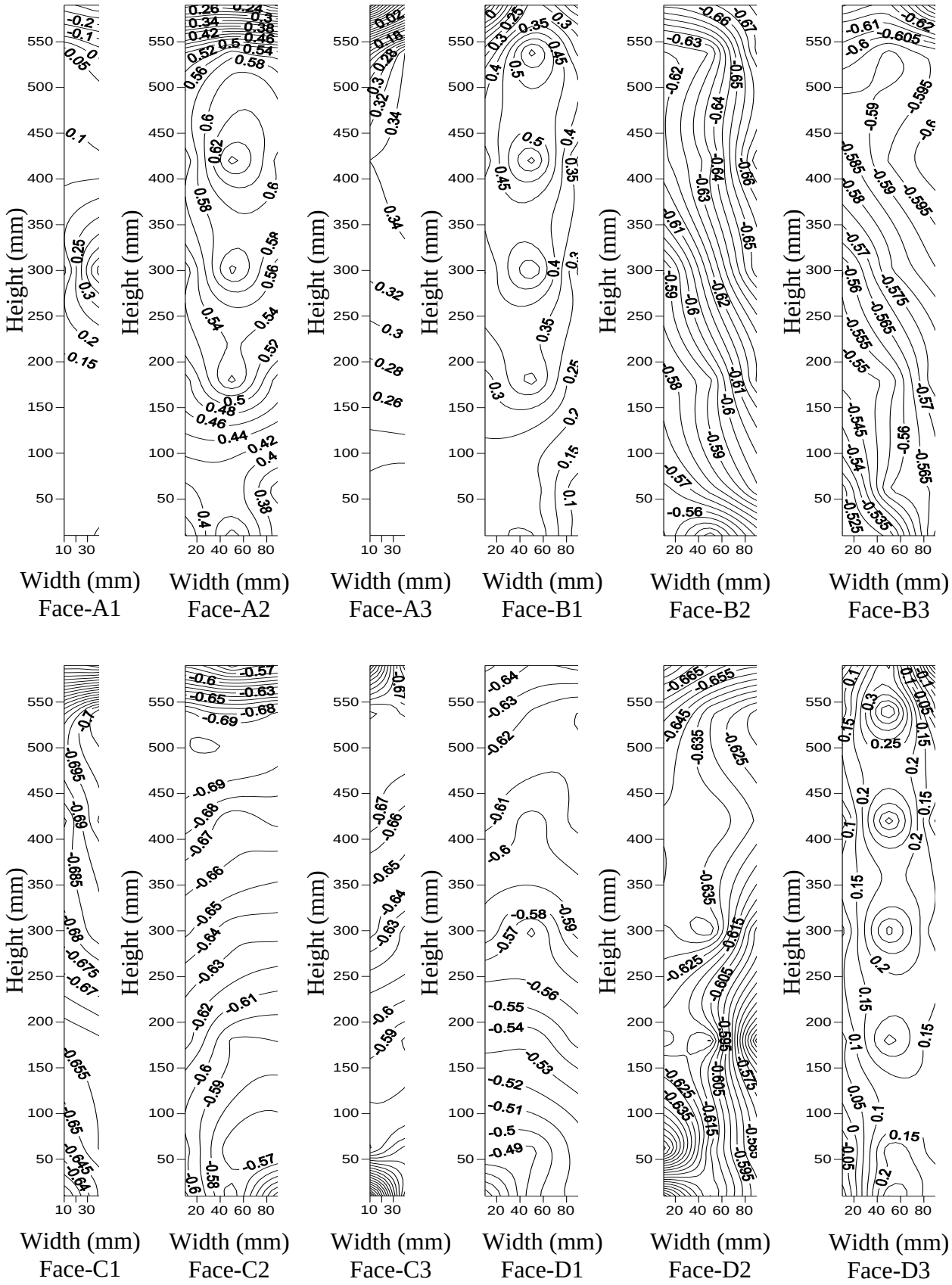


**Fig. 5.99 Distribution of mean wind pressure coefficients ($C_{p,mean}$) on different surfaces of model-C under no blockage interference condition**

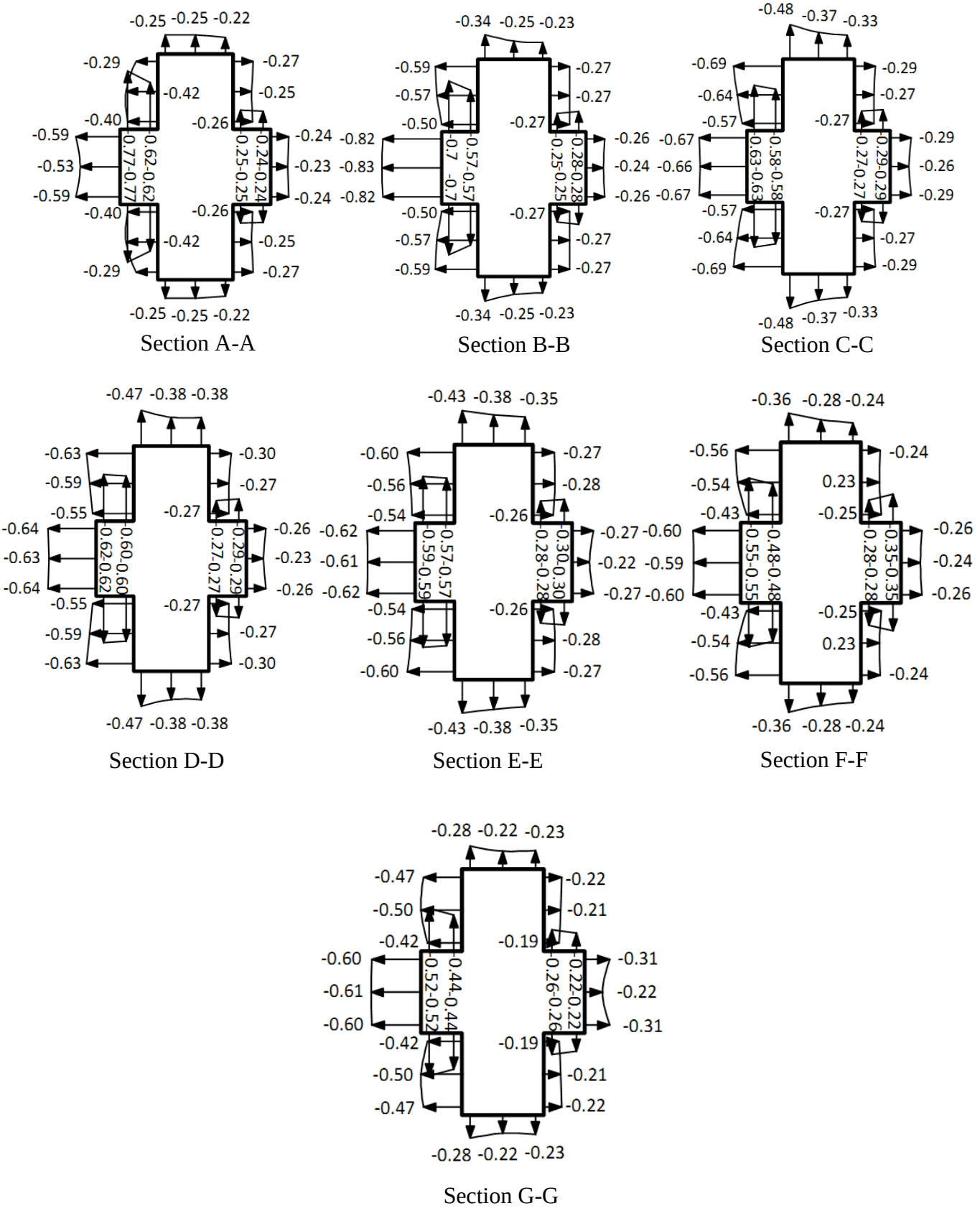


**Fig. 5.100 Cross-sectional variation of mean wind pressure coefficients ($C_{p,mean}$) on model-C in full blockage interference condition**

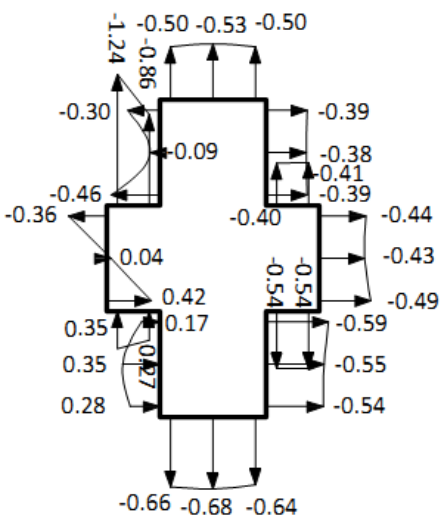


Section A-A

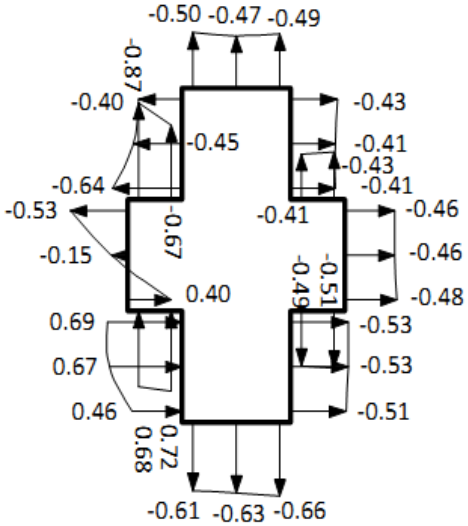


Section B-B

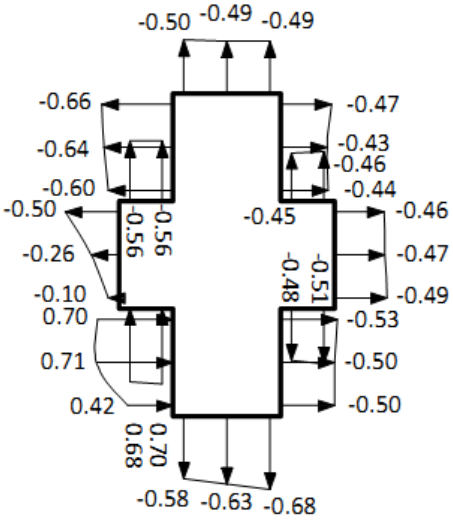


Section C-C

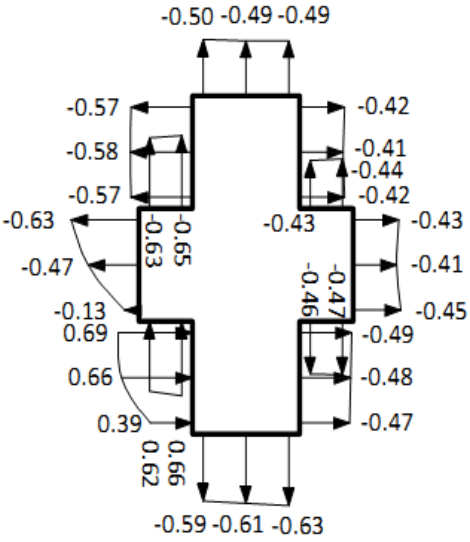


Section D-D

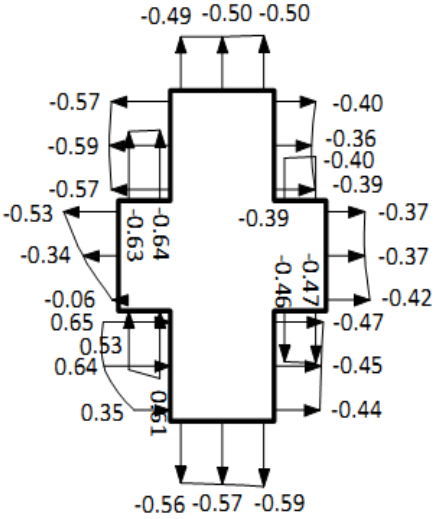


Section E-E

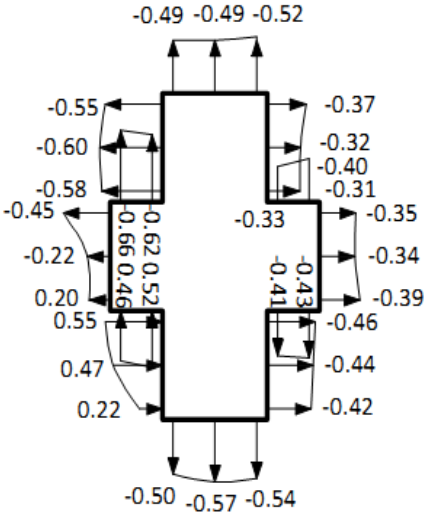


Section F-F

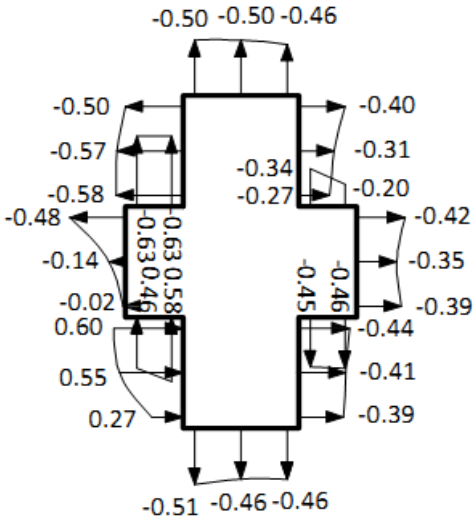


Section G-G

**Fig. 5.101 Cross-sectional variation of mean wind pressure coefficients ($C_{p,mean}$) on model-C in half blockage interference condition**

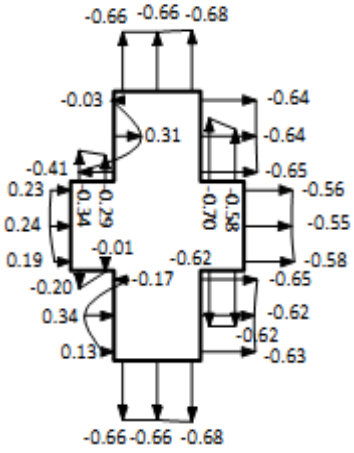


Section A-A

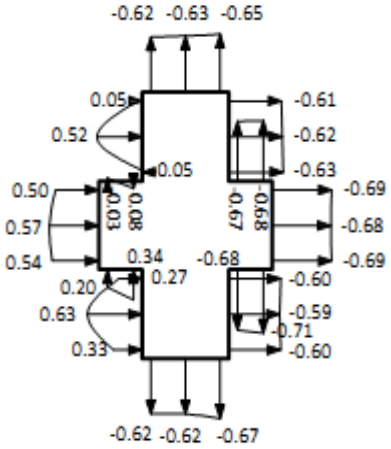


Section B-B

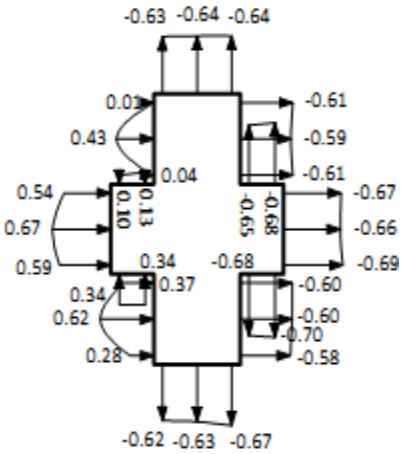


Section C-C

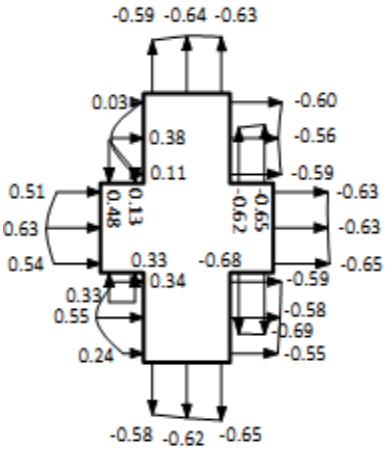


Section D-D

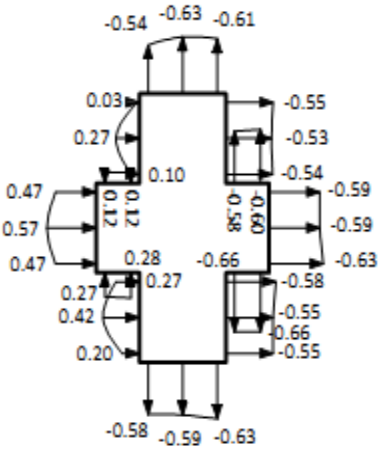


Section E-E

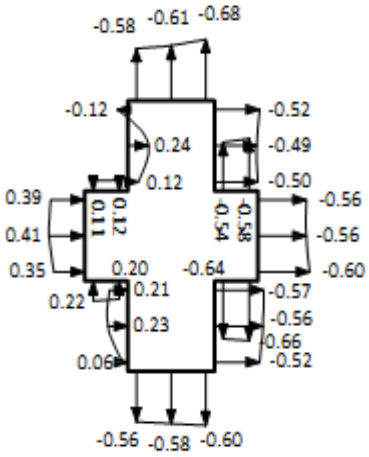


Section F-F

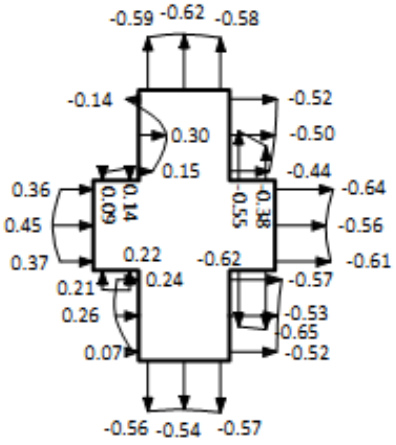


Section G-G

**Fig. 5.102 Cross-sectional variation of mean wind pressure coefficients ($C_{p,mean}$) on model-C in no blockage interference condition**

**Table 5.11 Interference effect on variation of $C_{p,mean}$ on face-A of building model-C**

| Pressure points | Mean wind pressure coefficients ($C_{p,mean}$) | | | |
|---|---|---|---|---|
| | Full blockage | Half blockage | No blockage | Isolated ($0^0$ wind incidence angle) |
| 1 | -0.62 | -0.86 | -0.29 | 0.02 |
| 2 | -0.77 | **-1.24** | **-0.34** | **-0.1** |
| 3 | -0.59 | -0.36 | 0.23 | 0.36 |
| 4 | -0.53 | 0.04 | 0.24 | 0.38 |
| 5 | -0.59 | 0.42 | 0.19 | 0.36 |
| 6 | -0.77 | 0.35 | -0.2 | **-0.1** |
| 7 | -0.62 | 0.27 | -0.01 | 0.02 |
| 8 | -0.57 | -0.67 | 0.08 | 0.47 |
| 9 | **-0.01** | -0.87 | -0.03 | 0.34 |
| 10 | -0.82 | -0.53 | 0.5 | 0.66 |
| 11 | **-0.83** | -0.15 | 0.57 | 0.66 |
| 12 | -0.82 | 0.4 | 0.54 | 0.66 |
| 13 | -0.01 | 0.68 | 0.2 | 0.34 |
| 14 | -0.57 | **0.72** | 0.34 | 0.47 |
| 15 | -0.58 | -0.56 | 0.13 | 0.46 |
| 16 | -0.63 | -0.56 | 0.1 | 0.46 |
| 17 | -0.67 | -0.5 | 0.54 | 0.67 |
| 18 | -0.66 | -0.26 | **0.67** | **0.71** |
| 19 | -0.67 | -0.1 | 0.59 | 0.67 |
| 20 | -0.63 | 0.68 | 0.34 | 0.46 |
| 21 | -0.58 | 0.7 | 0.34 | 0.46 |
| 22 | -0.6 | -0.65 | 0.13 | 0.43 |
| 23 | -0.62 | -0.63 | 0.48 | 0.41 |
| 24 | -0.64 | -0.63 | 0.51 | 0.59 |
| 25 | -0.63 | -0.47 | 0.63 | 0.63 |
| 26 | -0.64 | -0.13 | 0.54 | 0.59 |
| 27 | -0.62 | 0.62 | 0.33 | 0.41 |
| 28 | -0.6 | 0.66 | 0.33 | 0.43 |
| 29 | -0.57 | -0.64 | 0.12 | 0.36 |
| 30 | -0.59 | -0.63 | 0.12 | 0.37 |
| 31 | -0.62 | -0.53 | 0.47 | 0.53 |
| 32 | -0.61 | -0.34 | 0.57 | 0.58 |
| 33 | -0.62 | -0.06 | 0.47 | 0.53 |
| 34 | -0.59 | 0.53 | 0.27 | 0.37 |
| 35 | -0.57 | 0.61 | 0.28 | 0.36 |
| 36 | -0.48 | -0.62 | 0.12 | 0.34 |
| 37 | -0.55 | -0.66 | 0.11 | 0.34 |
| 38 | -0.6 | -0.45 | 0.39 | 0.43 |
| 39 | -0.59 | -0.22 | 0.41 | 0.49 |
| 40 | -0.6 | 0.2 | 0.35 | 0.43 |
| 41 | -0.55 | 0.46 | 0.22 | 0.34 |
| 42 | -0.48 | 0.52 | 0.2 | 0.34 |
| 43 | -0.44 | -0.63 | 0.14 | 0.38 |
| 44 | -0.52 | -0.63 | 0.09 | 0.35 |
| 45 | -0.6 | -0.48 | 0.36 | 0.47 |
| 46 | -0.61 | -0.14 | 0.45 | 0.52 |
| 47 | -0.6 | -0.02 | 0.37 | 0.47 |
| 48 | -0.52 | 0.46 | 0.21 | 0.35 |
| 49 | -0.44 | 0.58 | 0.22 | 0.38 |

### 5.3.4 Model-D (I-Shape-1)

Wind pressure distribution on the surfaces of model-D under 3 interference conditions (Fig. 5.103) are obtained and contours of $C_{p,mean}$ are plotted (Figs. 5.104 to 5.106). Distribution is similar to the models tested earlier. Figures 5.107 to 5.109 show cross-sectional variation of $C_{p,mean}$ at 7 sections along height.

Table 5.12 compares the values of $C_{p,mean}$ at 35 pressure points on face-A under 3 interference conditions with isolated case.

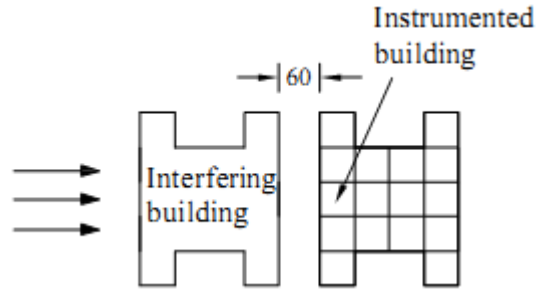


Full blockage interference condition

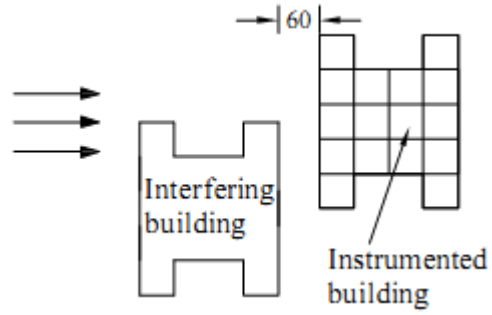


Half blockage interference condition

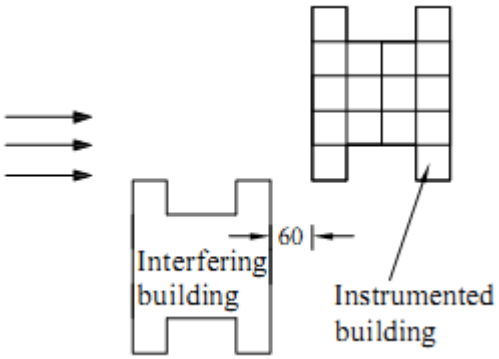


No blockage interference condition

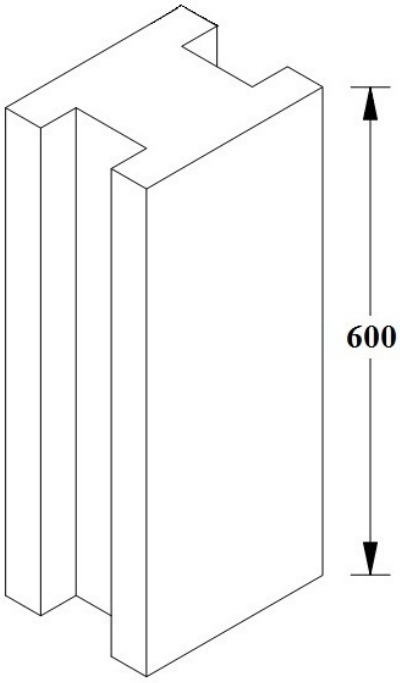


Isometric

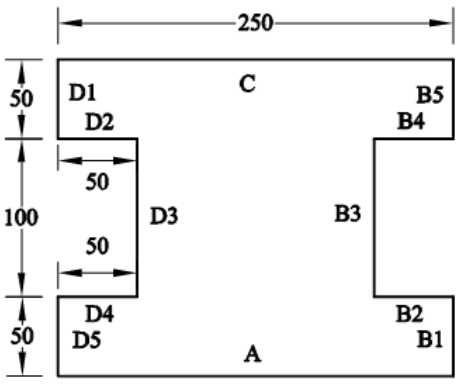


Plan

All dimensions are in mm

**Fig. 5.103 Details of model-D showing different wind interference conditions**

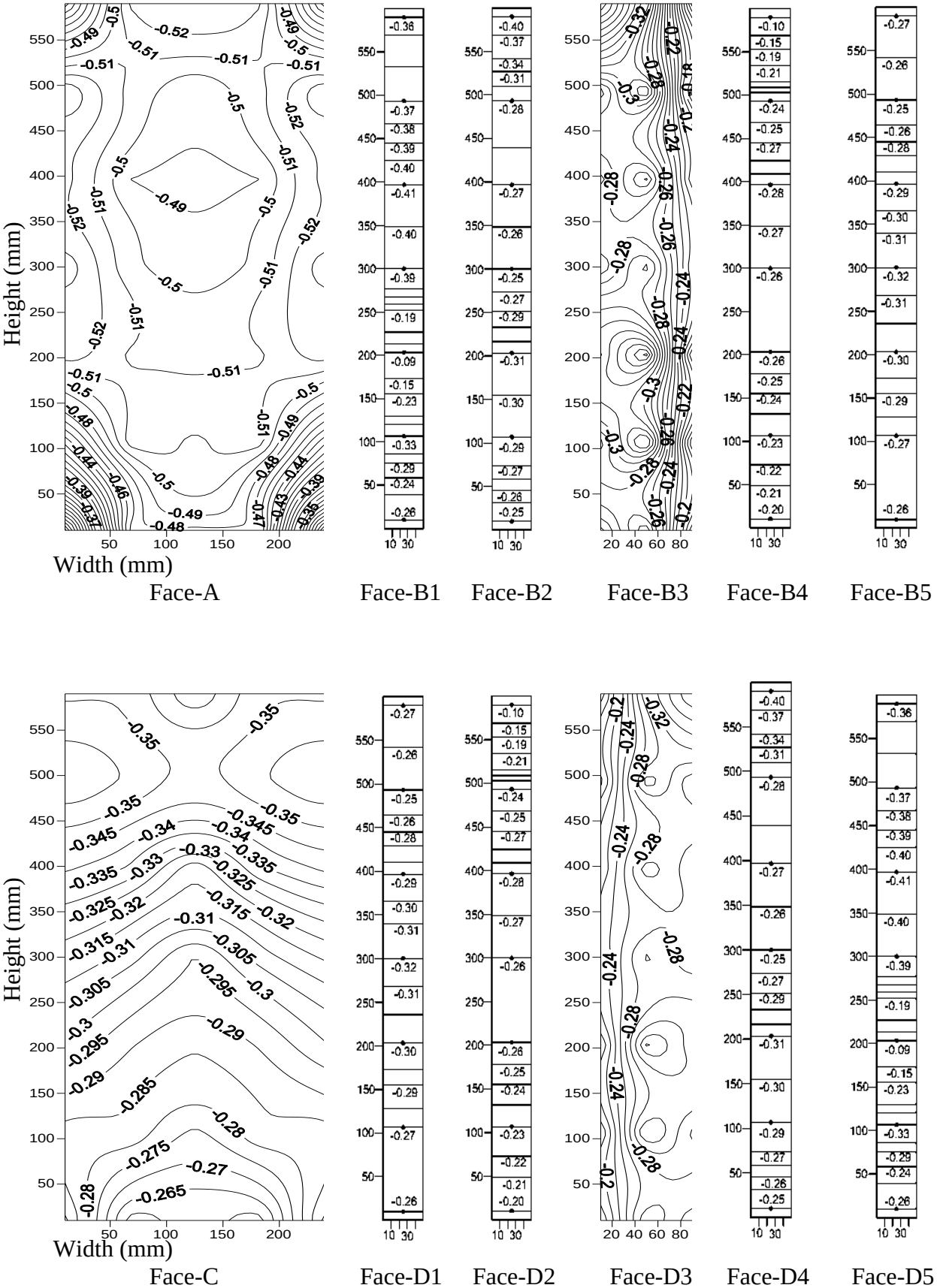


**Fig. 5.104 Distribution of mean wind pressure coefficients ($C_{p,mean}$) on different surfaces of model-D under full blockage interference condition**

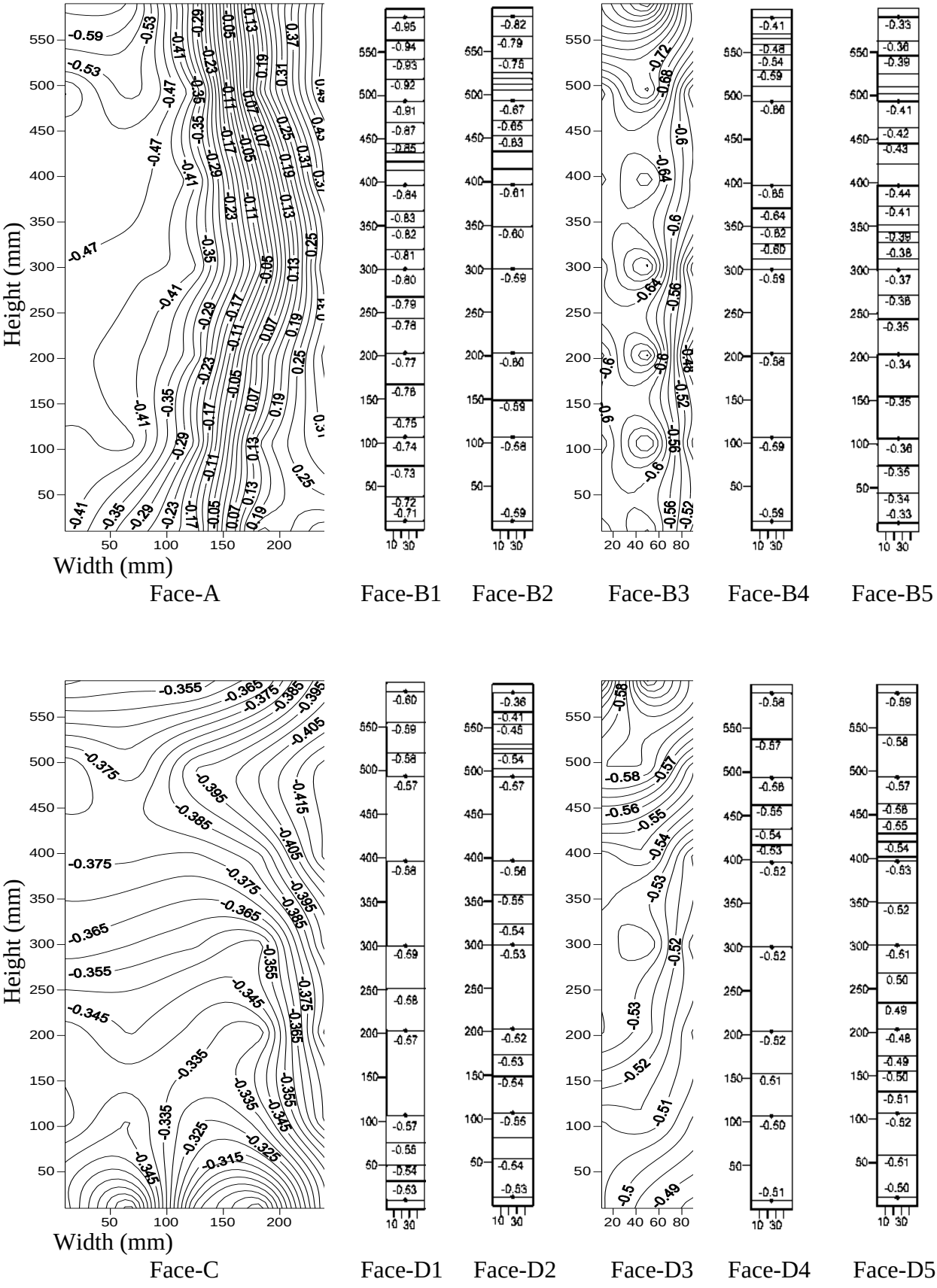


**Fig. 5.105 Distribution of mean wind pressure coefficients ($C_{p,mean}$) on different surfaces of model-D under half blockage interference condition**

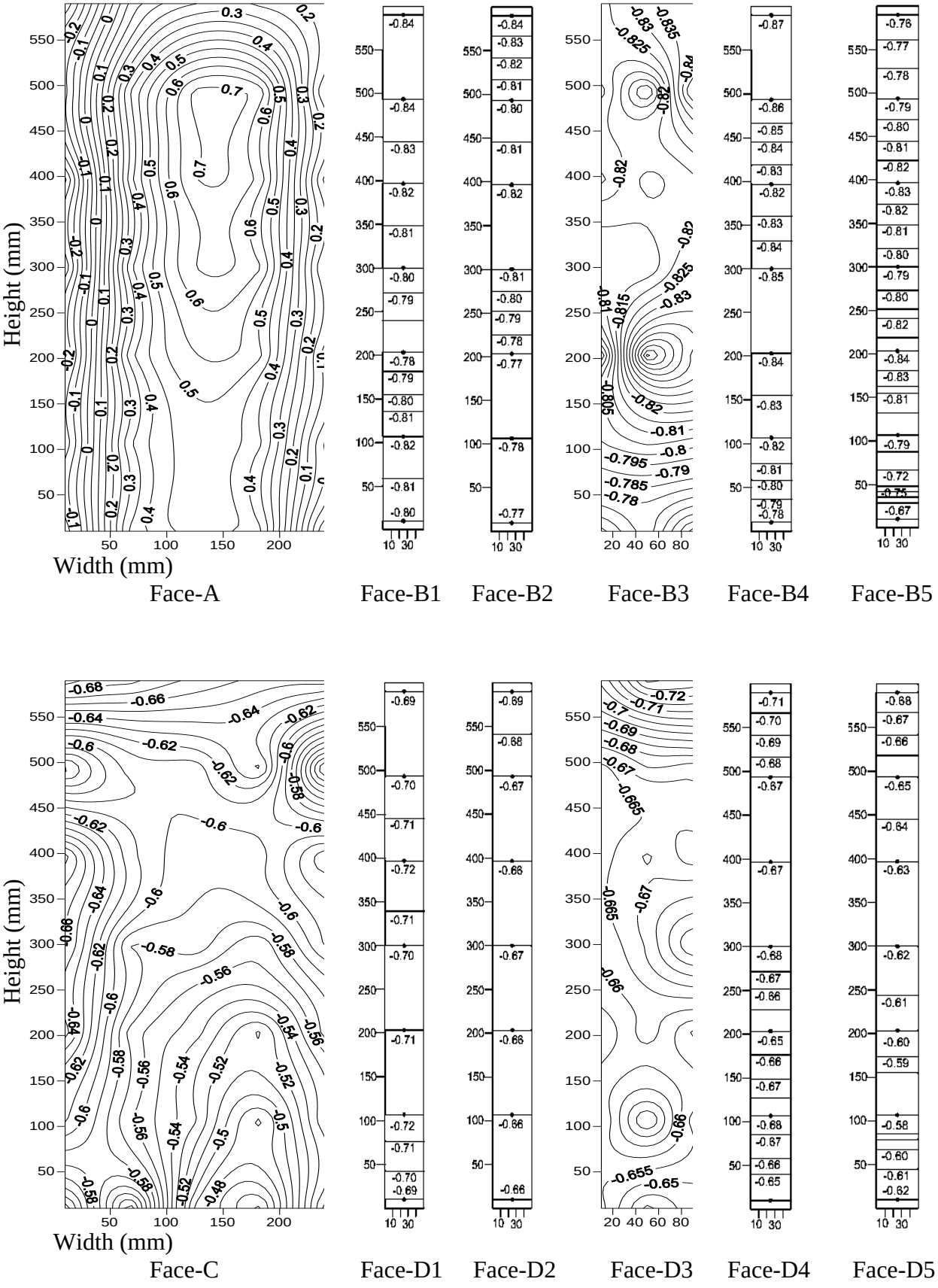


**Fig. 5.106 Distribution of mean wind pressure coefficients ($C_{p,mean}$) on different surfaces of model-D under no blockage interference condition**

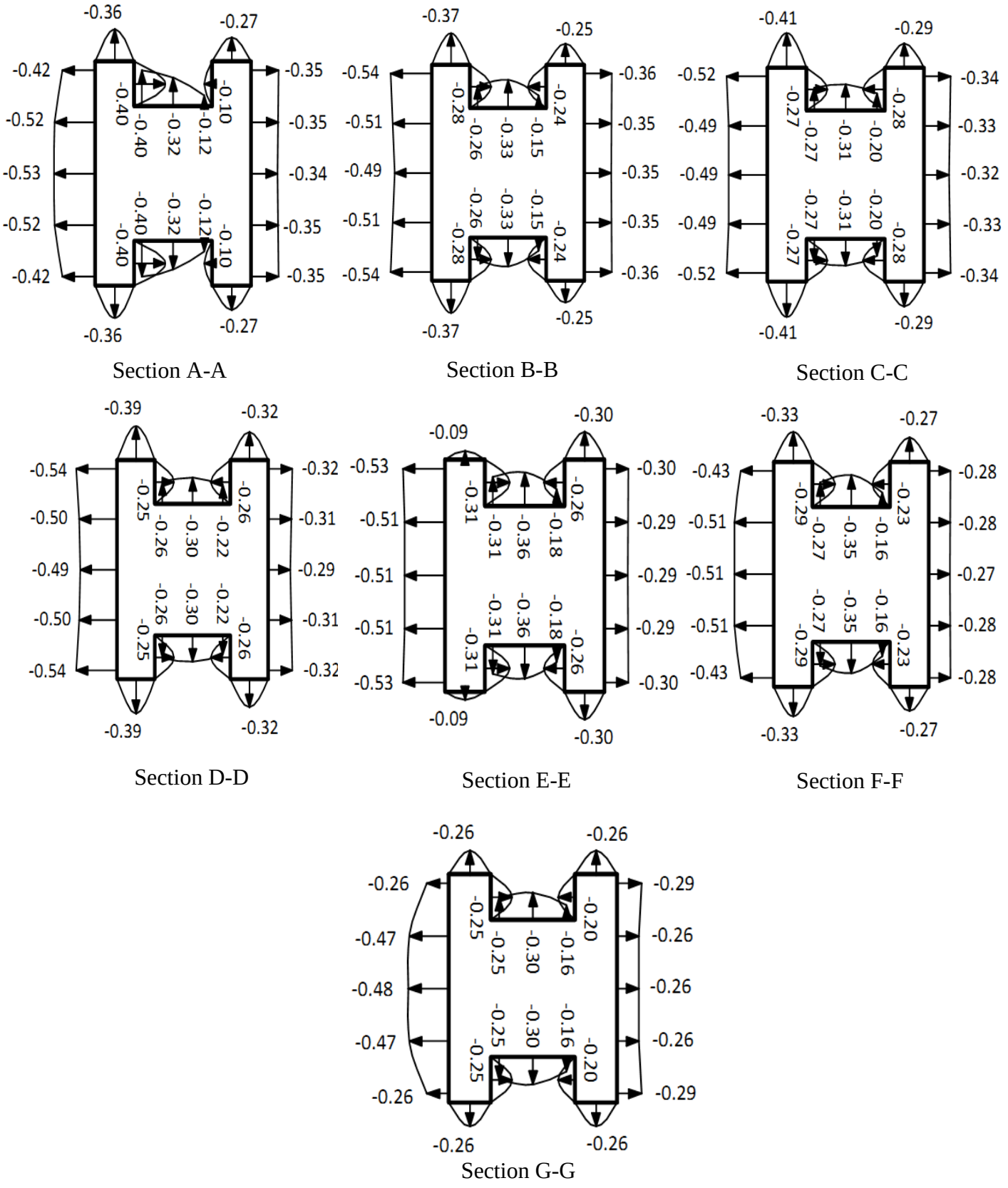


**Fig. 5.107 Cross-sectional variation of mean wind pressure coefficients ($C_{p,mean}$) on model-D in full blockage interference condition**

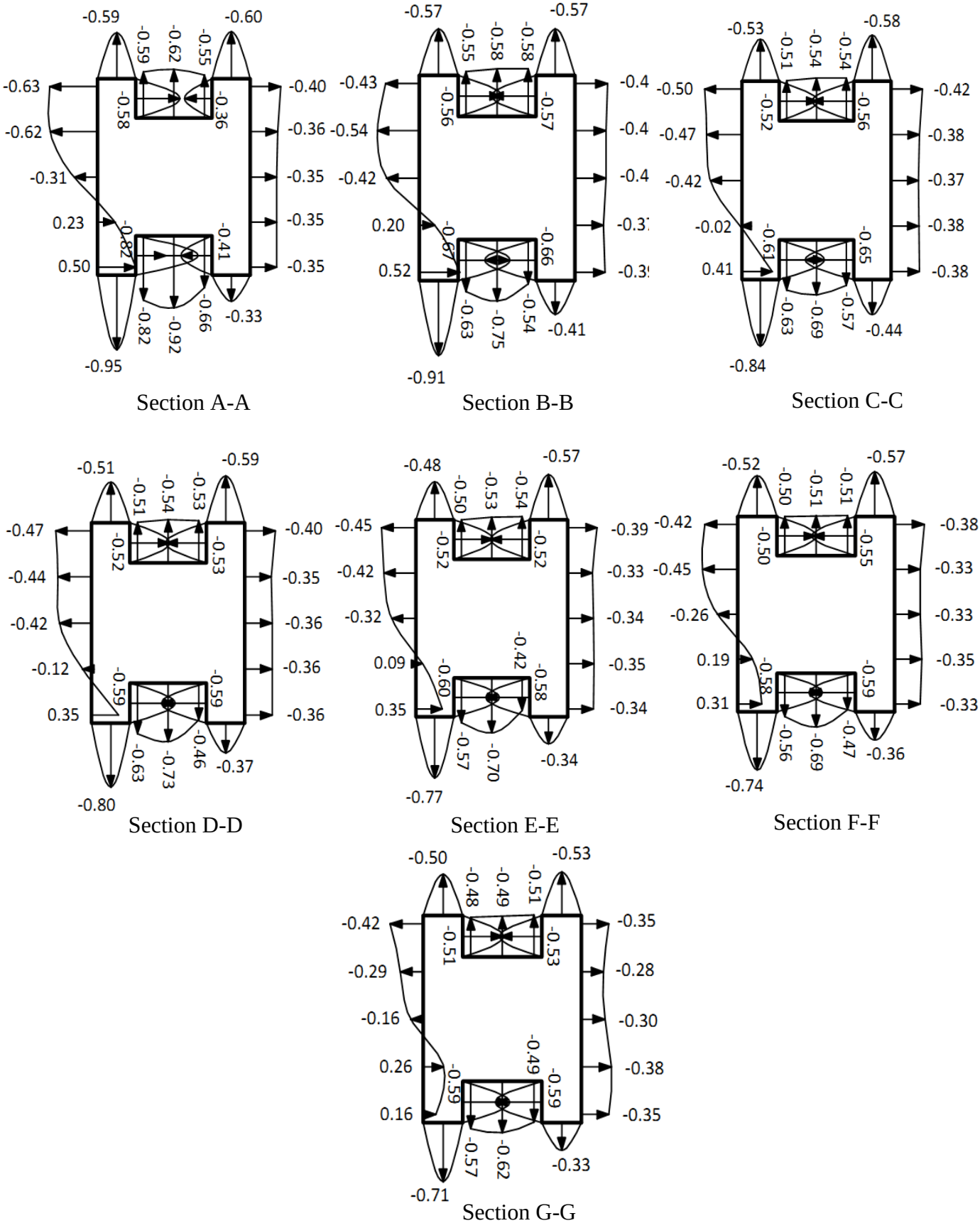


**Fig. 5.108 Cross-sectional variation of mean wind pressure coefficients ($C_{p,mean}$) on model-D in half blockage interference condition**

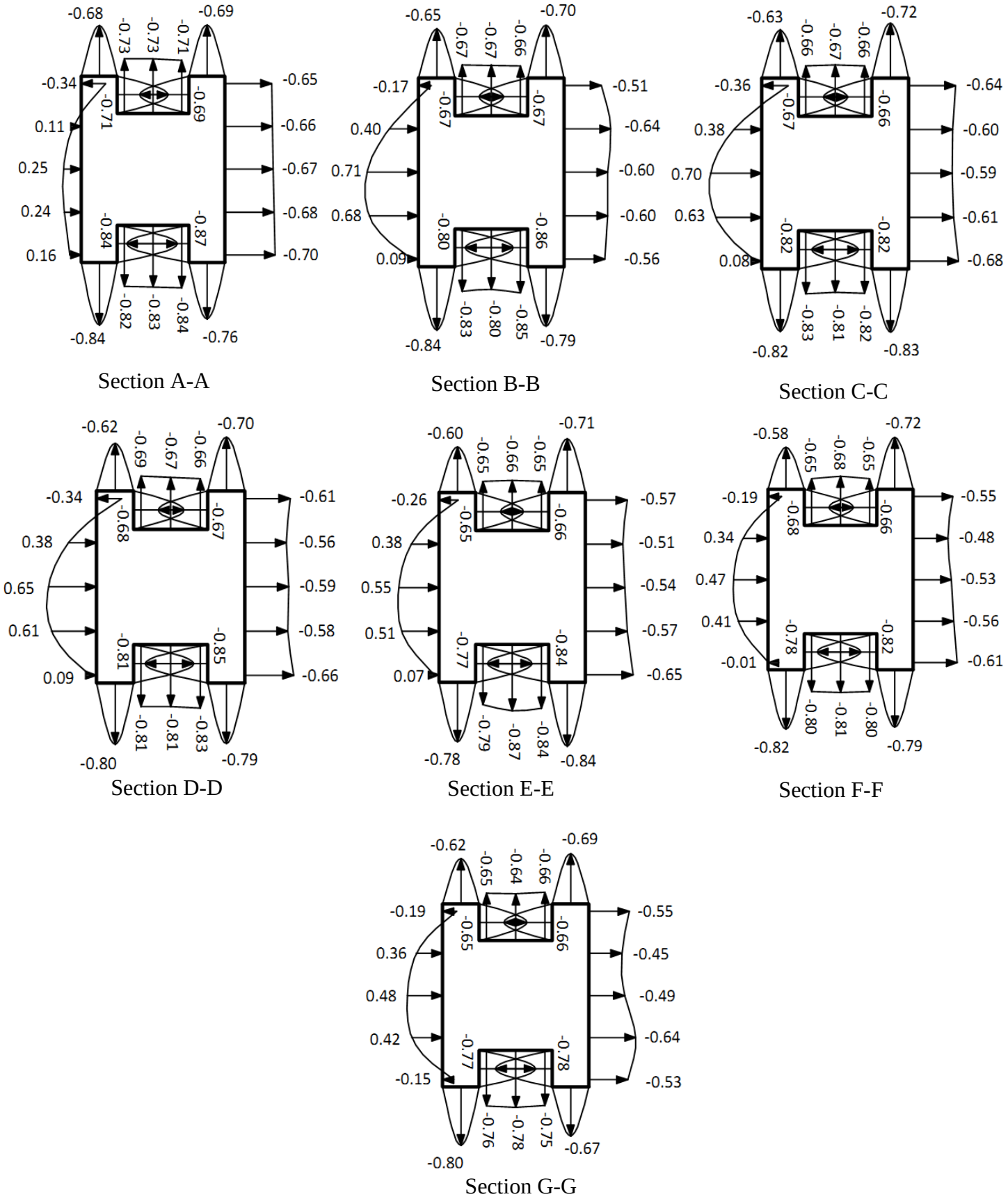


**Fig. 5.109 Cross-sectional variation of mean wind pressure coefficients ($C_{p,mean}$) on model-D in no blockage interference condition**

**Table 5.12 Interference effect on variation of $C_{p,mean}$ on face-A of building model-D**

| Pressure point no. | Mean wind pressure coefficients ($C_{p,mean}$) | | | |
|---|---|---|---|---|
| | Full blockage | Half blockage | No blockage | Isolated ($0^0$ wind incidence angle) |
| 1 | -0.42 | **-0.63** | -0.34 | 0.29 |
| 2 | -0.52 | -0.62 | 0.11 | 0.37 |
| 3 | -0.53 | -0.31 | 0.25 | 0.38 |
| 4 | -0.52 | 0.23 | 0.24 | 0.37 |
| 5 | -0.42 | 0.5 | 0.16 | 0.29 |
| 6 | **-0.54** | -0.43 | -0.17 | 0.51 |
| 7 | -0.51 | -0.54 | 0.4 | 0.58 |
| 8 | -0.49 | -0.42 | **0.71** | **0.76** |
| 9 | -0.51 | 0.2 | 0.68 | 0.58 |
| 10 | -0.54 | **0.52** | 0.09 | 0.51 |
| 11 | -0.52 | -0.5 | **-0.36** | 0.48 |
| 12 | -0.49 | -0.47 | 0.38 | 0.52 |
| 13 | -0.49 | -0.42 | 0.7 | 0.73 |
| 14 | -0.49 | -0.02 | 0.63 | 0.52 |
| 15 | -0.52 | 0.41 | 0.08 | 0.48 |
| 16 | -0.54 | -0.47 | -0.34 | 0.36 |
| 17 | -0.5 | -0.44 | 0.38 | 0.45 |
| 18 | -0.49 | -0.42 | 0.65 | 0.64 |
| 19 | -0.5 | -0.12 | 0.61 | 0.45 |
| 20 | -0.54 | 0.35 | 0.09 | 0.36 |
| 21 | -0.53 | -0.45 | -0.26 | 0.37 |
| 22 | -0.51 | -0.42 | 0.38 | 0.38 |
| 23 | -0.51 | -0.32 | 0.55 | 0.56 |
| 24 | -0.51 | 0.09 | 0.51 | 0.38 |
| 25 | -0.53 | 0.35 | 0.07 | 0.37 |
| 26 | -0.43 | -0.42 | -0.19 | 0.14 |
| 27 | -0.51 | -0.45 | 0.34 | 0.54 |
| 28 | -0.51 | -0.26 | 0.47 | 0.57 |
| 29 | -0.51 | 0.19 | 0.41 | 0.54 |
| 30 | -0.43 | 0.31 | -0.01 | 0.14 |
| 31 | **-0.26** | -0.42 | -0.19 | 0.06 |
| 32 | -0.47 | -0.29 | 0.36 | 0.57 |
| 33 | -0.48 | -0.16 | 0.48 | 0.65 |
| 34 | -0.47 | 0.26 | 0.42 | 0.57 |
| 35 | **-0.26** | 0.16 | -0.15 | **0.06** |

### 5.3.5 Model-F (Fish Shape-1)

Interference study between two models of model-F is carried out for 4 interference conditions namely back-to-back, back-to-front, front-to-back and front-to-front (Fig. 5.110). A gap of 60 mm is kept between 2 models in the direction of wind in all 4 cases.

Contours of $C_{p,mean}$ are shown in Figs. 5.111 to 5.114. It is noticed that rear face of the model, i.e. large face, is subjected to slightly less suction in case of back-to-back interference condition (Fig. 5.111) as compared to front-to-back condition (Fig. 5.113). Similarly, this face is subjected to slightly large suction in back-to-back interference condition (Fig. 5.112) as compared to front-to-front condition (Fig. 5.114). Cross-sectional variation of $C_{p,mean}$ are shown in Figs. 5.115 to 5.118.

Comparison of $C_{p,mean}$ at 14 pressure points on face-A of model-F for 4 interference conditions with isolated case is shown in Table 5.13.

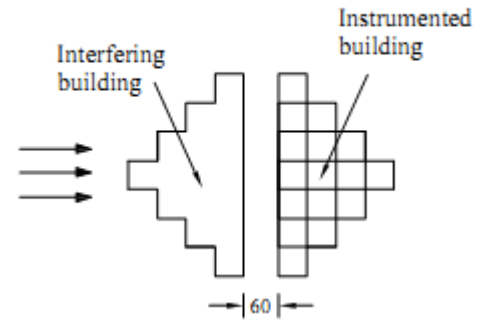


Back-to-back interference condition

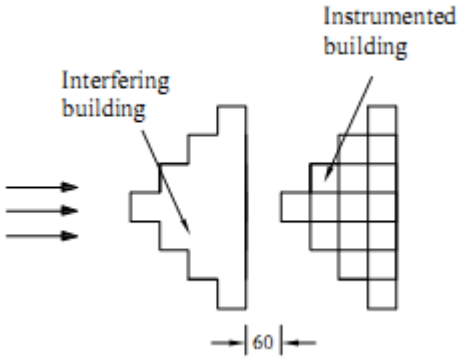


Back-to-front interference condition

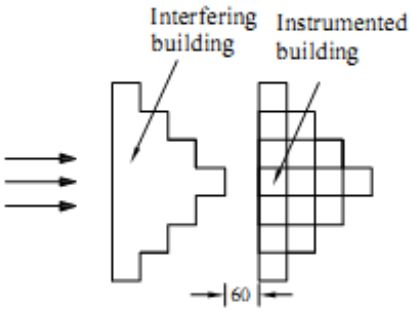


Front-to-back interference condition

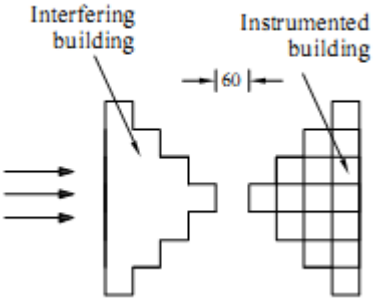


Front-to-front interference condition

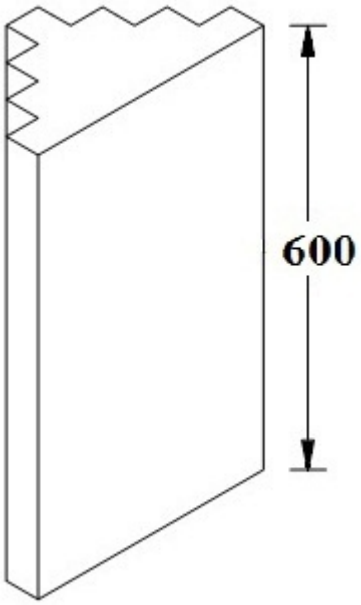


Isometric

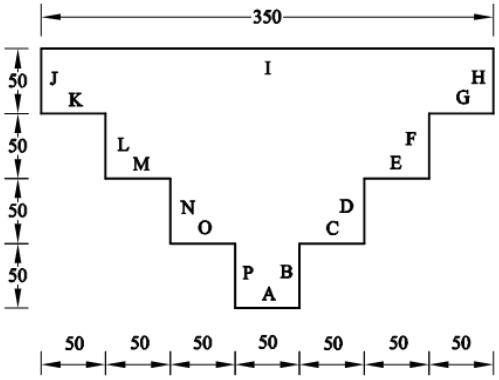


Plan

All dimensions are in mm

**Fig. 5.110 Details of model-F showing different interference conditions**

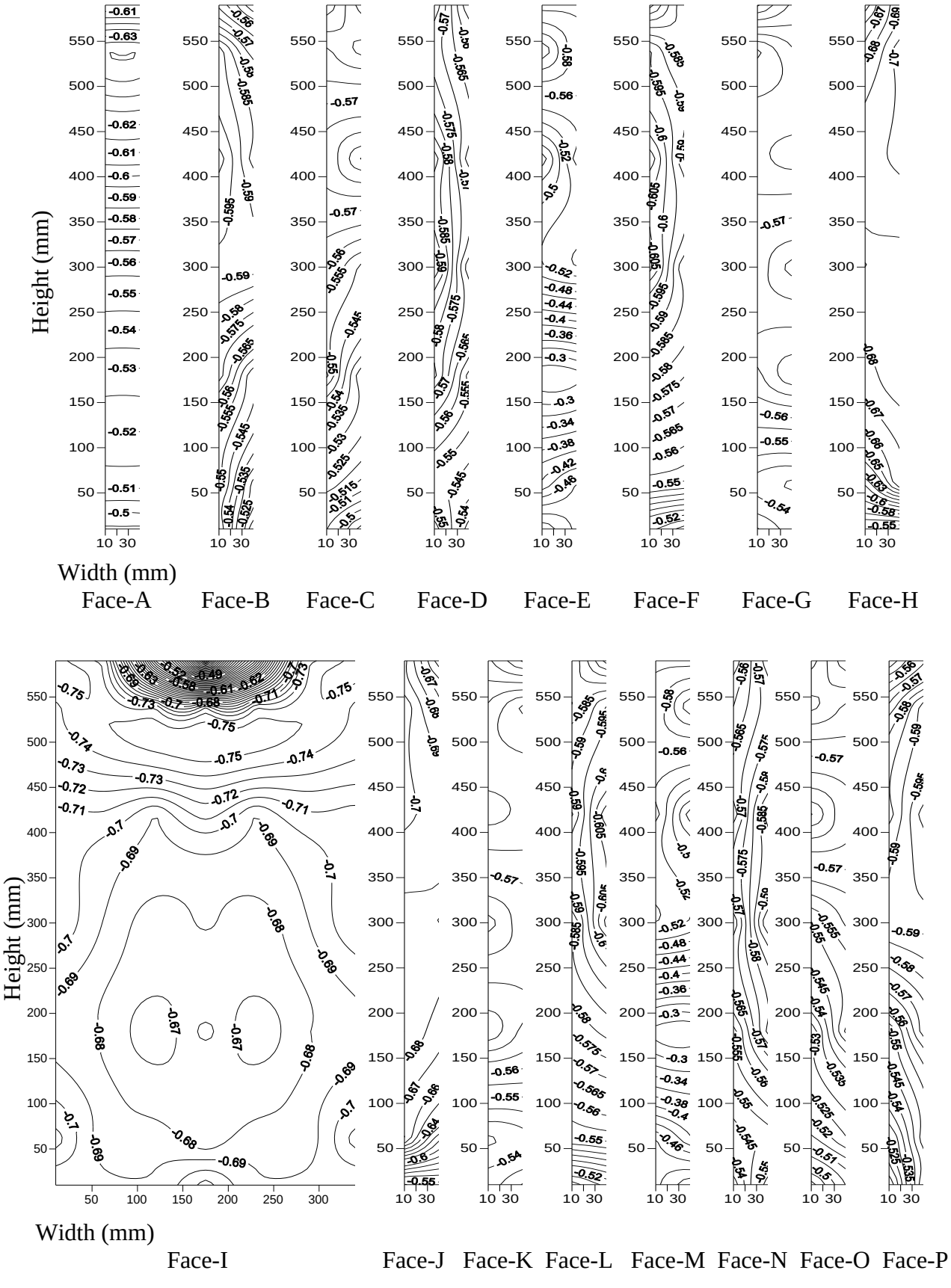


**Fig. 5.111 Distribution of mean wind pressure coefficients ($C_{p,mean}$) on different surfaces of model-F under back-to-back interference condition**

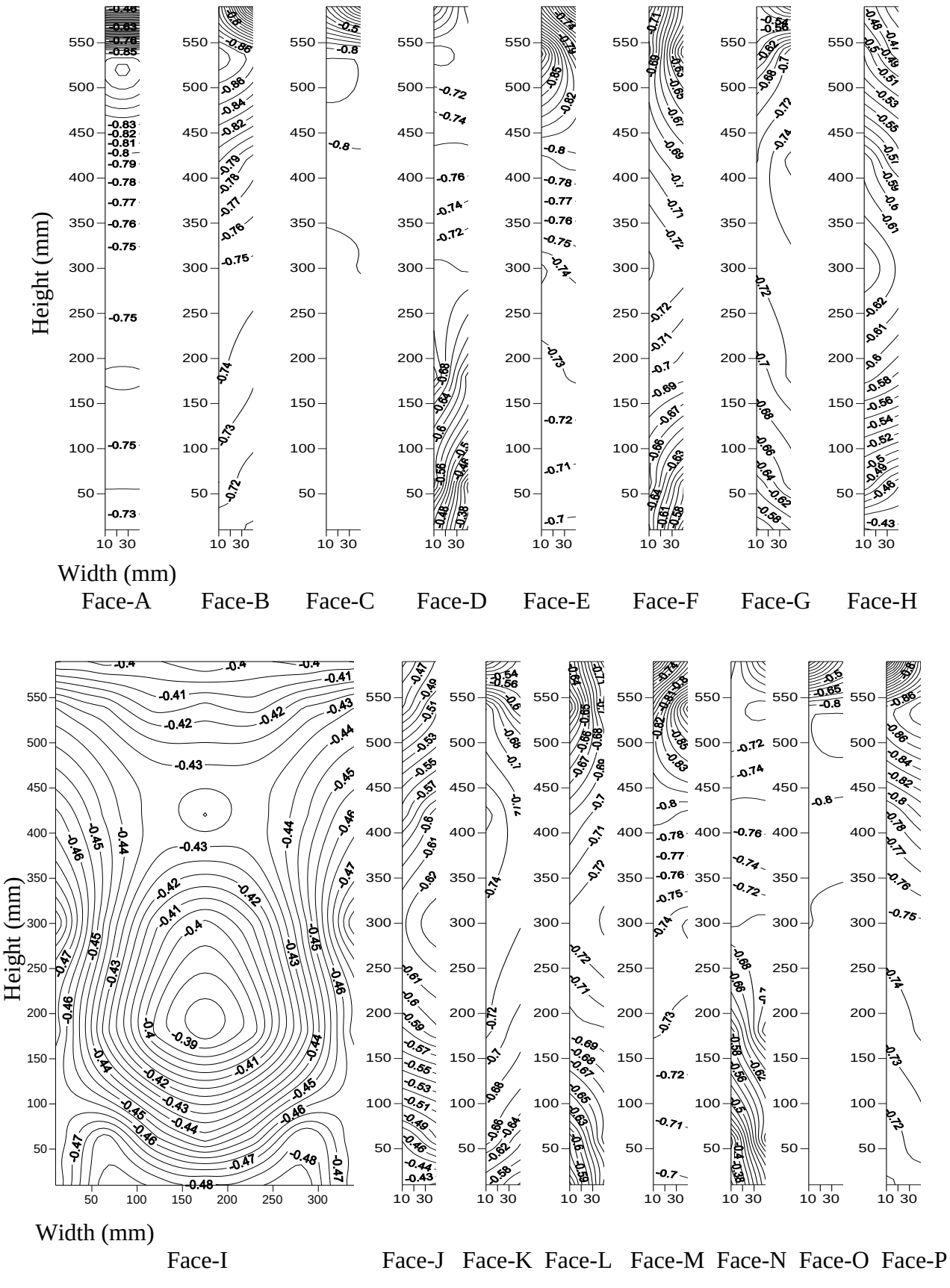


**Fig. 5.112 Distribution of mean wind pressure coefficients ($C_{p,mean}$) on different surfaces of model-F under back-to-front interference condition**

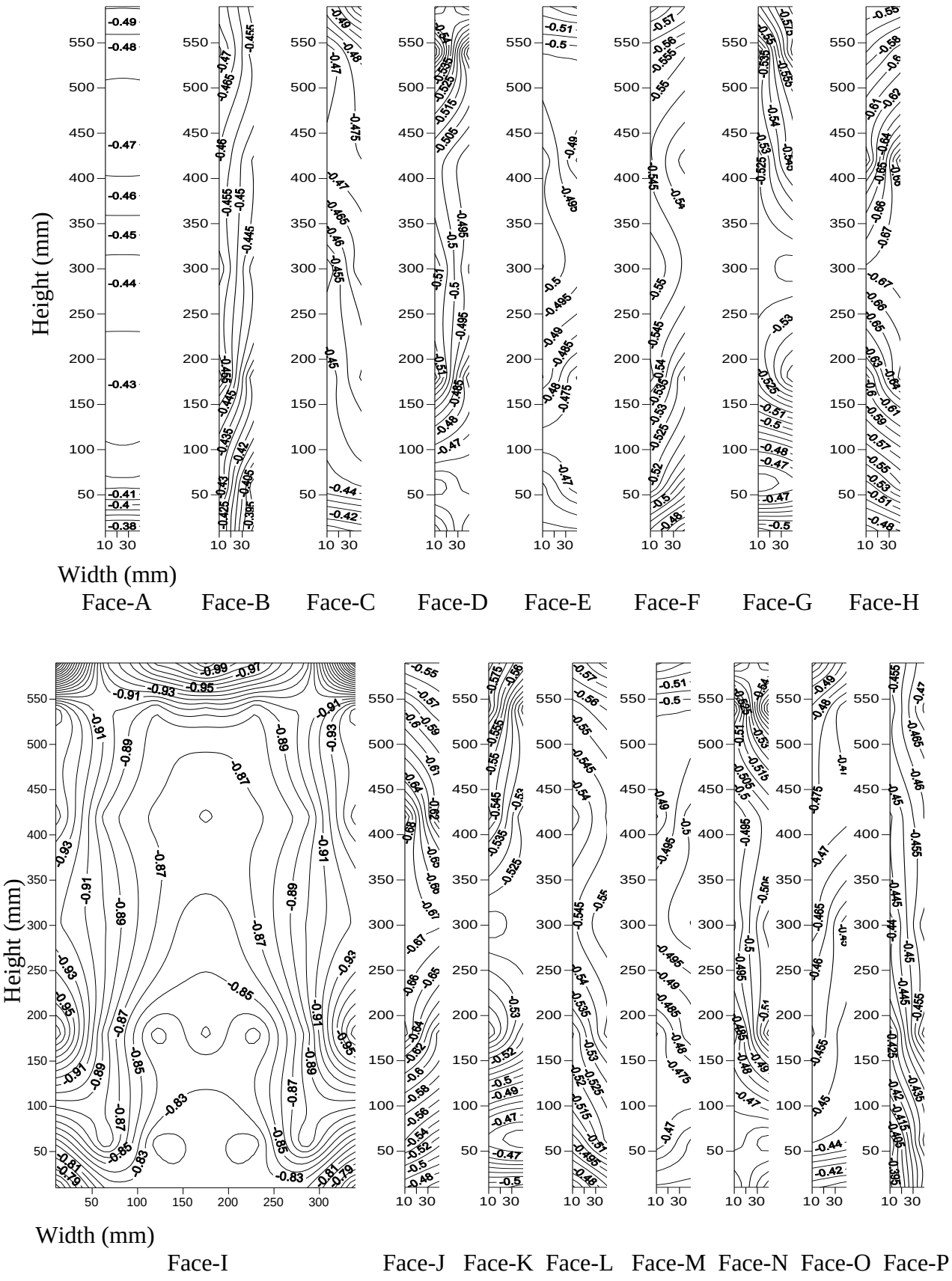


**Fig. 5.113 Distribution of mean wind pressure coefficients ($C_{p,mean}$) on different surfaces of model-F under front-to-back interference condition**

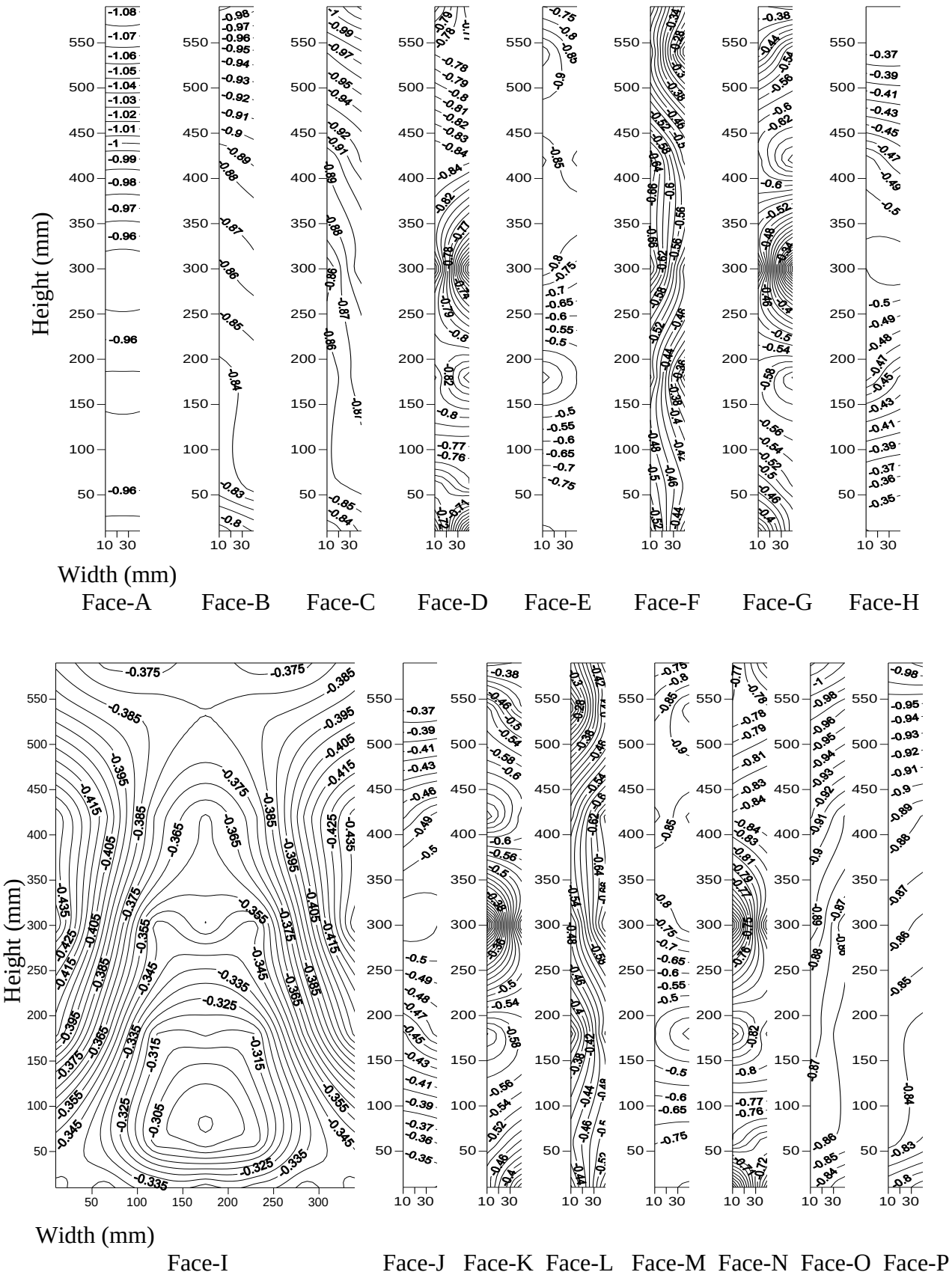


**Fig. 5.114 Distribution of mean wind pressure coefficients ($C_{p,mean}$) on different surfaces of model-F under front-to-front interference condition**

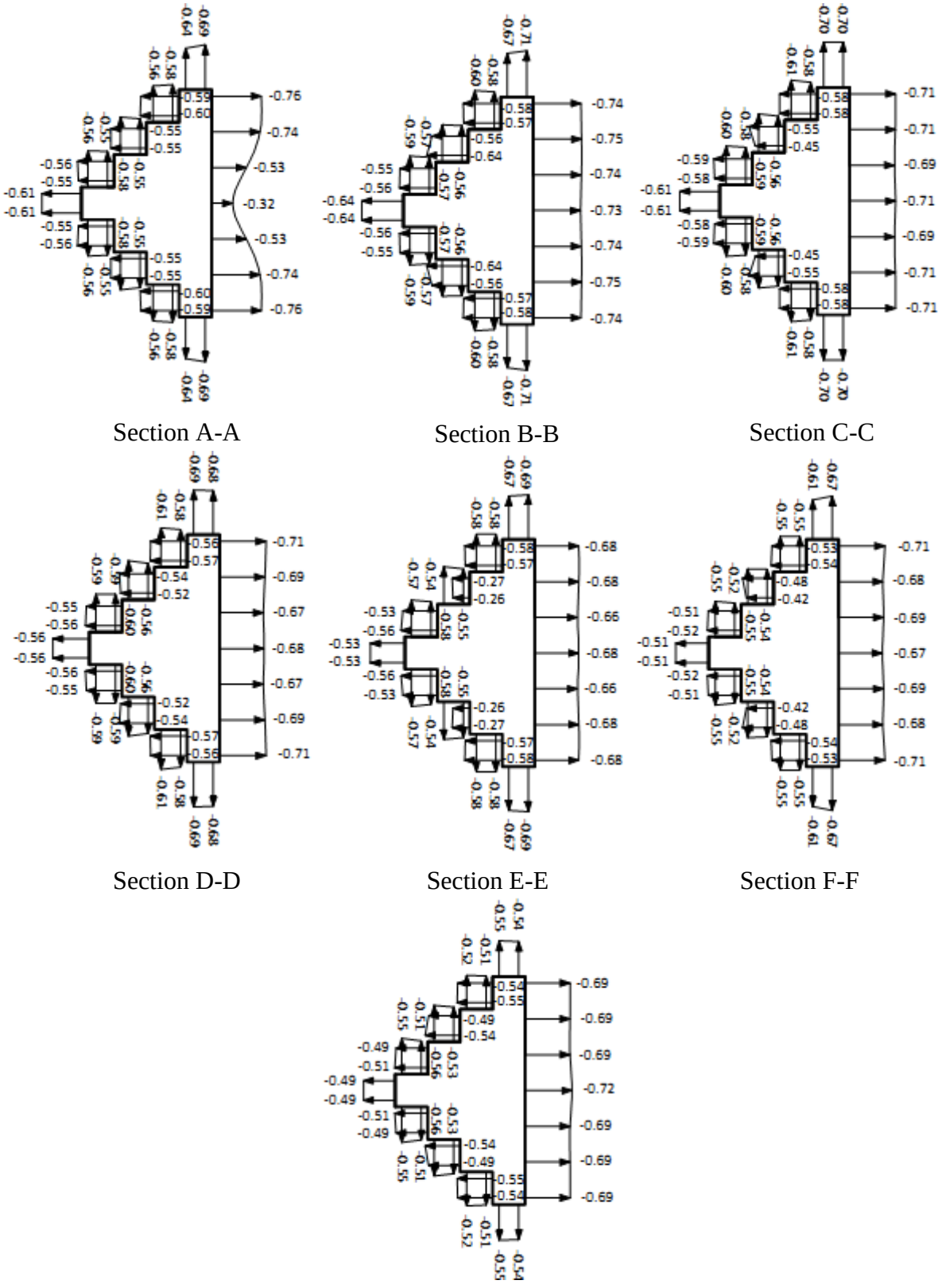


**Fig. 5.115 Cross-sectional variation of mean wind pressure coefficients ($C_{p,mean}$) on model-F in back-to-back interference condition**

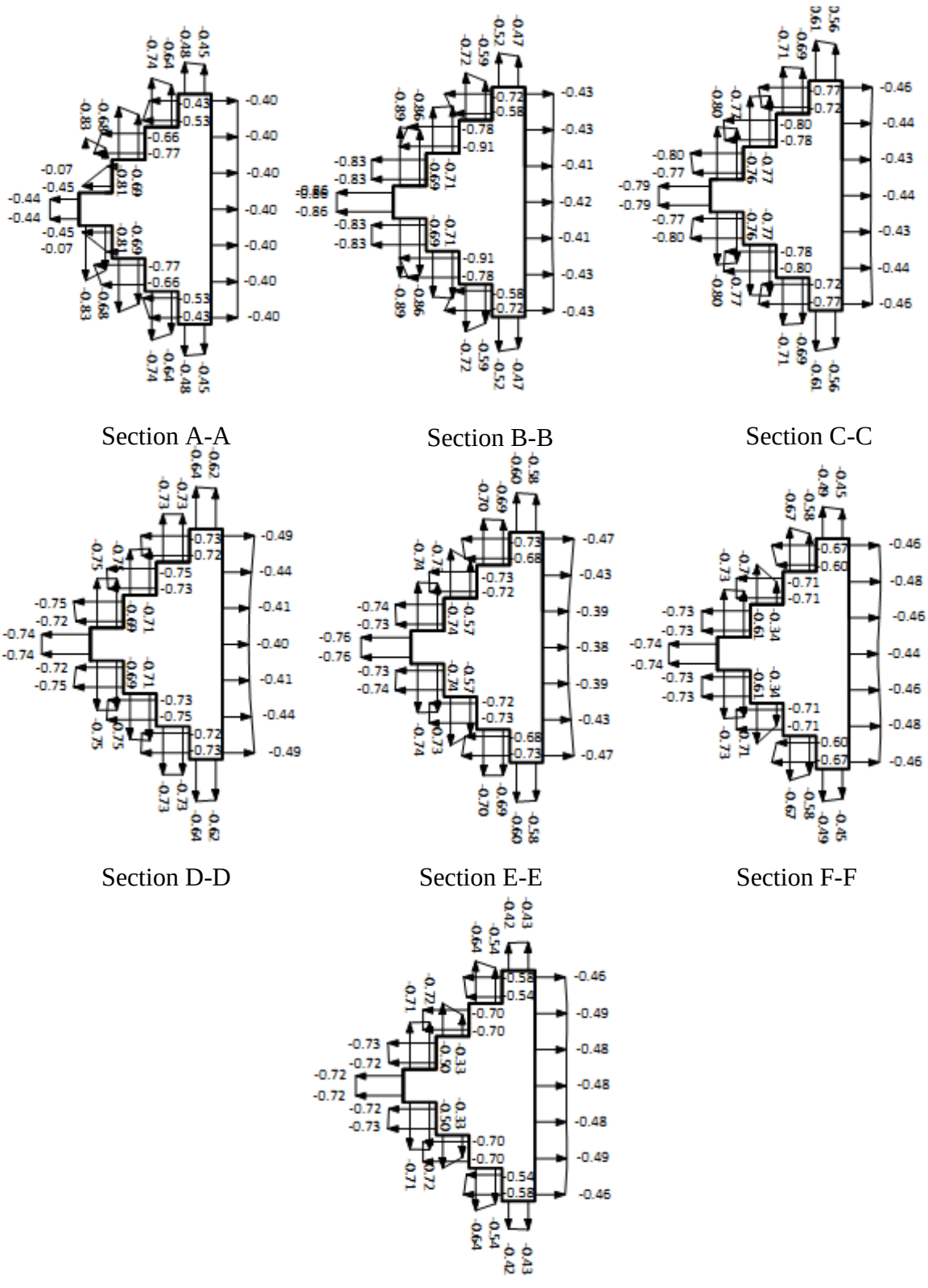


**Fig. 5.116 Cross-sectional variation of mean wind pressure coefficients ($C_{p,mean}$) on model-F in back-to-front interference condition**

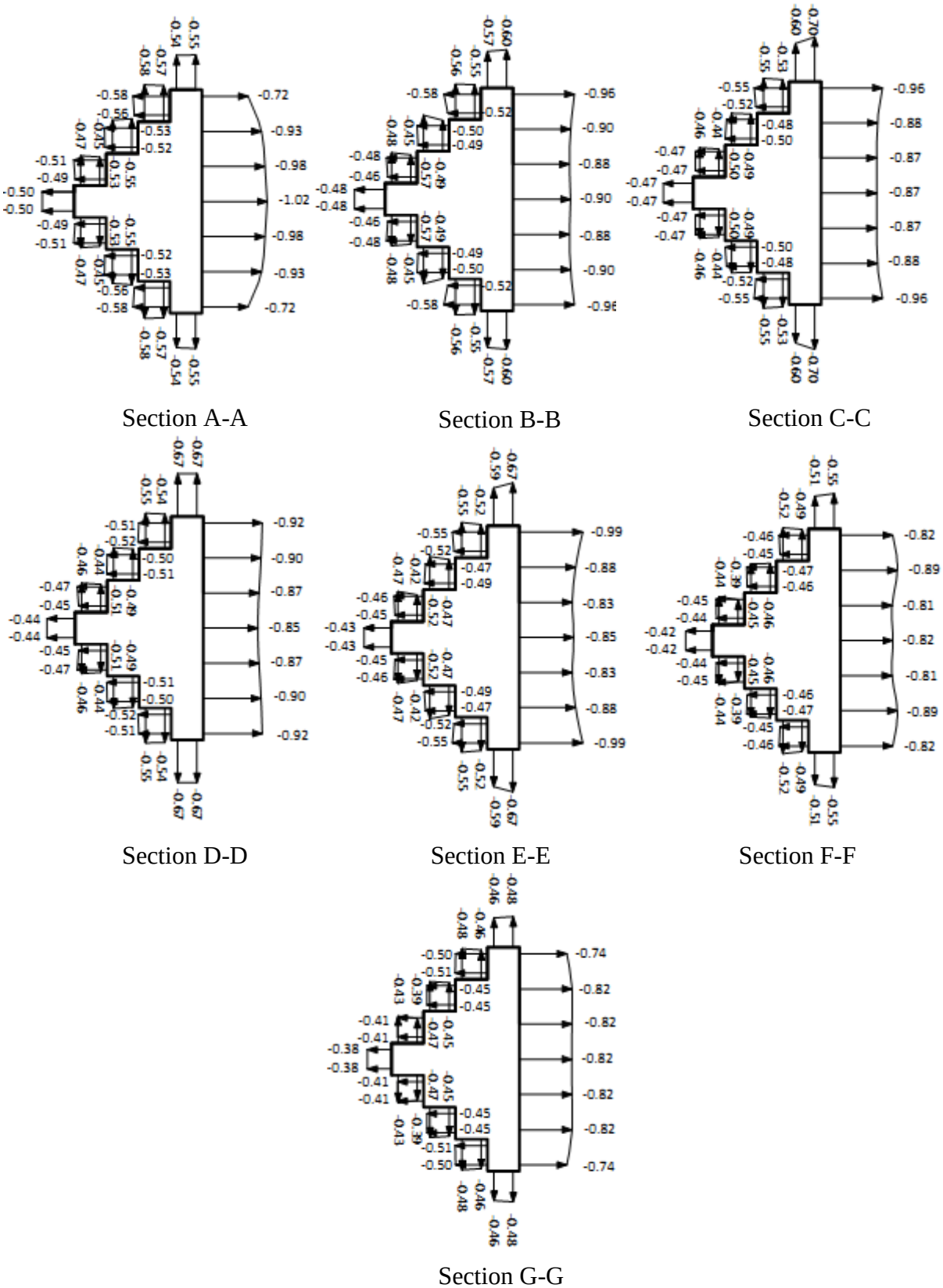


**Fig. 5.117 Cross-sectional variation of mean wind pressure coefficients ($C_{p,mean}$) on model-F in front-to-back interference condition**

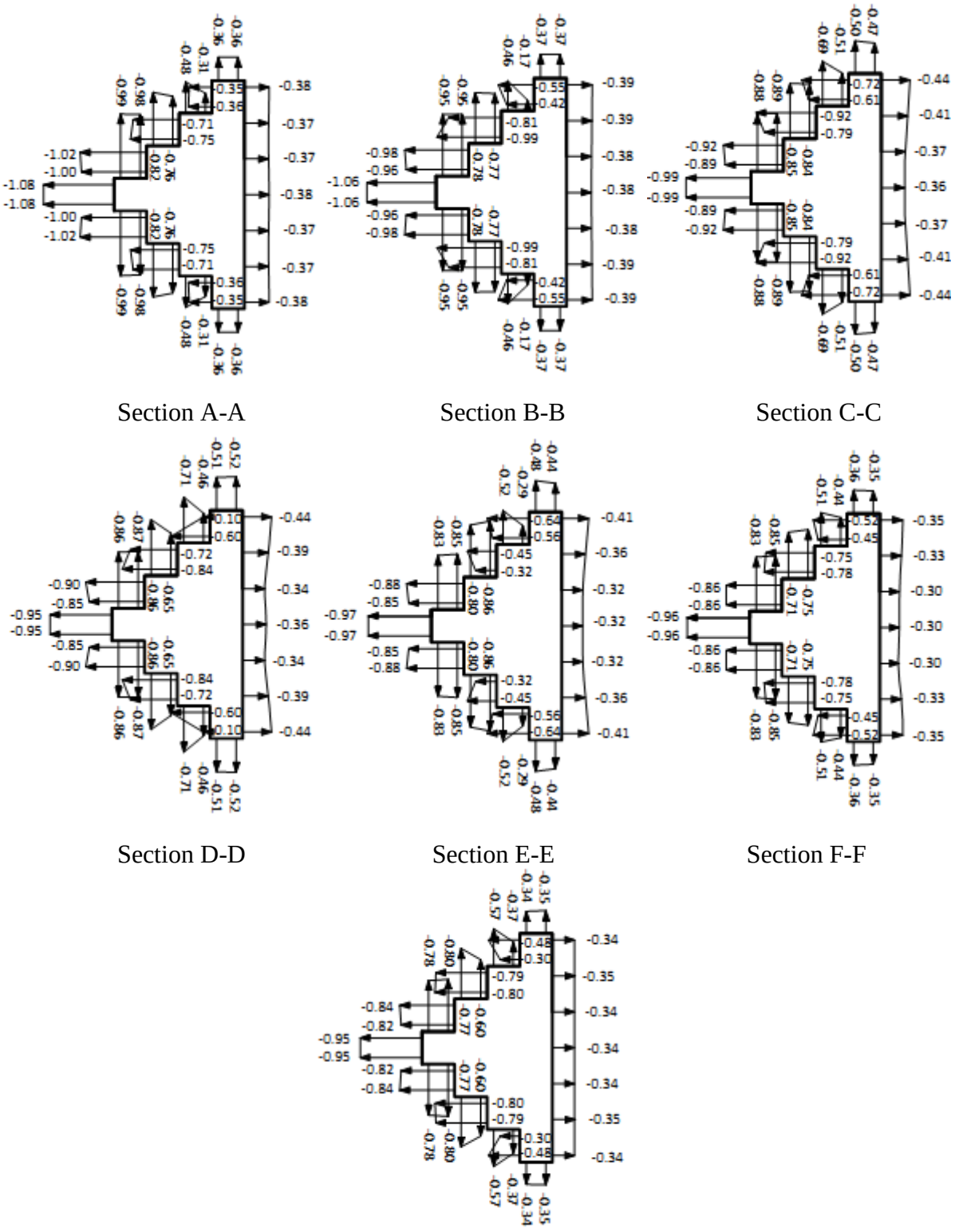


**Fig. 5.118 Cross-sectional variation of mean wind pressure coefficients ($C_{p,mean}$) on model-F in front-to-front interference condition**

**Table 5.13 Interference effect on variation of $C_{p,mean}$ on face-A of building model-F**

| Pressure point no. | Mean wind pressure coefficients ($C_{p,mean}$) | | | | |
|---|---|---|---|---|---|
| | Back to back | Back to front | Front to back | Front to front | Isolated ($0^0$ wind incidence angle) |
| 1 | -0.6 | -0.61 | -0.48 | -1.06 | 0.49 |
| 2 | -0.61 | -0.27 | **-0.51** | **-1.1** | 0.49 |
| 3 | **-0.64** | **-0.86** | -0.46 | -1.07 | **0.73** |
| 4 | **-0.64** | **-0.86** | -0.49 | -1.06 | **0.73** |
| 5 | -0.61 | -0.79 | -0.48 | -0.99 | 0.71 |
| 6 | -0.6 | -0.79 | -0.46 | -0.99 | 0.71 |
| 7 | -0.55 | -0.75 | -0.45 | -0.95 | 0.67 |
| 8 | -0.57 | -0.74 | -0.43 | -0.95 | 0.67 |
| 9 | -0.53 | -0.76 | -0.43 | -0.95 | 0.59 |
| 10 | -0.53 | -0.76 | -0.43 | -0.98 | 0.59 |
| 11 | -0.52 | -0.74 | -0.41 | -0.97 | **0.45** |
| 12 | -0.51 | -0.75 | -0.42 | -0.96 | **0.45** |
| 13 | -0.5 | -0.72 | **-0.36** | -0.97 | 0.47 |
| 14 | -0.49 | -0.72 | -0.39 | **-0.94** | 0.47 |

### 5.3.6 Model-G (Fish Shape-2)

Interfering model of model-G is placed on the upstream of instrumented model of model-G with a gap of 60 mm in 4 different interference conditions namely back-to-back, back-to-front, front-to-back and front-to-front (Fig. 5.119) to measure wind pressure distribution on all surfaces of model-G. Contours of $C_{p,mean}$ are shown in Figs 5.120 to 5.123 and cross-sectional variation in Figs. 5.124 to 5.127.

Comparison of $C_{p,mean}$ at 14 pressure points on face-A of model-G for various interference conditions with isolated condition is made in Table 5.14.

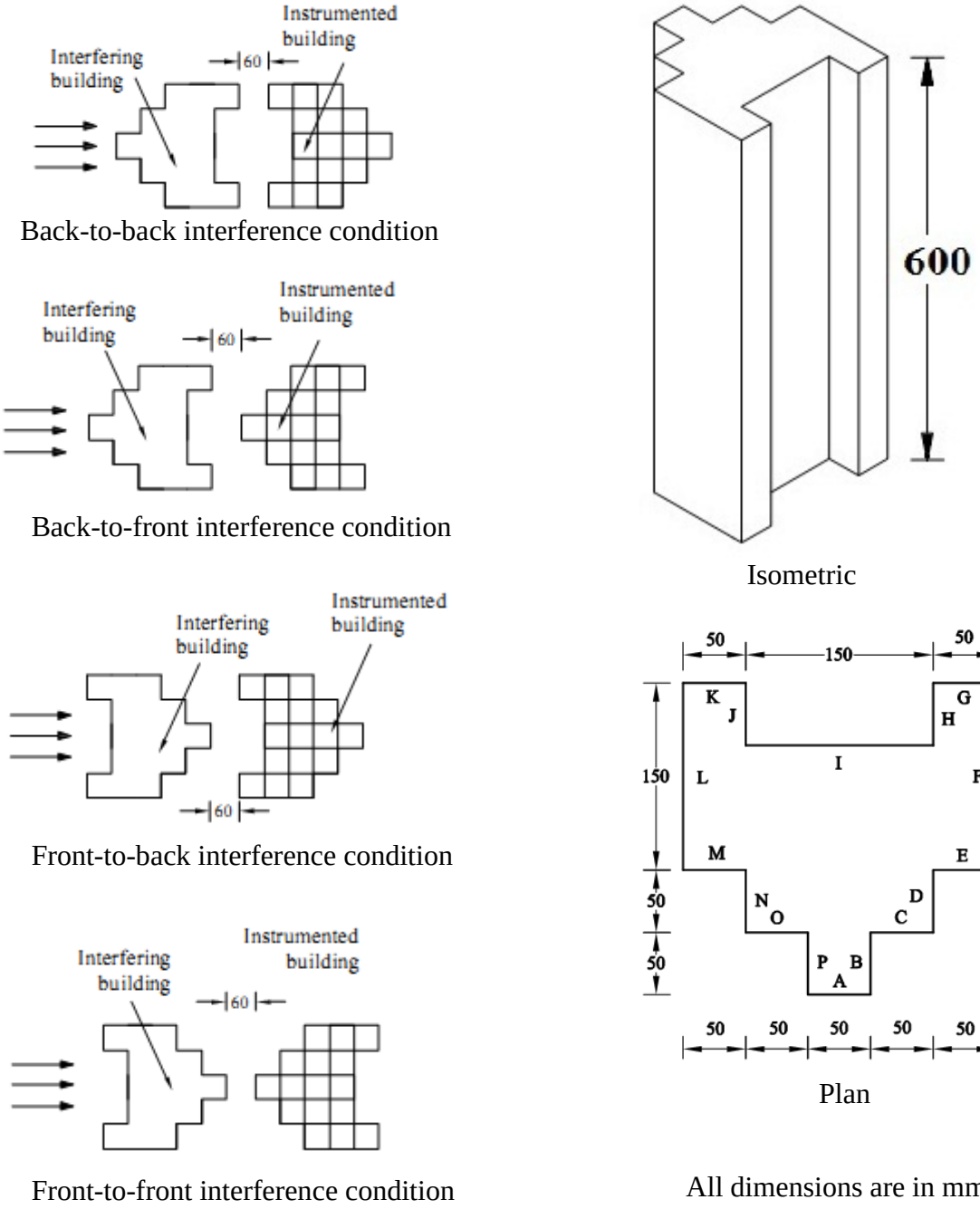


**Fig. 5.119 Details of model-G showing different interference conditions**

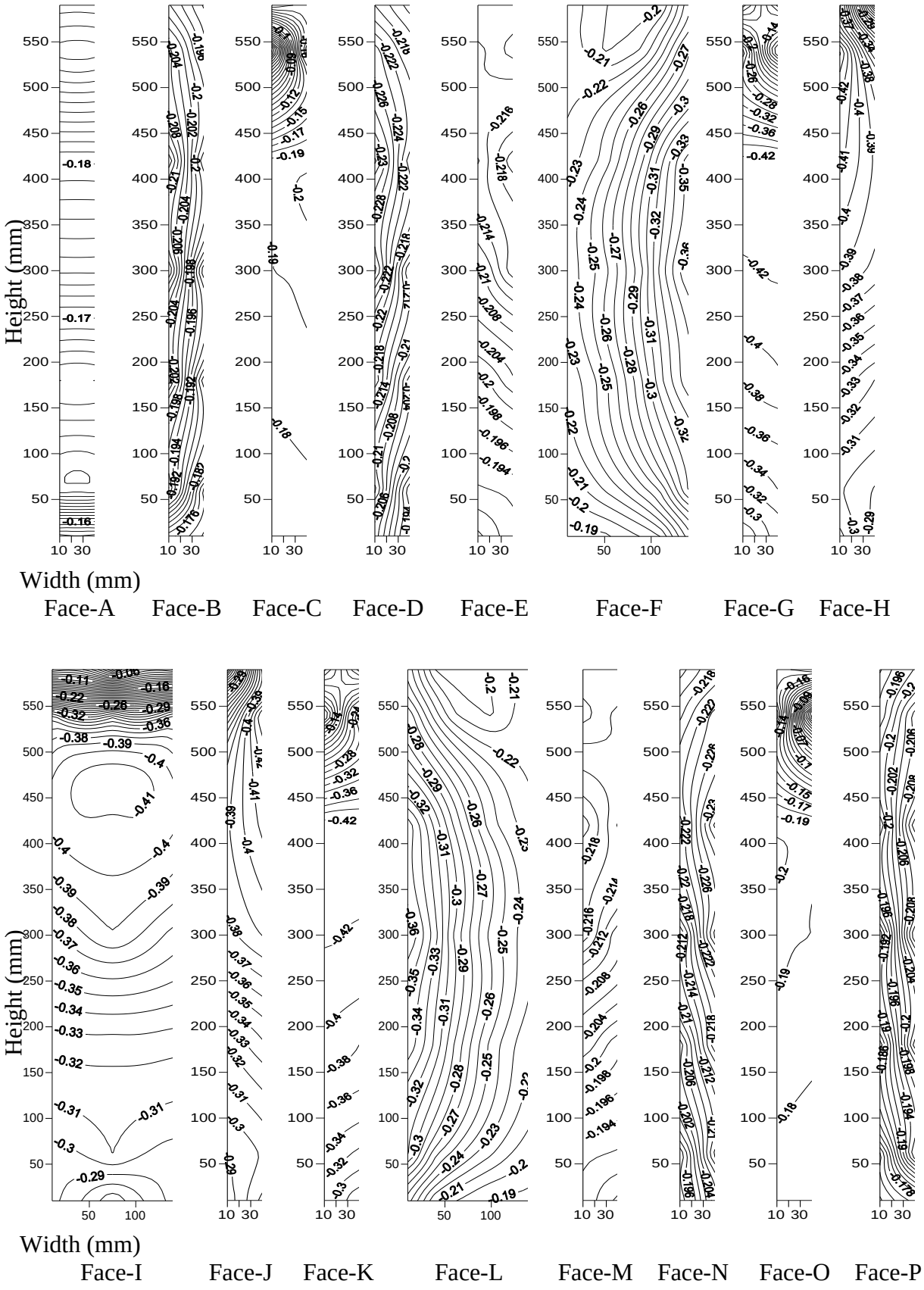


**Fig. 5.120 Distribution of mean wind pressure coefficients ($C_{p,mean}$) on different surfaces of model-G under back-to-back interference condition**

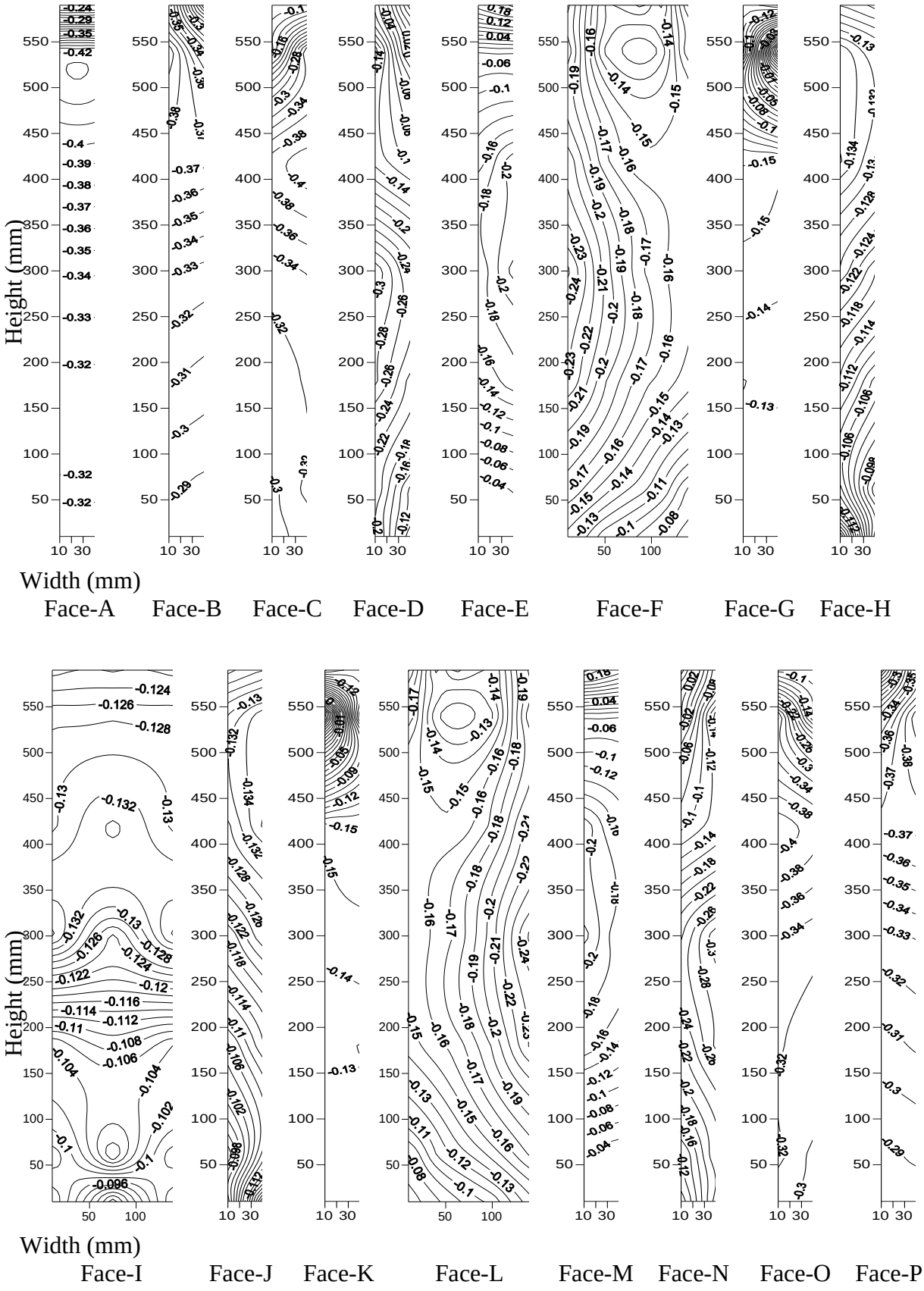


**Fig. 5.121 Distribution of mean wind pressure coefficients ($C_{p,mean}$) on different surfaces of model-G under back-to-front interference condition**

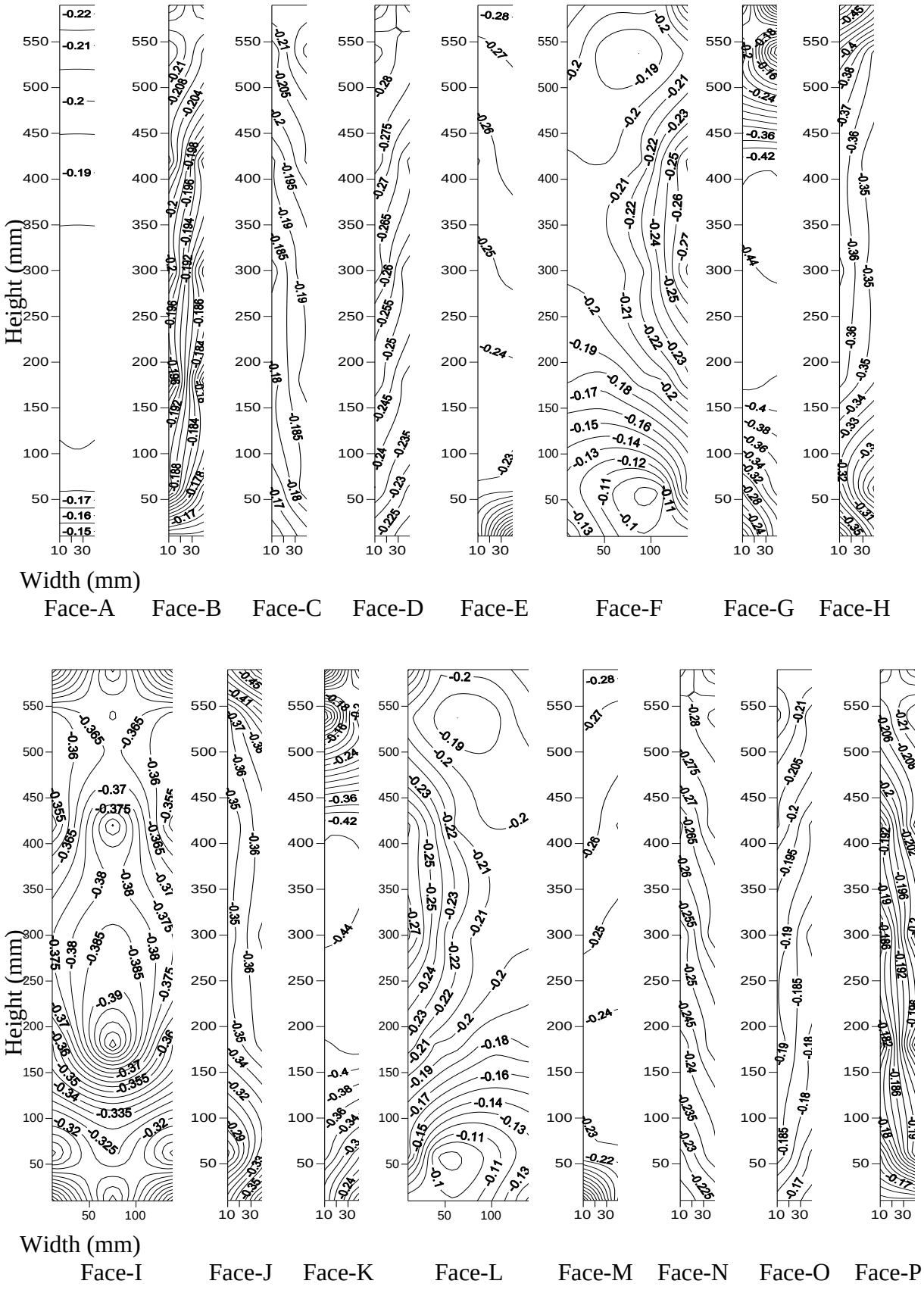


**Fig. 5.122 Distribution of mean wind pressure coefficients ($C_{p,mean}$) on different surfaces of model-G under front-to-back interference condition**

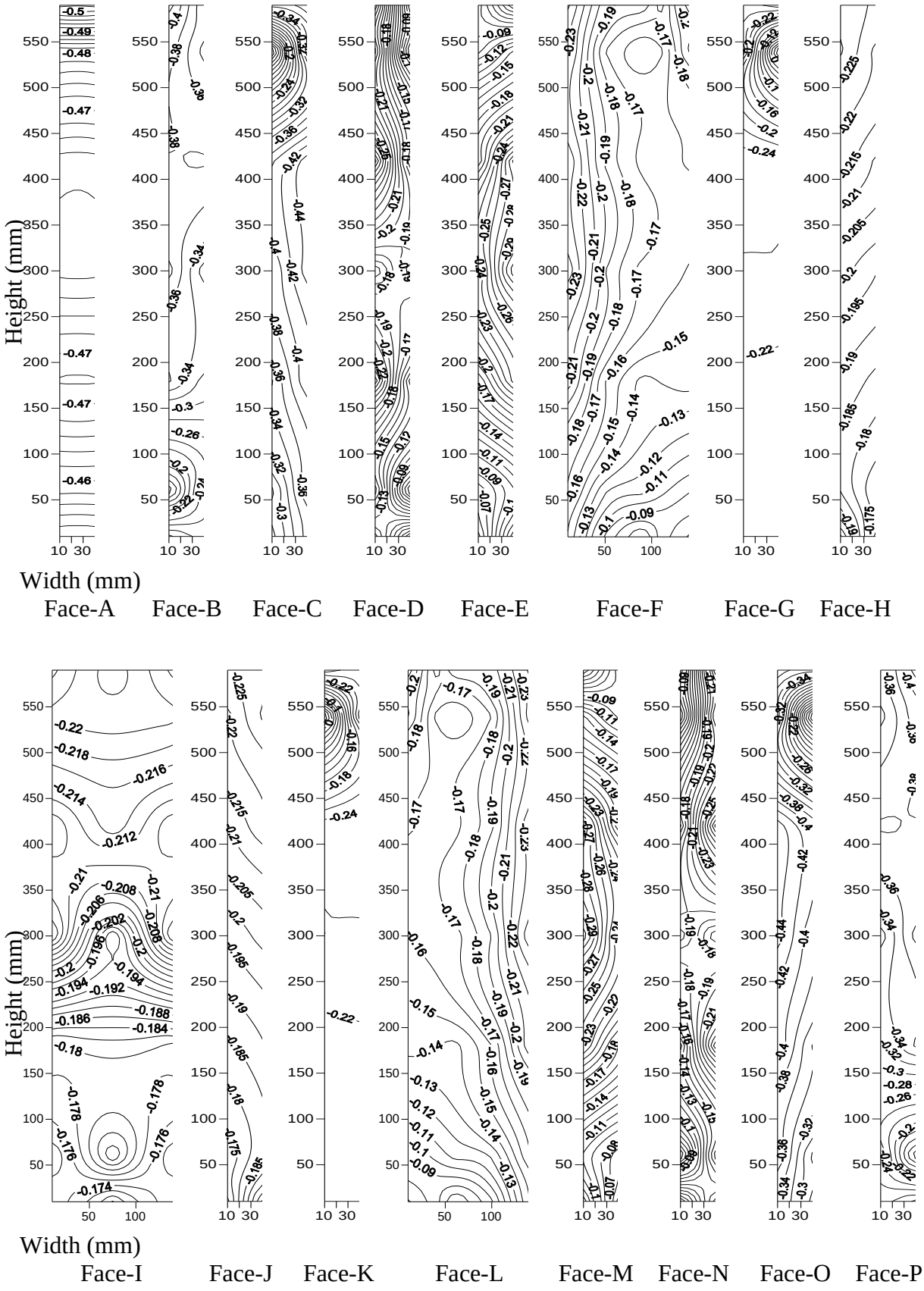


**Fig. 5.123 Distribution of mean wind pressure coefficients ($C_{p,mean}$) on different surfaces of model-G under front-to-front interference condition**

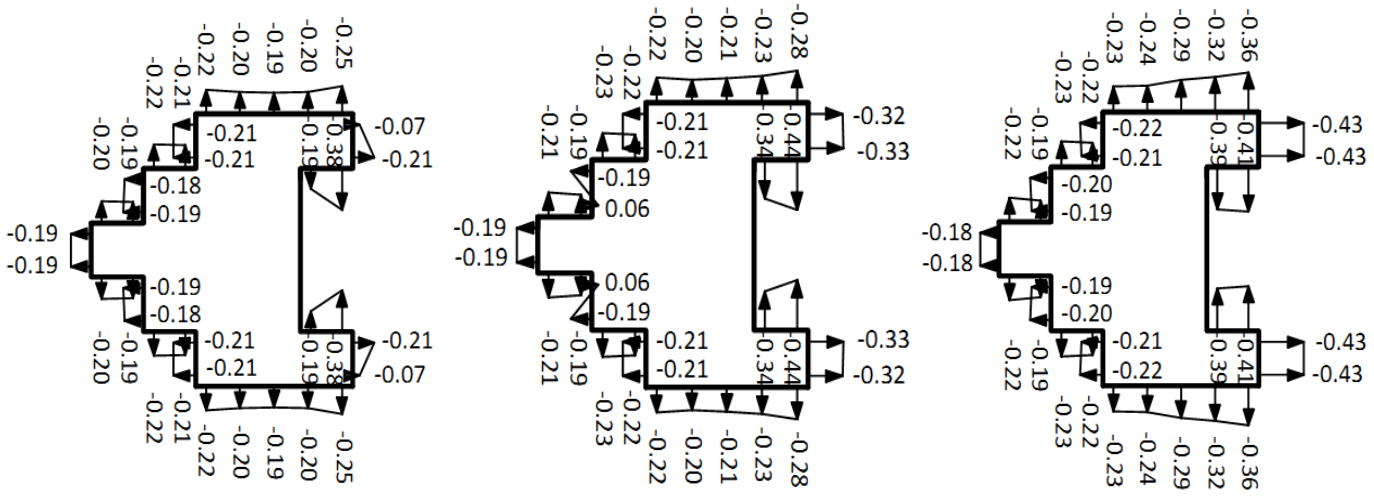


Section A-A Section B-B Section C-C

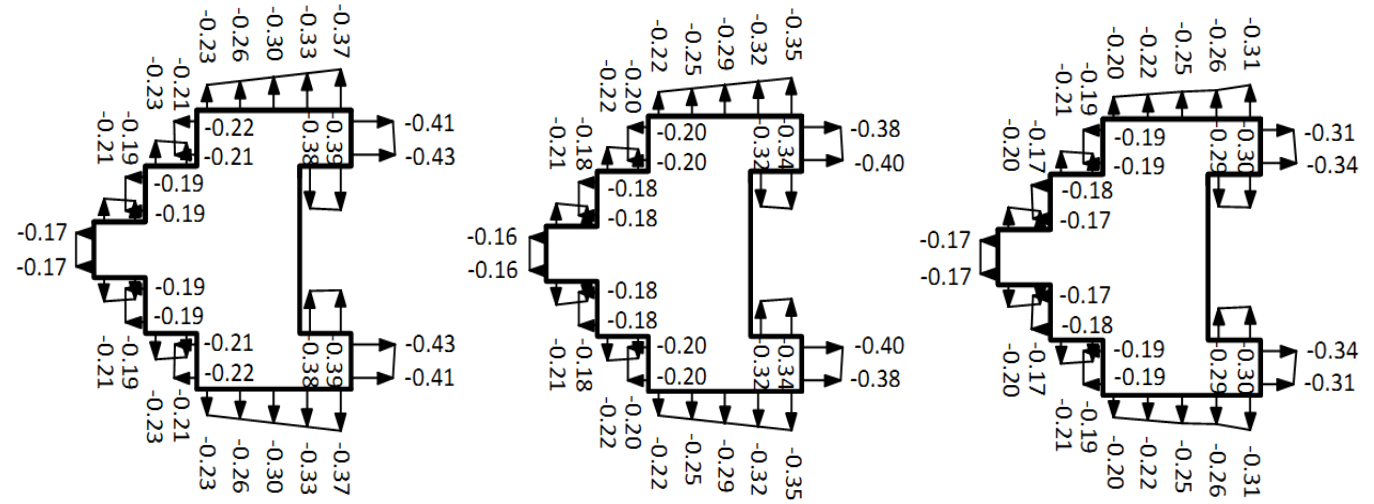


Section D-D Section E-E Section F-F

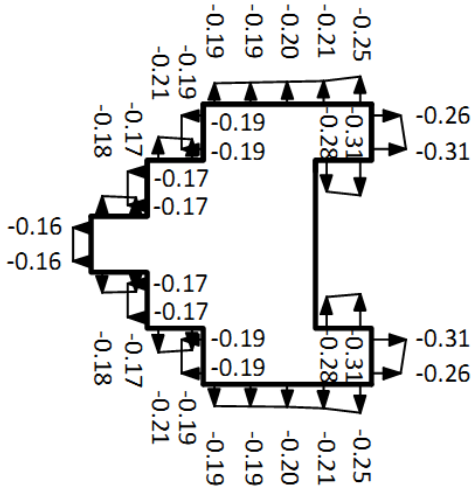


Section G-G

**Fig. 5.124 Cross-sectional variation of mean wind pressure coefficients ($C_{p,mean}$) on model-G in back-to-back interference condition**

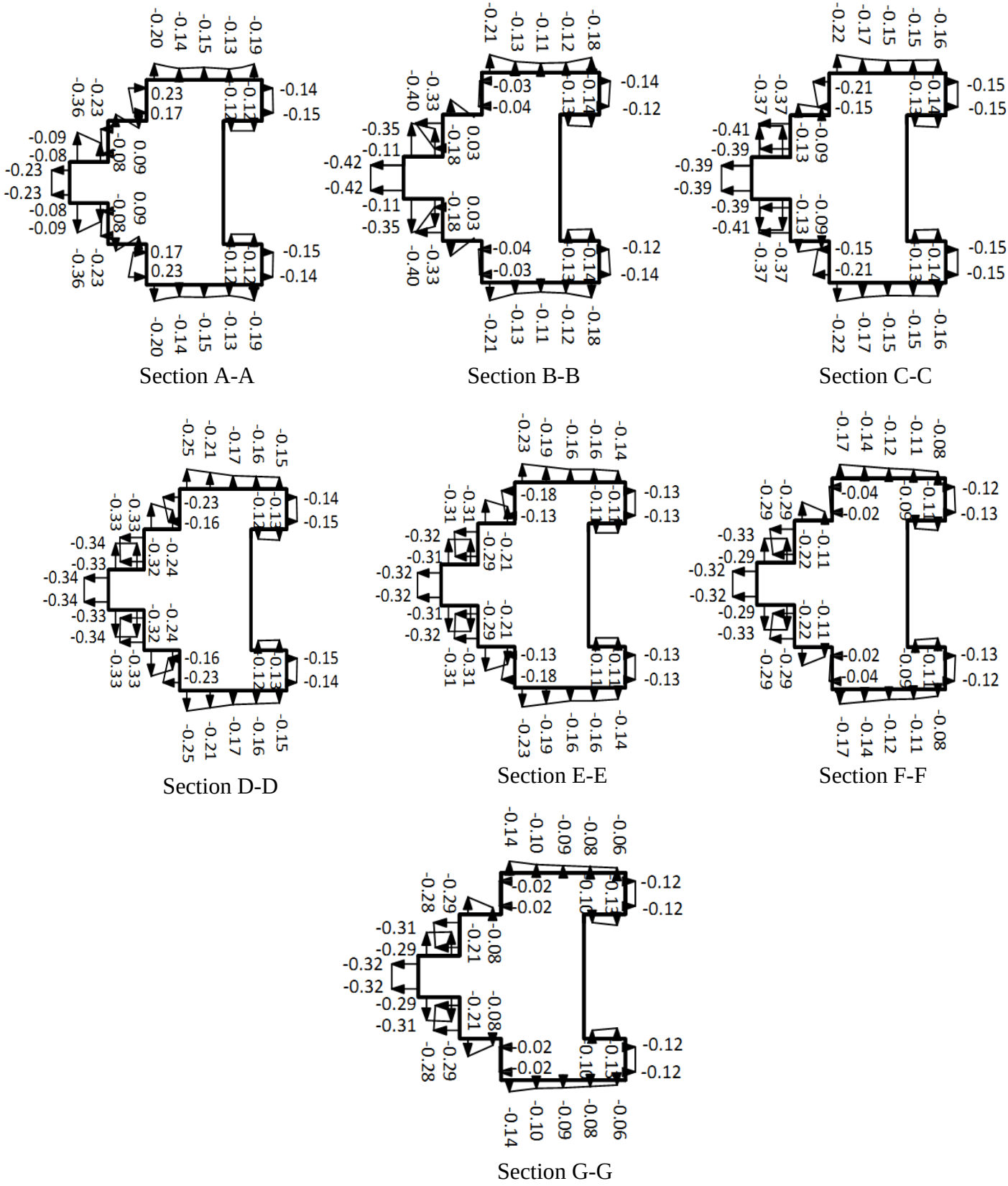


**Fig. 5.125 Cross-sectional variation of mean wind pressure coefficients ($C_{p,mean}$) on model-G in back-to-front interference condition**

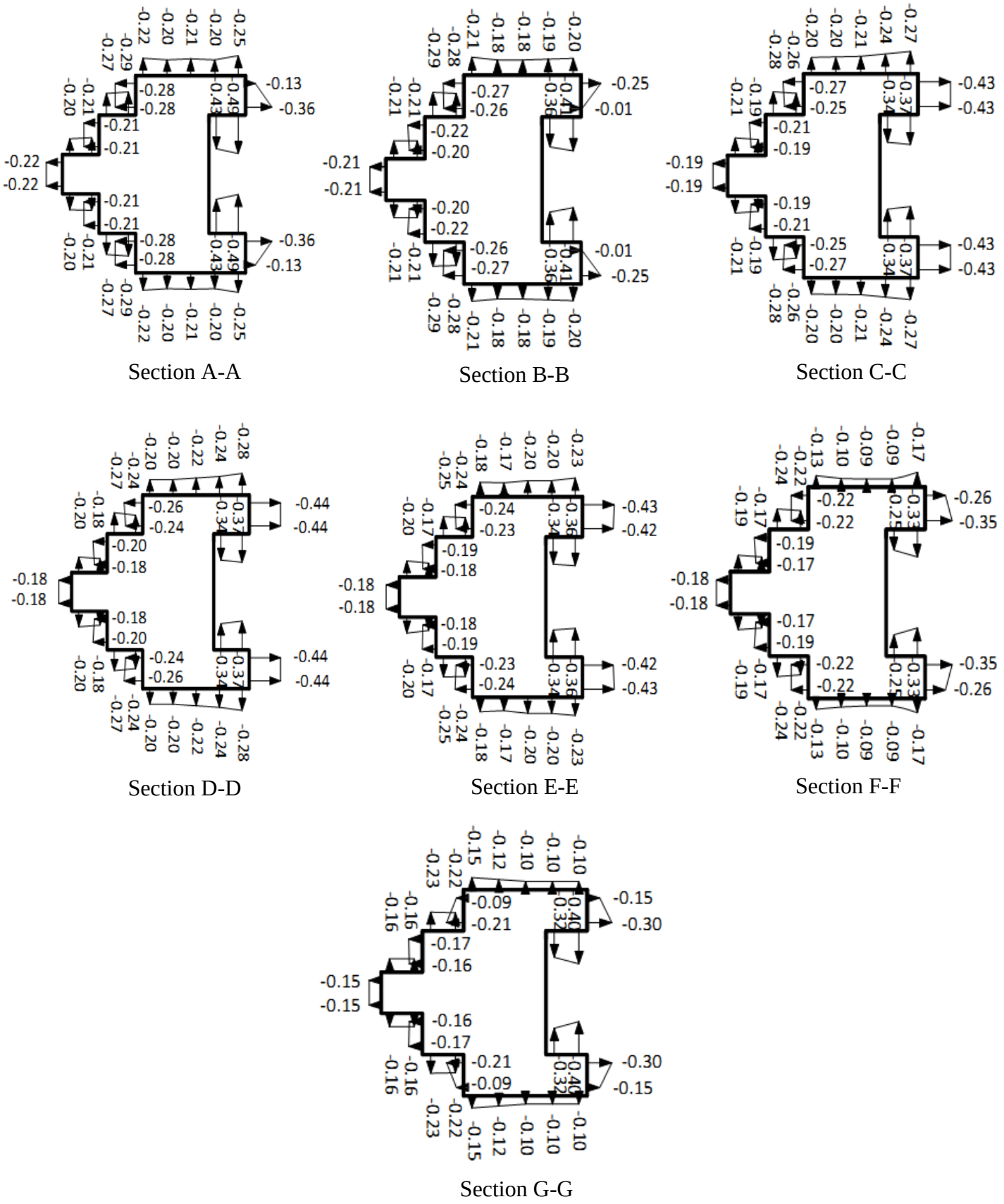


**Fig. 5.126 Cross-sectional variation of mean wind pressure coefficients ($C_{p,mean}$) on model-G in front-to-back interference condition**

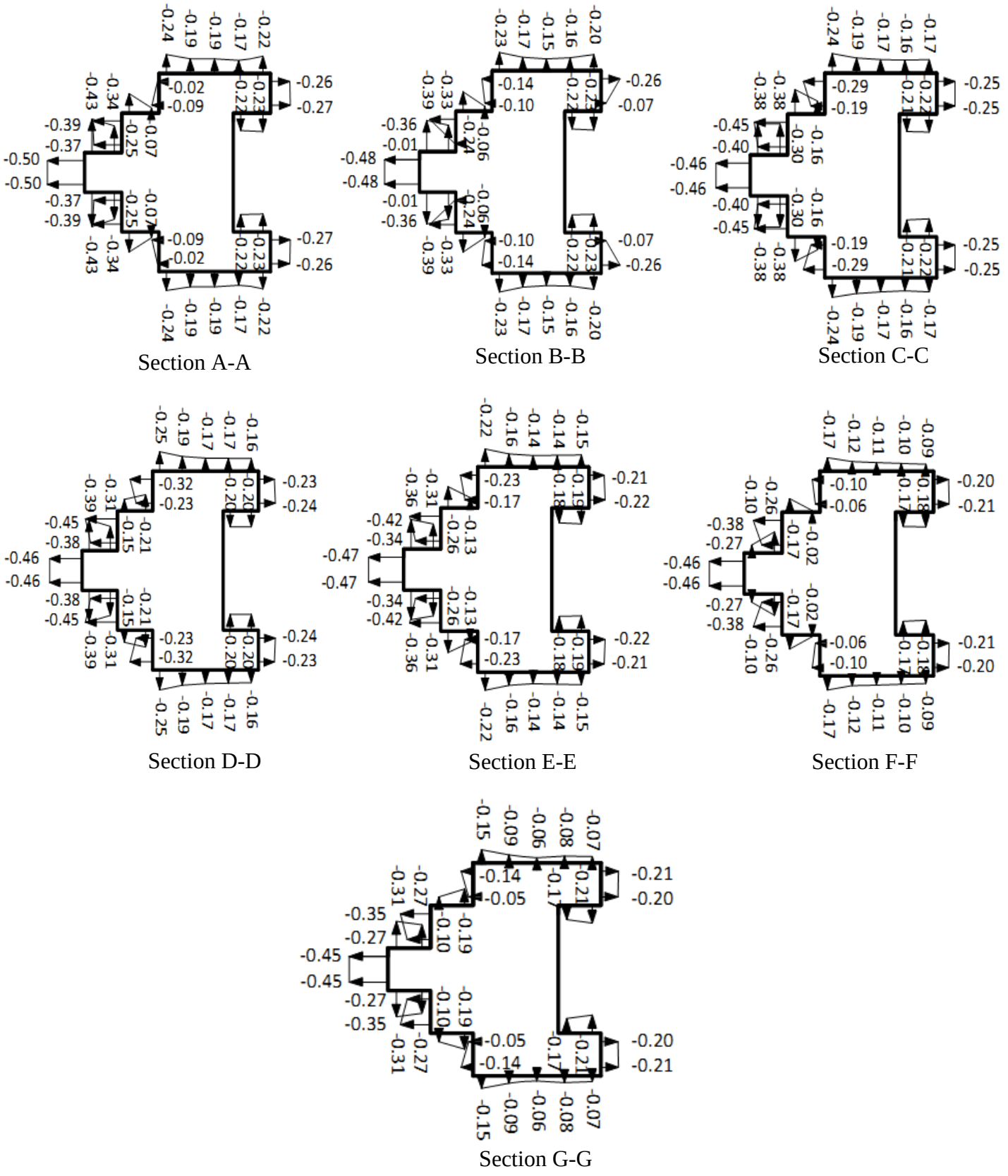


**Fig. 5.127 Cross-sectional variation of mean wind pressure coefficients ($C_{p,mean}$) on model-G in front-to-front interference condition**

**Table 5.14 Interference effect on variation of $C_{p,mean}$ on face-A of building model-G**

| Pressure point no. | Mean wind pressure coefficients ($C_{p,mean}$) | | | | |
|---|---|---|---|---|---|
| | **Back to back** | **Back to front** | **Front to back** | **Front to front** | **Isolated ($0^0$ wind incidence angle)** |
| 1 | -0.6 | -0.61 | -0.48 | -1.06 | 0.49 |
| 2 | -0.61 | **-0.27** | **-0.51** | -1.1 | 0.49 |
| 3 | **-0.64** | **-0.86** | -0.46 | **-1.07** | **0.73** |
| 4 | **-0.64** | **-0.86** | -0.49 | -1.06 | **0.73** |
| 5 | -0.61 | -0.79 | -0.48 | -0.99 | 0.71 |
| 6 | -0.6 | -0.79 | -0.46 | -0.99 | 0.71 |
| 7 | -0.55 | -0.75 | -0.45 | -0.95 | 0.67 |
| 8 | -0.57 | -0.74 | -0.43 | -0.95 | 0.67 |
| 9 | -0.53 | -0.76 | -0.43 | -0.95 | 0.59 |
| 10 | -0.53 | -0.76 | -0.43 | -0.98 | 0.59 |
| 11 | -0.52 | -0.74 | -0.41 | -0.97 | **0.45** |
| 12 | -0.51 | -0.75 | -0.42 | -0.96 | **0.45** |
| 13 | -0.5 | -0.72 | **-0.36** | -0.97 | 0.47 |
| 14 | **-0.49** | -0.72 | -0.39 | **-0.94** | 0.47 |

### 5.3.7 Model-H (Fish Shape-3)

Four interference conditions namely back-to-back, back-to-front, front-to-back and front-to-front under which wind pressures have been measured on the surfaces of the instrumented model of model-H are shown in Fig. 5.128. Results in the form of pressure contours are shown in Figs. 5.129 to 5.132 and in the form of cross-sectional variation in Figs. 5.133 to 5.136.

Table 5.15 compares the values of $C_{p,mean}$ in different cases.

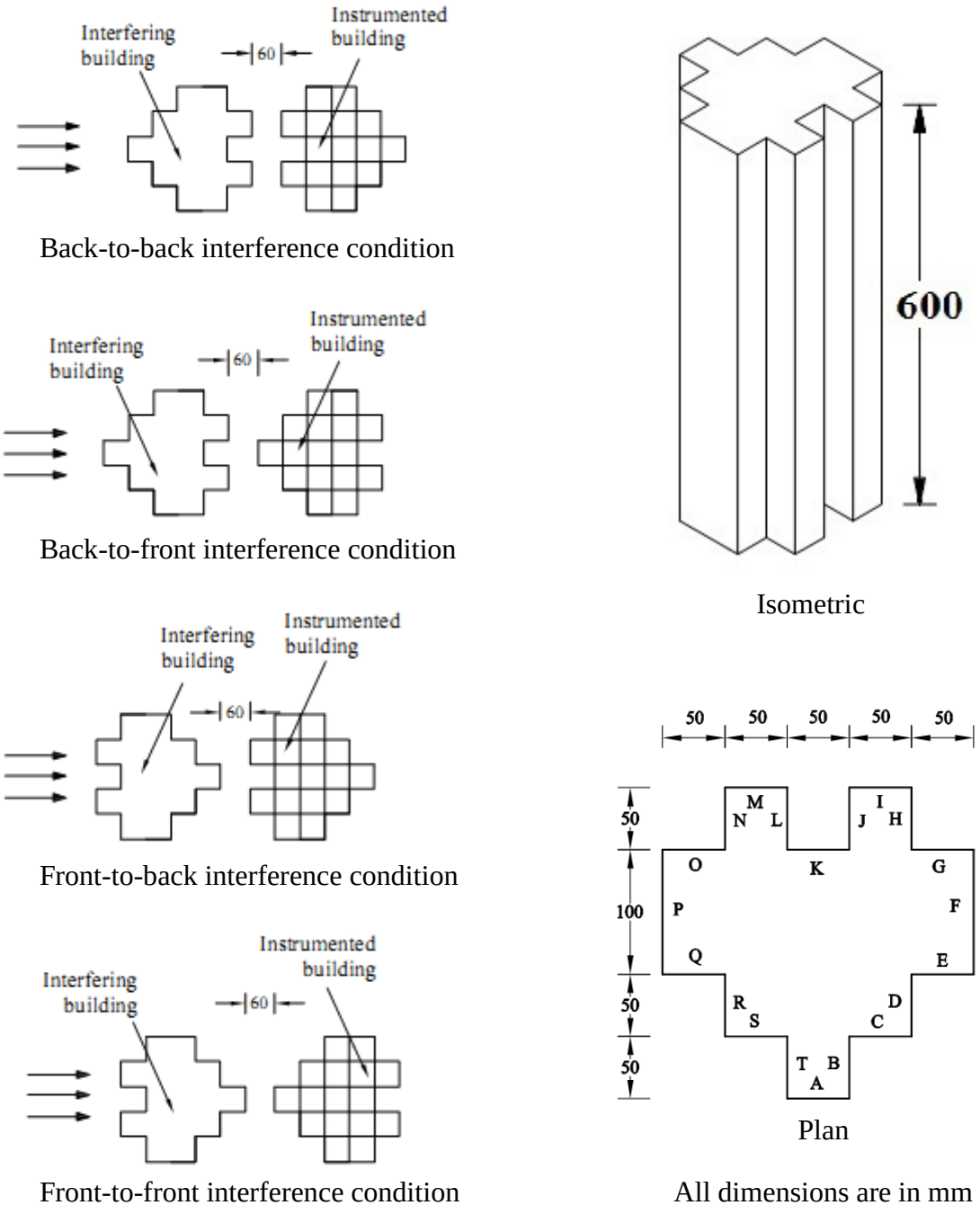


**Fig. 5.128 Details of model-H showing different interference conditions**

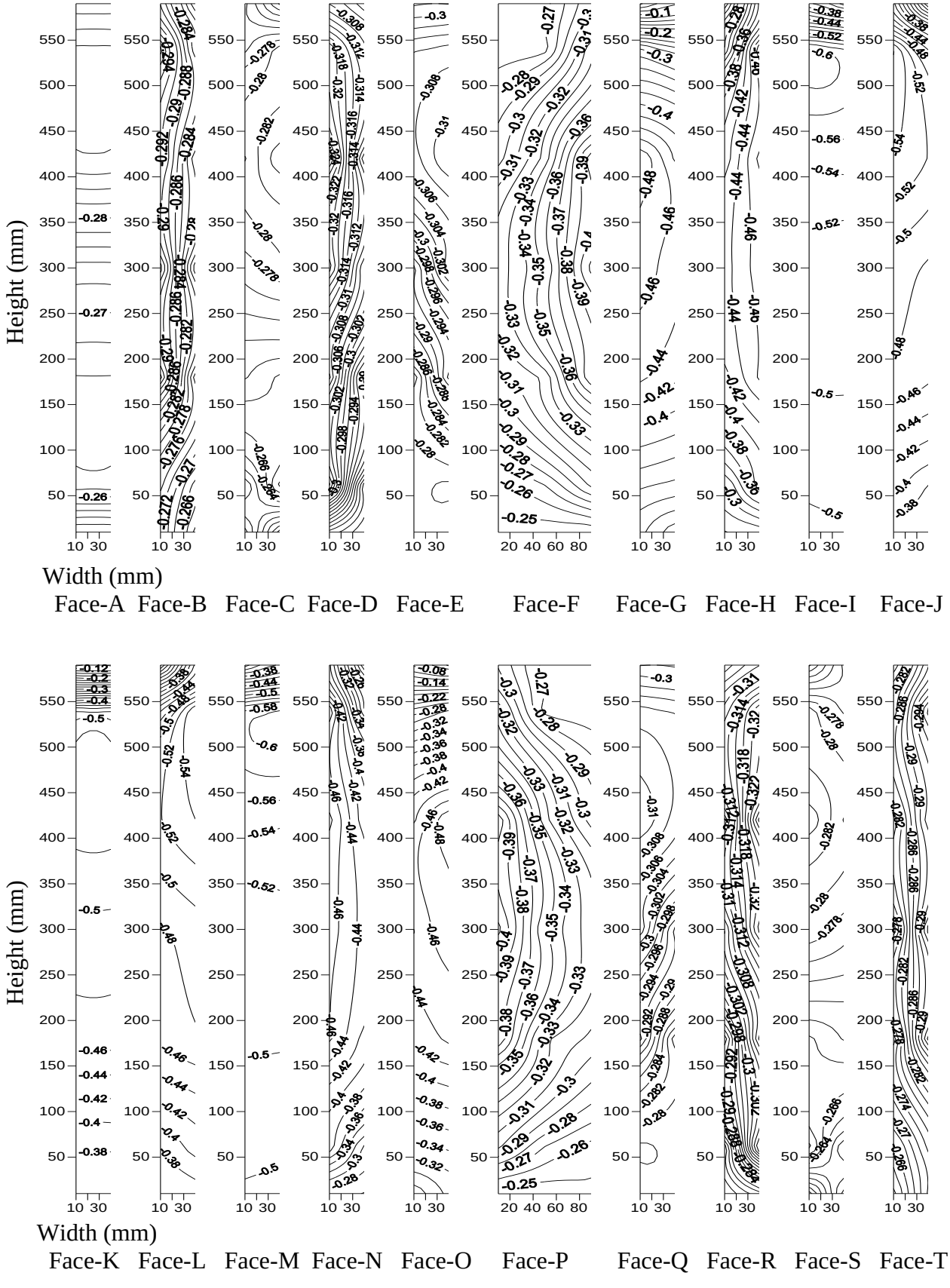


**Fig. 5.129 Distribution of mean wind pressure coefficients ($C_{p,mean}$) on different surfaces of model-H under back-to-back interference condition**

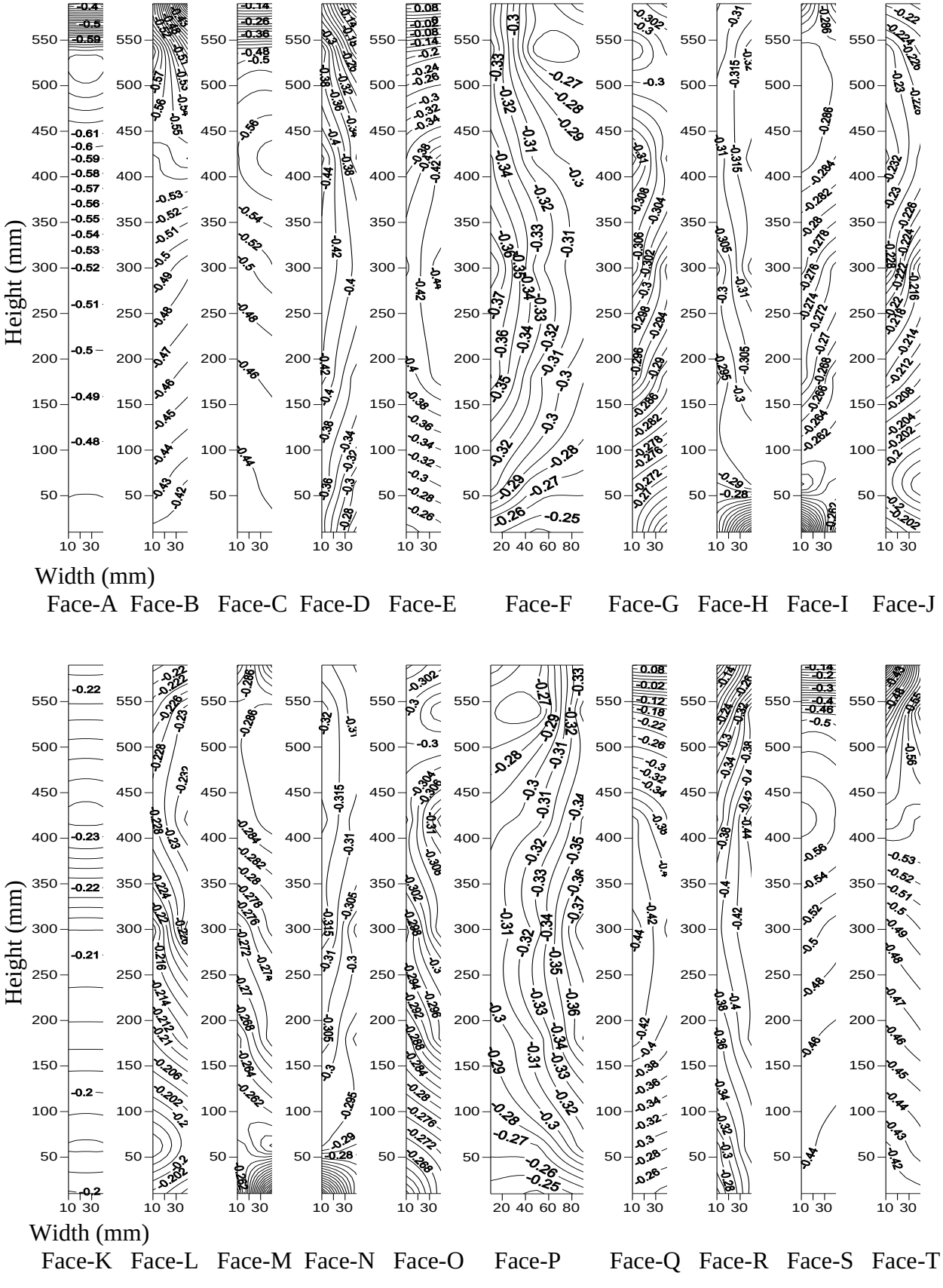


**Fig. 5.130 Distribution of mean wind pressure coefficients ($C_{p,mean}$) on different surfaces of model-H under back-to-front interference condition**

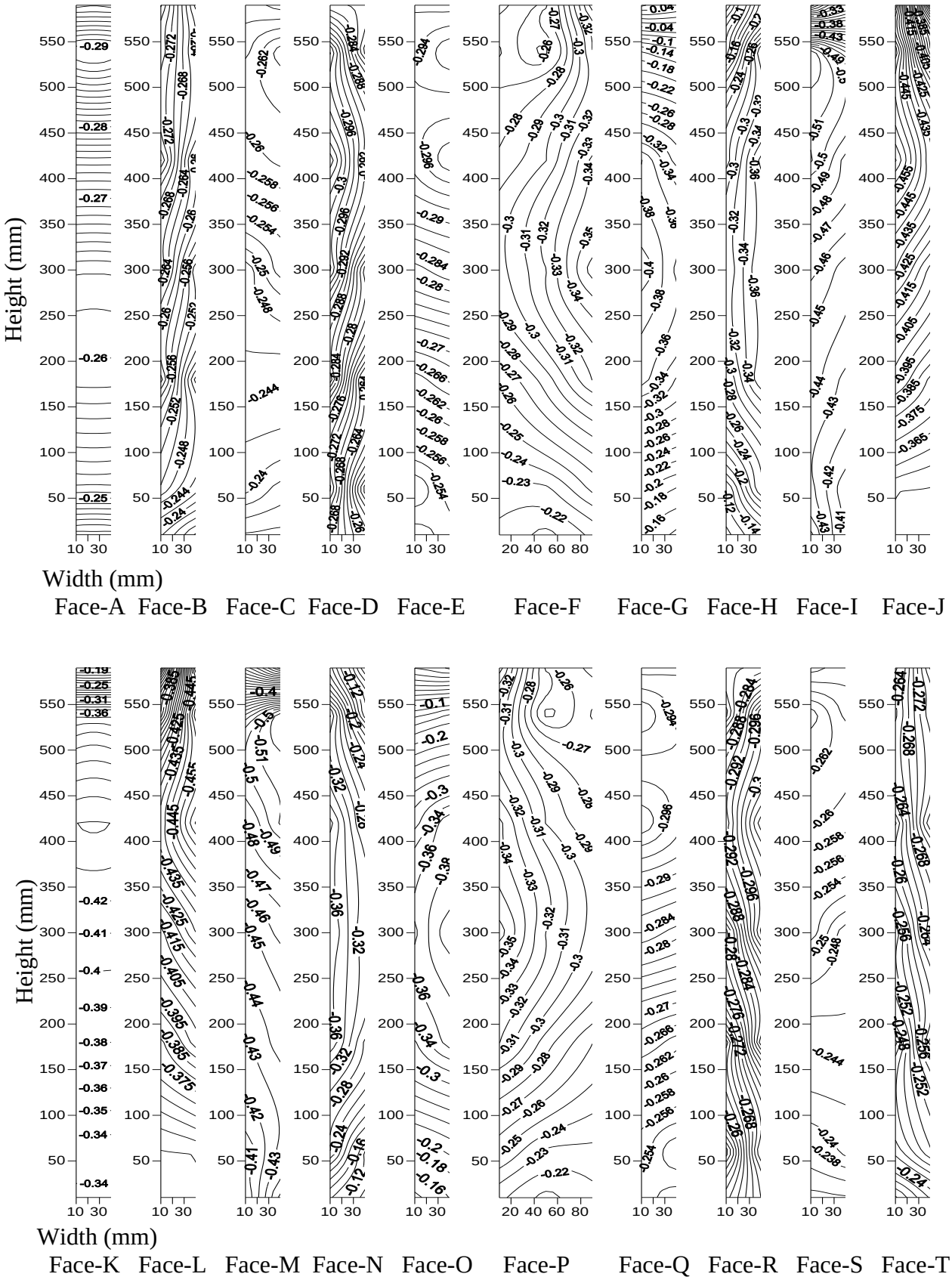


**Fig. 5.131 Distribution of mean wind pressure coefficients ($C_{p,mean}$) on different surfaces of model-H under front-to-back interference condition**

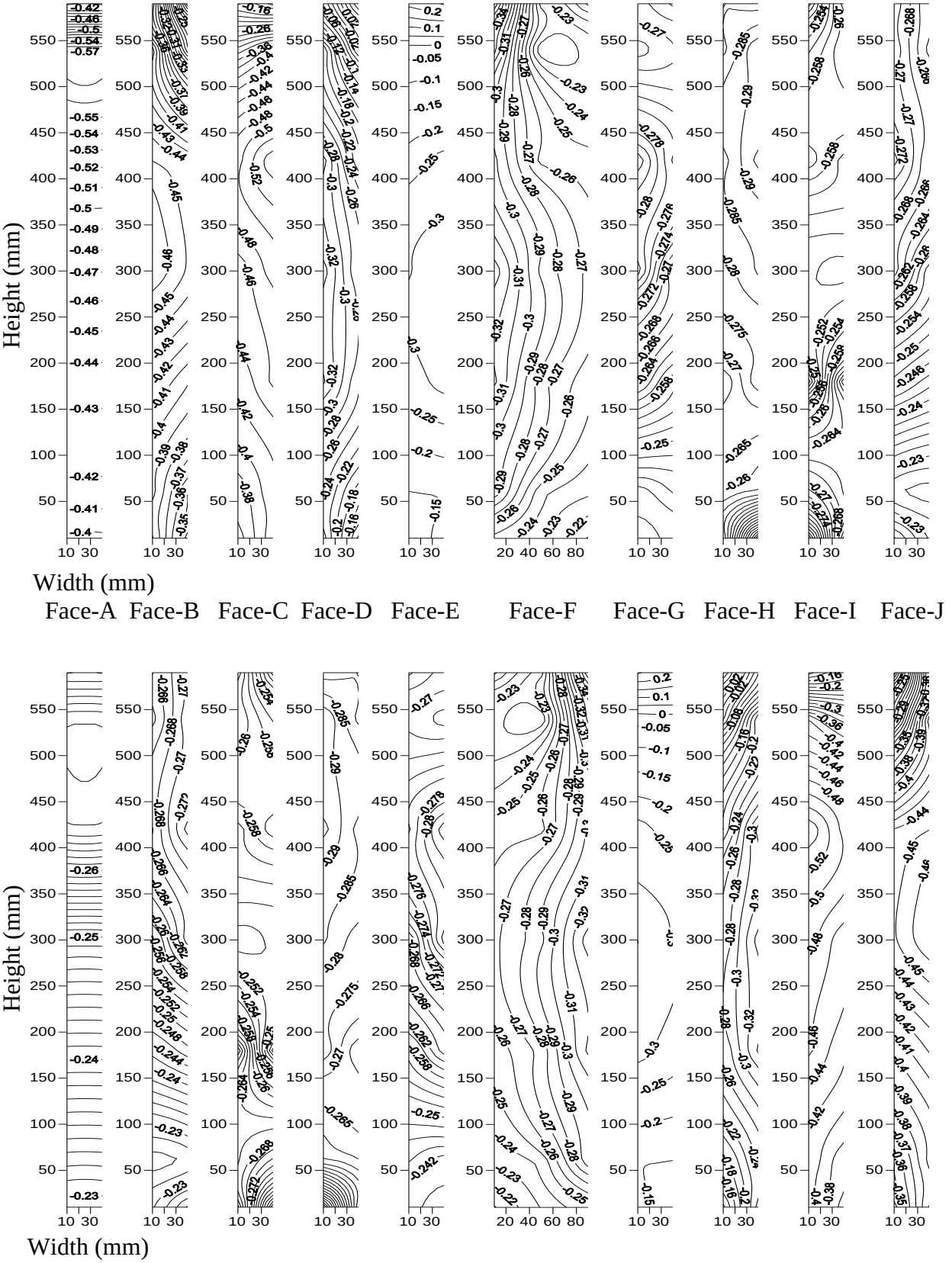


**Fig. 5.132 Distribution of mean wind pressure coefficients ($C_{p,mean}$) on different surfaces of model-H under front-to-front interference condition**

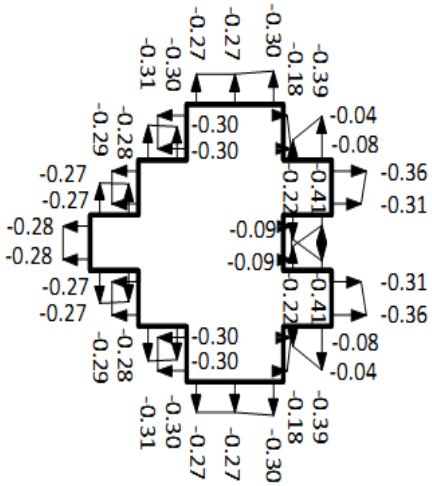

Section A-A

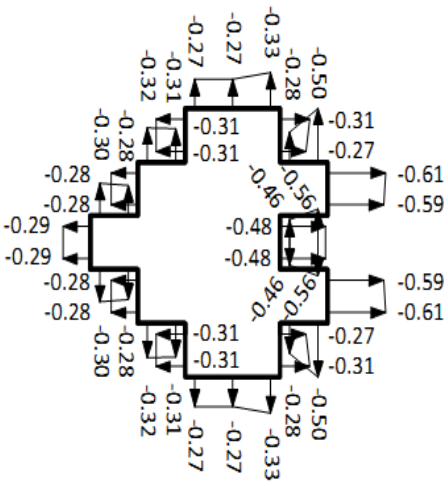

Section B-B

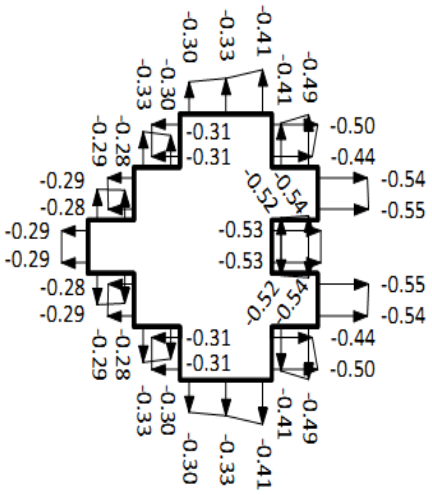

Section C-C

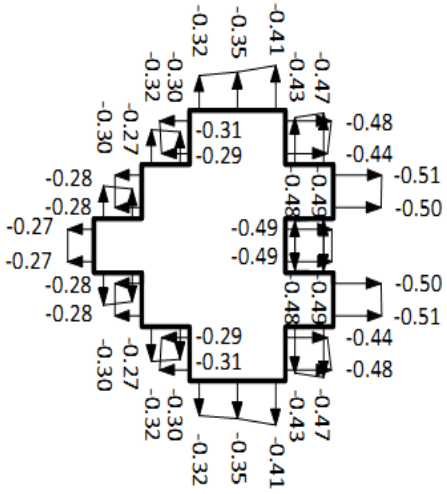

Section D-D

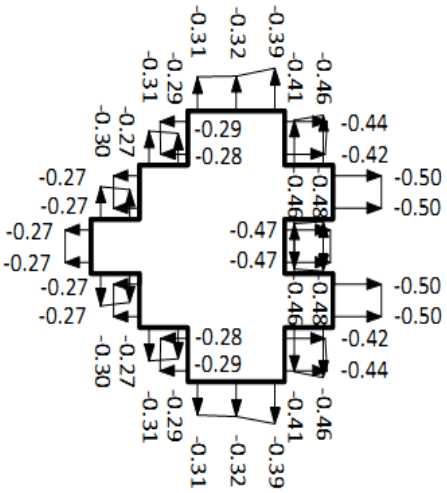

Section E-E

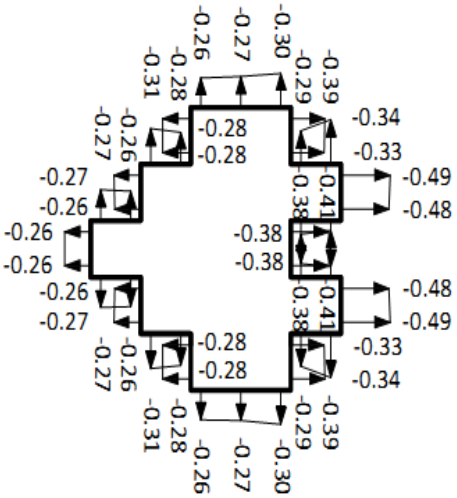

Section F-F

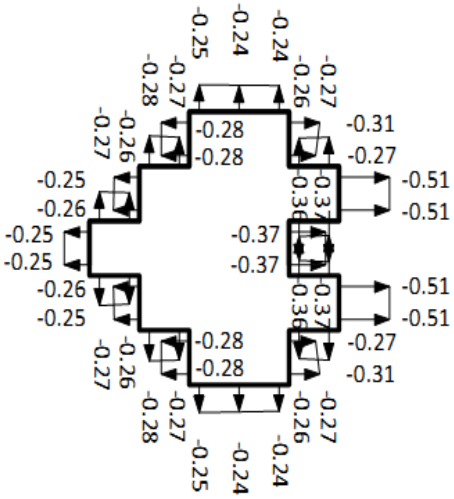

Section G-G

**Fig. 5.133 Cross-sectional variation of mean wind pressure coefficients ($C_{p,mean}$) on model-H in back-to-back interference condition**

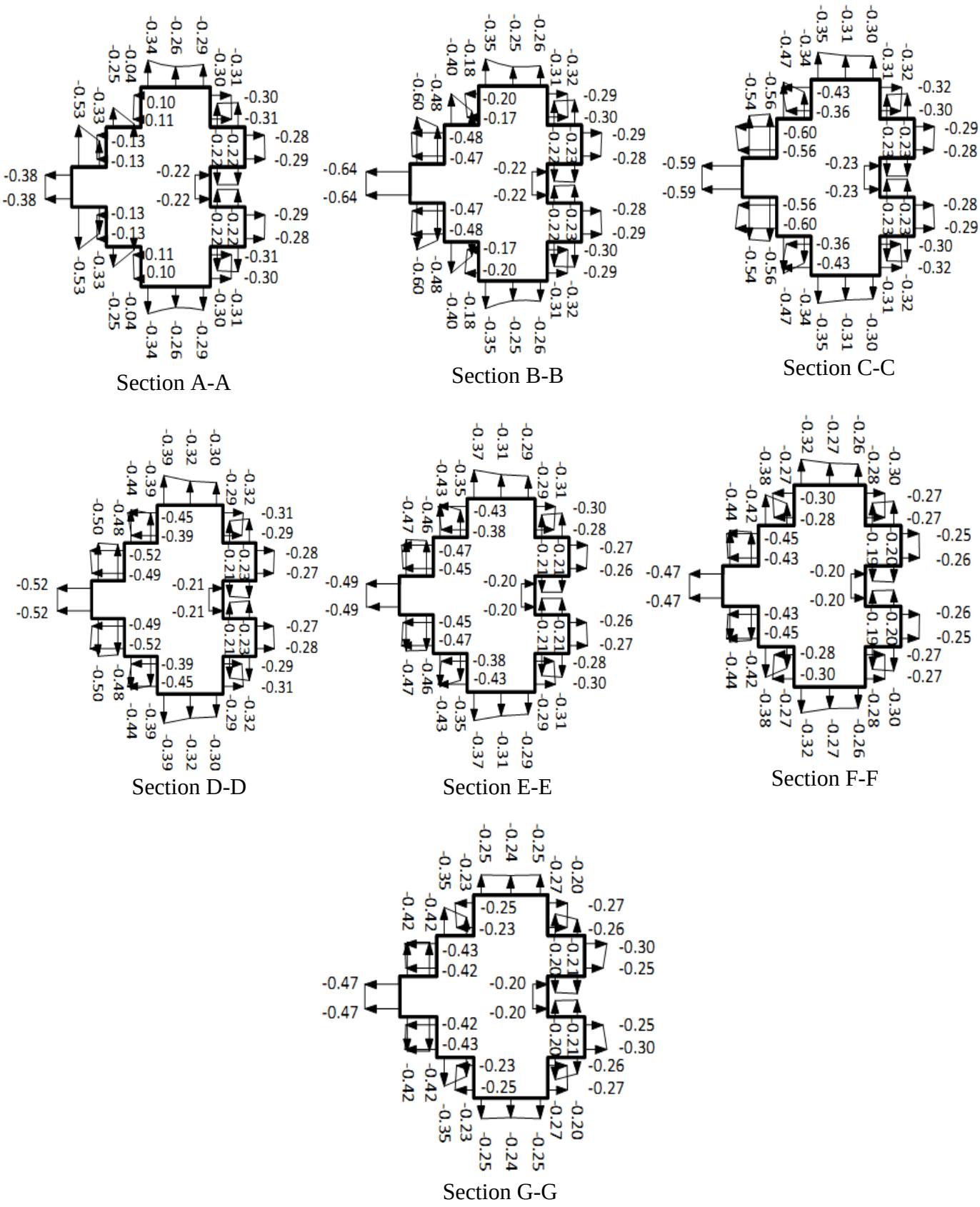


**Fig. 5.134 Cross-sectional variation of mean wind pressure coefficients ($C_{p,mean}$) on model-H in back-to-front interference condition**

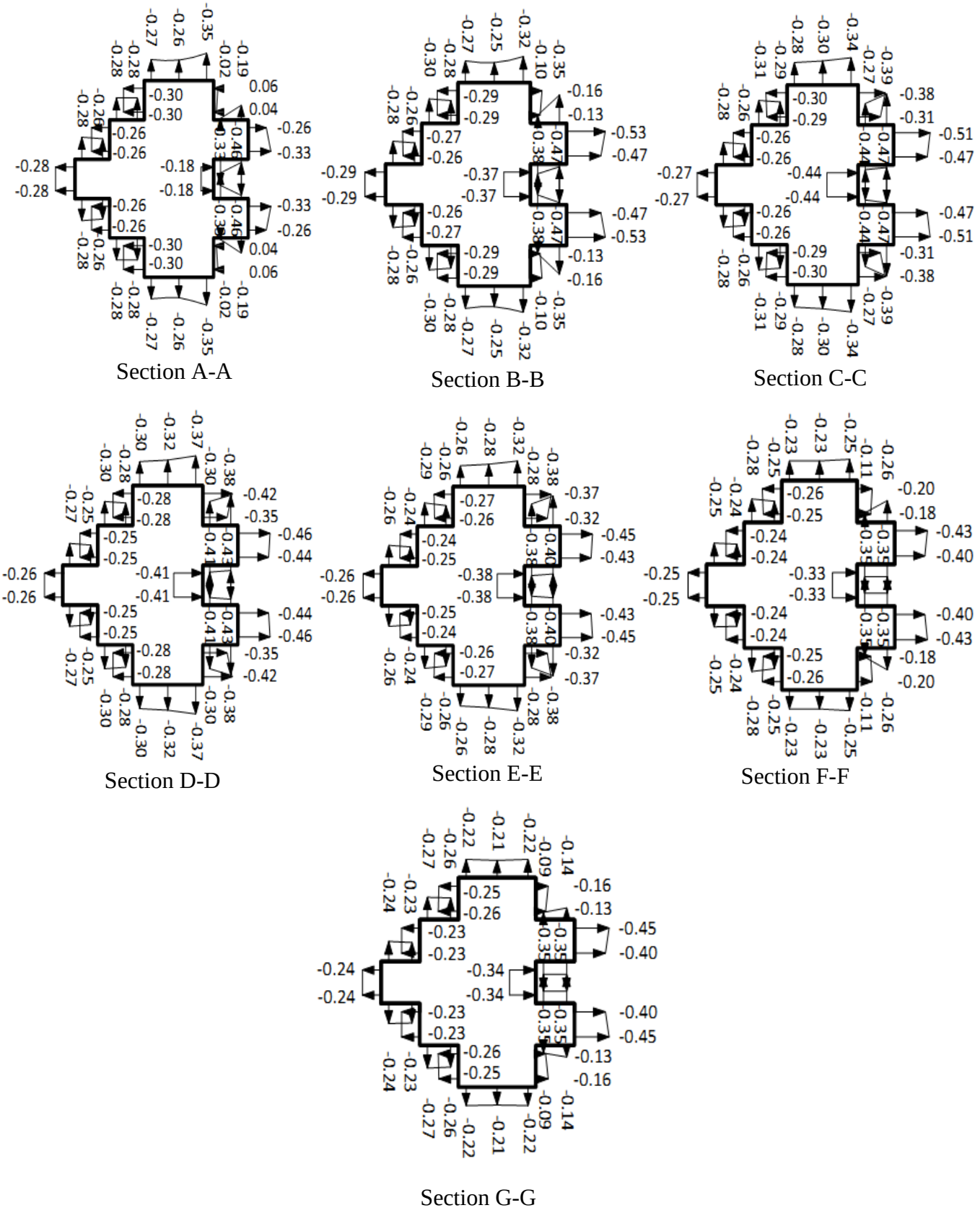


**Fig. 5.135 Cross-sectional variation of mean wind pressure coefficients ($C_{p,mean}$) on model-H in front-to-back interference condition**

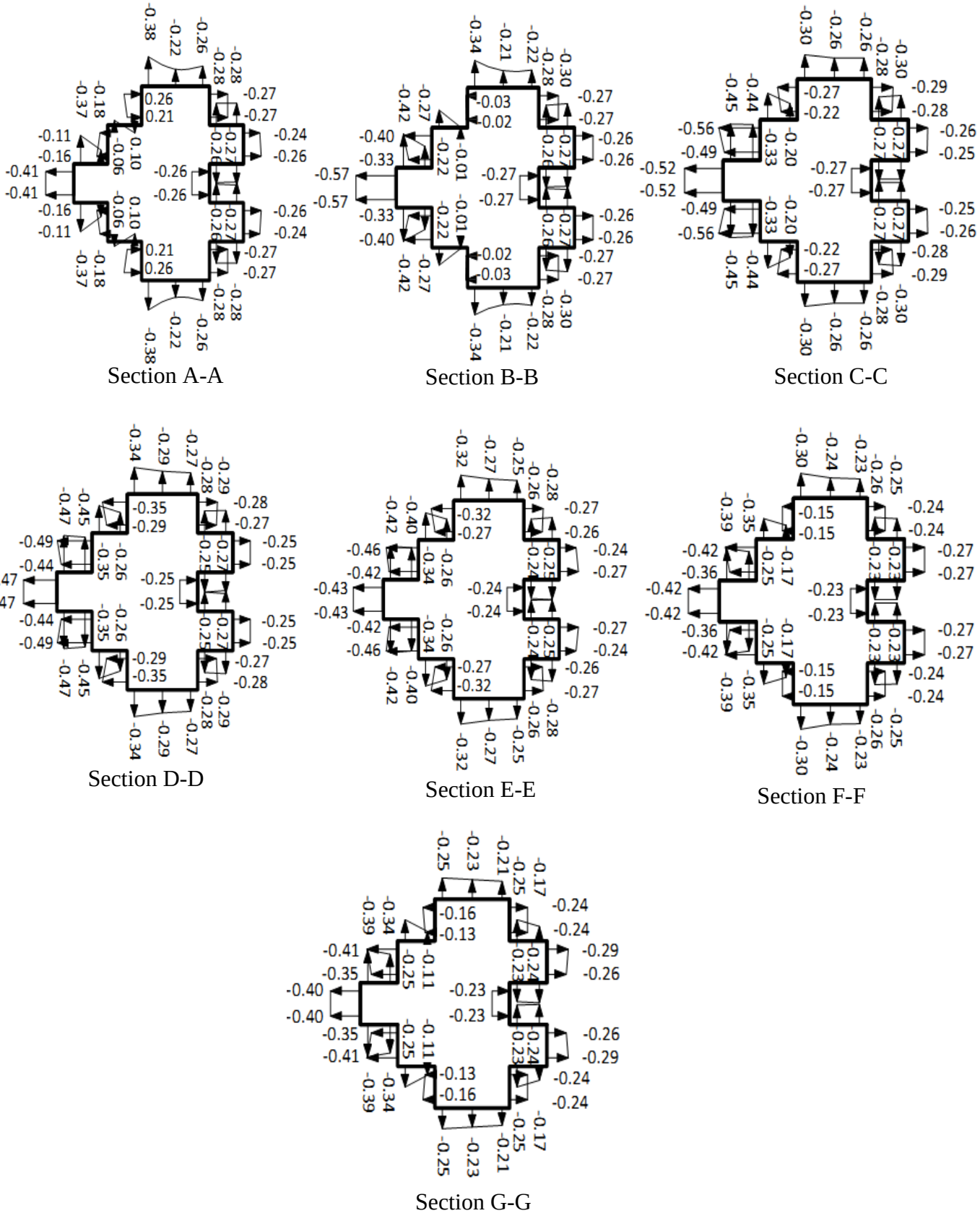


**Fig. 5.136 Cross-sectional variation of mean wind pressure coefficients ($C_{p,mean}$) on model-H in front-to-front interference condition**

**Table 5.15 Interference effect on variation of $C_{p,mean}$ on face-A of building model-H**

| Pressure point no. | Mean wind pressure coefficients ($C_{p,mean}$) | | | | |
|---|---|---|---|---|---|
| | Back to back | Back to front | Front to back | Front to front | Isolated ($0^0$ wind incidence angle) |
| 1 | -0.6 | -0.61 | -0.48 | -1.06 | 0.49 |
| 2 | -0.61 | **-0.27** | **-0.51** | **-1.1** | 0.49 |
| 3 | **-0.64** | **-0.86** | -0.46 | -1.07 | **0.73** |
| 4 | **-0.64** | **-0.86** | -0.49 | -1.06 | **0.73** |
| 5 | -0.61 | -0.79 | -0.48 | -0.99 | 0.71 |
| 6 | -0.6 | -0.79 | -0.46 | -0.99 | 0.71 |
| 7 | -0.55 | -0.75 | -0.45 | -0.95 | 0.67 |
| 8 | -0.57 | -0.74 | -0.43 | -0.95 | 0.67 |
| 9 | -0.53 | -0.76 | -0.43 | -0.95 | 0.59 |
| 10 | -0.53 | -0.76 | -0.43 | -0.98 | 0.59 |
| 11 | -0.52 | -0.74 | -0.41 | -0.97 | **0.45** |
| 12 | -0.51 | -0.75 | -0.42 | -0.96 | **0.45** |
| 13 | -0.5 | -0.72 | **-0.36** | -0.97 | 0.47 |
| 14 | **-0.49** | -0.72 | -0.39 | **-0.94** | 0.47 |

# Chapter - 6

# WIND RESPONSE ANALYSIS

## 6.1 GENERAL

The aim of the study is to evaluate the response of tall buildings with different cross-sectional shapes under wind loads obtained from the experimental measurements. All buildings are analyzed by linear static analysis method using STAAD.Pro software. The response of all building frames are obtained for various wind incidence angles both under isolated and interference conditions. The results obtained are presented in this chapter. The purpose of the study is to compare the response of tall buildings with different cross-sectional shapes under similar wind environment.

## 6.2 BUILDING DIMENSIONS

In all, buildings with 7 different cross-sectional shapes are considered for wind response analysis. The height and floor area of all prototype buildings are kept 60 m and 400 $m^2$ respectively. Each prototype building has 19 storeys with lowest storey height as 3.75 m and the height of the other storeys as 3.125 m each. All building frames are made of R.C.C. beams, slabs and columns. Table 6.1 gives the details of building and element dimensions. Grades of concrete and steel reinforcement used in prototype buildings are M-25 and Fe-415 respectively. Live load and floor finishing loads are taken as 4.0 $kN/m^2$ and 1.0 $kN/m^2$ respectively. The depth of the slab is taken as 150 mm.

**Table 6.1 Description of the buildings and frame elements**

| S.No. | Particulars | Details/Values |
|---|---|---|
| 1 | First storey height | 3.75 m |
| 2. | Remaining storey height | 3.125 m |
| 3. | Size of beams | 300 mm X 600 mm |
| 4. | Size of columns (from first storey to fifth storey) | 750 mm X 750 mm |
| 5. | Size of columns (from sixth storey to tenth storey) | 600 mm X 600 mm |
| 6. | Size of columns (from eleventh storey to fifteenth storey) | 500 mm X 500 mm |
| 7. | Size of columns (from sixteenth storey to nineteenth stoery) | 400 mm X 400 mm |
| 8. | Thickness of floor slab | 150 mm |

Square shape prototype building is assumed to have plan dimension of 20 m x 20 m. Bay width is taken as 5 m in both directions. Thus this building has 16 square blocks of 5 m x 5m dimension (Fig. 6.1). Plus Shape-1 prototype building is obtained by removing 2 square blocks from 2 corners of square shape building and placing them along another edge. Thus this building has plan dimensions of 20 m x 25 m (Fig. 6.2). This also represents rectangular plan building with corner cuts. Figure 6.3 indicates that Plus Shape-2 building has cross-sectional dimension of 20 m x 30 m.

I-shape-1 building has plan dimension of 20 m x 25 m as in the case of Plus Shape-1 building, but 4 blocks are placed differently at 4 corners.

Plan dimensions of Fish Shape-1, Fish Shape-2 and Fish Shape-3 buildings are 20 m x 35 m, 25 m x 25 m and 25 m x 25 m respectively (Figs. 6.5 to 6.7).

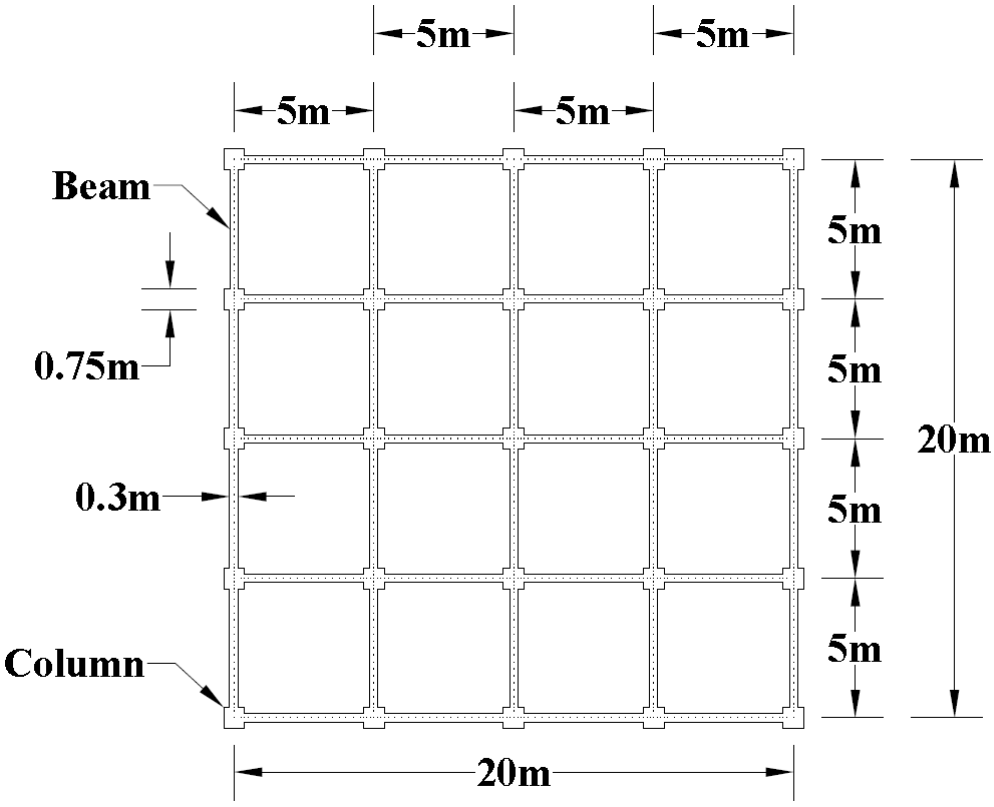


**Fig. 6.1 Ground floor plan of Square Shape building**

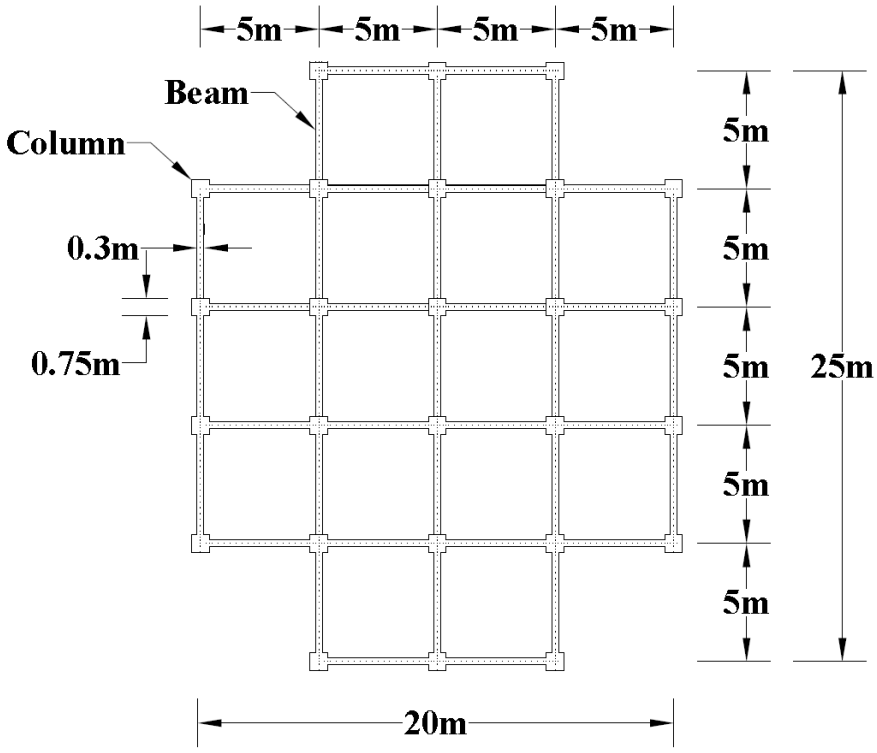


**Fig. 6.2 Ground floor plan of Plus Shape-1 building**

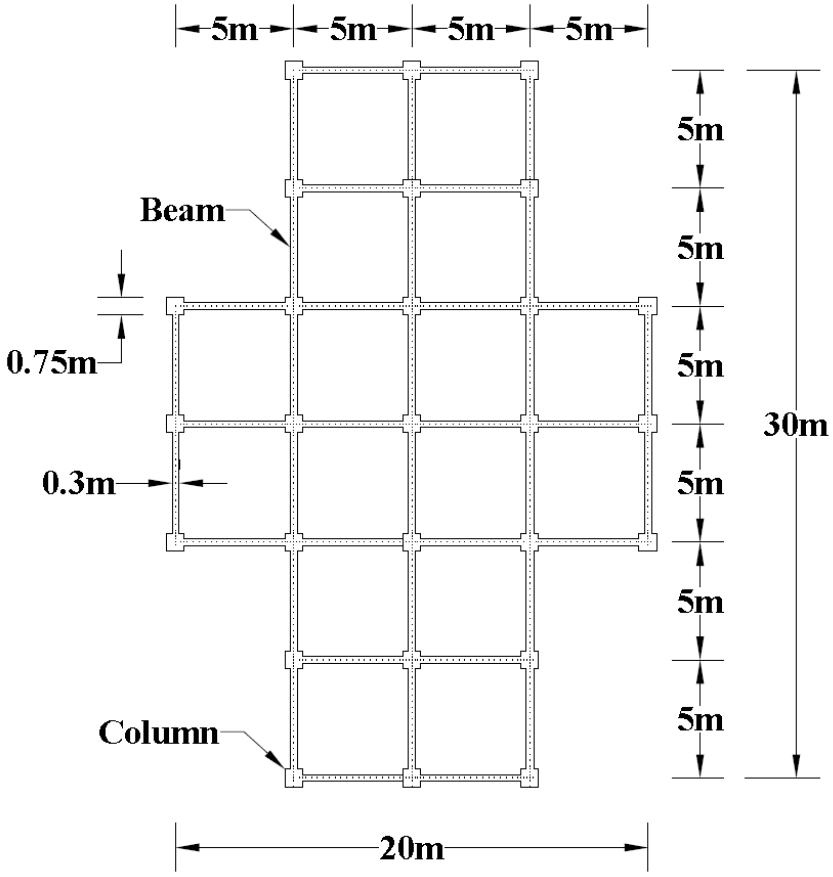


**Fig. 6.3 Ground floor plan of Plus Shape-2 building**

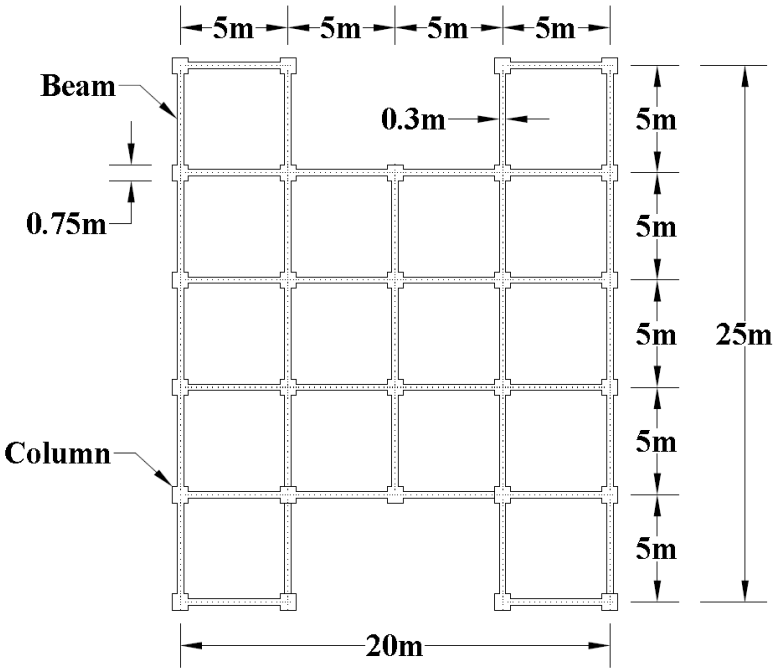


**Fig. 6.4 Ground floor plan of I-Shape-1 building**

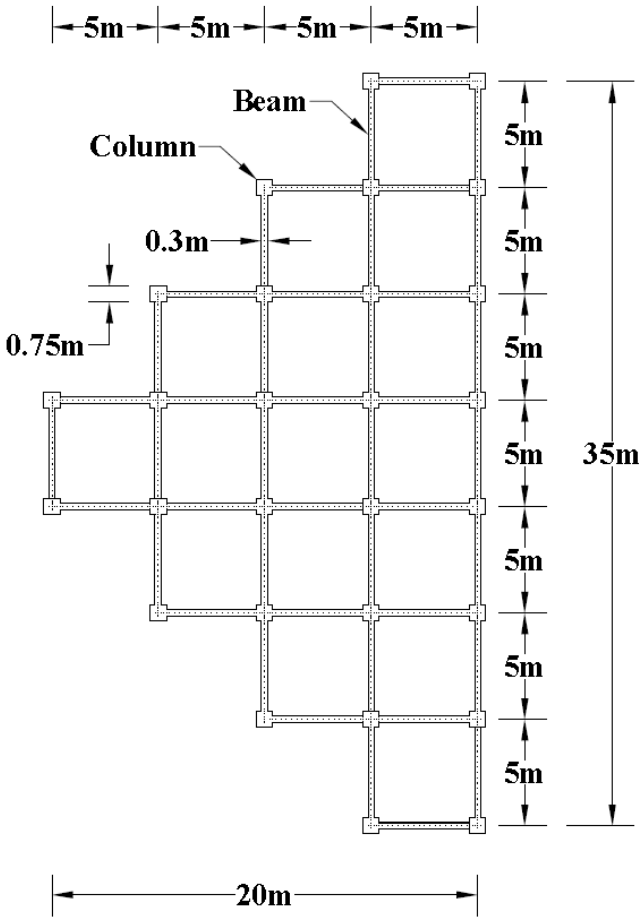


**Fig. 6.5 Ground floor plan of Fish Shape-1 building**

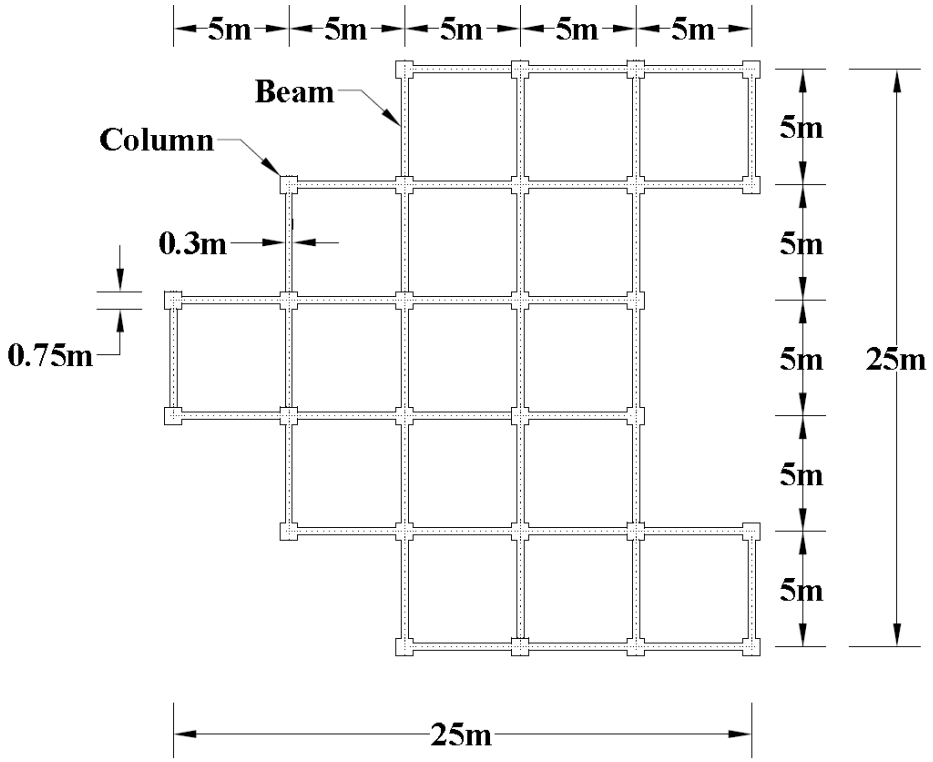


**Fig. 6.6 Ground floor plan of Fish Shape-2 building**

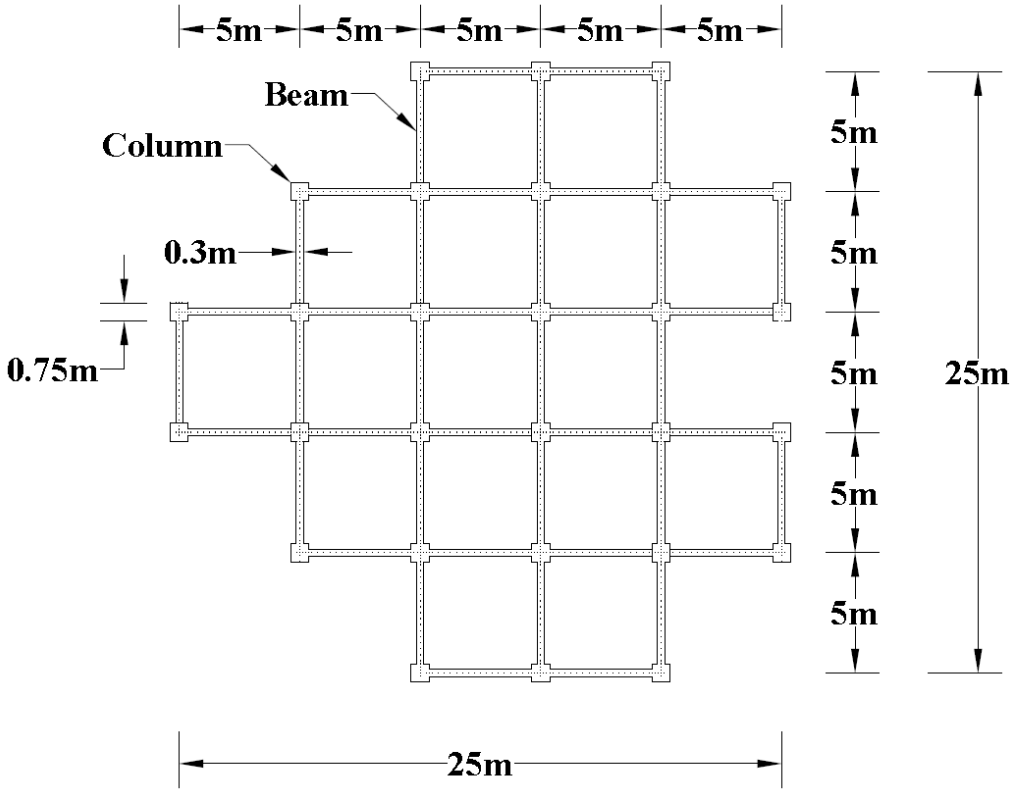


**Fig. 6.7 Ground floor plan of Fish Shape-3 building**

Figures 6.8 to 6.14 represent front elevations and isometric views of all seven prototype buildings.

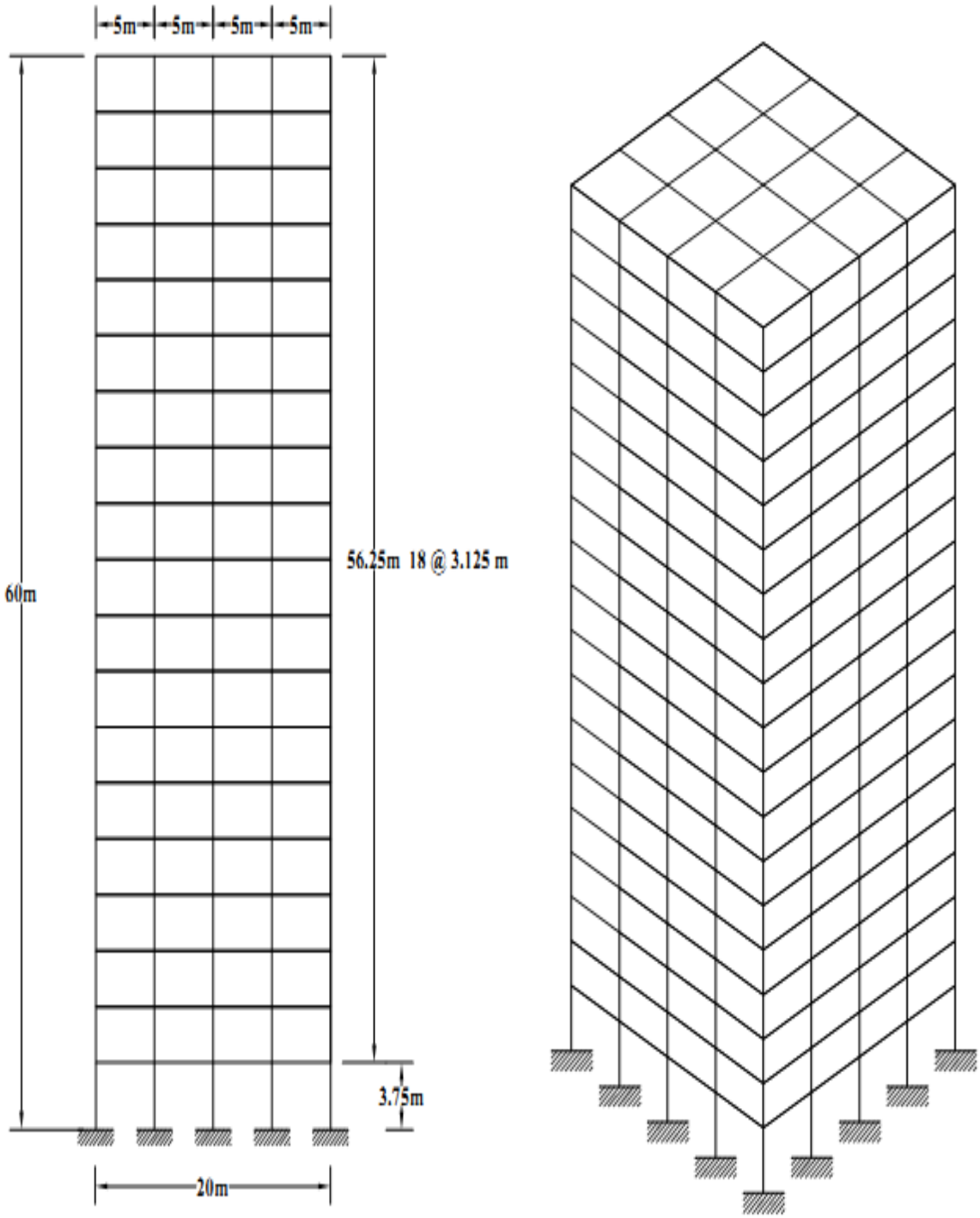


**Elevation** **Isometric View**

**Fig. 6.8 Elevation and isometric view of Square Shape building**

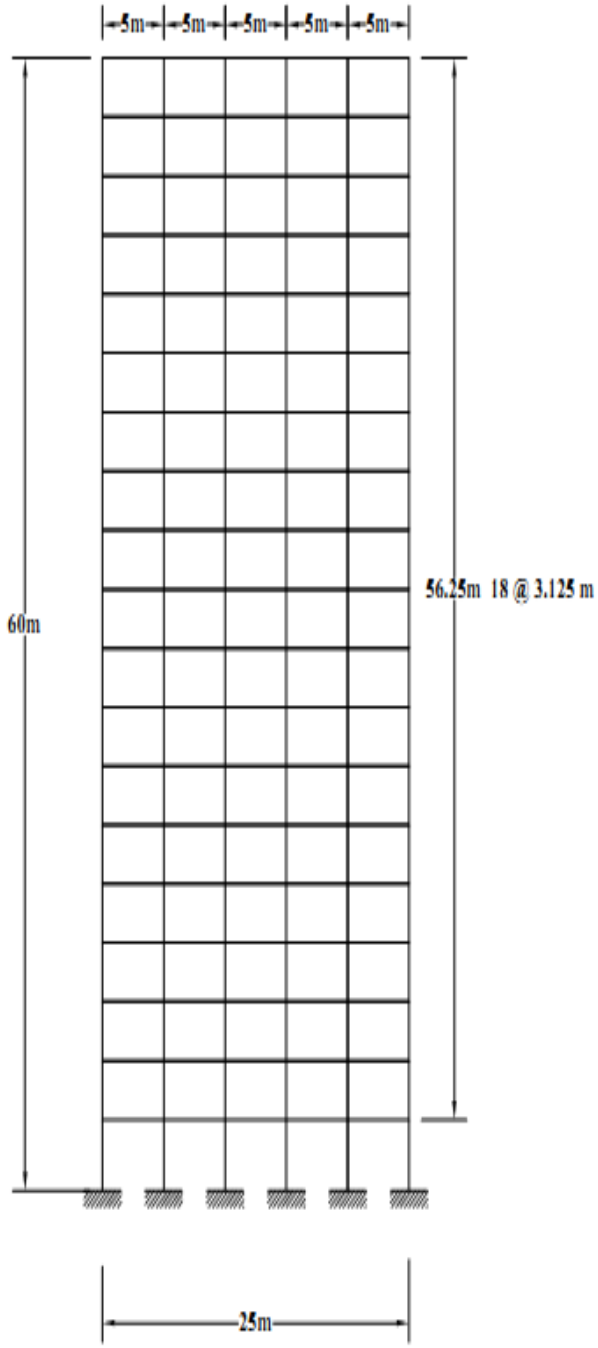


**Elevation**

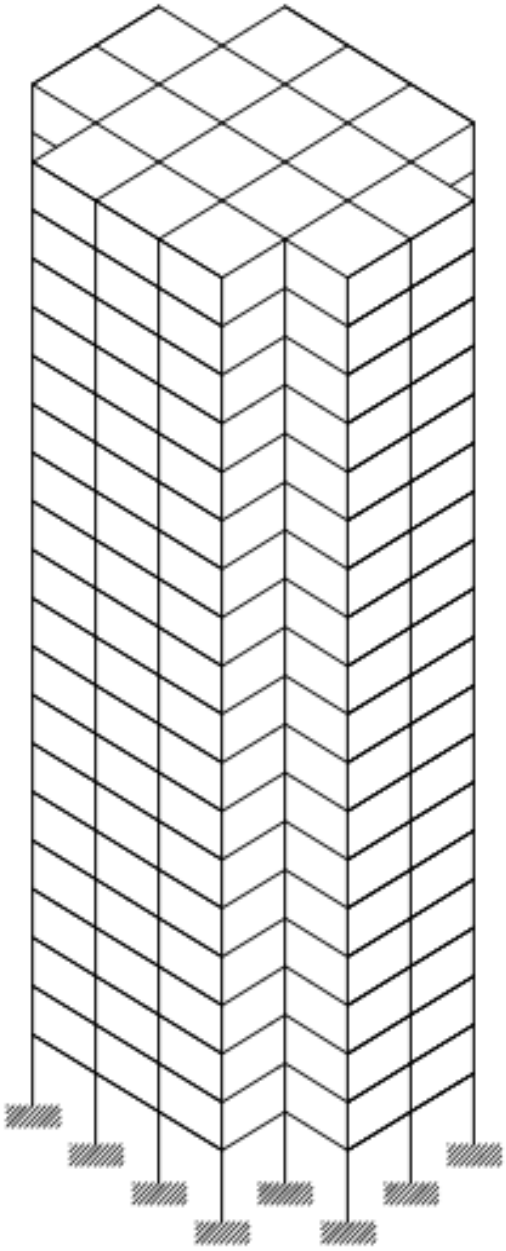

**Isometric View**

**Fig. 6.9 Elevation and isometric view of Plus Shape-1 building**

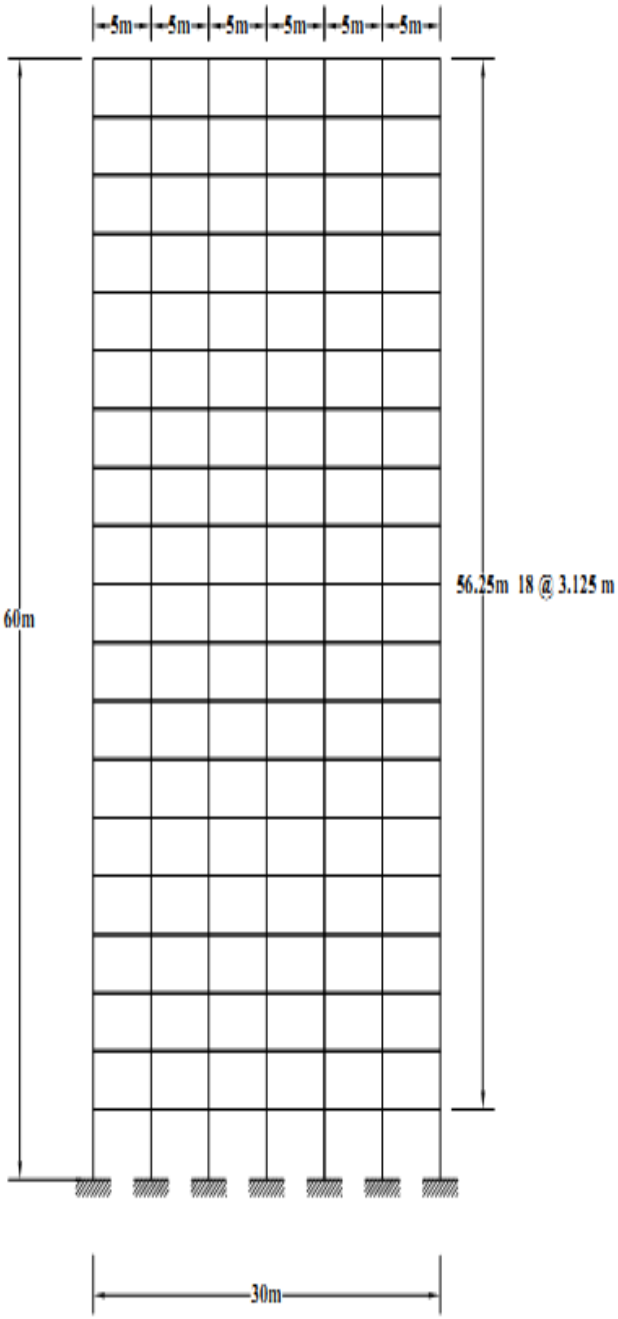


**Elevation**

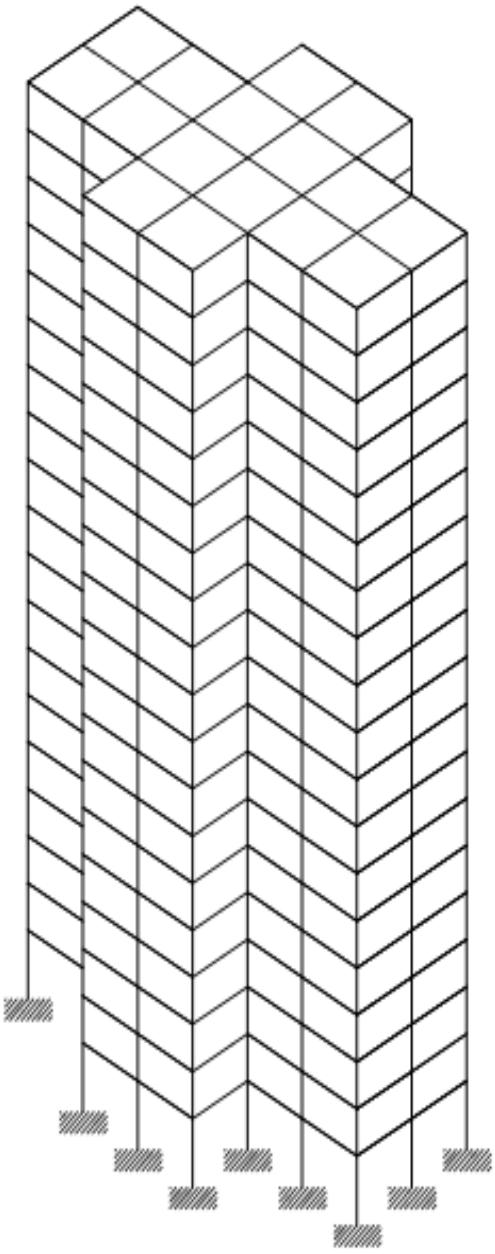

**Isometric View**

**Fig. 6.10 Elevation and isometric view of Plus Shape-2 building**

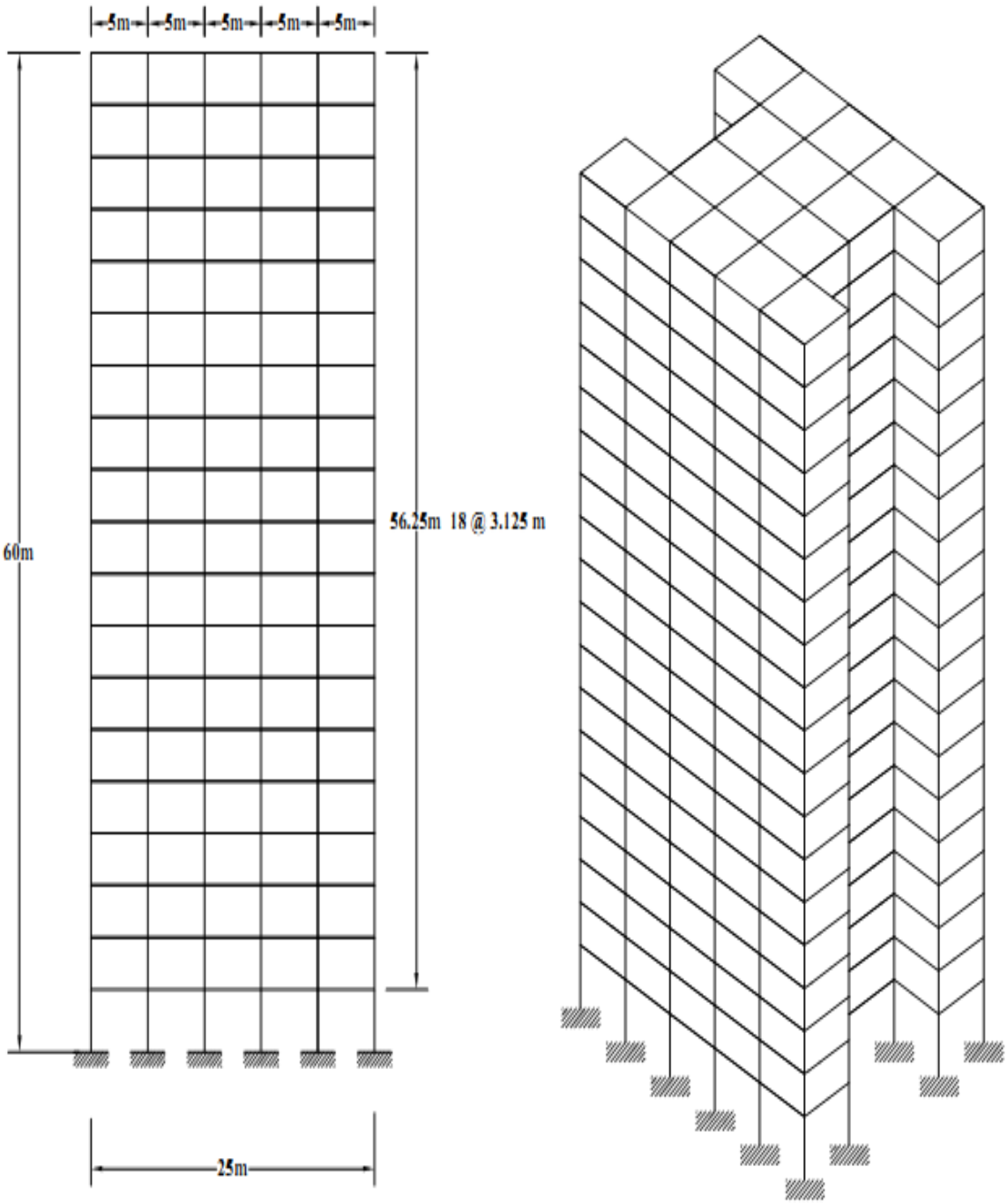


**Elevation** **Isometric View**

**Fig. 6.11 Elevation and isometric view of I-Shape-1 building**

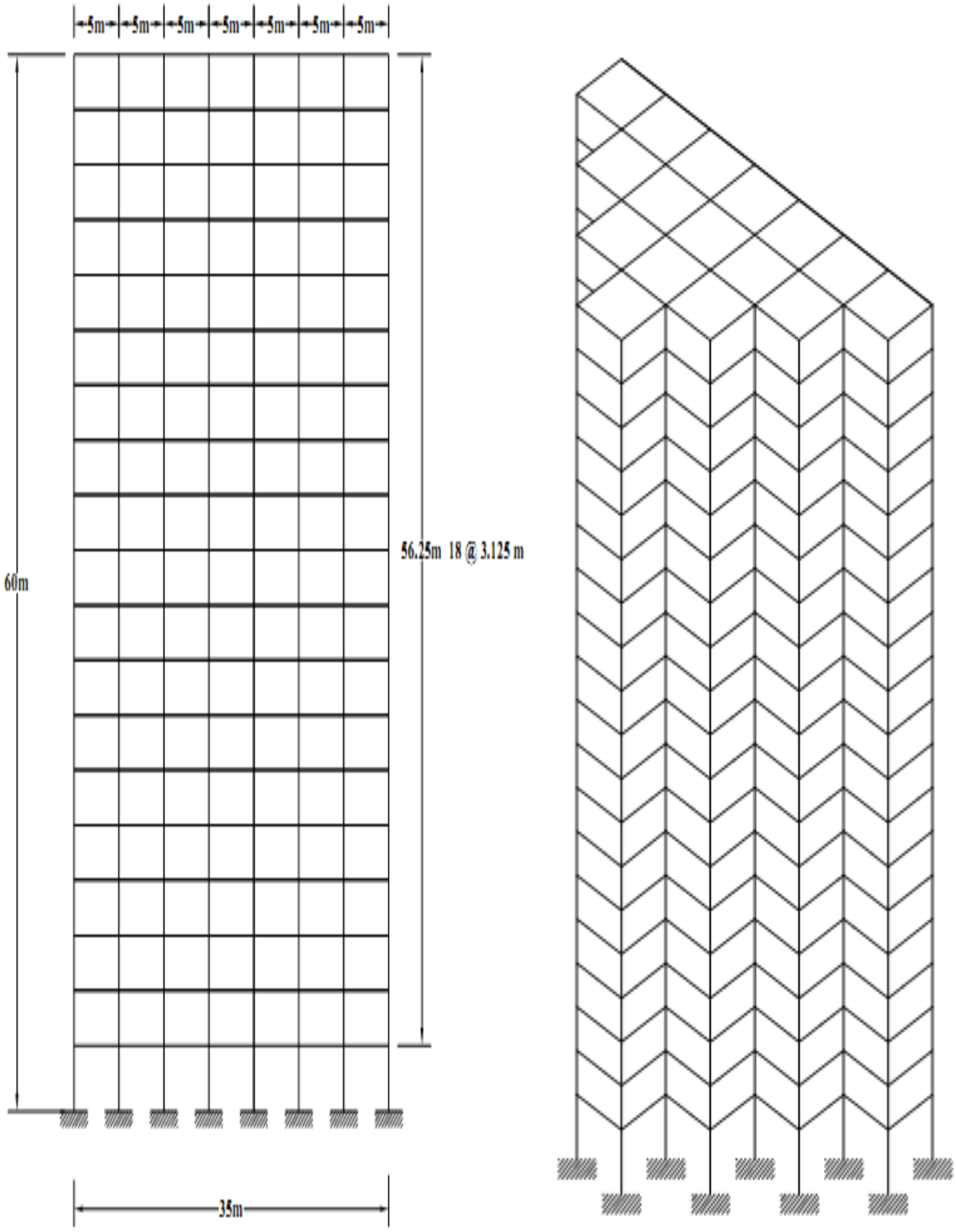


**Elevation** **Isometric View**

**Fig. 6.12 Elevation and isometric view of Fish Shape-1 building**

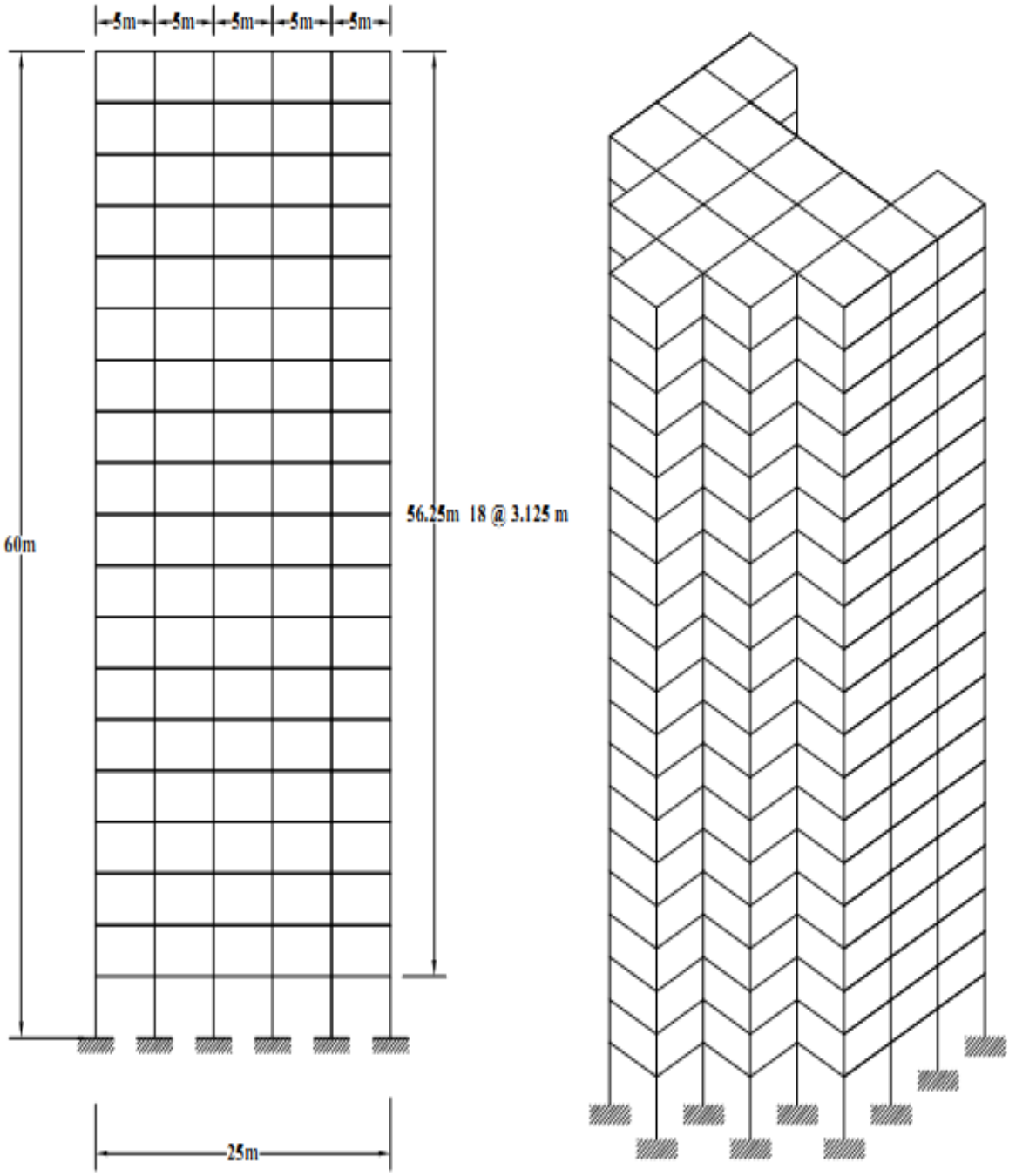


**Elevation** **Isometric View**

**Fig. 6.13 Elevation and isometric view of Fish Shape-2 building**

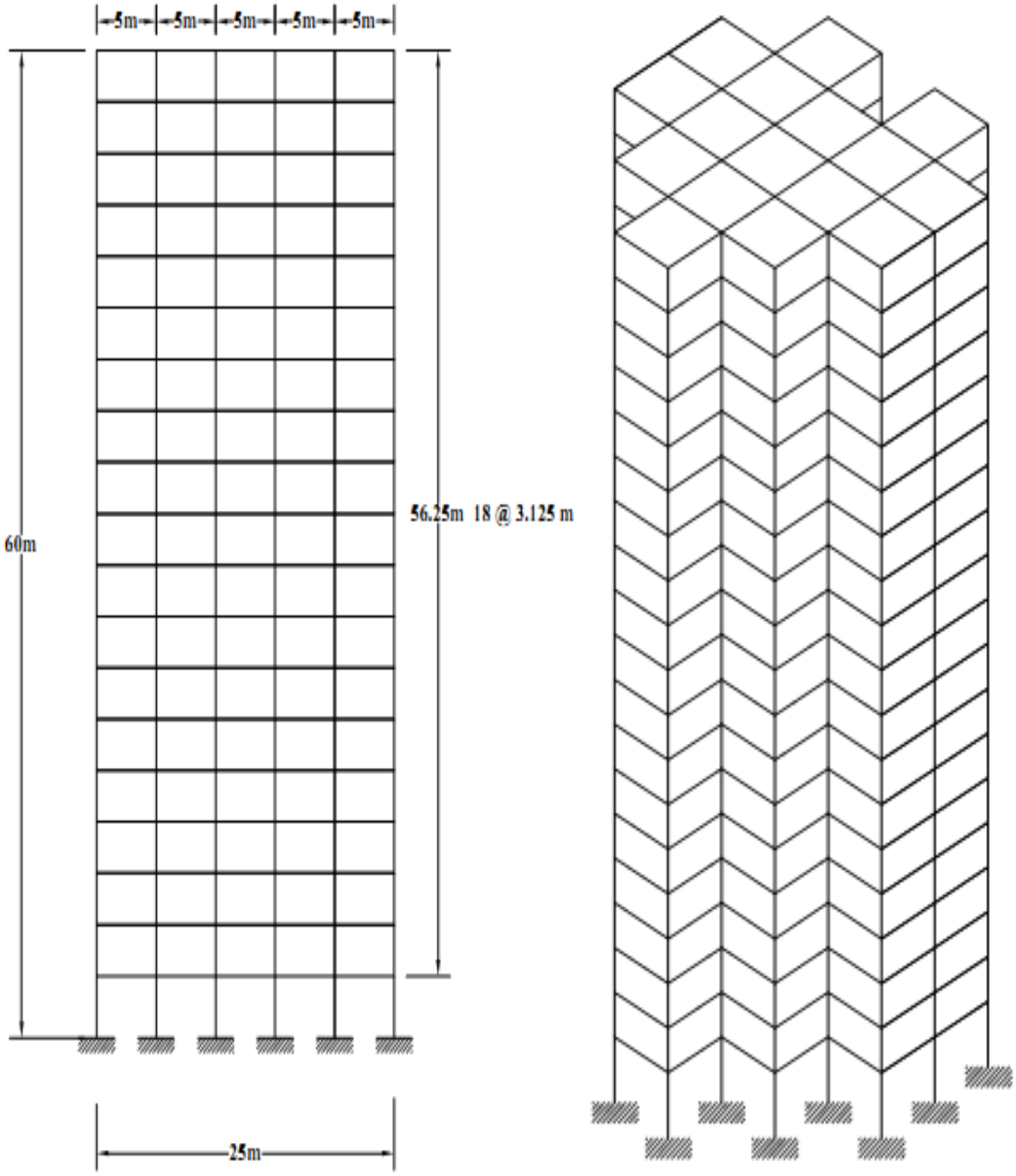


**Elevation** **Isometric View**

**Fig. 6.14 Elevation and isometric view of Fish Shape-3 building**

## 6.3 CALCULATION OF WIND LOADS ON PROTOTYPE BUILDINGS

Wind loads at each node of all seven prototype buildings are calculated from the experimentally obtained mean wind pressures at different pressure points on the building models. Method followed in evaluating wind load is described below.

**Step -1** Evaluation of pressure acting on model at various points as described in Chapter-3 using the expression

$$P_{r,mod} = 13.29\ X\ Baratron\ reading\ X\ Baratron\ range\ (\frac{N}{m^2}) \quad \text{..... (5.1)}$$

**Step -2** Evaluation of wind velocity at various levels on model during the wind tunnel test

**Step -3** Evaluation of wind velocity on prototype building at various storey levels using relation

$$\frac{\boldsymbol{u}}{\boldsymbol{u_0}} = \left(\frac{\boldsymbol{y}}{\boldsymbol{y_0}}\right)^{\boldsymbol{n}} \quad \text{..... (5.2)}$$

Where,

$y_0$ = atmospheric boundary layer depth

$u_0$ = free stream wind velocity corresponding to the boundary layer depth

y = any storey height

u = wind velocity on the structure at any height y

n = power law index

The building is considered to be located in terrain category – II and zone – V, open terrain with well scattered obstructions having heights generally between 1.5 to 10 m. The power law index obtained during the experiments is 0.22. As the building is in zone – V, the basic wind velocity at 10 m height above mean ground level is considered as 50 m/s for 50 year return period [IS : 875 (part - 3), 1987].

**Step – 4** Evaluation of pressure on prototype as

$$\frac{P_{ry,proto}}{P_{ry,mod}} = \left(\frac{V_{y,proto}}{V_{y,mod}}\right)^2$$

or,

$$P_{ry,proto} = P_{ry,mod}\ X \left(\frac{V_{y,proto}}{V_{y,mod}}\right)^2 \quad \text{..... (5.3)}$$

**Step – 5** Finally wind force at various nodal points is obtained as

$$F_{y,proto} = P_{ry,proto}\ X\ A_e \quad \text{..... (5.4)}$$

$F_{y,proto}$ = static load on the building structure at any height y corresponding to strip area $A_e$,

$P_{ry,proto}$ = pressure on the building at any height y,

$P_{ry,mod}$ = pressure on the corresponding model at any height y,

$V_{y,proto}$ = velocity on the corresponding building at any height y,

$V_{y,mod}$ = velocity on the corresponding model at any height y,

$A_e$ = effective frontal area (strip) area considered for the building at height y,

## 6.4 RESPONSE UNDER ISOLATED CONDITION

### 6.4.1 Square Shape Building

#### 6.4.1.1 Forces in columns

Response of square plan shape building (Fig. 6.8) subjected to wind loads under isolated condition is evaluated for 4 wind directions namely $0^0$, $30^0$, $60^0$ and $90^0$. In order to study the influence of wind incidence angles on the structural response, attention is given on certain internal stress resultants which includes axial force, twisting moment, Mx (global) and My (global) on three columns which are denoted as column-A, B and C (Figs. 6.15 to 6.26). In addition to these parameters, lateral deflections of these 3 columns in X-direction are also observed (Figs. 6.27 to 6.29). Effect of wind incidence angles on all these parameters are studied and reported in this article.

It is seen from Fig. 6.15 that axial force on central column i.e. column-A of square plan shape building increases linearly from top to bottom but does not vary with the change in wind incidence angle. Maximum axial force (6,800 kN) is observed at the ground level. In case of column-B (Fig. 6.16), axial force is not affected by wind incidence angle above 45 m height i.e. in top 25% of the height of the column. In the lower part, effect of wind incidence angle on axial force in column-B increases with decrease in height of the column. The axial force is minimum (5,200 kN) at $90^0$ wind incidence angle and it is maximum (5,800 kN) at $30^0$ wind incidence angle. For column-C (Fig. 6.17), variation of the axial force is similar to that of column-B, but maximum (4,600 kN) and minimum (4,400 kN) axial force are observed at $30^0$ and $90^0$ wind incidence angles repectively. Large variation due to wind incidence angle is seen in lower 75% height of the column above which the values match with each other.

Figure 6.18 shows the effect of the wind attack on twisting moment developed in central column i.e. column-A of square plan shape building. Due to symmetry of the structure almost zero torsional moment is observed along the height of the column at $0^0$ and $90^0$ wind incidence angles. Further, it is seen from the figure that torsional forces are large at other wind incidence angles. At $30^0$ and $60^0$ wind incidence angles, maximum twisting moment is noticed at around 17% height of the column from the base, and then torsional values suddenly drop to the bottom end. Almost zero torsion is observed near the top of the column in all the

cases. Figures 6.19 and 6.20 show the effect of the wind incidence angle on twisting moment on column-B and C respectively. Moment variation pattern in these cases are similar to column-A.

Figures 6.21 to 6.23 present comparison of the moment about 'X' axis (Mx) at different wind incidence angles on column-A, B and C respectively. It is seen from Fig. 6.21 that maximum Mx is observed at $30^0$ wind incidence angle and minimum moment i.e. zero at $90^0$ wind incidence angle in column-A. Variation of Mx with wind incidence angle in case of column-B and column-C are comparable (Figs. 6.22 and 6.23) with maximum value at $30^0$ wind incidence angle and minimum at $90^0$ angle. There is no influence of wind incidence angles on Mx near the top of these columns.

Figures 6.24 to 6.26 show the comparison of My, i.e. moment about 'Y' axis at varying wind incidence angles on column-A, B and C respectively. At $0^0$ wind incidence angle, zero moment is observed along the height of the column in case of column-A and B. Maximum My is observed in column-A and B at $90^0$ wind angle. In column-C, pattern of variation of moment My is different, but it is also maximum at $90^0$ wind angle and minimum at $0^0$ angle as in the case of column-A and B.

#### 6.4.1.2 Displacement of columns

Horizontal displacement of column-A, B and C at every floor level under different wind incidence angles are obtained during the analysis. The results are shown in Figs. 6.27 to 6.29. Maximum deflection in column-A and B is around 0.07% of height of the building and around 0.06% in column-C.

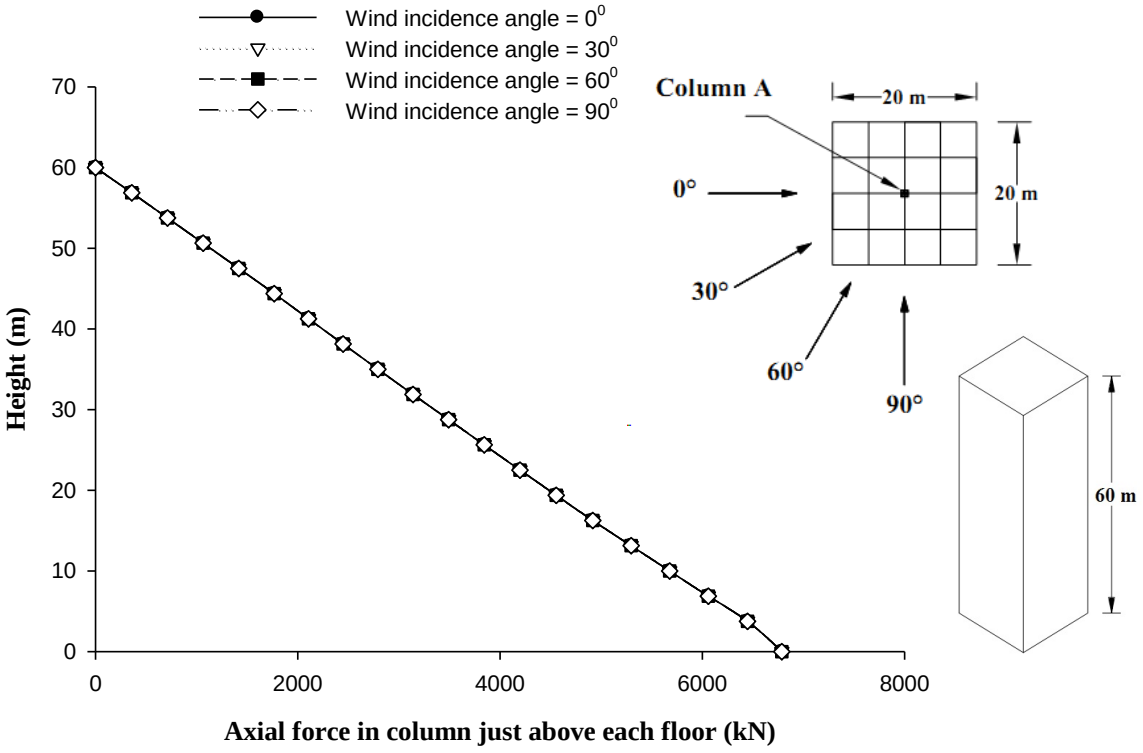


**Fig. 6.15 Effect of wind incidence angle on axial force in column-A of Square Shape building**

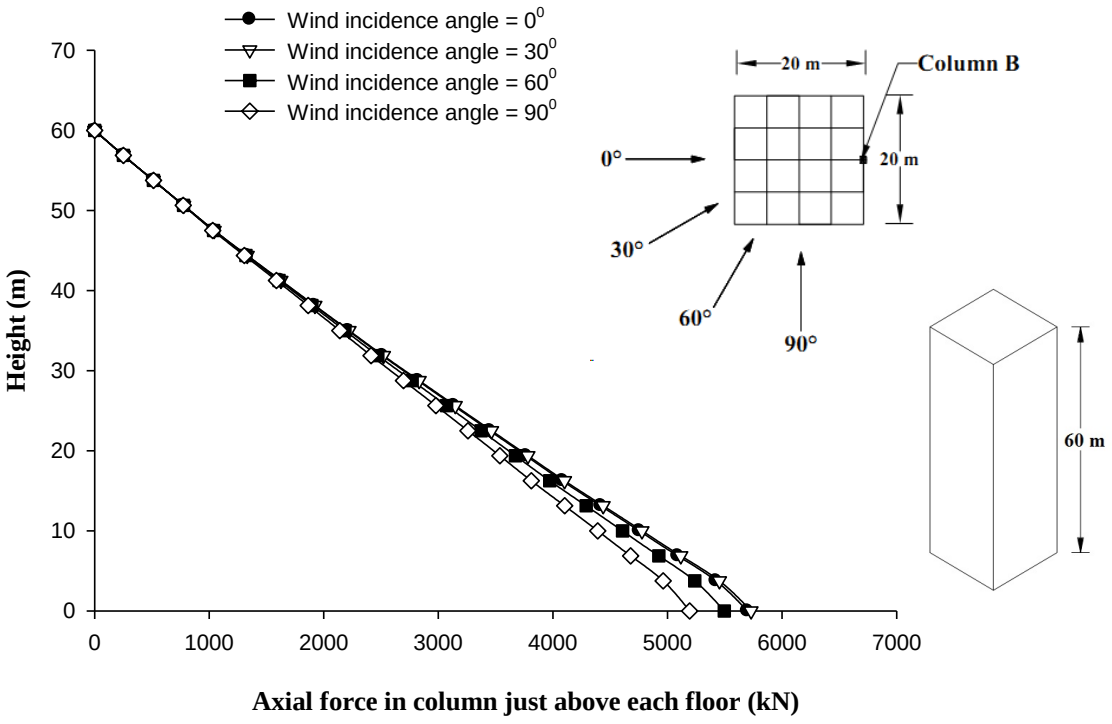


**Fig. 6.16 Effect of wind incidence angle on axial force in column-B of Square Shape building**

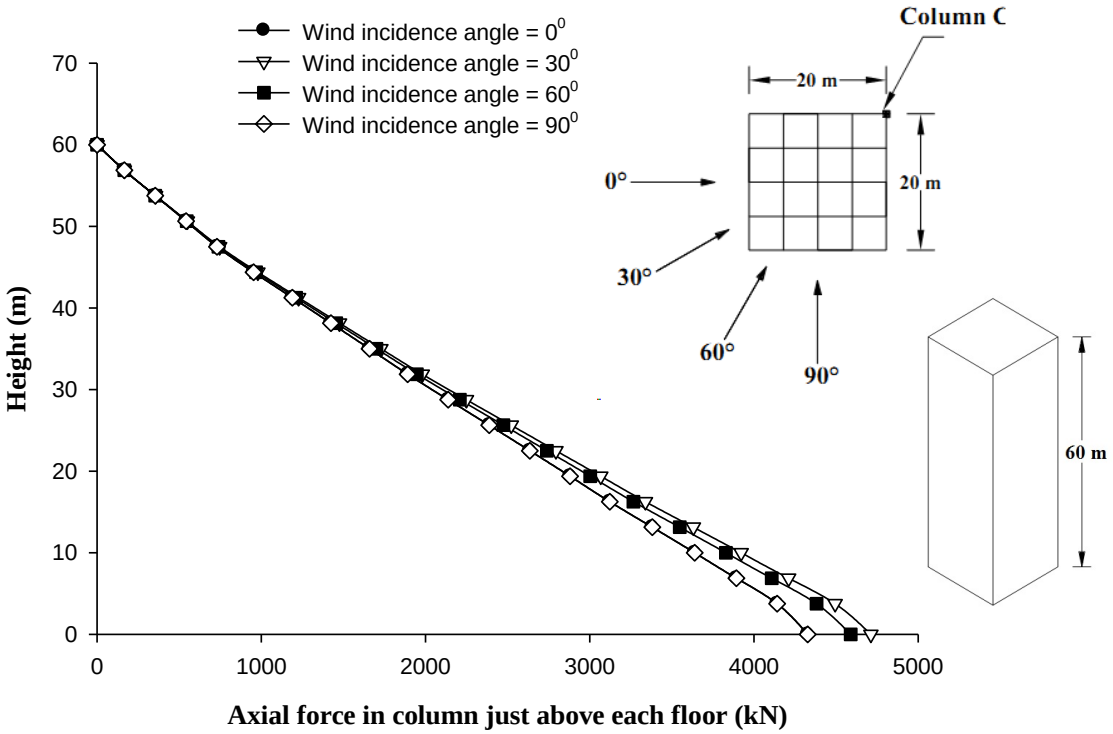


**Fig. 6.17 Effect of wind incidence angle on axial force in column-C of Square Shape building**

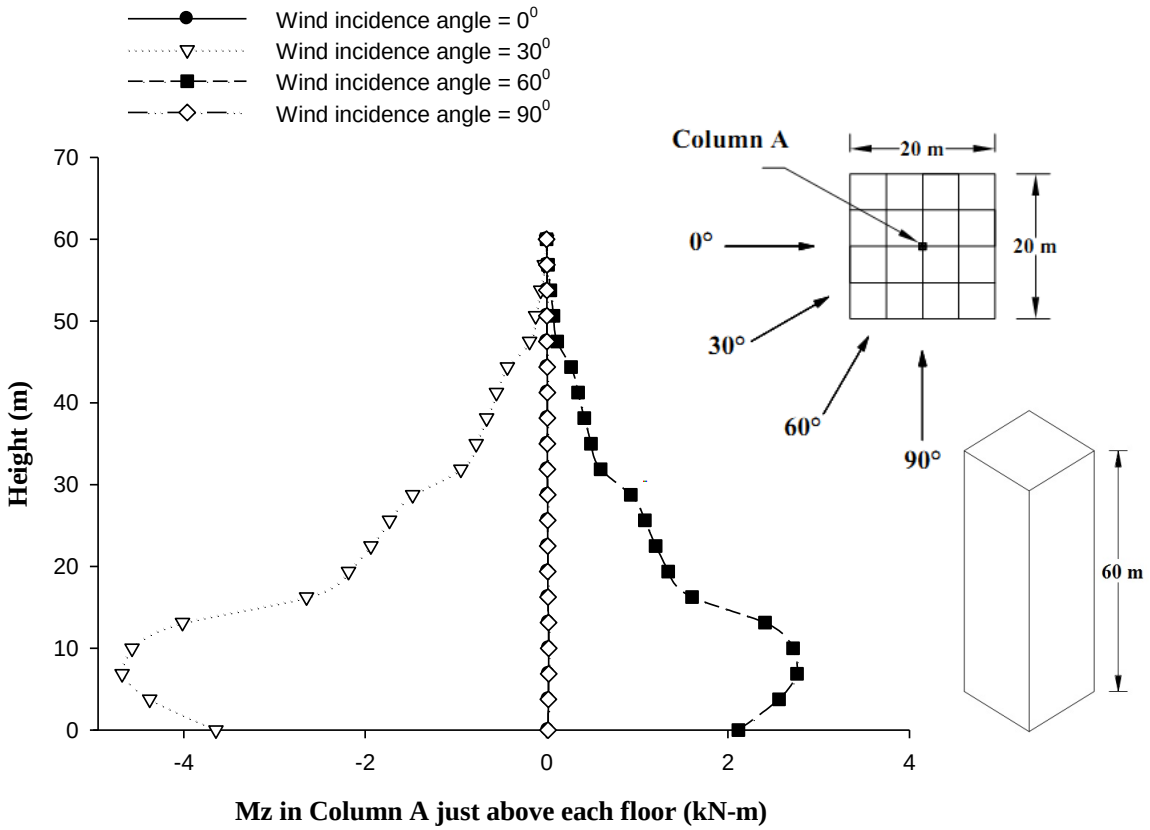


**Fig. 6.18 Effect of wind incidence angle on twisting moment Mz in column-A of Square Shape building**

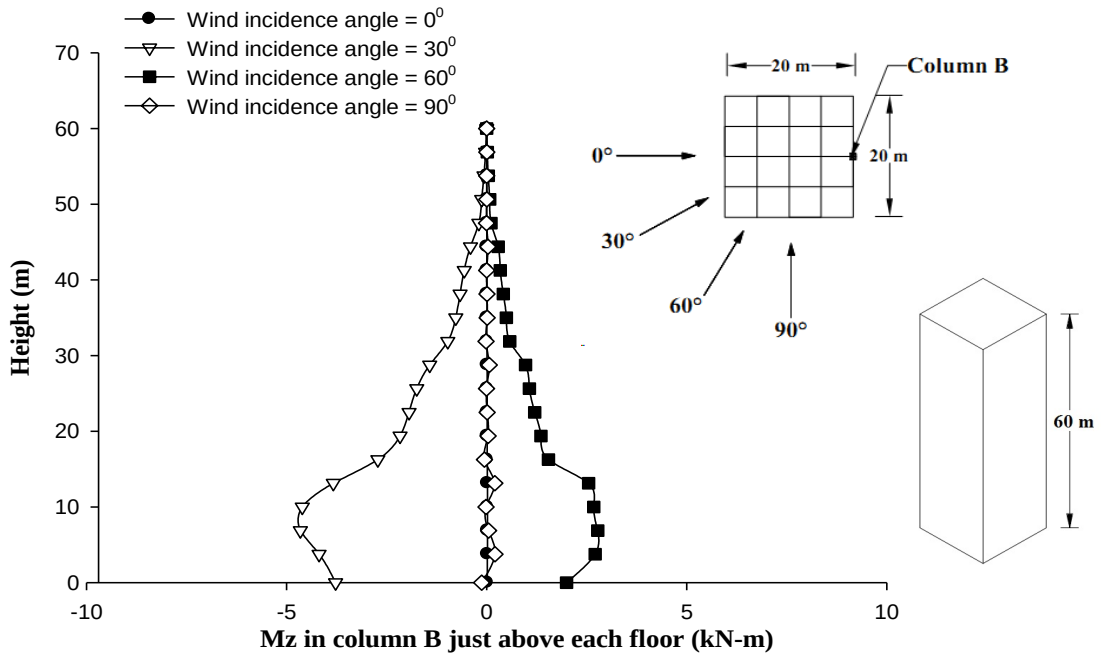


**Fig. 6.19 Effect of wind incidence angle on twisting moment Mz in column-B of Square Shape building**

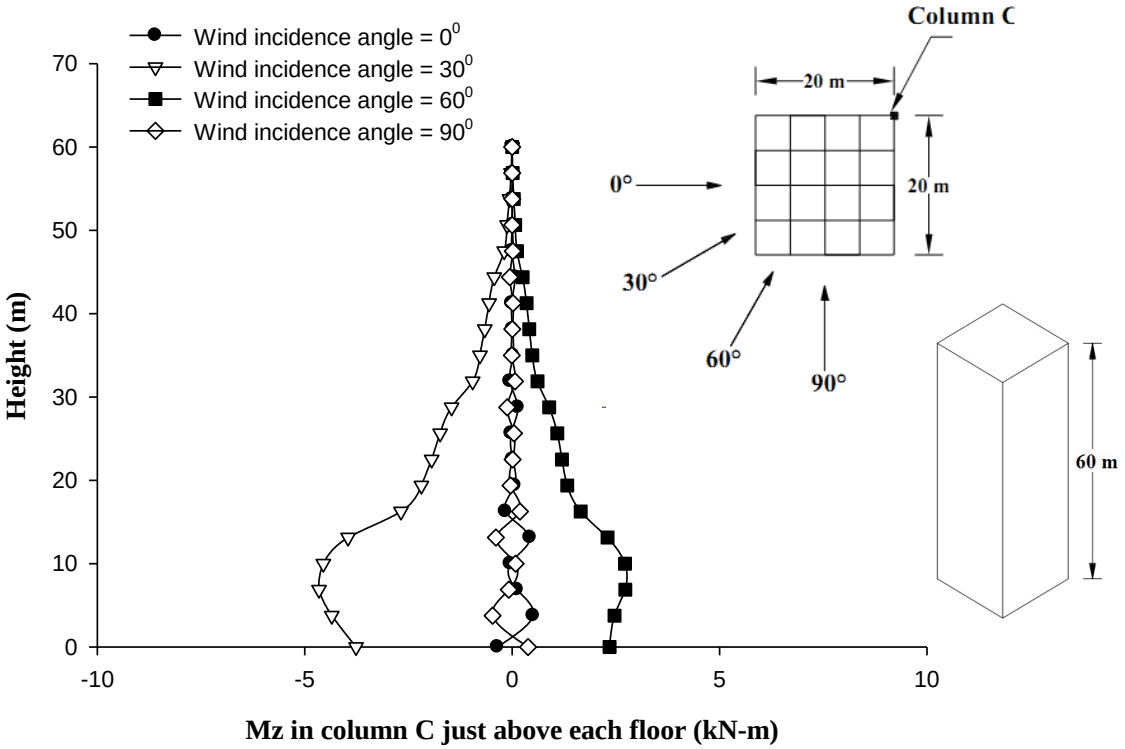


**Fig. 6.20 Effect of wind incidence angle on twisting moment Mz in column-C of Square Shape building**

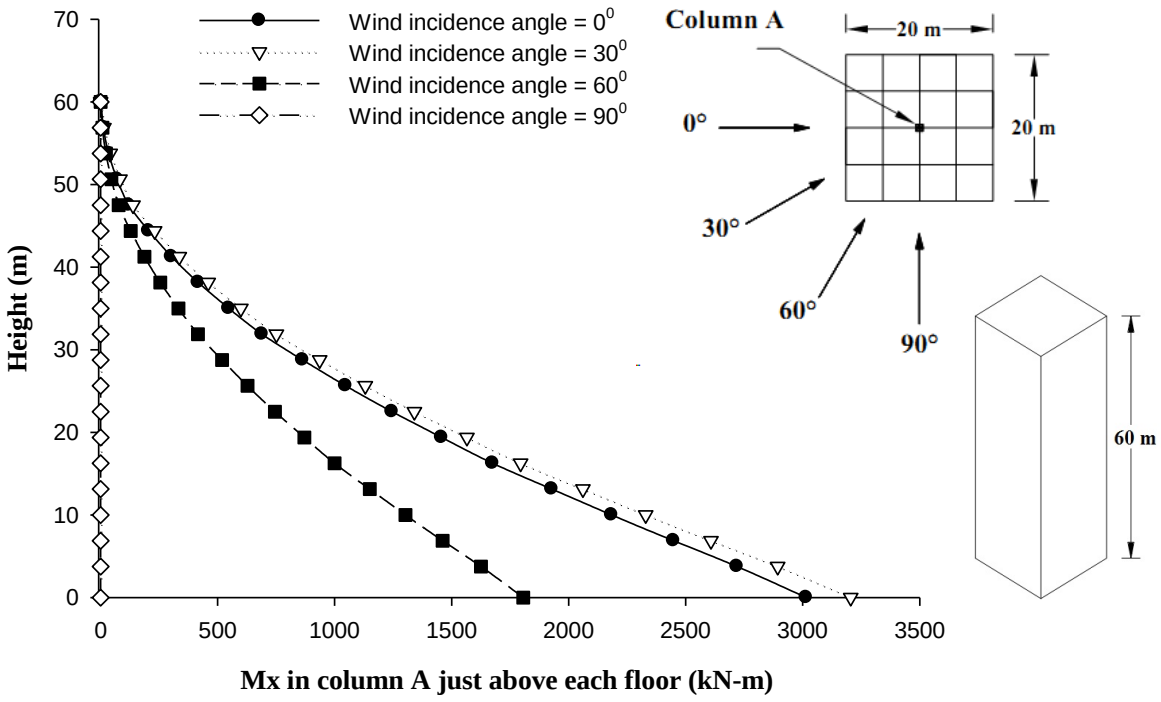


**Fig. 6.21 Effect of wind incidence angle on Mx (global) in column-A of Square Shape building**

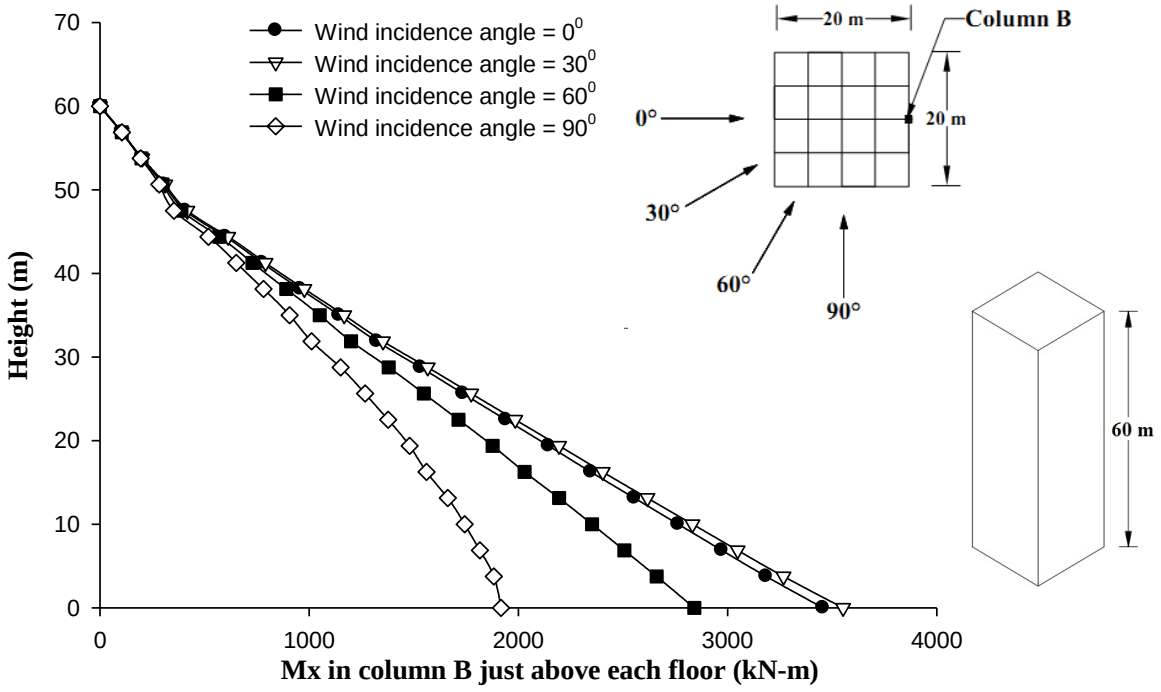


**Fig. 6.22 Effect of wind incidence angle on Mx (global) in column-B of Square Shape building**

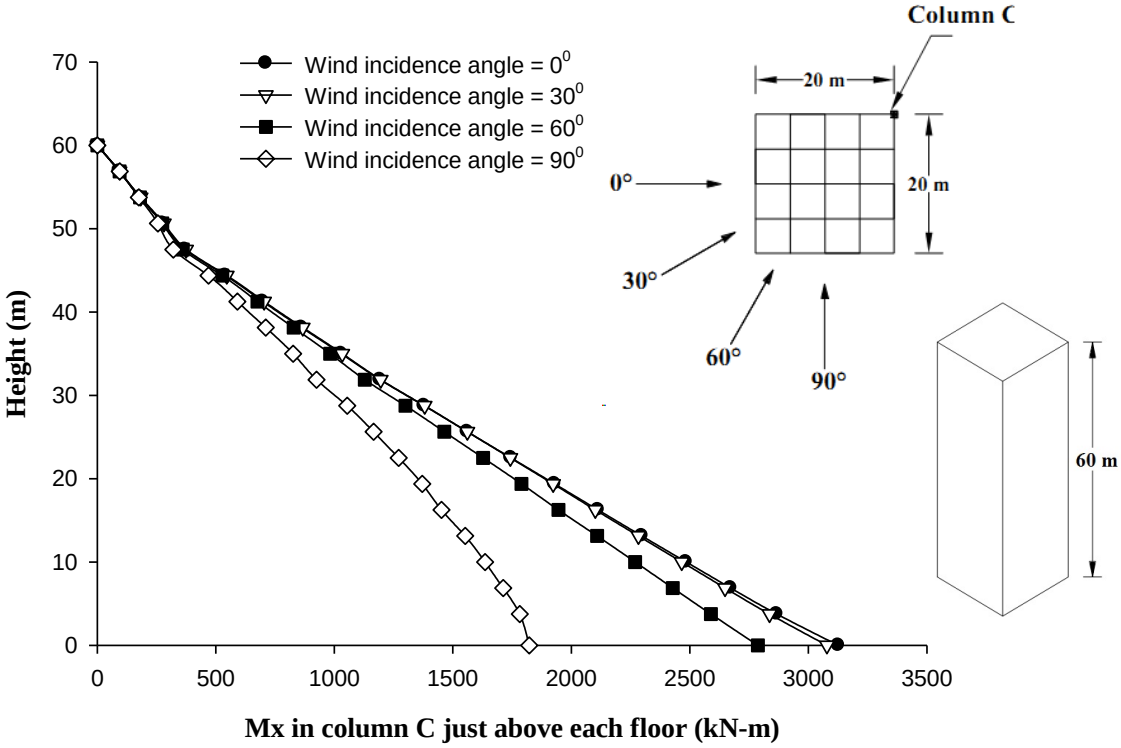


**Fig. 6.23 Effect of wind incidence angle on Mx (global) in column-C of Square Shape building**

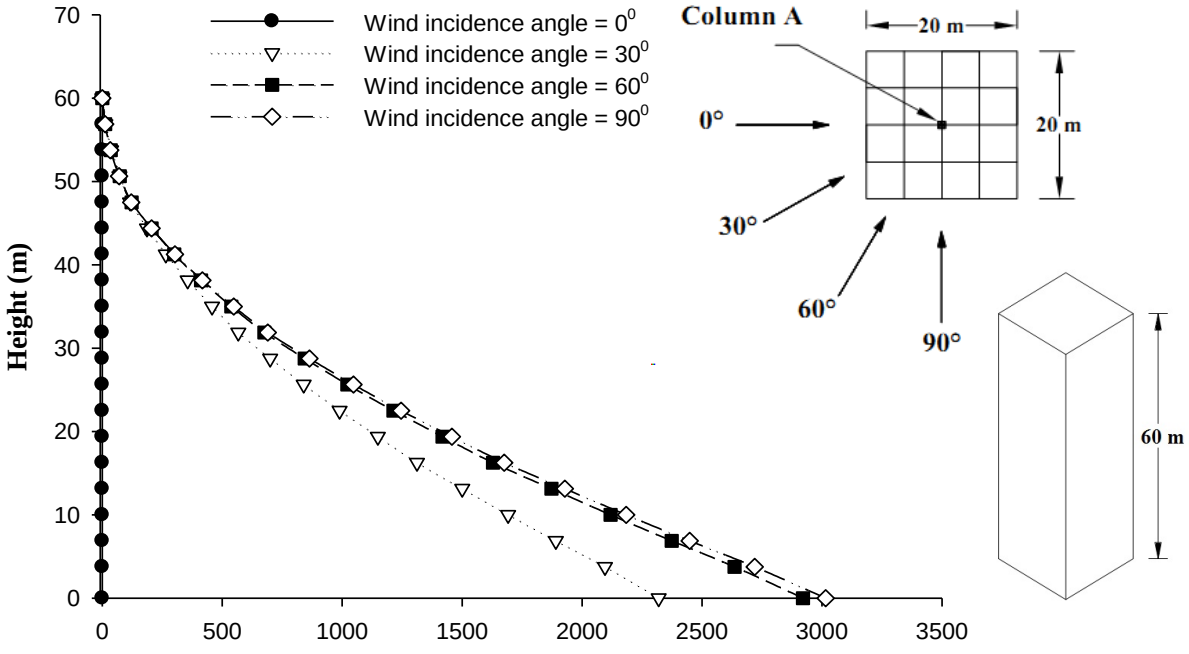


**Fig. 6.24 Effect of wind incidence angle on My (global) in column-A of Square Shape building**

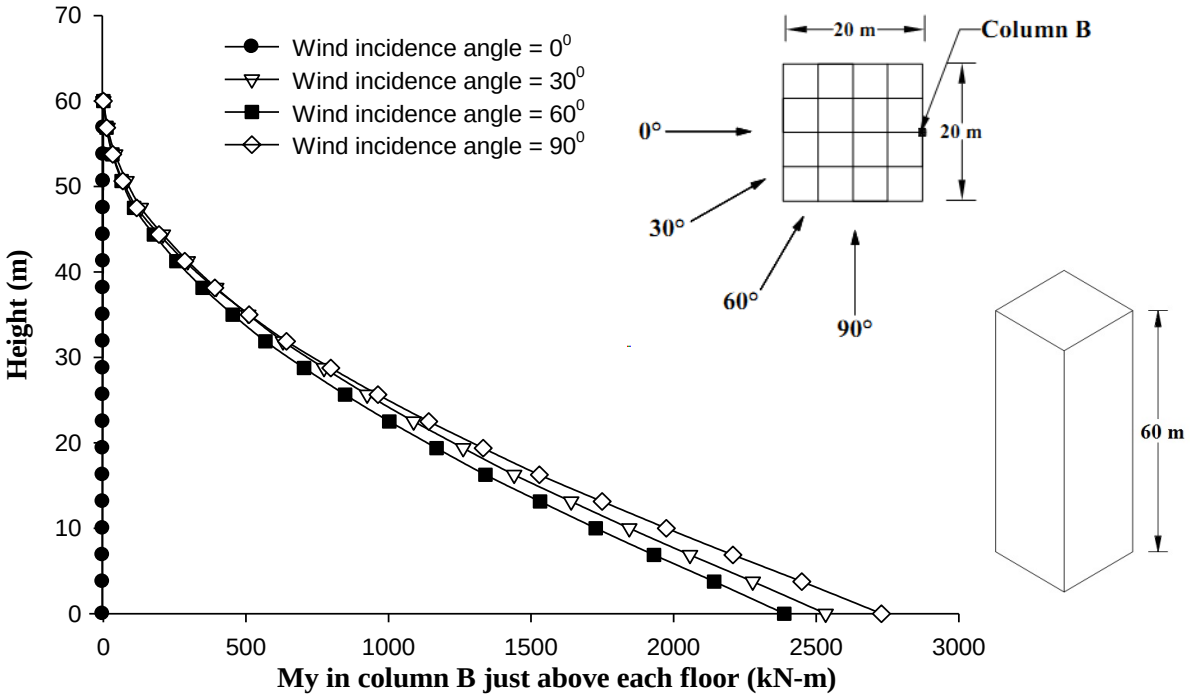


**Fig. 6.25 Effect of wind incidence angle on My (global) in column-B of Square Shape building**

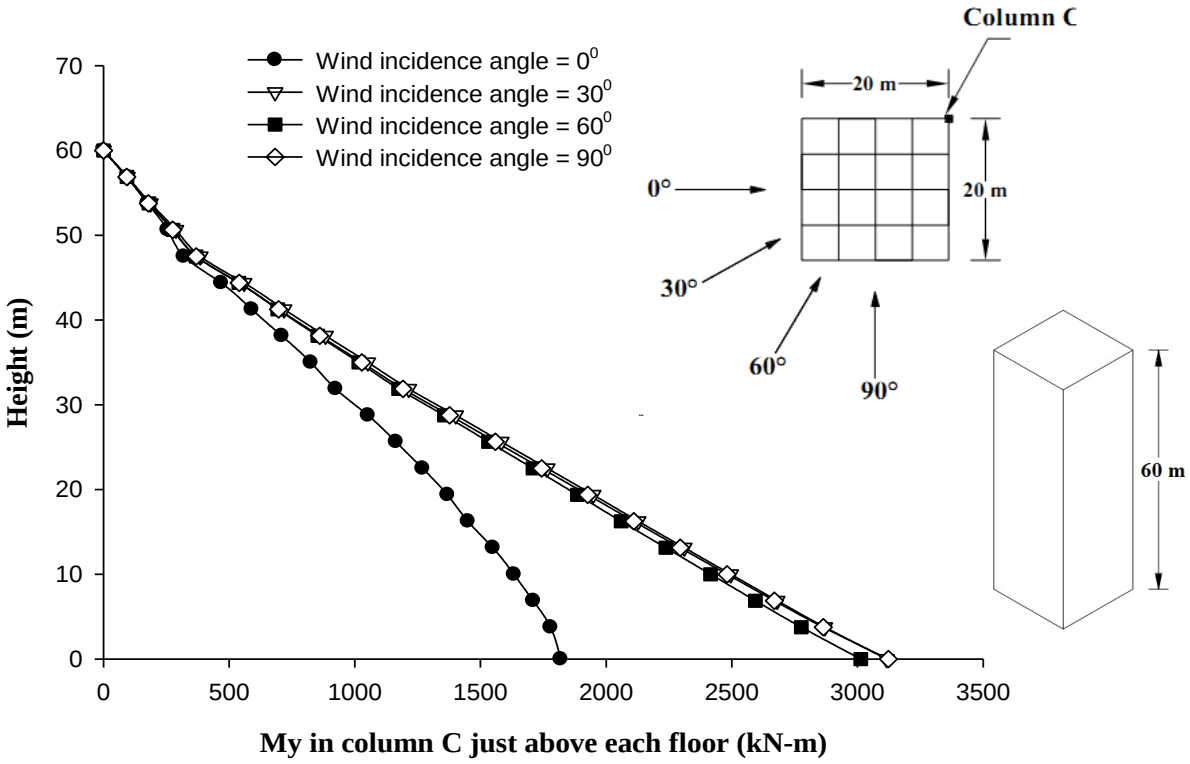


**Fig. 6.26 Effect of wind incidence angle on My (global) in column-C of Square Shape building**

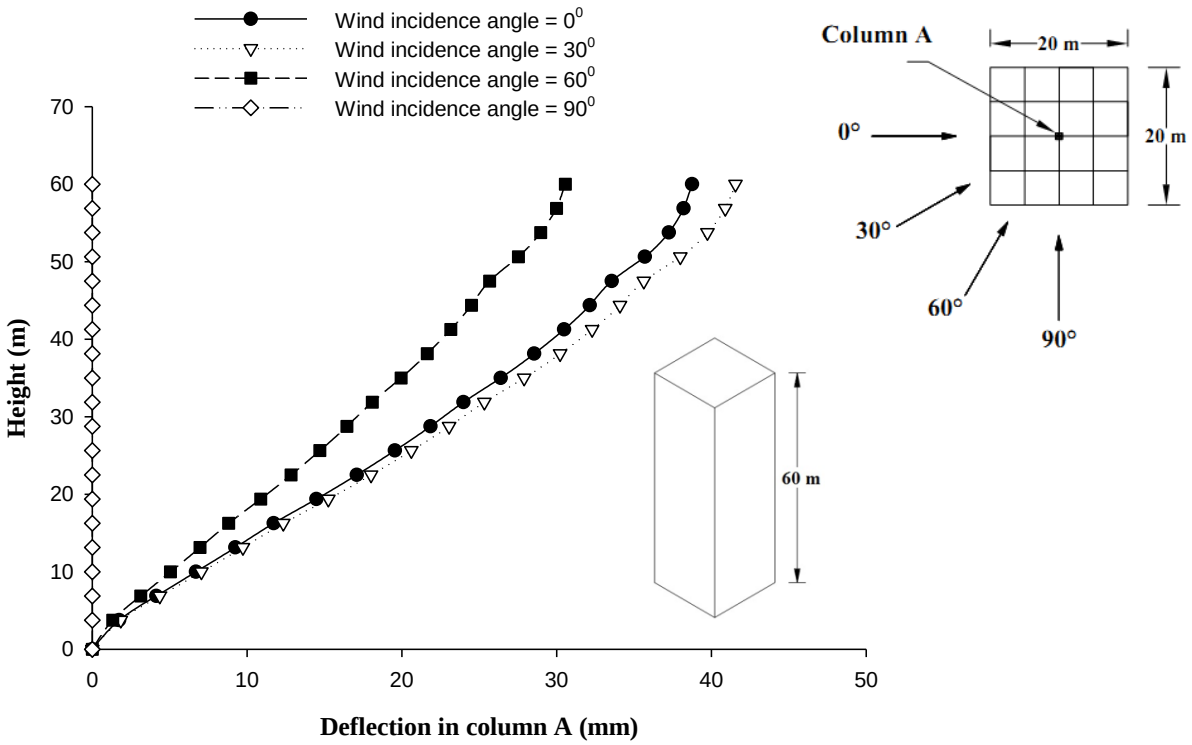


**Fig. 6.27 Effect of wind incidence angle on horizontal displacement of column-A of Square Shape building**

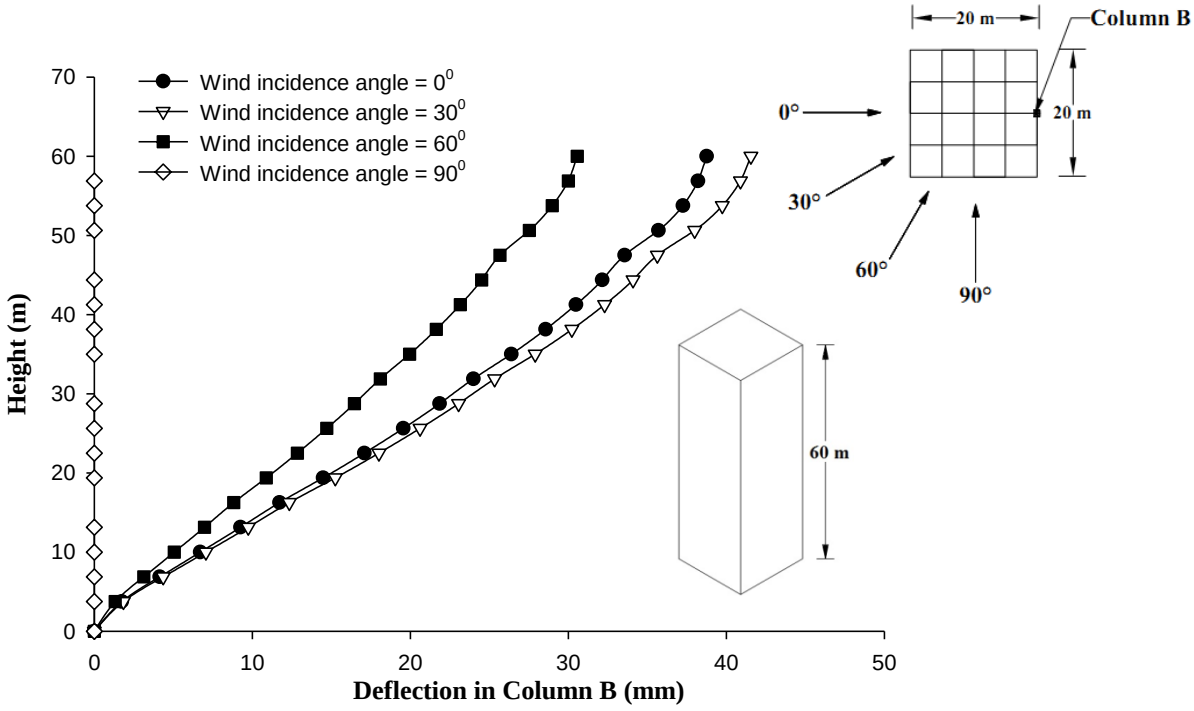


**Fig. 6.28 Effect of wind incidence angle on horizontal displacement of column-B of Square Shape building**

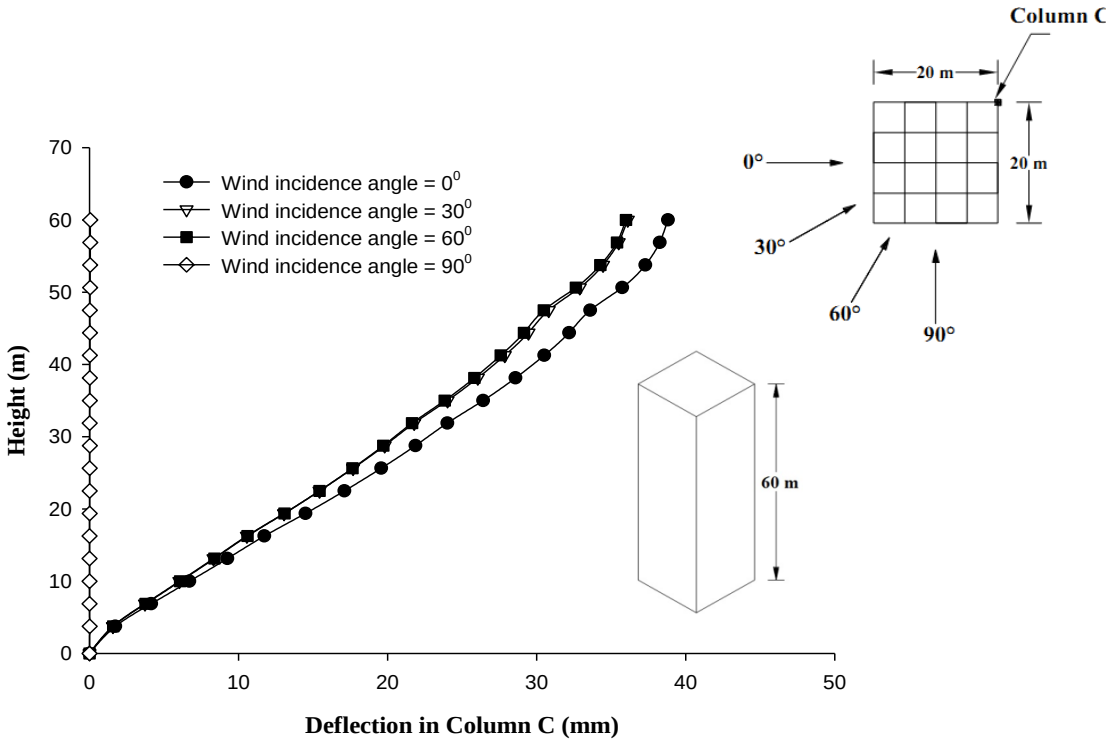


**Fig. 6.29 Effect of wind incidence angle on horizontal displacement of column-C of Square Shape building**

### 6.4.2 Plus Shape-1 Building

#### 6.4.2.1 Forces in columns

Response of Plus Shape-1 building is evaluated under different wind incidence angles namely $0^0$, $30^0$, $60^0$ and $90^0$. It is seen from Fig. 6.30 that axial force in column-A does not vary with wind incidence angle. It linearly increases from top to bottom. Axial force in lower parts of column-B and column-C are affected by wind directions, although of small magnitude (Figs. 6.31 and 6.32).

Figures 6.33 to 6.35 show the variation of twisting moment Mz with height of the building. It is observed from Fig. 6.33 that little amount ot torsional force is observed in column-A at $30^0$ wind attack, and for rest of wind incidence angles it is almost zero. Maximum twisting moment in column-B (Fig. 6.34) is observed at $60^0$ wind incidence angle with smaller values at other angles. Similar torsional forces are observed in case of column-C (Fig. 6.35).

Figures 6.36 to 6.38 show the moment about 'X' axis for column-A, B and C respectively. It can be seen from the figures that maximum moment Mx is observed at $0^0$ wind incidence angle and zero moment at $90^0$ wind incidence angle in all columns.

Effect of wind incidence angle on My in column-A, B and C are shown in Figs. 6.39, 6.40 and 6.41 respectively. Maximum moment and minimum moment are observed at $90^0$ and $0^0$ wind incidence angles respectively in all 3 columns. Numerically, value to My is maximum in column-B amongst these 3 columns and minimum in column-A.

#### 6.4.2.2 Displacement of columns

Horizontal displacement of column-A, B and C at every floor level under different wind incidence angles are obtained during the analysis. The results are shown in Figs. 6.42 to 6.44. As expected, maximum displacemtn in X-direction is observed at $0^0$ wind incidence angle and zero displacement at $90^0$ in all columns. Maximum deflection is around 0.07% of height of the building.

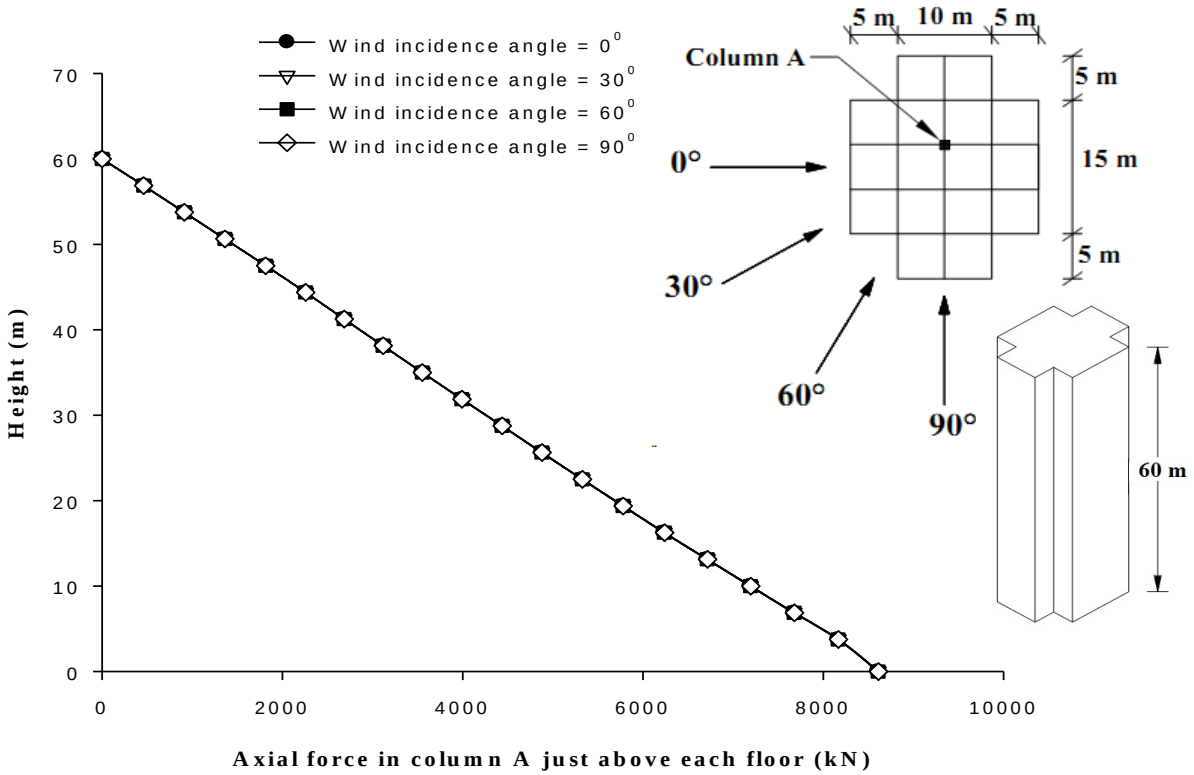


**Fig. 6.30 Effect of wind incidence angle on axial force in column-A of Plus Shape-1 building**

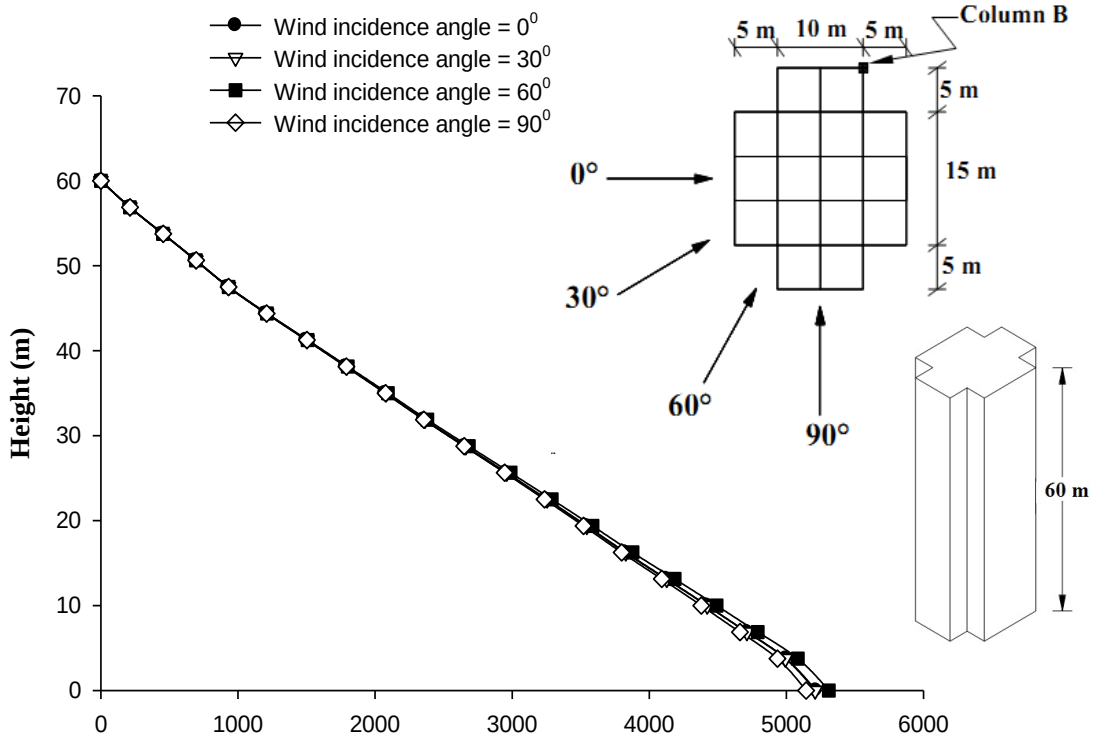


**Fig. 6.31 Effect of wind incidence angle on axial force in column-B of Plus Shape-1 building**

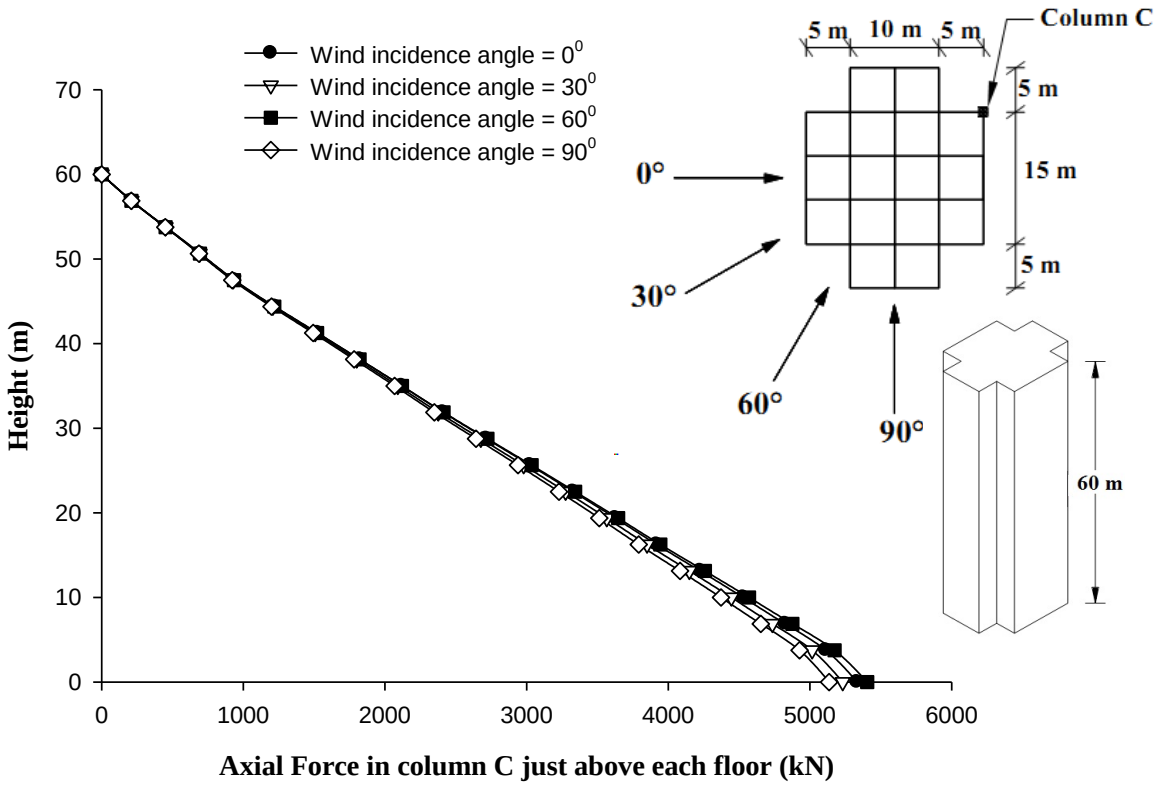


**Fig. 6.32 Effect of wind incidence angle on axial force in column-C of Plus Shape-1 building**

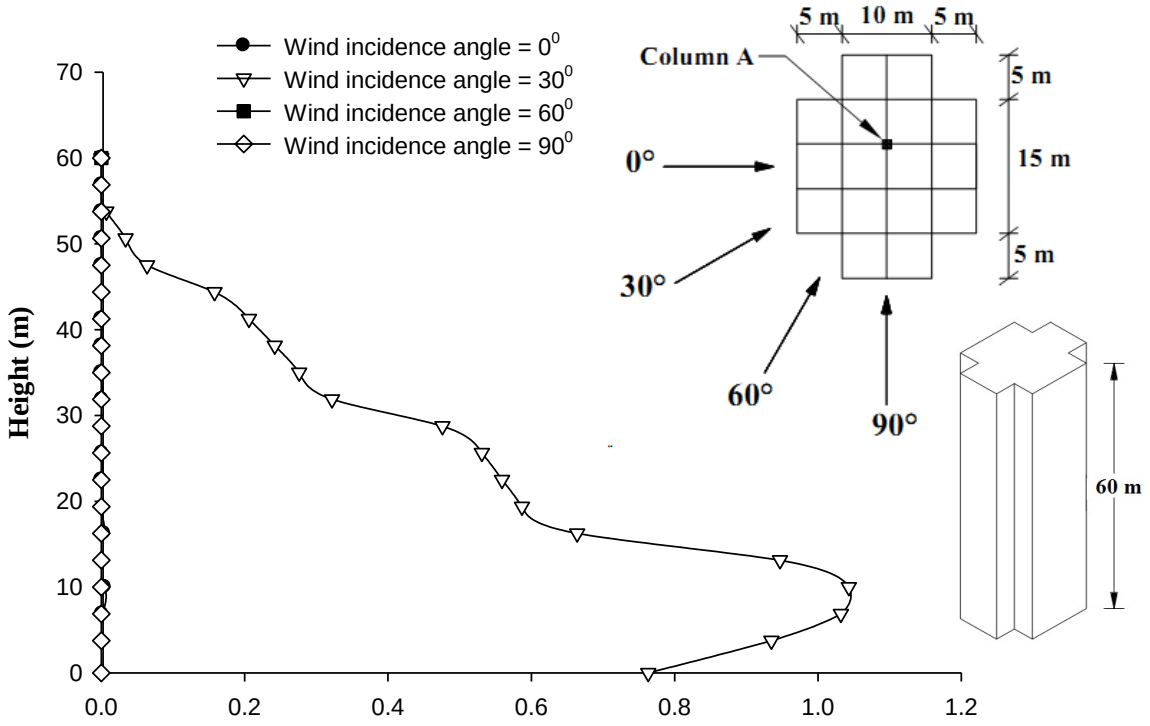


**Fig. 6.33 Effect of wind incidence angle on twisting moment Mz in column-A of Plus Shape-1 building**

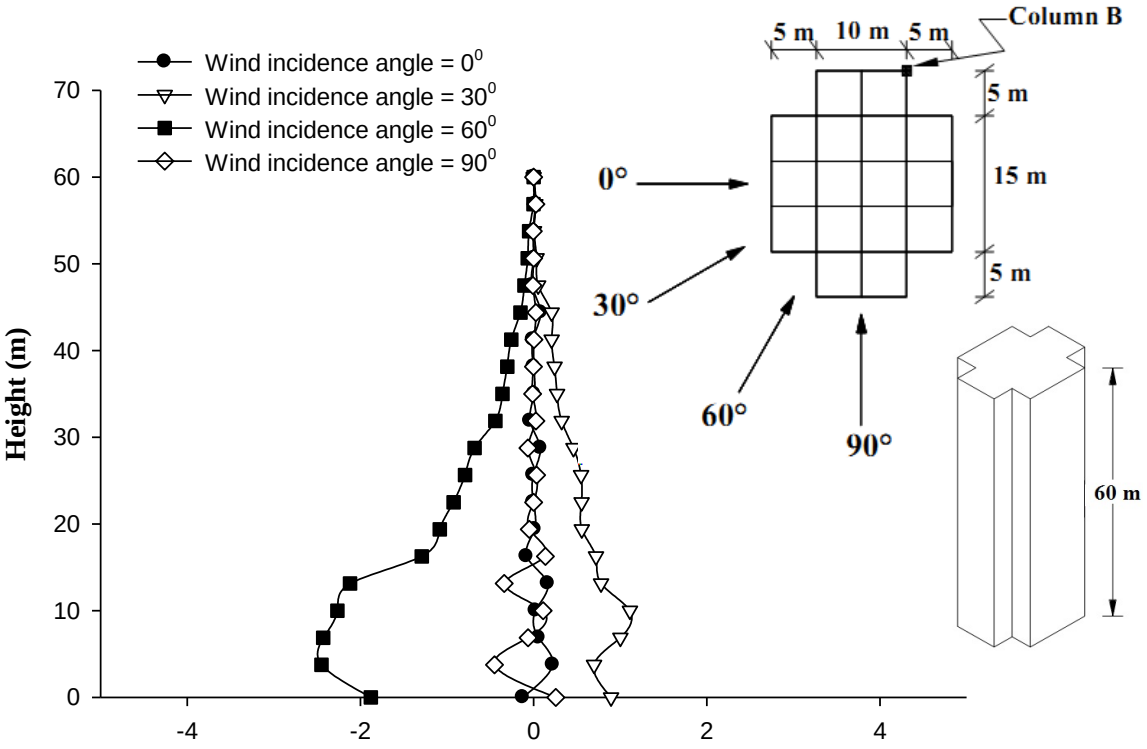


**Fig. 6.34 Effect of wind incidence angle on twisting moment Mz in column-B of Plus Shape-1 building**

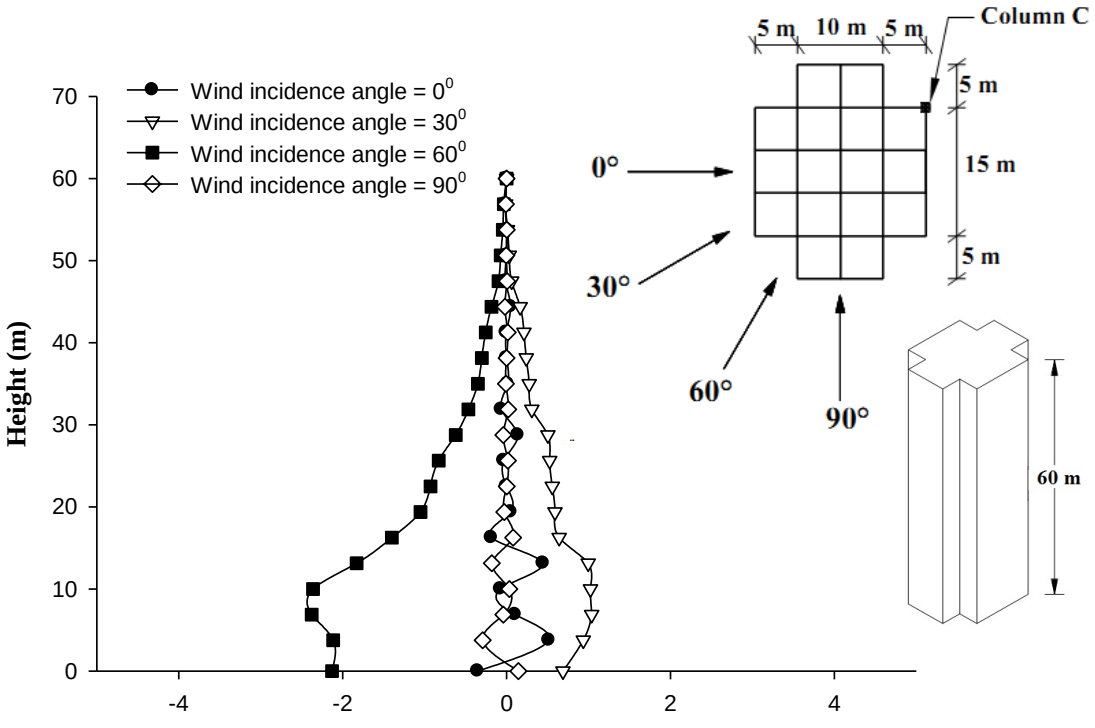


**Fig. 6.35 Effect of wind incidence angle on twisting moment Mz in column-C of Plus Shape-1 building**

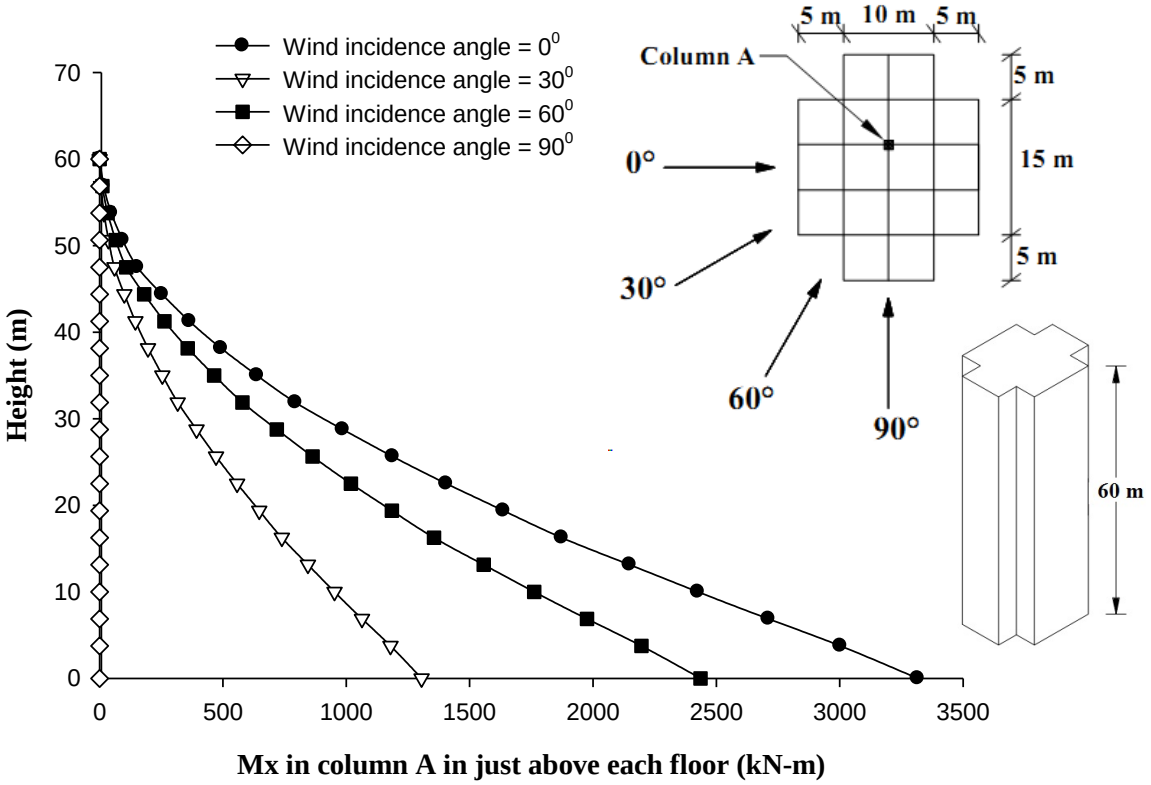


**Fig. 6.36 Effect of wind incidence angle on Mx (global) in column-A of Plus Shape-1 building**

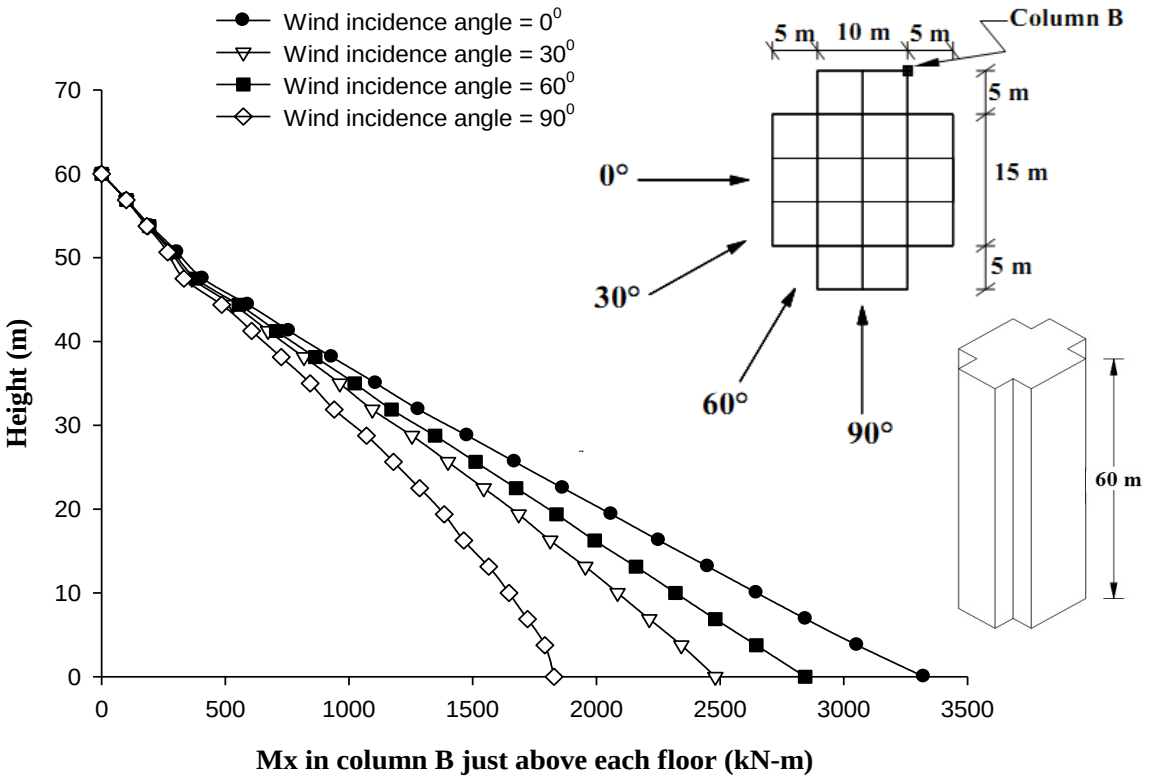


**Fig. 6.37 Effect of wind incidence angle on Mx (global) in column-B of Plus Shape-1 building**

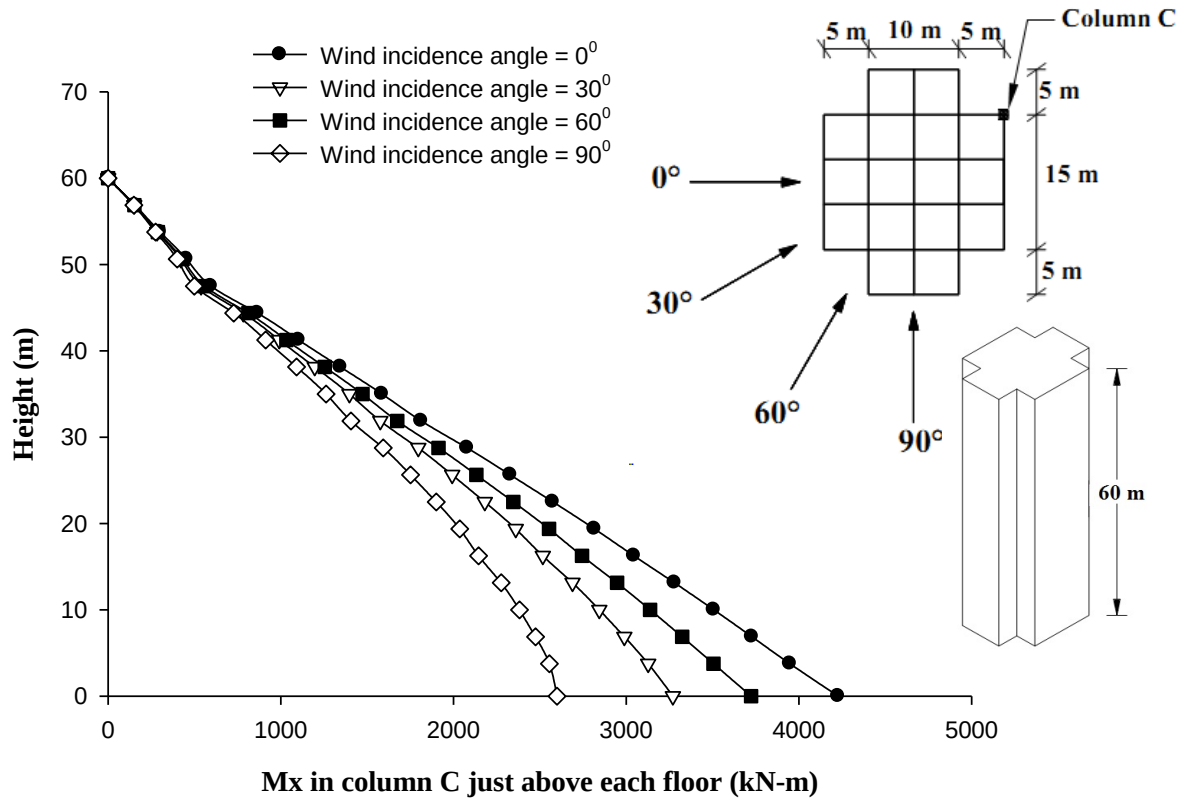


**Fig. 6.38 Effect of wind incidence angle on Mx (global) in column-C of Plus Shape-1 building**

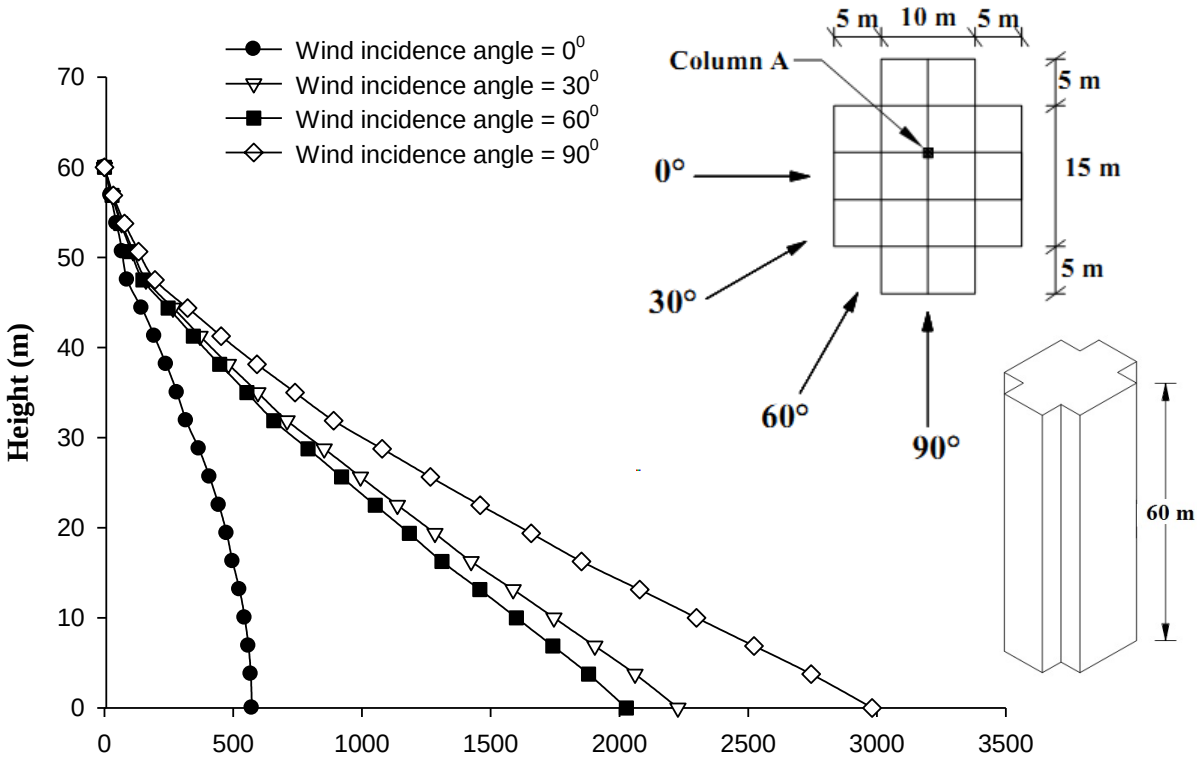


**Fig. 6.39 Effect of wind incidence angle on My (global) in column-A of Plus Shape-1 building**

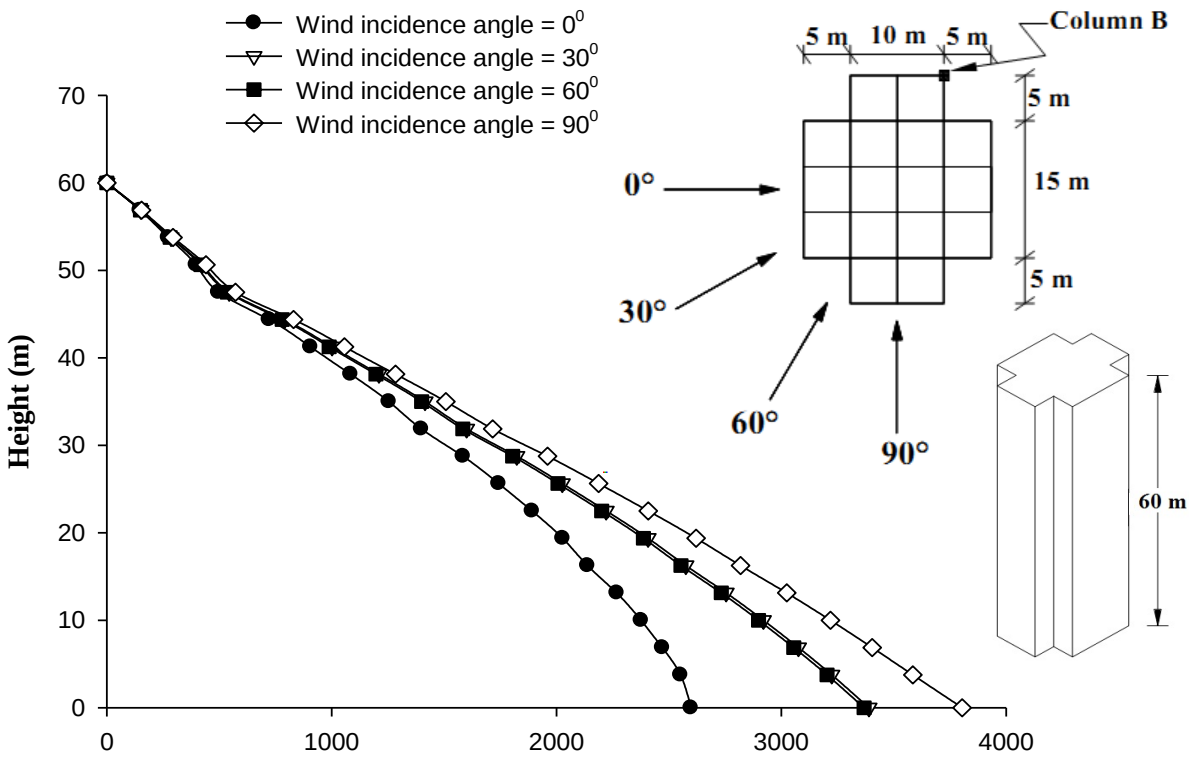


**Fig. 6.40 Effect of wind incidence angle on My (global) in column-B of Plus Shape-1 building**

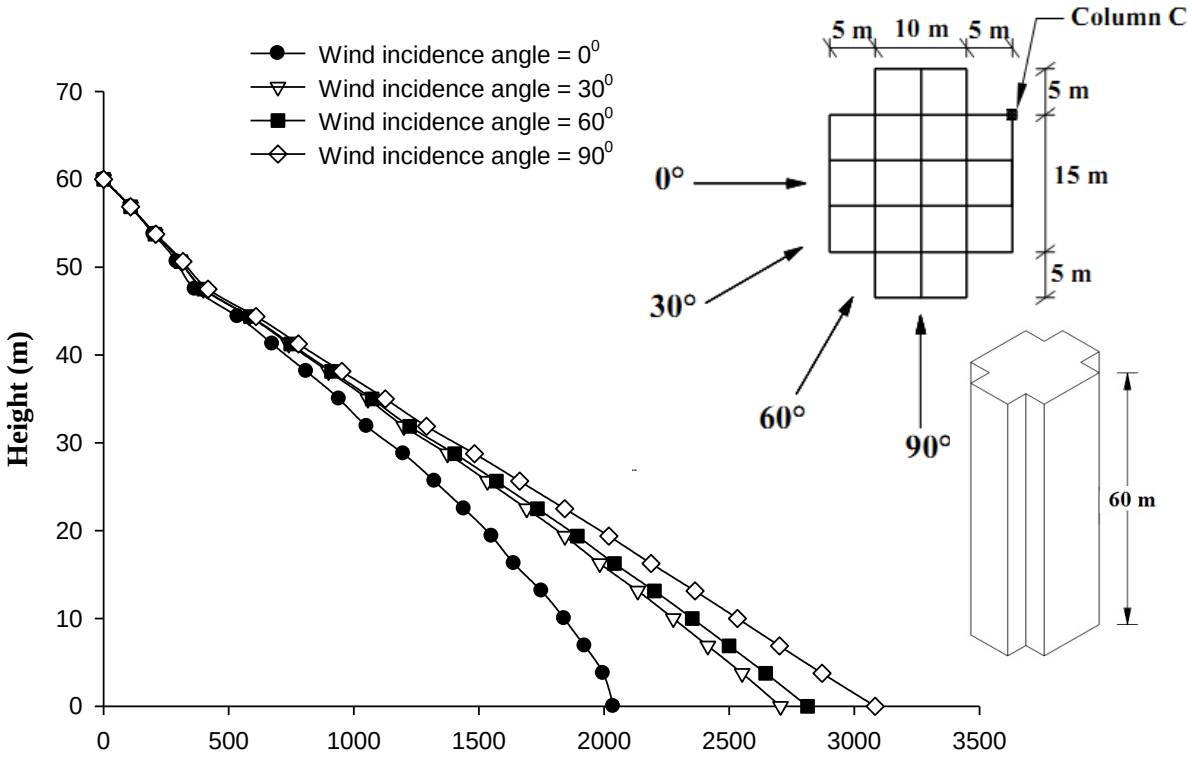


**Fig. 6.41 Effect of wind incidence angle on My (global) in column-C of Plus Shape-1 building**

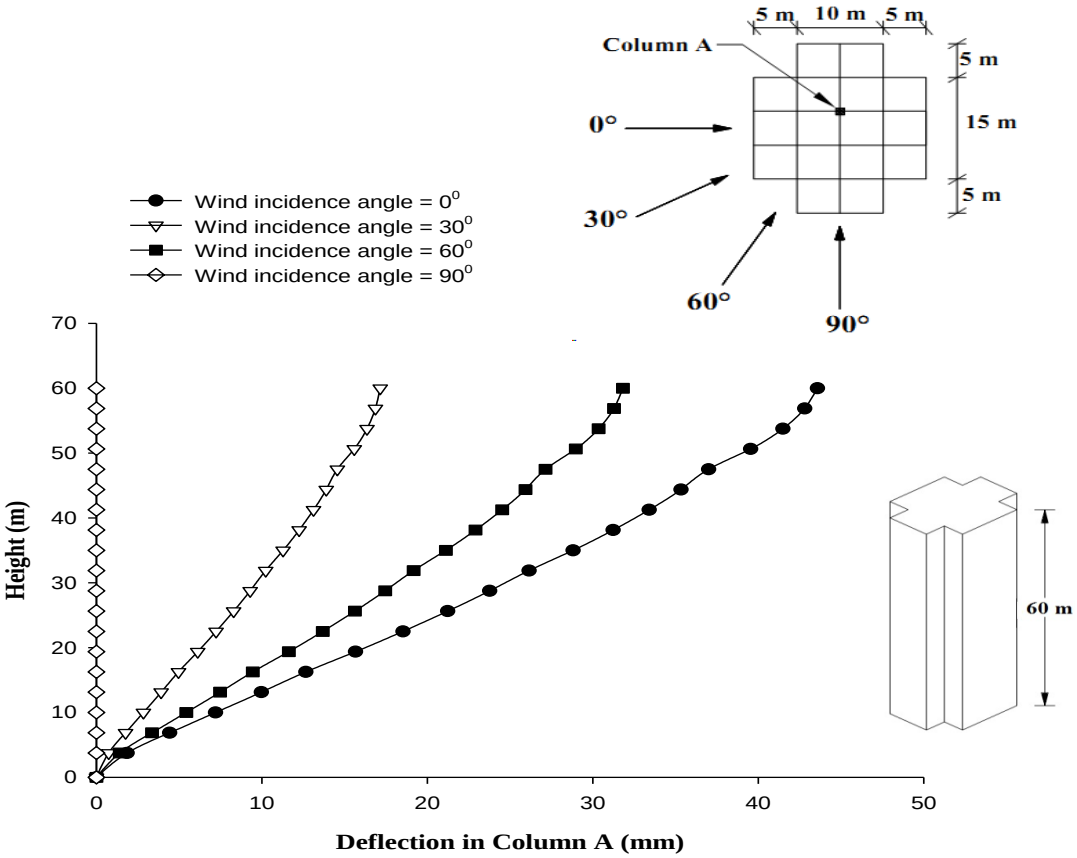


**Fig. 6.42 Effect of wind incidence angle on horizontal displacement of column-A of Plus Shape-1 building**

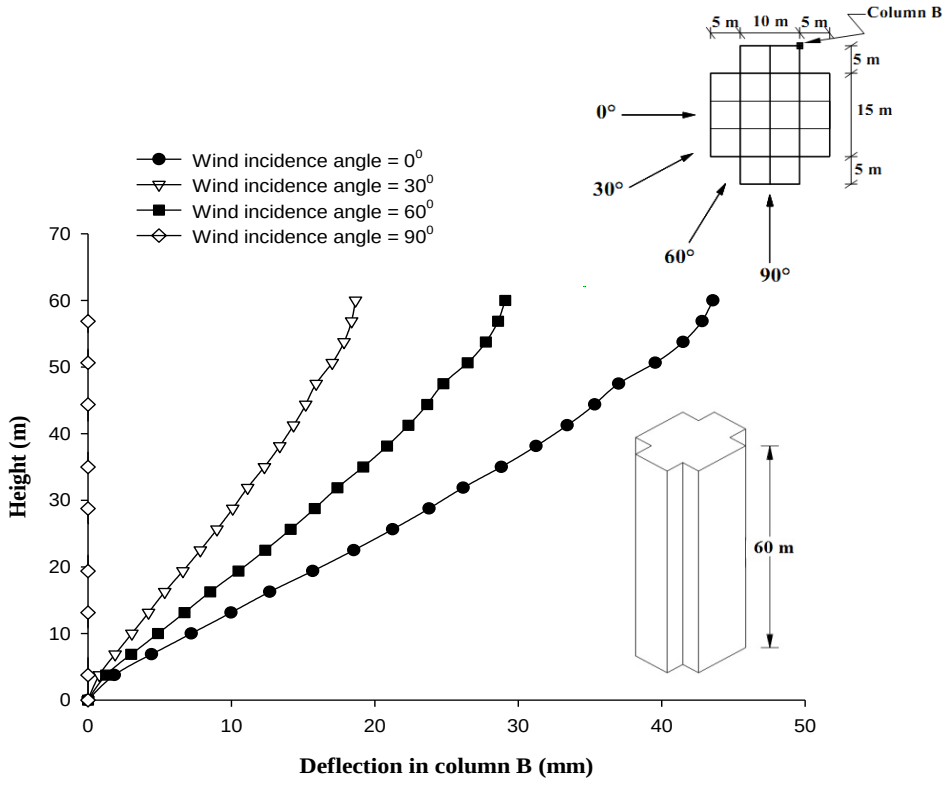


**Fig. 6.43 Effect of wind incidence angle on horizontal displacement of column-B of Plus Shape-1 building**

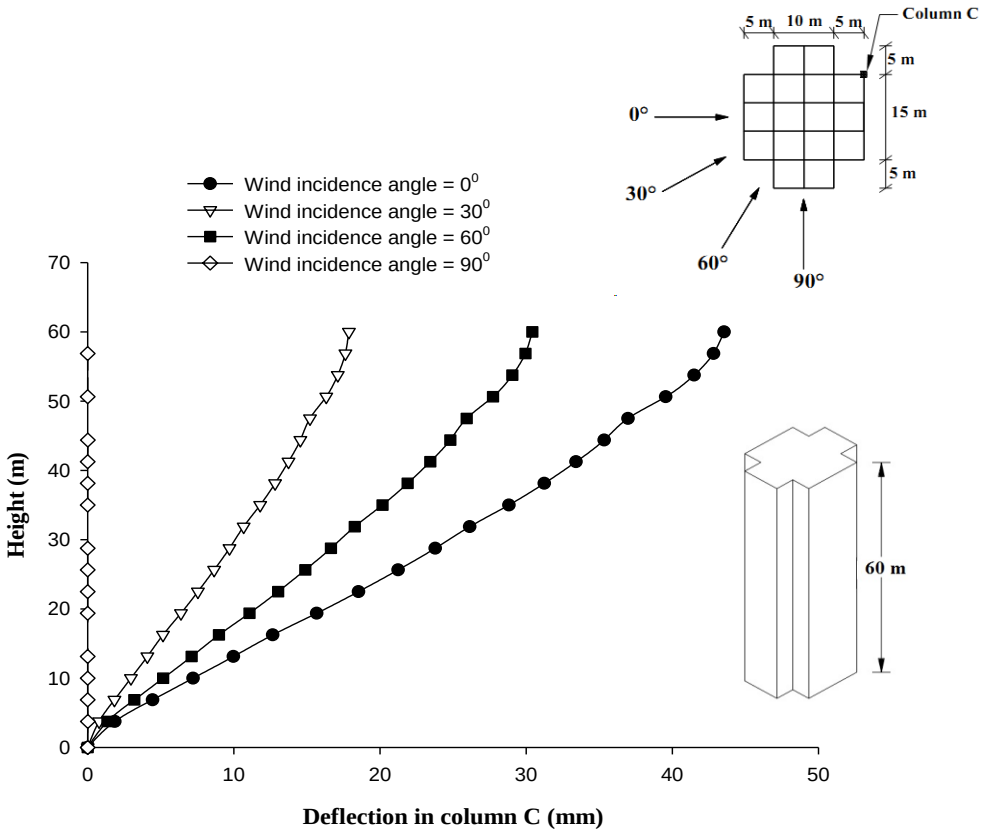


**Fig. 6.44 Effect of wind incidence angle on horizontal displacement of column-C of Plus Shape-1 building**

### 6.4.3 Plus Shape-2 Building

#### 6.4.3.1 Forces in columns

Effect of wind incidence angle on axial force in column-A, B and C can be seen in Figs. 6.45 to 6.47 respectively. In case of column-A (Fig. 6.45), maximum axial force is observed at $90^0$ wind incidence angle and minimum at $0^0$ degree wind incidence angle. Column-B (Fig. 6.46) is subjected to same axial force at every wind incidence angle. In case of column-C (Fig. 6.47), it is observed that maximum axial force is observed at $0^0$ wind incidence angle. However, axial force is same at all wind incidence angles above 80% height.

Figures 6.48 to 6.50 show variation of twisting moment (Mz) along the height of column-A, B and C of Plus Shape-2 building at varying angle of wind attack. Similar moment variation pattern is observed along the height of column-A, B and C. Mz is almost zero on column-A, B and C at $0^0$ and $90^0$ wind incidence angles and maximum at $60^0$ angle.

Moment about 'X' axis i.e. Mx and moment about 'Y' axis i.e. My are shown in Figs. 6.51 to 6.56 with respect to the varying wind incidence angle on column-A, B and C. In case of column-A both Mx and My are maximum at $90^0$ angle. Moment about 'X' axis in column-B is zero at $90^0$ angle and My is zero at $0^0$ wind incidence angle.

#### 6.4.3.2 Displacement of columns

Horizontal displacement of column-A, B and C at every floor level under different wind incidence angles are obtained during the analysis. The results are shown in Figs. 6.57 to 6.59. As expected, maximum displacement in X-direction is observed at $0^0$ wind incidence angle and zero displacement at $90^0$. Maximum deflection observed is around 0.125% of height of the building.

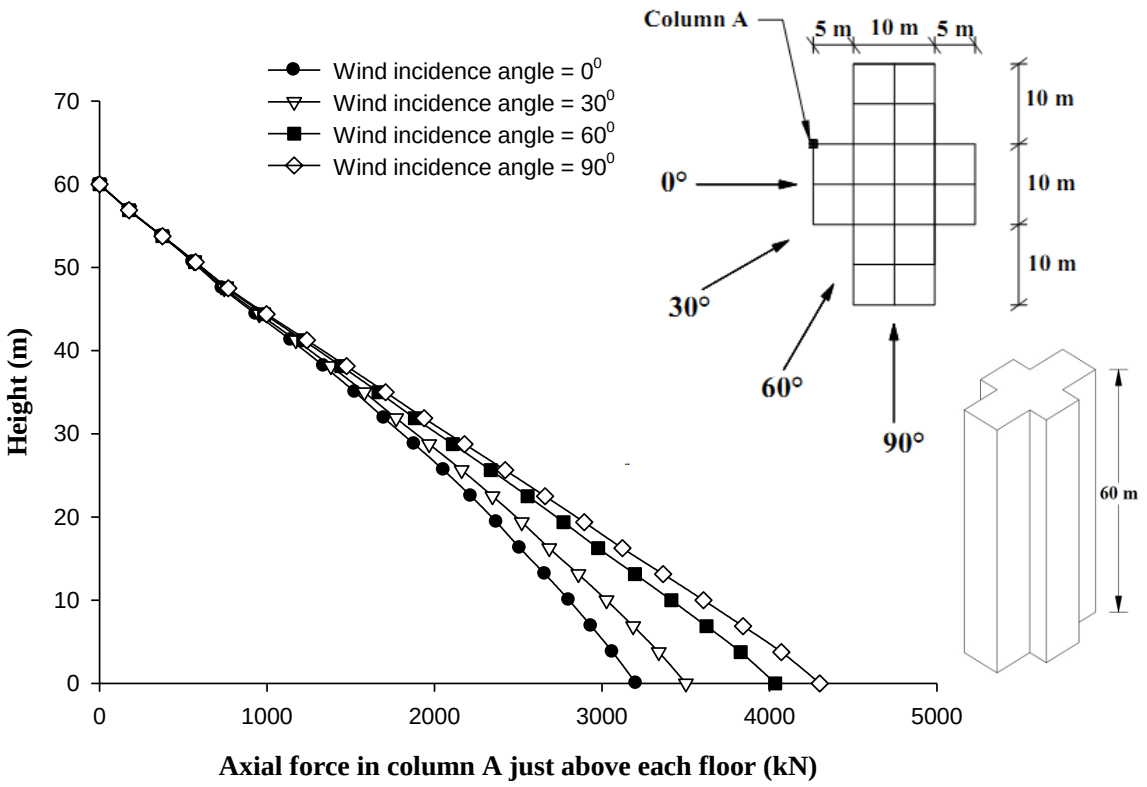


**Fig. 6.45 Effect of wind incidence angle on axial force in column-A of Plus Shape-2 building**

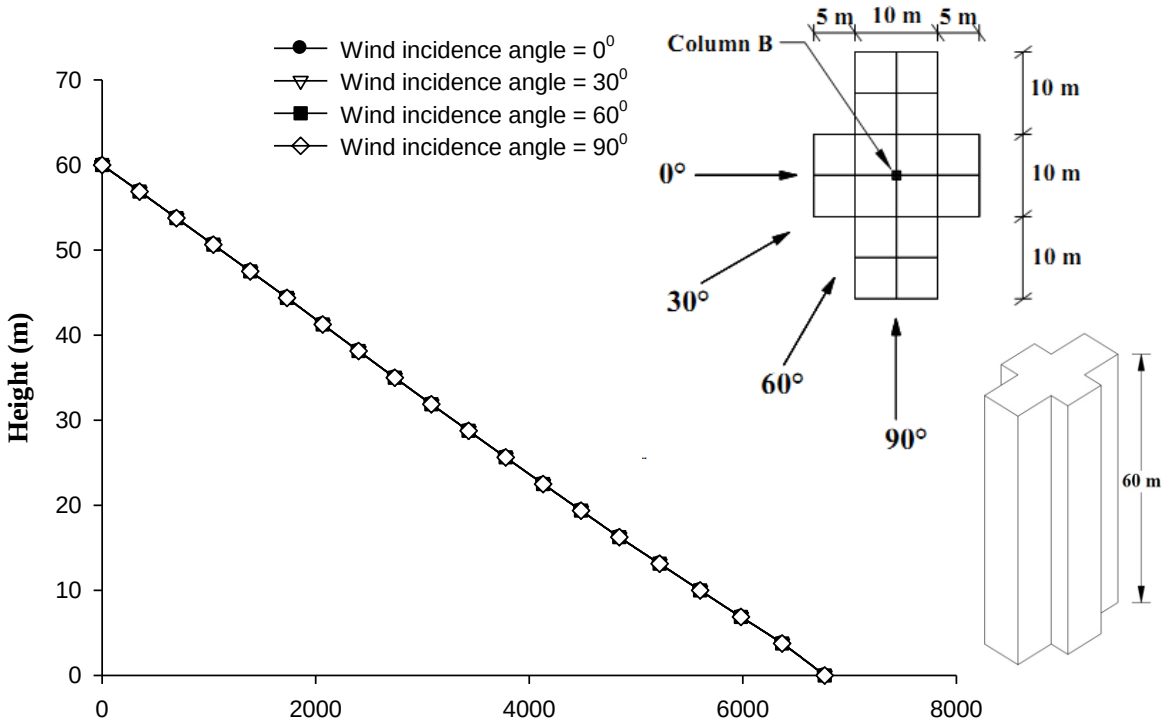


**Fig. 6.46 Effect of wind incidence angle on axial force in column-B of Plus Shape-2 building**

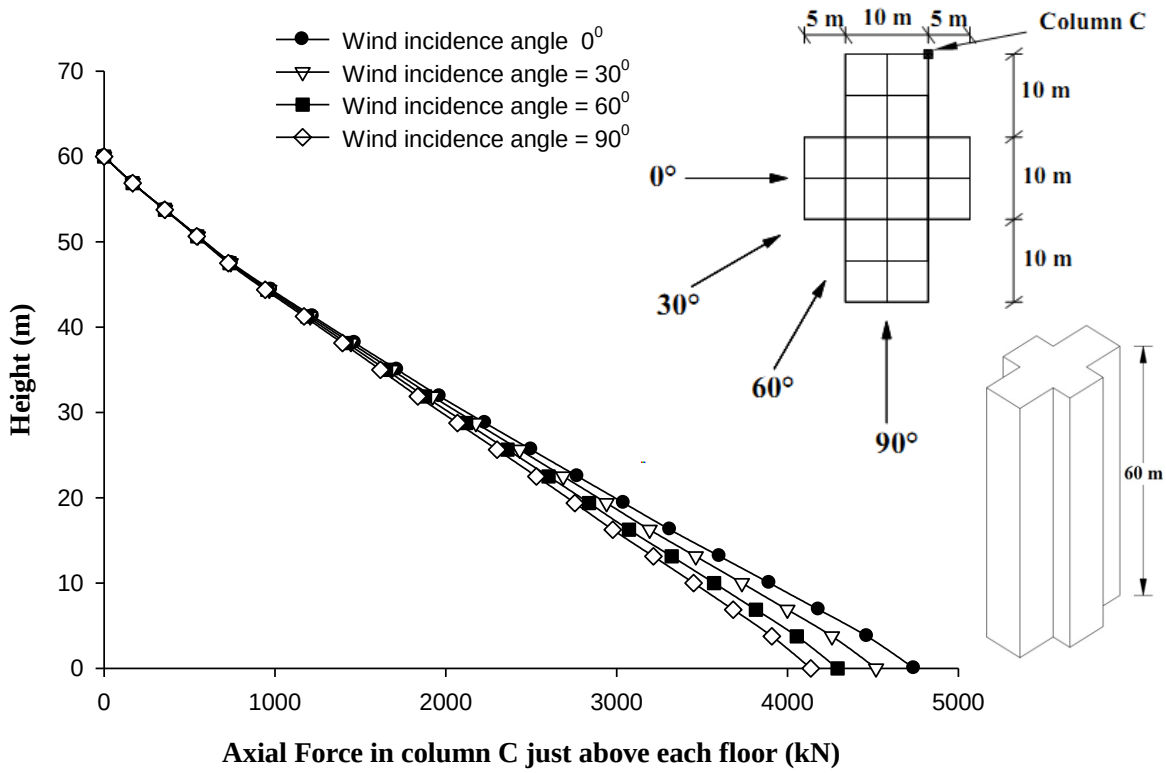


**Fig. 6.47 Effect of wind incidence angle on axial force in column-C of Plus Shape-2 building**

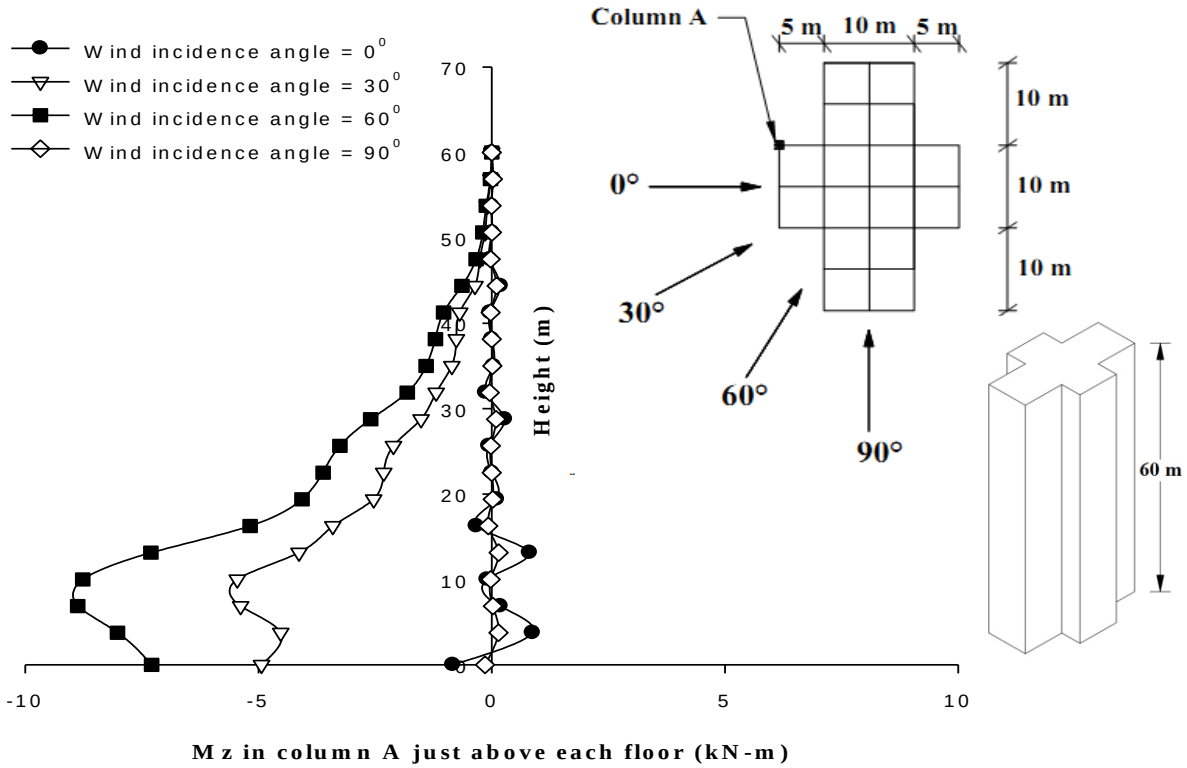


**Fig. 6.48 Effect of wind incidence angle on twisting moment Mz in column-A of Plus Shape-2 building**

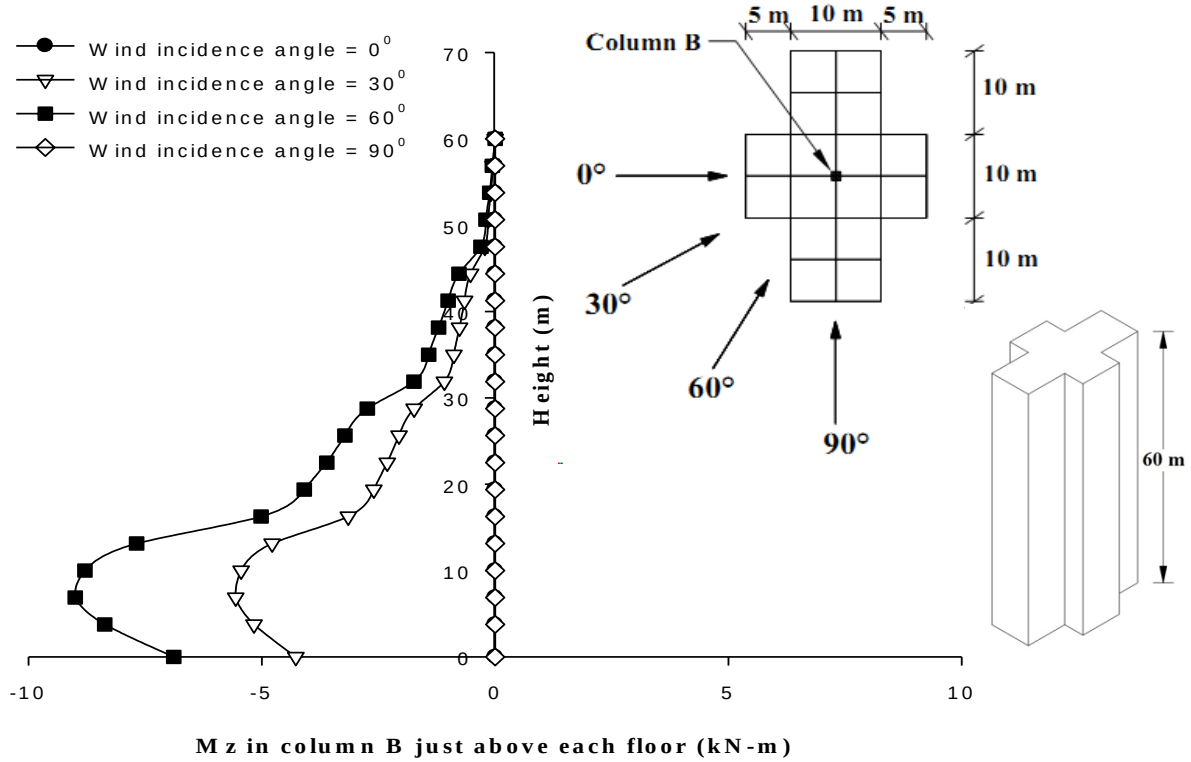


**Fig. 6.49 Effect of wind incidence angle on twisting moment Mz in column-B of Plus Shape-2 building**

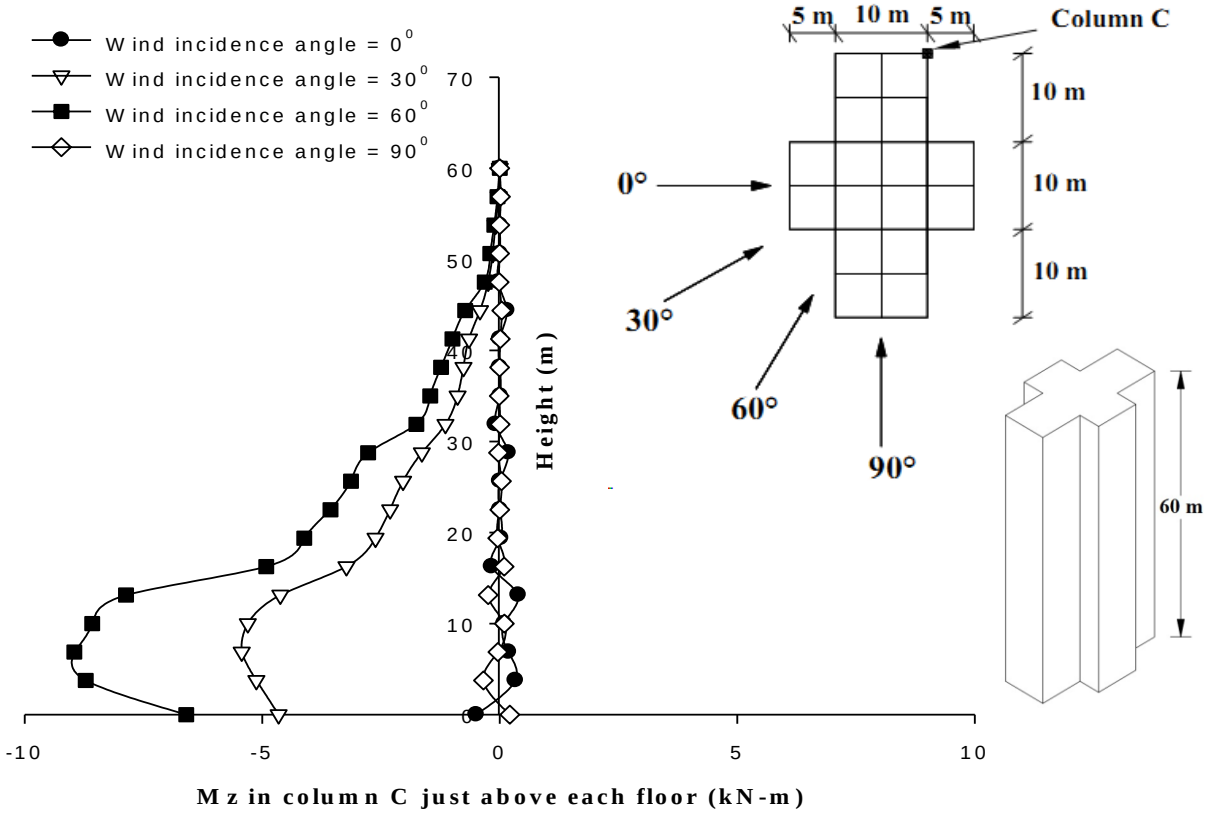


**Fig. 6.50 Effect of wind incidence angle on twisting moment Mz in column-C of Plus Shape-2 building**

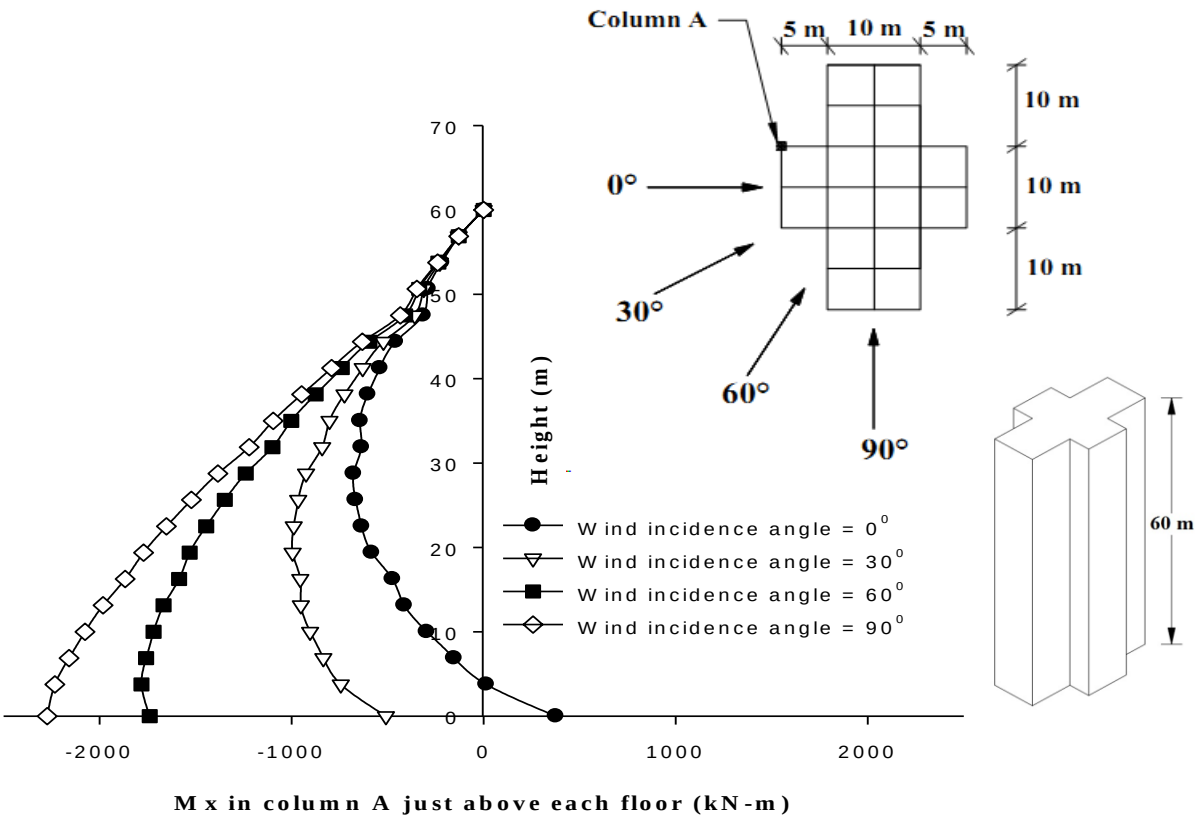


**Fig. 6.51 Effect of wind incidence angle on Mx (global) in column-A of Plus Shape-2 building**

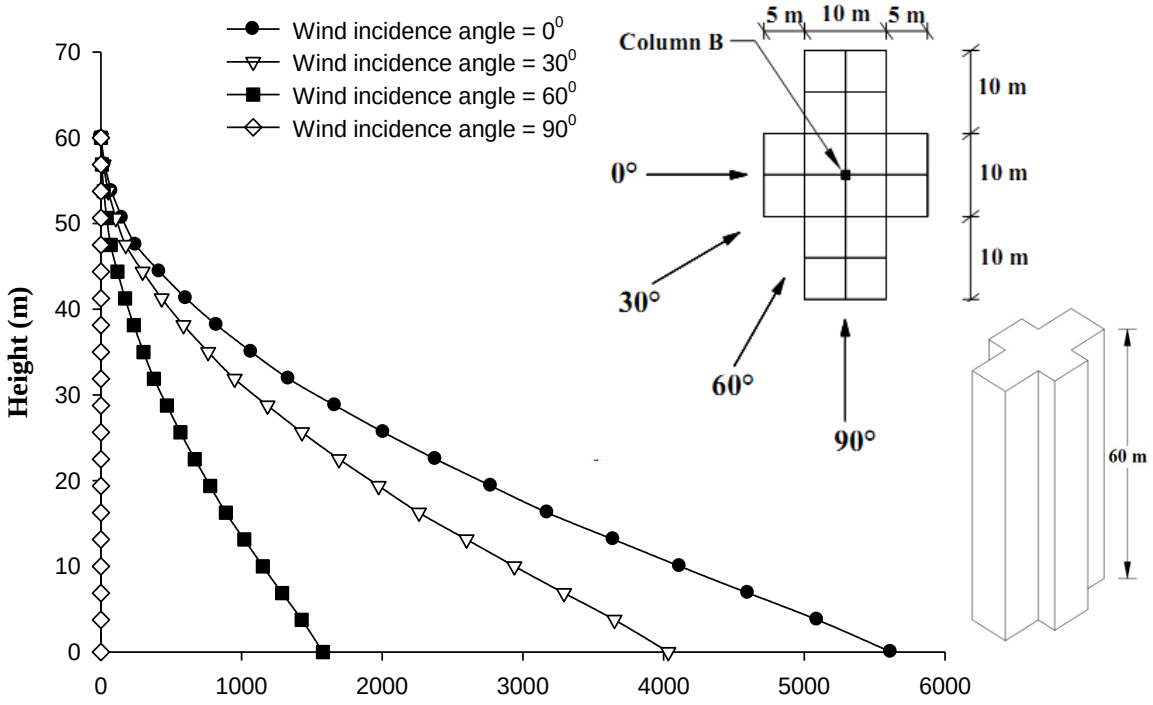


**Fig. 6.52 Effect of wind incidence angle on Mx (global) in column-B of Plus Shape-2 building**

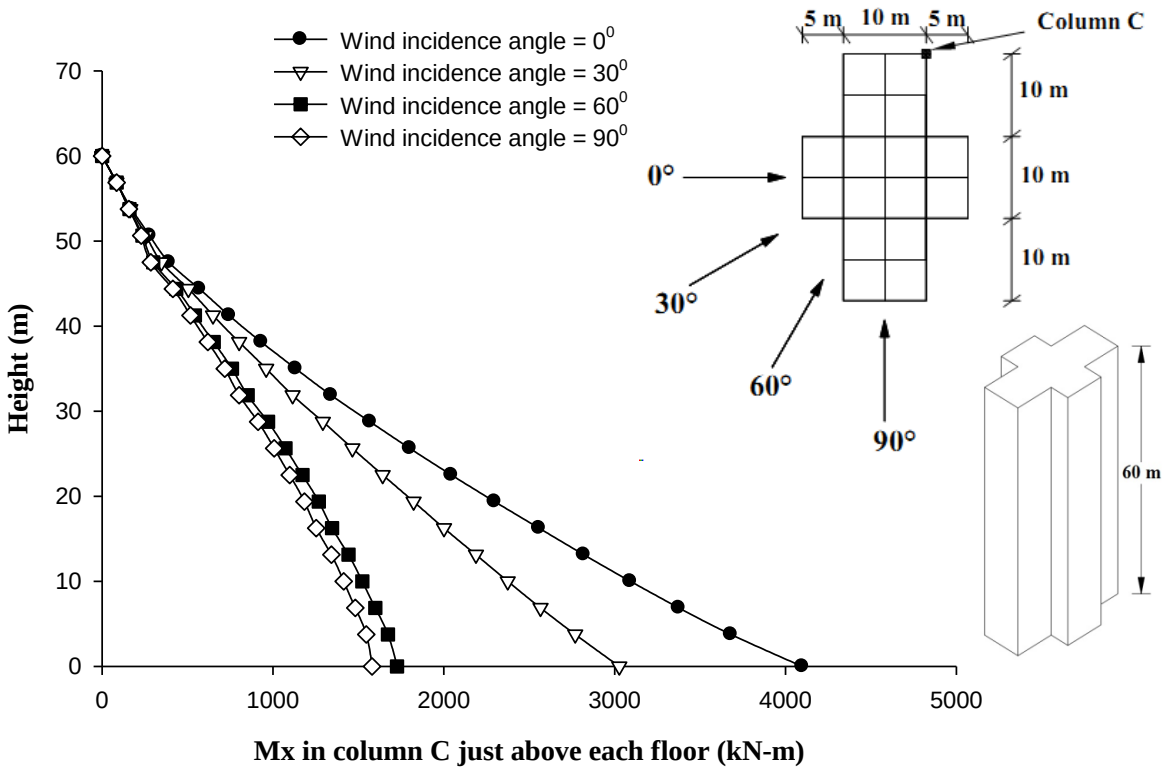


**Fig. 6.53 Effect of wind incidence angle on Mx (global) in column-C of Plus Shape-2 building**

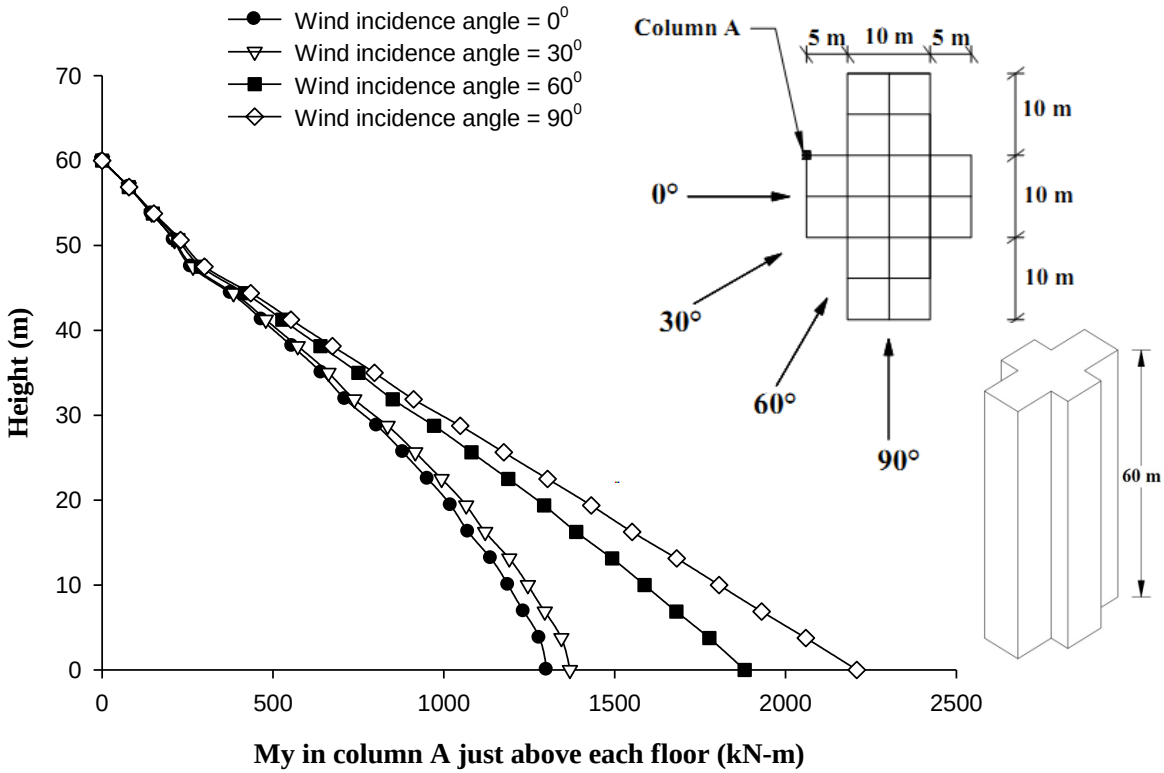


**Fig. 6.54 Effect of wind incidence angle on My (global) in column-A of Plus Shape-2 building**

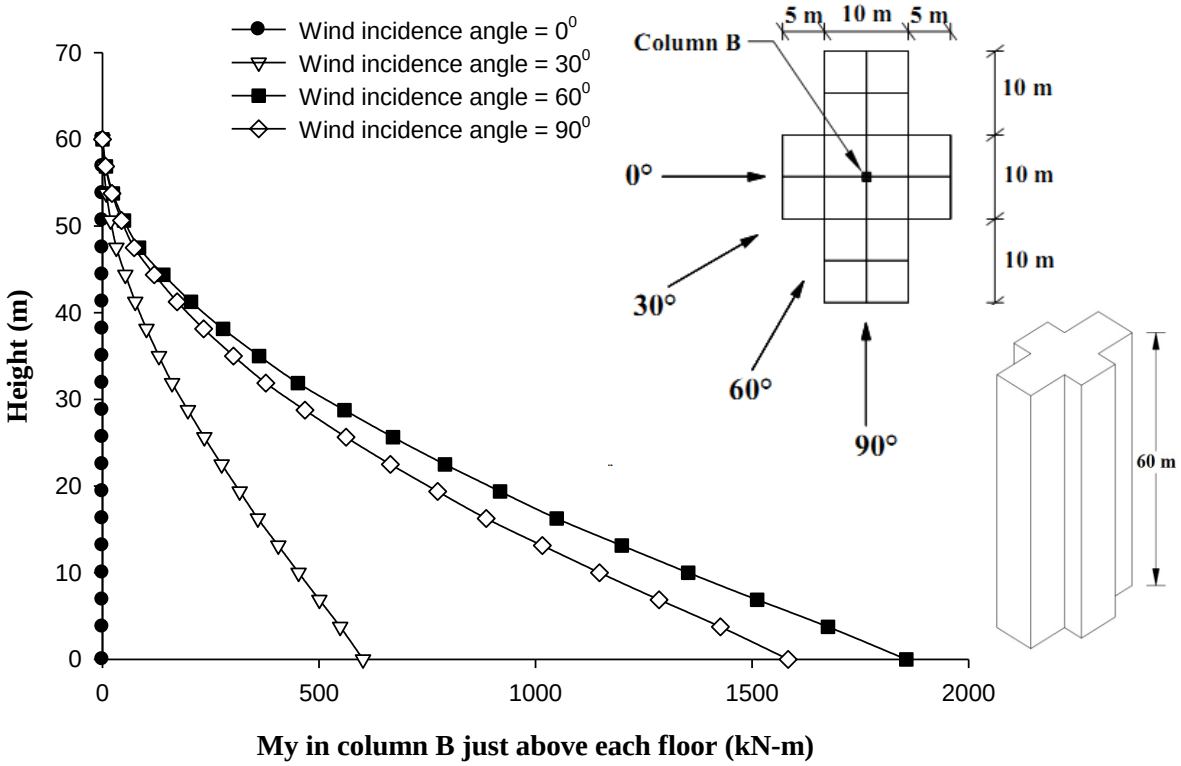


**Fig. 6.55 Effect of wind incidence angle on My (global) in column-B of Plus Shape-2 building**

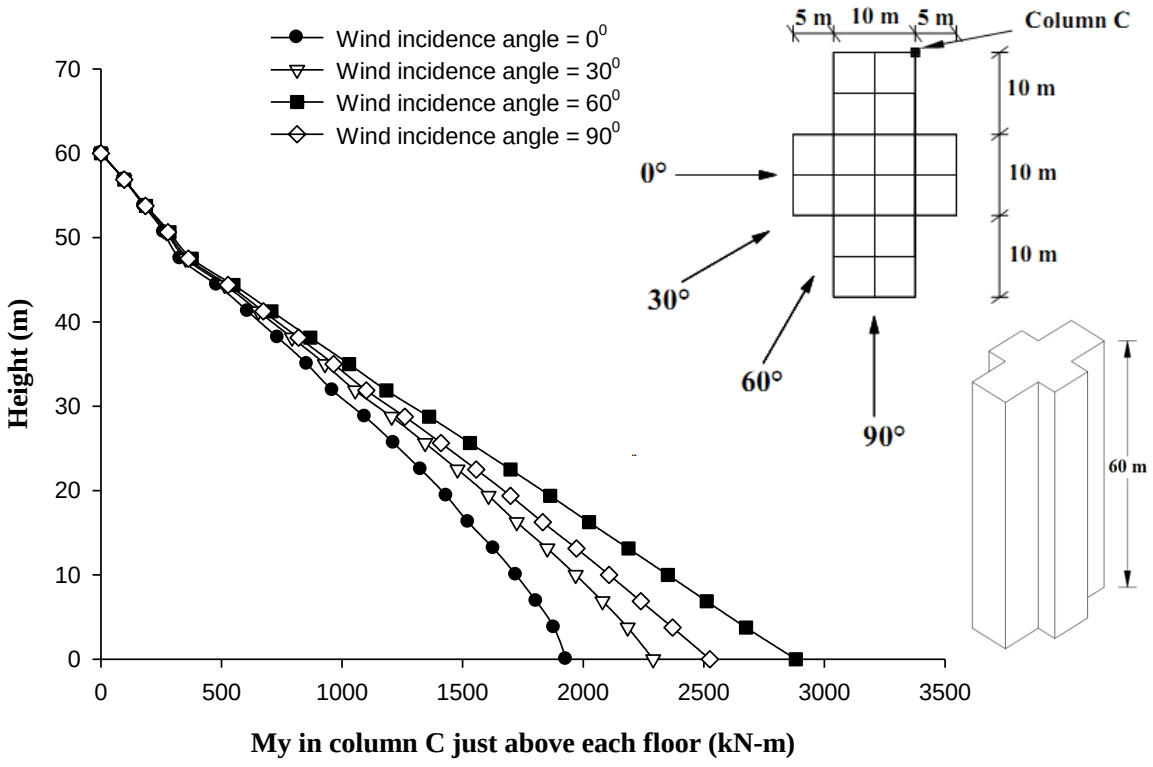


**Fig. 6.56 Effect of wind incidence angle on My (global) in column-C of Plus Shape-2 building**

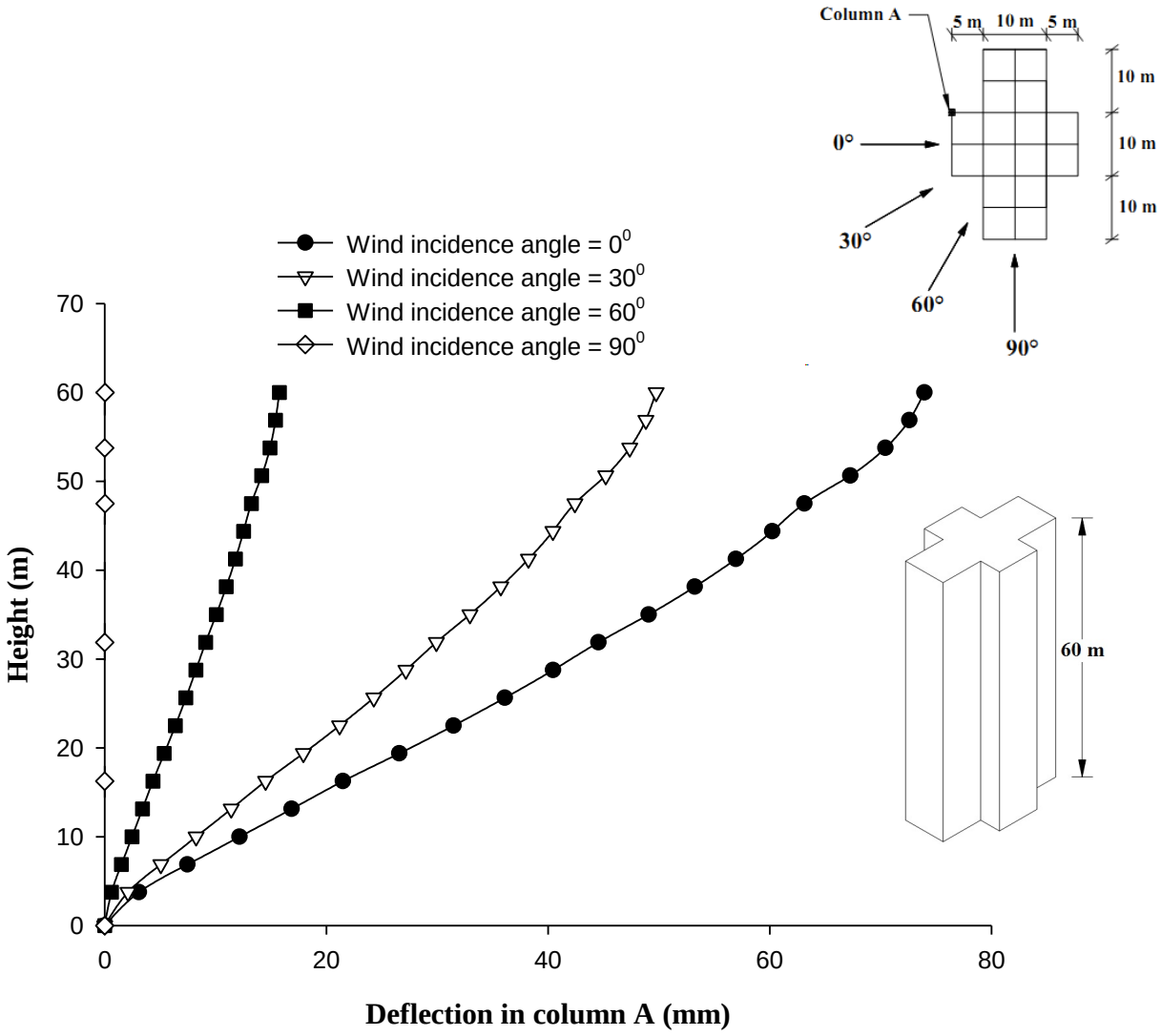


**Fig. 6.57 Effect of wind incidence angle on horizontal displacement of column-A of Plus Shape-2 building**

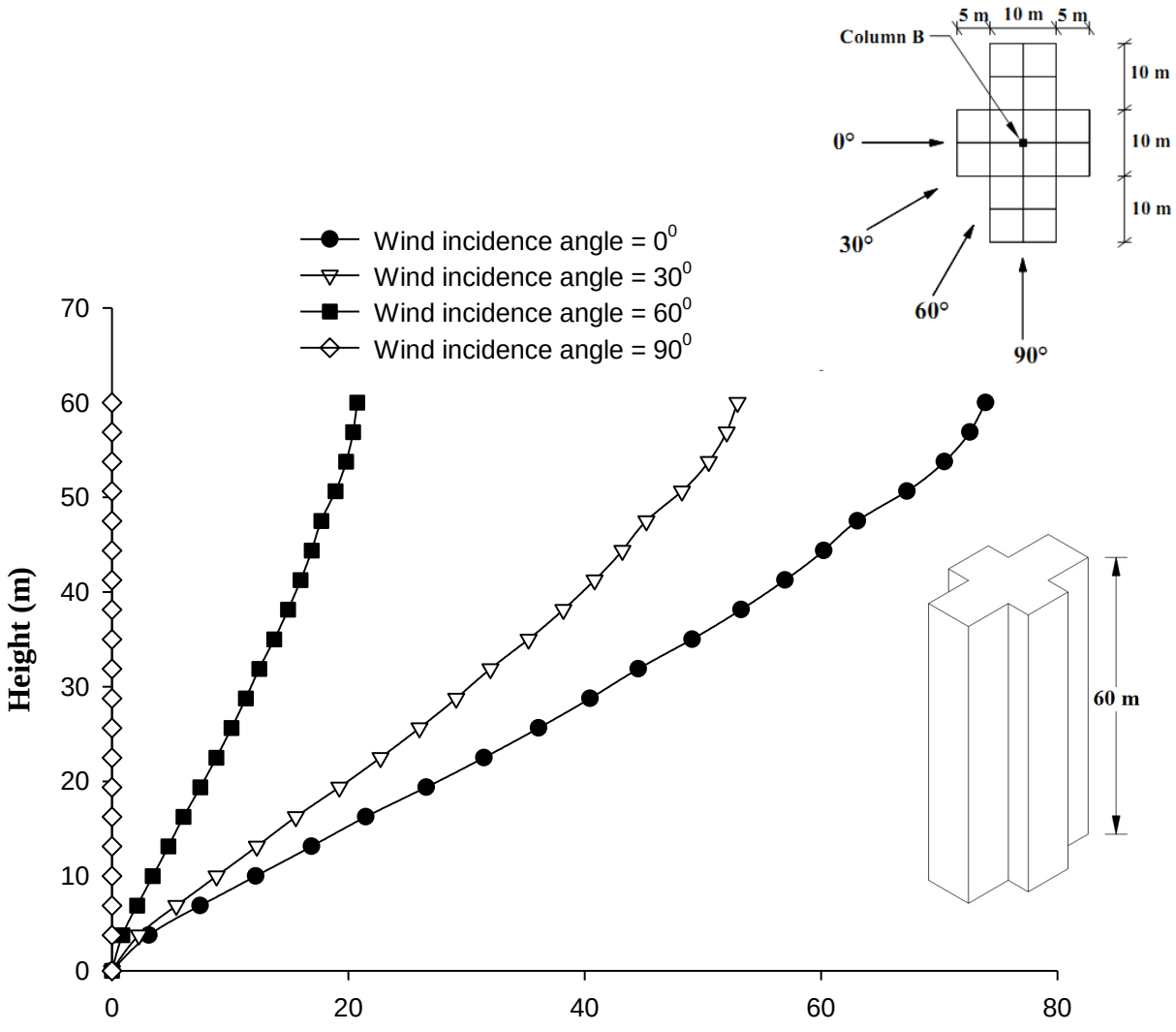


**Fig. 6.58 Effect of wind incidence angle on horizontal displacement of column-B of Plus Shape-2 building**

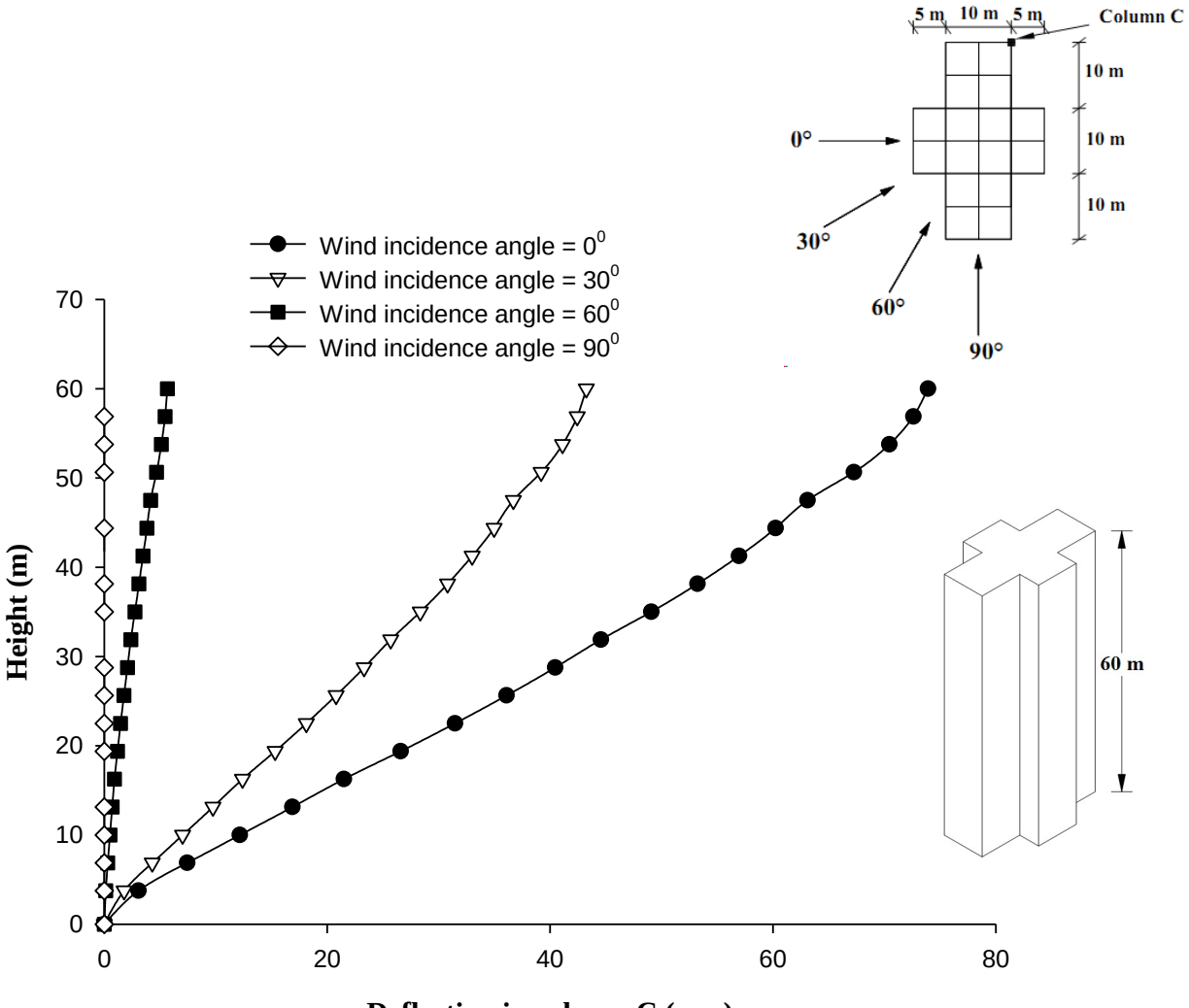


**Fig. 6.59 Effect of wind incidence angle on horizontal displacement of column-C of Plus Shape-2 building**

### 6.4.4 I-Shape-1 Building

#### 6.4.4.1 Forces in columns

Axial force in column-A, B and C of I-shape-1 building at different wind incidence angles are shown in Figs. 6.60 to 6.62 respectively. In case of column-A (Fig. 6.60), axial force gradually increases with increase in wind incidence angle in the lower 80% height of the column. Above 80% height, axial force is same at all wind incidence angles. In case of column-B (Fig. 6.61), axial force remains same at all wind incidence angles. For column-C (Fig. 6.62), axial force is approximately similar at $30^0$ and $60^0$ wind incidence angles. Maximum axial force is observed at $60^0$ wind incidence angle and minimum at $90^0$ angle.

Figures 6.63 to 6.65 show the variarion of torsional moment Mz along the height of column-A, B and C at varying angle of wind attack. At $0^0$ and $90^0$ wind incidence angles, twisting moment is zero and it is maximum at $30^0$ wind incidence angle.

Moment about 'X' axis i.e. Mx is plotted along the height and is shown in Figs. 6.66 to 6.68 for column-A, B and C respectively. Mx is minimum at $0^0$ wind incidence angle in column-A which increases with increase in wind incidence angle (Fig. 6.66). It is maximum at $90^0$ wind angle of attack. In case of column-B (Fig. 6.67), it is observed that zero moment occurs at $90^0$ wind incidence angle and maximum moment at $0^0$ wind incidence angle. For column-C (Fig. 6.68), maximum moment is observed at $0^0$ wind incidence angle and minimum at $90^0$ angle.

Moment about 'Y' axis i.e. My is plotted along the height with respect to wind incidence angle for column-A, B and C shown in Figs. 6.69 to 6.71 respectively. For column-A (Fig. 6.69), almost same values of My is observed at $60^0$ and $90^0$ wind incidence angles. Similar moment variation pattern is observed along the height of column-B and C. Moment My is maximum at $60^0$ angle and is minimum at $0^0$ angle in case of column-B as well as column-C.

#### 6.4.4.2 Displacement of columns

Horizontal displacement of column-A, B and C at every floor level under different wind incidence angles are obtained during the analysis. The results are shown in Figs. 6.72 to 6.74. As expected, maximum displacement in X-direction is observed at $0^0$ wind incidence angle and zero displacement at $90^0$. Maximum deflection is around 0.09% of building height in all columns.

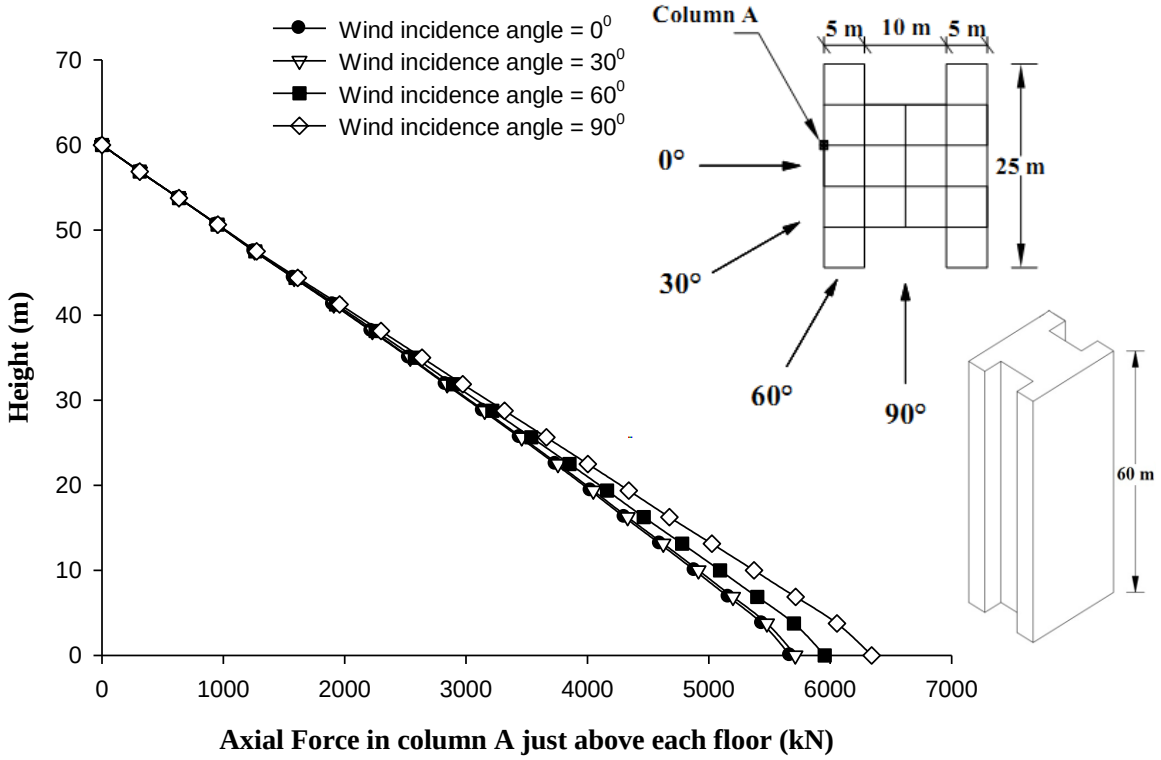


**Fig. 6.60 Effect of wind incidence angle on axial force in column-A of I-Shape-1 building**

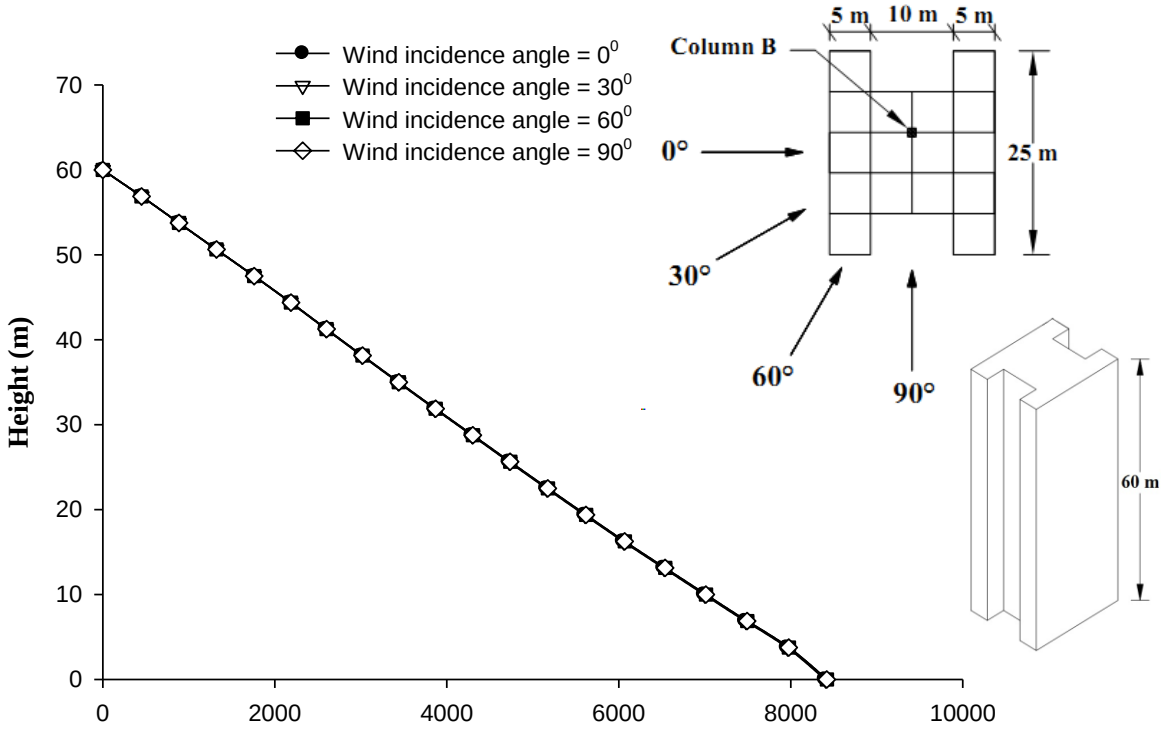


**Fig. 6.61 Effect of wind incidence angle on axial force in column-B of I-Shape-1 building**

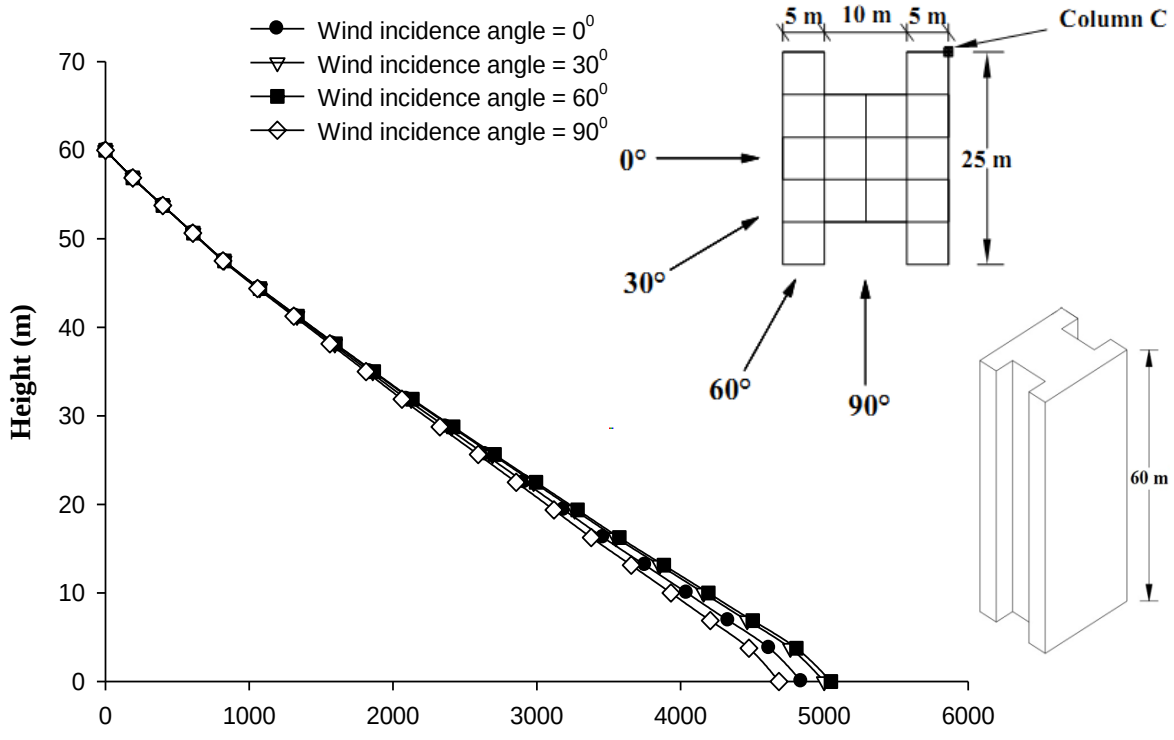


**Axial Force in column C just above each floor (kN)**

**Fig. 6.62 Effect of wind incidence angle on axial force in column-C of I-Shape-1 building**

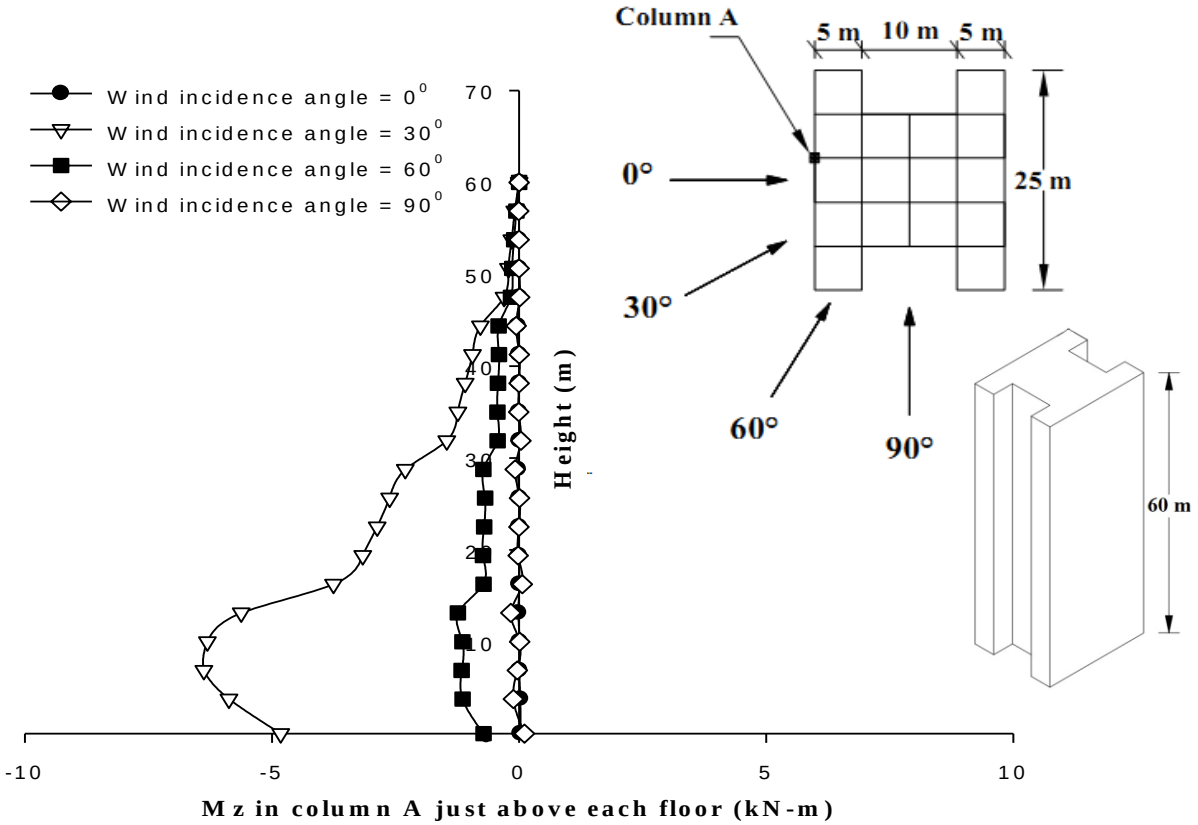


**Mz in column A just above each floor (kN-m)**

**Fig. 6.63 Effect of wind incidence angle on twisting moment Mz in column-A of I-Shape-1 building**

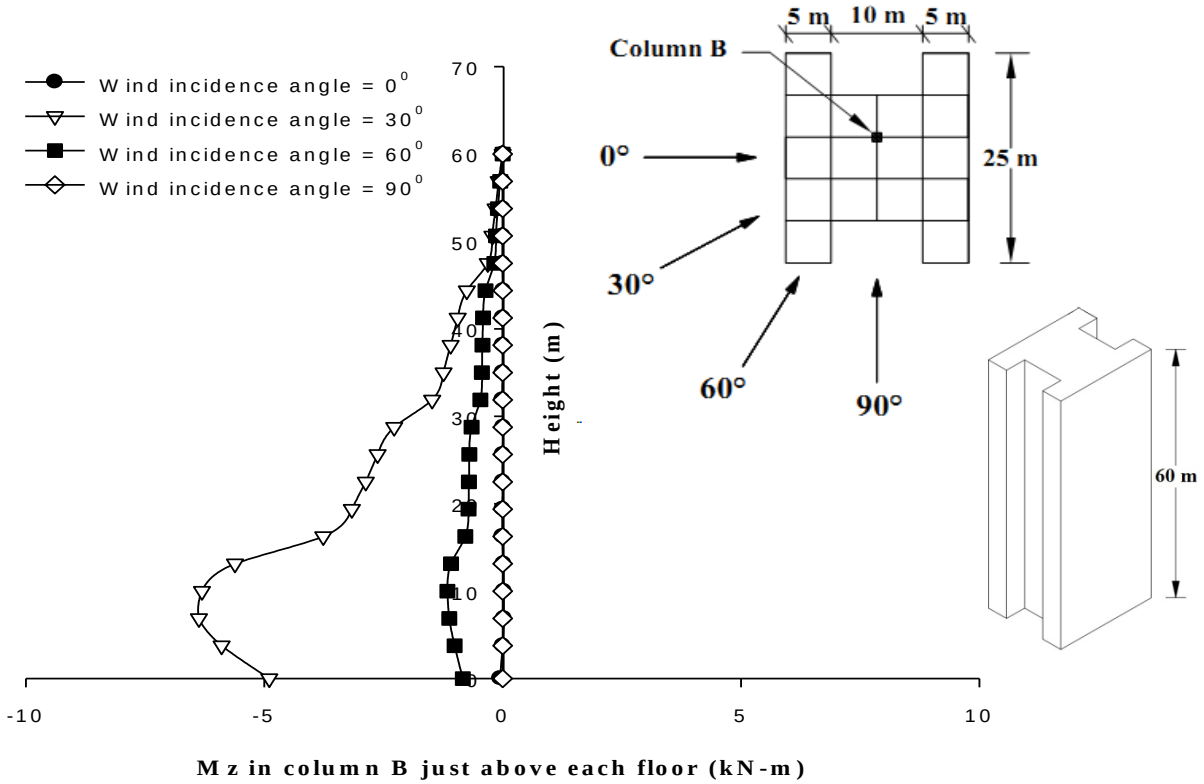


**Fig. 6.64 Effect of wind incidence angle on twisting moment Mz in column-B of I-Shape-1 building**

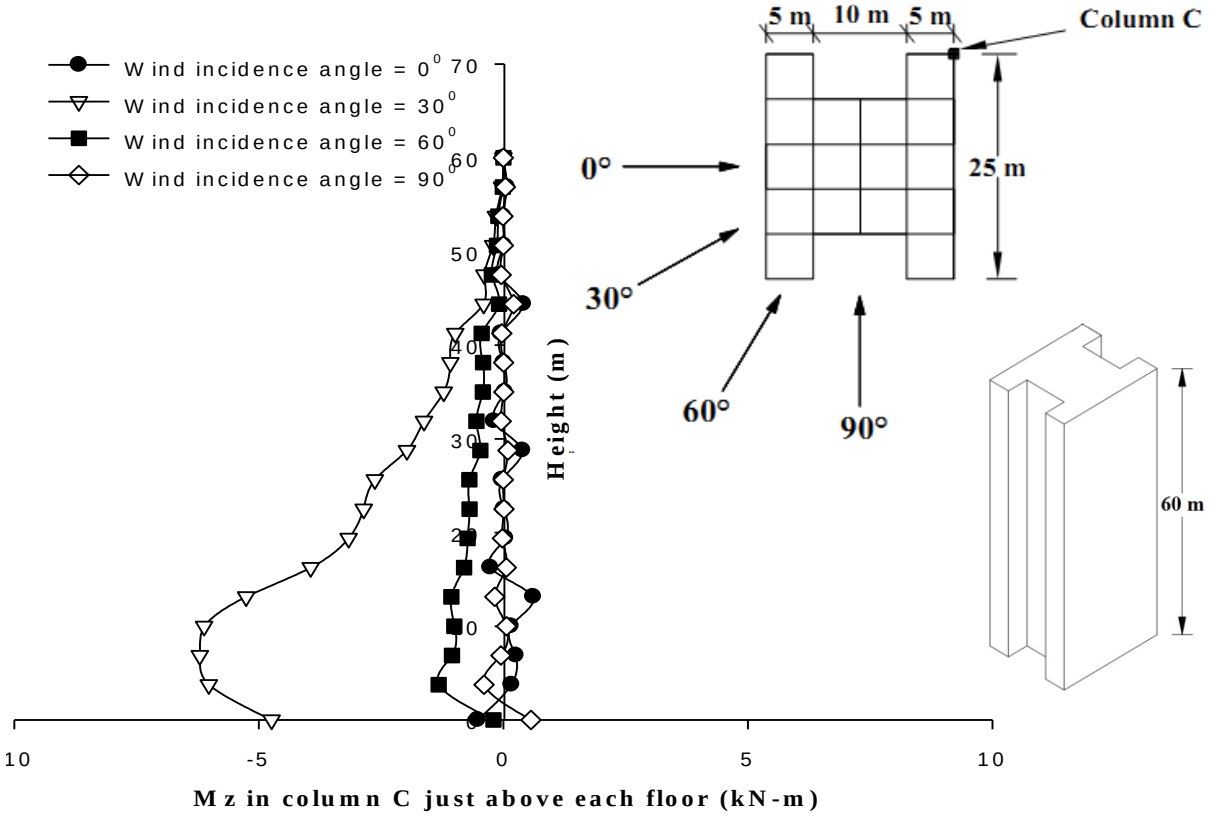


**Fig. 6.65 Effect of wind incidence angle on twisting moment Mz in column-C of I-Shape-1 building**

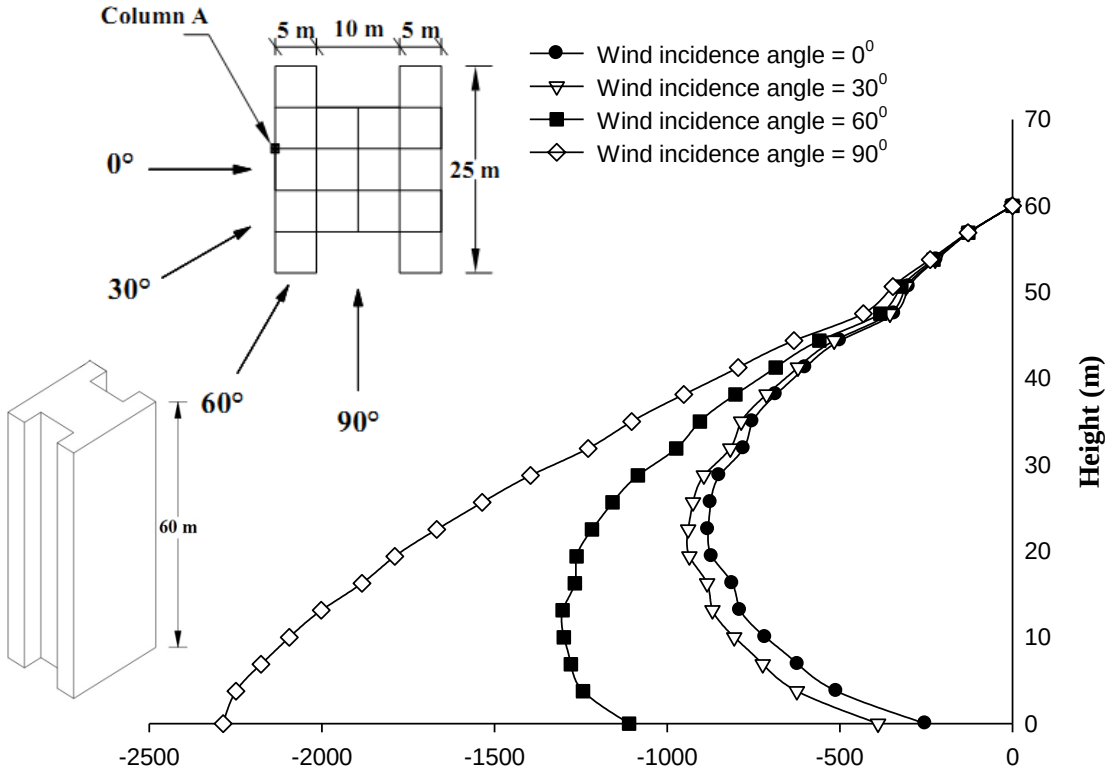


**Fig. 6.66 Effect of wind incidence angle on Mx (global) in column-A of I-Shape-1 building**

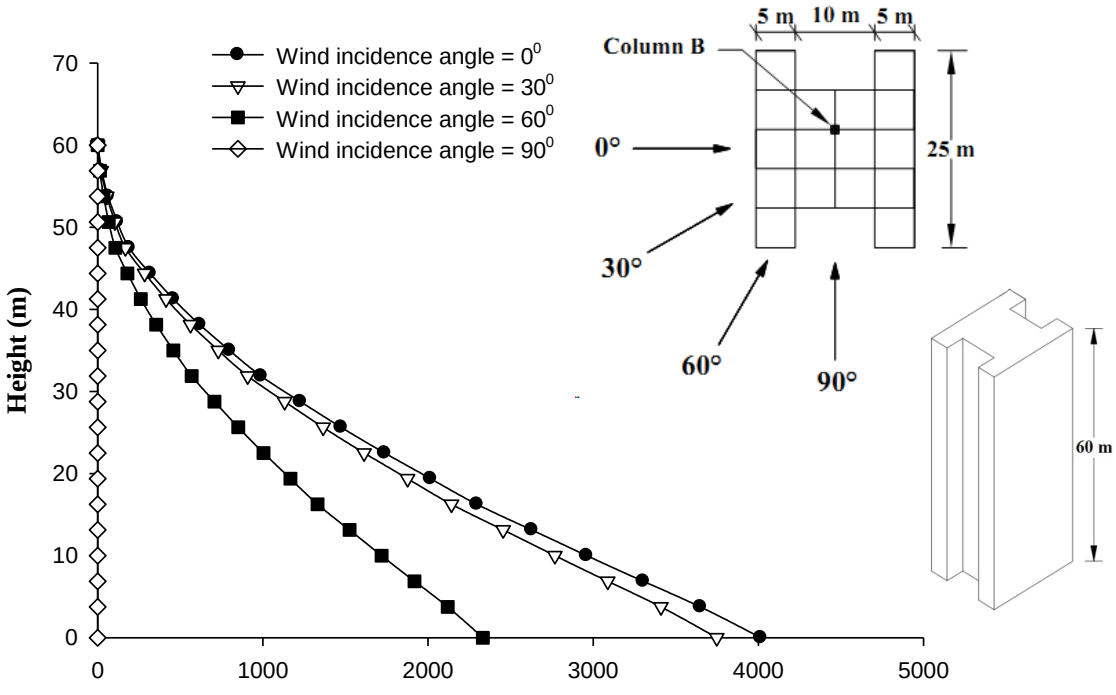


**Fig. 6.67 Effect of wind incidence angle on Mx (global) in column-B of I-Shape-1 building**

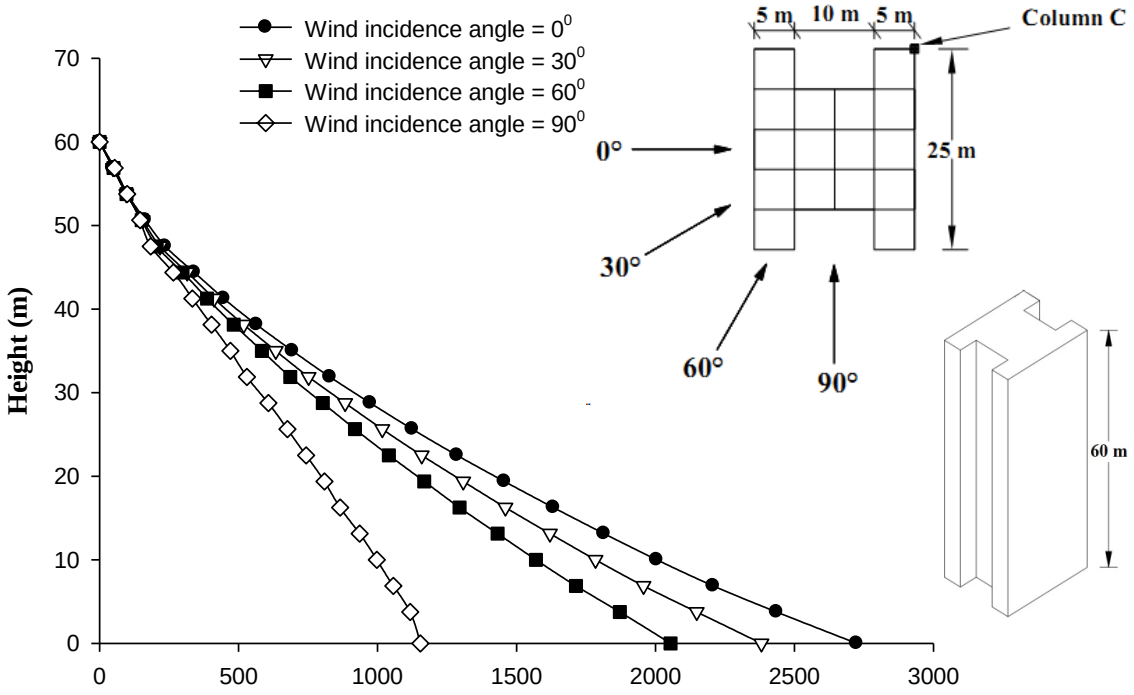


**Mx in column C just above each floor (kN-m)**

**Fig. 6.68 Effect of wind incidence angle on Mx (global) in column-C of I-Shape-1 building**

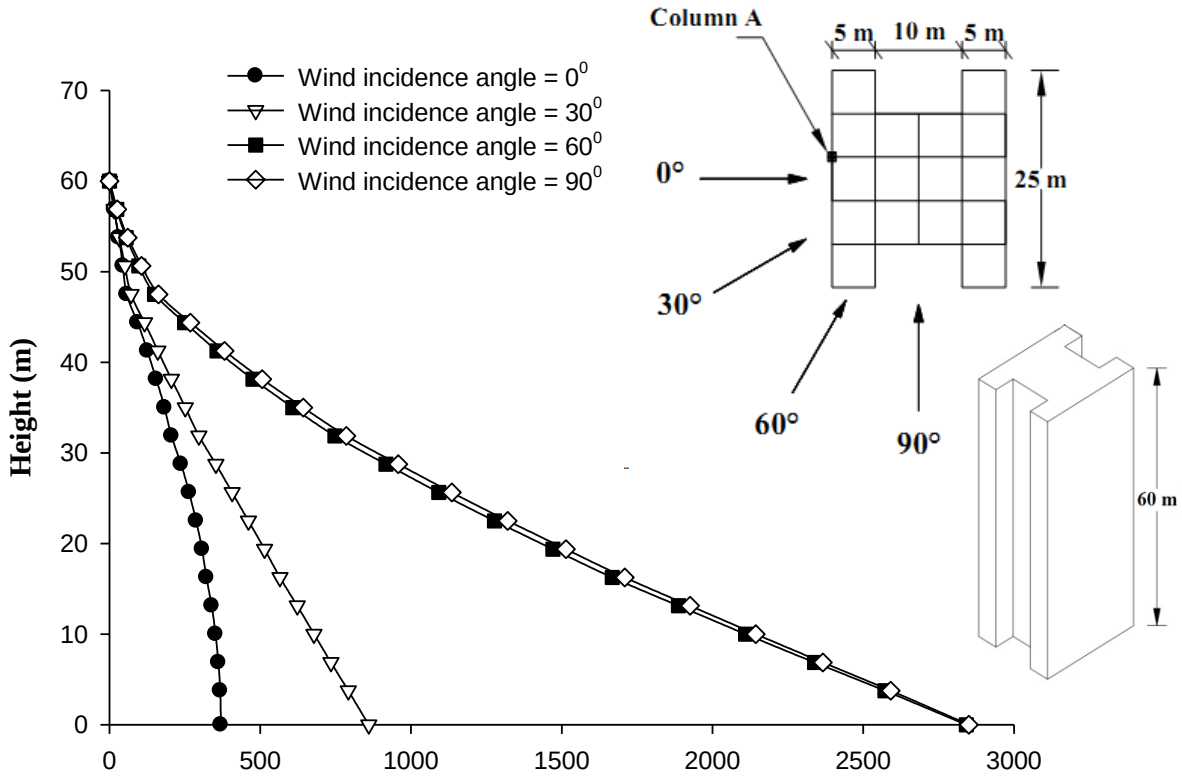


**My in column A just above each floor (kN-m)**

**Fig. 6.69 Effect of wind incidence angle on My (global) in column-A of I-Shape-1 building**

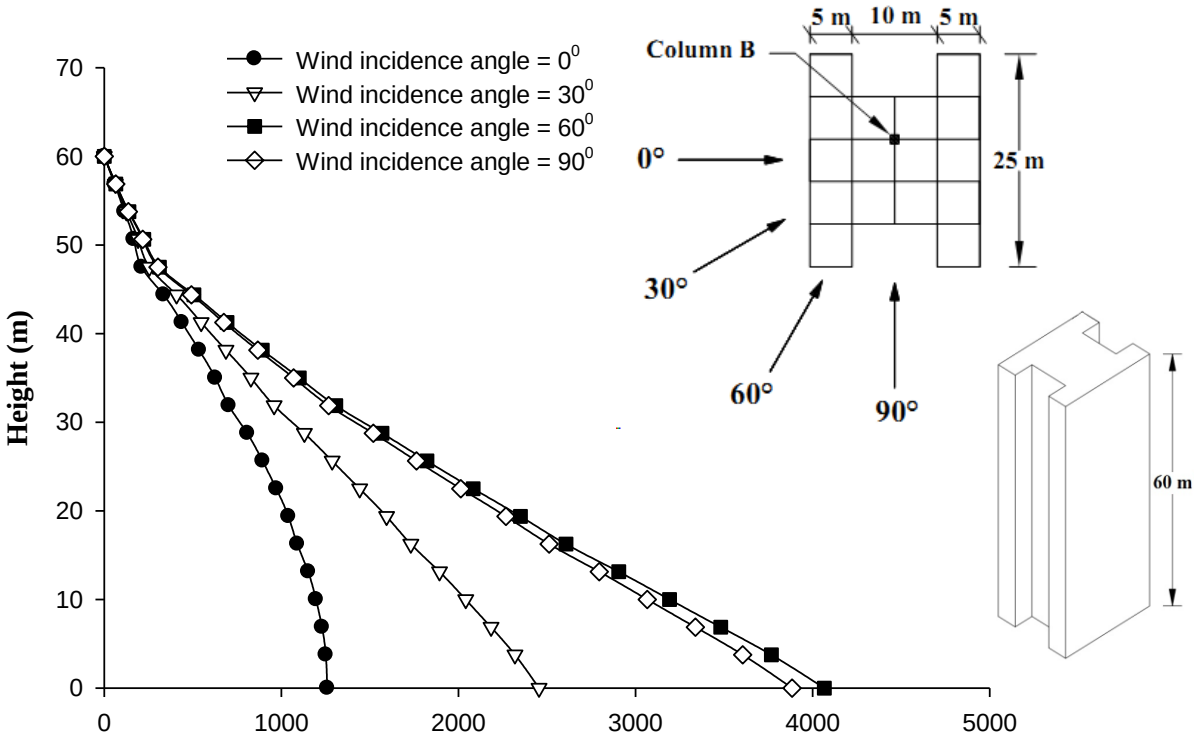


**Fig. 6.70 Effect of wind incidence angle on My (global) in column-B of I-Shape-1 building**

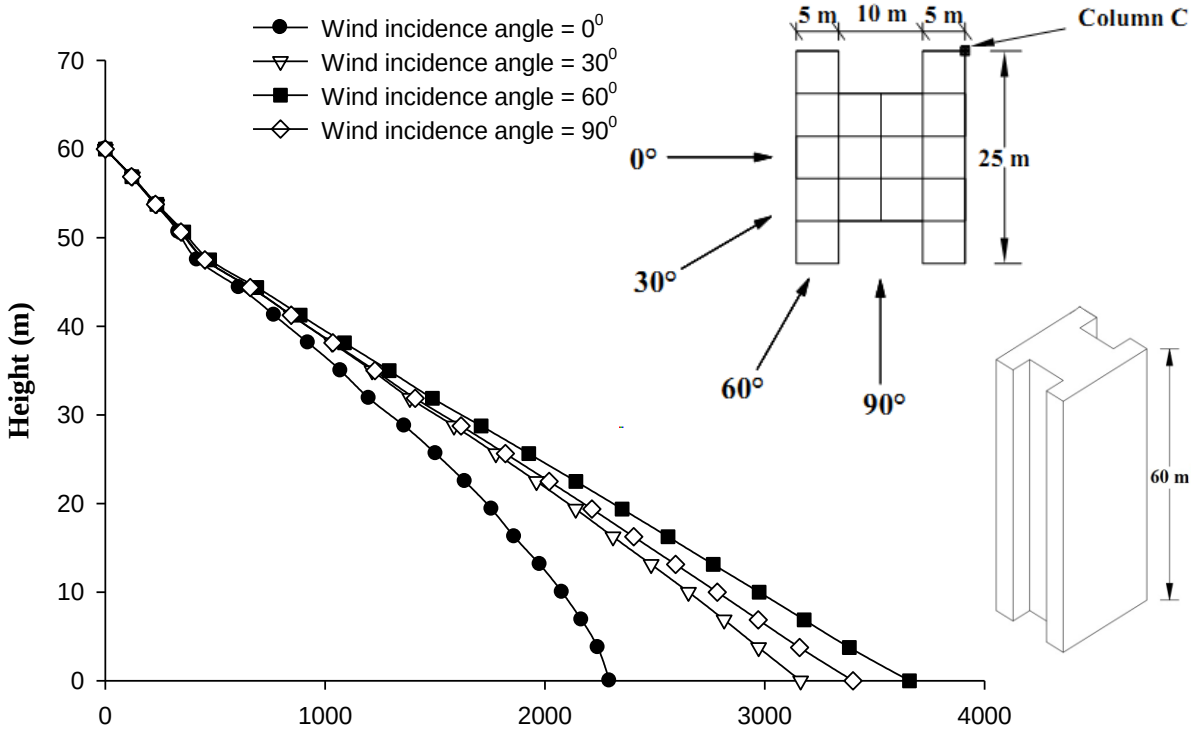


**Fig. 6.71 Effect of wind incidence angle on My (global) in column-C of I-Shape-1 building**

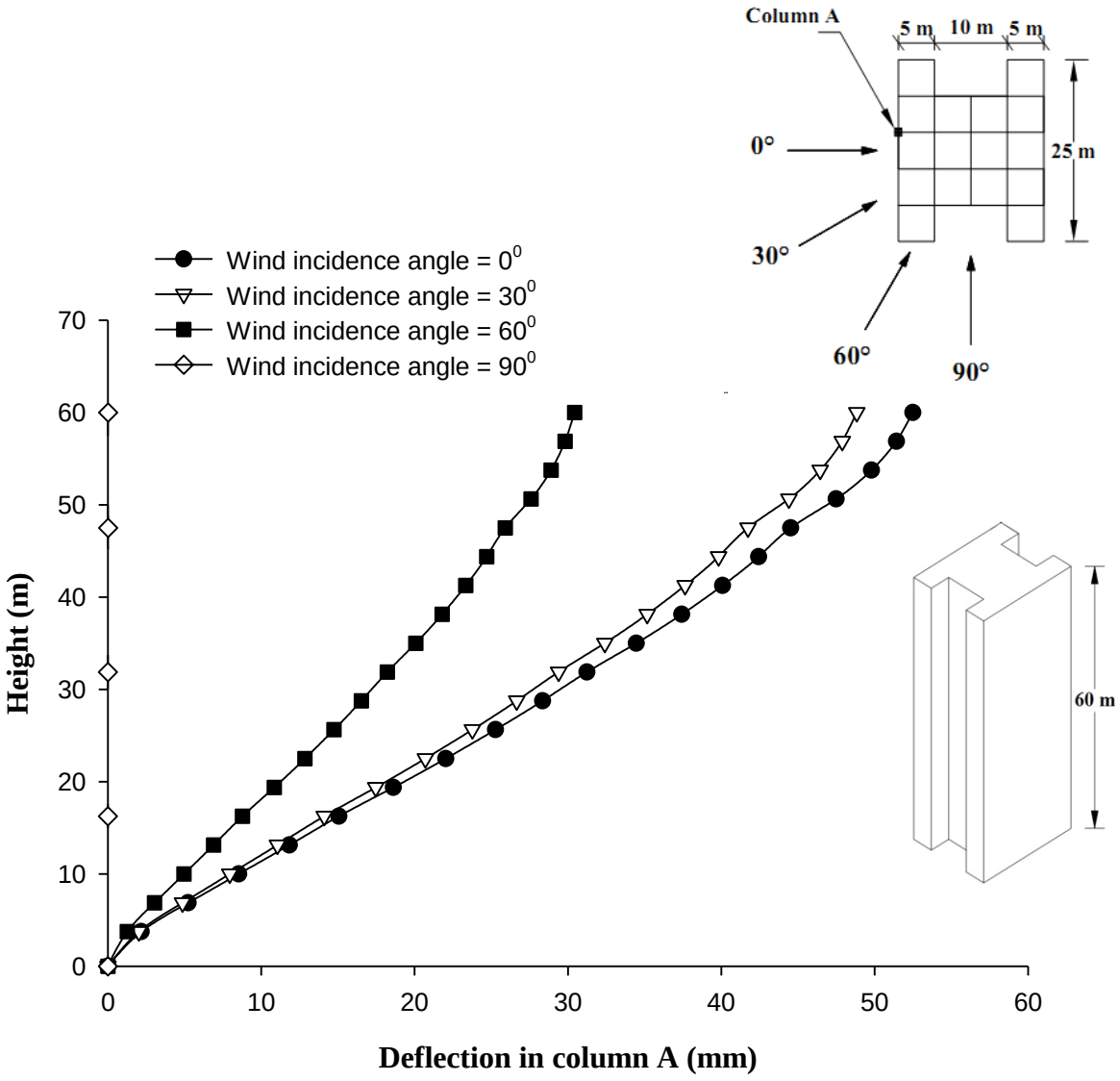


**Fig. 6.72 Effect of wind incidence angle on horizontal displacement of column-A of I-Shape-1 building**

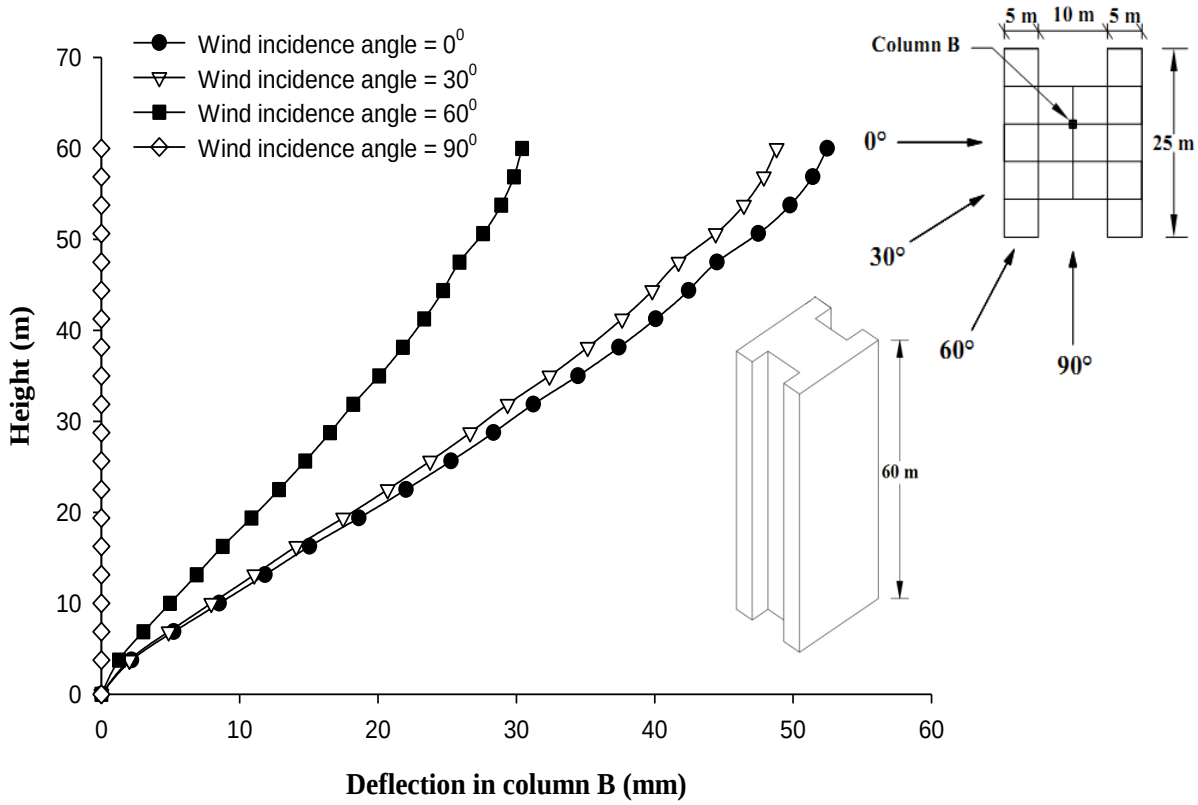


**Fig. 6.73 Effect of wind incidence angle on horizontal displacement of column-B of I-Shape-1 building**

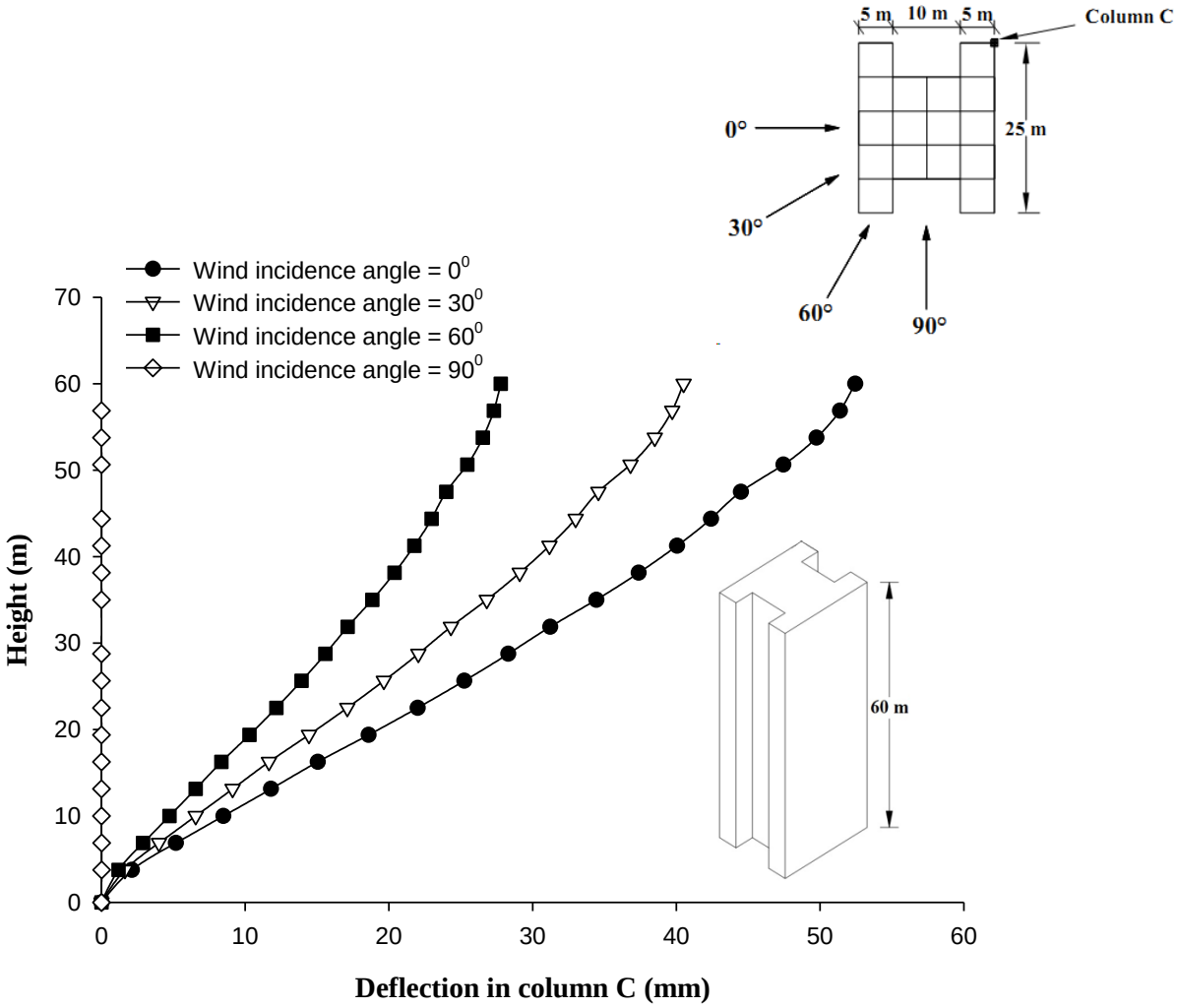


**Fig. 6.74 Effect of wind incidence angle on horizontal displacement of column-C of I-Shape building**

### 6.4.5 Fish Shape-1 Building

#### 6.4.5.1 Forces in columns

Figures 6.75 to 6.77 present the comparison of axial force on three typical columns namely column-A, B and C of Fish Shape-1 building respectively. Axial force in all columns is highly affected by wind incidence angle. In case of column-A (Fig. 6.75), minimum axial force is observed at $0^0$ wind incidence angle which increases gradually with increase in wind incidence angle. In case of column-B (Fig. 6.76), it is observed that maximum axial force is observed at $0^0$ wind incidence angle and minimum at $180^0$. Maximum axial force is observed at $60^0$ wind incidence angle in case of column-C (Fig. 6.77).

Torsional moment Mz developed in column-A, B and C are shown in Figs. 6.78 to 6.80 respectively. Similar moment variation pattern is observed in all columns with maximum twisting moment at $150^0$ wind incidence angle. Twisting moment is zero near top portion of the columns.

Moment about 'X' axis i.e. Mx plotted along height is shown in Figs. 6.81 to 6.83 for column-A, B and C respectively. Moment Mx is maximum at $180^0$ wind incidence angle and minimum at $0^0$ in case of column-A. For column-B and C similar pattern is observed for moment Mx with maximum value at $0^0$ wind incidence angle but difference in magnitude is large.

My i.e. moment about 'Y' axis are plotted in Figs. 6.84 to 6.86 along the height for column-A, B and C respectively. From 80% height to top end, same moment variation is observed at all wind incidence angles in case of column-A, B and C but the magnitude is different for lower parts. For column-A, maximum moment is observed at $90^0$ wind incidence angle and minimum at $0^0$ wind incidence angle. For column-B and C, maximum moment is approximately same.

#### 6.4.5.2 Displacement of columns

In case of Fish Shape-1 building, deflection of columns are not exactly zero, but close to zero (Figs. 6.87 to 6.89) at $90^0$ angle. It is maximum at $0^0$ wind incidence angle.

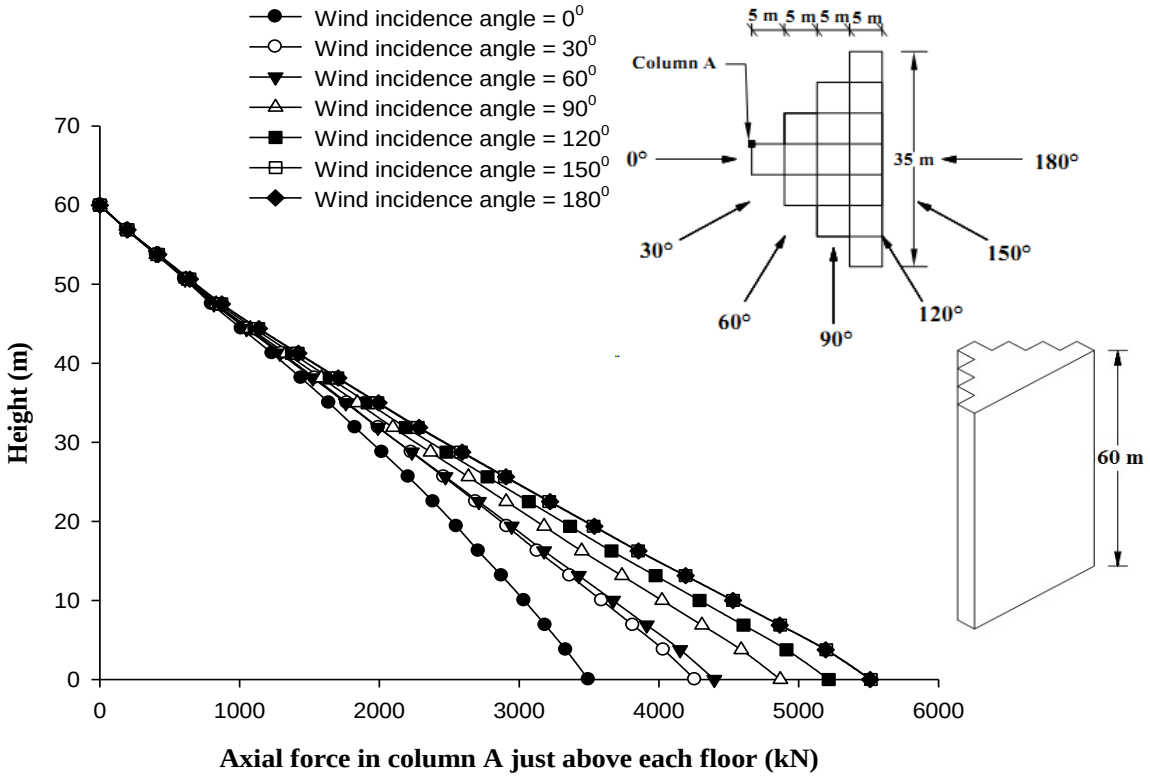


**Fig. 6.75 Effect of wind incidence angle on axial force in column-A of Fish Shape-1 building**

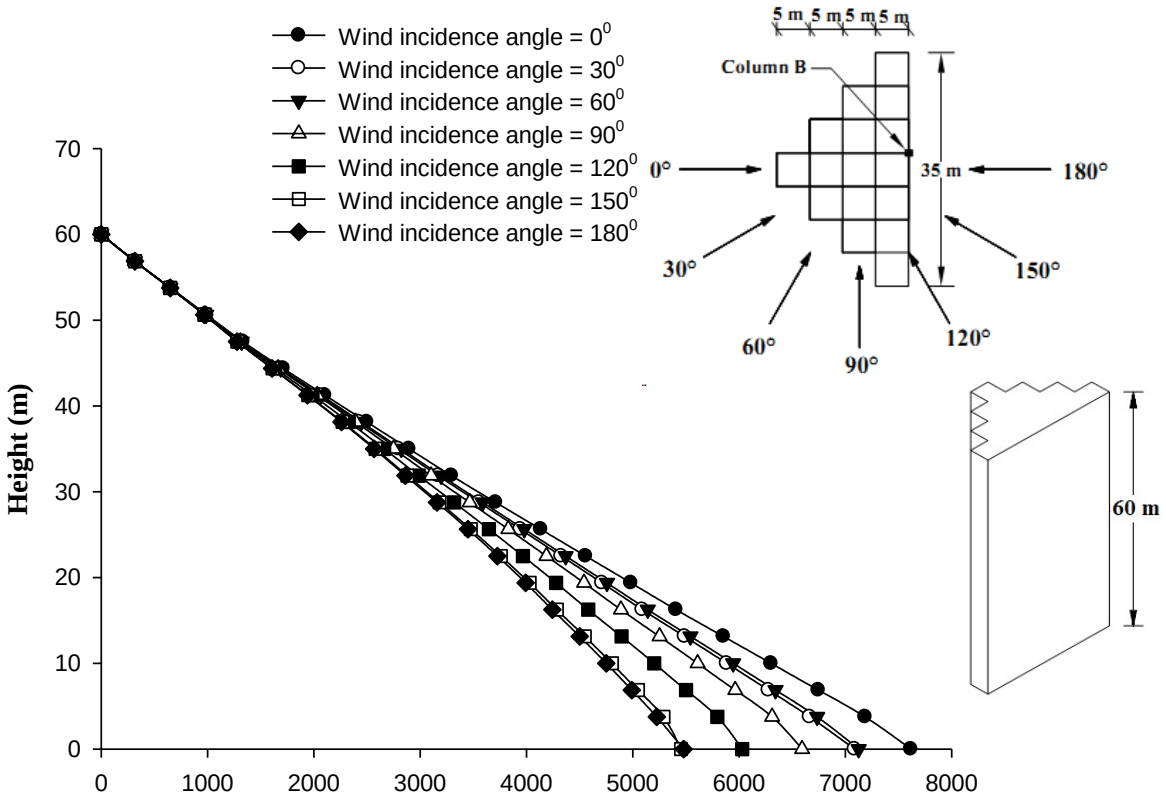


**Fig. 6.76 Effect of wind incidence angle on axial force in column-B of Fish Shape-1 building**

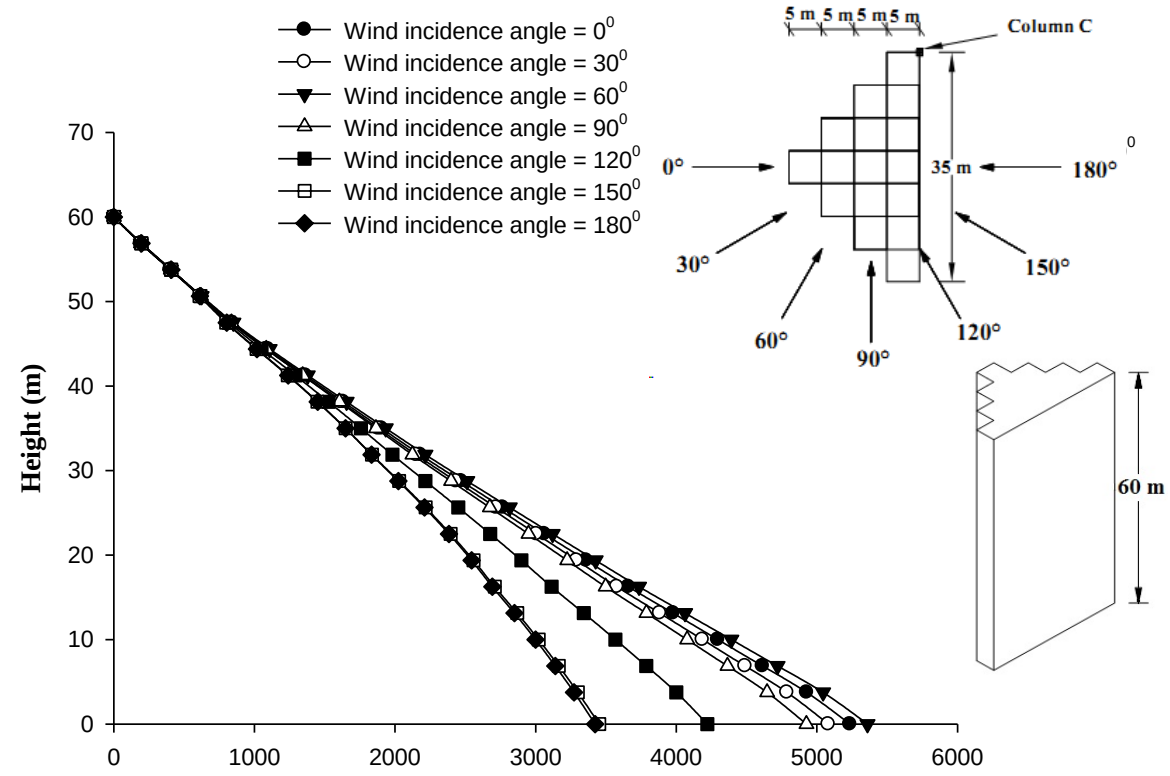


**Axial force in column C just above each floor (kN)**

**Fig. 6.77 Effect of wind incidence angle on axial force in column-C of Fish Shape-1 building**

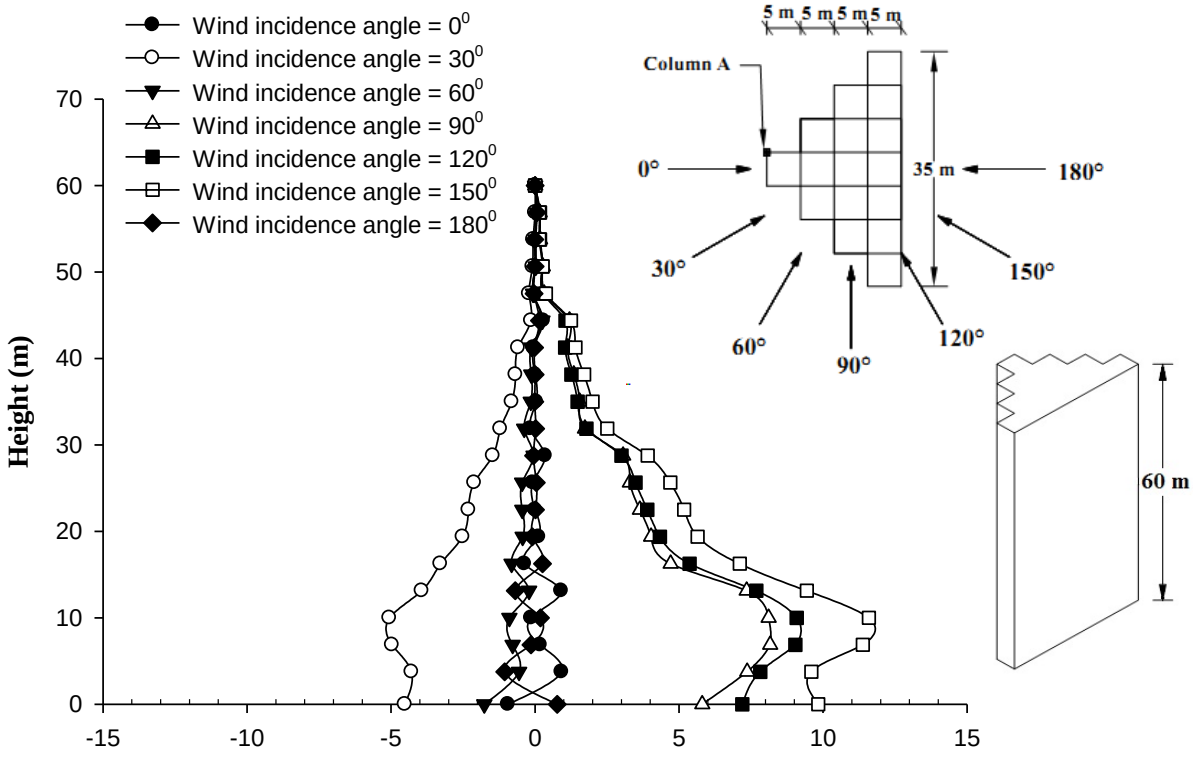


**Mz in column A just above each floor (kN-m)**

**Fig. 6.78 Effect of wind incidence angle on twisting moment Mz in column-A of Fish Shape-1 building**

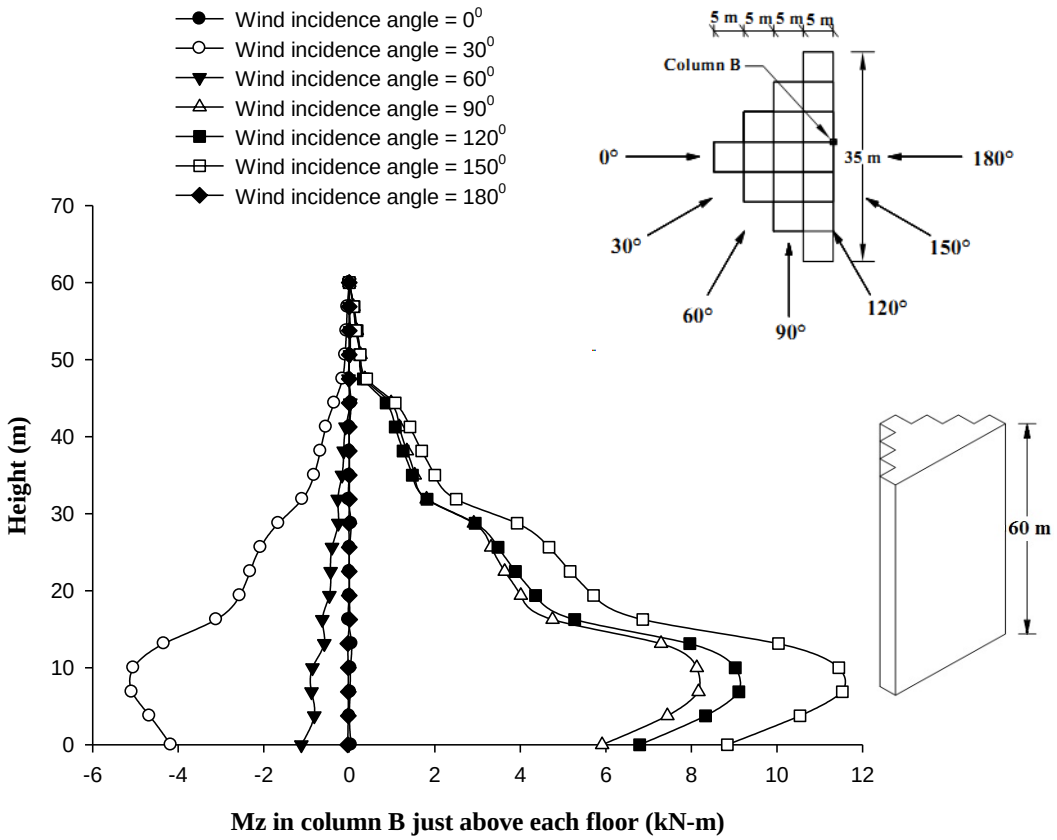


**Fig. 6.79 Effect of wind incidence angle on twisting moment Mz in column-B of Fish Shape-1 building**

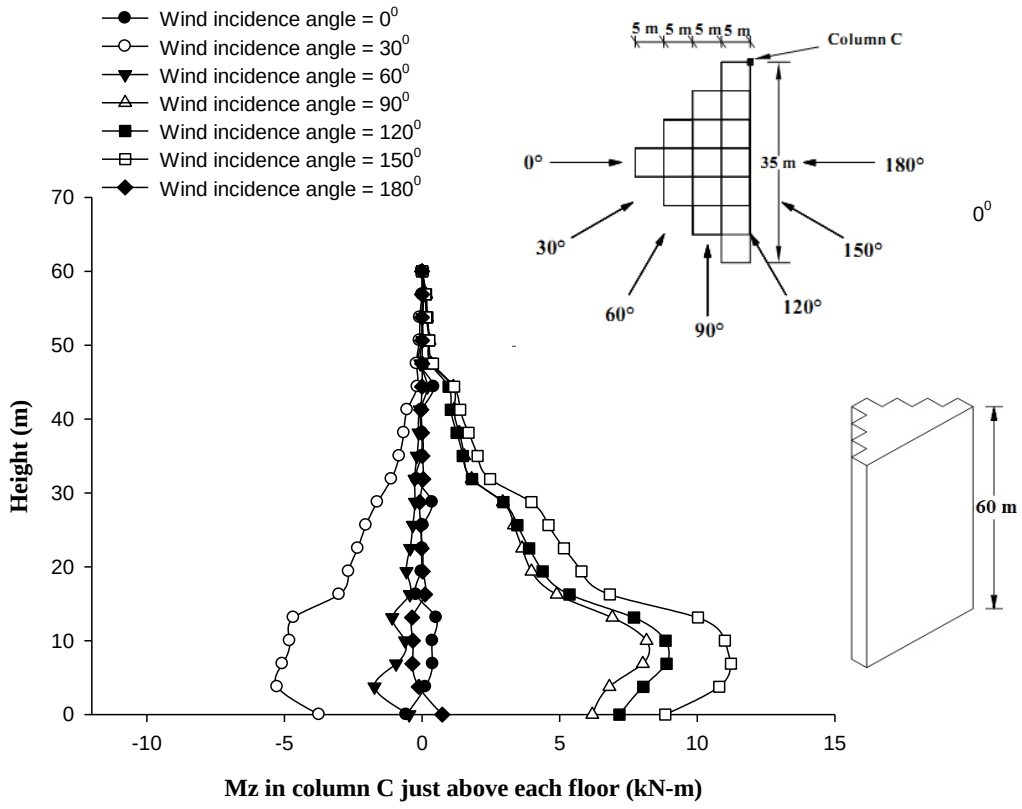


**Fig. 6.80 Effect of wind incidence angle on twisting moment in column-C of Fish Shape-1 building**

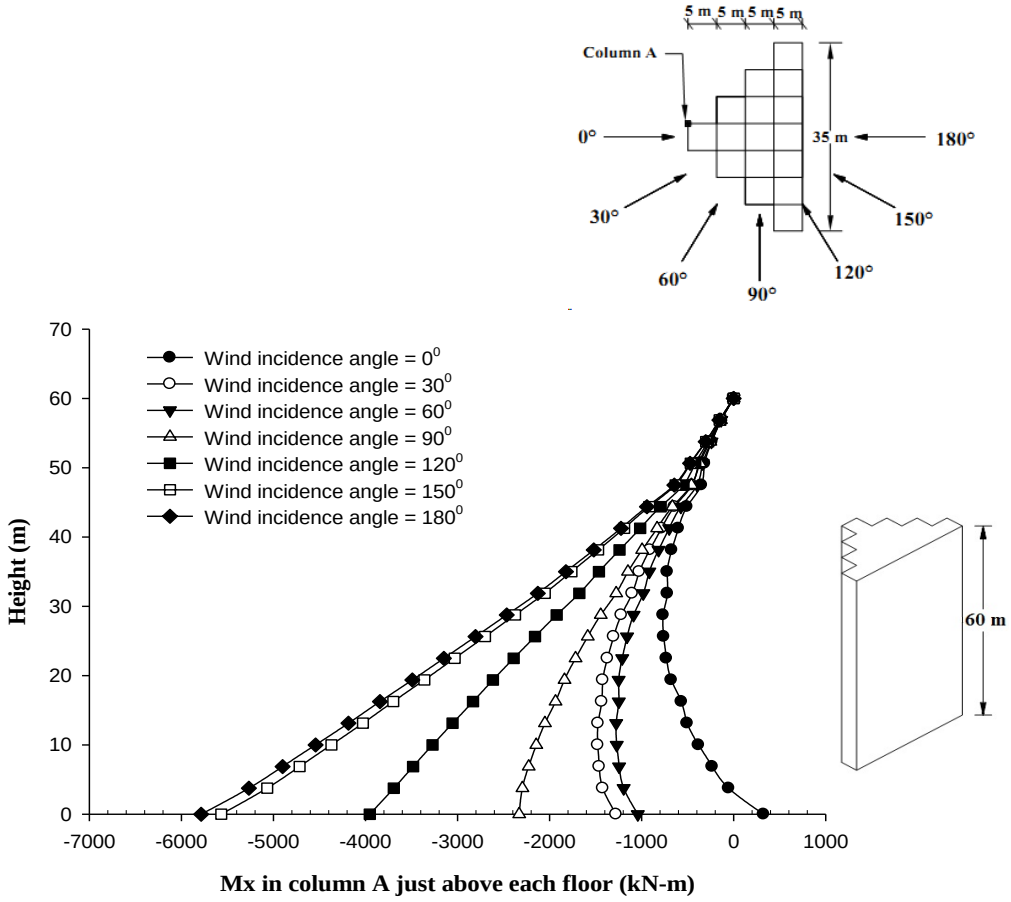


**Fig. 6.81 Effect of wind incidence angle on Mx (global) in column-A of Fish Shape-1 building**

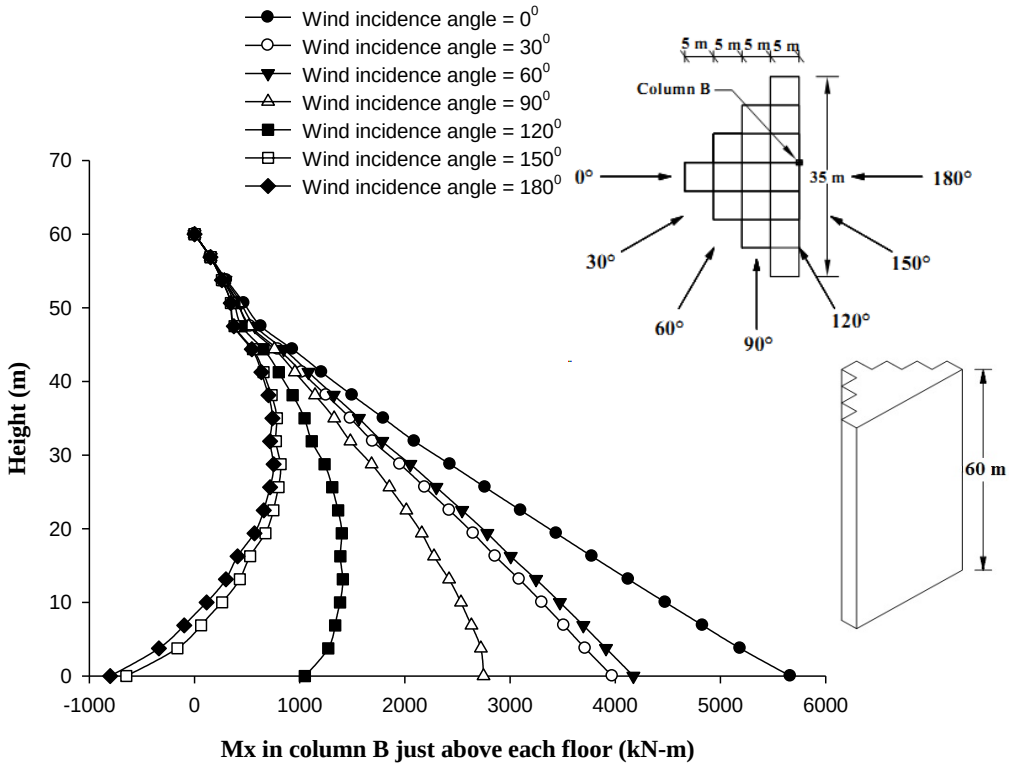


**Fig. 6.82 Effect of wind incidence angle on Mx (global) in column-B of Fish Shape-1 building**

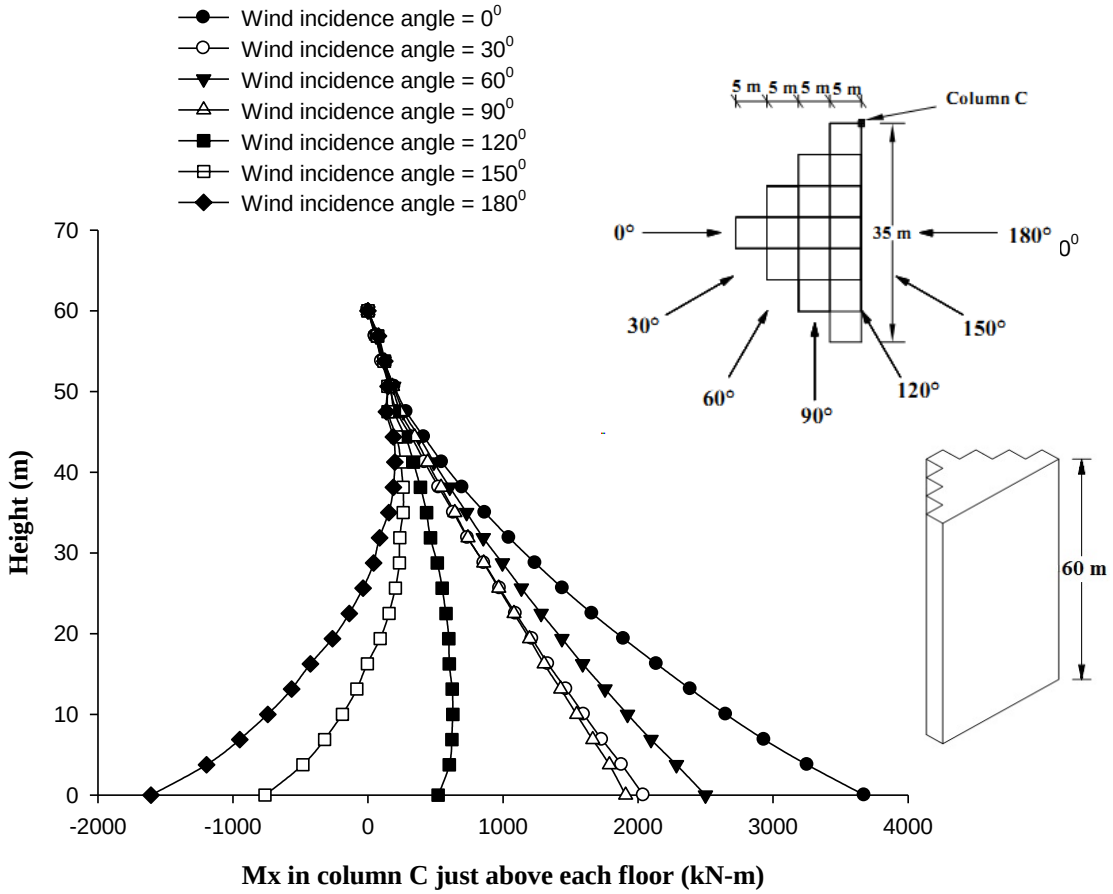


**Fig. 6.83 Effect of wind incidence angle on Mx (global) in column-C of Fish Shape-1 building**

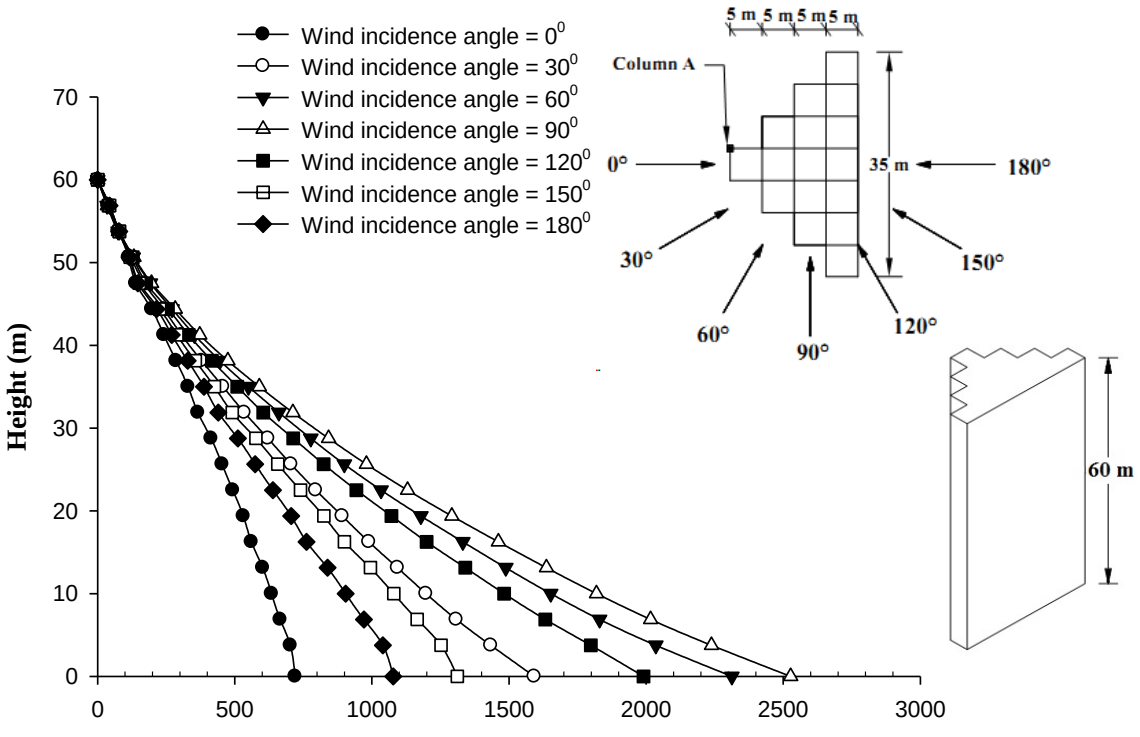


**Fig. 6.84 Effect of wind incidence angle on My (global) in column-A of Fish Shape-1 building**

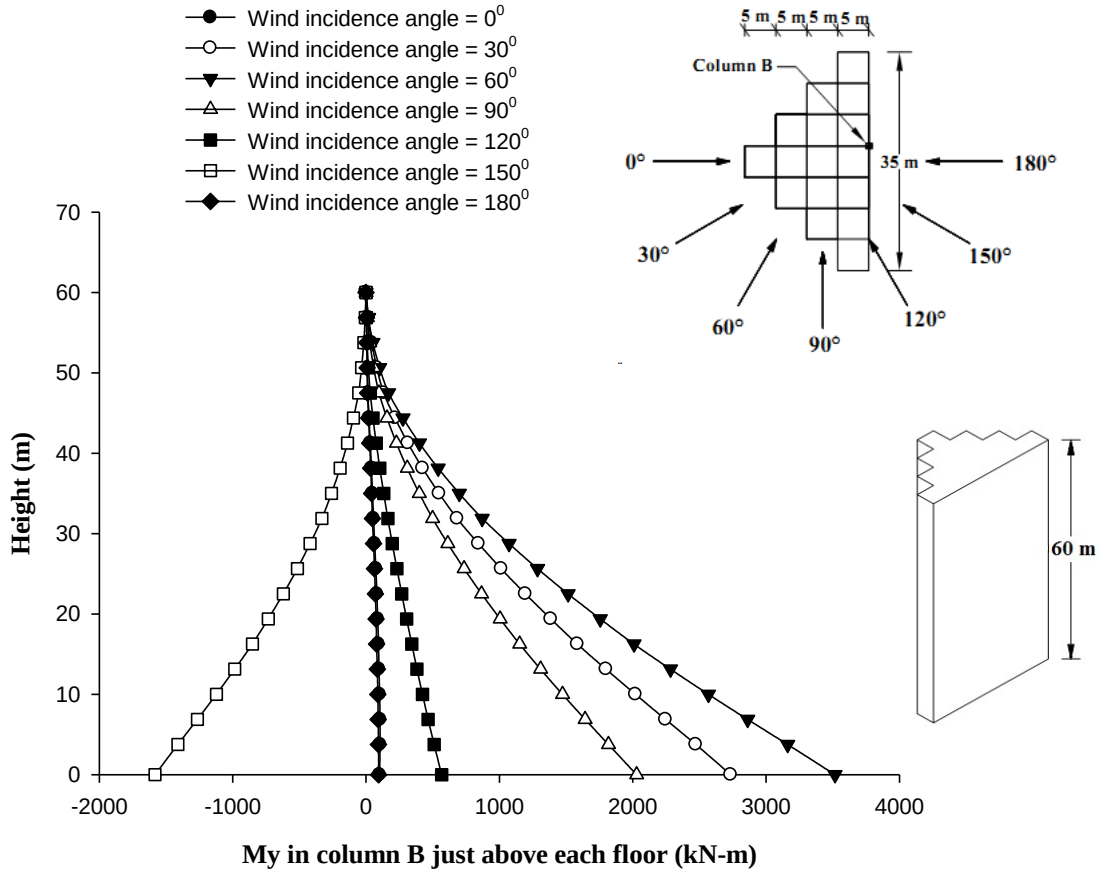


**Fig. 6.85 Effect of wind incidence angle on My (global) in column-B of Fish Shape-1 building**

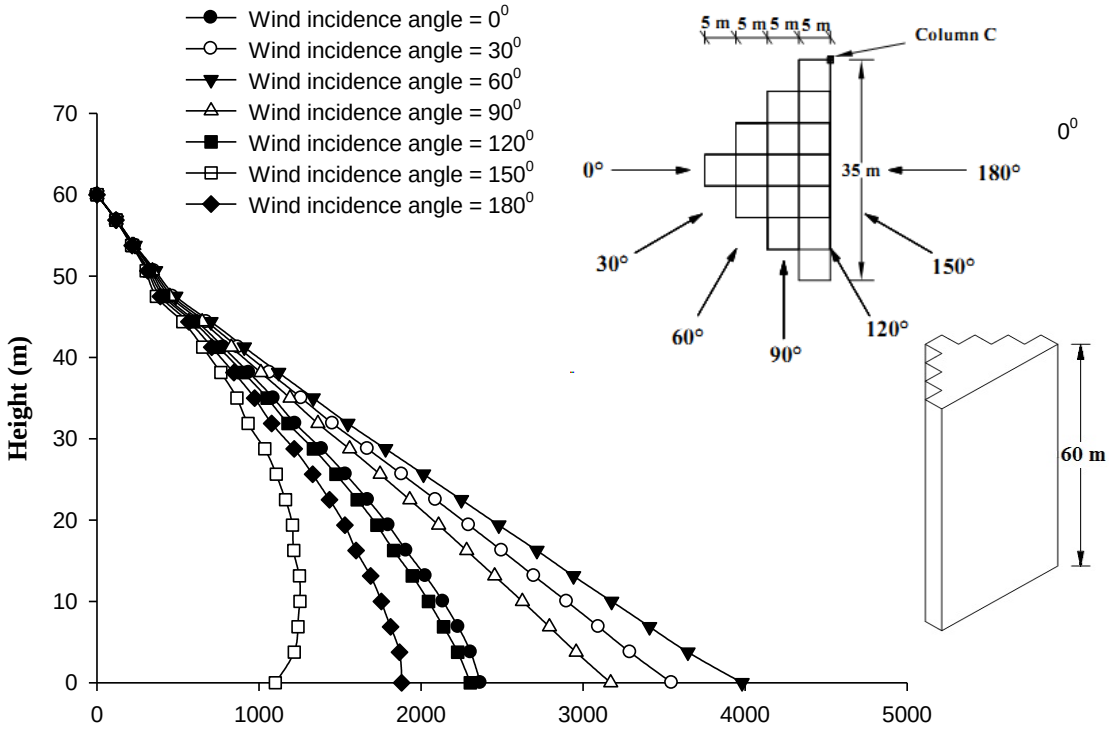


**Fig. 6.86 Effect of wind incidence angle on My (global) in column-C of Fish Shape building**

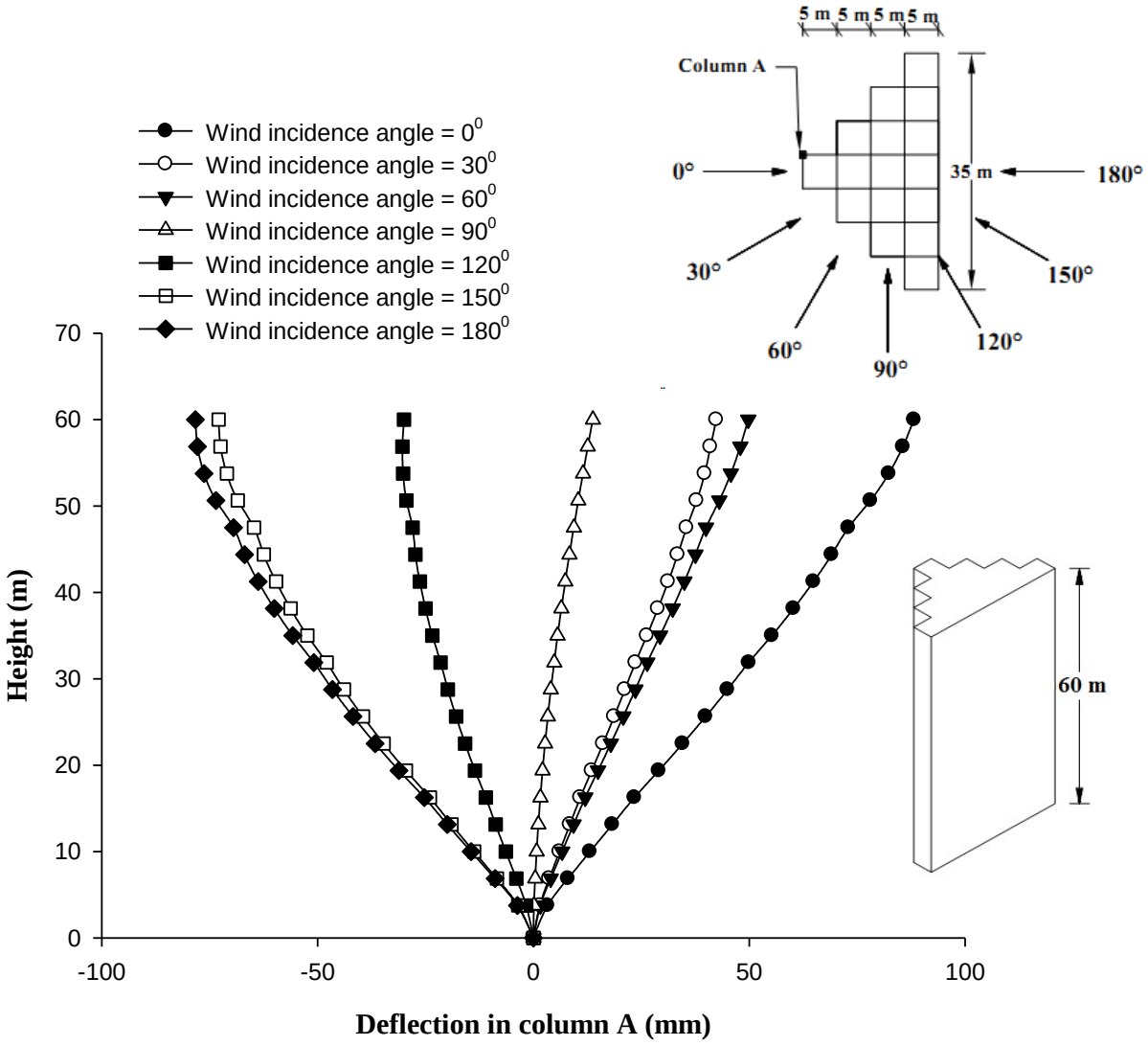


**Fig. 6.87 Effect of wind incidence angle on horizontal displacement of column-A of Fish Shape-1 building**

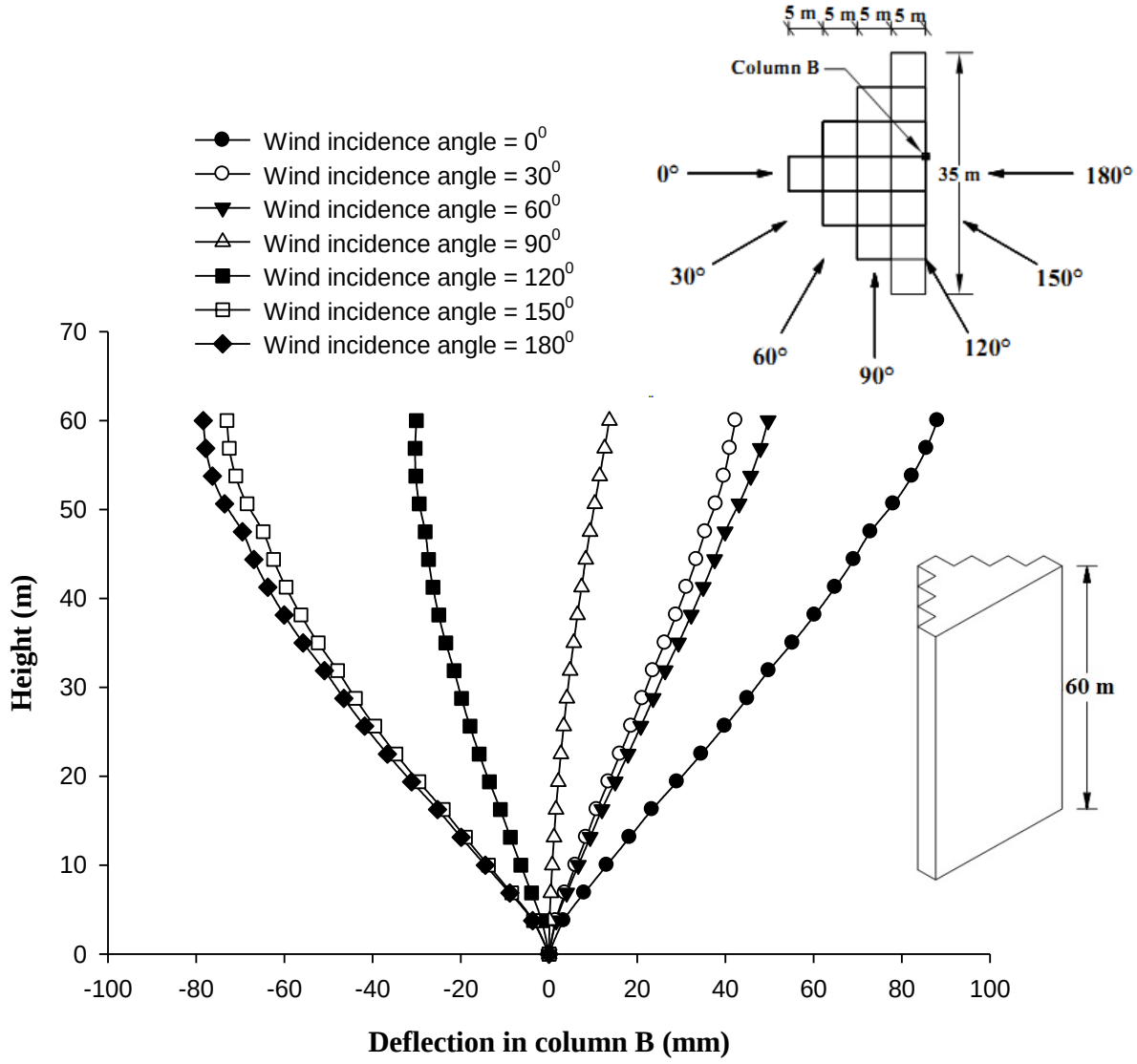


**Fig. 6.88 Effect of wind incidence angle on horizontal displacement of column-B of Fish Shape-1 building**

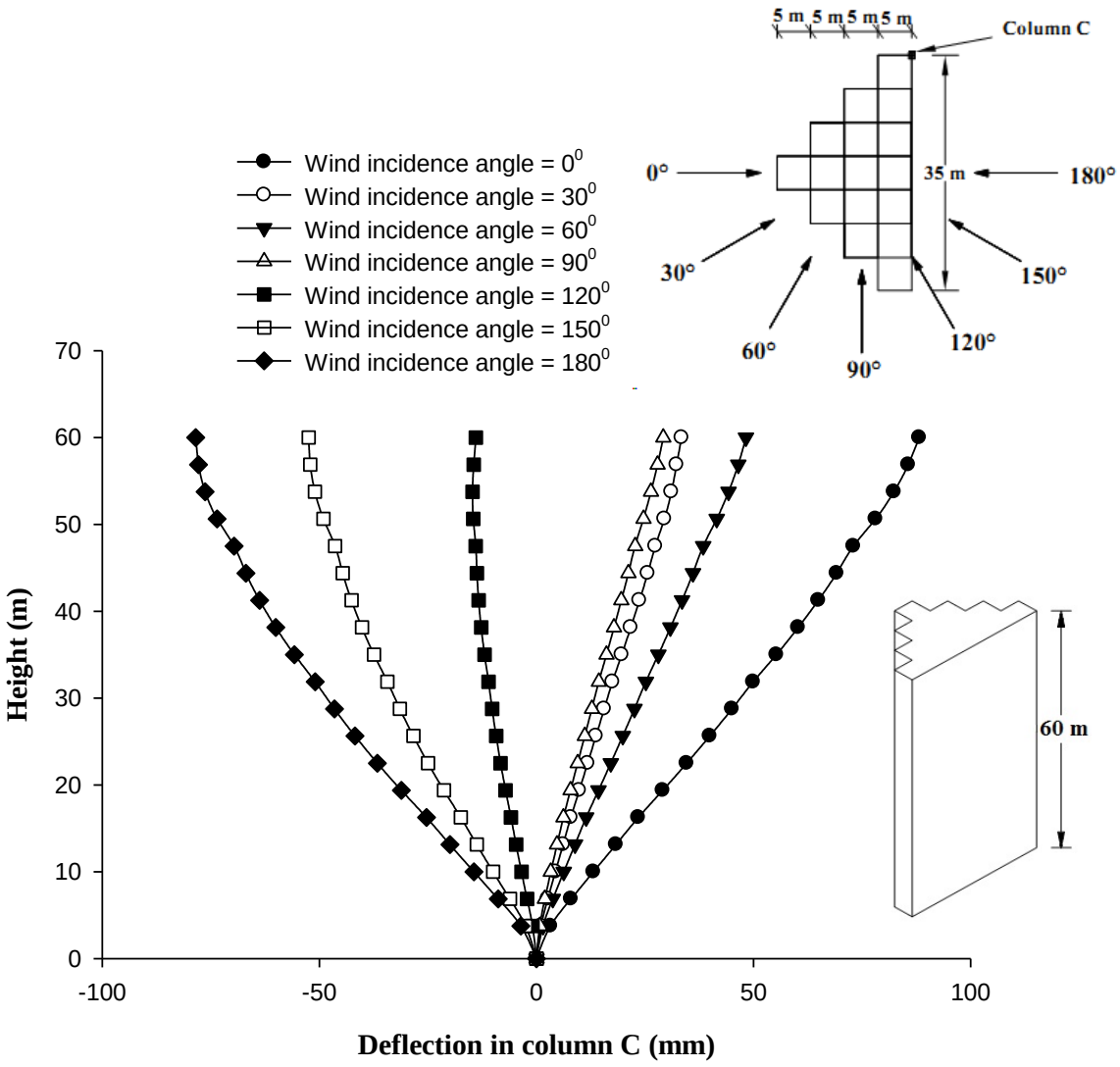


**Fig. 6.89 Effect of wind incidence angle on horizontal displacement of column-C of Fish Shape-1 building**

### 6.4.6 Fish Shape-2 Building

#### 6.4.6.1 Forces in columns

Variation of axial force in column-A, B and C with wind incidence angle is shown in Figs. 6.90 to 6.92. Influence of wind incidence angle on axial force in columns is not much.

Figures 6.93 to 6.95 represents variation of torsional moment Mz in these three columns with angle of wind attack. It is maximum in all columns at $120^0$ wind angle followed by its value at $90^0$ angle.

Effects of wind incidence angle on moment about 'X' i.e. Mx can be seen in Figs 6.96 to 6.98 for column-A, B and C respectively. Variation of My, i.e. moment about 'Y' axis is shown in Figs. 6.99 to 6.101. Mx is highly influenced by wind incidence angle. It is maximum at $180^0$ wind angle in column-A, whereas it is maximum at $0^0$ angle in column-B and C. My is also highly influenced by wind direction. It is maximum at $90^0$ angle in column-A with very close values at $60^0$ angle. In case of column-B and C, it is maximum at $60^0$ angle.

#### 6.4.6.2 Deflections of columns

In case of Fish Shape-2 building (Figs. 6.102 to 6.104), horizontal deflection is maximum at $180^0$ angle in all columns. It is almost zero at $90^0$ angle.

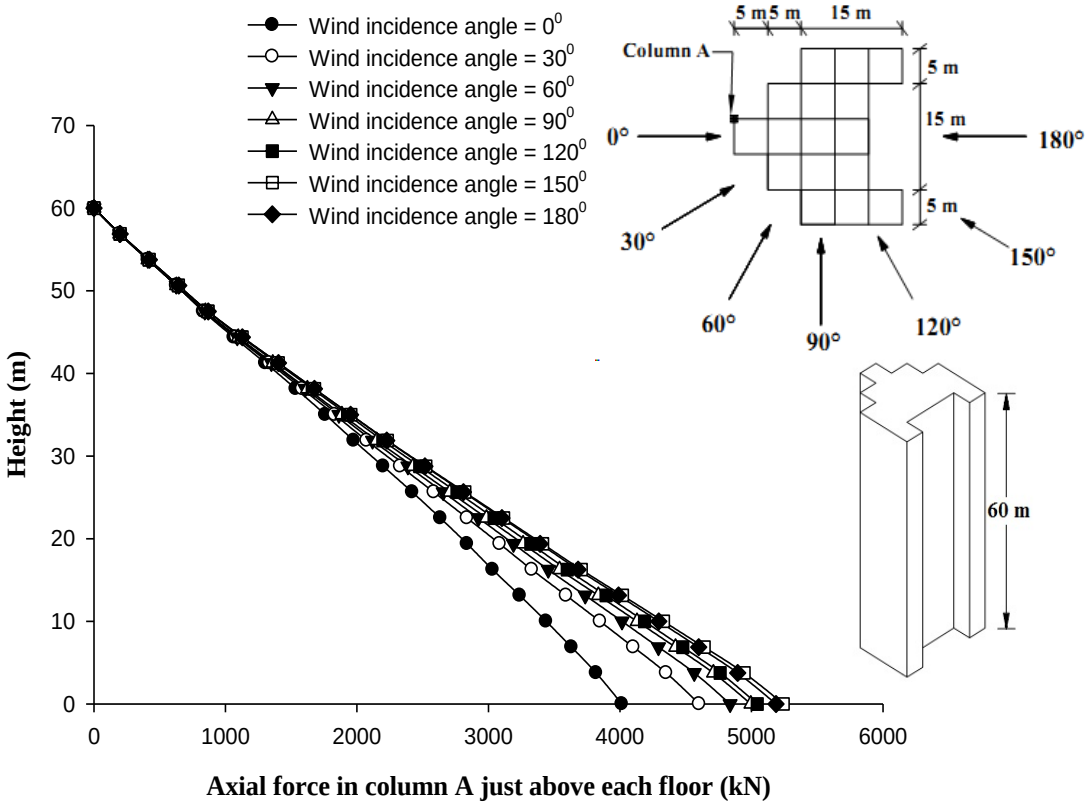


**Fig. 6.90 Effect of wind incidence angle on axial force in column-A of Fish Shape-2 building**

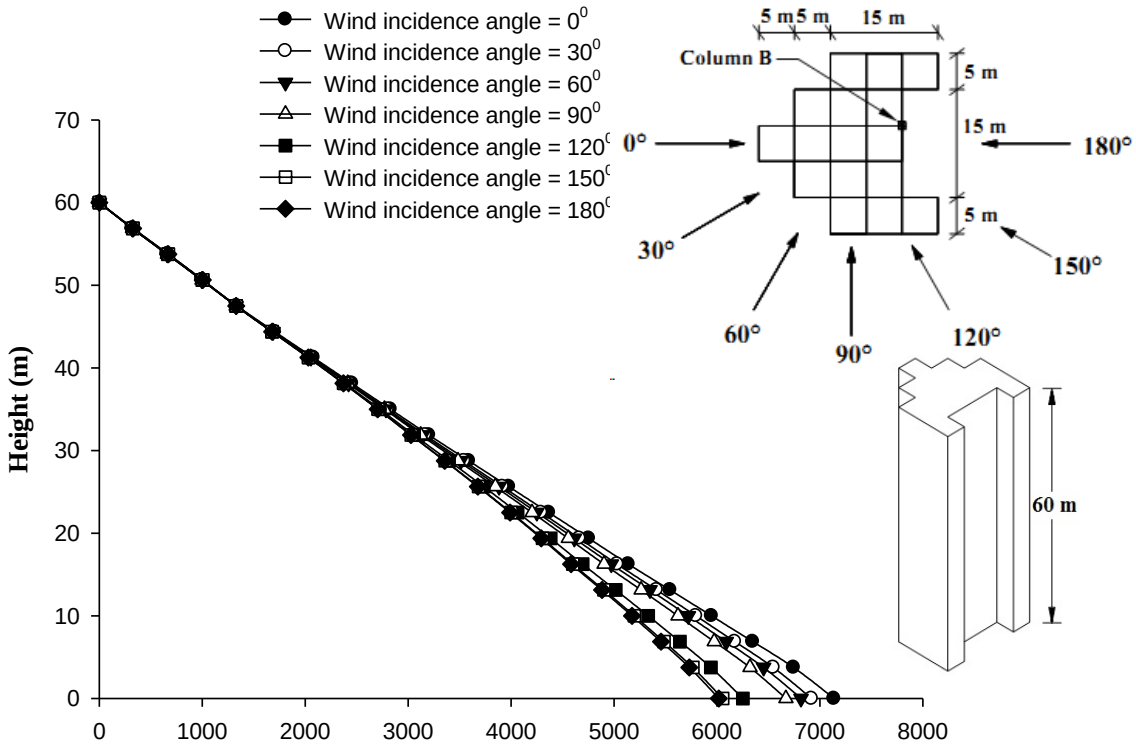


**Fig. 6.91 Effect of wind incidence angle on axial force in column-B of Fish Shape-2 building**

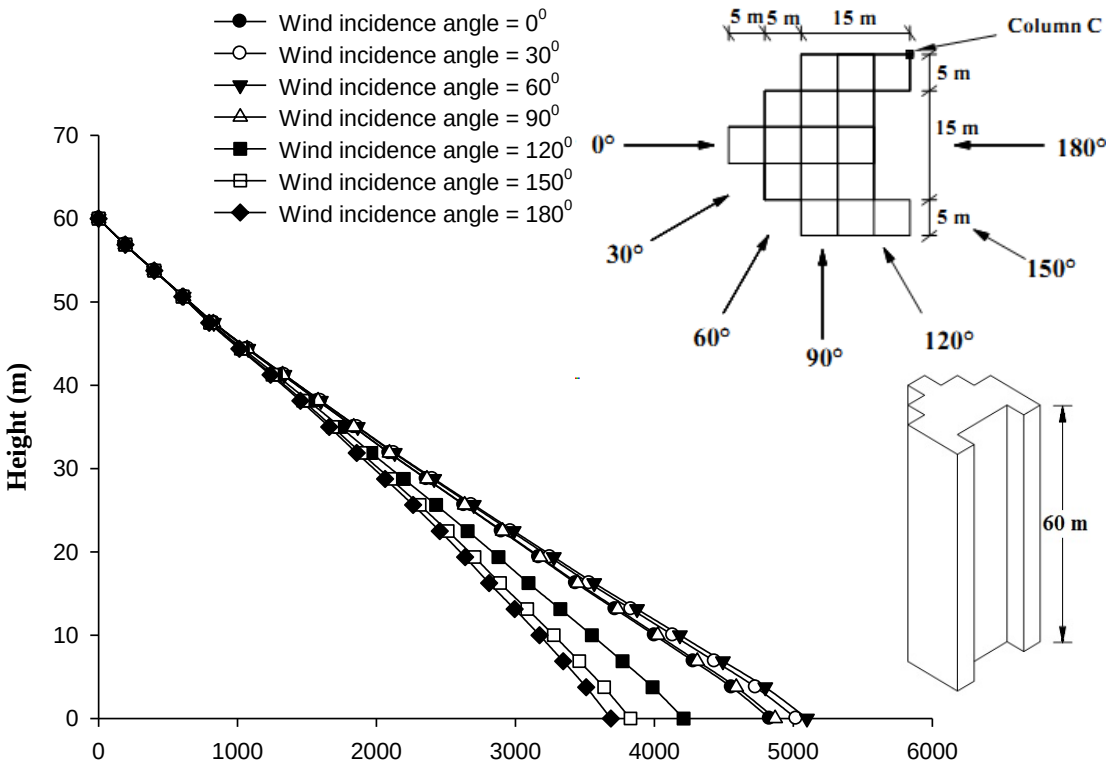


**Fig. 6.92 Effect of wind incidence angle on axial force in column-C of Fish Shape-2 building**

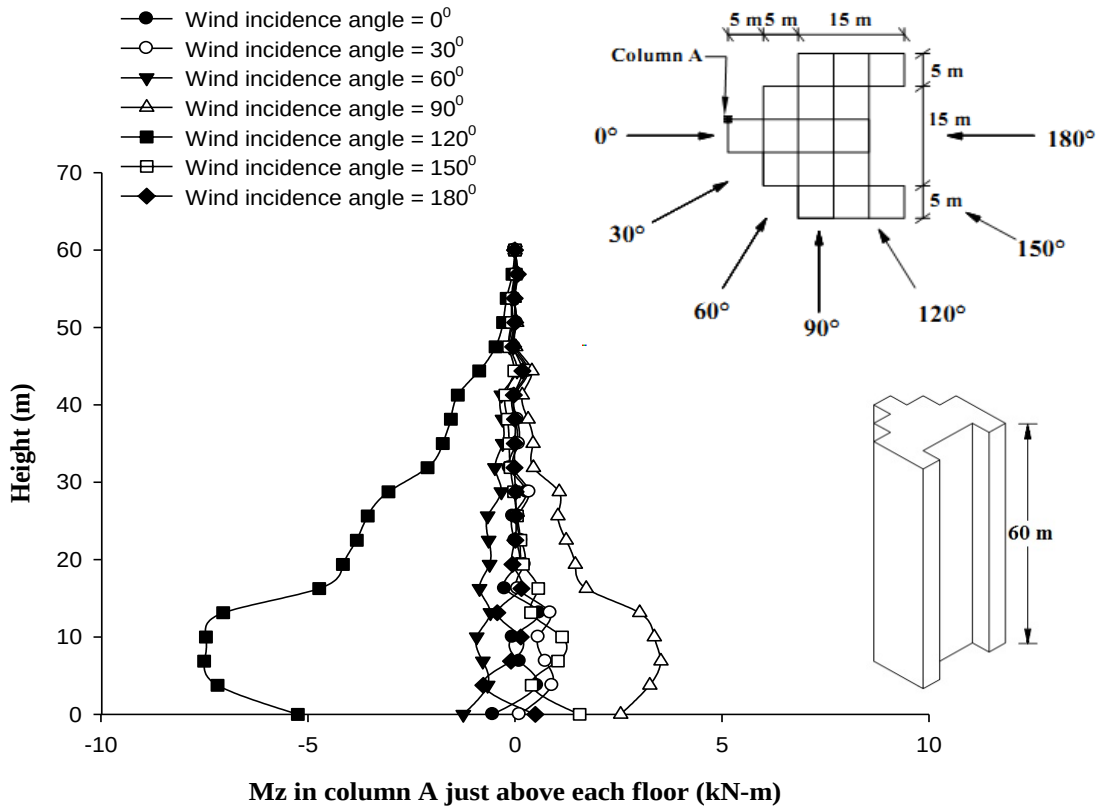


**Fig. 6.93 Effect of wind incidence angle on twisting moment Mz in column-A of Fish Shape-2 building**

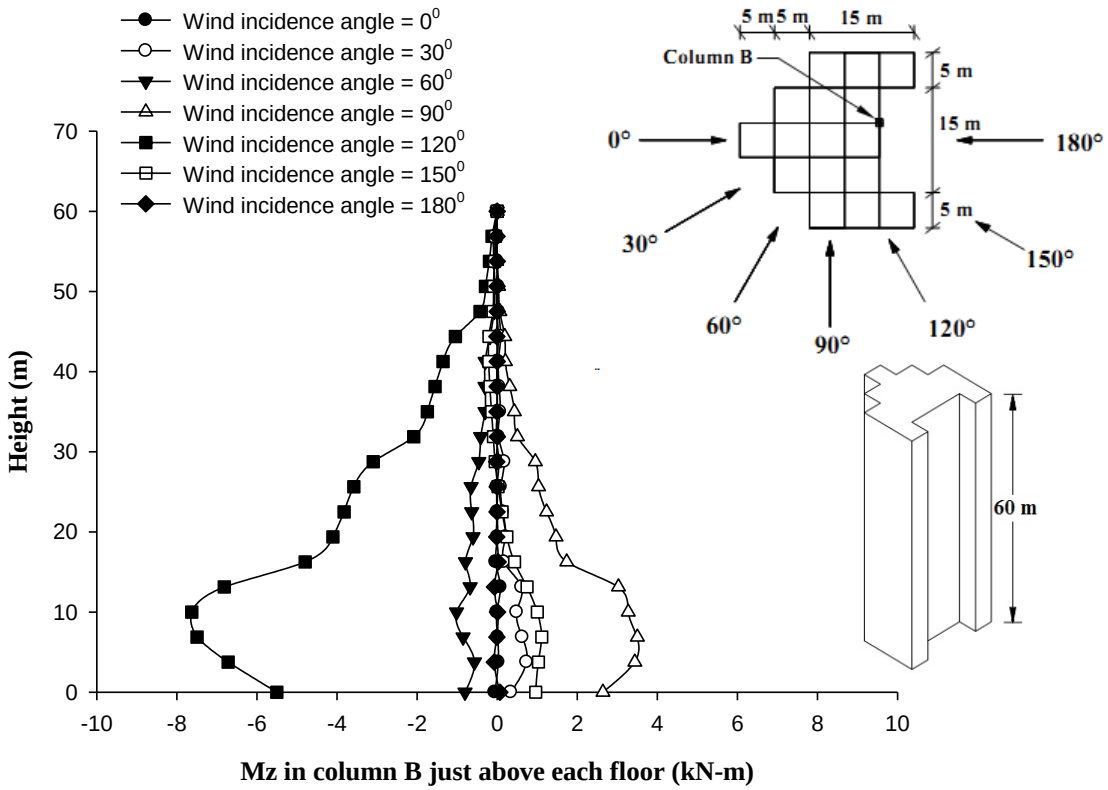


**Fig. 6.94 Effect of wind incidence angle on twisting moment Mz in column-B of Fish Shape-2 building**

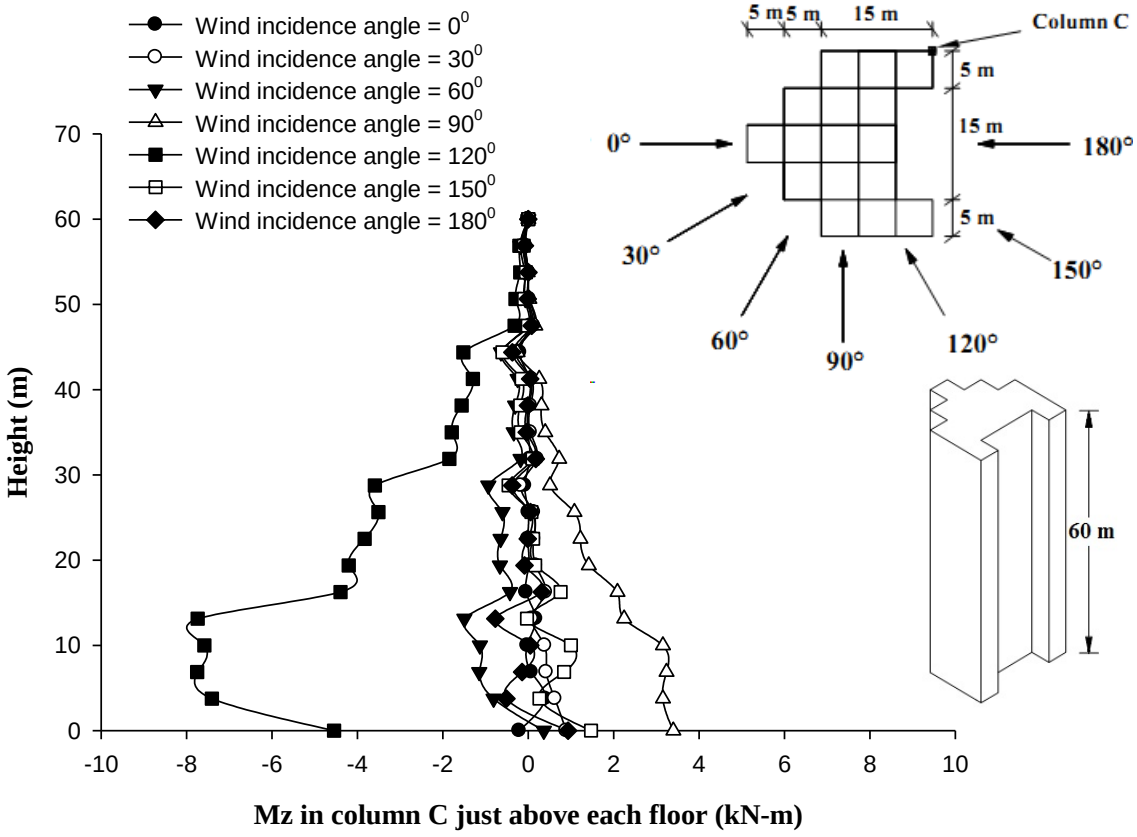


**Fig. 6.95 Effect of wind incidence angle on twisting moment Mz in column-C of Fish Shape-2 building**

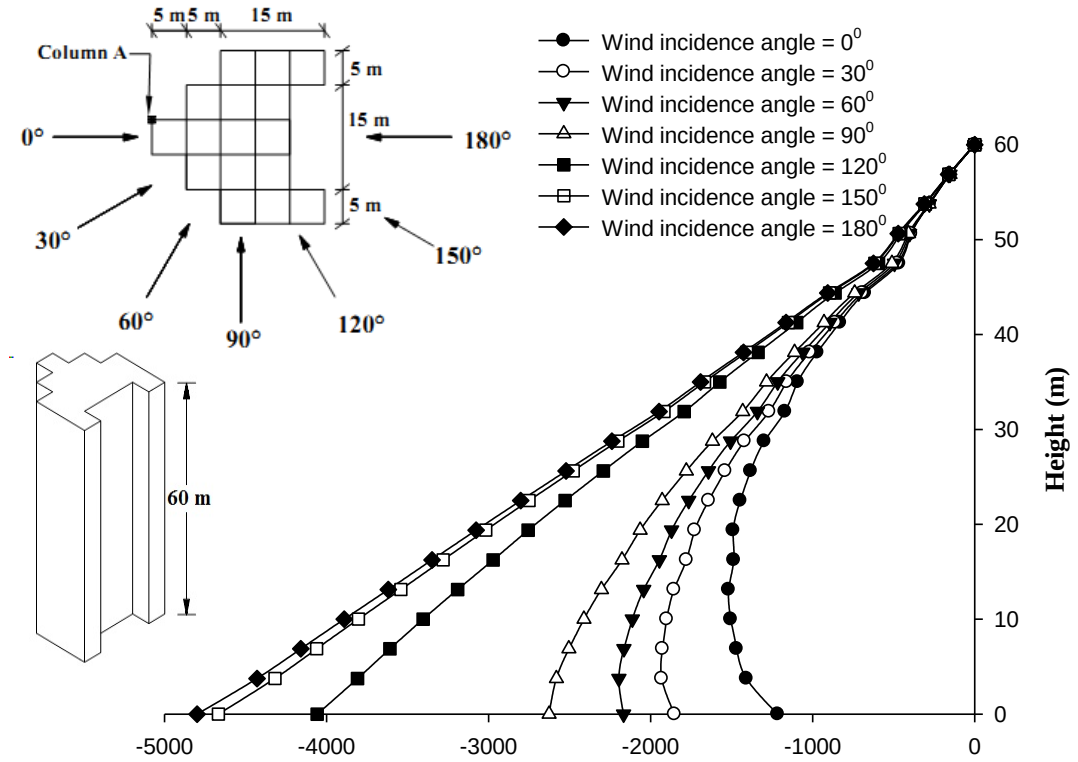


**Fig. 6.96 Effect of wind incidence angle on Mx (global) in column-A of Fish Shape-2 building**

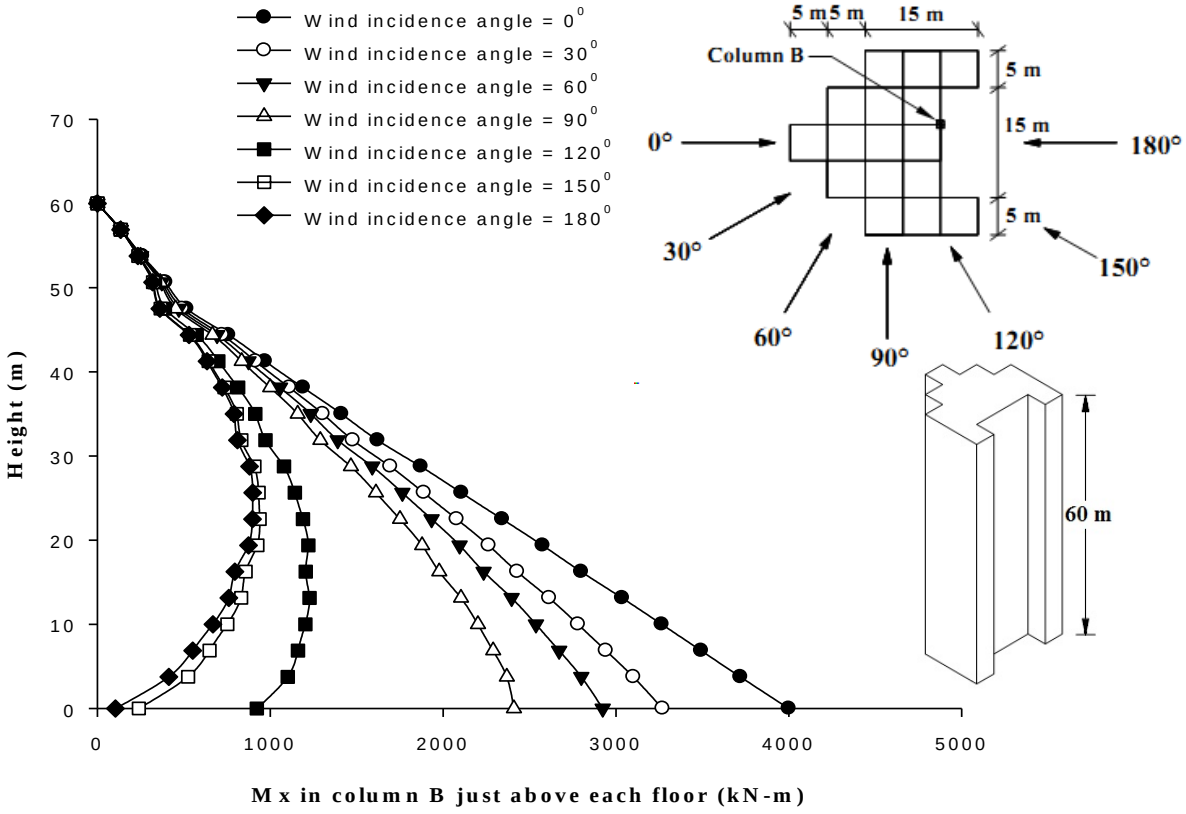


**Fig. 6.97 Effect of wind incidence angle on Mx (global) in column-B of Fish Shape-2 building**

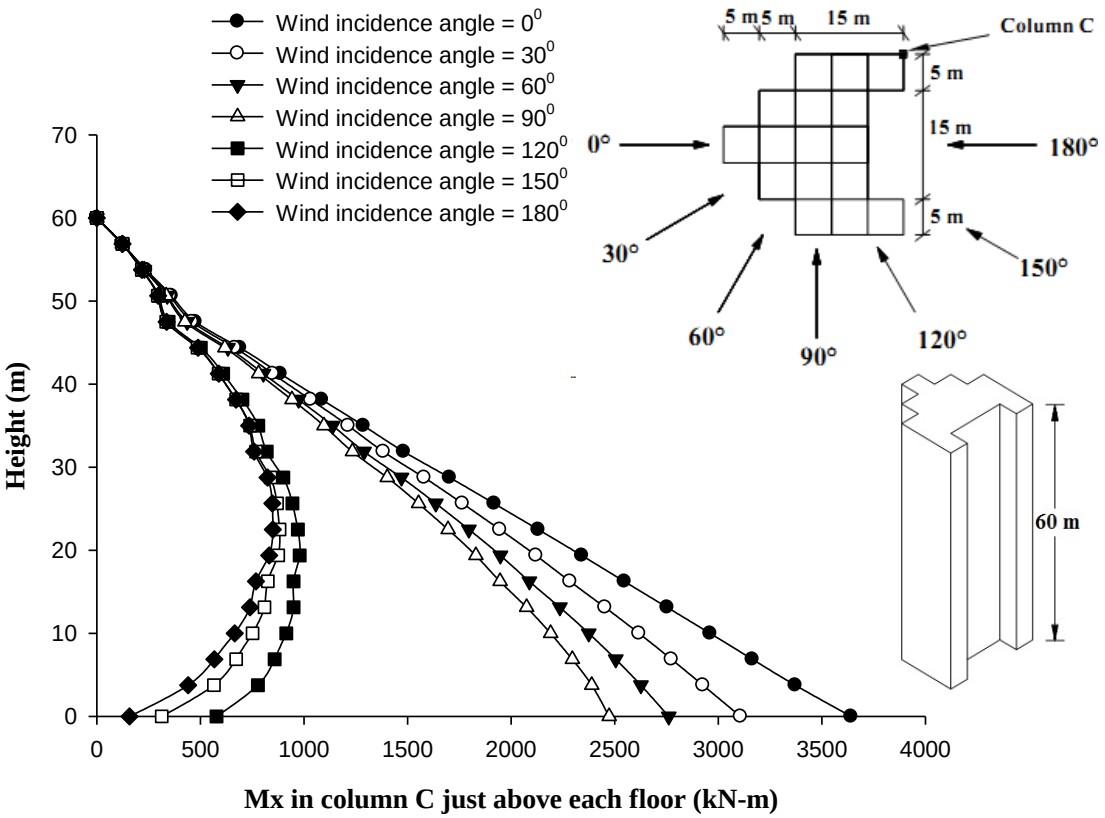


**Fig. 6.98 Effect of wind incidence angle on Mx (global) in column-C of Fish Shape-2 building**

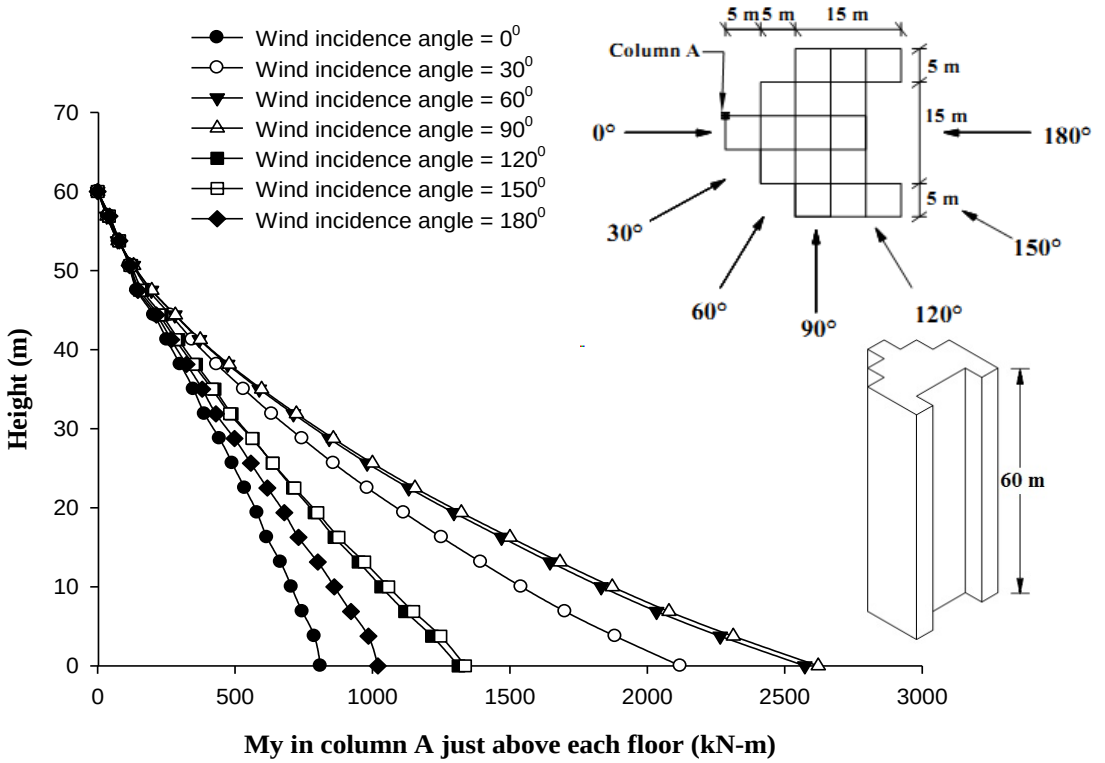


**Fig. 6.99 Effect of wind incidence angle on My (global) in column-A of Fish Shape-2 building**

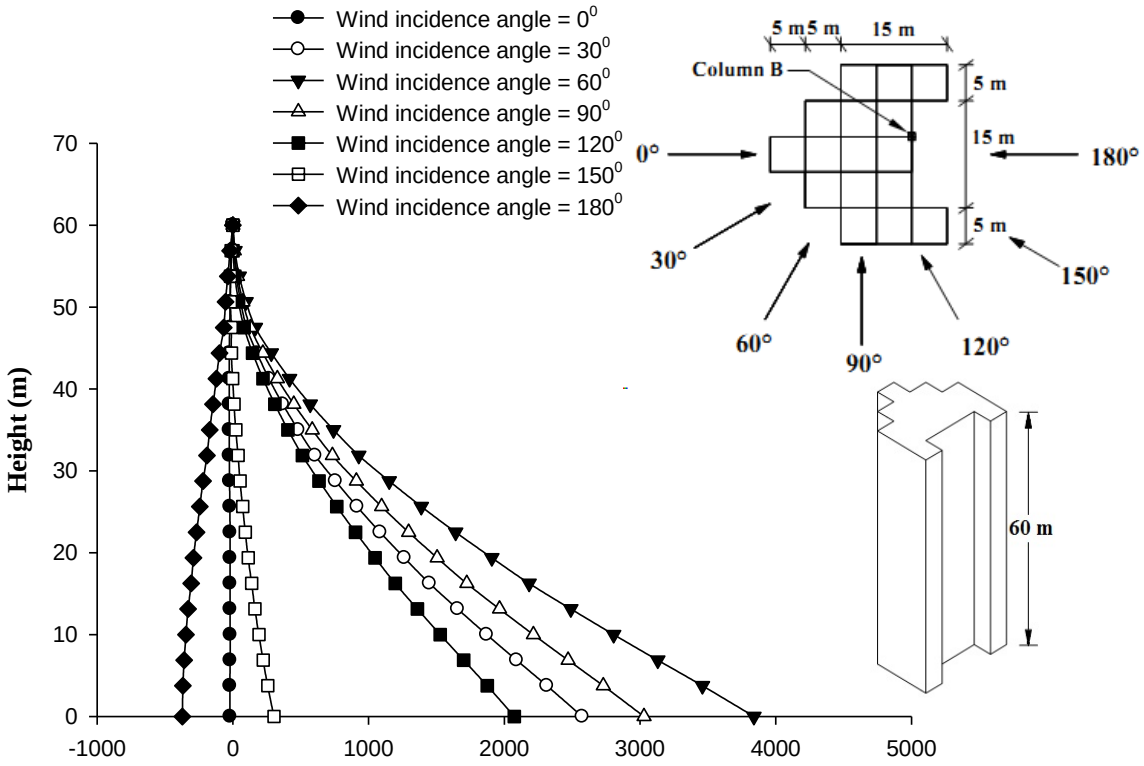


**Fig. 6.100 Effect of wind incidence angle on My (global) in column-B of Fish Shape-2 building**

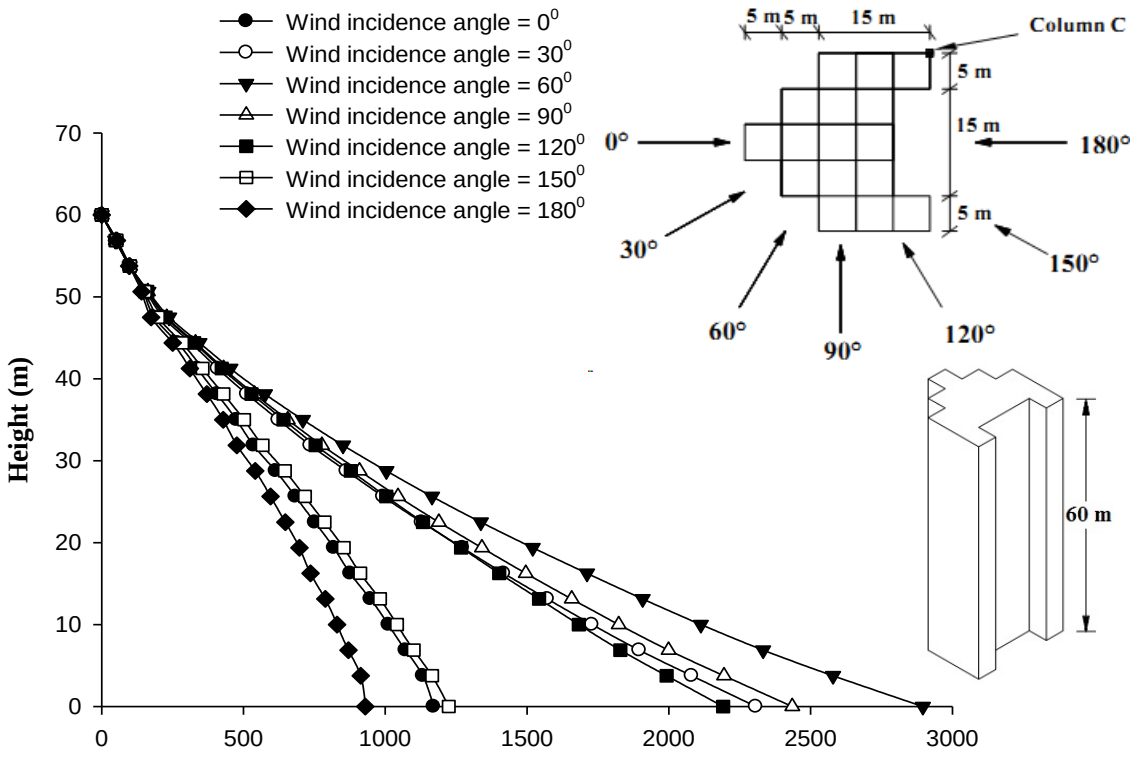


**Fig. 6.101 Effect of wind incidence angle on My (global) in column-C of Fish Shape-2 building**

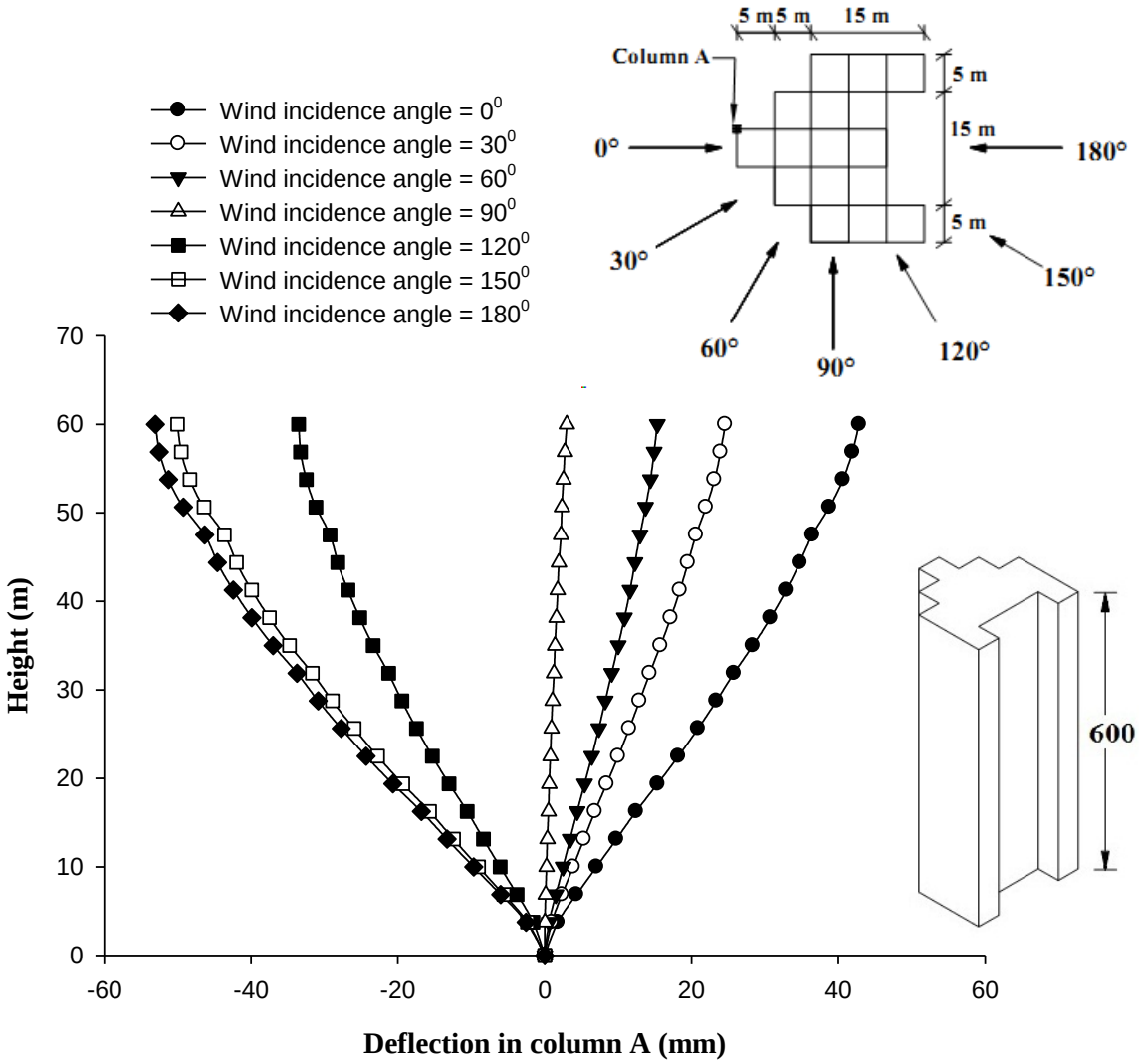


**Fig. 6.102 Effect of wind incidence angle on horizontal displacement column-A of Fish Shape-2 building**

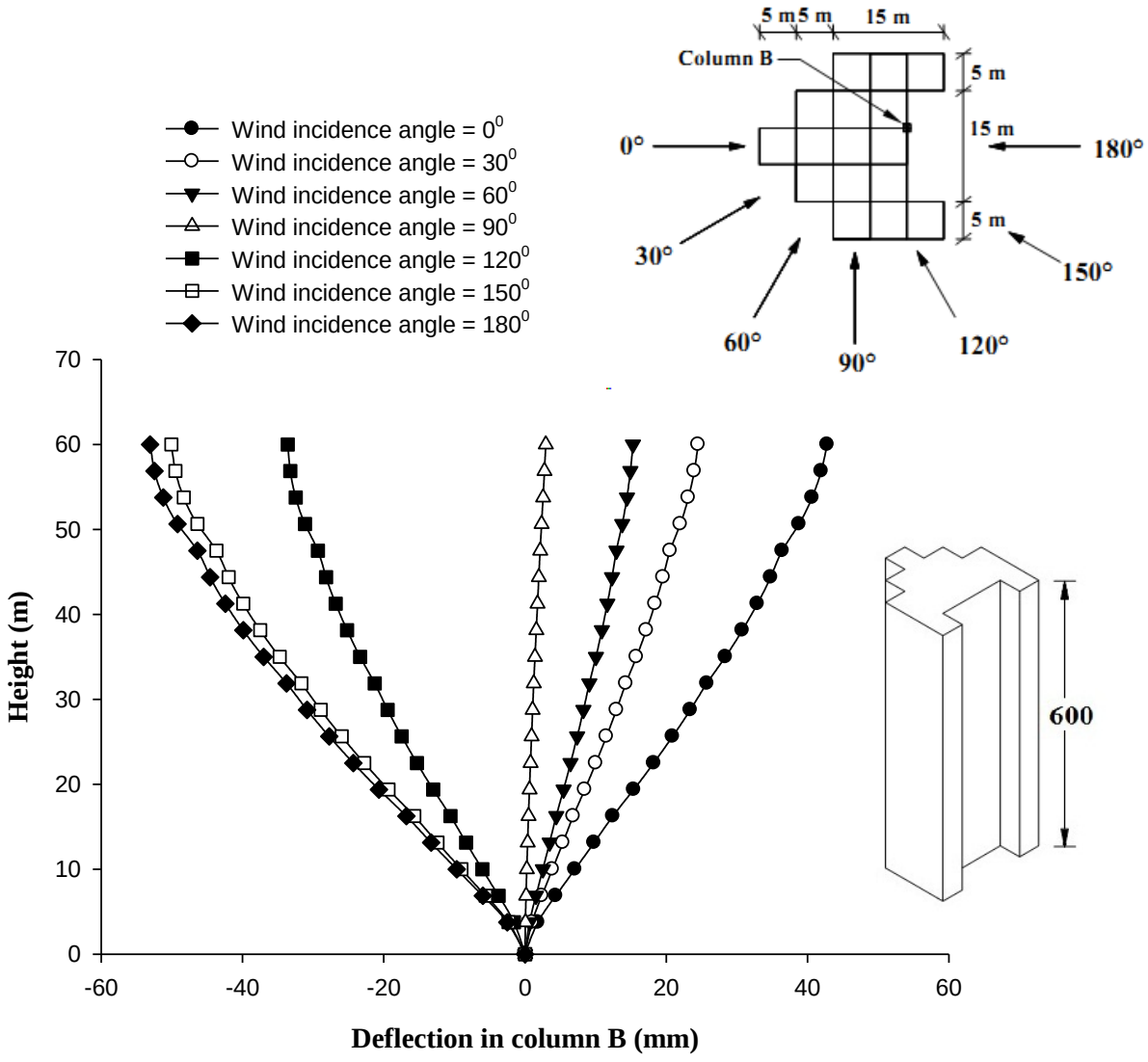


**Fig. 6.103 Effect of wind incidence angle on horizontal displacement of column-B of Fish Shape-2 building**

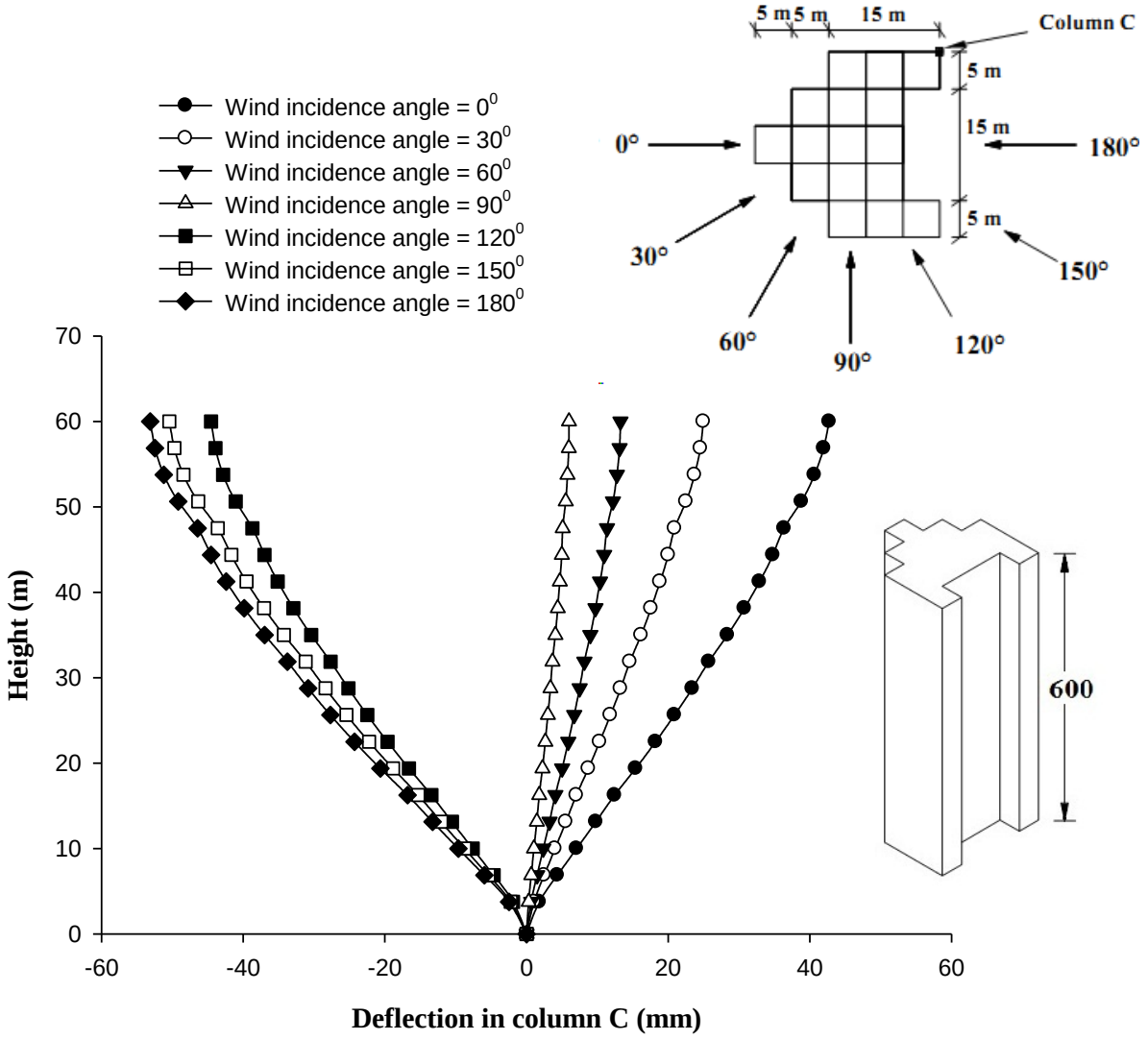


**Fig. 6.104 Effect of wind incidence angle on horizontal displacement of column-C of Fish Shape-2 building**

### 6.4.7 Fish Shape-3 Building

#### 6.4.7.1 Forces in columns

Response of Fish Shape-3 building under wind loads at 7 wind incidence angles is obtained and variation of axial force, twisting moment Mz, moment about 'X' axis i.e. Mx and moment about 'Y' axis i.e. My with wind incidence angle are plotted in Figs. 6.105 to 6.116.

Axial force in face column, i.e. column-A and corner column, i.e. column-C are affected by wind incidence angles. Whereas axial force is maximum at $150^0$ wind angle in column-A, it is maximum at $60^0$ angle in column-C. Axial force in central column, i.e. column-B, is not affected by wind incidence angle.

Twisting moment, Mz, is maximum at $90^0$ angle in all three columns.

Moment about 'X' axis, i.e. Mx in column-B and C is maximum at $0^0$ wind incidence angle. My is maximum at $90^0$ angle in all three columns.

#### 6.4.7.2 Deflections of columns

Horizontal displacement in X-direction in case of Fish Shape-3 building in all three columns is highly influenced by wind direction. It is maximum at $180^0$ angle followed by the value at $0^0$ angle (Figs. 6.117 to 6.119). It is minimum at $90^0$ angle.

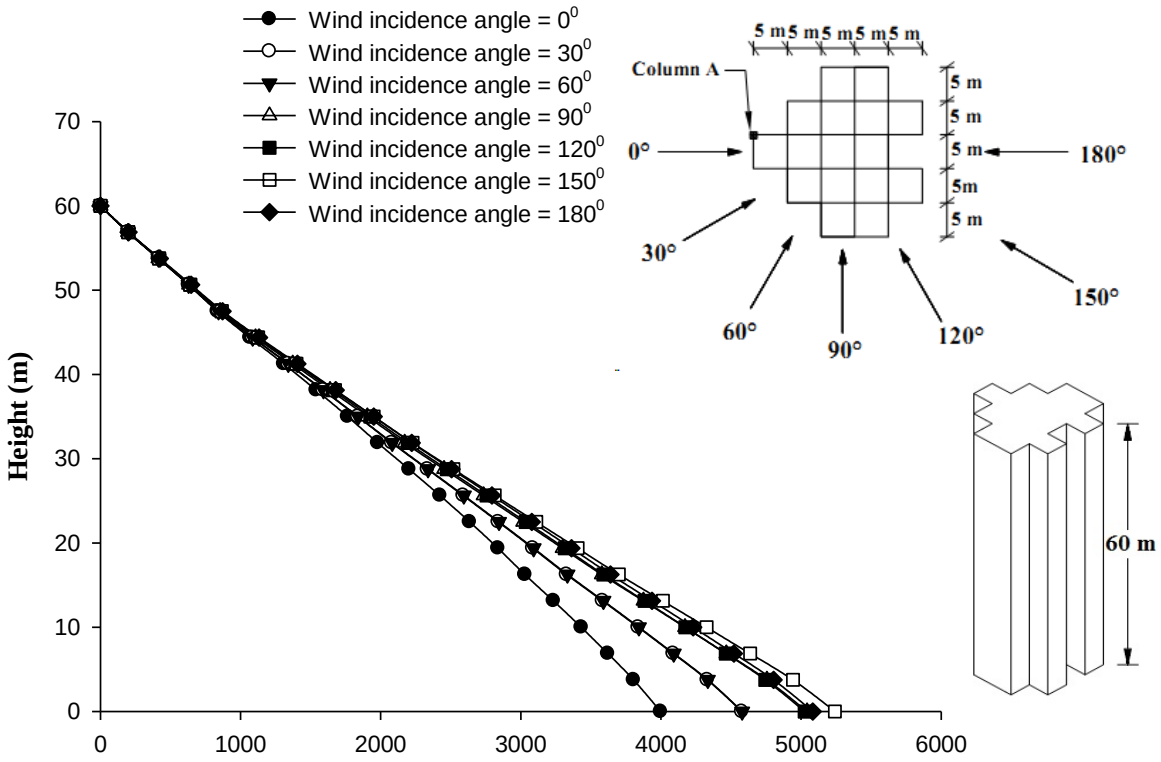


**Fig. 6.105 Effect of wind incidence angle on axial force in column-A of Fish shape-3 building**

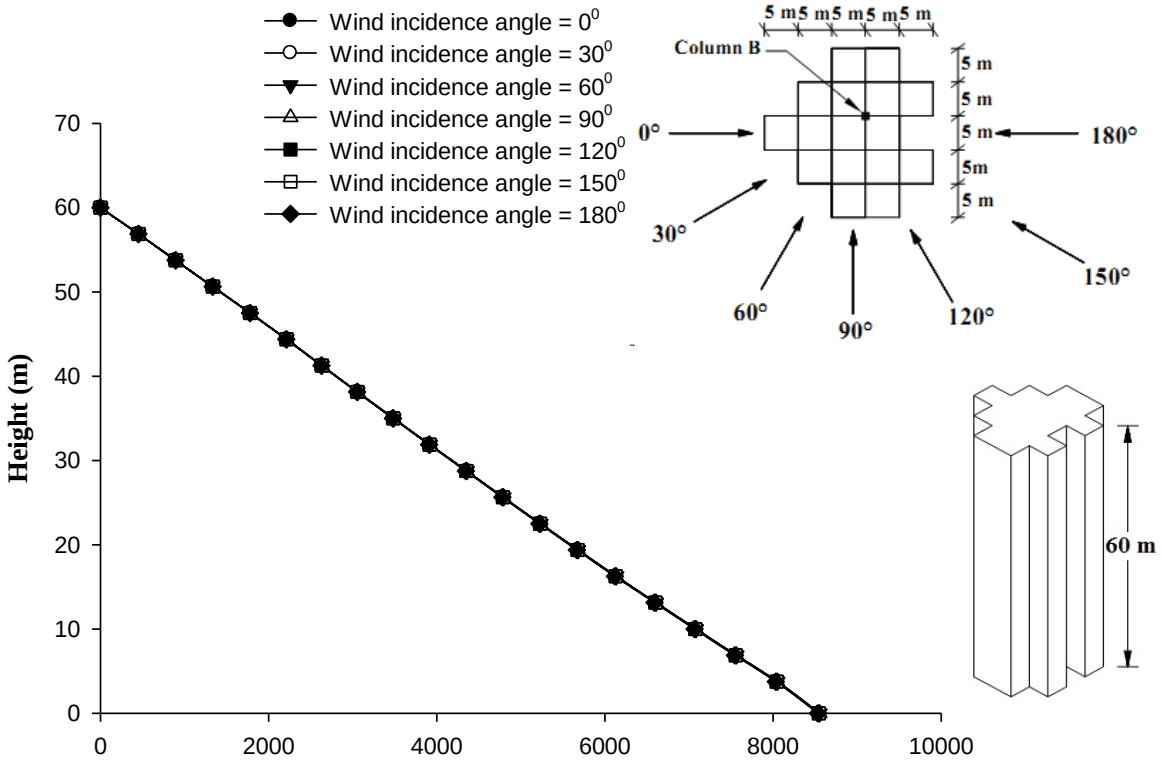


**Fig. 6.106 Effect of wind incidence angle on axial force in column-B of Fish shape-3 building**

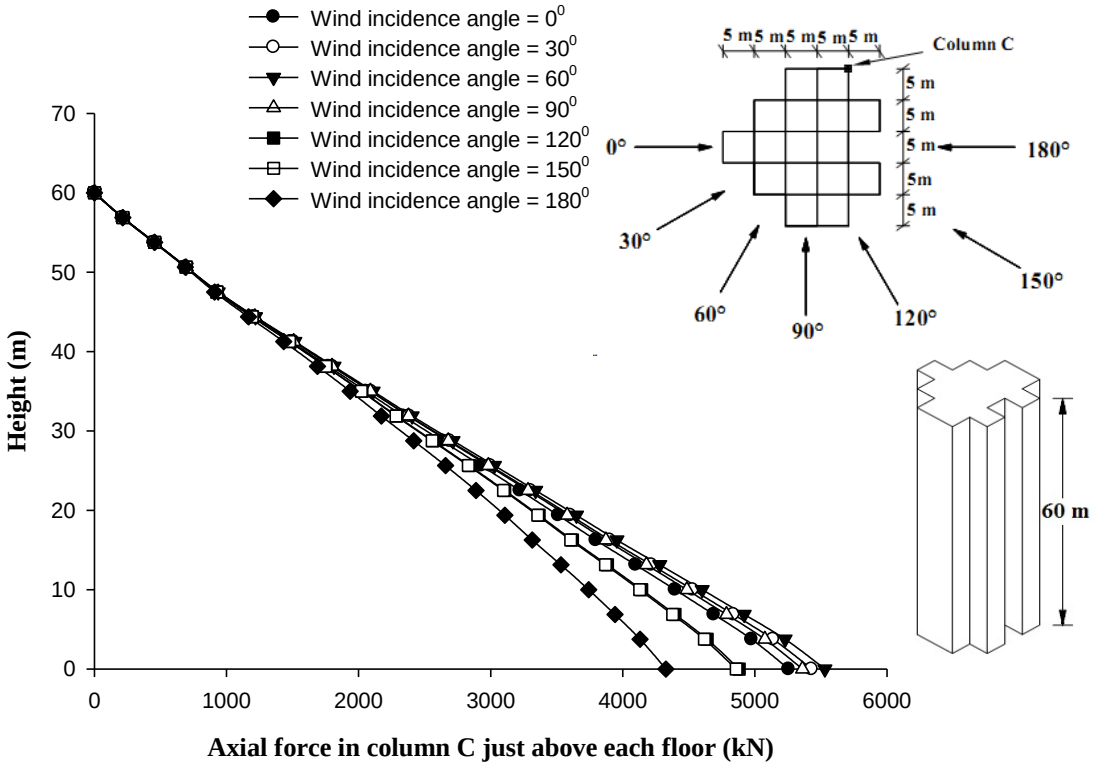


**Fig. 6.107 Effect of wind incidence angle on axial force in column-C of Fish Shape-3 building**

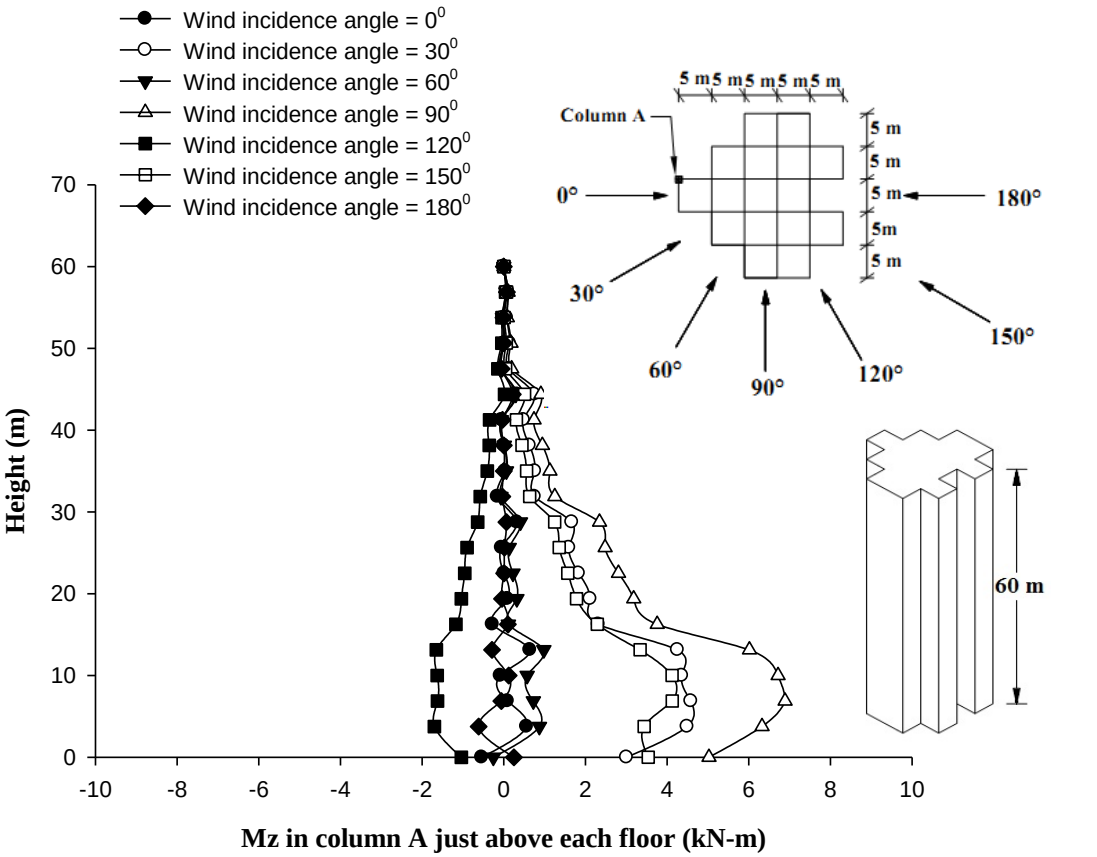


**Fig. 6.108 Effect of wind incidence angle on twisting moment Mz in column-A of Fish Shape-3 building**

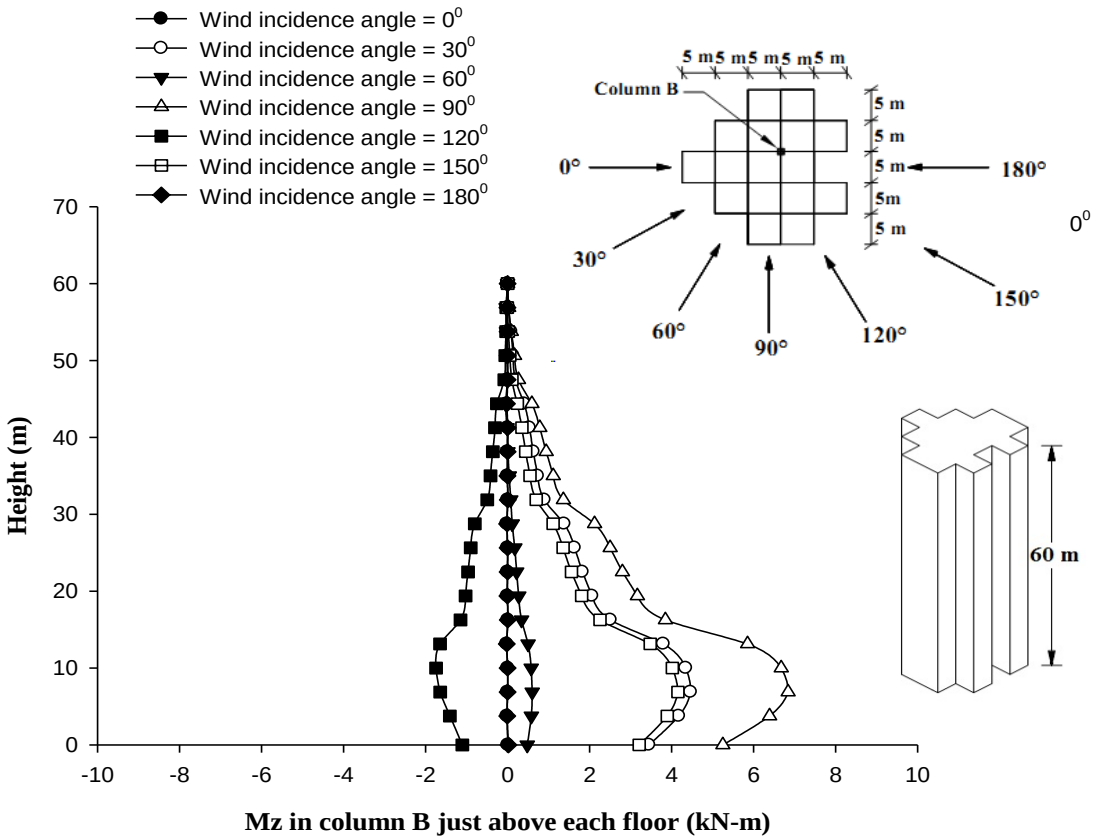


**Fig. 6.109 Effect of wind incidence angle on twisting moment Mz in column-B of Fish Shape-3 building**

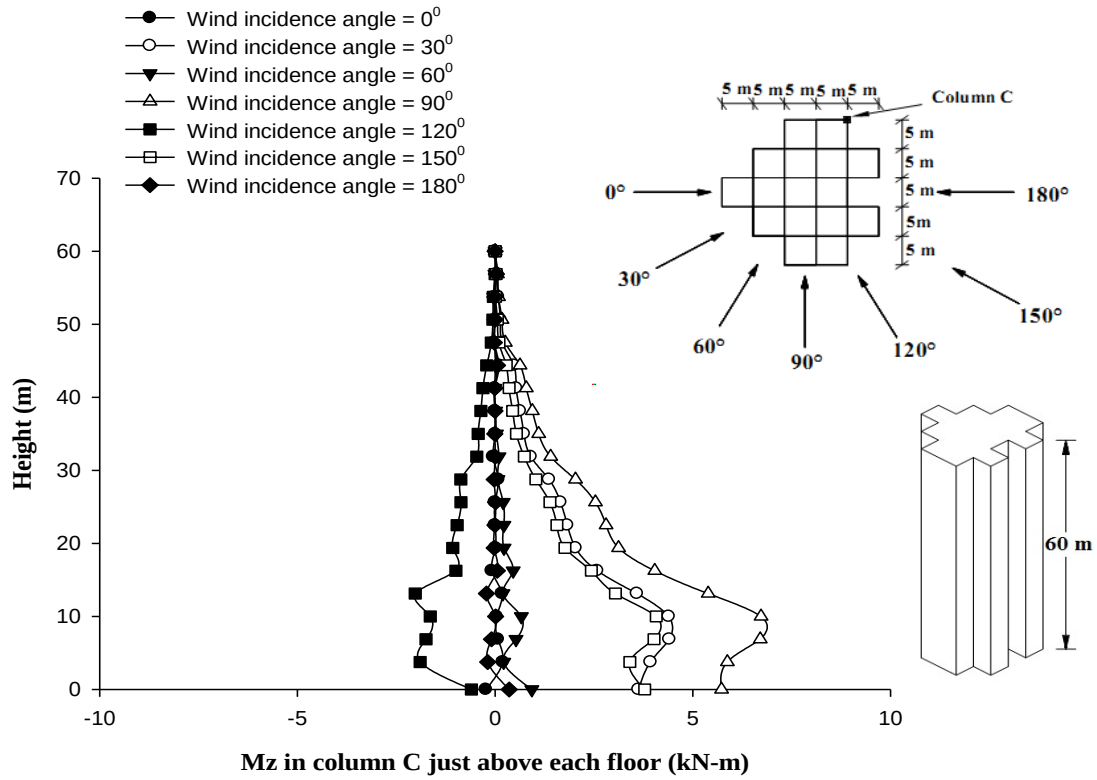


**Fig. 6.110 Effect of wind incidence angle on twisting moment Mz in column-C of Fish Shape-3 building**

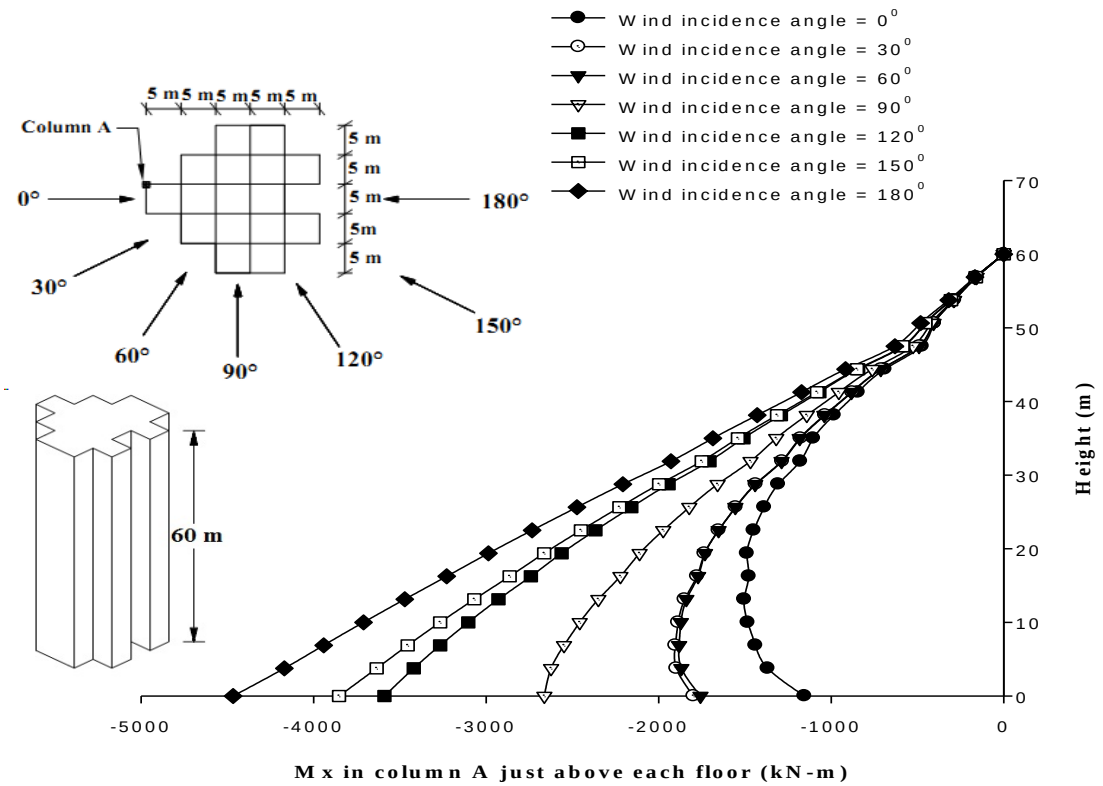


**Fig. 6.111 Effect of wind incidence angle on Mx (global) in column-A of Fish Shape-3 building**

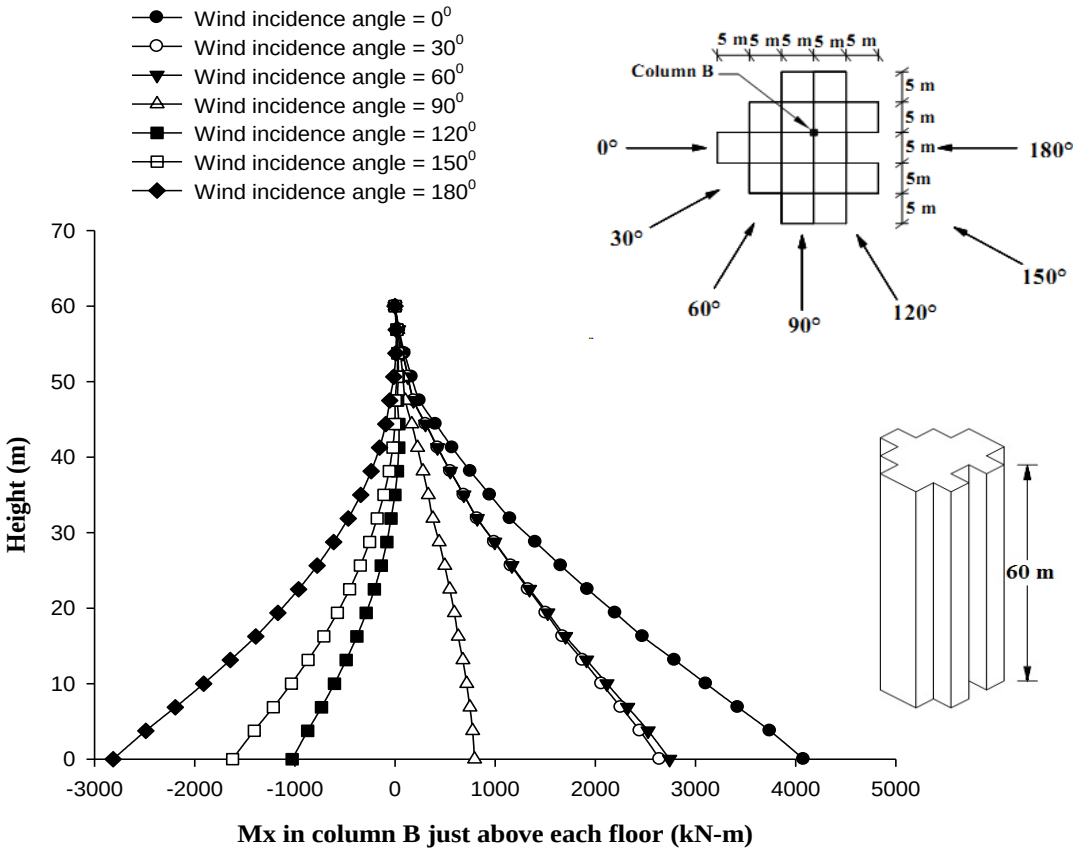


**Fig. 6.112 Effect of wind incidence angle on Mx (global) in column-B of Fish Shape-3 building**

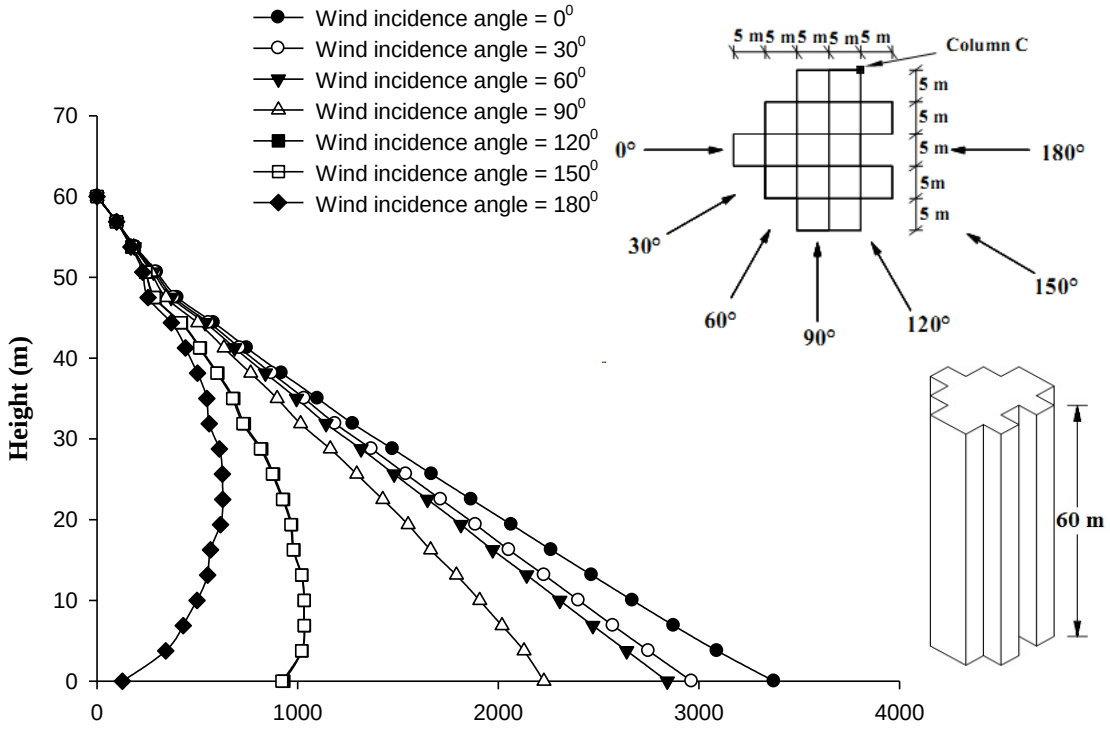


Mx in column C just above each floor (kN-m)

**Fig. 6.113 Effect of wind incidence angle on Mx (global) in column-C of Fish Shape-3 building**

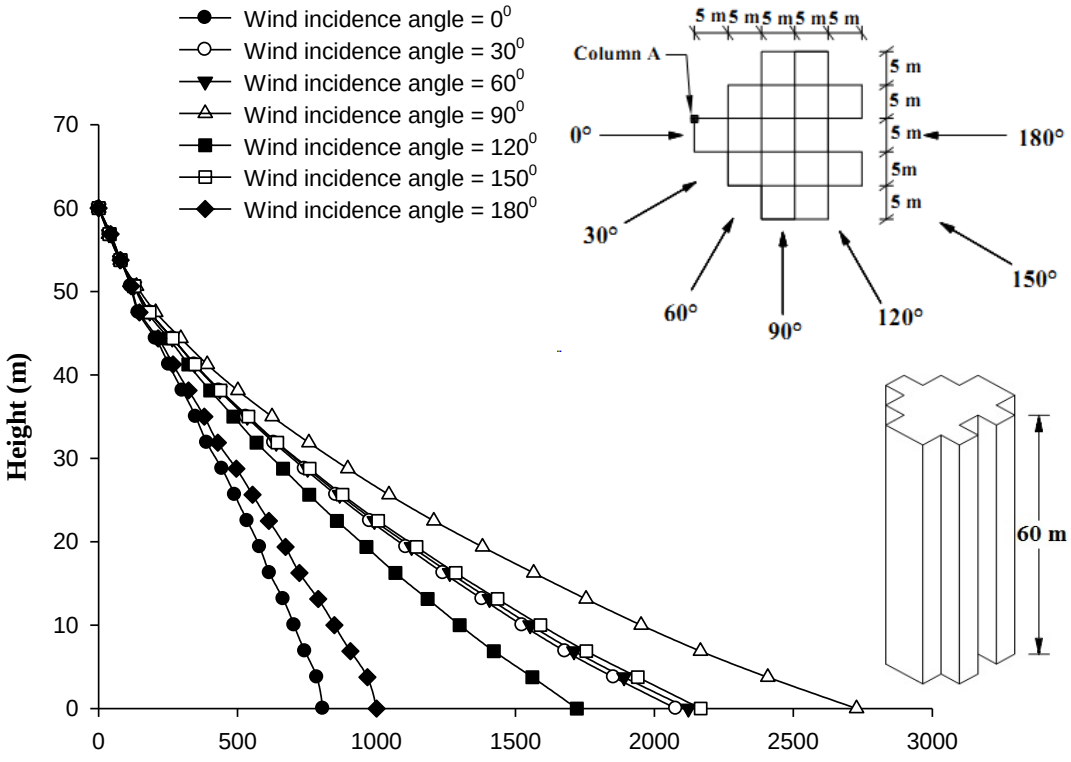


My in column A just above each floor (kN-m)

**Fig. 6.114 Effect of wind incidence angle on My (global) in column-A of Fish Shape-3 building**

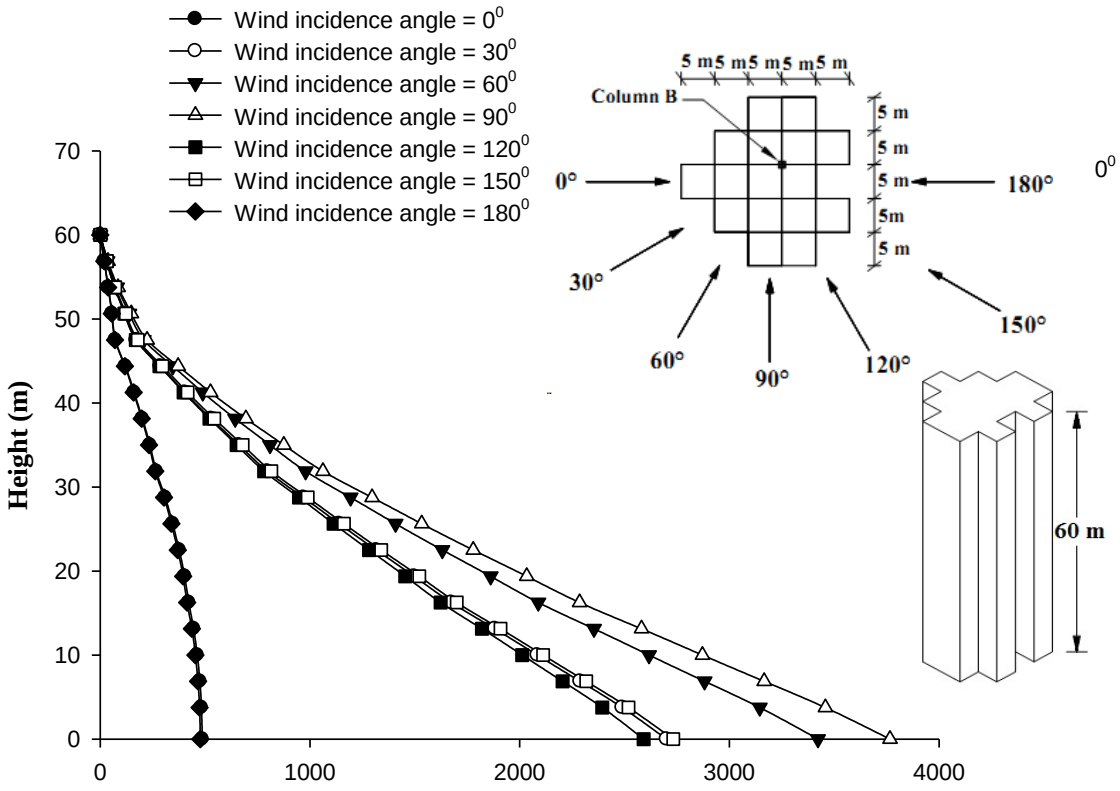


**Fig. 6.115 Effect of wind incidence angle on My (global) in column-B of Fish Shape-3 building**

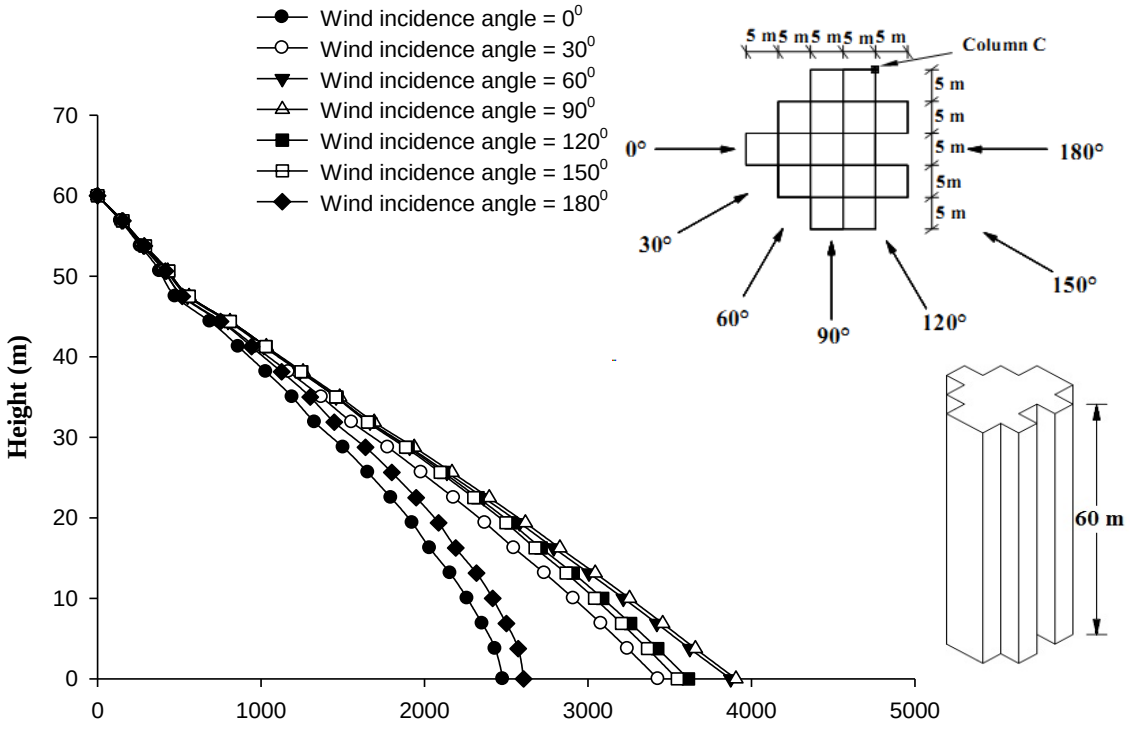


**Fig. 6.116 Effect of wind incidence angle on My (global) in column-C of Fish Shape-3 building**

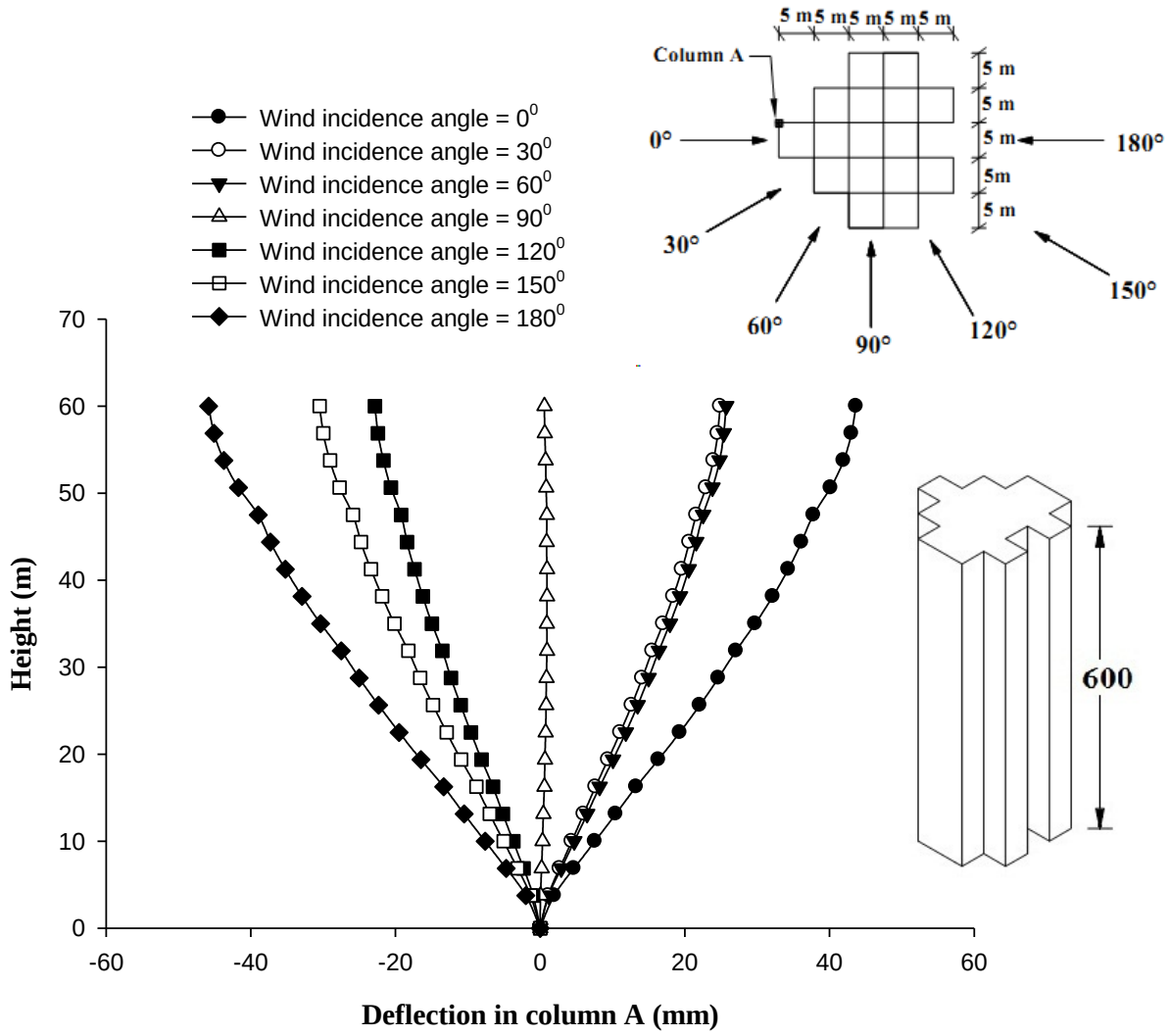


**Fig. 6.117 Effect of wind incidence angle on horizontal displacement of column-A of Fish Shape-3 building**

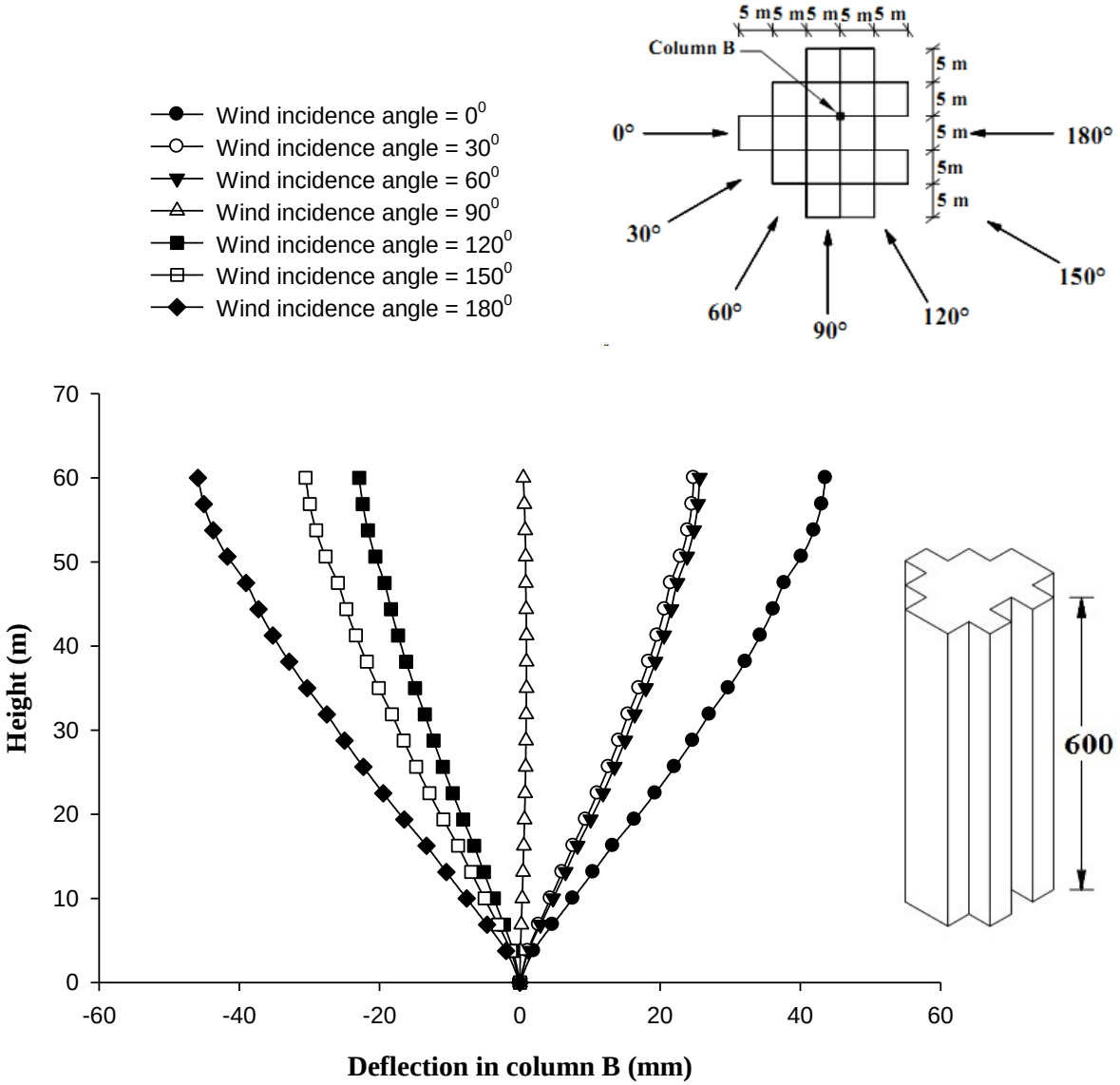


**Fig. 6.118 Effect of wind incidence angle on horizontal displacement of column-B of Fish Shape-3 building**

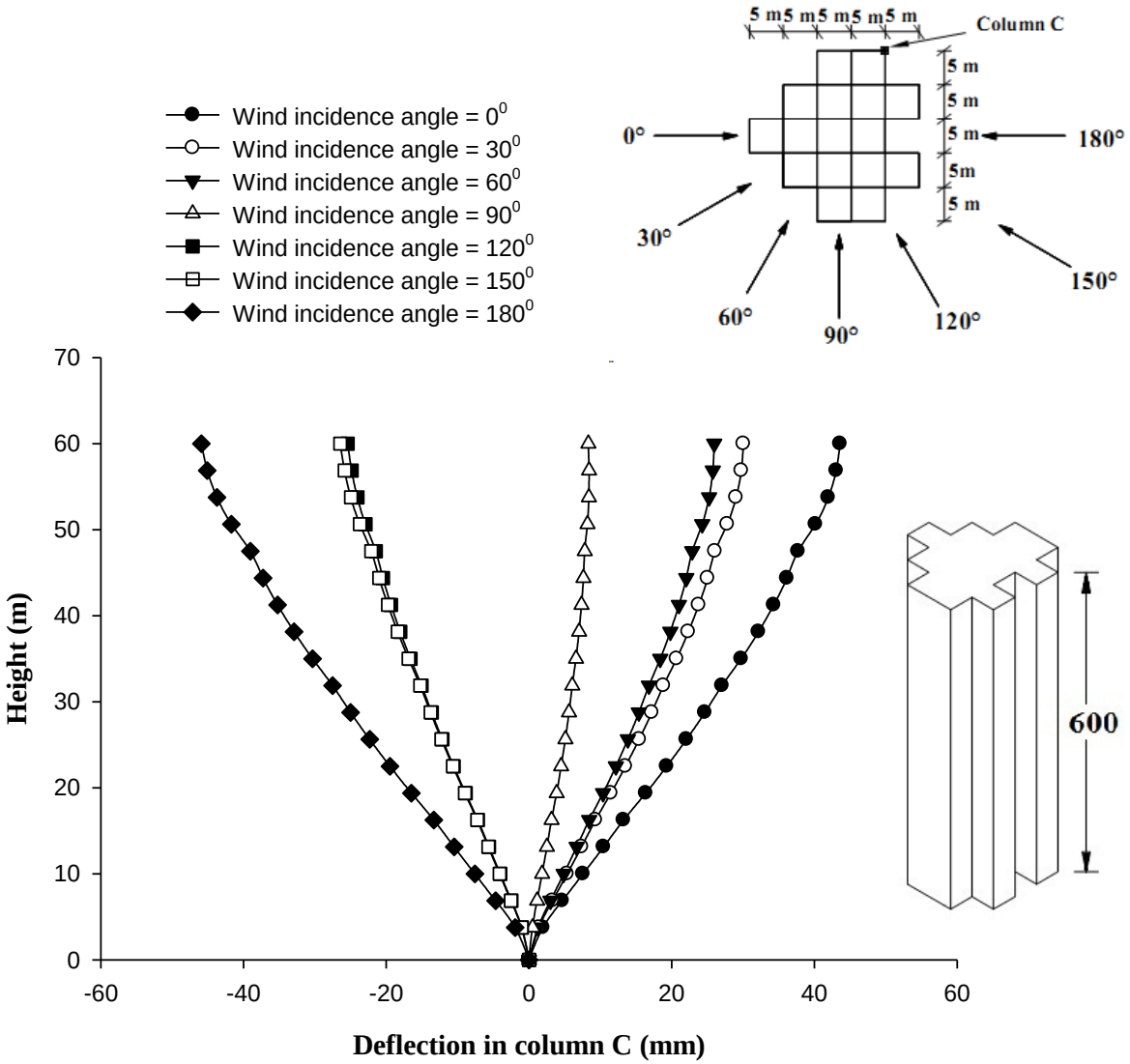


**Fig. 6.119 Effect of wind incidence angle on horizontal displacement of column-C of Fish Shape-3 building**

## 6.5 RESPONSE UNDER INTERFERENCE CONDITION

### 6.5.1 Square Shape Building

#### 6.5.1.1 Forces in Columns

Response of square shape building is measured under three interference conditions also namely full blockage, half blockage and no blockage (Fig. 6.120). Figures 6.121 to 6.123 show the effect of interfering building on axial forces in case of column-A, B and C respectively. In case of column-A i.e. central column, axial force remains same at each interference condition (Fig. 6.121). There is no effect of interfering building on axial force in central column. In case of column-B, i.e. edge column (Fig. 6.122), minimum axial force is observed in full blockage interference condition and maximum at no blockage interference condition which is as close as value in isolated condition. In case of column-C, i.e. corner column (Fig. 6.123), similar variation pattern of axial force is observed but the magnitudes are slightly less than that in column-B. In full blockage interference condition, the square shape building is fully covered by interfering building and hence the axial forces in column-B and C are minimum in this condition. Values of axial force in column-B and C in no blockage condition are quite close to respective value of axial force in isolated condition. At other two interference conditions, value of axial force is less than that in isolated condition, which indicates that there is advantage of shielding in case of axial force in columns.

Wind interference effect on twisting moment Mz is shown in Figs. 6.124 to 6.126 for column-A, B and C respectively. Similar moment variation pattern is observed in all columns with maximum twisting moment under half blockage condition. It is further noticed that Mz is maximum at around 17% height from the bottom end and zero at the top end.

Moment about ‘X’ axis i.e. Mx plotted along the height is shown in Figs. 6.127 to 6.129 on column-A, B and C respectively. Maximum moment is observed in column-A at no blockage interference condition which is very close in magnitude to the value in case of isolated condition (Fig. 6.127). In case of column-B (Fig. 6.128) maximum moment is observed at no blockage interference condition and minimum at full blockage condition. In case of column-C, Mx is almost zero in full blockage condition and maximum at no blockage condition (Fig. 6.129). Moment My i.e. moment about ‘Y’ axis are shown for column-A, B and C in Figs 6.130 to 6.132 respectively. Figure 6.130 indicates that maximum moment is observed in column-A at no blockage interference condition followed by its value at half blockage condition. My is zero at full blockage interference condition as well as isolated condition. In case of column-B (Fig. 6.131) and column-C (Fig. 6.132), maximum moment is observed at half blockage wind interference condition and minimum at full blockage condition.

#### 6.5.1.2 Displacement of columns

In case of interference conditions, horizontal displacement in X-direction of all three columns in Square Shape building is less than that in case of isolated condition. In case of full blockage interference condition, the building and thus all three columns move in –ve X-direction (Figs. 6.133 to 6.135).

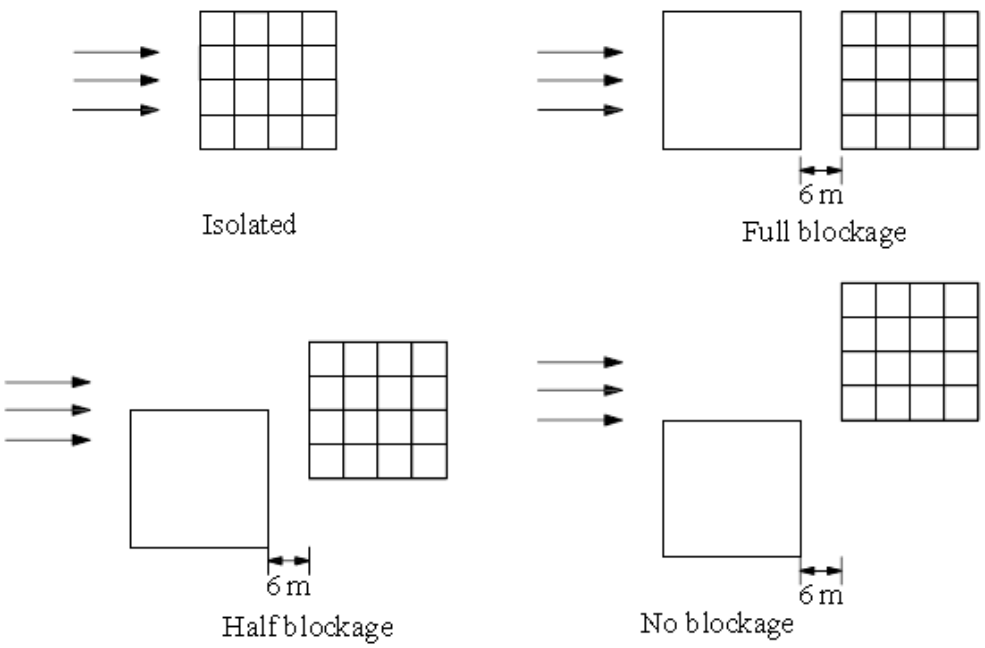


**Fig. 6.120 Relative position of square shape buildings under different interference conditions**

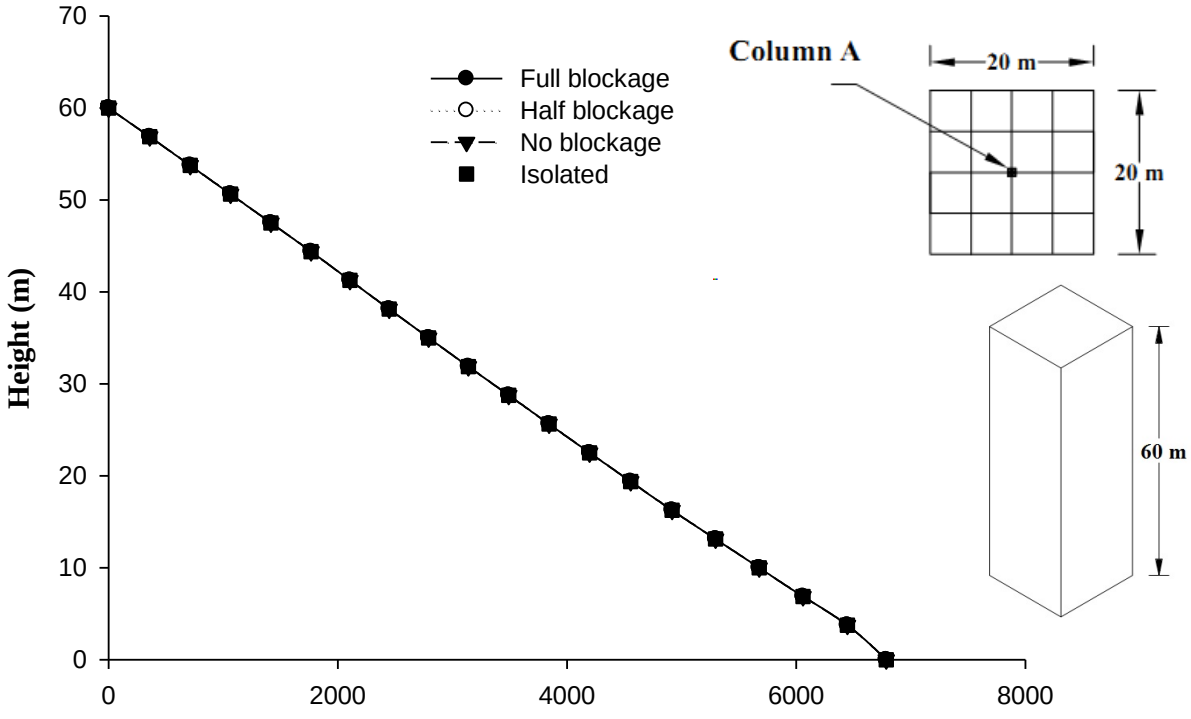


**Fig. 6.121 Interference effect on axial force in column-A of Square Shape building**

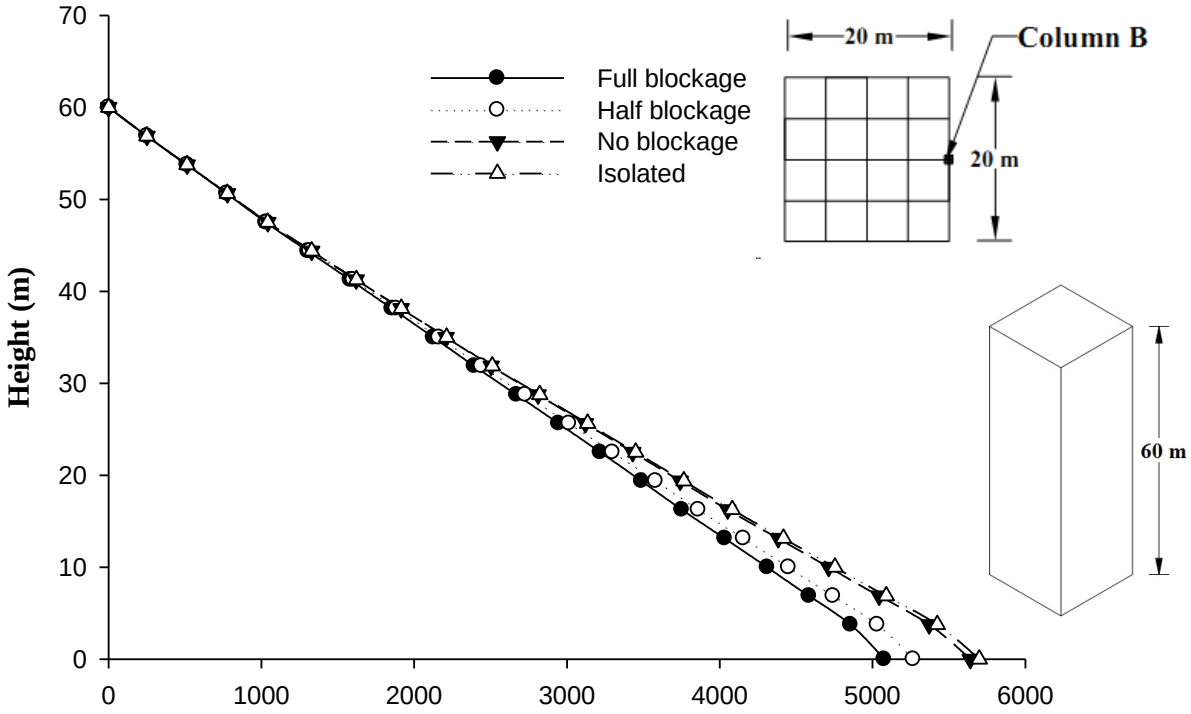


**Fig. 6.122 Interference effect on axial force in column-B of Square Shape building**

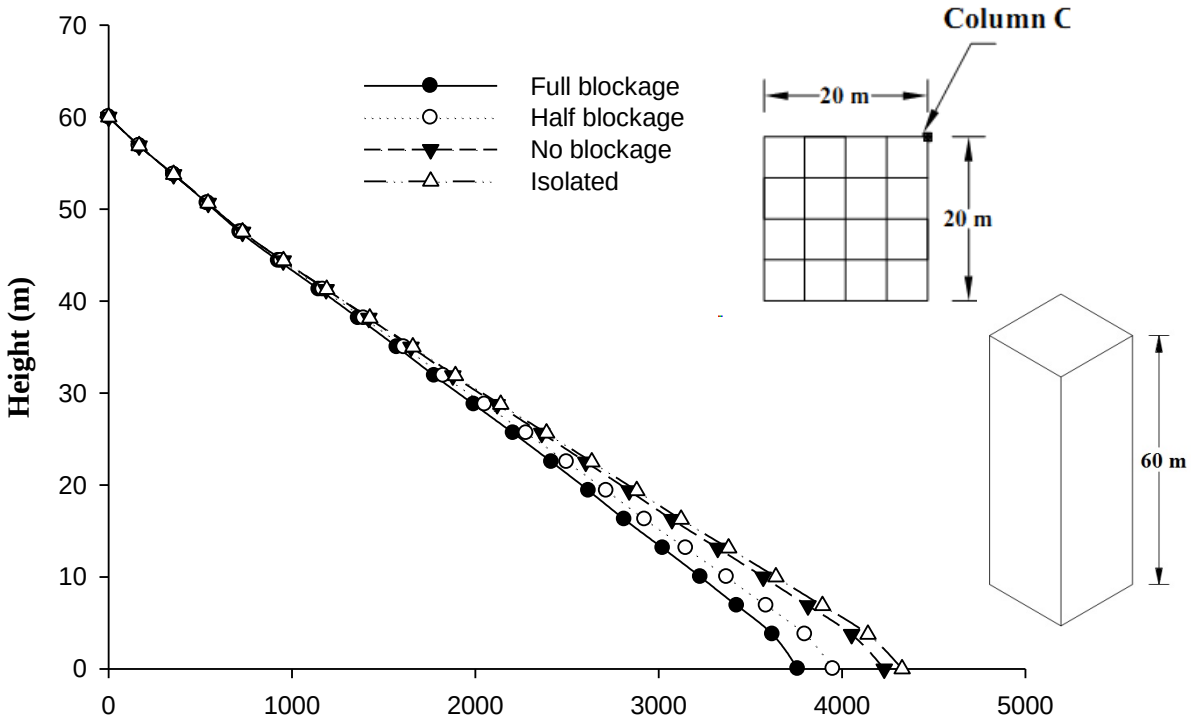


**Fig. 6.123 Interference effect on axial force in column-C of Square Shape building**

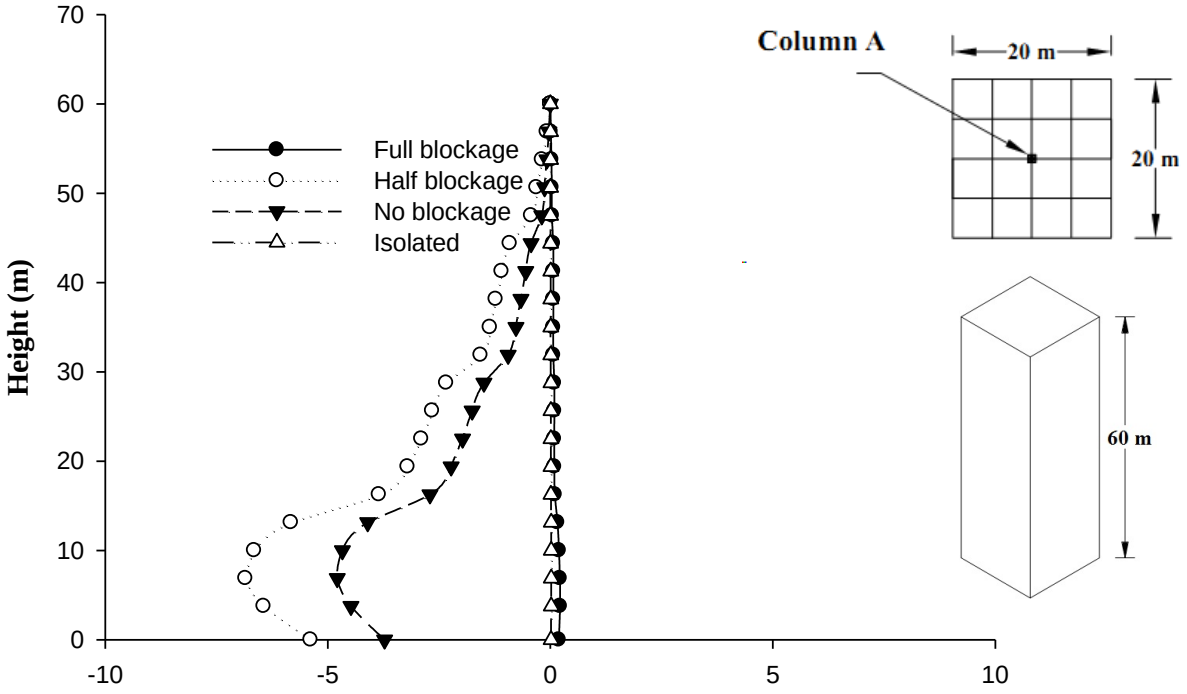


**Mz in column A just above each floor (kN-m)**

**Fig. 6.124 Interference effect on twisting moment Mz in column-A of Square Shape building**

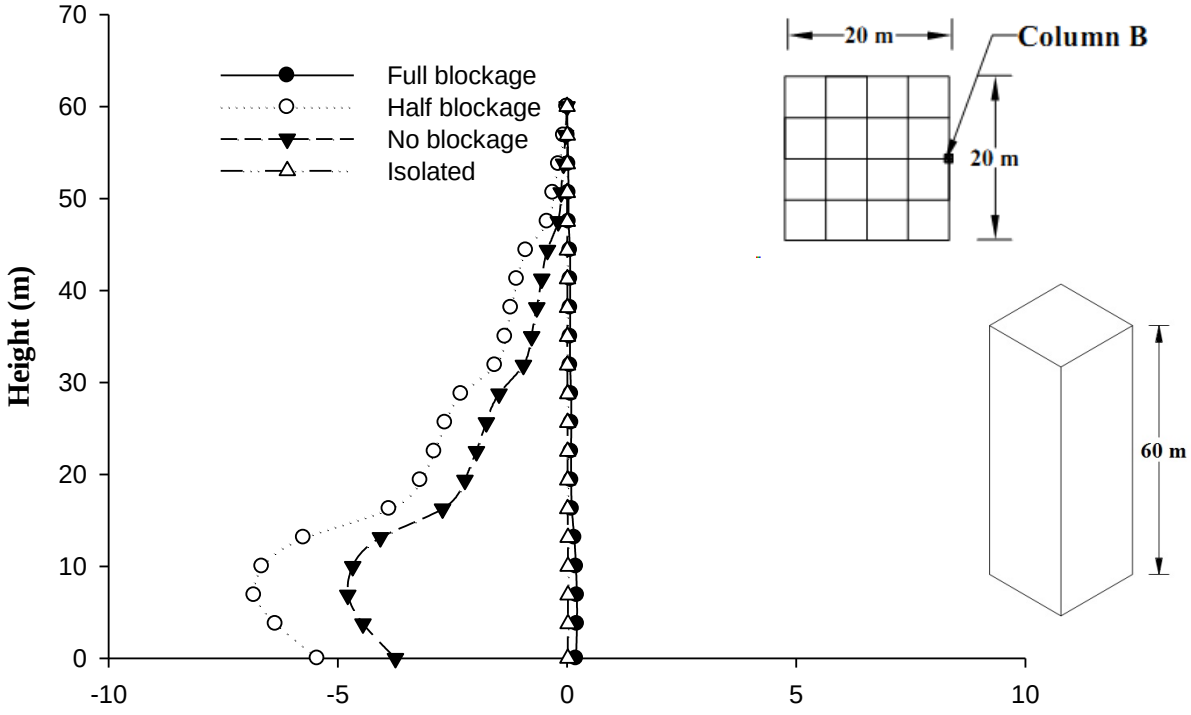


**Mz in column B just above each floor (kN)**

**Fig. 6.125 Interference effect on twisting moment Mz in column-B of Square Shape building**

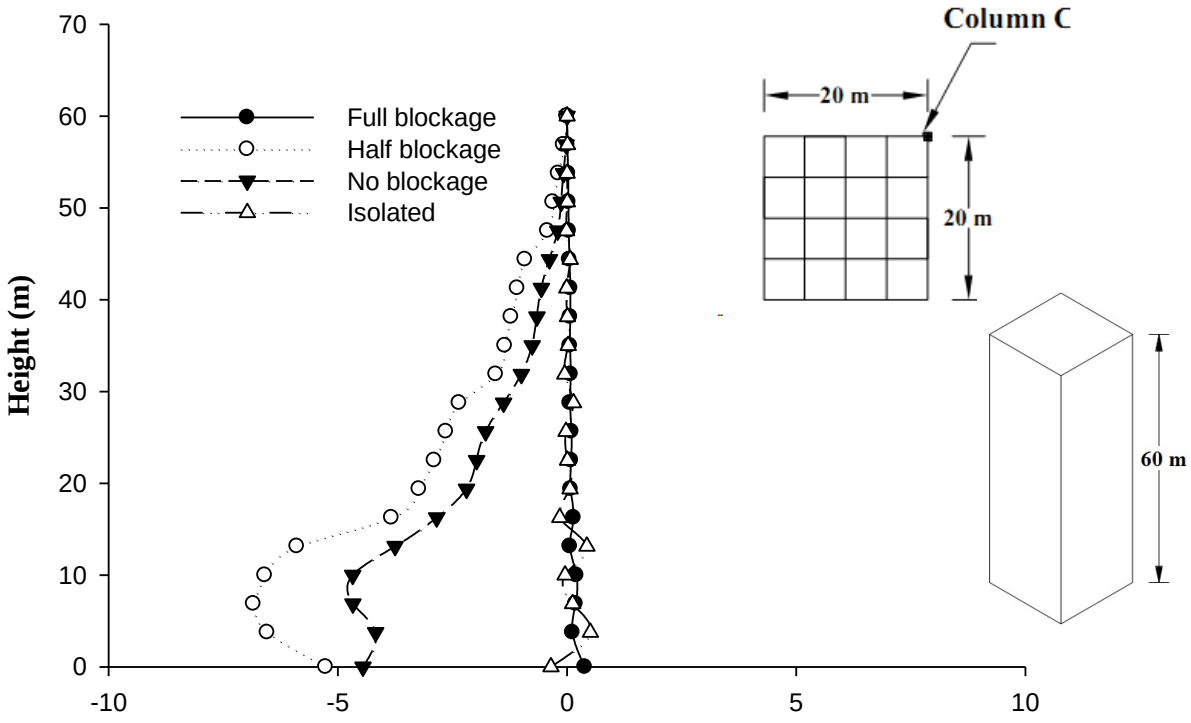


**Mz in column C just above each floor (kN)**

**Fig. 6.126 Interference effect on twisting moment Mz in column-C of Square Shape building**

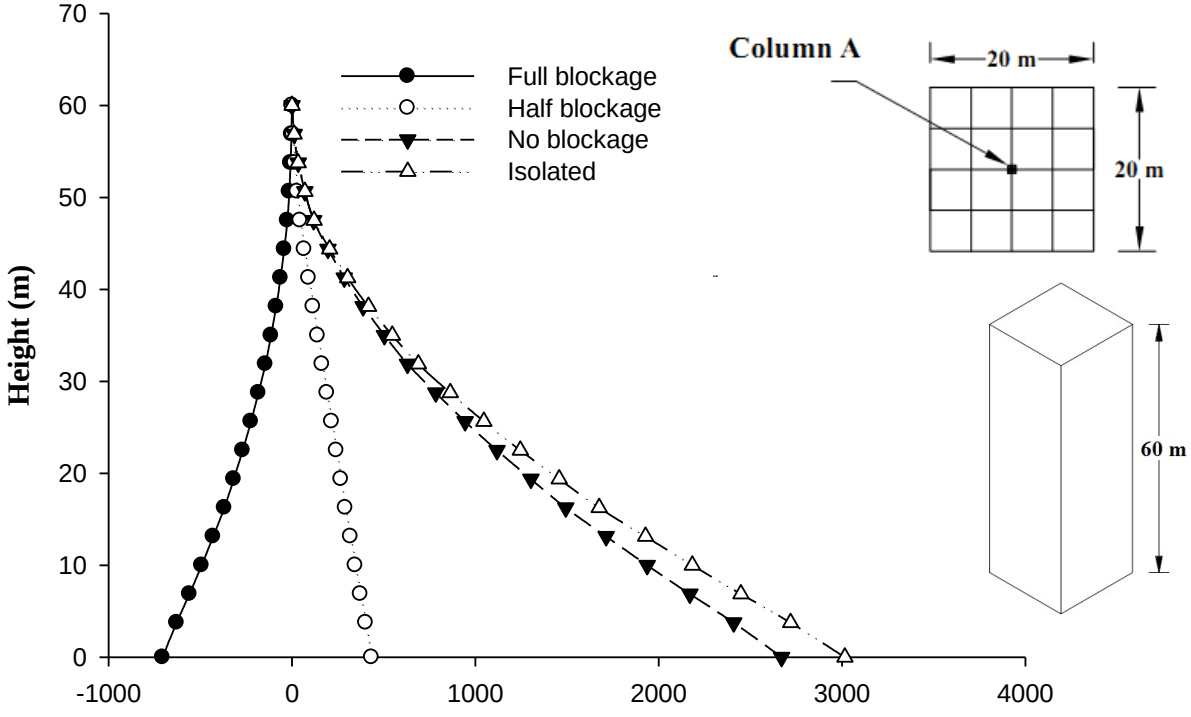


**Mx in column A just above each floor (kN-m)**

**Fig. 6.127 Interference effect on Mx (global) in column-A of Square Shape building**

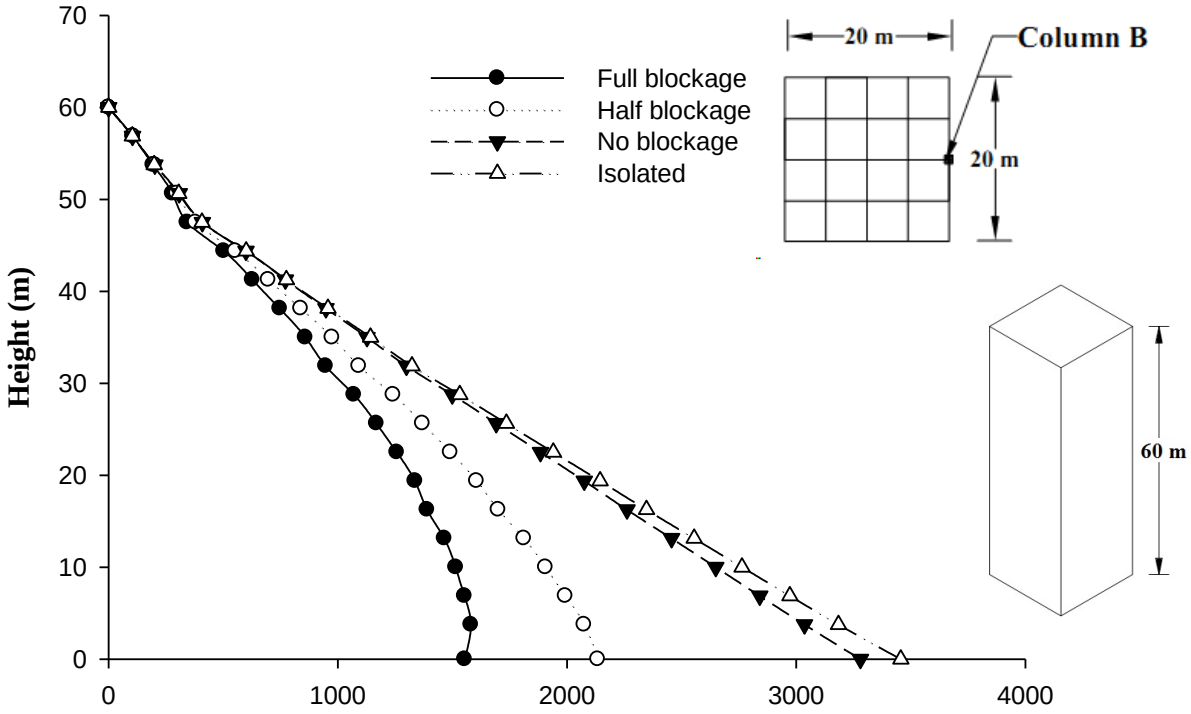


**Fig. 6.128 Interference effect on Mx (global) in column-B of Square Shape building**

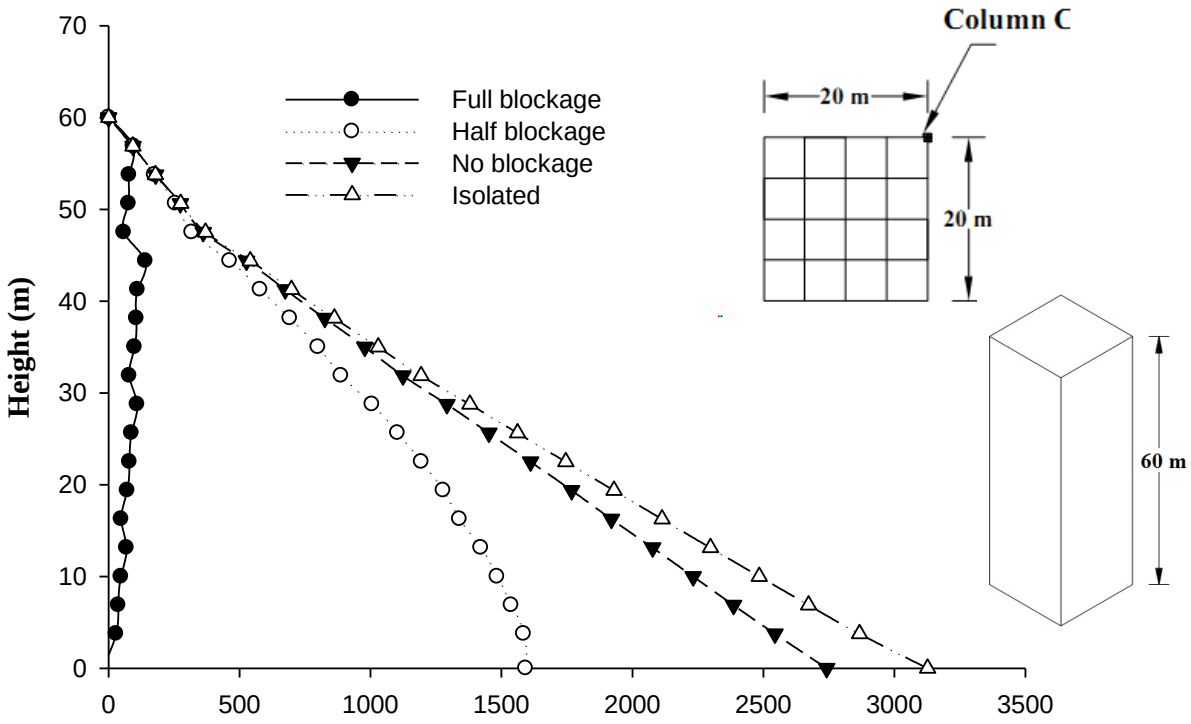


**Fig. 6.129 Interference effect on Mx (global) in column-C of Square Shape building**

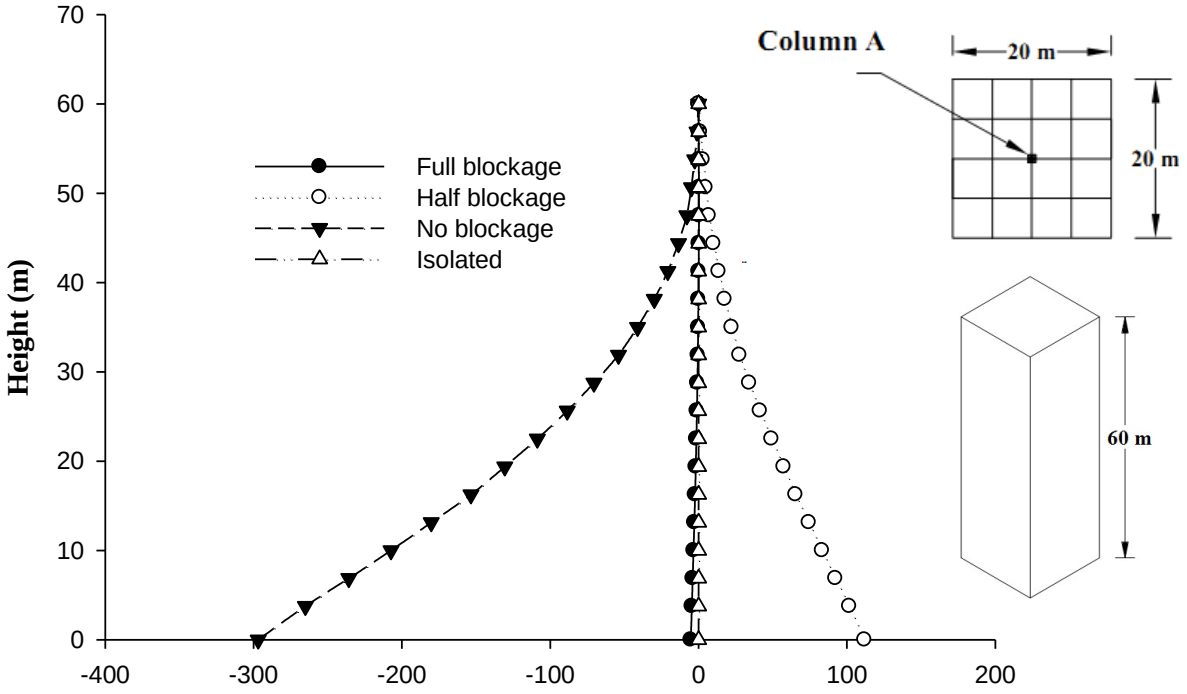


**Fig. 6.130 Interference effect on My (global) in column-A of Square Shape building**

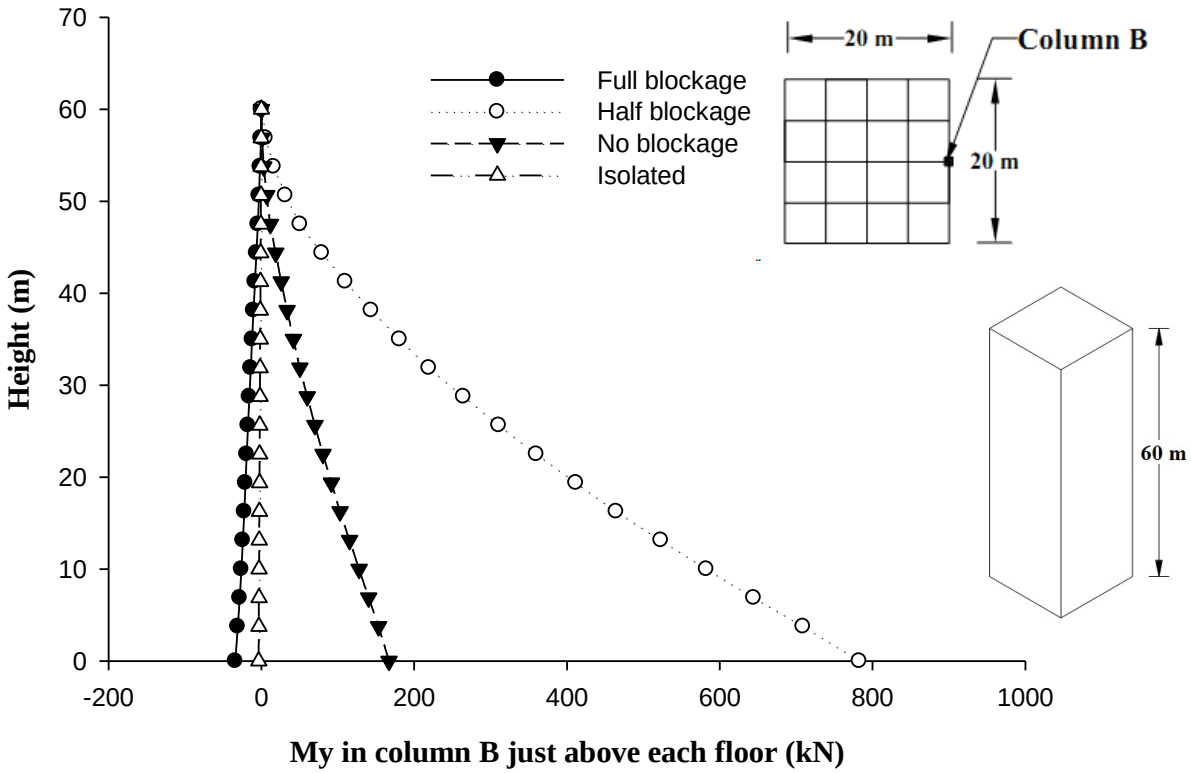


**Fig. 6.131 Interference effect on My (global) in column-B of Square Shape building**

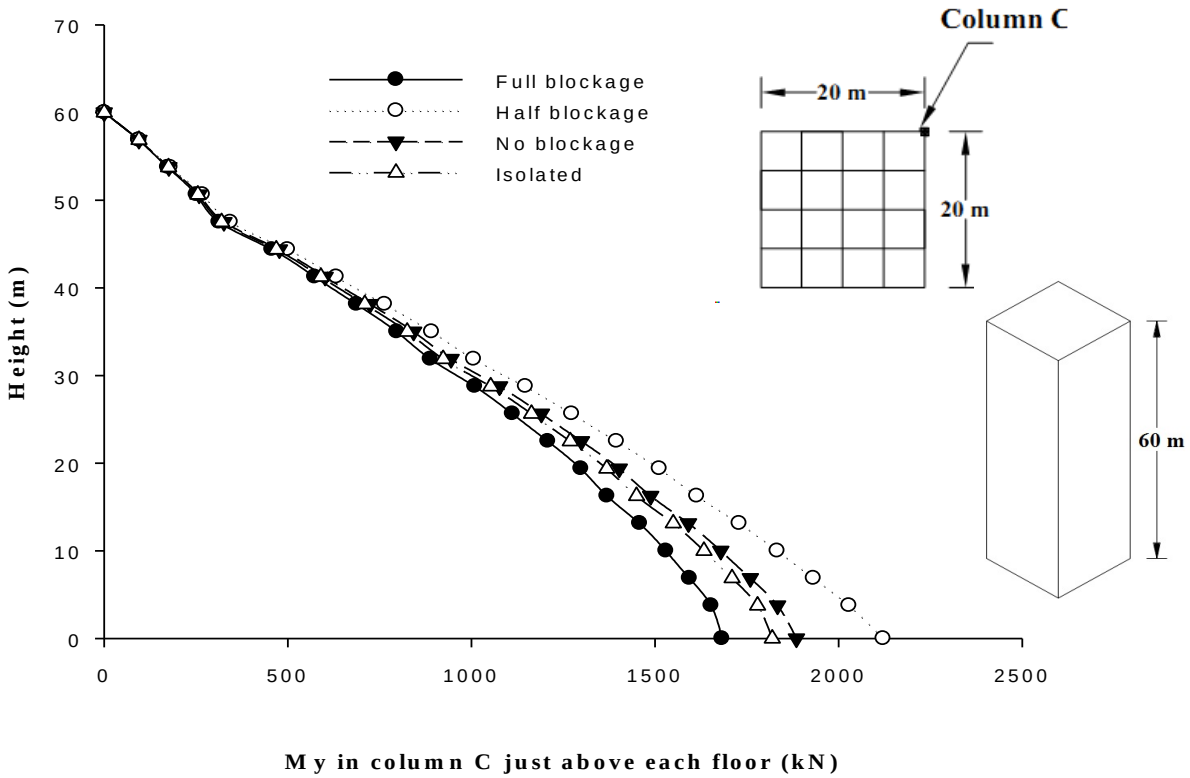


**Fig. 6.132 Interference effect on My (global) in column-C of Square Shape building**

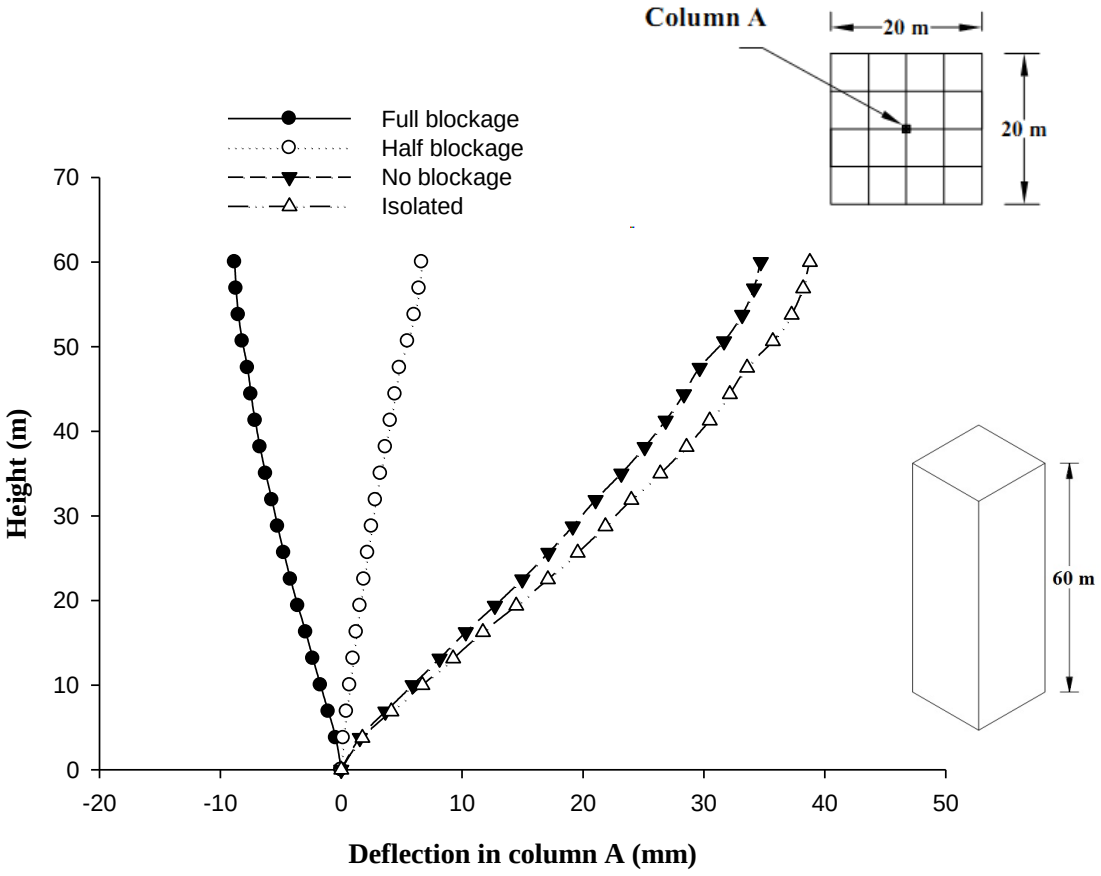


**Fig. 6.133 Interference effect on horizontal displacment of column-A of Square Shape building**

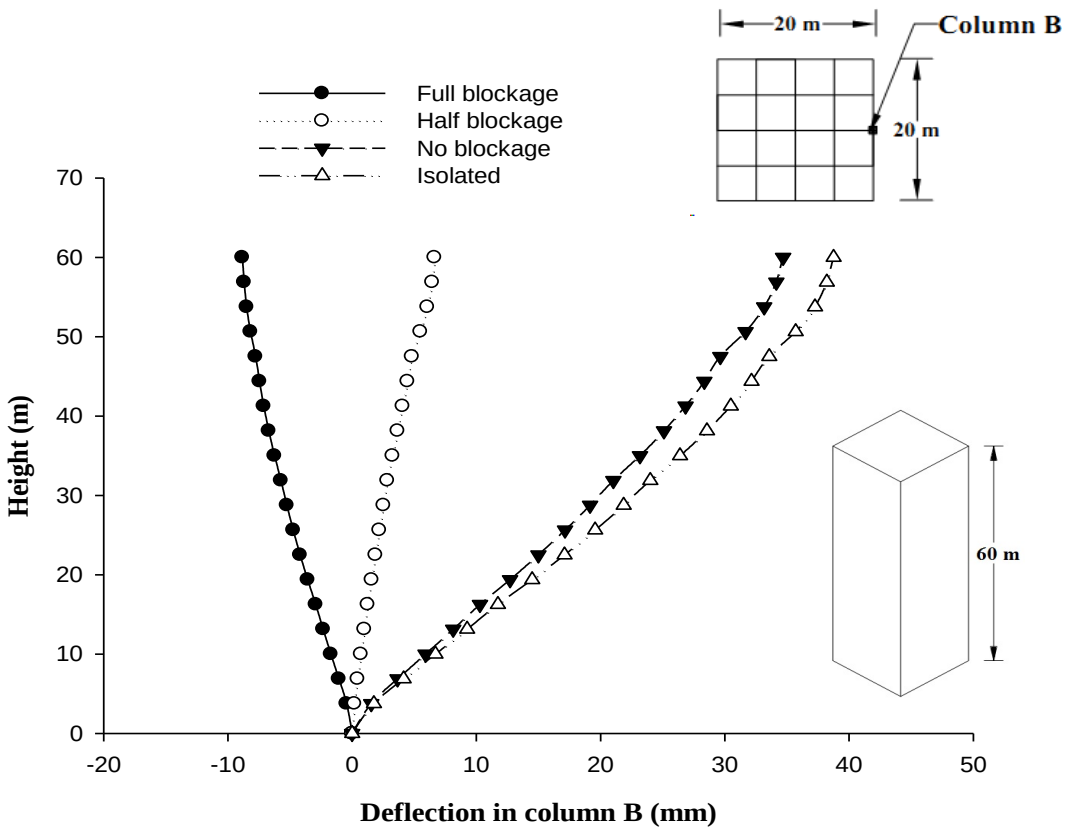


**Fig. 6.134 Interference effect on horizontal displacment of column-B of Square Shape building**

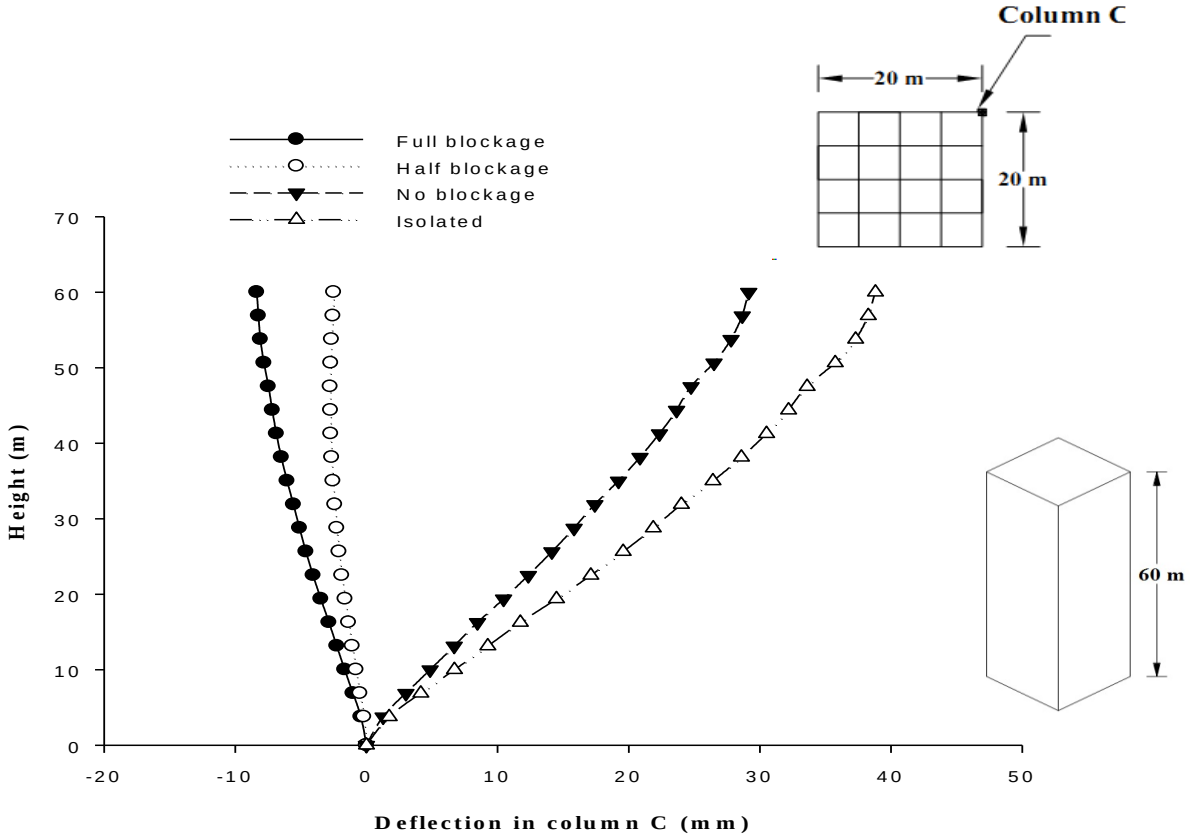


**Fig. 6.135 Interference effect on horizontal displacment of column-C of Square Shape building**

### 6.5.2 Plus Shape-1 Building

#### 6.5.2.1 Forces in columns

As in the case of Square Shape building, response of Plus Shape-1 building is also obtained under three interference conditions namely full blockage, half blockage and no blockage (Fig. 6.136). Interference effect on axial force is observed in column-A, B and C. Axial force values are similar at all interference conditions along height in case of column-A (Fig. 6.137). Maximum axial force observed in column-A of this building is greater than that in Square Shape building. In case of column-B (Fig. 6.138) and column-C (Fig. 6.139), there is very small effect of interference on axial force.

Variation of twisting moment pattern are similar for all columns namely column-A, B and C, as shown in Figs. 6.140 to 6.142 respectively. Maximum torsional moment is observed at half blockage interference condition and at around 10% height from the bottom end. In case of isolated and full blockage wind interference condition, torsional moment is almost zero thoroughout the height.

Figures 6.143 to 6.145 show the variation of moment Mx along height for column-A, B and C respectively. Figure 6.143 indicates that maximum moment is observed at isolated condition in case of column-A and minimum moment Mx is observed at full blockage wind interference condition. There is very small effect of interference on Mx in column-B. Similarly there is large effect of interference on My in column-A (Fig. 6.146), but there is small effect on My in column-B (Fig. 6.147) and column-C (Fig. 6.148).

#### 6.5.2.2 Displacment of columns

As in the case of Plus Shape-1 building, all three columns have –ve deflection in full blockage interference condition. Similarly, numerical values of deflection in all interference conditions are less than that in case of isolated condition (Figs. 6.149 to 6.151).

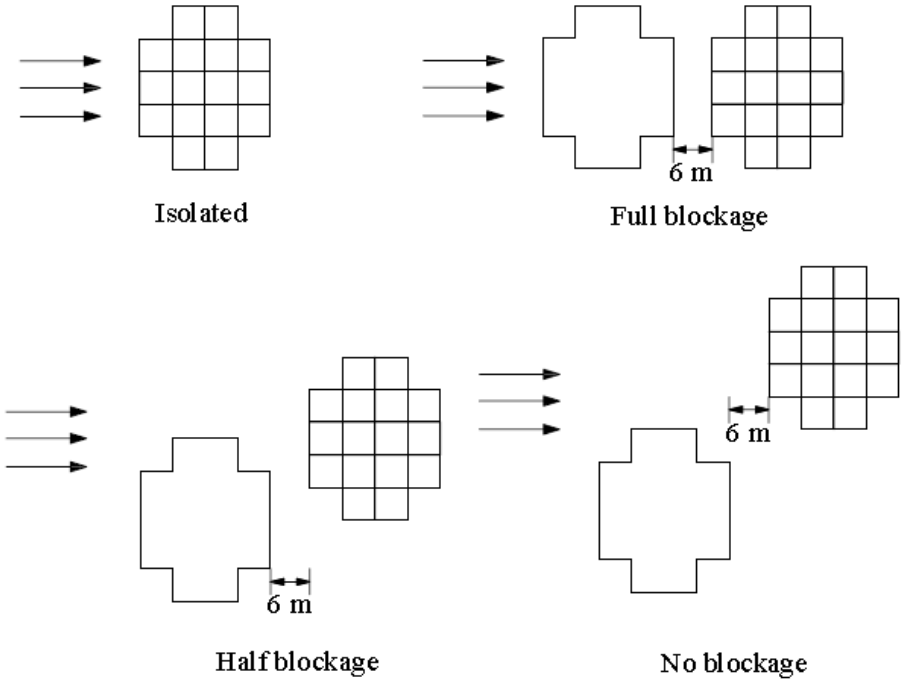


**Fig. 6.136 Relative position of Plus Shape-1 buildings under different interference conditions**

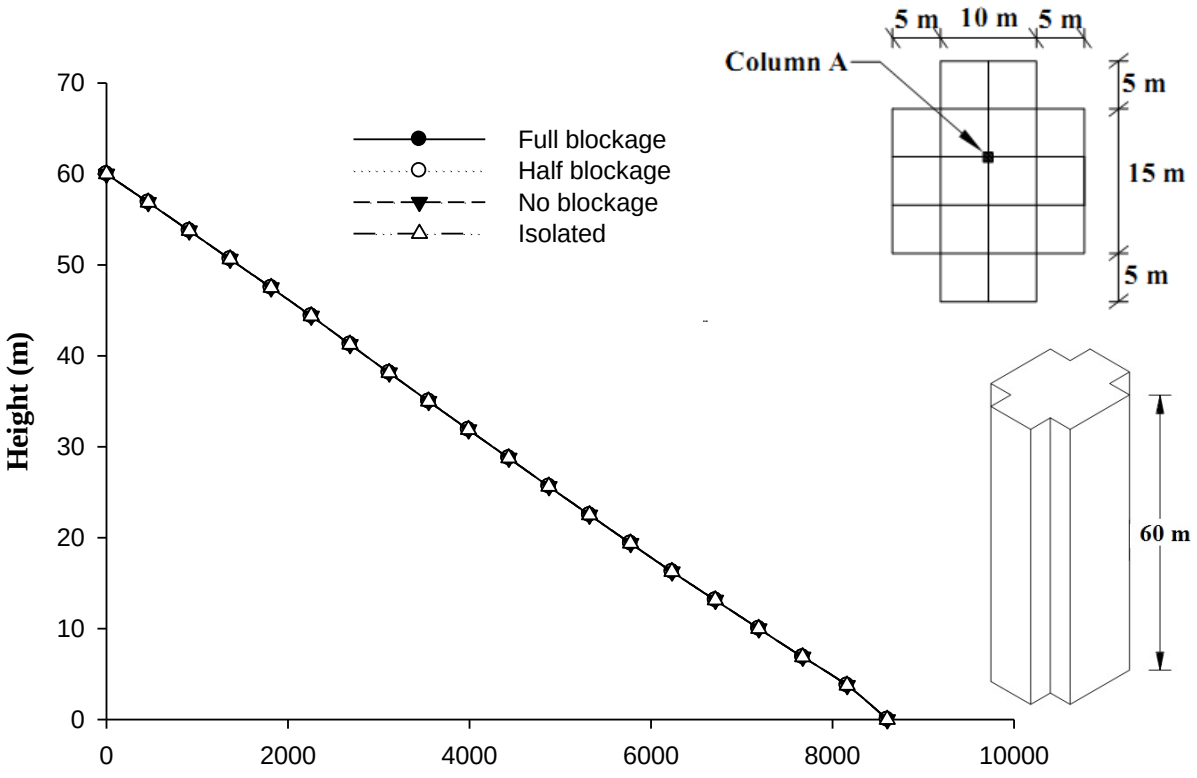


**Fig. 6.137 Interference effect on axial force in column-A of Plus Shape-1 building**

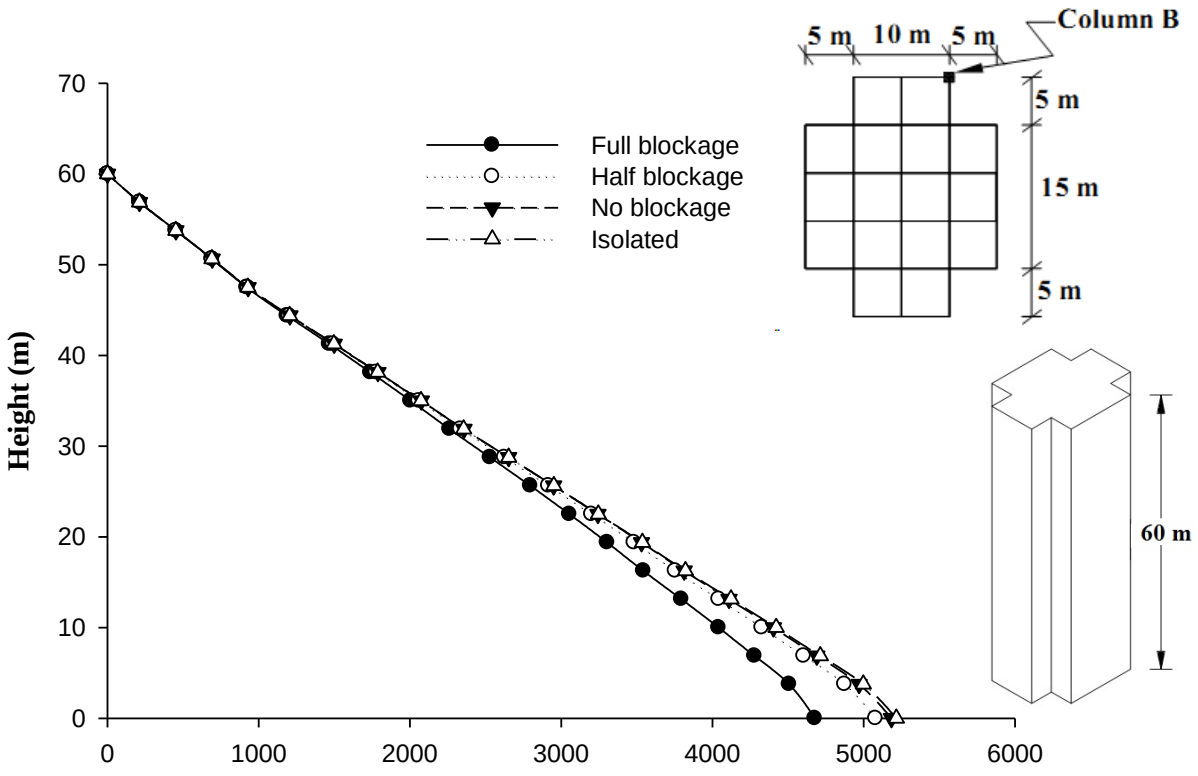


**Fig. 6.138 Interference effect on axial force in column-B of Plus Shape-1 building**

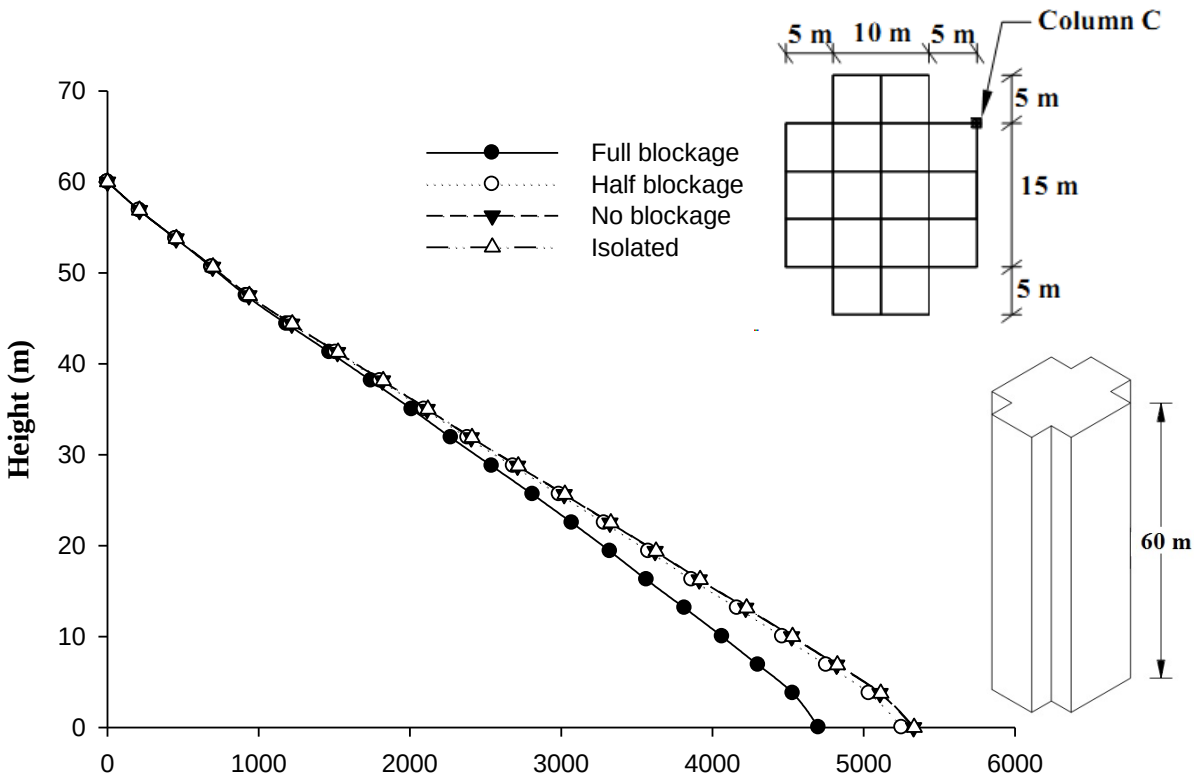


**Fig. 6.139 Interference effect on axial force in column-C of Plus Shape-1 building**

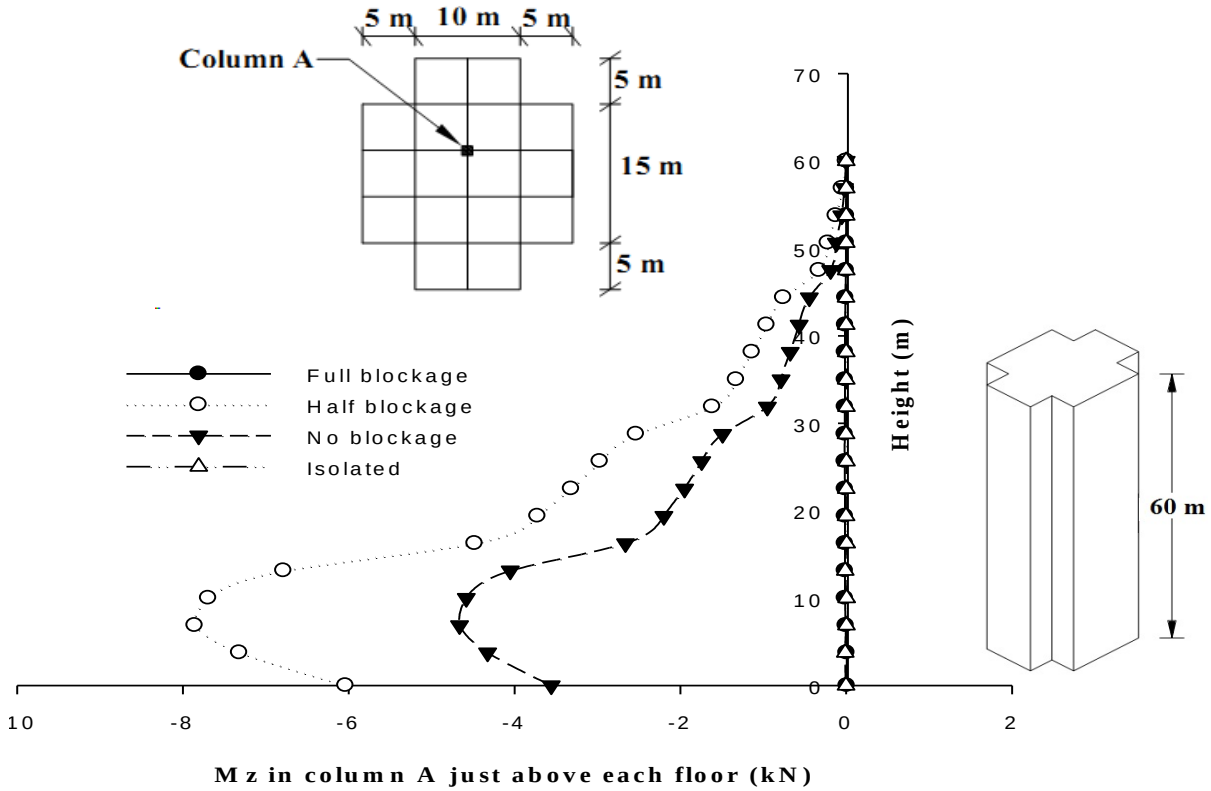


**Fig. 6.140 Interference effect on twisting moment Mz in column-A of Plus Shape-1 building**

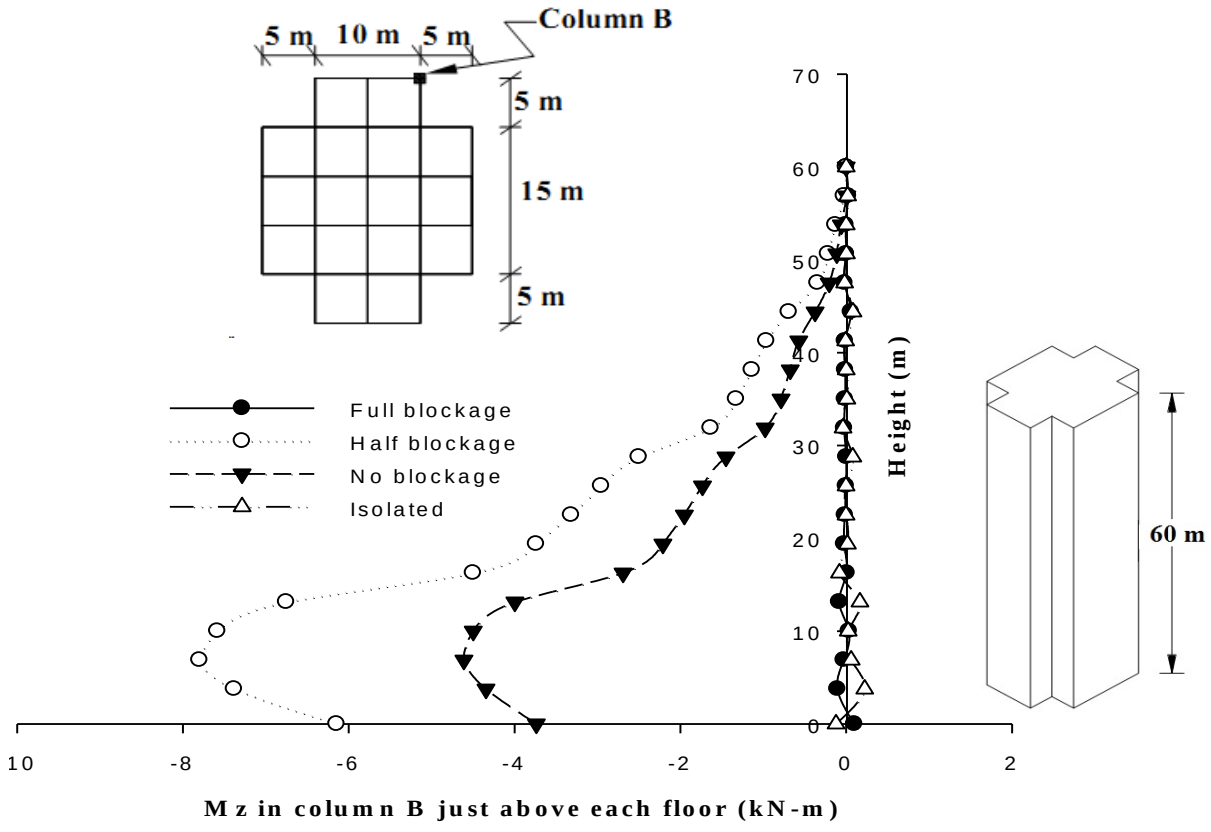


**Fig. 6.141 Interference effect on twisting moment Mz in column-B of Plus Shape-1 building**

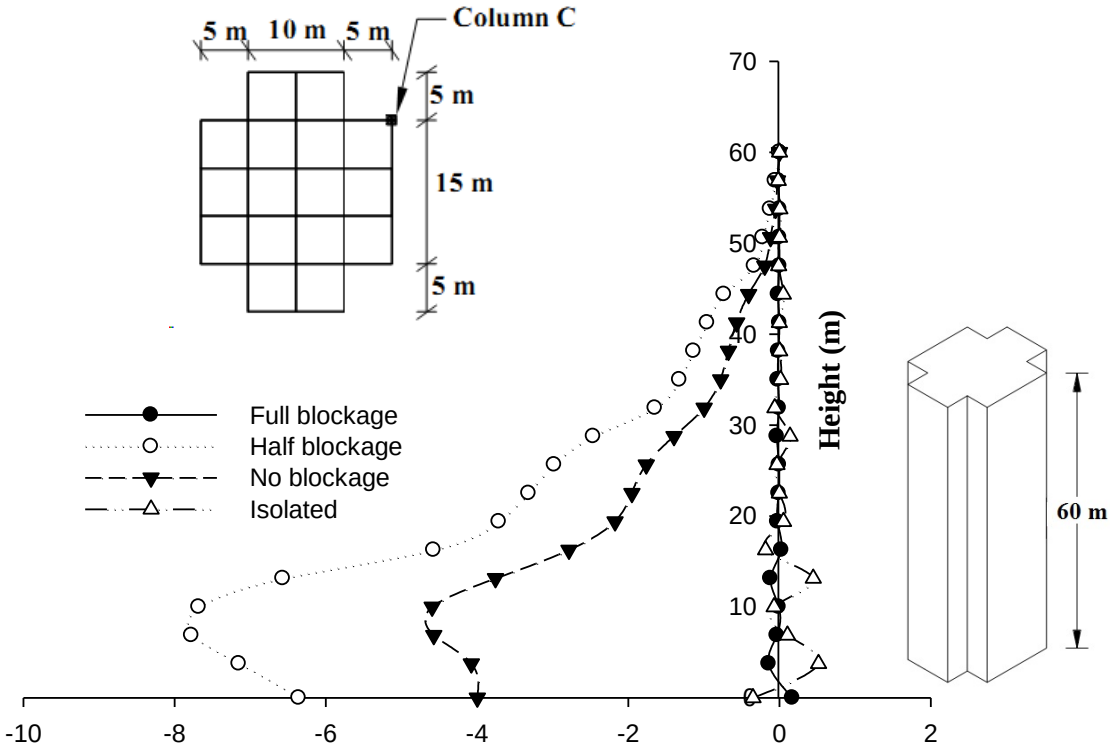


**Fig. 6.142 Interference effect on twisting moment Mz in column-C of Plus Shape-1 building**

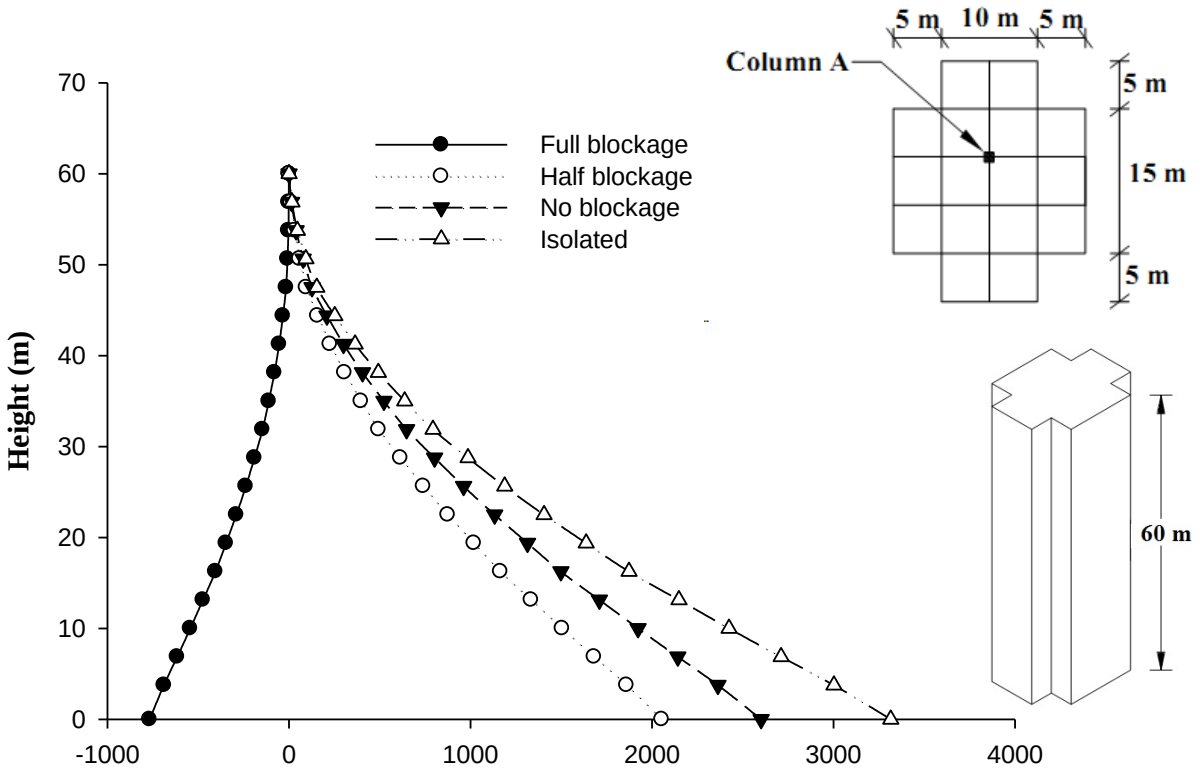


**Fig. 6.143 Interference effect on Mx (global) in column-A of Plus Shape-1 building**

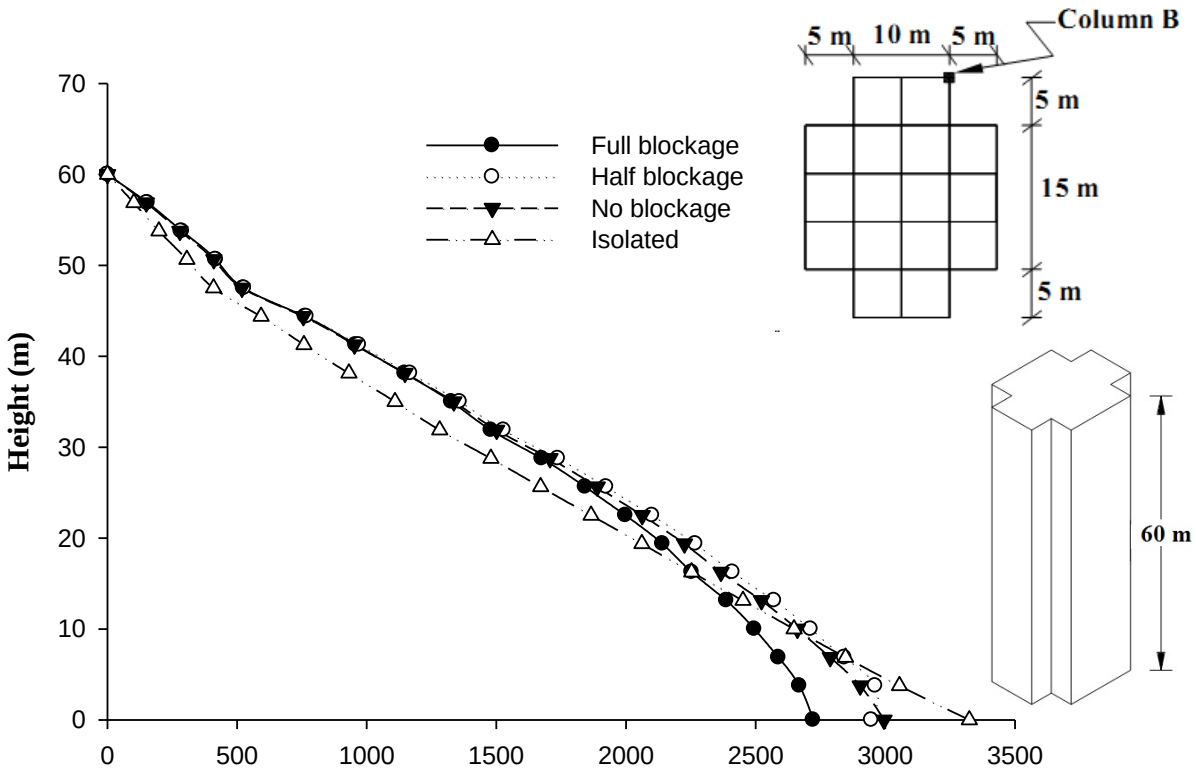


**Fig. 6.144 Interference effect on Mx (global) in column-B of Plus Shape-1 building**

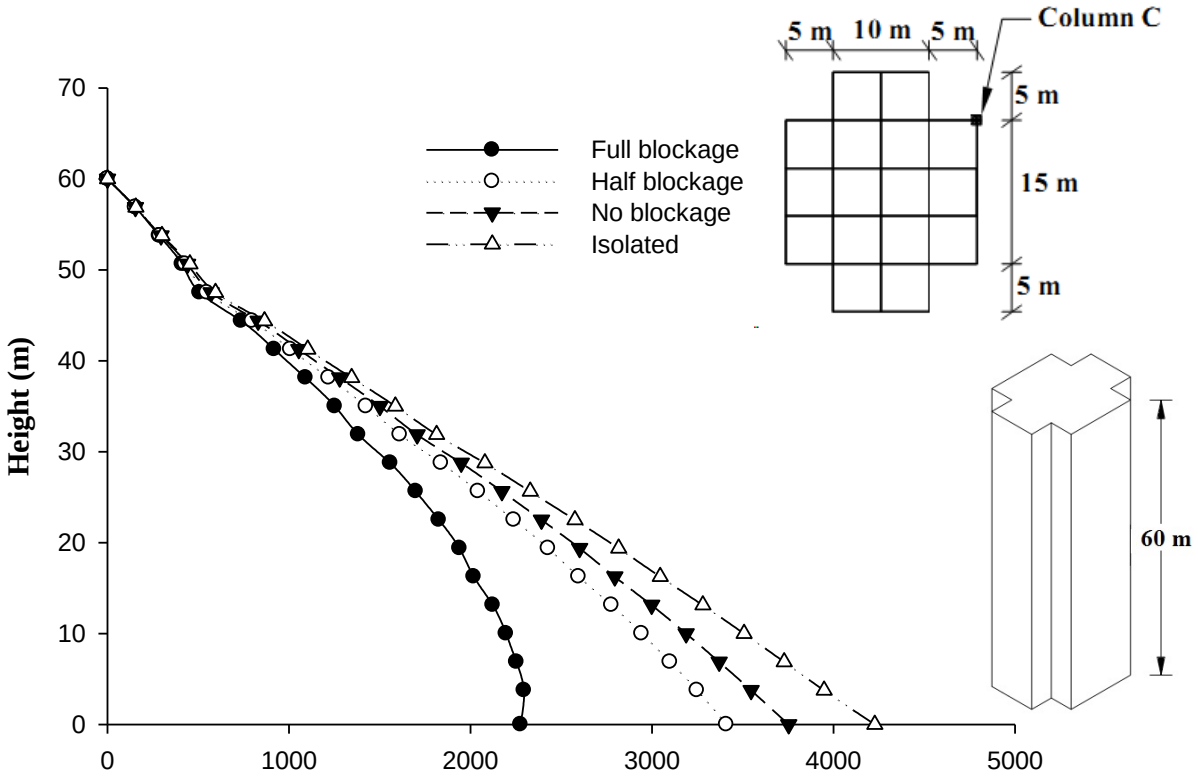


**Fig. 6.145 Interference effect on Mx (global) in column-C of Plus Shape-1 building**

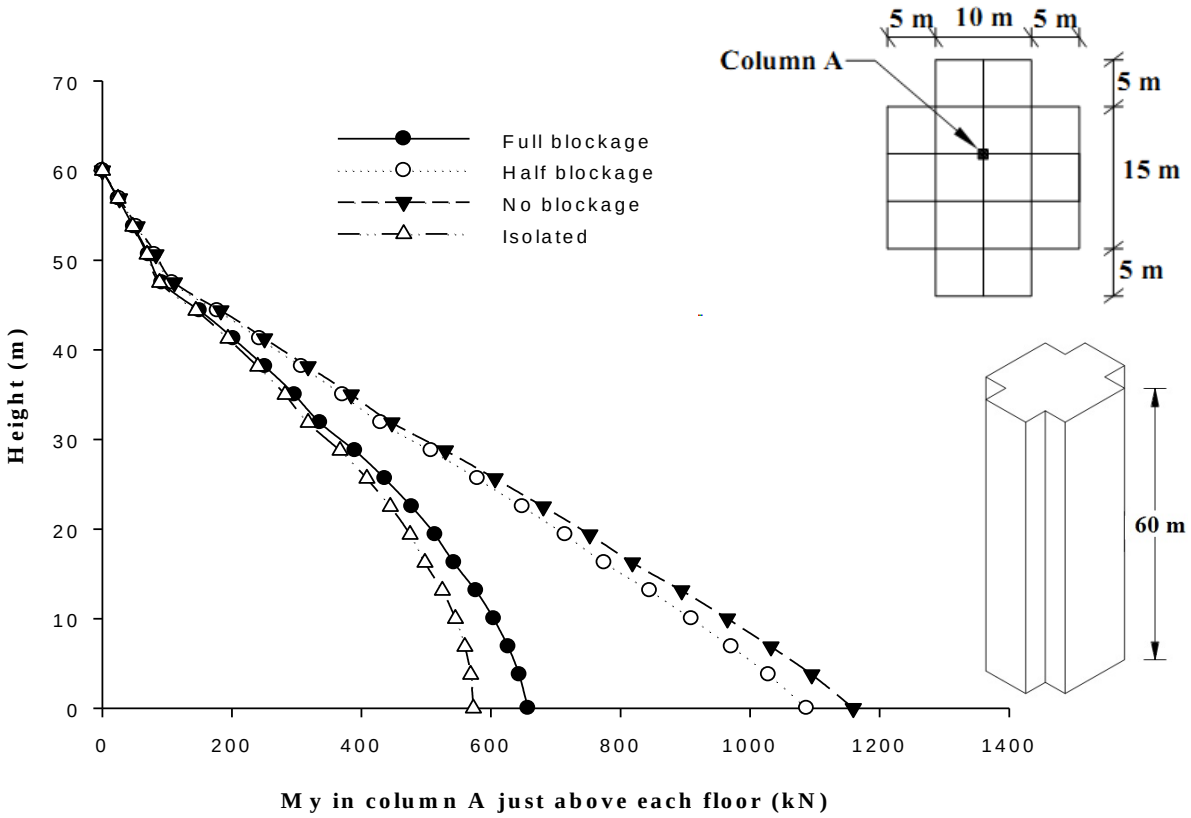


**Fig. 6.146 Interference effect on My (global) in column-A of Plus Shape-1 building**

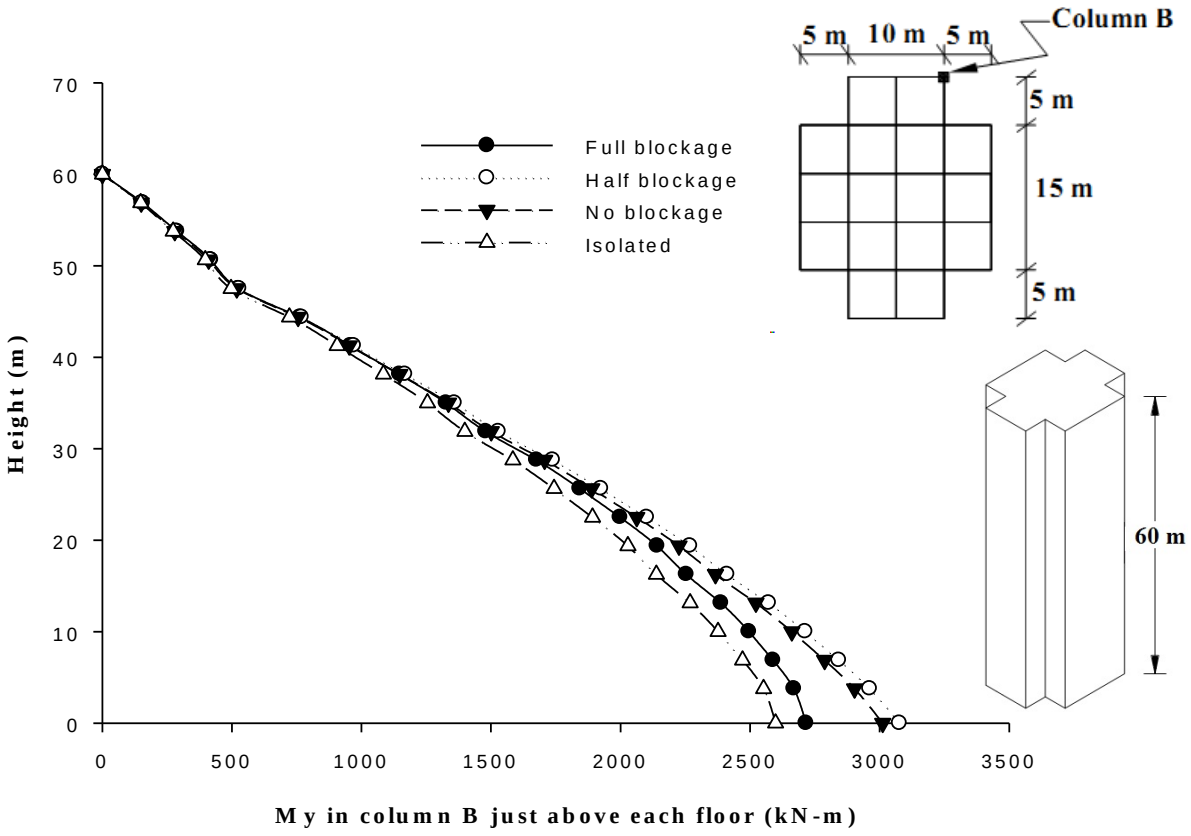


**Fig. 6.147 Interference effect on My (global) in column-B of Plus Shape-1 building**

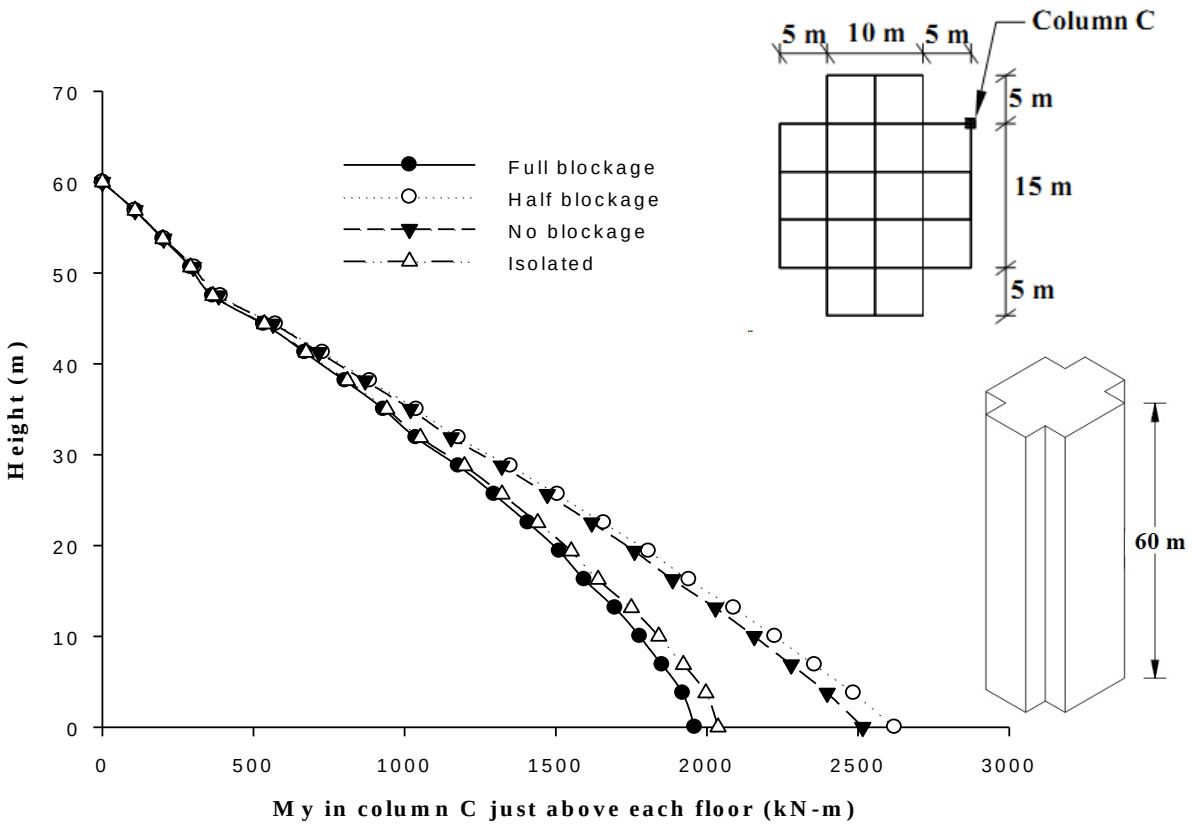


**Fig. 6.148 Interference effect on My (global) in column-C of Plus Shape-1 building**

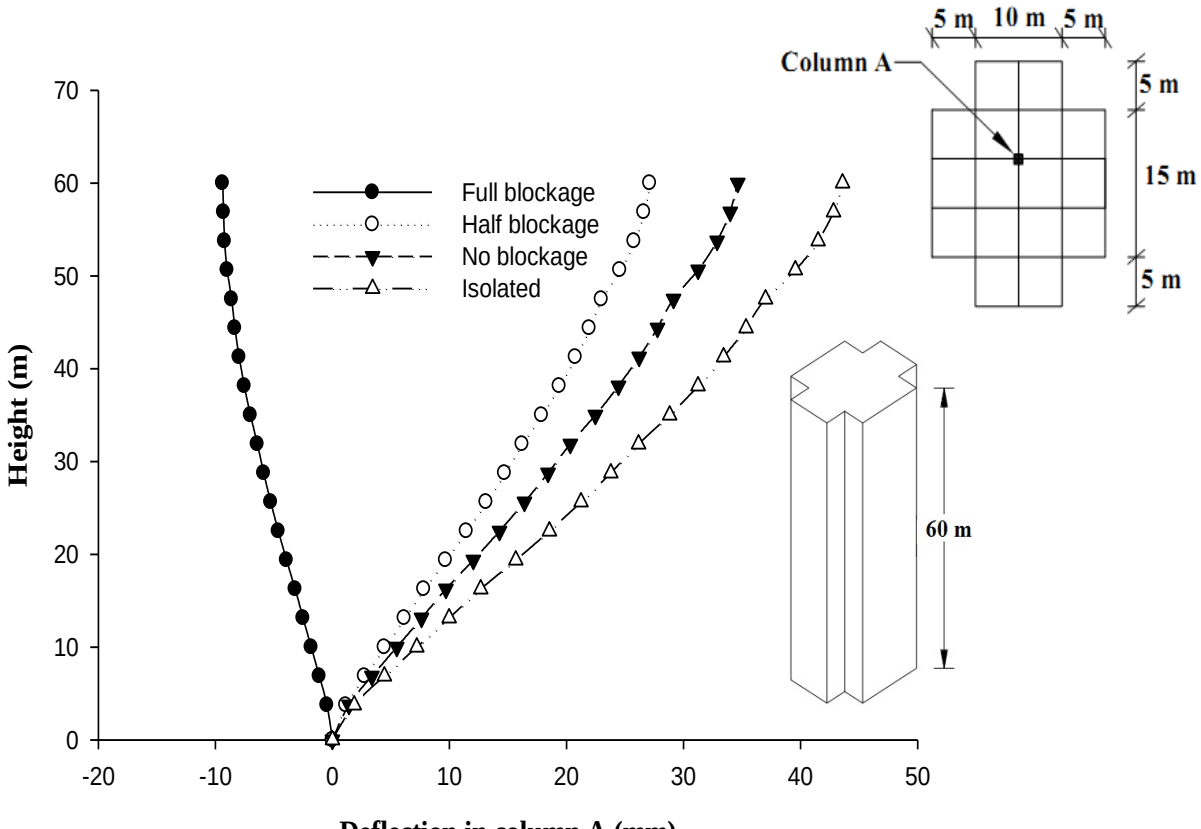


**Fig. 6.149 Interference effect on horizontal displacment of column-A of Plus Shape-1 building**

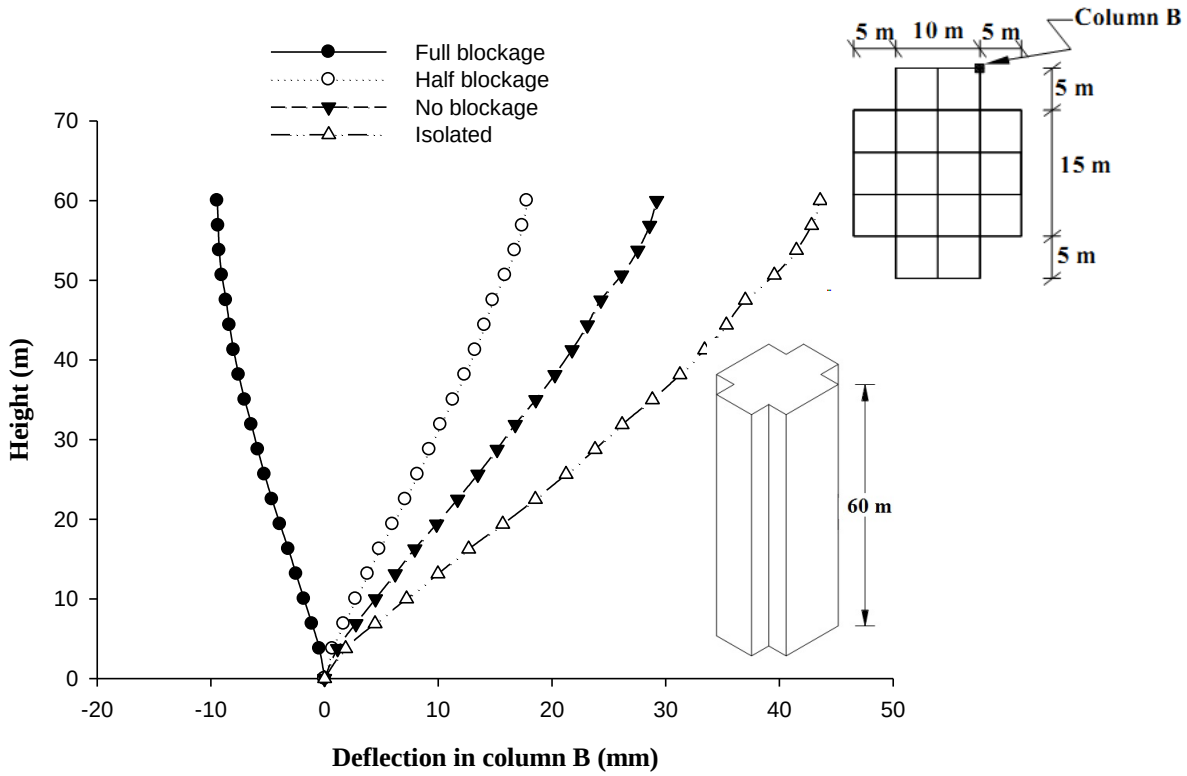


**Fig. 6.150 Interference effect on horizontal displacment of column-B of Plus Shape-1 building**

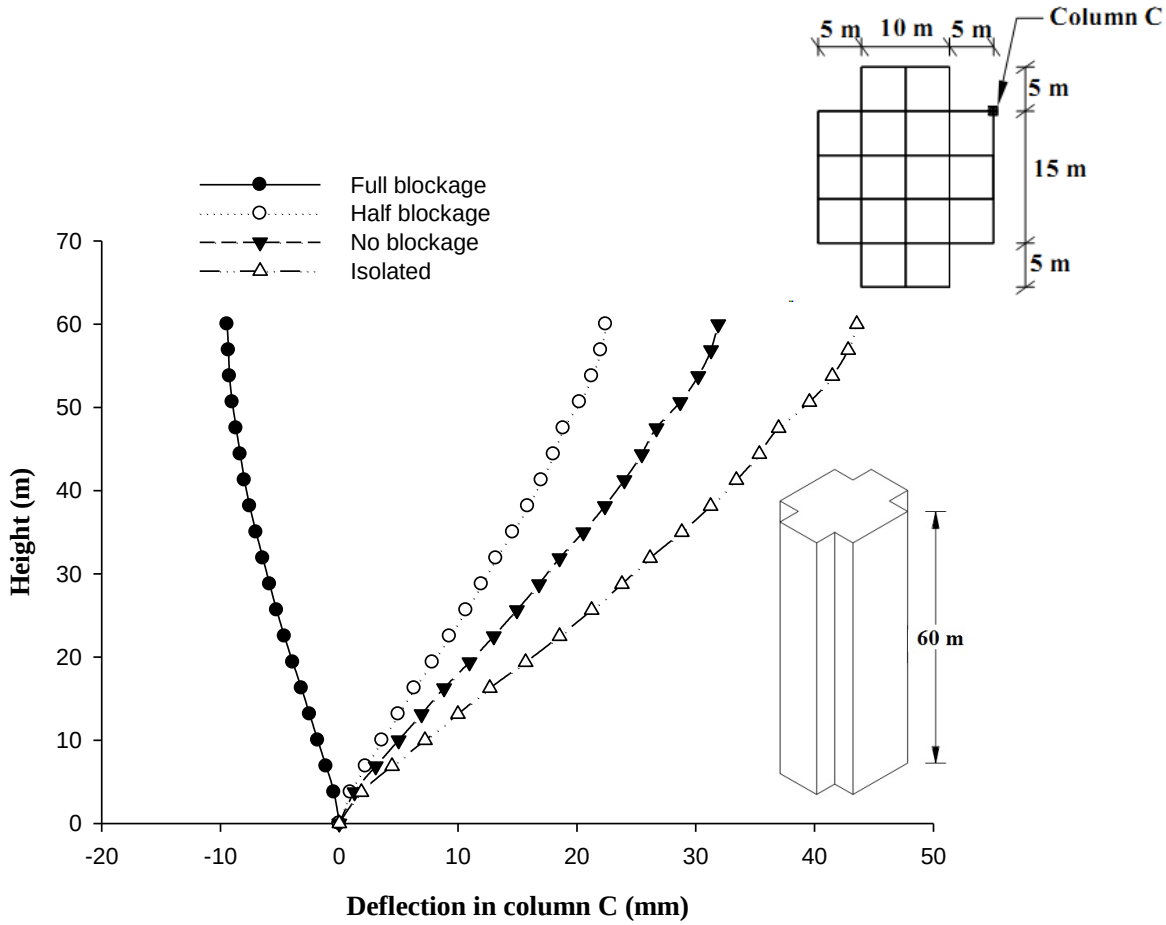


**Fig. 6.151 Interference effect on horizontal displacment in column-C of Plus Shape-1 building**

### 6.5.3 Plus Shape-2 Building

#### 6.5.3.1 Forces in columns

Effects of interference (Fig. 6.152) on axial force in column-A, B and C of Plus Shape-2 building can be seen in Figs. 6.153 to 6.155 respectively. It is noticed that whereas axial force in edge column i.e. column-A and corner column i.e. column-C are affected by interference conditions, the same in central column i.e. column-B is not affected. Variation of Mz due to interference can be seen in Figs. 6.156 to 6.158. It is maximum in half blockage interference condition. Further, values of twisting moment in other conditions are almost zero. Influence of interference on Mx is shown in Figs. 6.159 to 6.161 and on My in Figs. 6.162 to 6.164. Mx in case of all three columns are highly influenced by blockage condition. It in case of edge column, i.e. column-A is maximum at full blockage interference condition. It is maximum in isolated condition in case of central column, i.e. column-B and corner column, i.e. column-C. Values of Mx in no blockage condition in both these columns are slightly less than that in isolated condition.

Moment about 'Y' axis, i.e. My is not affected much by blockage condition in case of edge column i.e. column-A. Its value is maximum in half blockage condition in both central and corner columns, i.e. column-B and C.

#### 6.5.3.2 Displacment of columns

Columns in Plus Shape-2 building also show similar deflection pattern as Square Shape and Plus Shape-1 buildings (Figs. 6.165 to 6.167). All three columns under consideration show maximum deflection in isolated condition. Values of deflection in no blockage condition are slightly smaller than but close to corresponding values in isolated condition.

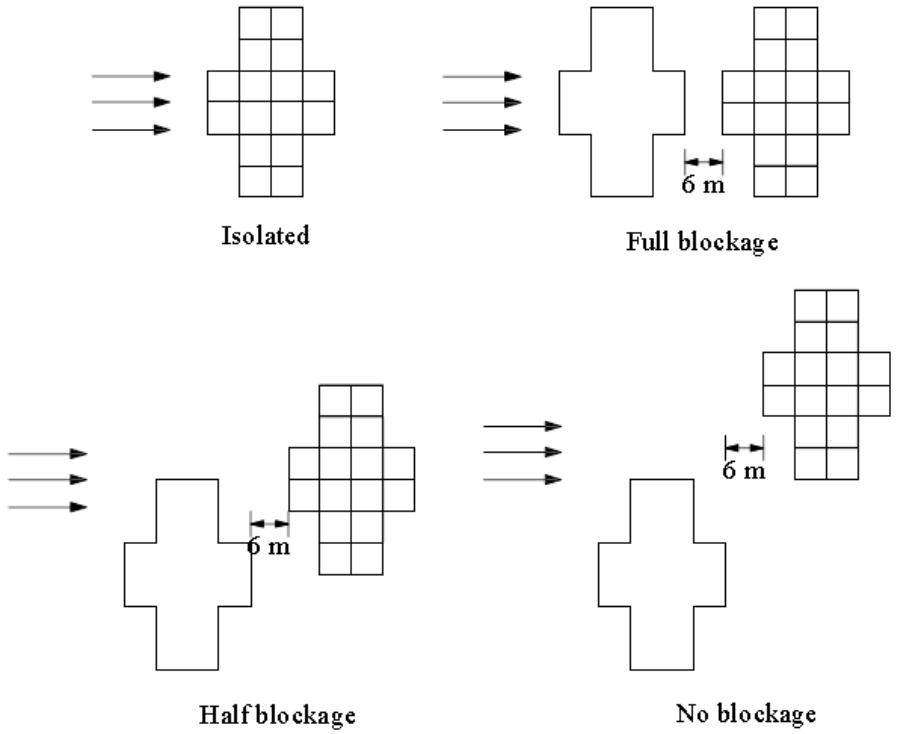


**Fig. 6.152 Relative position of Plus Shape-2 buildings under different interference conditions**

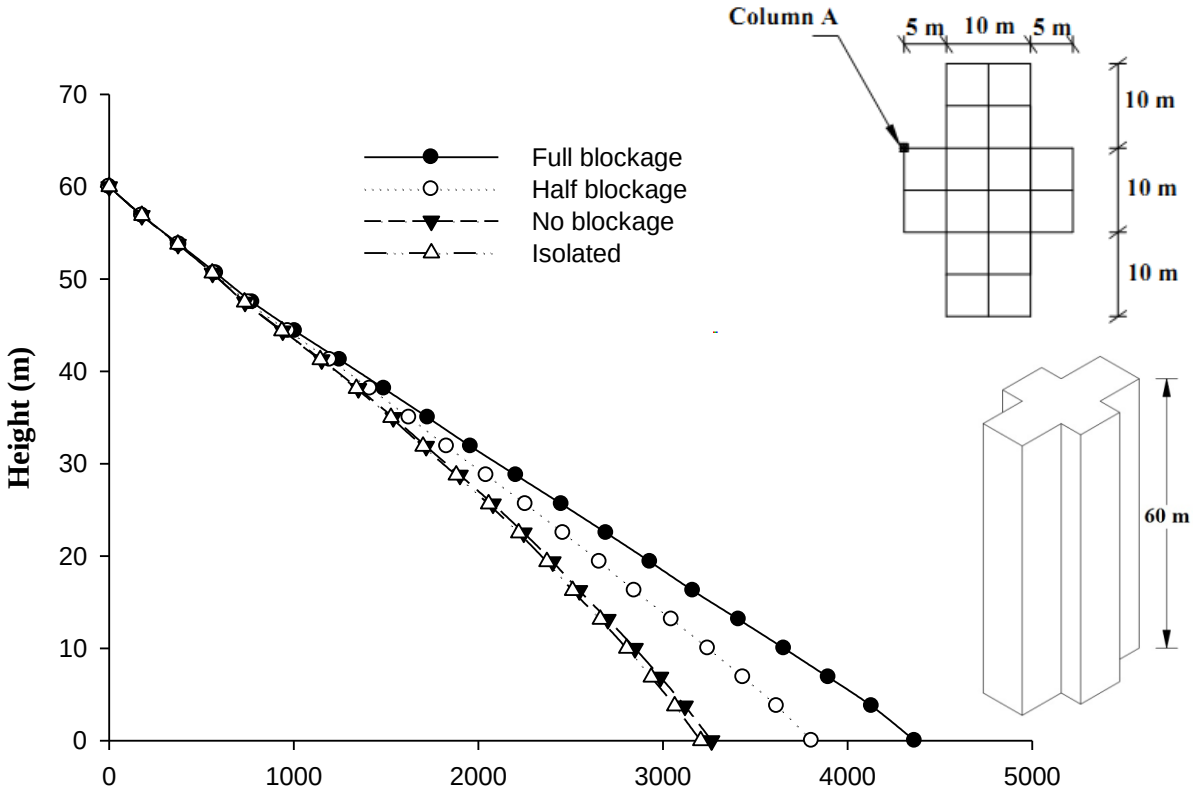


**Fig. 6.153 Interference effect on axial force in column-A of Plus Shape-2 building**

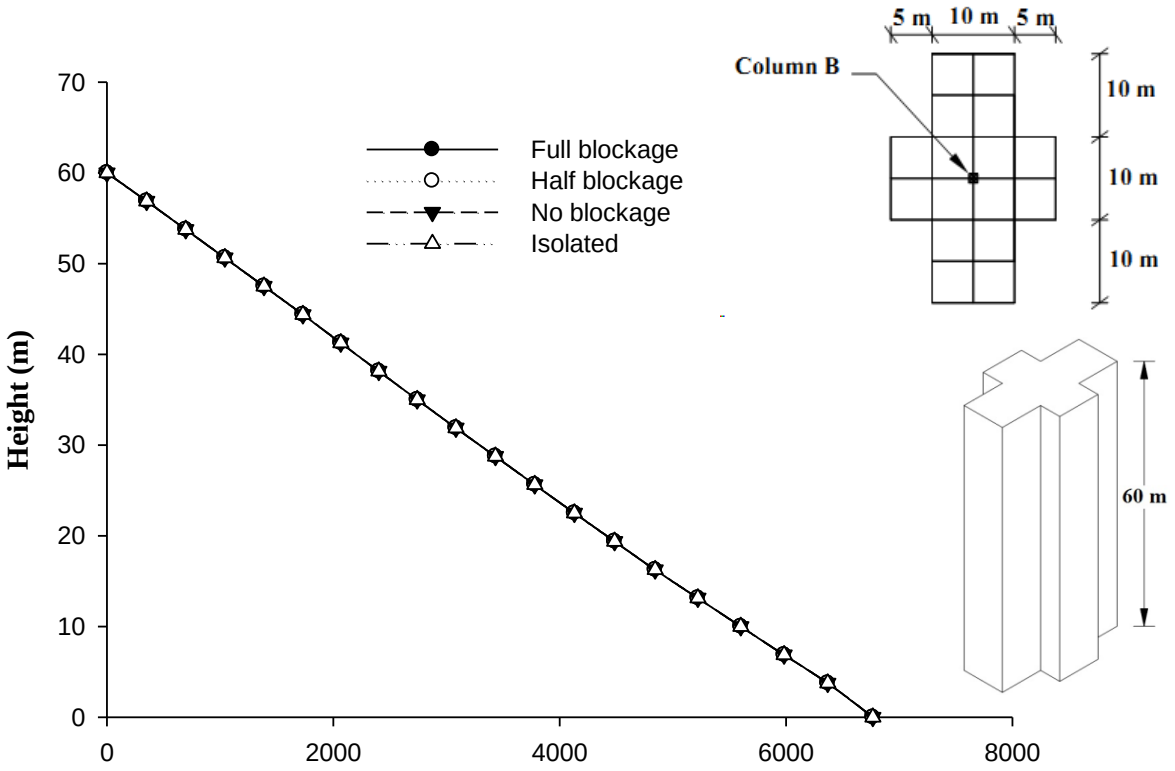


**Axial force in column B just above each floor (kN)**

**Fig. 6.154 Interference effect on axial force in column-B of Plus Shape-2 building**

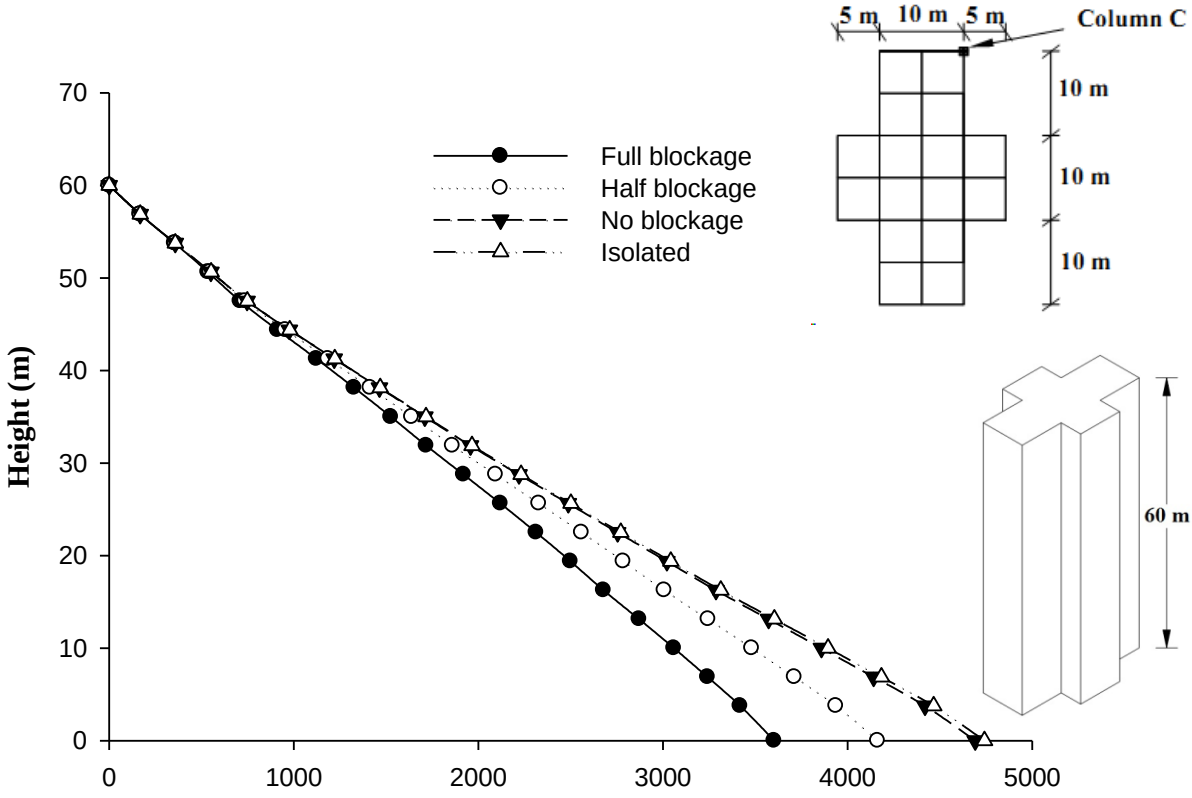


**Axial force in column C just above each floor (kN)**

**Fig. 6.155 Interference effect on axial force in column-C of Plus Shape-2 building**

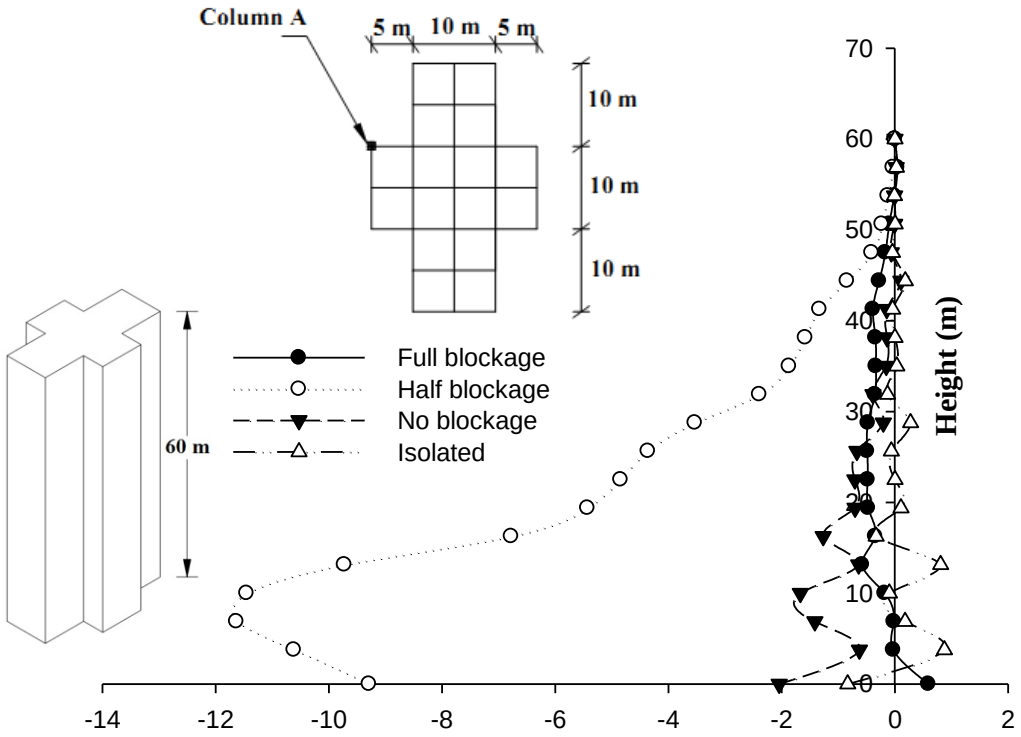


**Mz in column A just above each floor (kN-m)**

**Fig. 6.156 Interference effect on twisting moment Mz in column-A of Plus Shape-2 building**

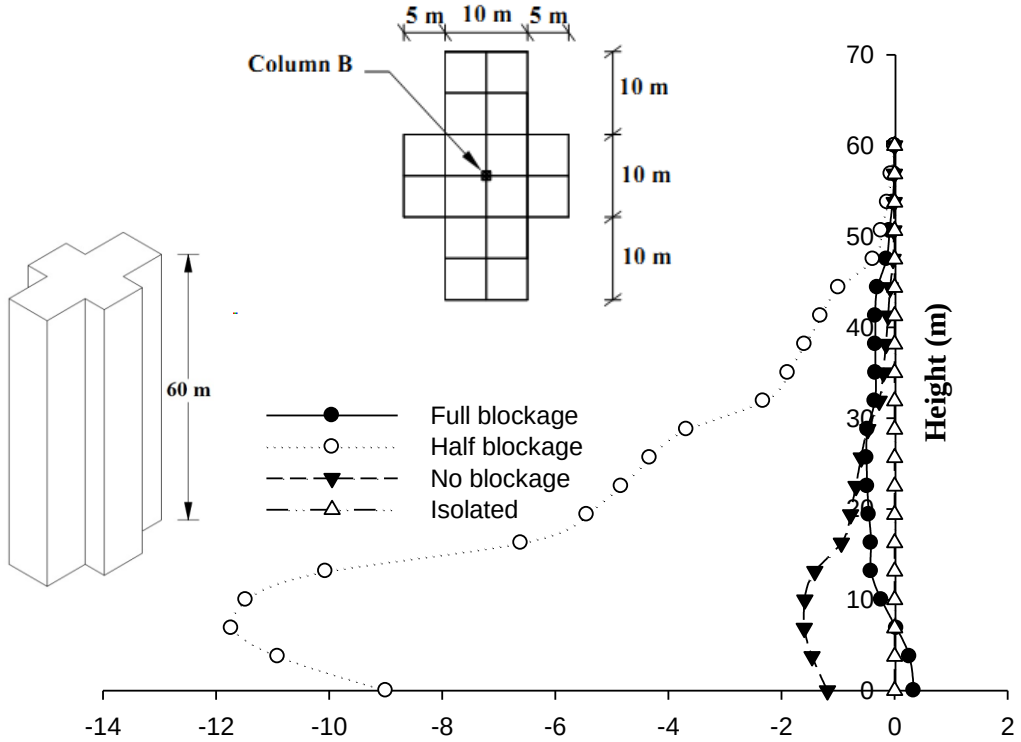


**Mz in column B just above each floor (kN-m)**

**Fig. 6.157 Interference effect on twisting moment Mz in column-B of Plus Shape-2 building**

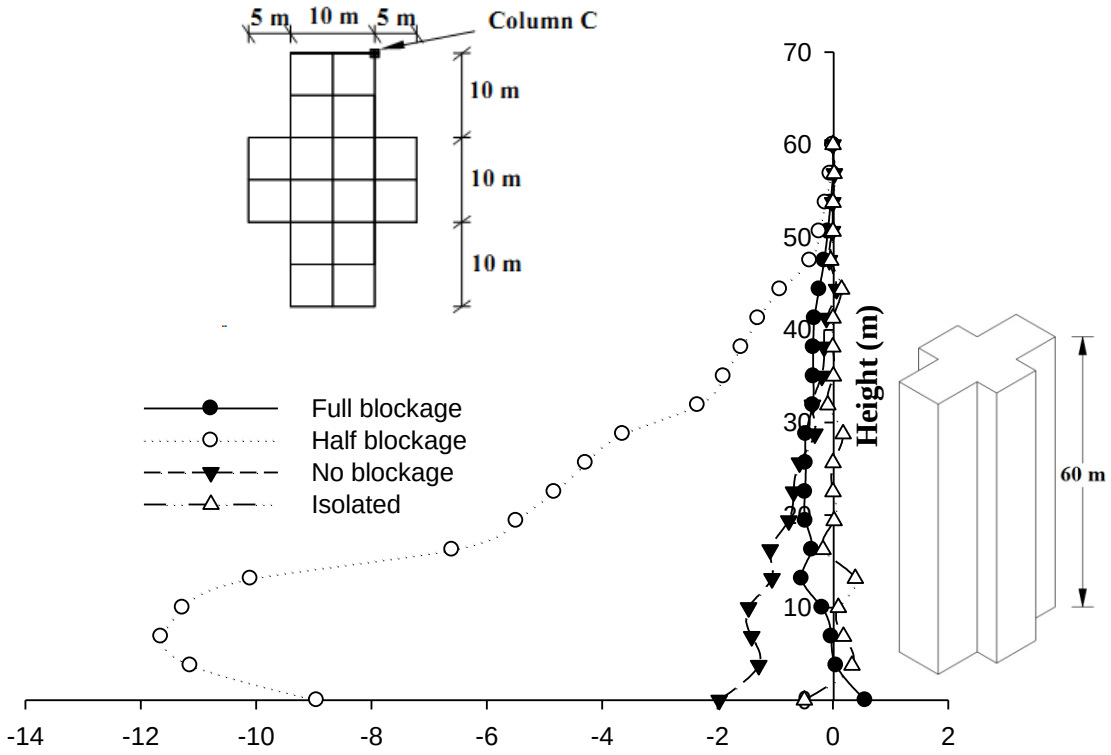


**Mz in column C just above each floor (kN-m)**

**Fig. 6.158 Interference effect on twisting moment Mz in column-C of Plus Shape-2 building**

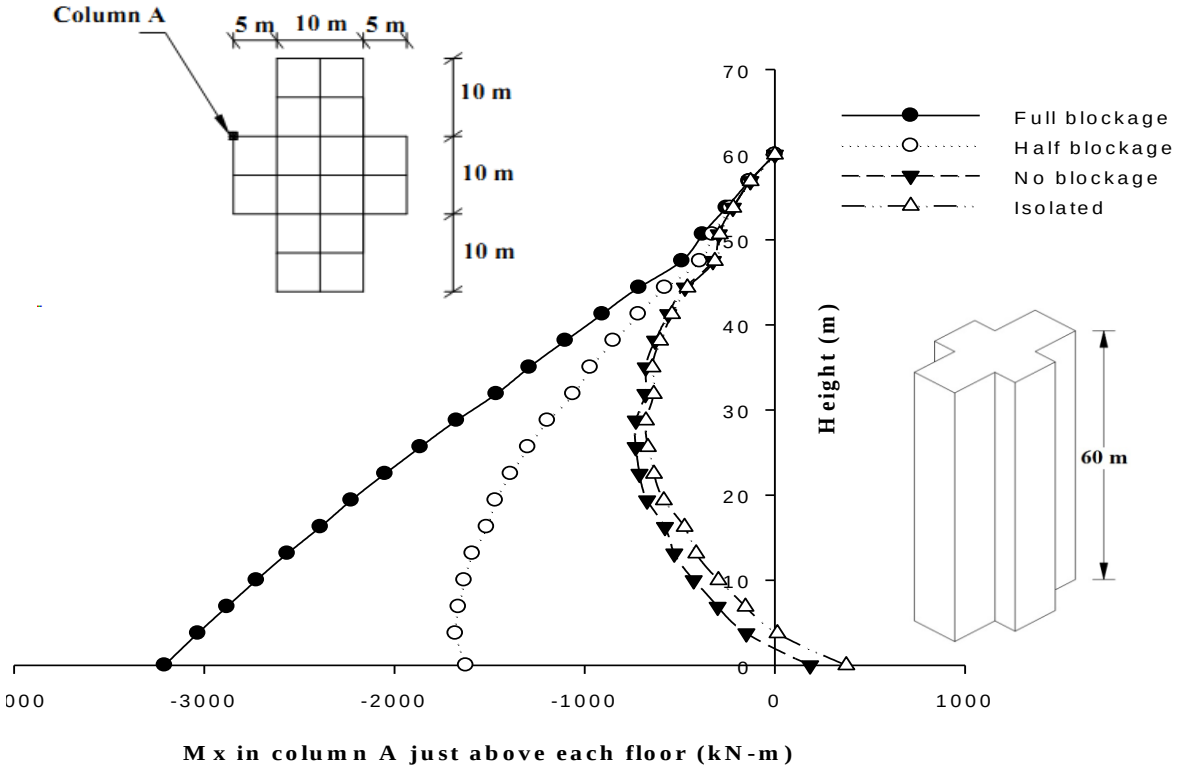


**Fig. 6.159 Interference effect on Mx (global) in column-A of Plus Shape-2 building**

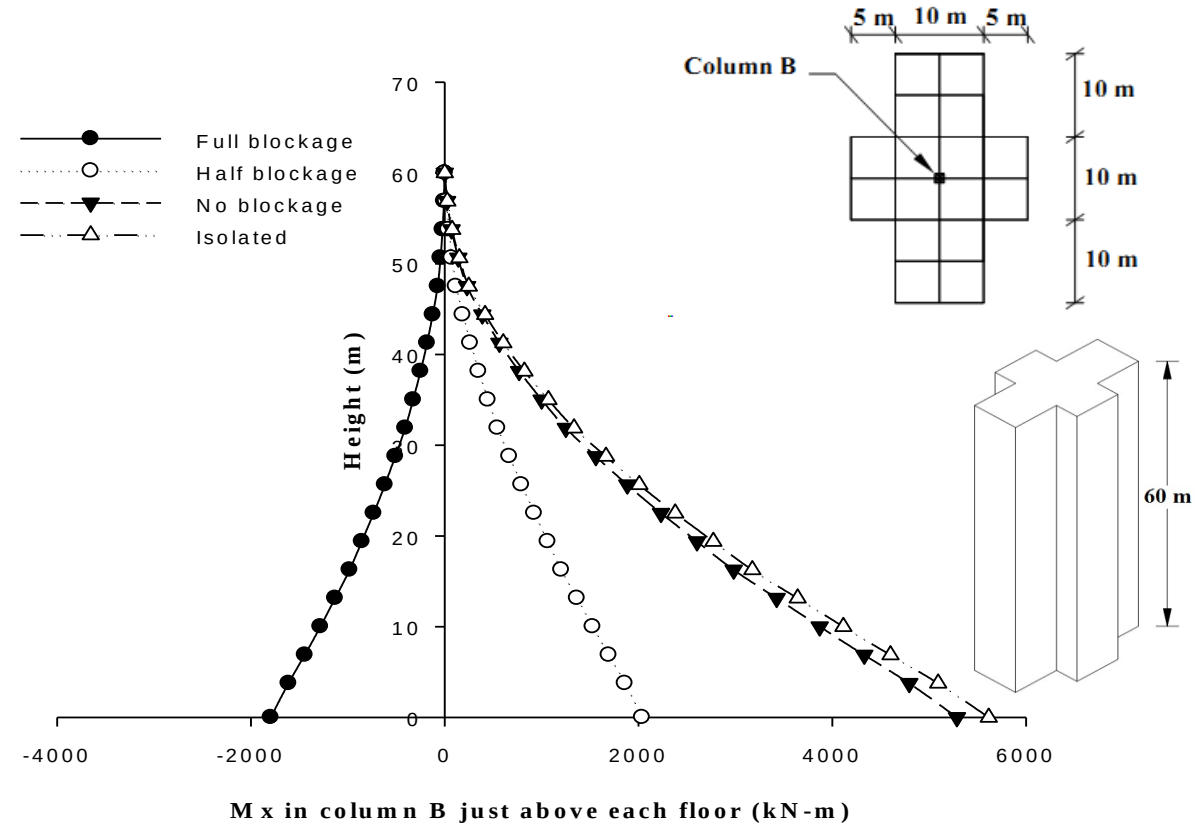


**Fig. 6.160 Interference effect on Mx (global) in column-B of Plus Shape-2 building**

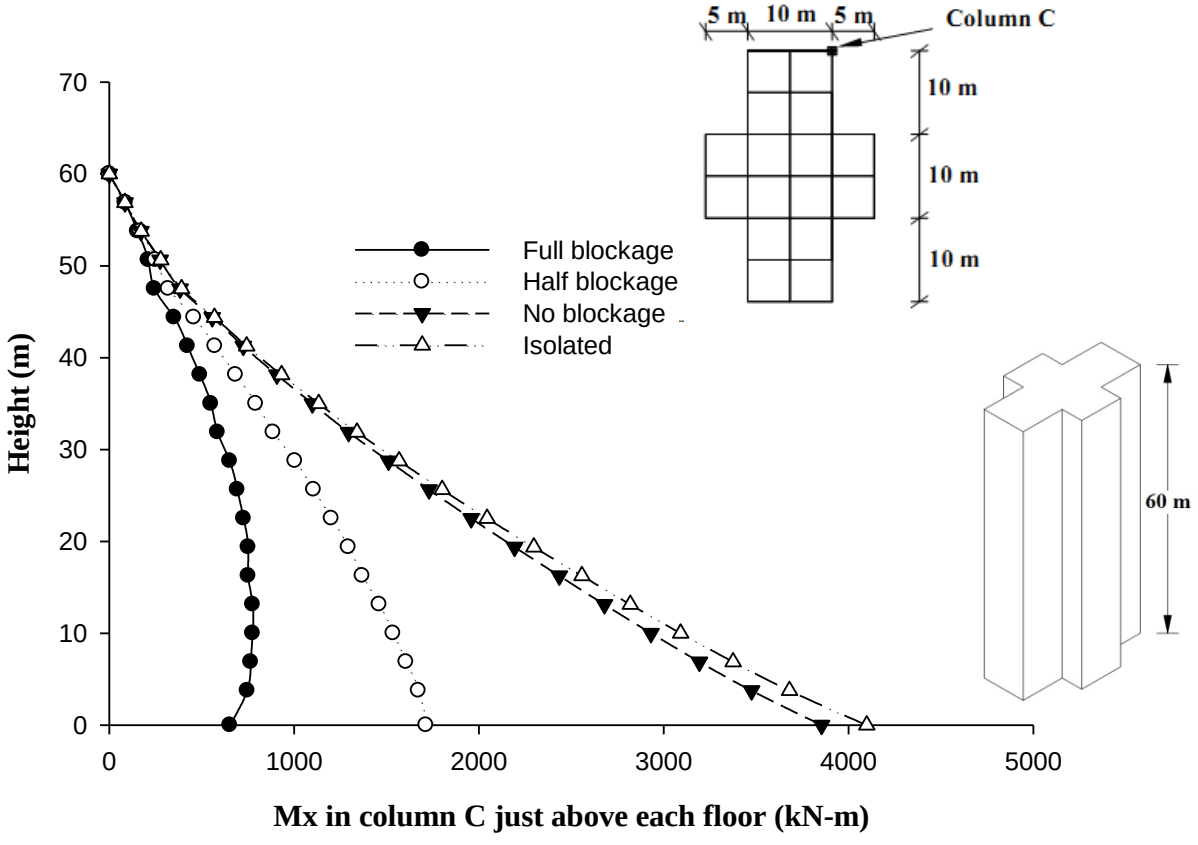


**Fig. 6.161 Interference effect on Mx (global) in column-C of Plus Shape-2 building**

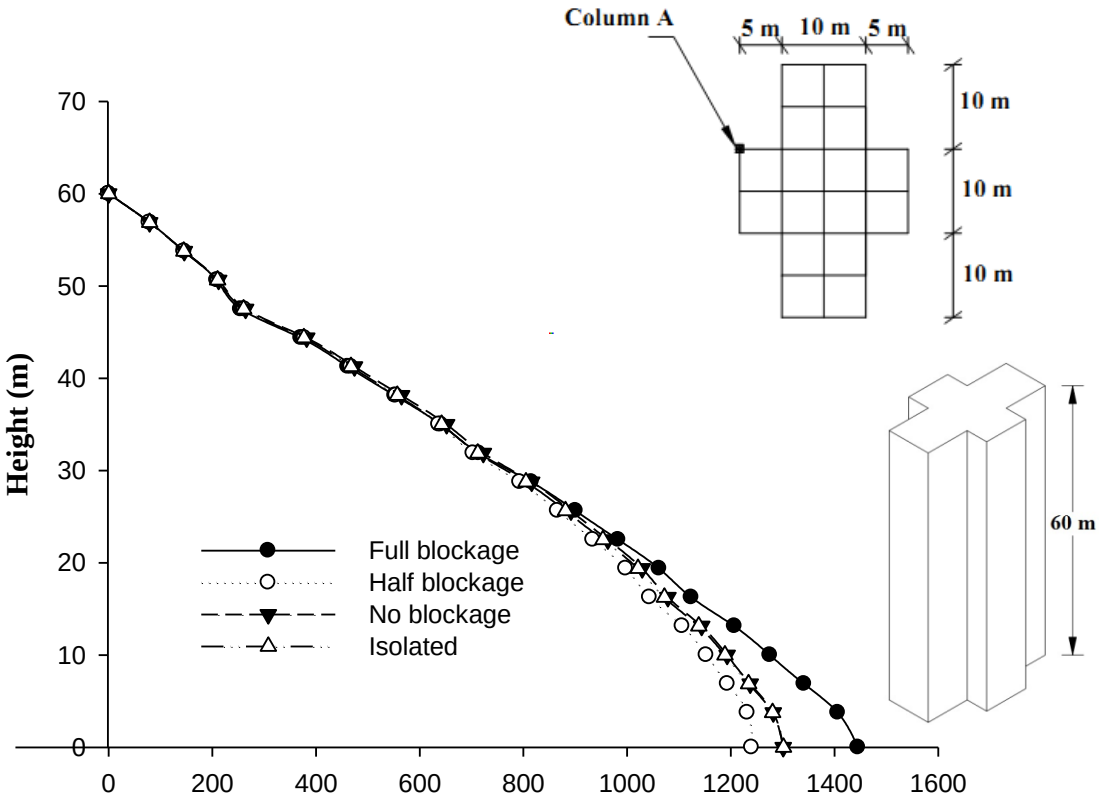


**Fig. 6.162 Interference effect on My (global) in column-A of Plus Shape-2 building**

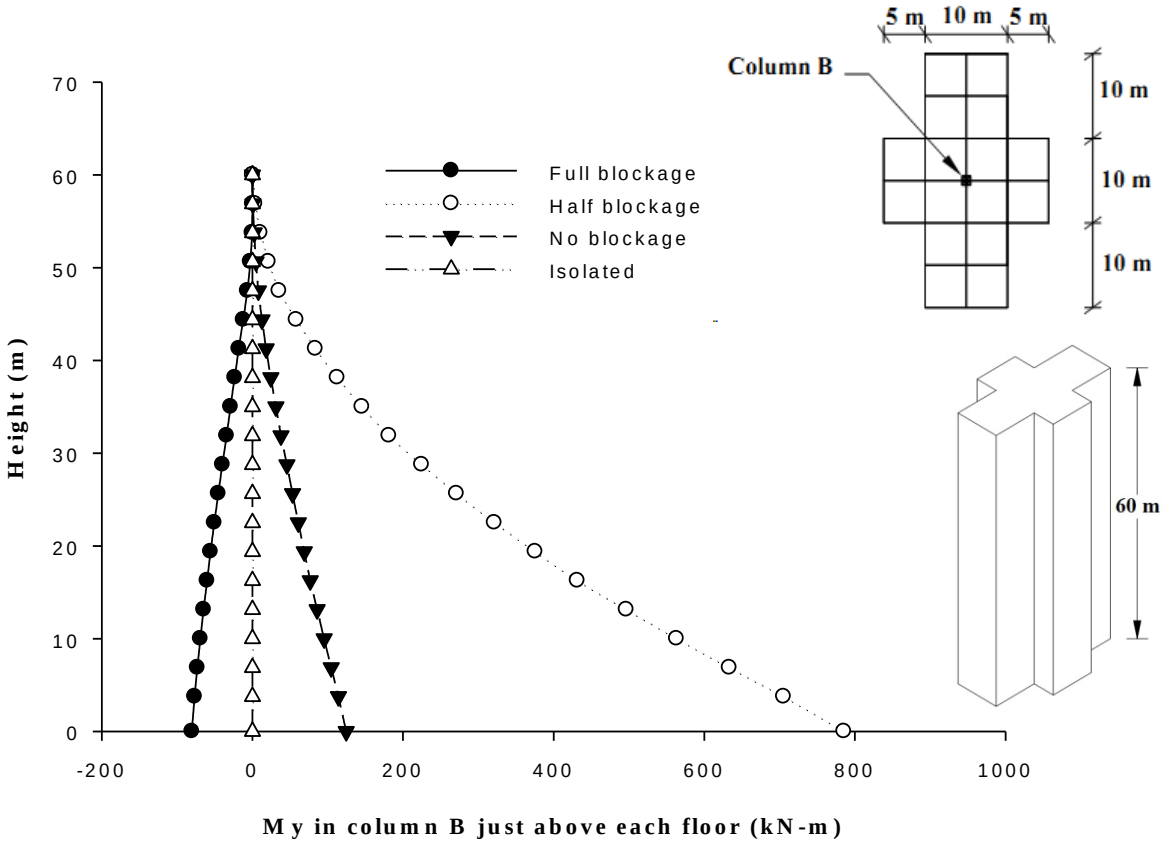


**Fig. 6.163 Interference effect on My (global) in column-B of Plus Shape-2 building**

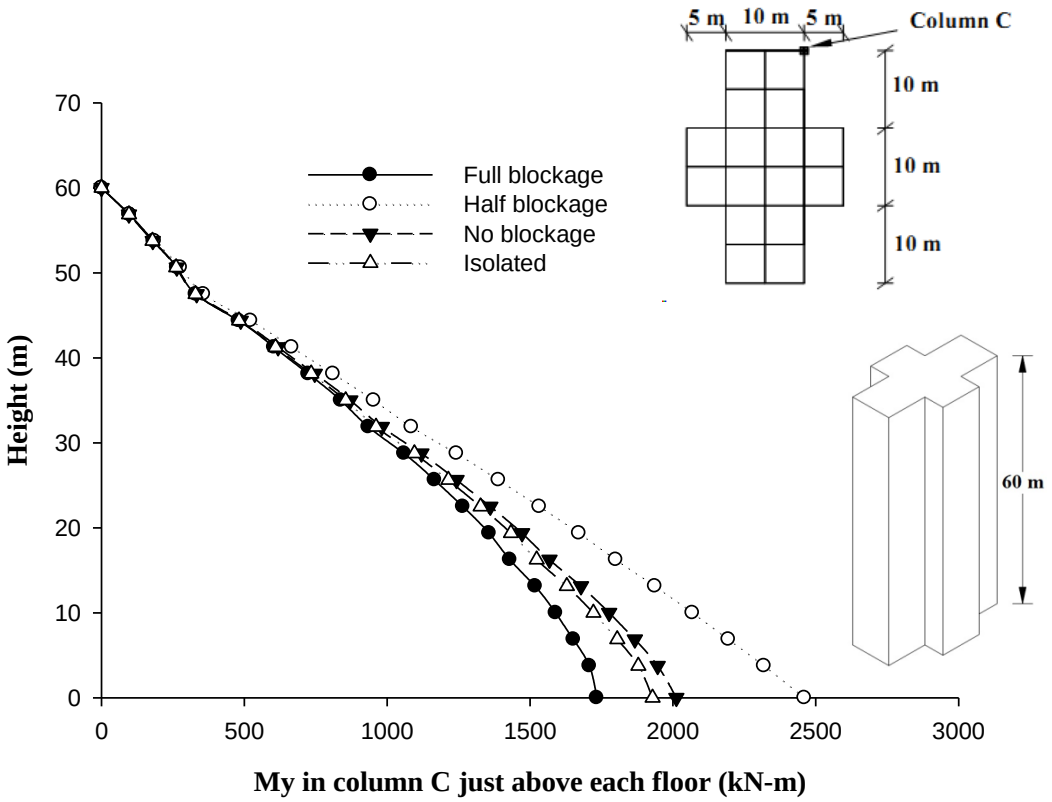


**Fig. 6.164 Interference effect on My (global) in column-C of Plus Shape-2 building**

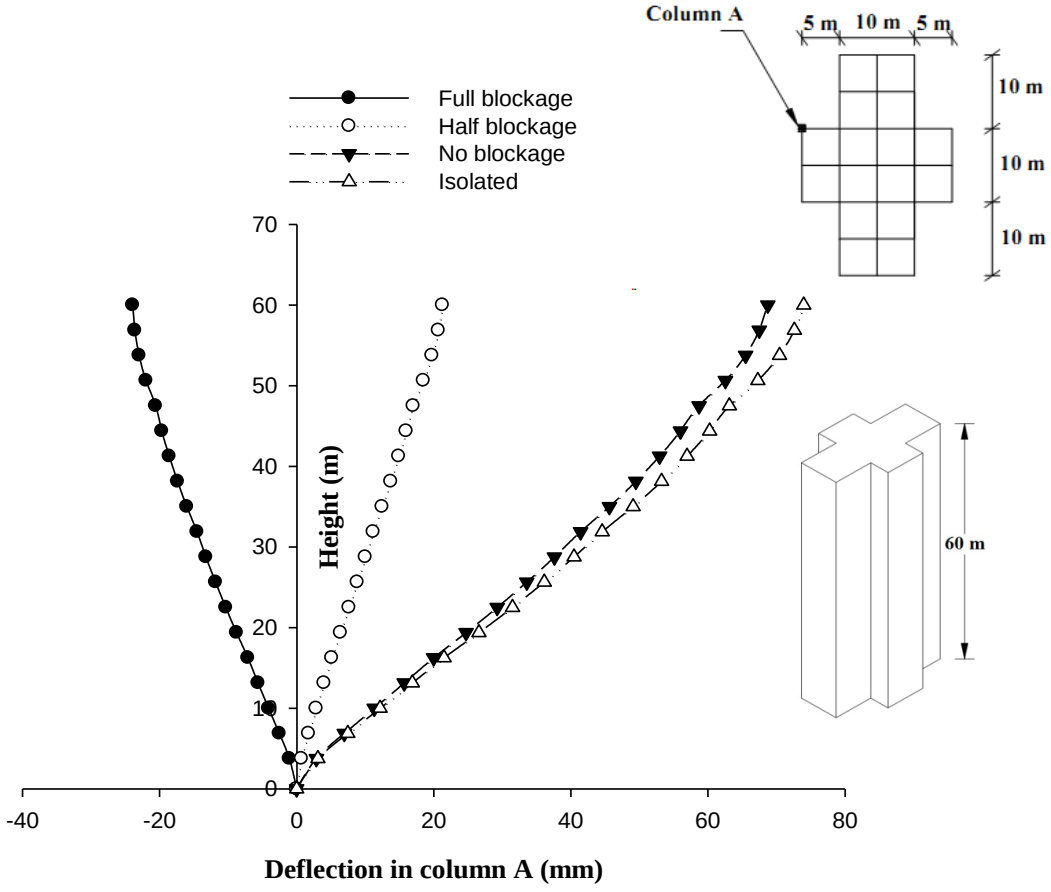


**Fig. 6.165 Interference effect on horizontal displacment of column-A of Plus Shape-2 building**

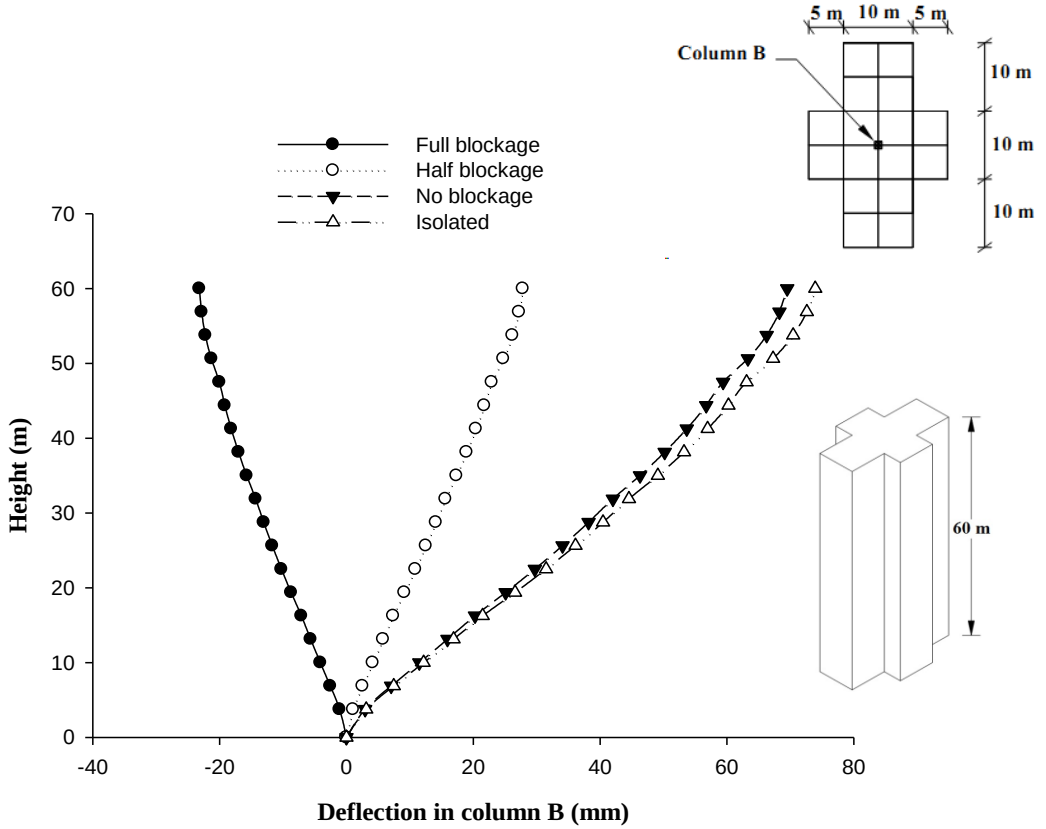


**Fig. 6.166 Interference effect on horizontal displacment of column-B of Plus Shape-2 building**

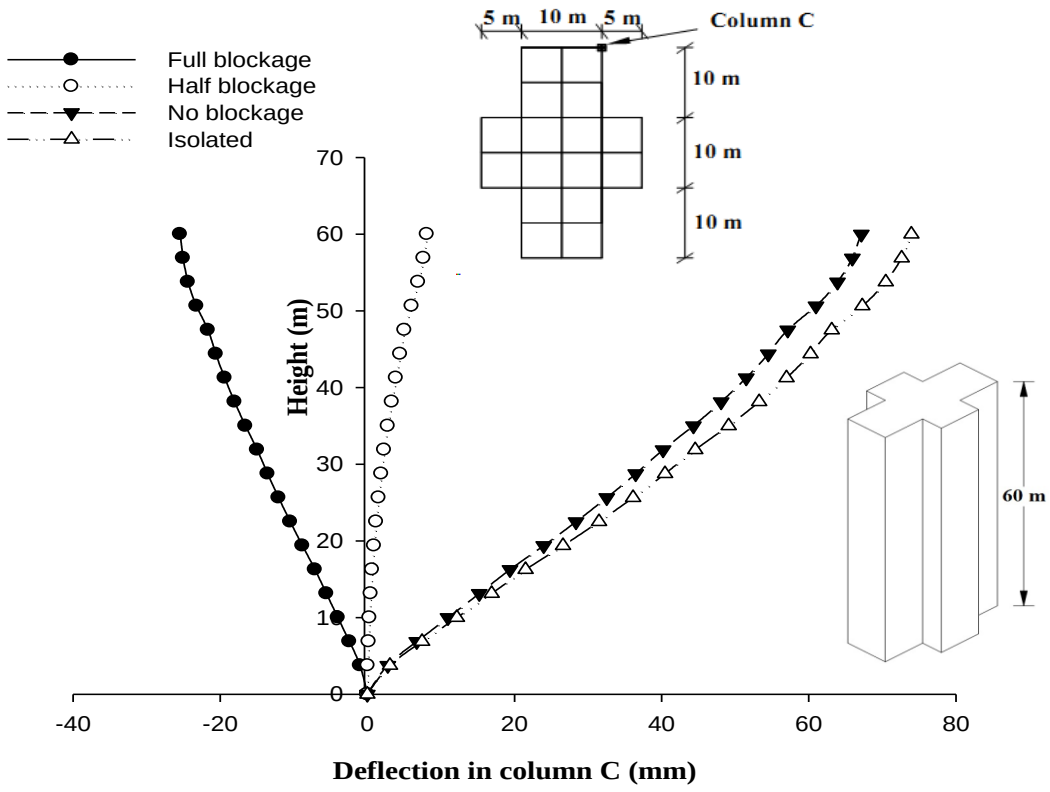


**Fig. 6.167 Interference effect on horizontal displacement of column-C of Plus Shape-2 building**

### 6.5.4 I-Shape-1 Building

#### 6.5.4.1 Forces in columns

Figures 6.169 to 6.180 show the results of force and moments for column-A, B and C in isolated condition and three interference conditions namely full blockage, half blockage and no blockage (Fig. 6.168). Axial force, twisting moment, moment about 'X' and 'Y' axis, all are plotted along the height to check the effects of wind forces at each floor of I-Shape-1 building. Figures 6.169 to 6.171 show the plot of axial force in column-A, B and C respectively. Whereas blockage conditions have no effect on axial force in central column i.e. column-B, it have small effects on axial forces in edge column i.e. column-A and corner column i.e. column-C.

Variation of twisting moment Mz can be seen in Figs. 6.172 to 6.174. All three columns under consideration are subjected to similar values of twisting moment at different interference conditions. All of them are subjected to maximum twisting moment in half blockage condition.

Moment about 'X' axis i.e. Mx is shown in Figs. 6.175 to 6.177 for column-A, B and C respectively. There is large influence of interference on moment about 'X' axis in all columns. Whereas Mx in edge column is maximum at full blockage condition, its values in central column and corner column are maximum at isolated condition. Values of Mx in these two columns in no blockage condition are slightly less than those in isolated condition.

Moment My drawn with repsect to height are shown in Figs. 6.178 to 6.180. My in column-A and column-C is maximum in half blockage condition. Its value in column-B is maximum in full blockage condition which is as close as the value in isolated condition.

#### 6.5.4.2 Displacement of columns

In case of I-Shape-1 building also, all three columns move in –ve X-direction at full blockage condition (Figs. 6.181 to 6.183). Deflection in +ve X-direction is maximum at isolated condition in all columns, followed by its value in no blockage condition.

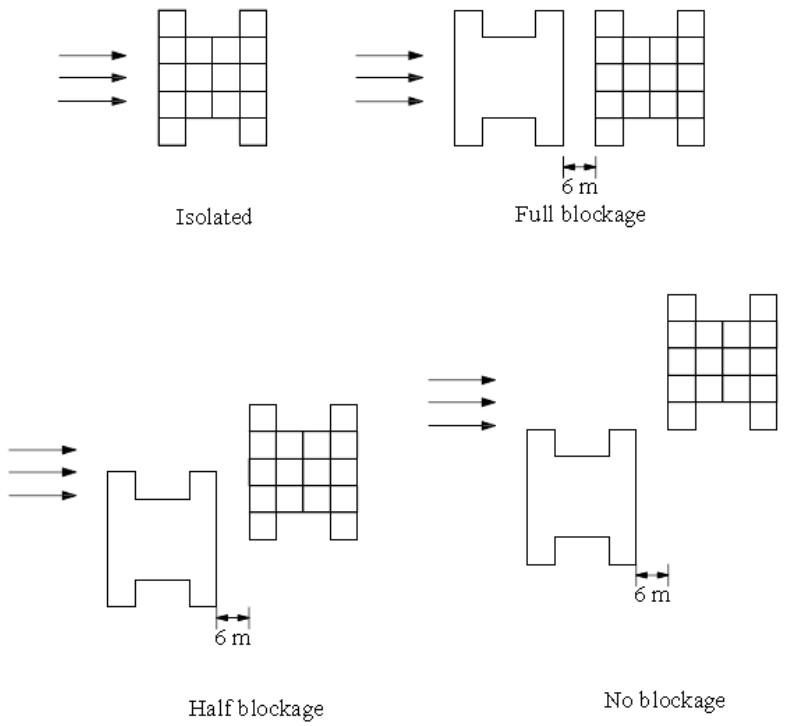


**Fig. 6.168 Relative position of I-Shape-1 buildings under different interference conditions**

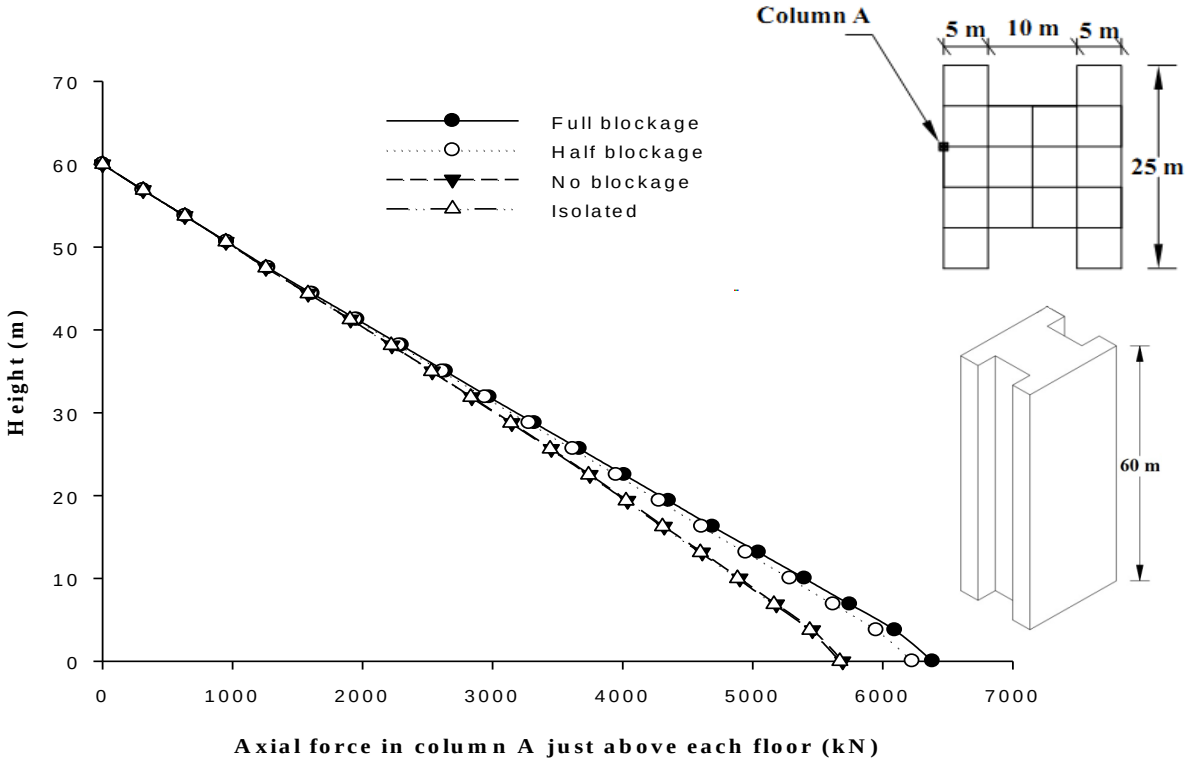


**Fig. 6.169 Interference effect on axial force in column-A of I-Shape-1 building**

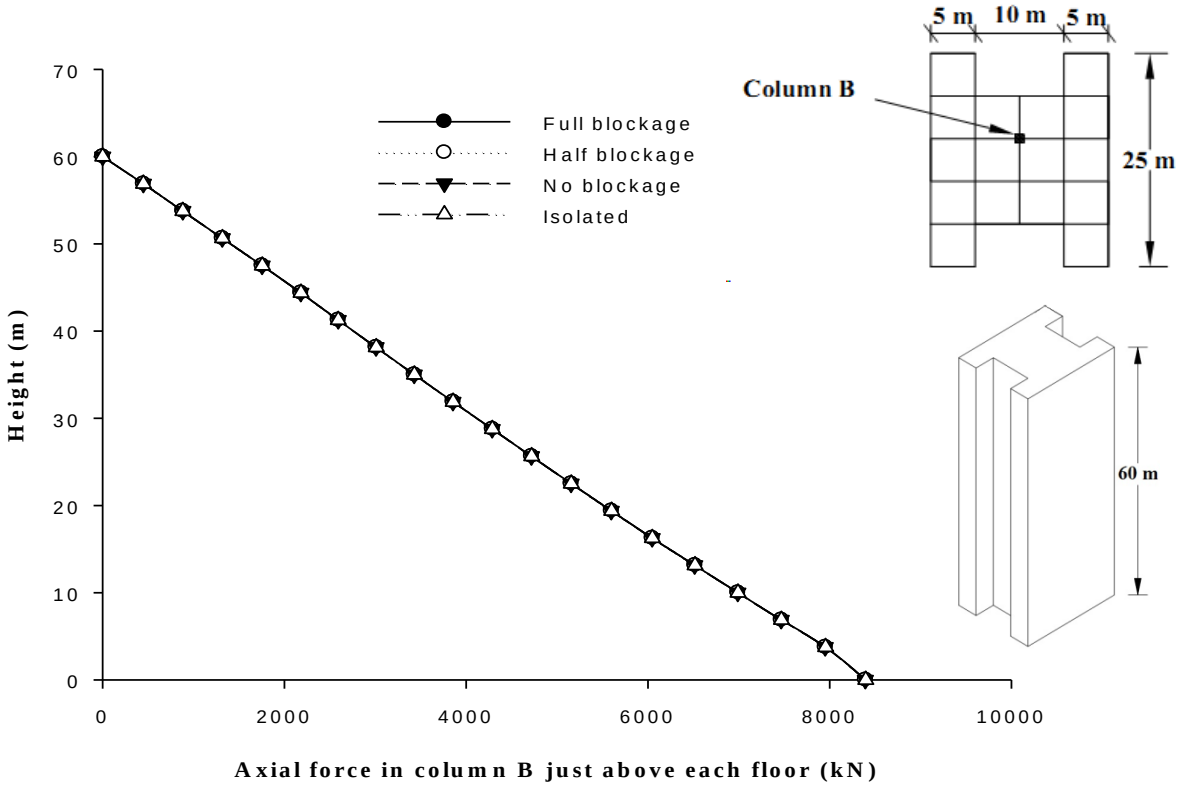


**Fig. 6.170 Interference effect on axial force in column-B of I-Shape-1 building**

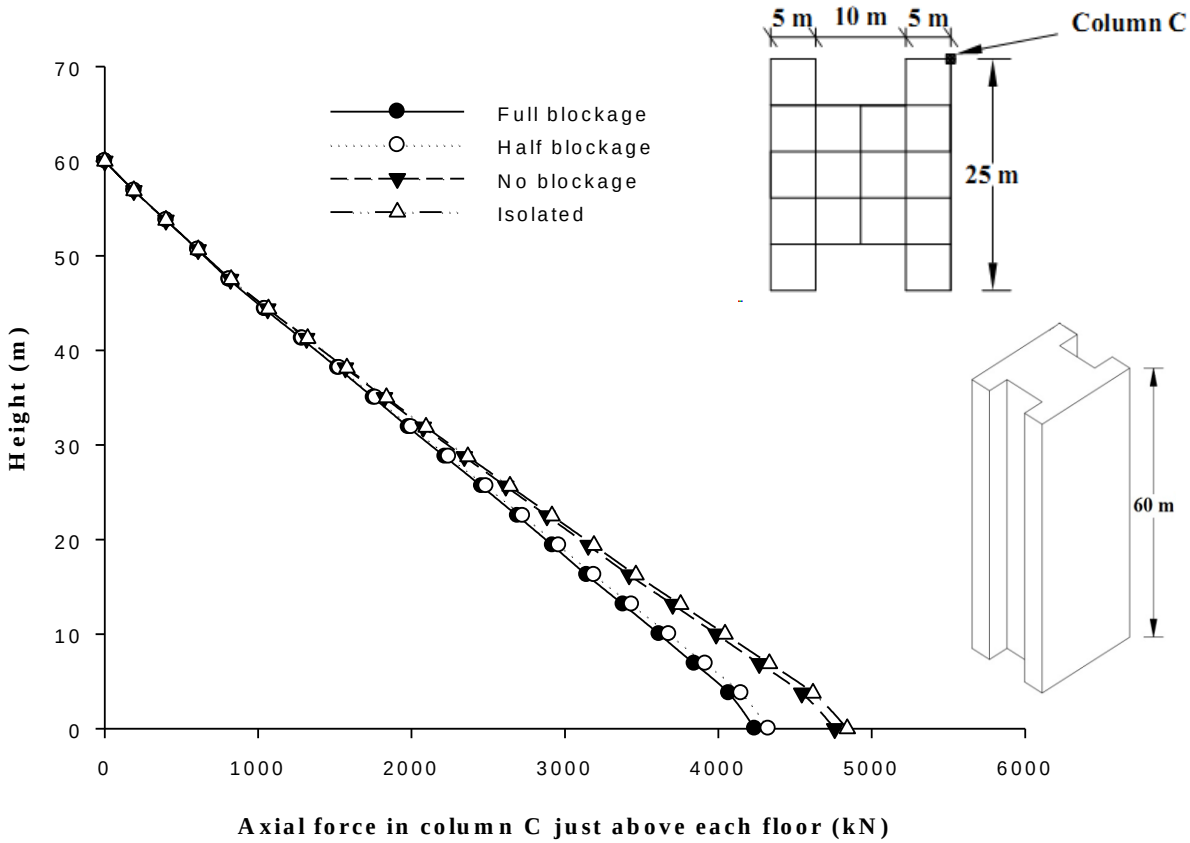


**Fig. 6.171 Interference effect on axial force in column-C of I-Shape-1 building**

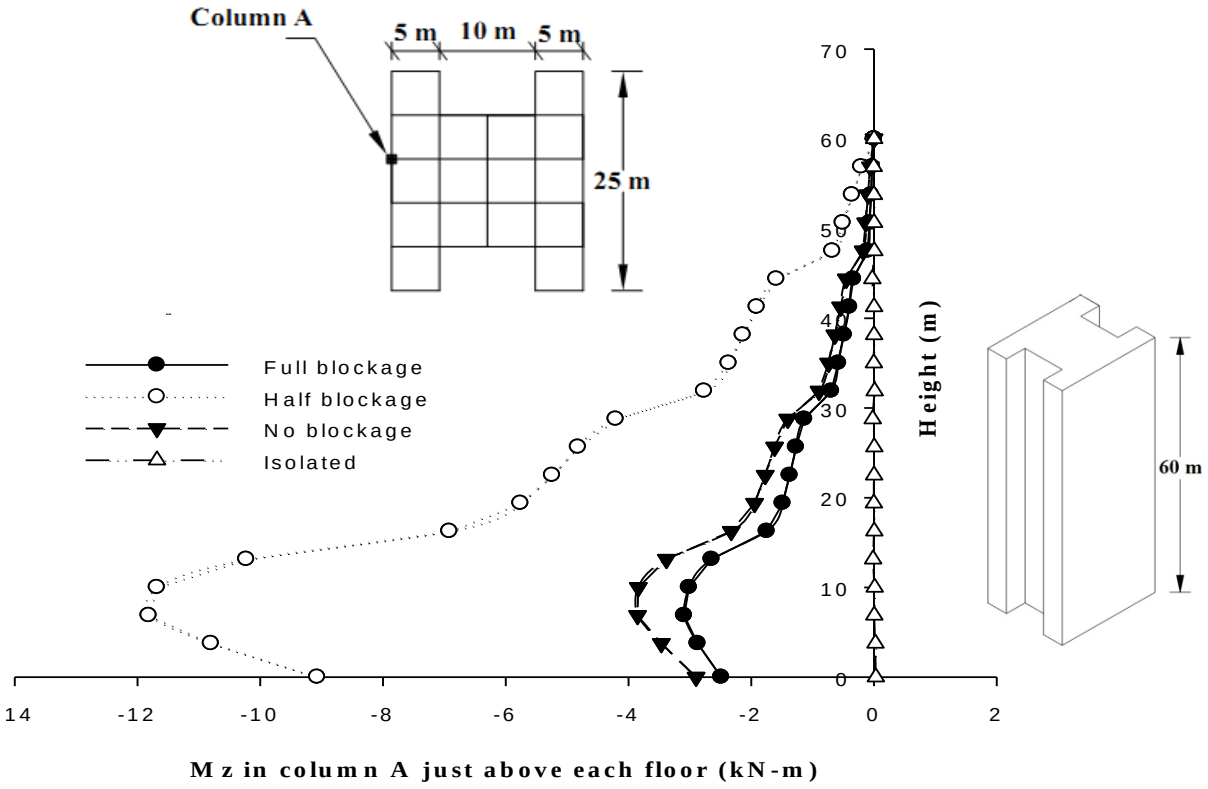


**Fig. 6.172 Interference effect on twisting moment Mz in column-A of I-Shape-1 building**

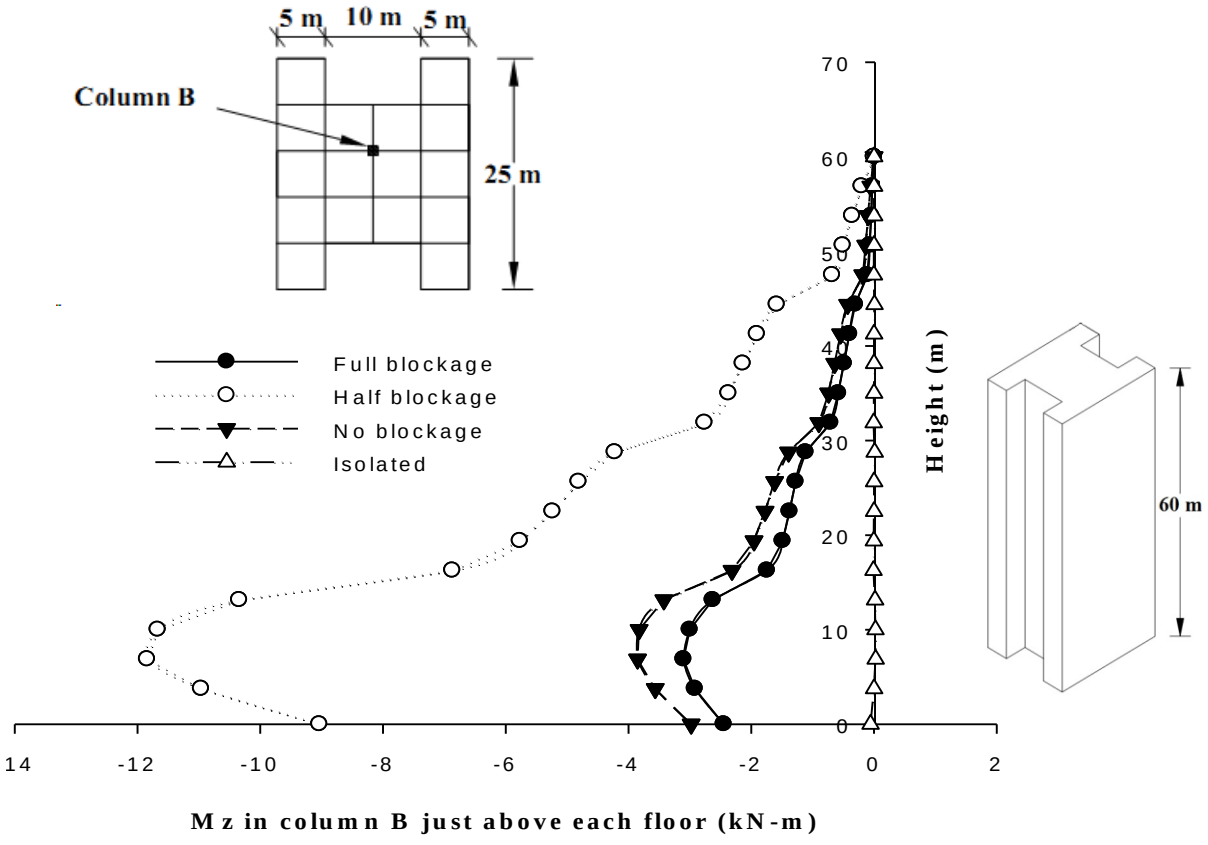


**Fig. 6.173 Interference effect on twisting moment Mz in column-B of I-Shape-1 building**

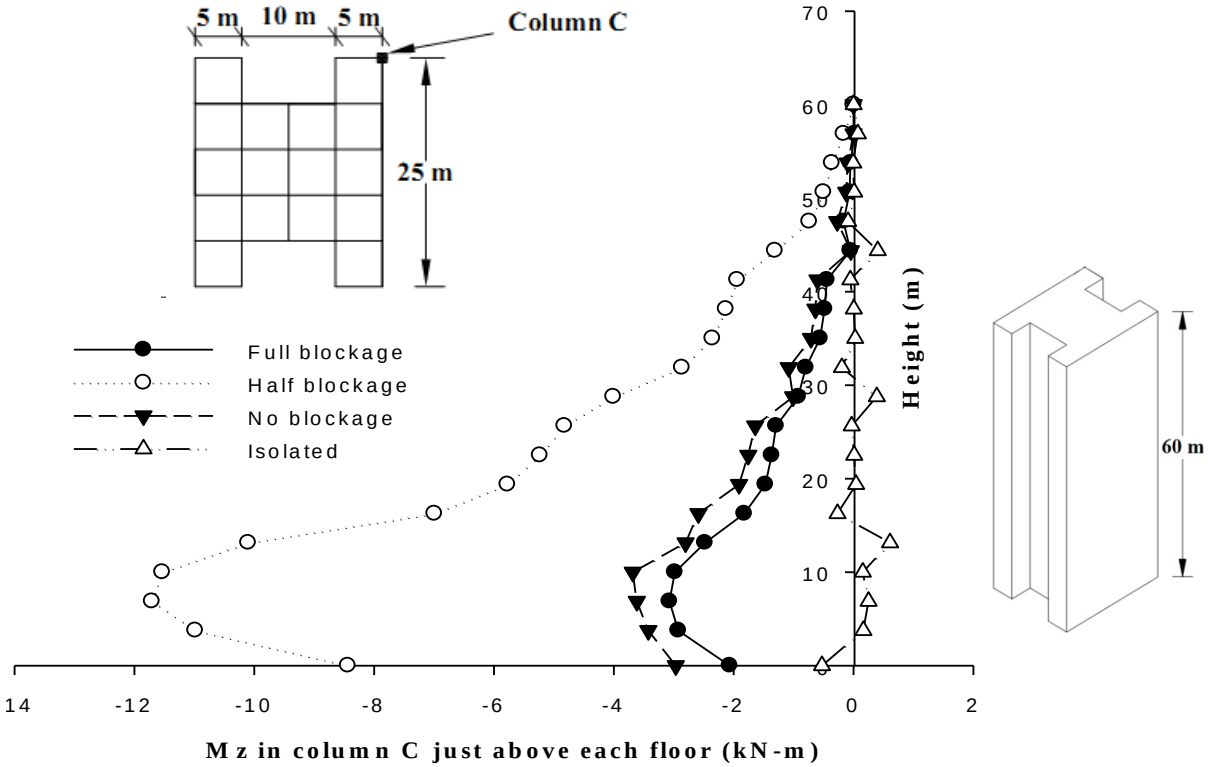


**Fig. 6.174 Interference effect on twisting moment Mz in column-C of I-Shape-1 building**

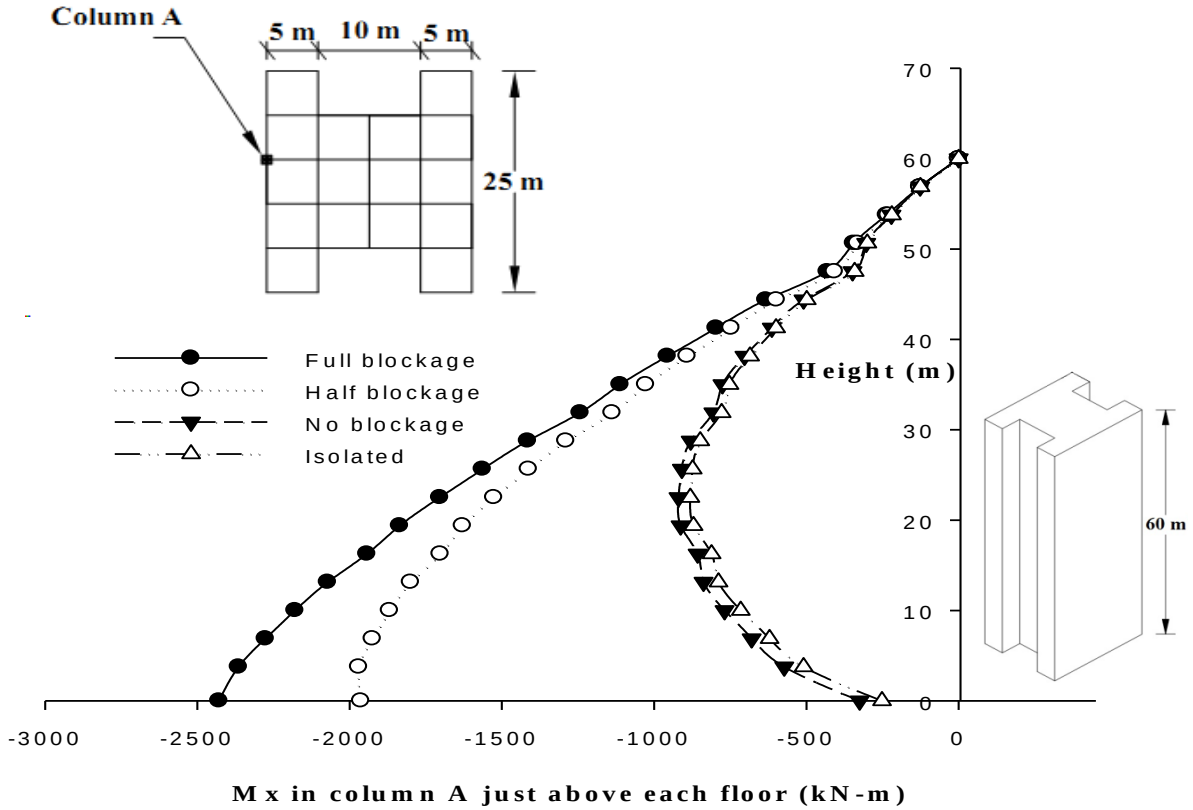


**Fig. 6.175 Interference effect on Mx (global) in column-A of I-Shape-1 building**

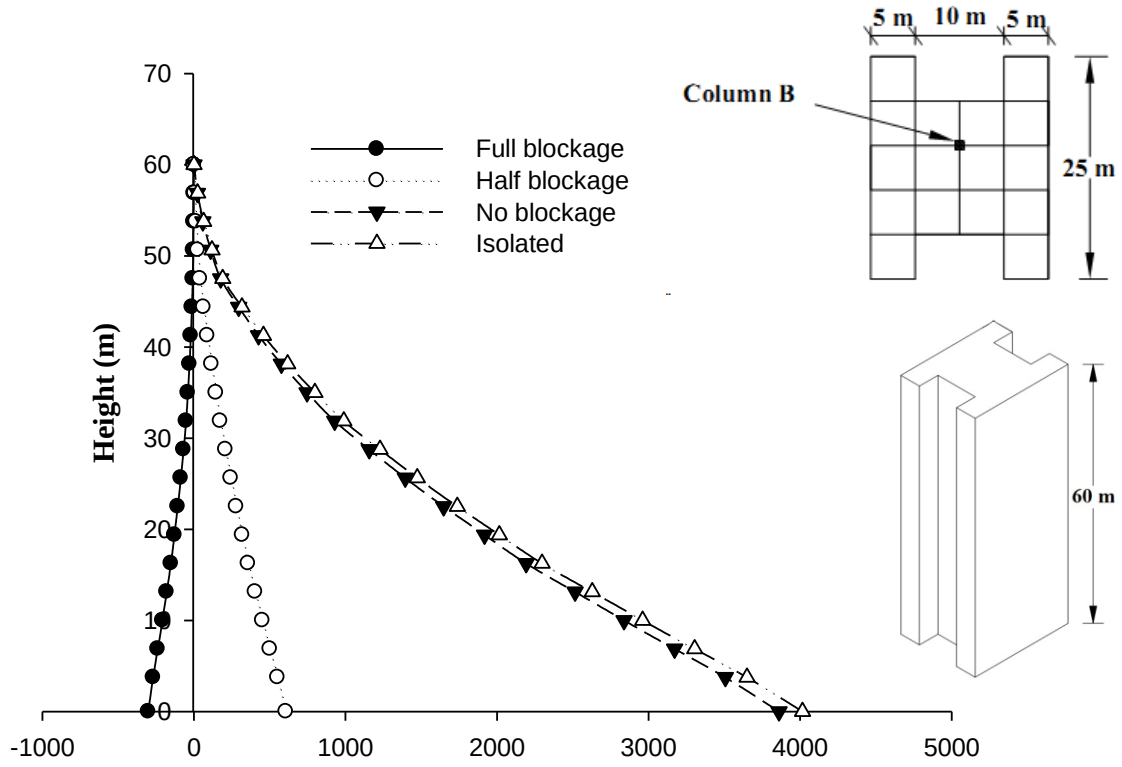


**Fig. 6.176 Interference effect on Mx (global) in column-B of I-Shape-1 building**

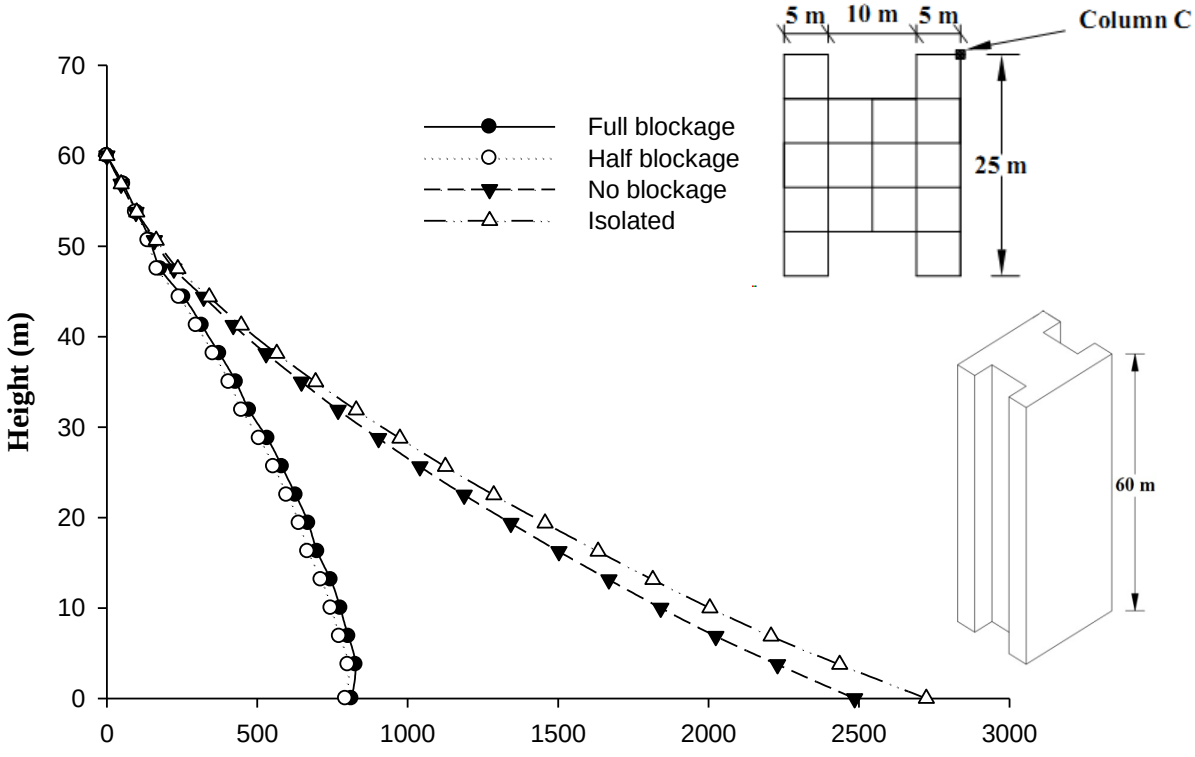


**Fig. 6.177 Interference effect on Mx (global) in column-C of I-Shape-1 building**

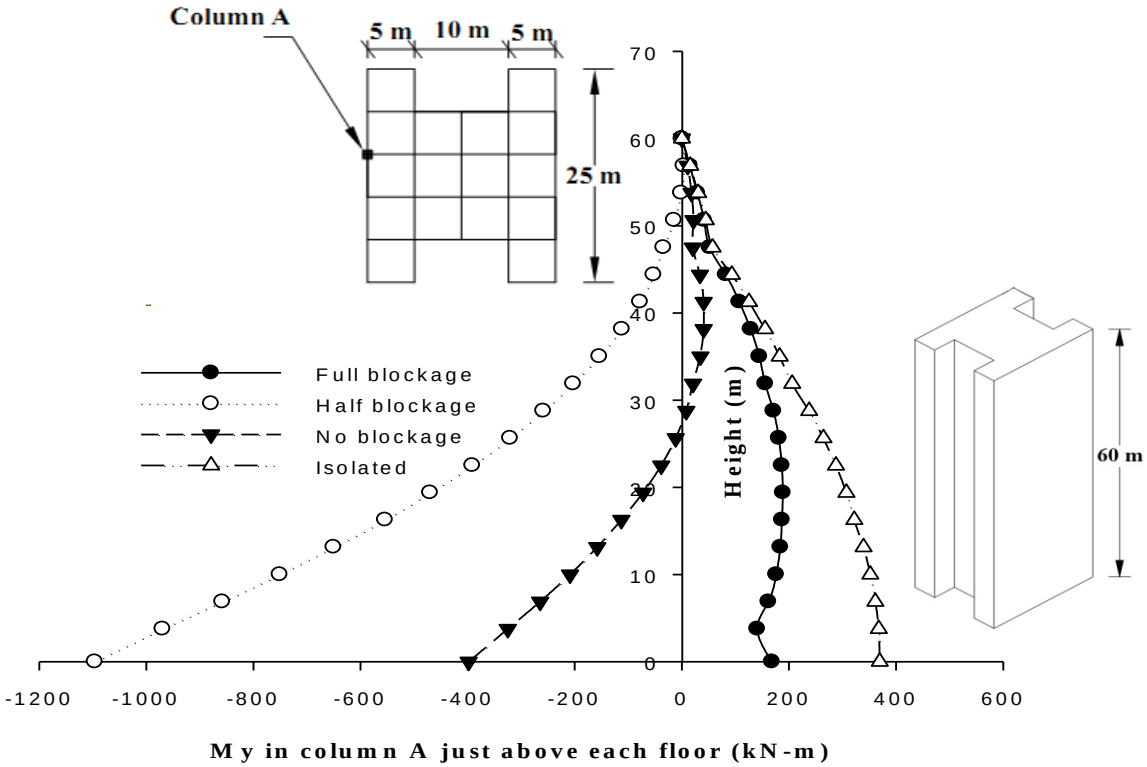


**Fig. 6.178 Interference effect on My (global) in column-A of I-Shape-1 building**

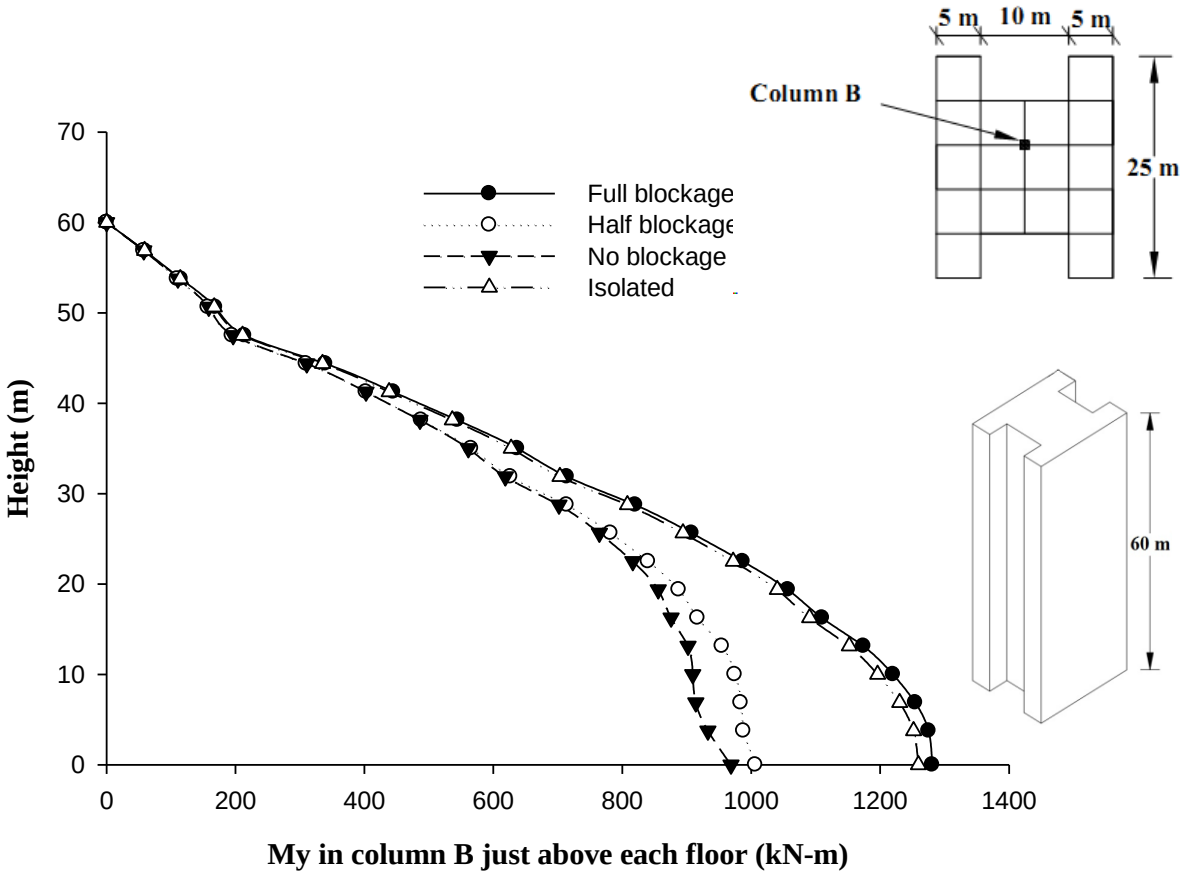


**Fig. 6.179 Interference effect on My (global) in column-B of I-Shape-1 building**

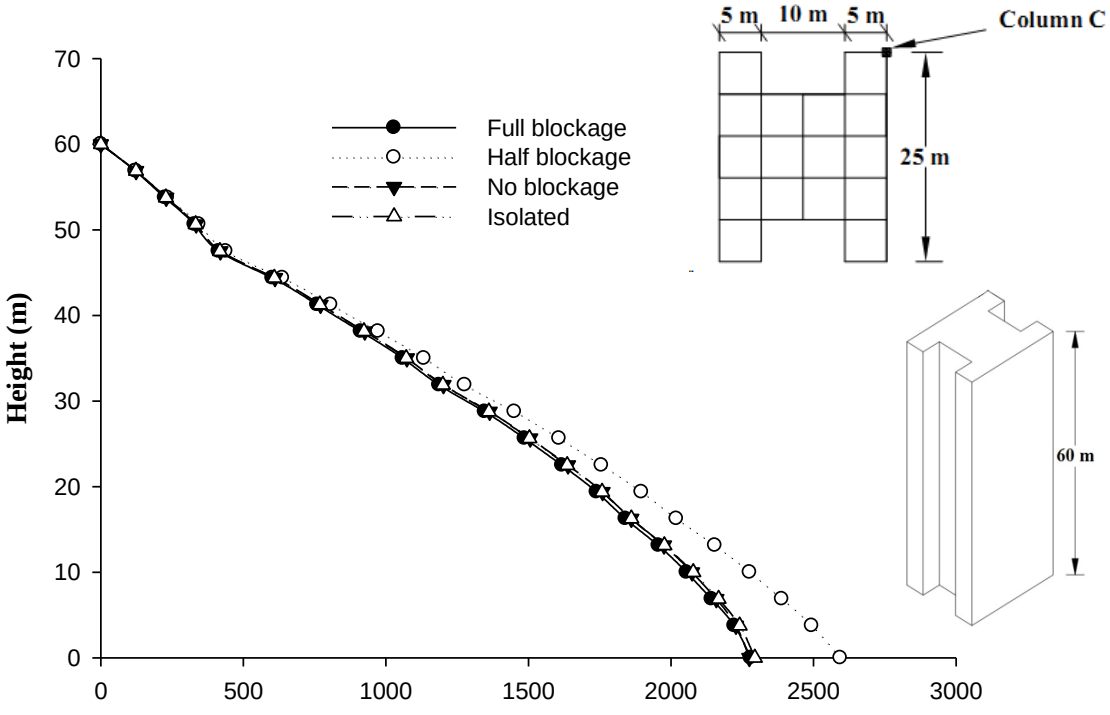


**Fig. 6.180 Interference effect on My (global) in column-C of I-Shape-1 building**

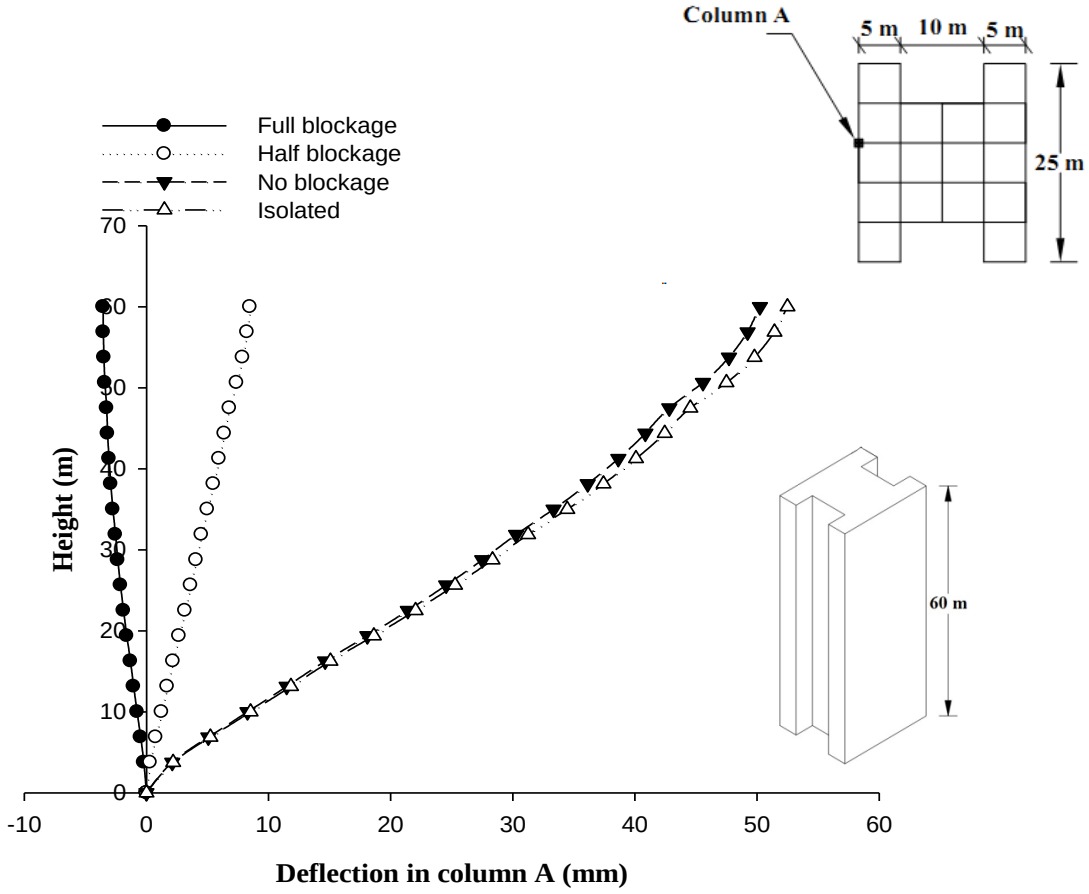


**Fig. 6.181 Interference effect on horizonta displacment of column-A of I-Shape-1 building**

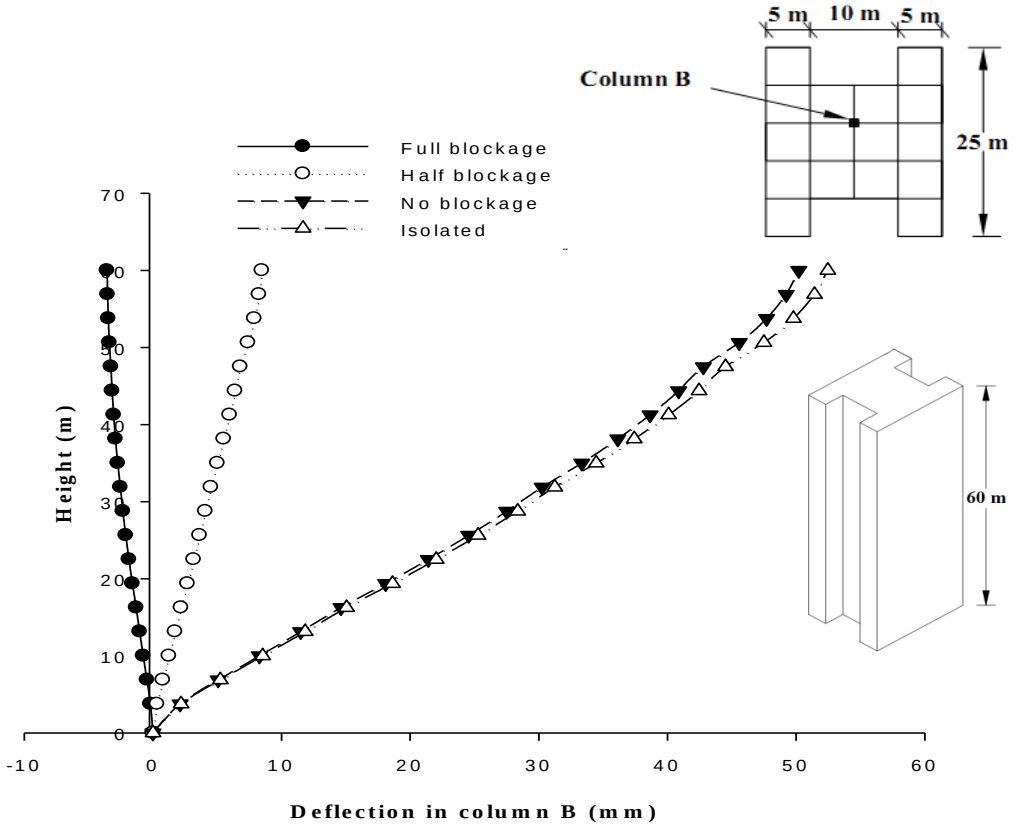


**Fig. 6.182 Interference effect on horizontal displacment of column-B of I-Shape-1 building**

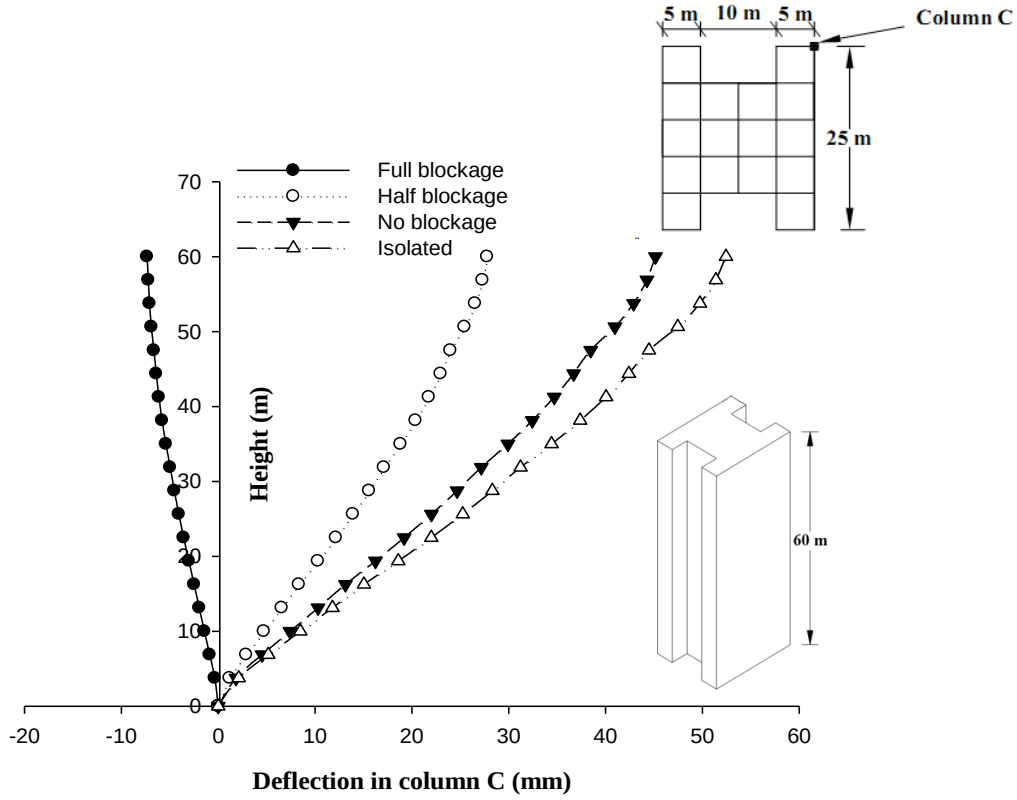


**Fig. 6.183 Interference effect on horizontal displacment of column-C of I-Shape-1 building**

### 6.5.5 Fish Shape-1 Building

#### 6.5.5.1 Forces in columns

Axial forces in column-A, B and C are calculated under wind load at four wind interference conditions namely back-to-back, back-to-front, front-to-back and front-to-front for Fish Shape-1 building and compared the values with those of 2 isolated cases namely $0^0$ and $180^0$ wind attack (Fig. 6.184). Variation of axial force along height is shown for column-A, B and C in Figs. 6.185 to 6.187 respectively. Axial force in front column i.e. column-A is maximum in isolated $180^0$ case. Axial force in back edge column i.e. column-B and back corner column i.e. column-C are maximum at isolated $0^0$ condition.

Moment about 'X' axis i.e. Mx along the height are shown in Figs. 6.188 to 6.190. It is highly influenced by interference condition. Mx is maximum at isolated $180^0$ condition in column-A, isolated $0^0$ condition in column-B and C.

Figures 6.191 to 6.193 show the variation of moment My with respect to height in case of column-A, B and C respectively. Influence of interference condition on My is not much.

#### 6.5.5.2 Displacement of columns

Response of Fish Shape-1 building is obtained under 2 isolated conditions and 4 interference conditions. Horizontal displacements of all three columns in all four interference conditions are less than those in two isolated conditions (Figs. 6.194 to 6.196).

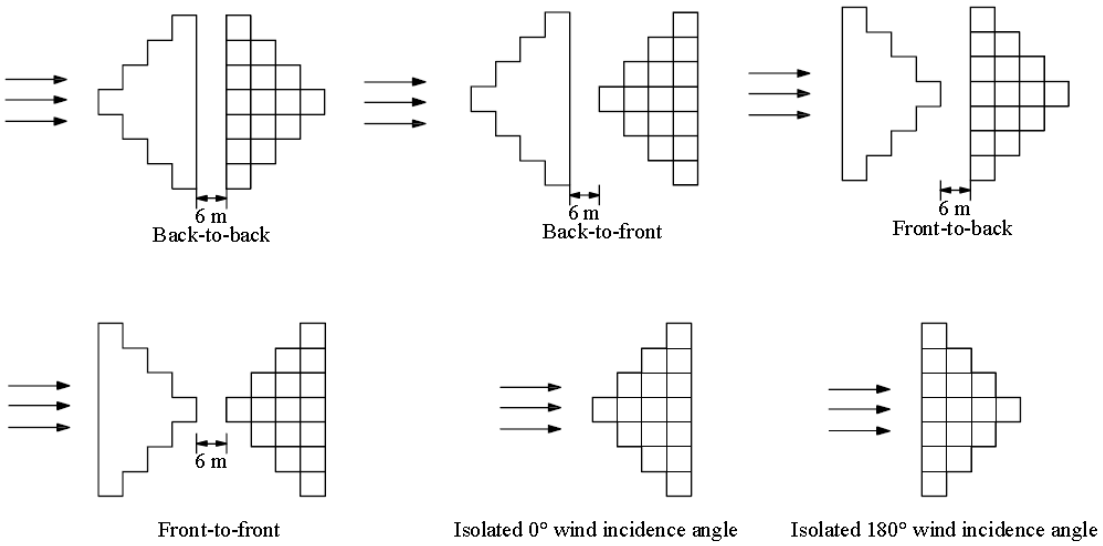


**Fig. 6.184 Relative position of Fish Shape-1 buildings under different interference conditions**

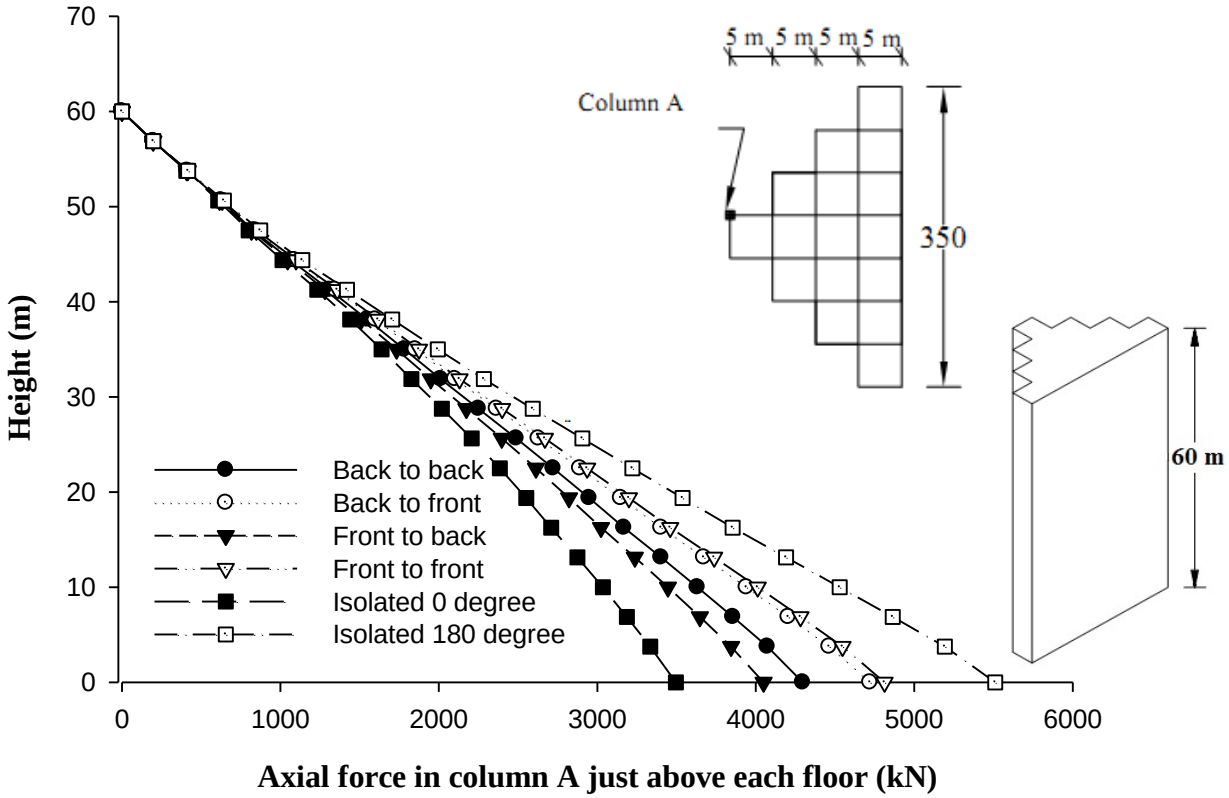


**Fig. 6.185 Interference effect on axial force in column-A of Fish Shape-1 building**

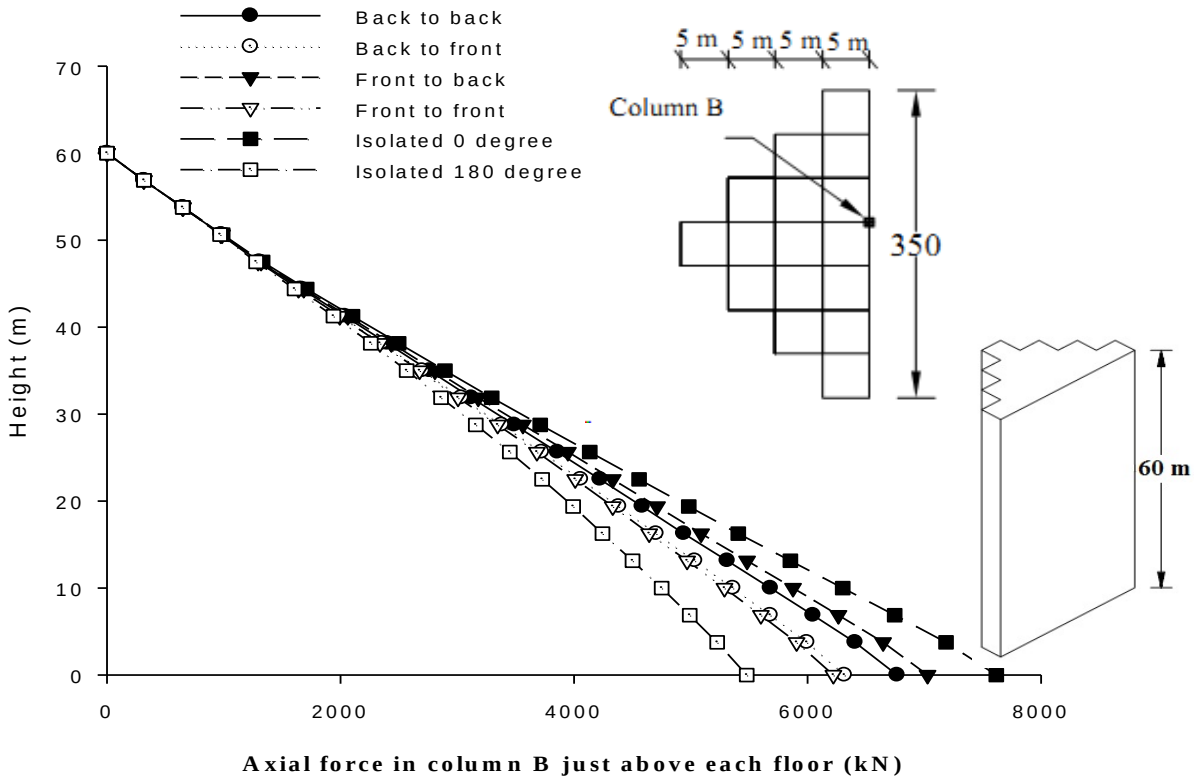


**Fig. 6.186 Interference effect on axial force in column-B of Fish Shape-1 building**

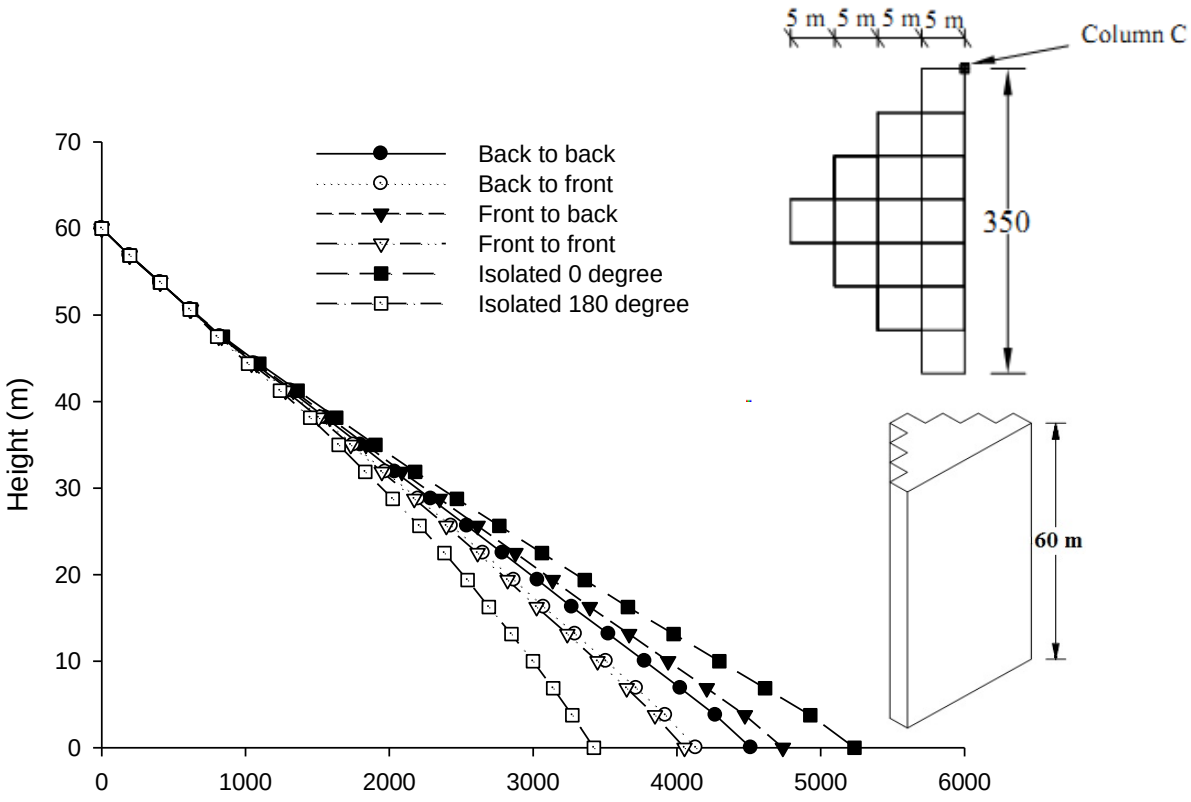


**Fig. 6.187 Interference effect on axial force in column-C of Fish Shape-1 building**

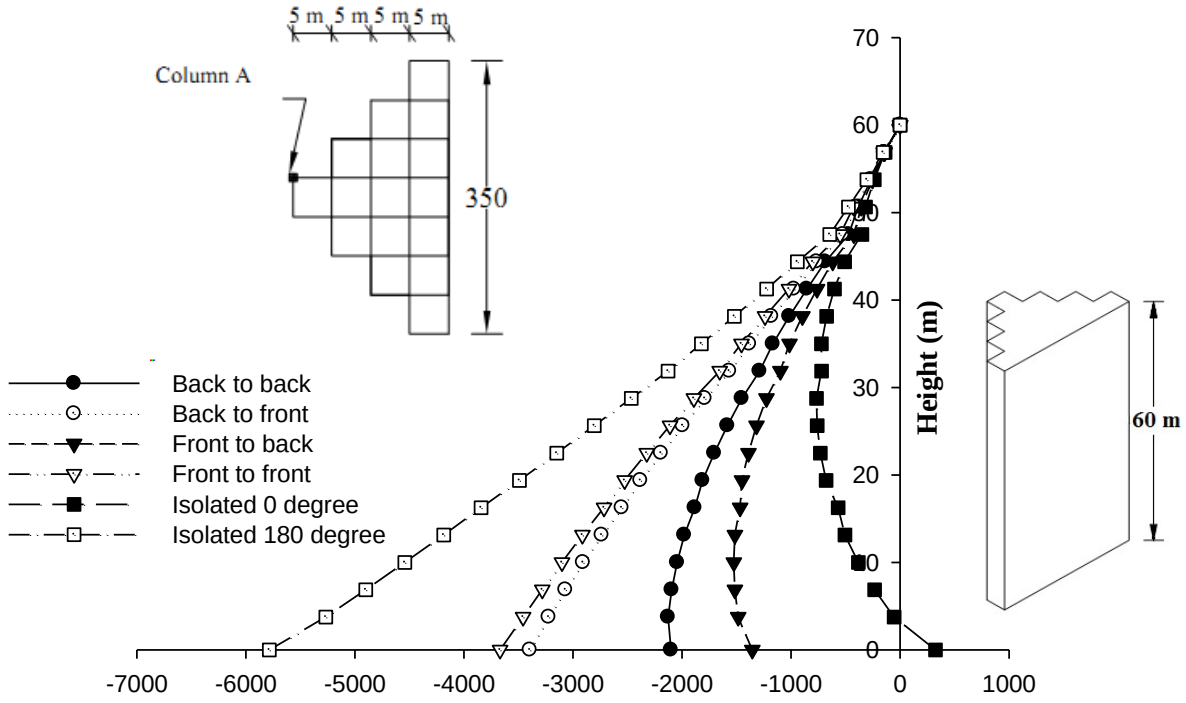


**Fig. 6.188 Interference effect on Mx (global) in column-A of Fish Shape-1 building**

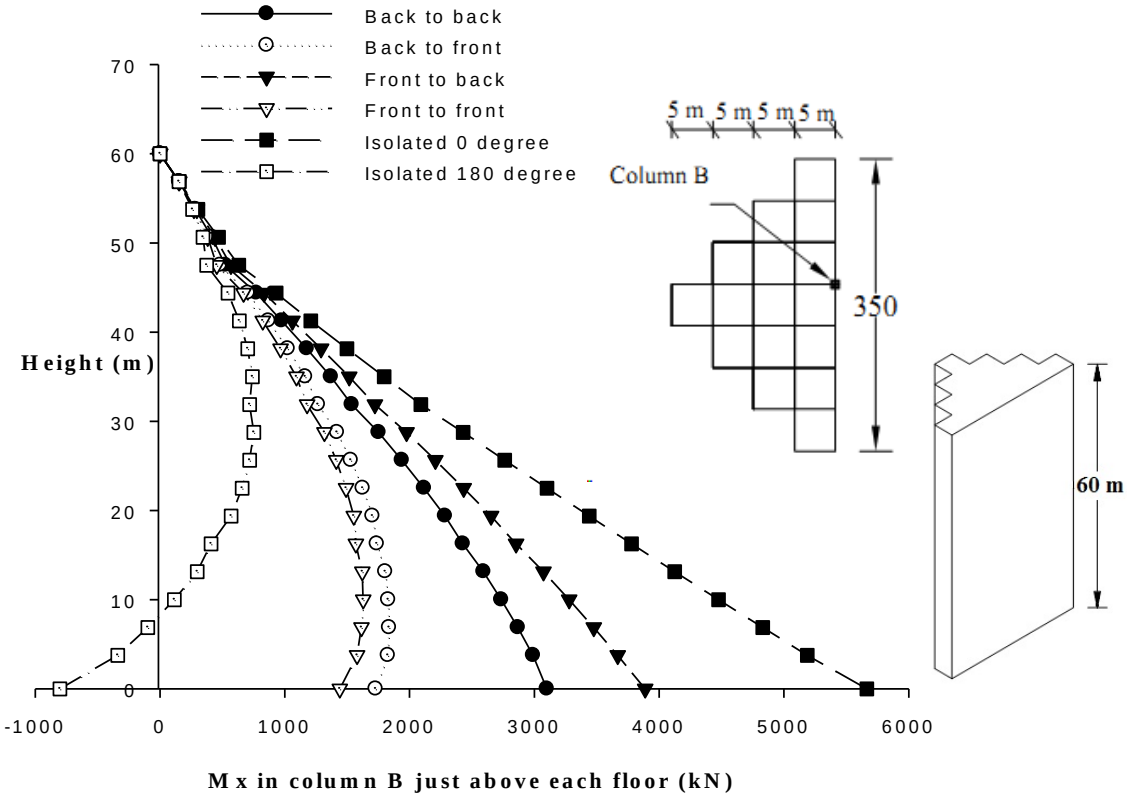


**Fig. 6.189 Interference effect on Mx (global) in column-B of Fish Shape-1 building**

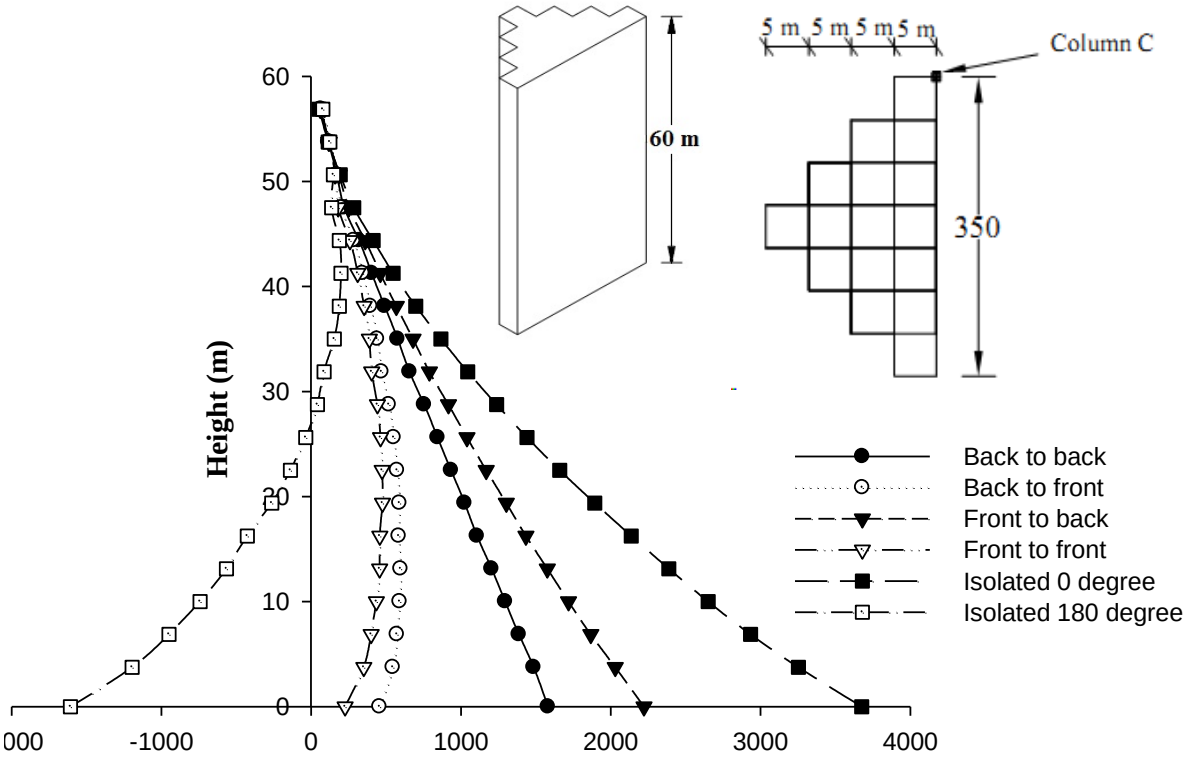


**Mx in column C just above each floor (kN-m)**

**Fig. 6.190 Interference effect on Mx (global) in column-C of Fish Shape-1 building**

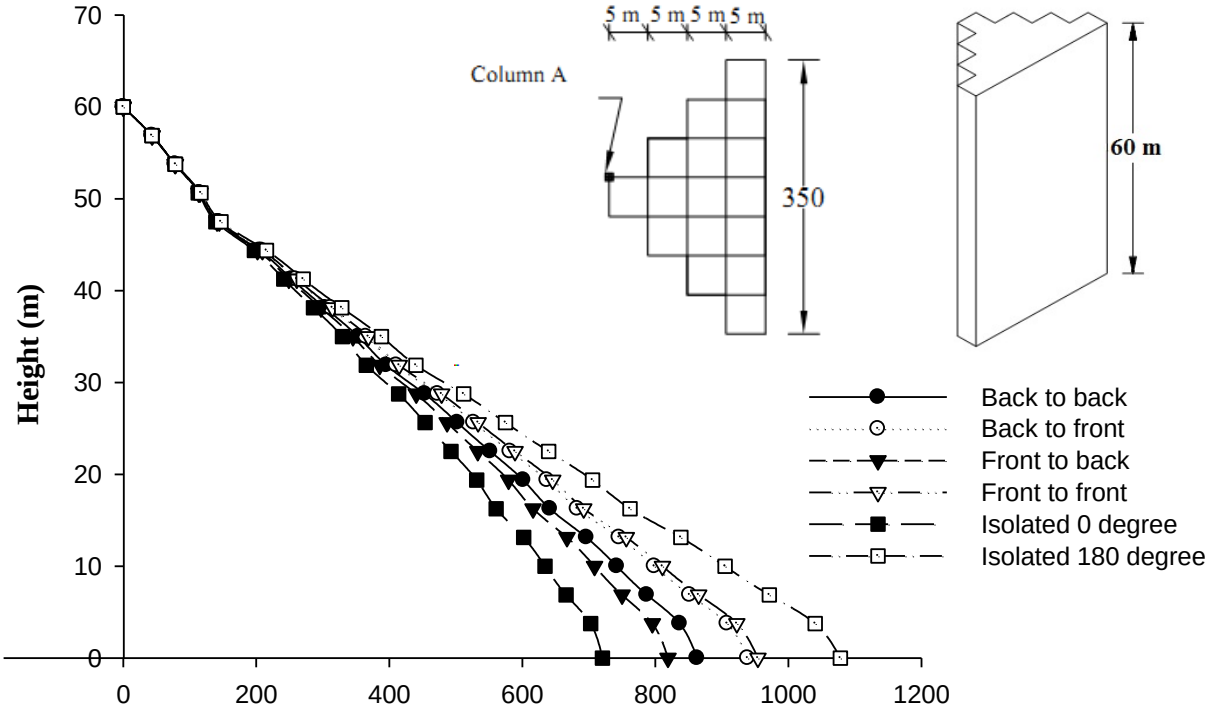


**My in column A just above each floor (kN-m)**

**Fig. 6.191 Interference effect on My (global) in column-A of Fish Shape-1 building**

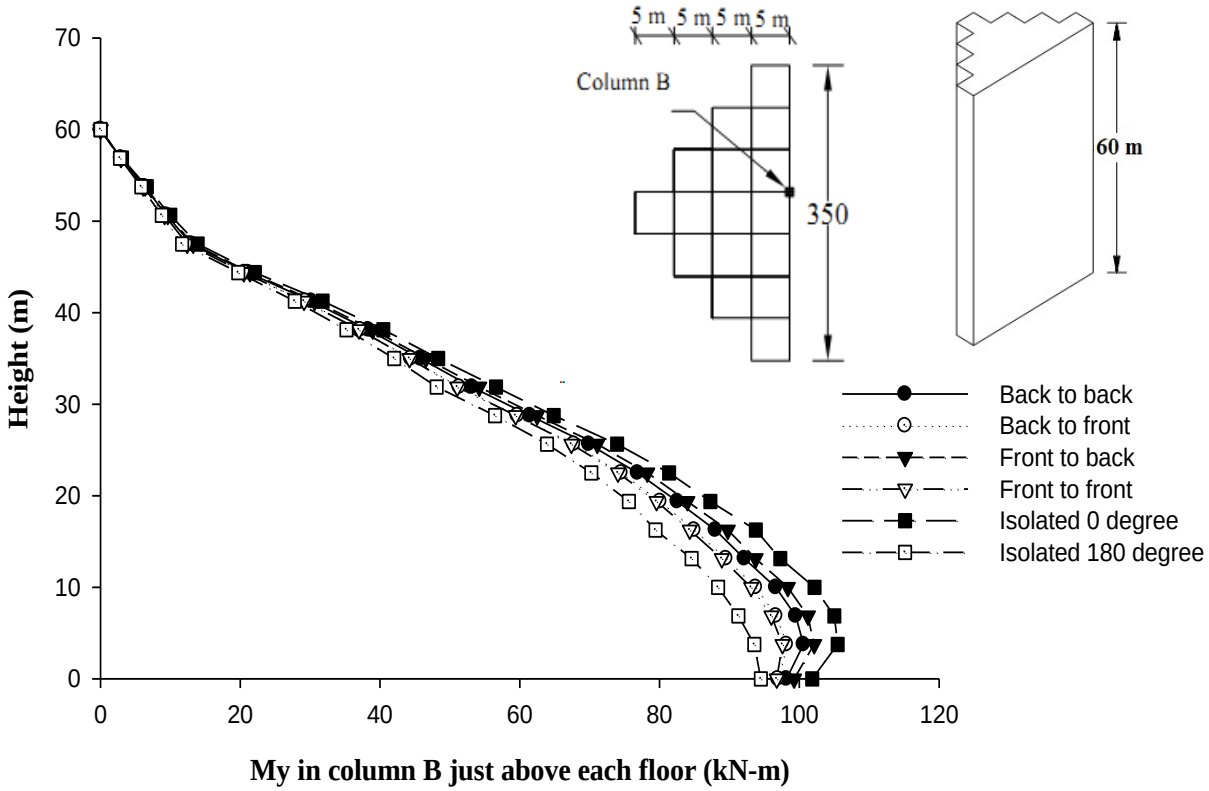


**Fig. 6.192 Interference effect on My (global) in column-B of Fish Shape-1 building**

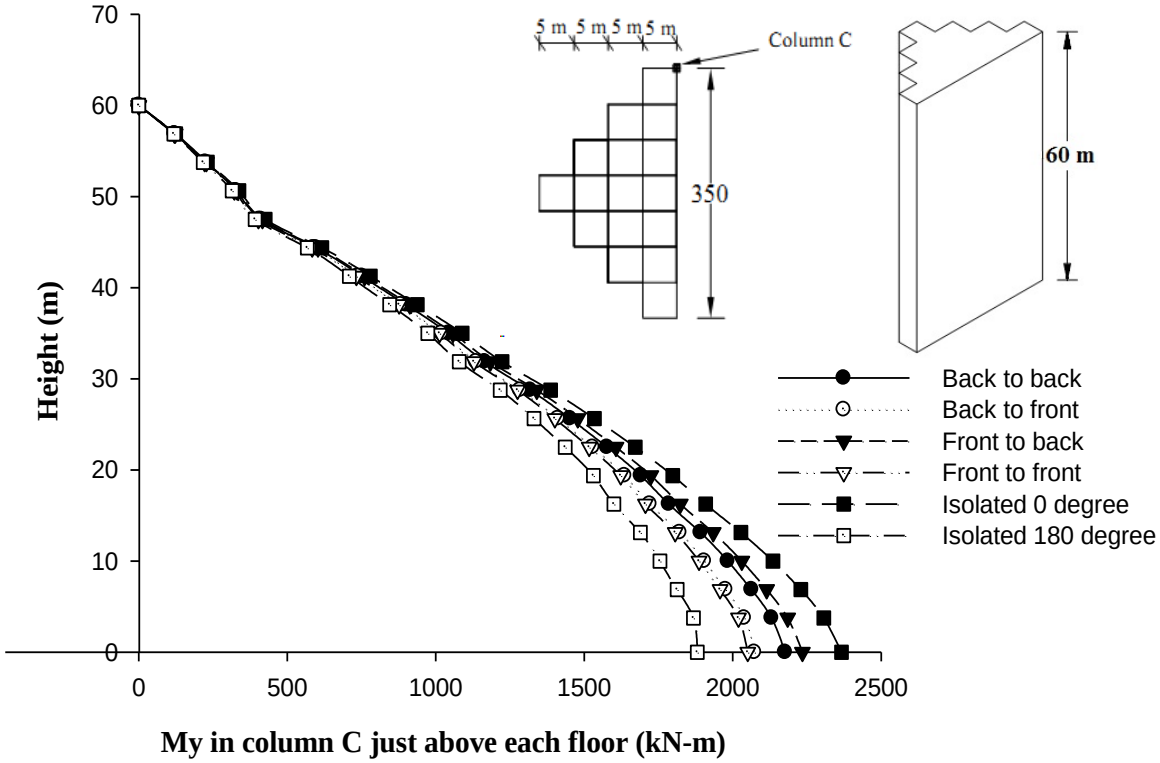


**Fig. 6.193 Interference effect on My (global) in column-C of Fish Shape-1 building**

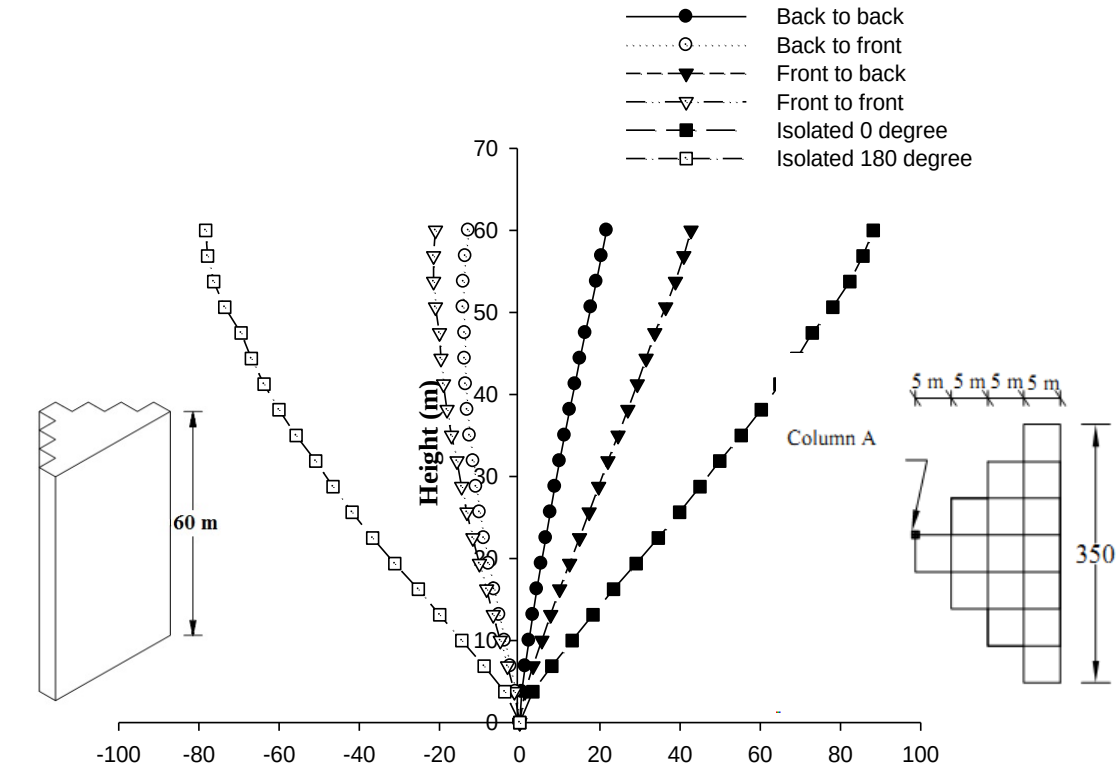


**Fig. 6.194 Interference effect on horizontal displacment of column-A of Fish Shape-1 building**

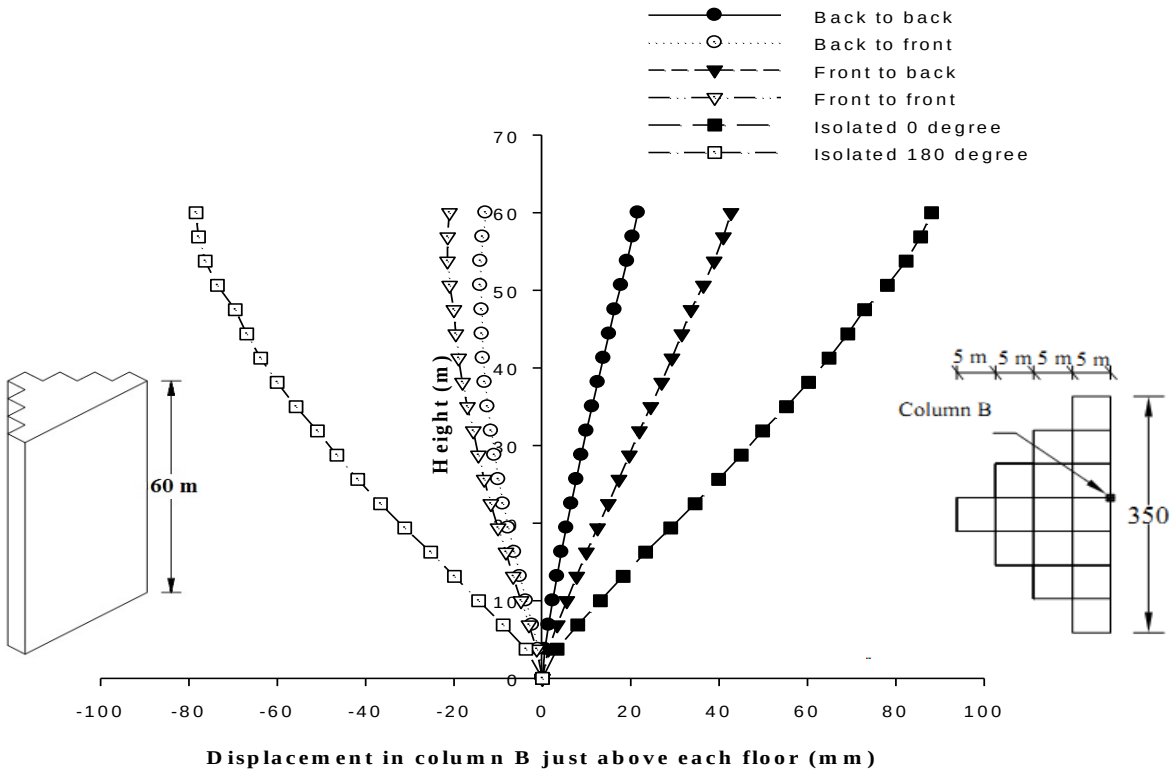


**Fig. 6.195 Interference effect on horizontal displacment of column-B of Fish Shape-1 building**

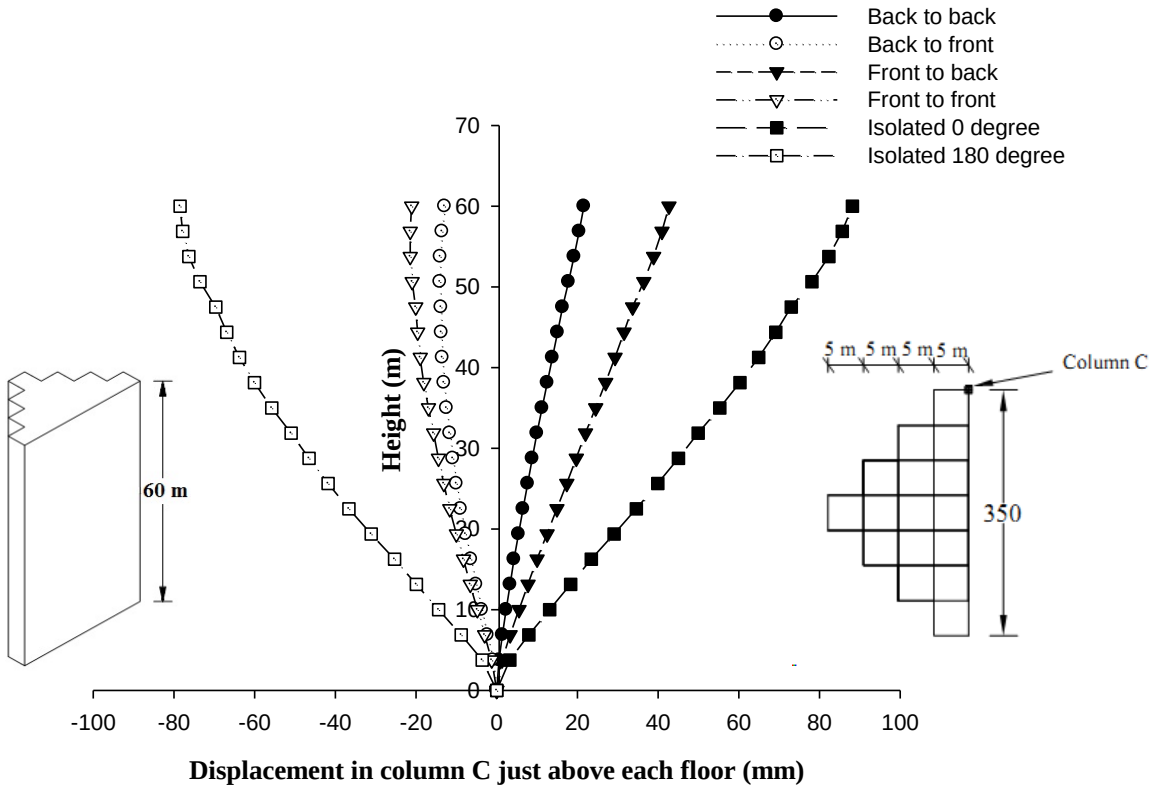


**Fig. 6.196 Interference effect on horizontal displacment of column-C of Fish Shape-1 building**

### 6.5.6 Fish Shape-2 Building

#### 6.5.6.1 Forces in columns

Analytical results for Fish Shape-2 building are shown in Figs. 6.198 to 6.206. Axial force in face column, i.e. column-A is maximum at isolated $180^0$ condition. Axial force in back edge column, i.e. column-B and back corner column i.e. column-C are maximum at isolated $0^0$ condition. Values of axial force in all three columns fall between the values for isolated $0^0$ and isolated $180^0$ condition.

There is large effect of interference on the values of moment about 'X' axis in all three columns. Mx is maximum in isolated $180^0$ condition in column-A, in isolated $0^0$ condition in column-B and C

There is not much influence of blockage on My in column-A and C. Its influence on column-B is large.

#### 6.5.6.2 Displacement of columns

Interference effect on horizontal displacement of columns in Fish Shape-2 building can be seen in Figs. 6.207 to 6.209. Horizontal displacements in interference conditions in all columns are less than corresponding values in isolated condition, which implies that blockage is beneficial so far as deflection of columns is concerned. Maximum displacement is observed in isolated $180^0$ case followed by isolated $0^0$ condition.

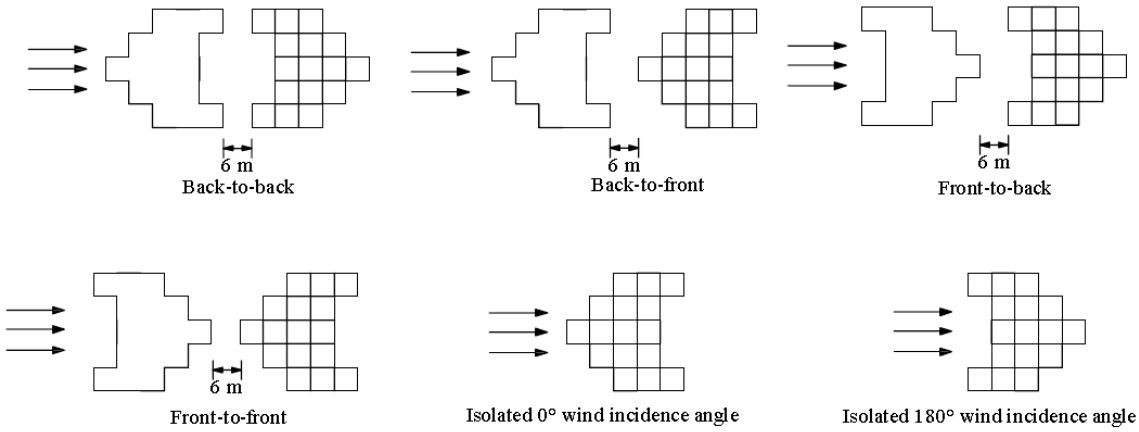


**Fig. 6.197 Relative position of Fish Shape-2 buildings under different interference conditions**

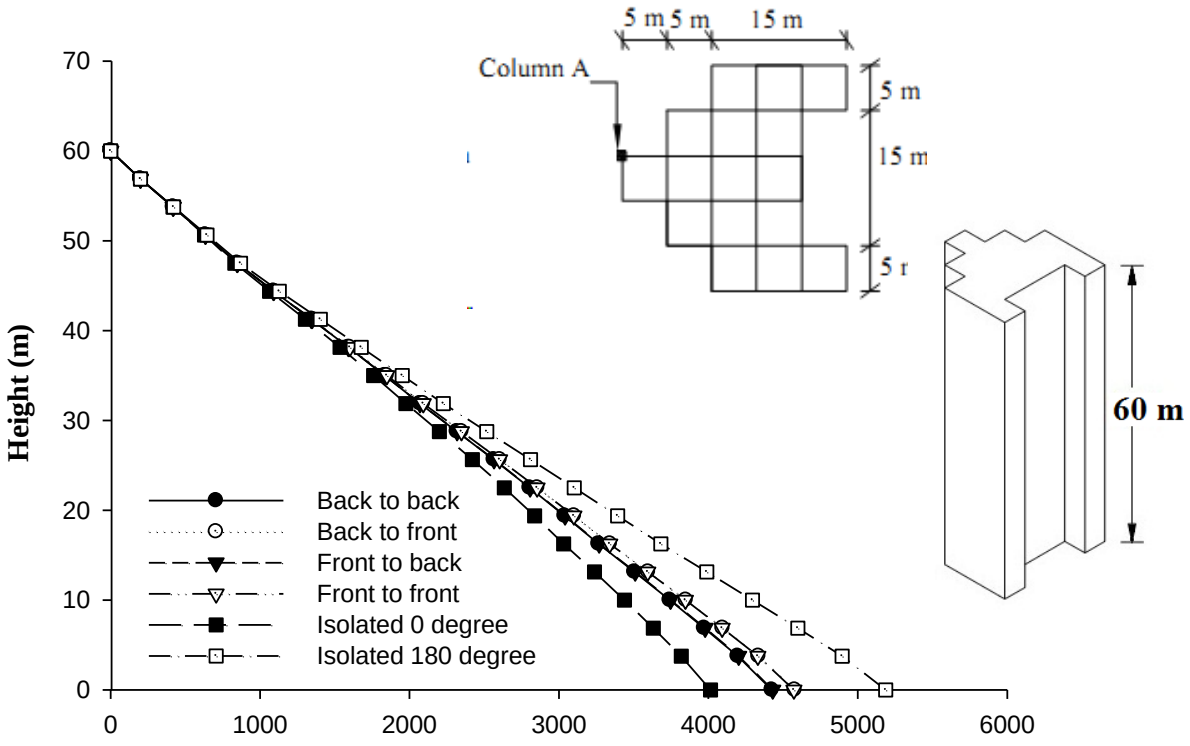


**Fig. 6.198 Interference effect on axial force in column-A of Fish Shape-2 building**

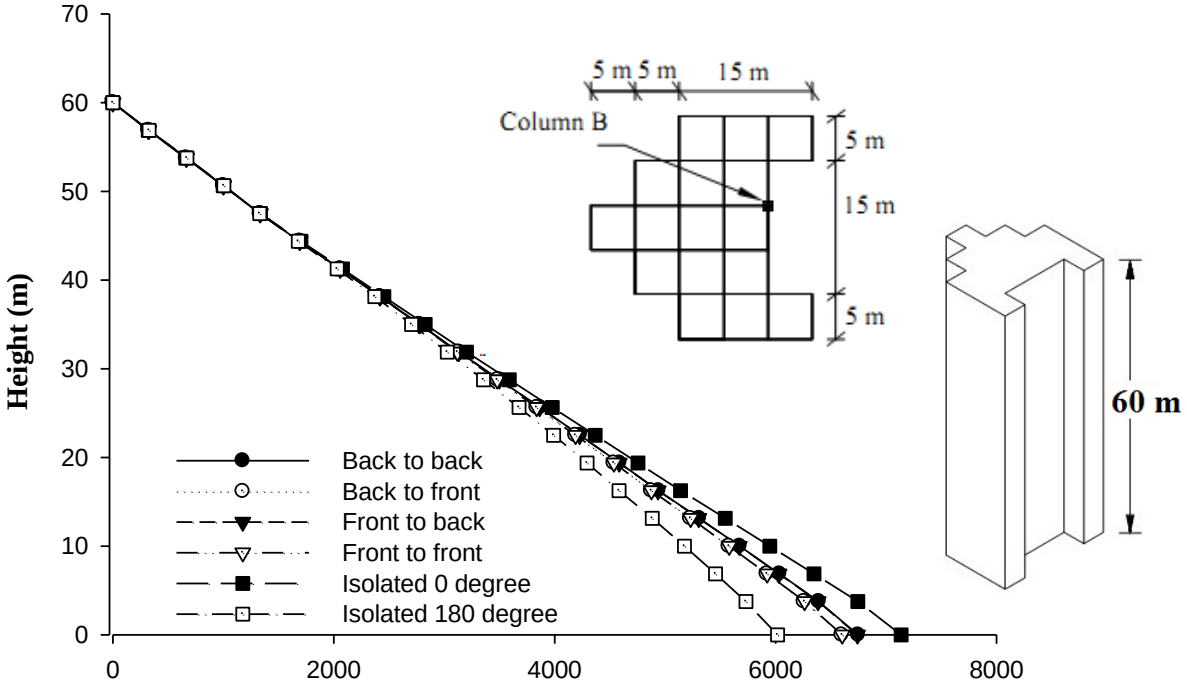


**Axial force in column B just above each floor (kN)**

**Fig. 6.199 Interference effect on axial force in column-B of Fish Shape-2 building**

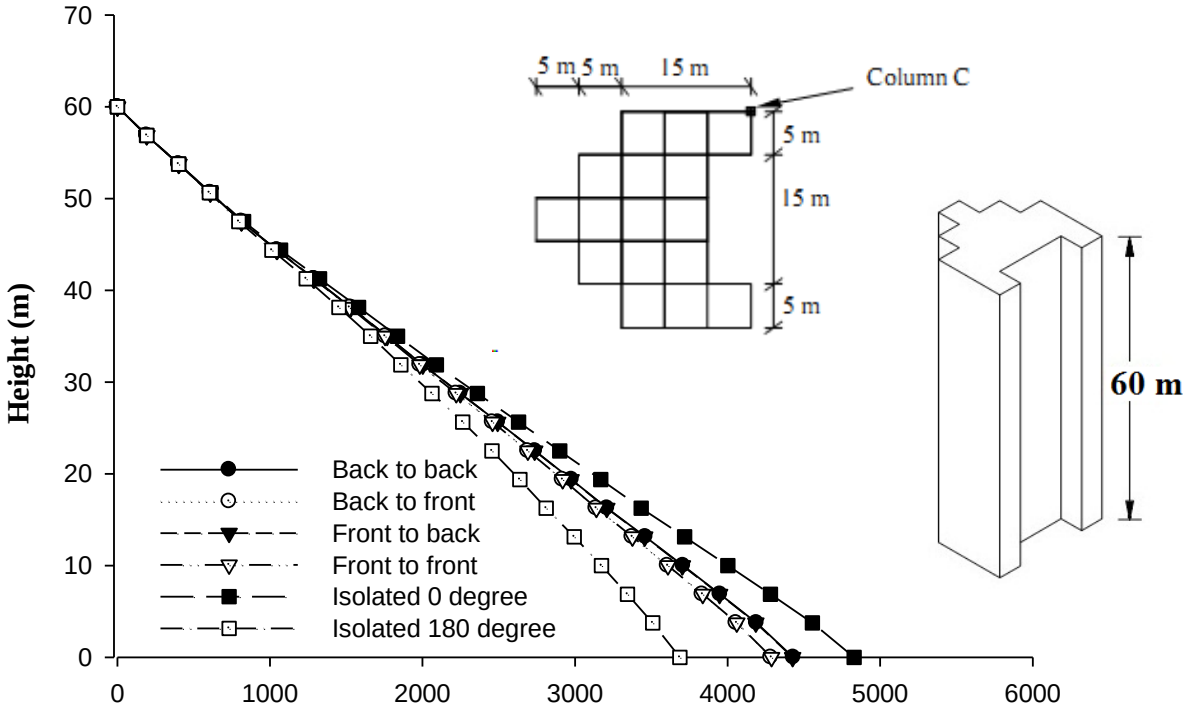


**Axial force in column C just above each floor (kN)**

**Fig. 6.200 Interference effect on axial force in column-C of Fish Shape-2 building**

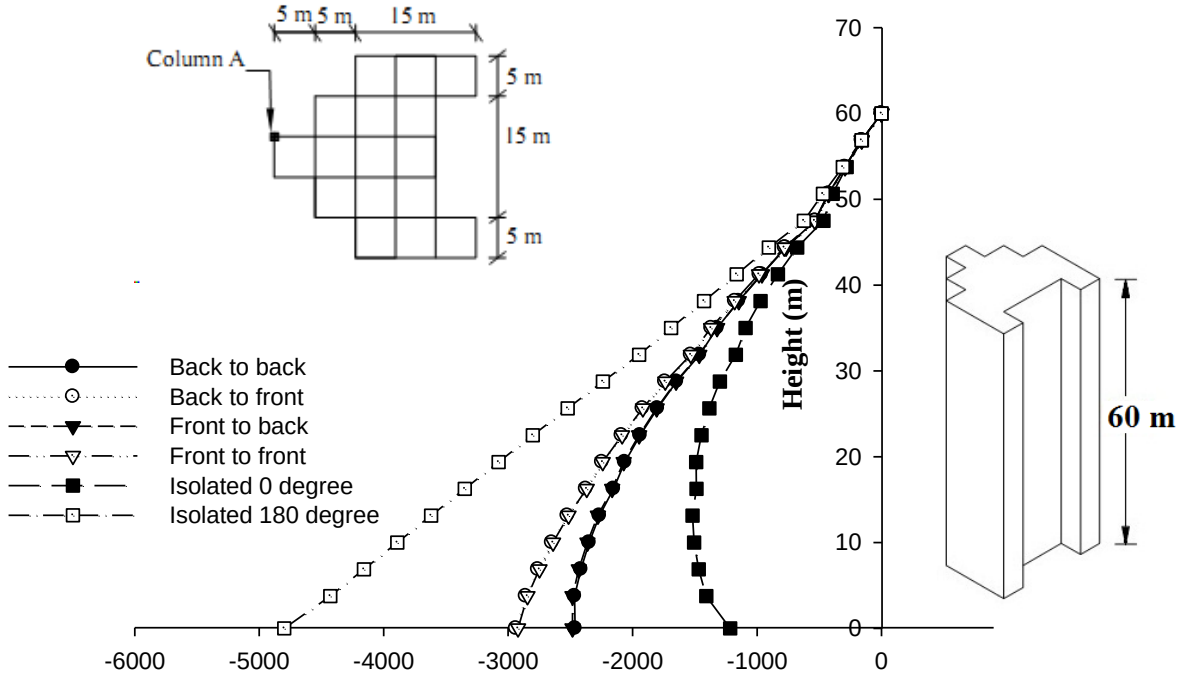


**Mx in column A just above each floor (kN-m)**

**Fig. 6.201 Interference effect on Mx (global) in column-A of Fish Shape-2 building**

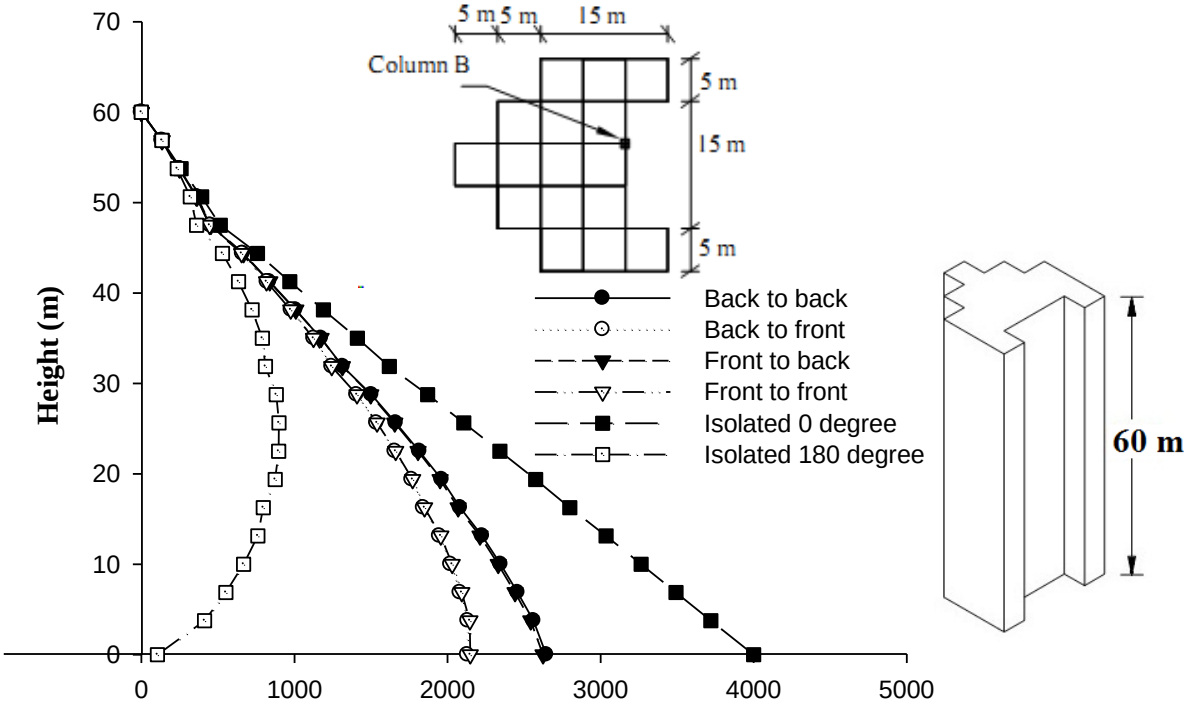


**Mx in column B just above each floor (kN-m)**

**Fig. 6.202 Interference effect on Mx (global) in column-B of Fish Shape-2 building**

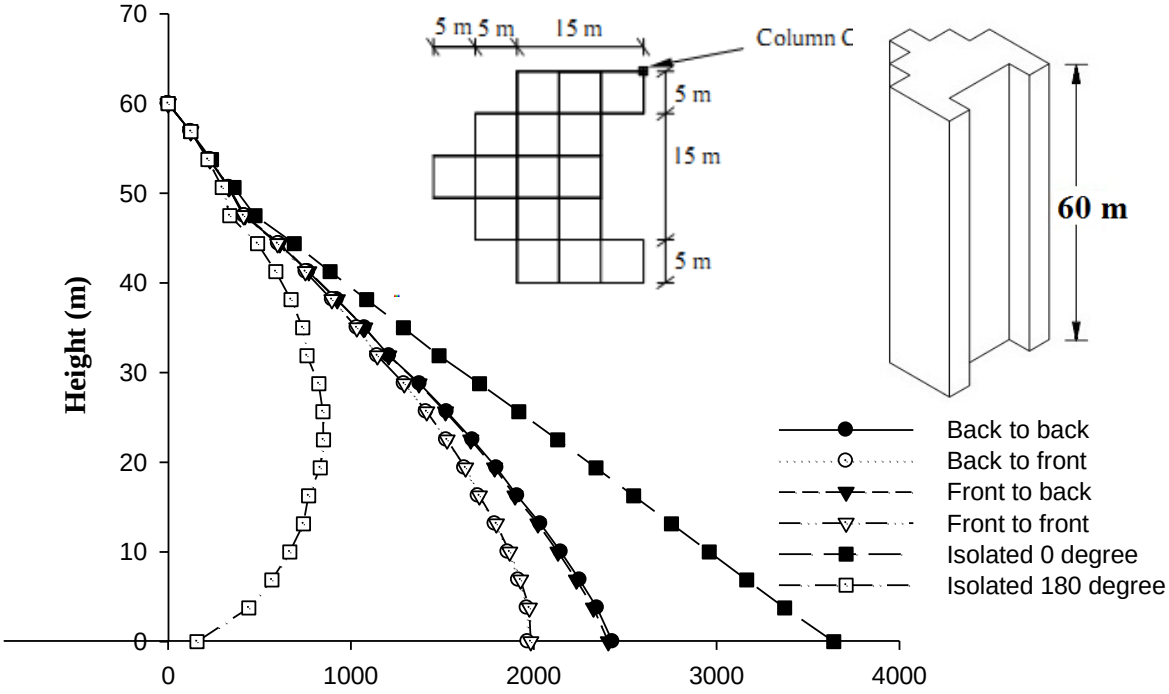


**Mx in column C just above each floor (kN-m)**

**Fig. 6.203 Interference effect on Mx (global) in column-C of Fish Shape-2 building**

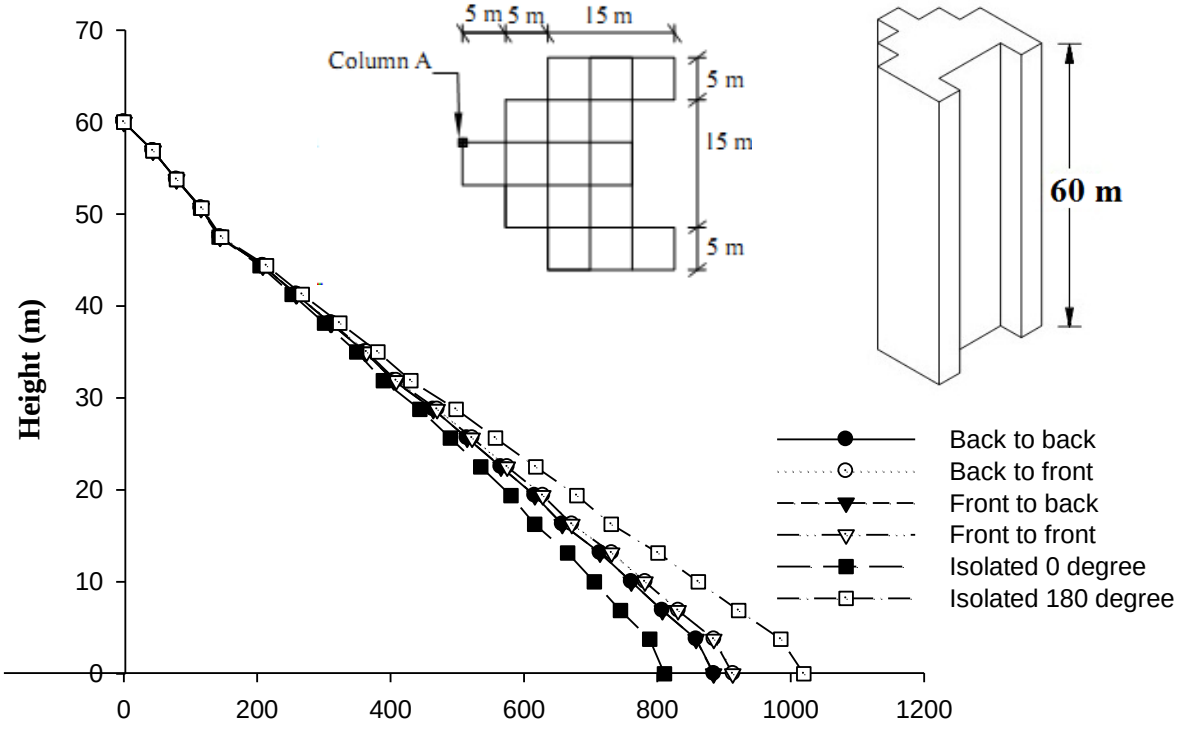


**My in column A just above each floor (kN-m)**

**Fig. 6.204 Interference effect on My (global) in column-A of Fish Shape-2 building**

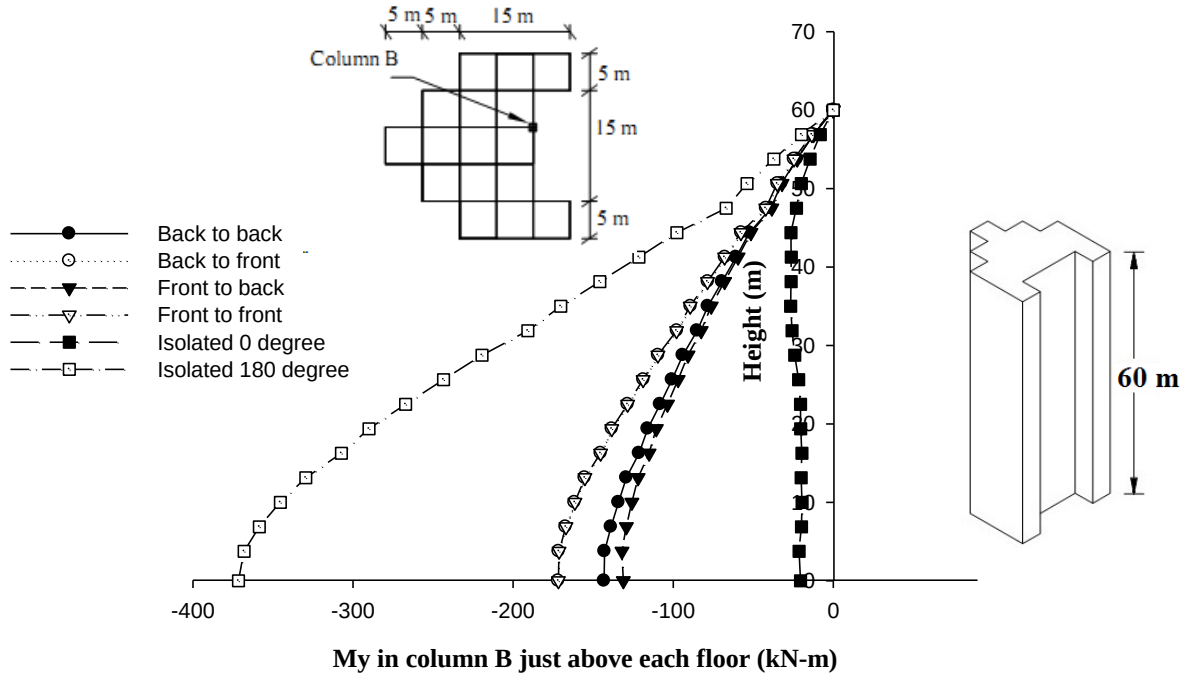


**Fig. 6.205 Interference effect on My (global) in column-B of Fish Shape-2 building**

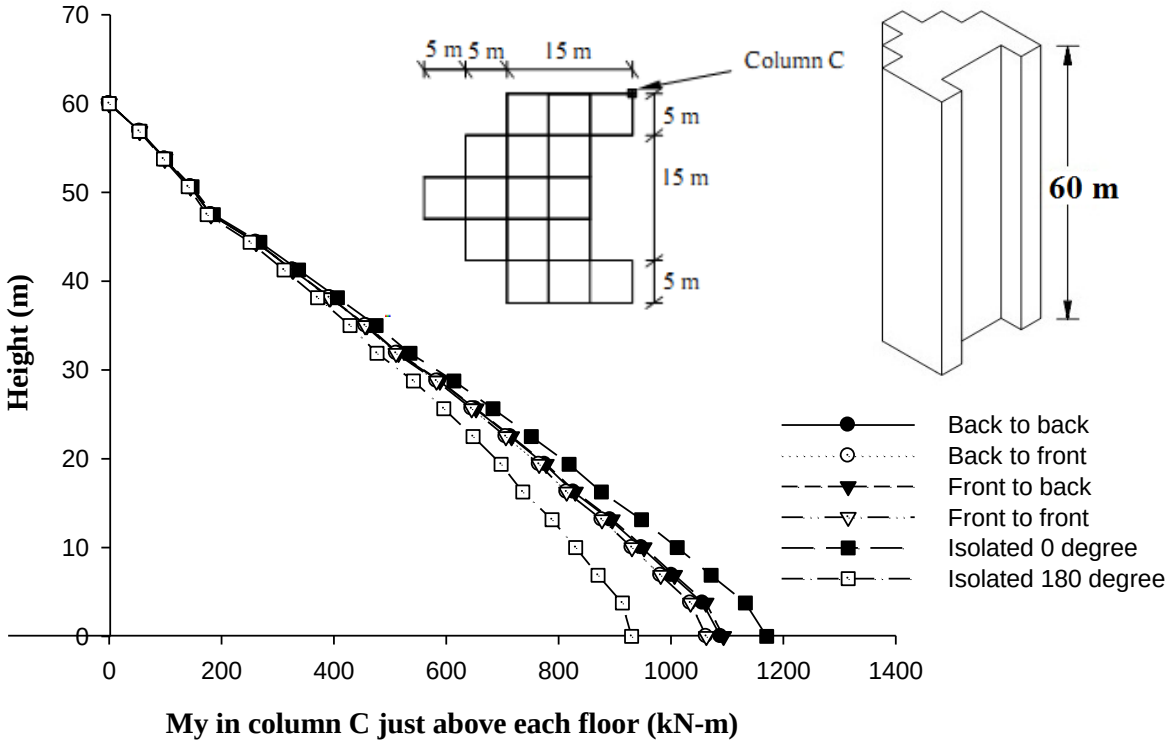


**Fig. 6.206 Interference effect on My (global) in column-C of Fish Shape-2 building**

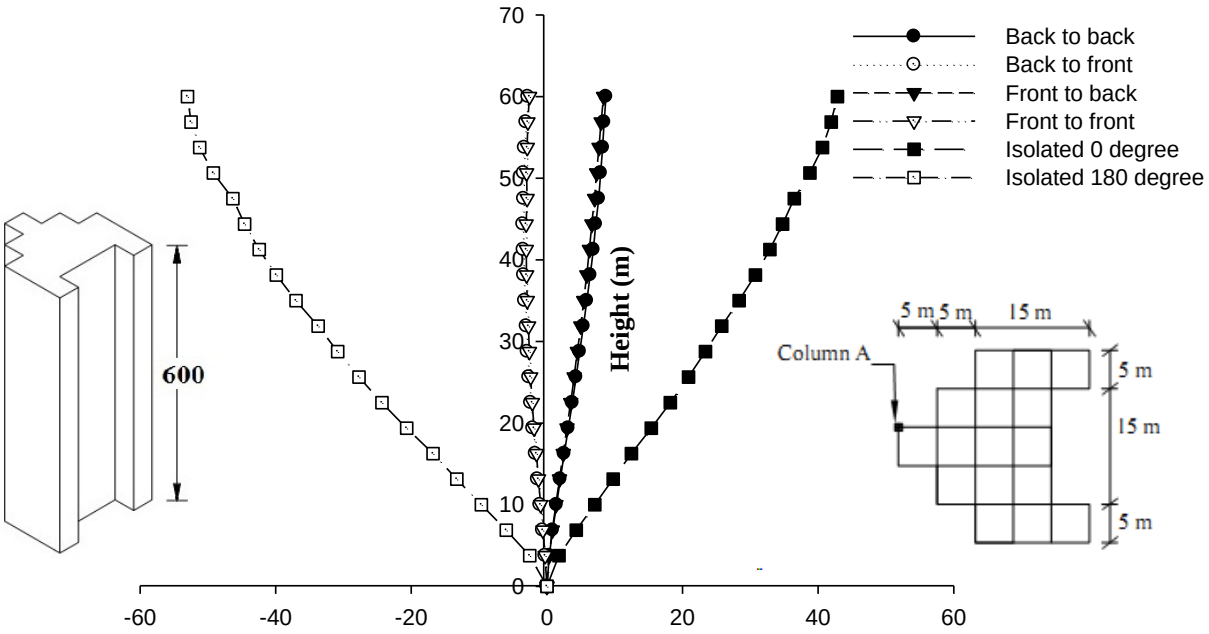


**Displacement in column A just above each floor (mm)**

**Fig. 6.207 Interference effect on horizontal displacement of column-A of Fish Shape-2 building**

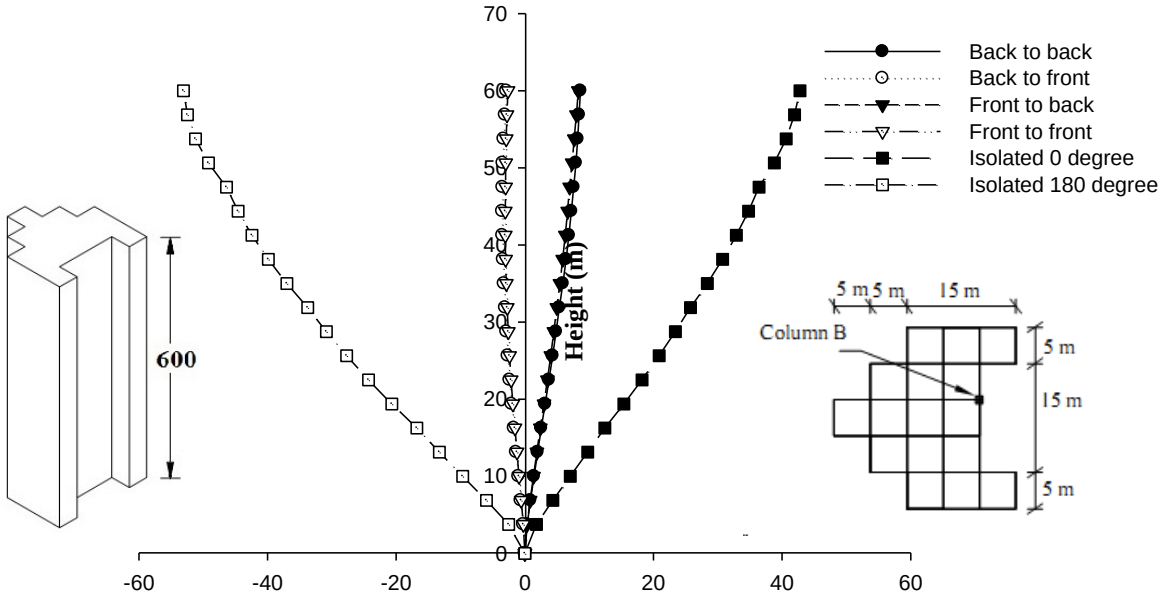


**Displacement in column B just above each floor (mm)**

**Fig. 6.208 Interference effect on horizontal displacement of column-B of Fish Shape-2 building**

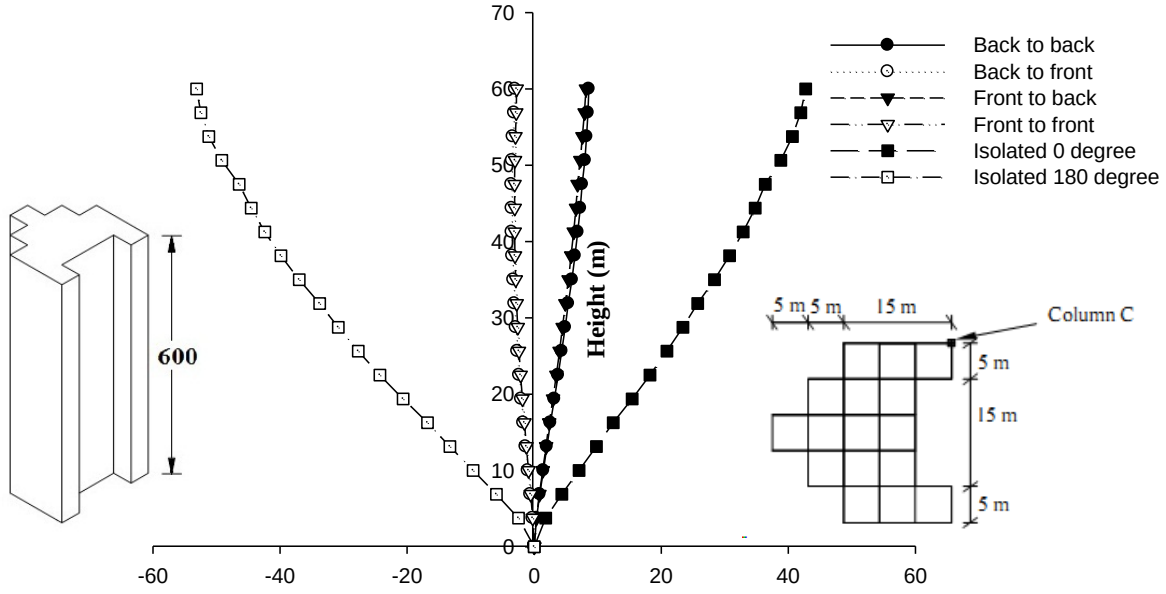


**Fig. 6.209 Interference effect on horizontal displacement of column-C of Fish Shape-2 building**

### 6.5.7 Fish Shape-3 Building

#### 6.5.7.1 Forces in columns

Wind interference effects on forces in column-A, B and C of Fish Shape-3 building can be seen in Figs. 6.211 to 6.219. Whereas axial forces in column-A and column-C are affected by blockage condition, axial force in column-B is not affected.

Moments about 'X' axis, i.e. Mx in all columns are influenced by interference condition. There is reduction in values of Mx due to interference. Blockage has not much of influence on My values.

#### 6.5.7.2 Displacement of columns

Figures 6.220 to 6.222 show the deflected shapes of column-A, B and C respectively under 4 interference conditions and 2 isolated conditions. Deflection values in interference conditions are very small as compared to those in isolated conditions. Deflection values in isolated $180^0$ condition are slightly more than corresponding values in isolated $0^0$ condition in all 3 columns.

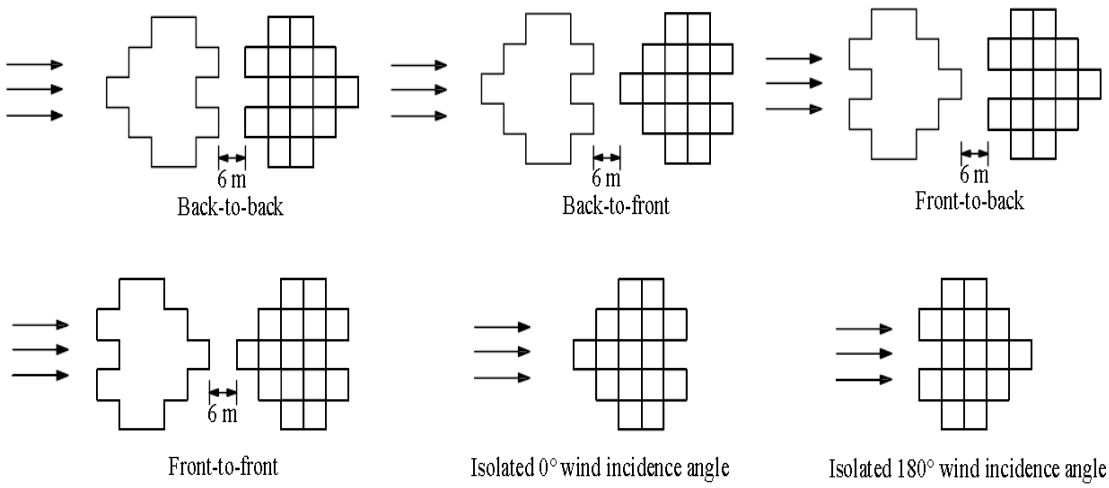


**Fig. 6.210 Relative position of Fish Shape-3 buildings under different interference conditions**

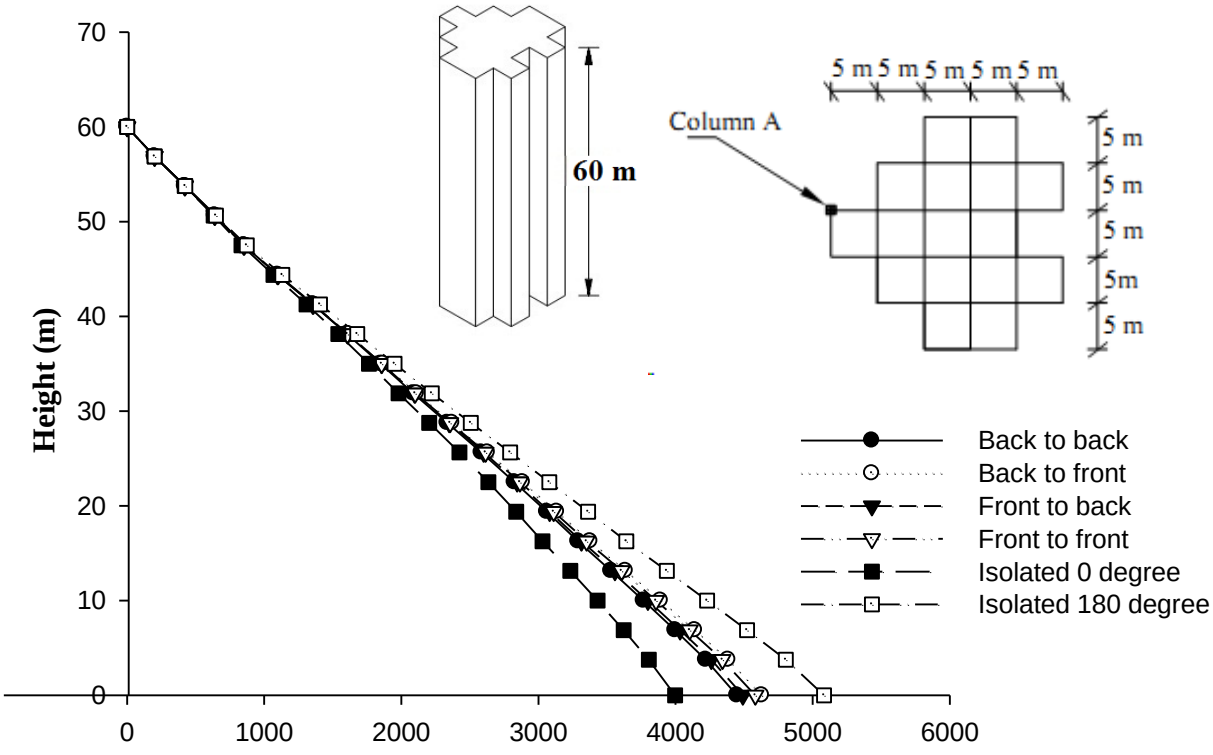


**Fig. 6.211 Interference effect on axial force in column-A of Fish Shape-3 building**

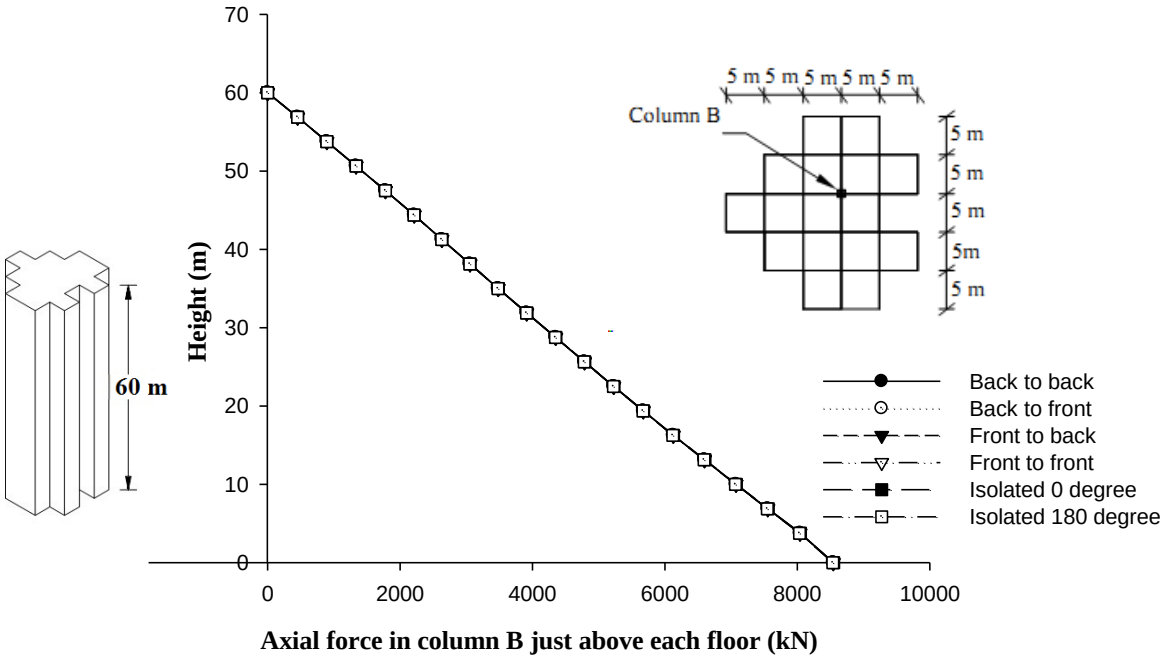


**Fig. 6.212 Interference effect on axial force in column-B of Fish Shape-3 building**

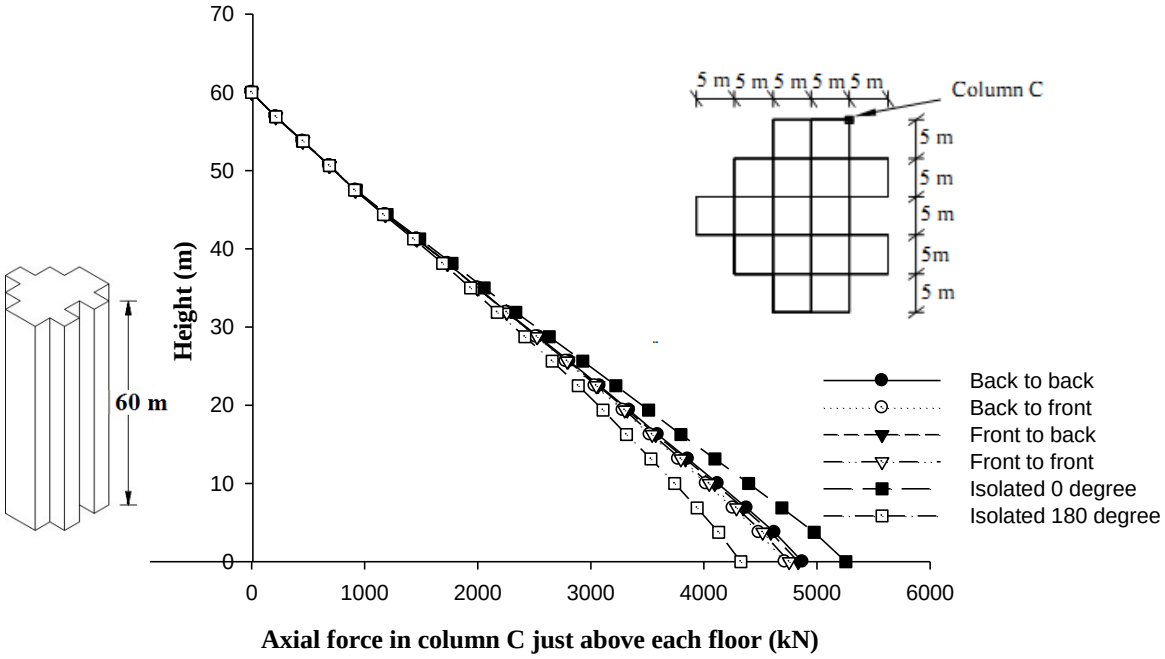


**Fig. 6.213 Interference effect on axial force in column-C of Fish Shape-3 building**

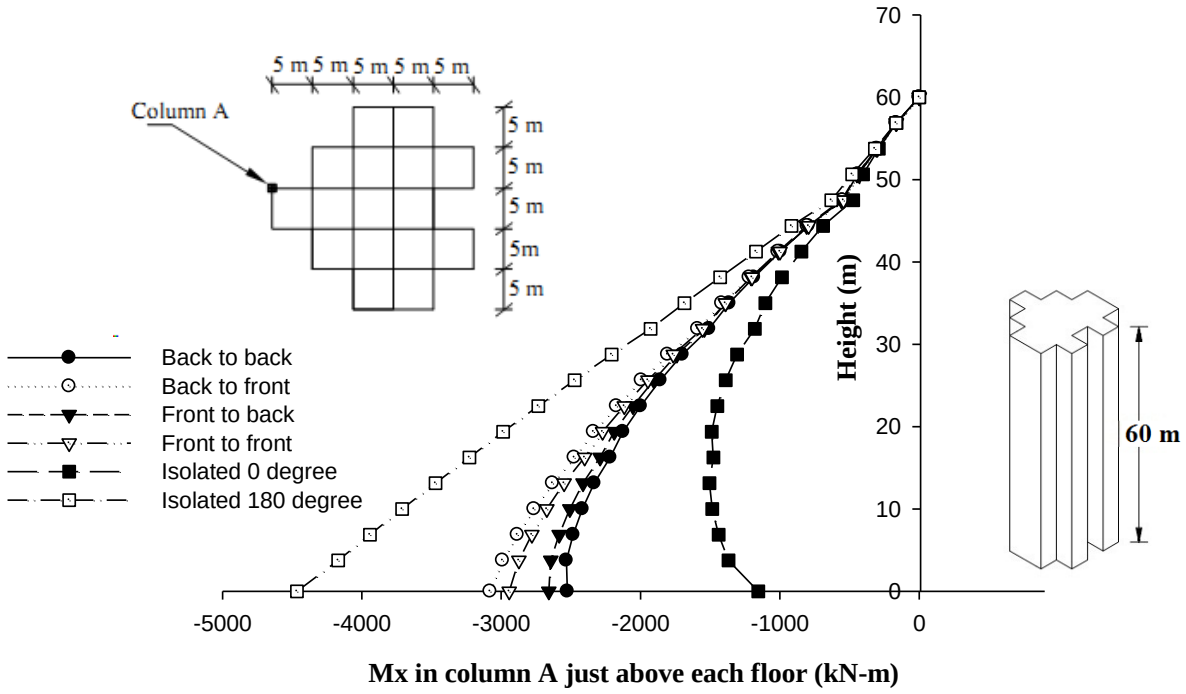


**Fig. 6.214 Interference effect on Mx (global) in column-A of Fish Shape-3 building**

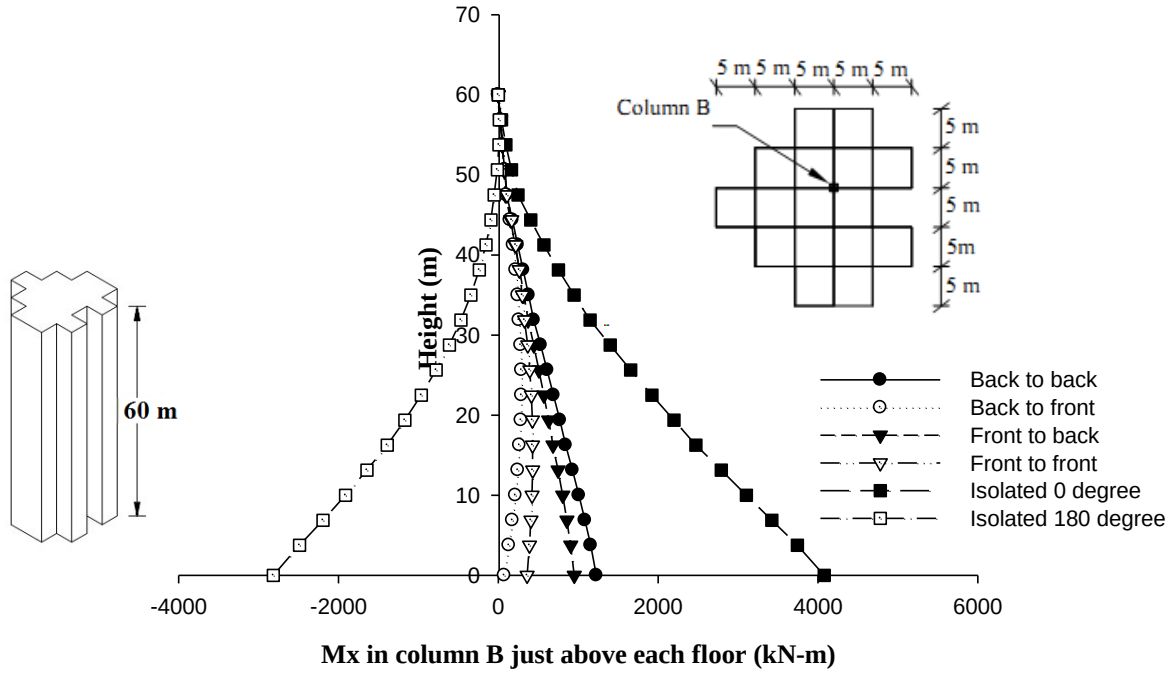


**Fig. 6.215 Interference effect on Mx (global) in column-B of Fish Shape-3 building**

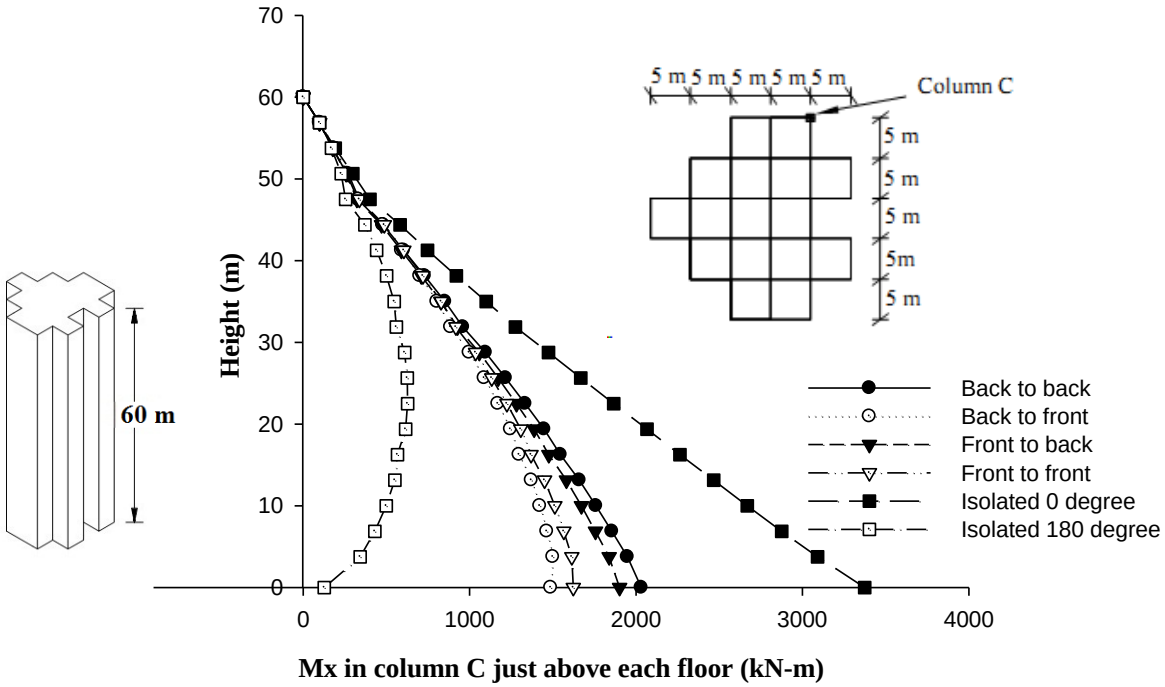


**Fig. 6.216 Interference effect on Mx (global) in column-C of Fish Shape-3 building**

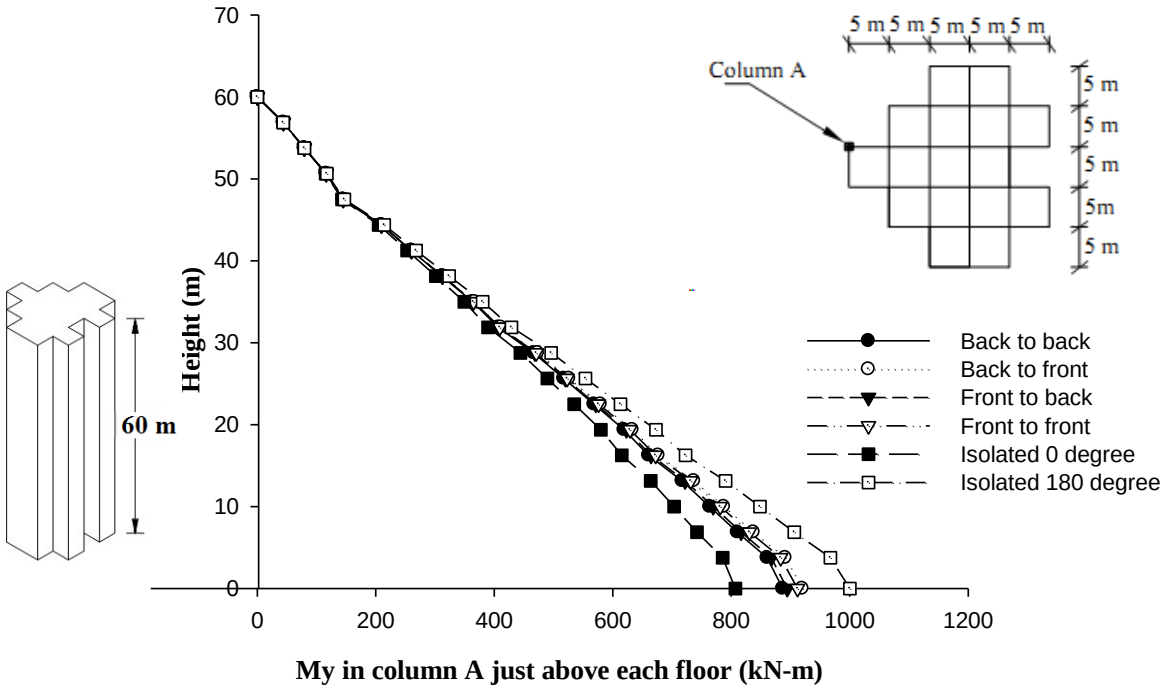


**Fig. 6.217 Interference effect on My (global) in column-A of Fish Shape-3 building**

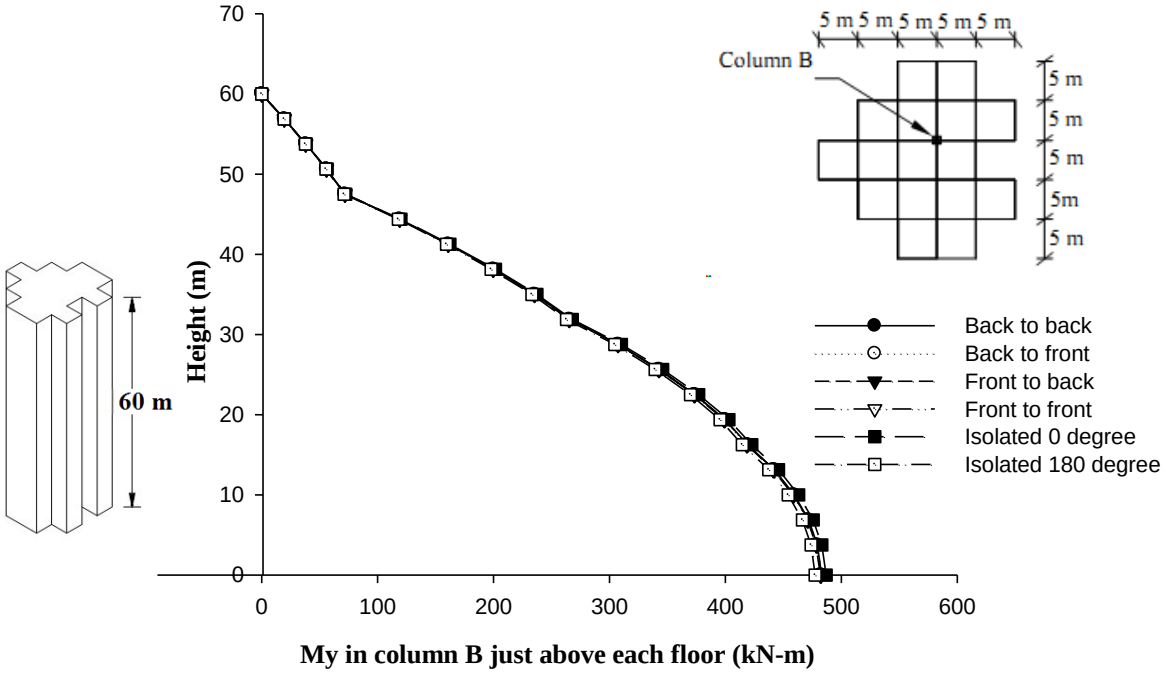


**Fig. 6.218 Interference effect on My (global) in column-B of Fish Shape-3 building**

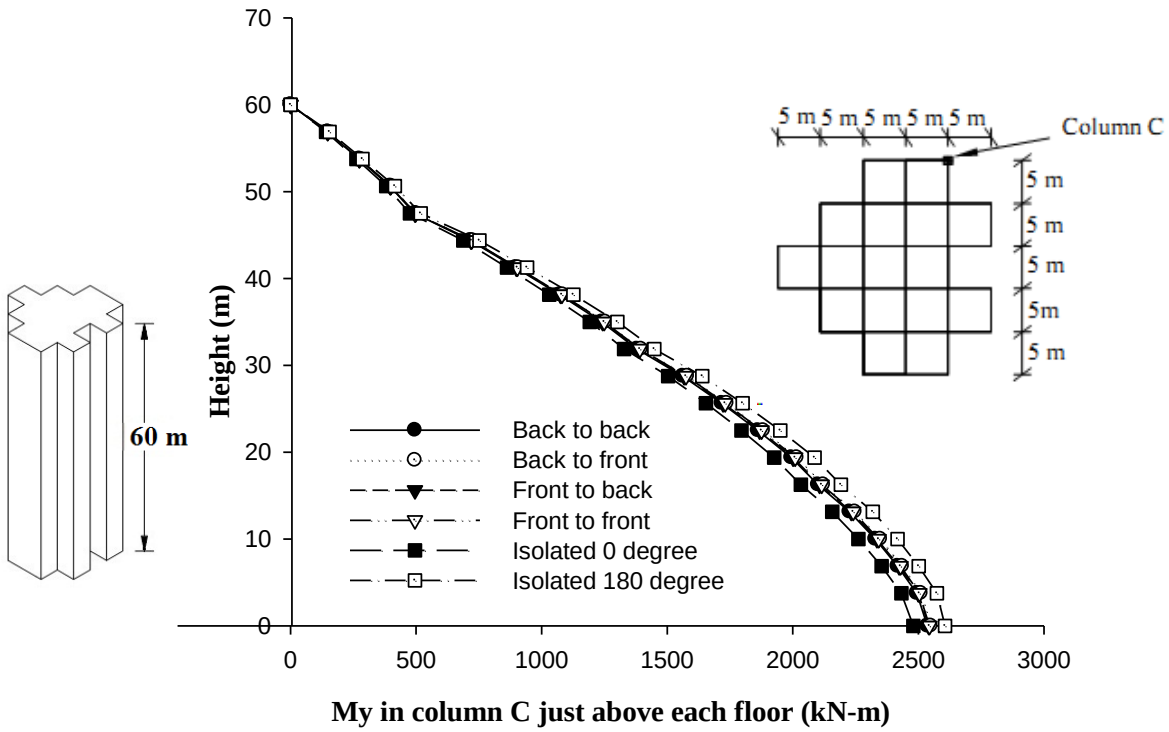


**Fig. 6.219 Interference effect on My (global) in column-C of Fish Shape-3 building**

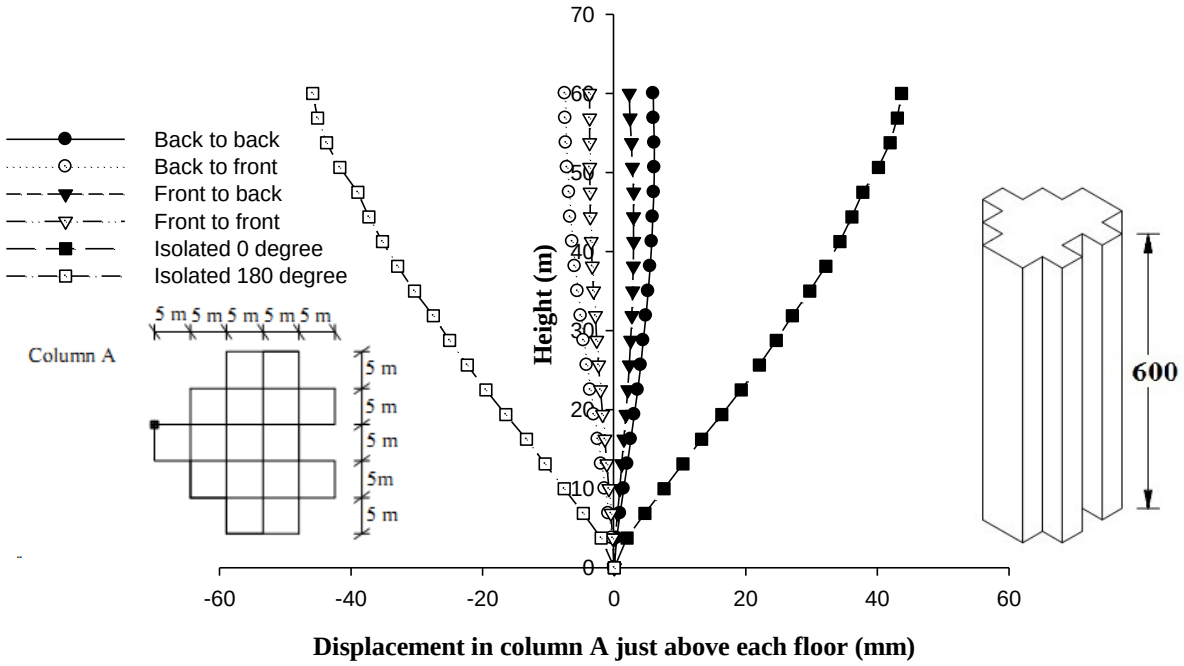


**Fig. 6.220 Interference effect on horizontal displacement of column-A of Fish Shape-3 building**

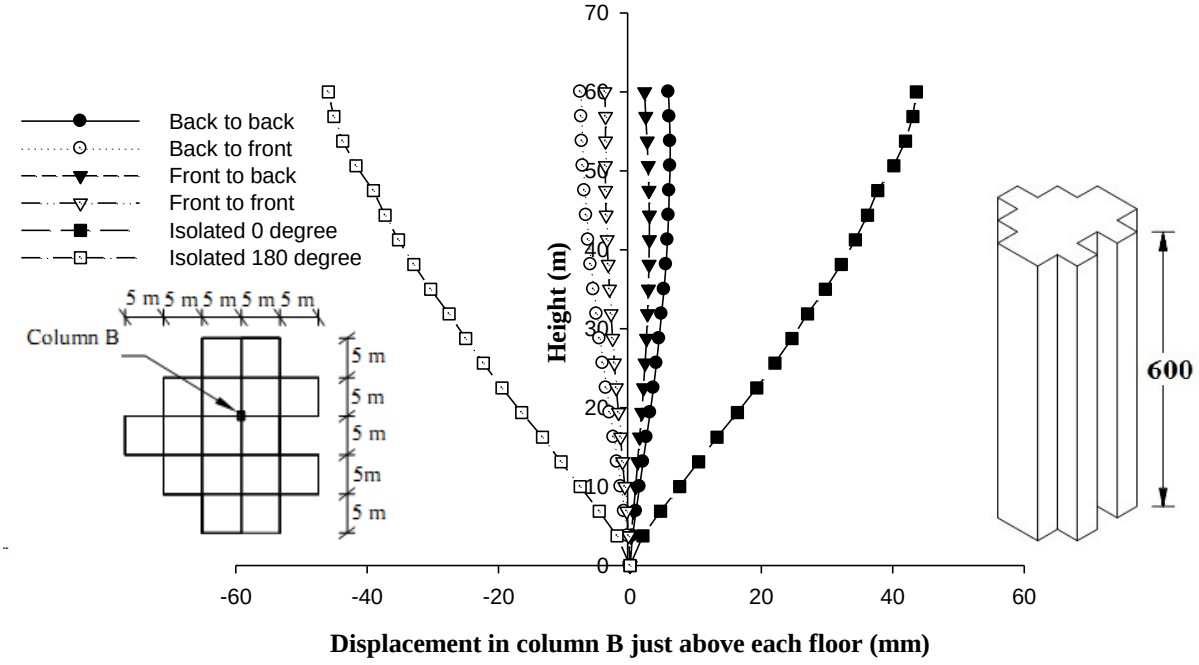


**Fig. 6.221 Interference effect on horizontal displacement of column-B of Fish Shape-3 building**

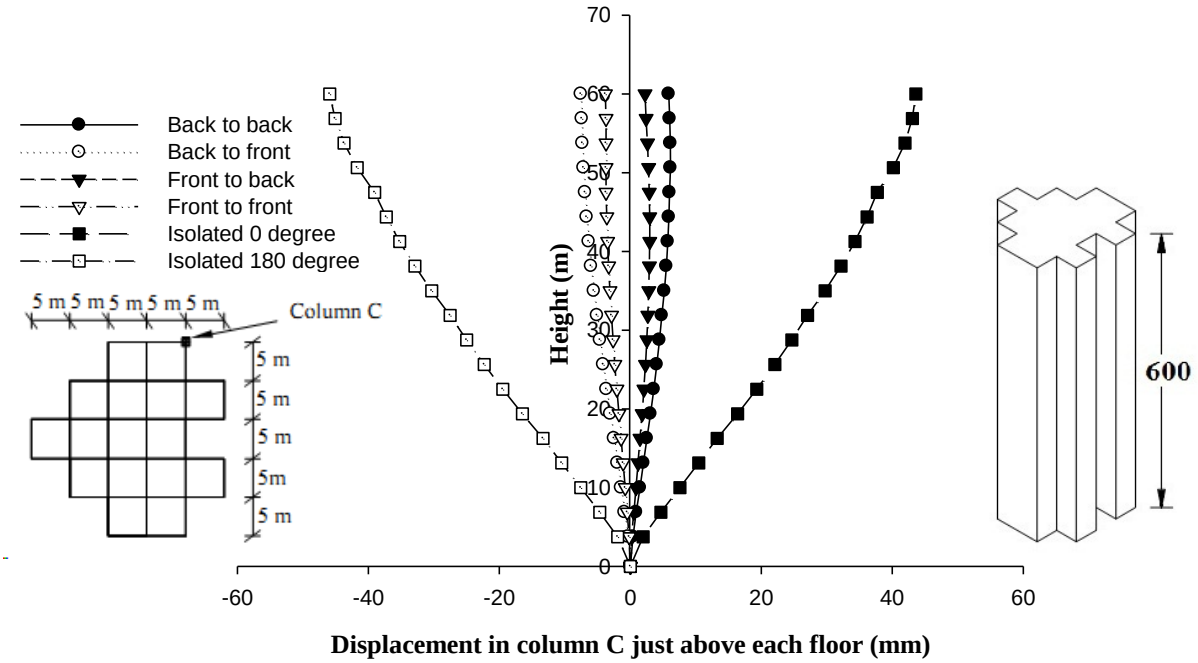


**Fig. 6.222 Interference effect on horizontal displacement in column-C of Fish Shape-3 building**

# Chapter - 7

# CONCLUSIONS

## 7.1 GENERAL

The preceding chapter of this thesis covers a study of the effects of wind on high-rise buildings with different cross-sectional shapes. Detailed study is made to determine the peak pressure around the buildings and behavior of building on wind loads. The rigid models are used for force measurement and Perspex sheet models are used for pressure measurement. A high degree of accuracy achieved in the present wind tunnel study. Response study is also made to compute the along-wind and across-wind mean wind response of such buildings.

On the basis of experimental and analytical studies carried out, significant findings of the present study are summarized below.

## 7.2 EXPERIMENTAL STUDY - FORCE MEASUREMENTS

### 7.2.1 Isolated Condition

#### 7.2.1.1 Square Shape building

1. Base shear $F_x$, i.e. along wind force is maximum at $45^0$ wind incidence angle, i.e. when wind hits perpendicular to the diagonal.
2. Base shear $F_y$, i.e. across wind force is maximum at $30^0$ and $75^0$ wind incidence angles.
3. Twisting moment $M_z$ is maximum at $15^0$ and $75^0$ wind angles.
4. There is negligible effect of wind incidence angle on the value of drag force coefficient $C_d$.

#### 7.2.1.2 Plus Shape-1 building

1. Base shear $F_x$ is maximum at $45^0$ wind angle and minimum at $75^0$.
2. Base shear $F_y$ is maximum at $60^0$ angle.
3. Twisting moment $M_z$ is maximum at $30^0$ angle.
4. $C_d$ varies significantly with wind angle.

#### 7.2.1.3 Plus Shape-2 building

1. Base shear $F_x$ is maximum at $0^0$ wind incidence angle and it falls sharply from $0^0$ to $90^0$ angles.
2. Base shear Fy is maximum at $15^0$ angle.
3. Twisting moment $M_z$ is maximum at $60^0$ wind incidence angle.

4. $C_d$ is maximum at $0^0$ wind incidence angle which falls drastically with increase in wind angle.

#### 7.2.1.4 I-Shape-1 building

1. Value of $F_x$ is maximum at $45^0$ angle.
2. Variation of $F_x$ between $0^0$ and $45^0$ is small as compared to its variation between $45^0$ and $90^0$ wind incidence angles.
3. $F_y$ is maximum at $15^0$ wind angle.
4. $M_z$ is maximum at $30^0$ angle.
5. $C_d$ is not much affected by wind incidence angle.

#### 7.2.1.5 I-Shape-2 building

1. $F_x$ is maximum at $45^0$ angle with small variation between $0^0$ and $45^0$, as compared to the variation between $45^0$ and $90^0$.
2. $F_y$ is maximum at $75^0$ angle.
3. $M_z$ is maximum at $15^0$ and $75^0$ angles.
4. There is very small influence of wind incidence angle on the value of $C_d$.

#### 7.2.1.6 Fish Shape-1 building

1. $F_x$ is maximum at $180^0$ wind incidence angle.
2. $F_y$ is maximum at an angle between $135^0$ and $150^0$.
3. $M_z$ is maximum at $90^0$ angle.
4. $C_d$ is highly influenced by wind incidence angle and it is maximum at $180^0$ wind angle.

#### 7.2.1.7 Fish Shape-2 building

1. $F_x$ is maximum at $75^0$ wind incidence angle.
2. Fy is maximum at $45^0$, $90^0$ and $135^0$ angles.
3. $M_z$ is maximum at $135^0$ angle.
4. $C_d$ is highly affected by wind incidence angle.

#### 7.2.1.8 Fish Shape-3 building

1. Effect of wind incidence angle on $F_x$ is small.
2. $F_x$ is maximum at $90^0$ angle.
3. $F_y$ is maximum at $135^0$ angle.
4. $M_z$ is maximum at $90^0$ wind angle.
5. Effect of wind incidence angle on $C_d$ is not appreciable.

#### 7.2.1.9 Comparison of forces on buildings with different cross -sectional shapes

1. I-shape-2 building is subjected to maximum along wind force i.e. $F_x$, followed by Plus shape building which is very close in magnitude.
2. I-shape-1 building is subjected to intermediate value of $F_x$.
3. Square shape and Plus shape-1 buildings are subjected to minimum $F_x$.
4. Maximum value of $F_x$ in case of I-Shape-2 building is almost 1.5 times that on I-Shape-1 building and 1.8 times that on square shape and Plus Shape-1 buildings.
5. Variation of $F_x$ with wind incidence angle is maximum in case of Plus Shape-2 building where maximum value of $F_x$ is almost 3 times minimum value.
6. Out of Fish Shape-1, Fish Shape-2 and Fish Shape-3 buildings, along wind force, i.e. $F_x$ is maximum on Fish Shape-1 building.
7. $F_x$ on Fish Shape-2 and Fish Shape-3 buildings varies within a small range with wind incidence angle as compared to variation of $F_x$ on Fish Shape-1 building.
8. It is not only $F_x$, twisting moment $M_z$ is also maximum on I-Shape-2 building.
9. Out of Fish shape-1, Fish shape-2 and Fish shape-3 buildings, Mz is maximum on Fish Shape-1 building as is the case with $F_x$ also.
10. Drag coefficient $C_d$ is maximum on Plus Shape-2 building out of square shape, Plus Shapes and I-shapes buildings in isolated condition.
11. $C_d$ on Fish Shape-1 building is maximum out of all Fish Shape buildings in isolated condition.

### 7.2.2 Interference Condition

#### 7.2.2.1 Square Shape building

1. Both base shears i.e. $F_x$ and $F_y$, and thus both base moments i.e. $M_x$ and $M_y$ are maximum in no blockage wind interference condition.
2. Twisting moment $M_z$ is maximum in half blockage condition followed by no blockage condition.
3. Drag coefficient $C_d$ is maximum in no blockage condition.

#### 7.2.2.2 Plus Shape-1 building

1. Both $F_x$ and $F_y$ are maximum in no blockage condition.
2. $M_z$ is maximum in half blockage condition.
3. $C_d$ is maximum in no blockage condition.

#### 7.2.2.3 Plus Shape-2 building

1. $F_x$ and $M_y$ are maximum no blockage condition.

2. $F_y$, $M_x$ and $M_z$ are maximum in half blockage condition.
3. $C_d$ is maximum in no blockage condition.

#### 7.2.2.4 I-Shape-1 building

1. $F_x$ and $M_y$ are maximum in no blockage condition.
2. Values of $F_y$ and $M_x$ are not influenced by interference conditions.
3. $M_z$ is maximum in half blockage condition.
4. $C_d$ is maximum in no blockage condition.

#### 7.2.2.5 I-Shape-2 building

1. Both base shears i.e. $F_x$ and $F_y$, both base moments i.e. $M_x$ and $M_y$, and twisting moment $M_z$ are maximum in no blockage condition.
2. Drag coefficient $C_d$ is also maximum in no blockage condition.

#### 7.2.2.6 Fish Shape-1 building

1. $F_x$ and $M_y$ are maximum at front-to-back condition.
2. $F_y$, $M_x$ and $M_z$ are maximum at front-to-front condition.
3. $C_d$ is maximum at front-to-back condition.

#### 7.2.2.7 Fish Shape-2 building

1. $F_x$, $M_y$ and $M_z$ are maximum at front-to-back condition.
2. $F_y$ and $M_x$ are maximum at front-to-back condition.
3. Although $C_d$ value is maximum at front-to-back condition, its values at other interference conditions also are of almost same magnitude.

#### 7.2.2.8 Fish Shape-3 building

1. $F_x$, $F_y$, $M_x$ and $M_y$ are maximum at back-to-back condition.
2. $M_z$ is maximum at back-to-front condition.
3. $C_d$ is maximum in Back-to-back condition.

#### 7.2.2.9 Comparison of $C_d$ on buildings with different cross-sectional shapes

1. In interference condition, out of Square Shape, Plus Shapes and I-Shapes buildings, I-Shape-2 building has maximum $C_d$ in full blockage and no blockage conditions.
2. $C_d$ is maximum on Plus Shape-1 building in half blockage wind interference condition.
3. All Fish Shape buildings have almost same $C_d$ in back-to-back wind interference condition.

4. Amongst all Fish Shape buildings, Fish Shape-1 building has maximum $C_d$ in all remaining three interference conditions.

## 7.3 EXPERIMENTAL STUDY - PRESSURE MEASUREMENTS

### 7.3.1 Isolated Condition

#### 7.3.1.1 Square Shape building

1. When wind flow is perpendicular to the windward face, pressure occurs on it and suction occurs on all other faces.
2. The positive wind pressure observed on windward face increase from bottom to near top edge of the face due to increase in wind velocity with height.
3. Maximum positive pressure is observed along the center line of the windward face which decreases towards the edges.
4. Near the top edge of windward face, pressure reduces due to upwash.
5. Suction on side faces reduces towards leeward edge.
6. Leeward face is subjected to uniform suction.
7. Values of pressure and suction on all faces changes with change in wind incidence angle.

#### 7.3.1.2 Plus Shape-1 building

1. Pressure occurs on windward face and suction occurs on parallel side faces and leeward face under wind incidence angle of $0^0$.
2. Even cut corners on windward faces are subjected to suction.
3. Pressure on windward face decreases with the increase in wind incidence angle.
4. Maximum suction is observed in a cut corner on leeward side at a skew angle of wind attack.
5. Maximum pressure on Plus Shape-1 building is less than that on Square Shape building.
6. Value of maximum suction on Plus Shape-1 building is greater than that on Square Shape building.

#### 7.3.1.3 Plus Shape-2 building

1. Entire windward face including cut corners are subjected to pressure due to long length of cut corners, when wind hits perpendicular to long wall.
2. Suction is noticed on parallel side faces and leeward faces.
3. At skew angles and also when wind hits perpendicular to a short wall, most of the surfaces are subjected to suction.

#### 7.3.1.4 I-Shape-1 building

1. When wind hits the building perpendicular to long wall, windward face is subjected to pressure. Side faces and leeward face are subjected to suction.
2. Suction is maximum in the cut regions on side walls.
3. At other wind angles, very small portion of the building is subjected to pressure. Most of the areas are subjected to suction.

#### 7.3.1.5 Fish Shape-1 building

1. When wind hits the stepped face, all cut corners are subjected to pressure including side faces.
2. It is only last side face and leeward face, which are subjected to suction.
3. When wind hits the flat surface, perpendicular to it, only windward flat surface is subjected to pressure and all other areas are subjected to suction.

#### 7.3.1.6 Fish Shape-2 building

1. When wind hits the pointed end of the building, windward cuts are subjected to pressure and all other surfaces are subjected to suction.
2. When wind hits the tail end, this surface is subjected to pressure and all other surfaces are subjected to suction.
3. Pressure in the channel part is greater than corresponding value in case of Fish Shape-1 building.
4. Even suction on side walls in this case is more than that in case of Fish Shape-1 building.

#### 7.3.1.7 Fish Shape-3 building

1. When pointed end of Fish Shape-3 building is subjected to wind, both windward and leeward faces are subjected to pressure and suction respectively of same magnitude of Fish Shape-2 building.
2. When wind hits the tail end, side faces are subjected to suction of smaller magnitude as compared to Fish Shape-2 building.

### 7.3.2 Interference Condition

#### 7.3.2.1 Square Shape building

1. When wind flows in full blockage interference condition, all surfaces of the building are subjected to suction with larger suction on windward face.
2. Maximum suction occurs near ¾ height from the bottom on windward face.

3. Part of the windward face is subjected to pressure and part suction under half blockage interference condition.
4. Although almost entire windward face is subjected to pressure under no blockage interference condition, the distribution is not symmetrical.
5. Suction on side faces and leeward face is higher in magnitude in no blockage condition as compared to the other two cases.

#### 7.3.2.2 Plus Shape-1 building

1. In full blockage interference condition, all faces are subjected to suction, with maximum suction on windward face near the top edge of the building.
2. At half blockage interference condition, leeward face and side faces are subjected to suction whereas, windward face is subjected to partly pressure and partly suction.
3. Almost entire windward face is subjected to pressure at no blockage interference condition.

#### 7.3.2.3 Plus Shape-2 building

1. All surfaces are subjected to suction in full blockage interference condition.
2. Part of windward face is subjected to pressure and part suction at half blockage interference condition.
3. At no blockage interference condition, windward face is subjected to positive pressure.
4. Suction on leeward face is maximum in no blockage interference condition.

#### 7.3.2.4 I-Shape-1 building

1. In full blockage interference condition, all faces of the building are subjected to suction.
2. In half blockage interference condition, windward face is subjected to partly pressure and partly suction.
3. Almost entire windward face is subjected to pressure in no blockage interference condition.
4. Out of three interference condition, suction on leeward face is maximum in no blockage interference condition.

#### 7.3.2.5 Fish Shape-1 building

1. Maximum suction occurs on large face at front-to-back interference condition.
2. Large face is subjected to minimum suction at front-to-front interference condition.

#### 7.3.2.6 Fish Shape-2 building

1. Suction on all faces vary with interference condition.
2. Minimum suction on rear face occurs at front-to-back interference condition.

#### 7.3.2.7 Fish Shape-3 building

1. All faces are subjected to suction in all interference conditions.
2. Maximum suction on rear face occurs at back-to-back interference condition.

## 7.4 WIND RESPONSE ANALYSIS

### 7.4.1 Isolated Condition

#### 7.4.1.1 Square Shape building

1. Out of column-A, B and C, column-A i.e. central column, is subjected to maximum axial force.
2. Axial force in column-A is not influenced by wind incidence angle.
3. In case of column-B and C, i.e. edge column and corner column, influence of wind incidence angle is predominant in lower 75% height of the columns.
4. All three columns, namely column-A, B and C are subjected to maximum twisting at $30^0$ wind incidence angle, followed by its value at $60^0$ angle.
5. Twisting moment in all three columns are maximum at around 17% height of the column from the base.
6. Moment about X-axis in all three columns are maximum at $30^0$ wind incidence angle.
7. Moment about Y-axis in all three columns are maximum at $90^0$ wind incidence angle.
8. Central column, i.e. column-A and edge column, i.e. column-B are subjected to maximum deflection at $30^0$ wind incidence angle, whereas corner column, i.e. column-C is subjected to maximum deflection at $0^0$ angle.
9. Maximum deflection in column-A and B is around 0.07% of height of the building whereas it is around 0.06% in case of column-C.

#### 7.4.1.2 Plus Shape-1 building

1. Axial force in central column, i.e. column-A is not influenced by wind incidence angle.
2. Axial force in lower parts of end columns namely column-B and column-C are affected by wind direction, although of small magnitude.
3. End columns are subjected to maximum twisting at $60^0$ wind incidence angle.
4. Moment about X-axis is maximum at $0^0$ wind incidence angle and minimum at $90^0$ angle in all three columns.

5. Moment about Y-axis is maximum at $90^0$ angle and minimum at $0^0$ in all columns.
6. Out of these three columns, column-B is subjected to maximum $M_y$, whereas column-C is subjected to maximum $M_x$.
7. Maximum displacement in X-direction is observed at $0^0$ wind incidence angle and zero displacement at $90^0$ angles in all three columns.
8. Maximum deflection is around 0.07% of height of the building in all columns.

#### 7.4.1.3 Plus Shape-2 building

1. Axial force in central column, i.e. column-B is not influenced by wind incidence angle.
2. End columns are subjected to maximum axial force at $0^0$ or $90^0$ angle depending upon its location.
3. All columns are subjected to maximum twisting at $60^0$ wind incidence angle.
4. Moment about X and Y axes are highly influenced by wind direction.
5. All three columns under consideration are subjected to maximum deflection at $0^0$ wind incidence angle, with value being around 0.125% of height of the building.

#### 7.4.1.4 I shape-1 building

1. Axial force in edge column, i.e. column-A remains same in all wind incidence angle above 80% height.
2. Below 80% height, axial force in column-A increases with wind incidence angle. Thus it is minimum at $0^0$ and maximum at $90^0$ angle.
3. Axial force in central column, i.e. column-B is not affected by wind incidence angle.
4. In case of corner column, i.e. column-C, axial force is maximum at $60^0$ angle and minimum at $90^0$ angle.
5. Twisting moment, $M_z$, is maximum at $30^0$ wind incidence angle in all columns. $M_z$ is almost zero at all other angles.
6. Moment about X-axis is minimum at $0^0$ angle and maximum at $90^0$ angle in column-A.
7. Mx in column-B is maximum at $0^0$ angle and zero at $90^0$ angle. It is maximum at $0^0$ angle and minimum at $90^0$ in column-C.
8. Effect of wind incidence angle on $M_y$ is similar on all three columns. It is maximum at $60^0$ angle and minimum at $0^0$ angle.
9. All columns show maximum deflection at $0^0$ angle. It reduces with increase in wind angle and becomes zero at $90^0$ angle.

10. Maximum deflection is about 0.09% of building height in all columns.

#### 7.4.1.5 Fish Shape-1 building

1. Axial force in all columns are highly influenced by wind incidence angle.
2. Wind incidence angle, causing maximum axial force varies with location of column.
3. Whereas edge column, i.e. column-B is subjected to maximum axial force at $0^0$ angle, corner column, i.e. column-C is subjected to maximum axial force at $60^0$ angle.
4. Twisting moment, $M_z$, is maximum in all three columns under consideration at $150^0$ wind incidence angle.
5. Moment about X-axis is maximum at $180^0$ angle and minimum at $0^0$ angle in case of column-A.
6. $M_x$ is maximum at $0^0$ angle in case of column-B and C with larger value in column-B than column-C.
7. Moment about Y-axis, i.e. $M_y$, is maximum at $90^0$ and minimum at $0^0$ wind incidence angle in column-A.
8. $M_y$ in column-B and C are maximum at $60^0$ angle with almost same value.
9. All three columns show maximum horizontal deflection at $0^0$ wind incidence angle which is followed by its value at $180^0$ angle.
10. Influence of wind incidence angle on the horizontal deflection is a lot.

#### 7.4.1.6 Fish Shape-2 building

1. Influence of wind incidence angle on axial force in columns is not much.
2. Twisting moment is maximum in all three columns at $120^0$ wind incidence angle followed by its value at $90^0$ angle.
3. Moment about X-axis, i.e. $M_x$, is highly influenced by wind incidence angle.
4. $M_x$ is maximum at $180^0$ angle in face column, i.e. column-A, whereas it is maximum at $0^0$ angle on tail columns i.e. column-B and C.
5. $M_y$ is maximum at $60^0$ angle in all three columns.
6. Horizontal deflections in all columns are maximum at $180^0$ angle and are almost zero at $90^0$ angle.

#### 7.4.1.7 Fish Shape-3 building

1. Axial force in face column and corner columns are affected by wind incidence angles.
2. Axial force in central column is not affected by wind direction.
3. Twisting moment is maximum at $90^0$ angle in all columns under consideration.

4. Moment about X-axis is maximum at $0^0$ angle and moment about Y-axis at $90^0$ angle in all three columns.
5. Horizontal deflection is maximum at $180^0$ angle and minimum at $90^0$ angle in all three columns.

### 7.4.2 Interference Condition

#### 7.4.2.1 Square Shape building

1. There is no effect of interference on axial force in central column.
2. Both edge column and corner column show similar pattern of axial force variation under interference conditions with minimum value of axial force in full blockage condition and maximum at no blockage condition.
3. Values of axial force in no blockage condition are quite close to respective value of axial force in isolated condition in case of both edge column and corner column.
4. Similar twisting moment variation pattern is observed in all three columns under consideration with maximum value under half blockage condition.
5. Twisting moment in all the columns are maximum at around 17% height from the bottom.
6. Moment about X-axis is maximum in no blockage interference condition in all columns which is very close in magnitude to the value in case of isolated condition.
7. Moment about Y-axis in central column is maximum at no blockage interference condition, followed by its value at half blockage condition.
8. In case of edge column and corner column, moment about Y-axis is maximum at half blockage condition and is minimum at full blockage condition.
9. Horizontal displacements of all three columns in X-direction under consideration in all interference conditions are less than respective value in isolated condition.
10. Horizontal displacement is minimum in half blockage interference condition.
11. In case of full blockage interference condition, the entire building moves in negative X-direction.

#### 7.4.2.2 Plus Shape-1 building

1. Axial force in central column is not affected by interference condition.
2. Axial force in corner columns are affected by interference condition, although the influence is very small.
3. All three columns under consideration are subjected to maximum twisting moment in half blockage interference condition.

4. Maximum twisting moment in all columns occurs at around 10% height from the base.
5. Moment about X-axis is maximum in isolated condition and minimum in full blockage condition.
6. Effect of interference on moment about X-axis is maximum in central column.
7. There is large effect of interference on moment about Y-axis in central column, although its effect on corner columns is small.
8. The entire building moves in negative X-direction in full blockage interference condition.
9. Numerical values of deflection in all interference conditions are less than that in isolated condition in all columns under consideration.

#### 7.4.2.3 Plus Shape-2 building

1. Axial forces in edge column and corner columns are affected by interference conditions. However, the same in central column is not affected.
2. Twisting moment in all three columns under consideration are maximum in half blockage interference condition.
3. Values of twisting moment in other blockage conditions are almost zero.
4. Moment about X-axis in edge column is maximum at full blockage interference condition.
5. In case of central column and end columns, moment about X-axis is maximum in isolated condition followed by its value in no blockage condition.
6. Moment about Y-axis is not affected much by blockage condition in case of edge column.
7. In case of both central and corner columns, moment about Y-axis is maximum in half blockage condition.
8. All three columns under consideration show maximum deflection in isolated condition followed by its values in no blockage condition.

#### 7.4.2.4 I-Shape-1 building

1. Axial force in central column is not affected by interference conditions.
2. Blockage conditions have small effects on axial forces in edge column and corner column.
3. All three columns under consideration are subjected to maximum twisting moment in half blockage condition.

4. Whereas moment about X-axis in edge column is maximum at full blockage condition, its values in central column and corner column are maximum at isolated condition.
5. Moment about Y-axis in edge column and corner column are maximum in half blockage condition. Its value in central column is maximum in full blockage condition.
6. Horizontal deflection in all three columns is maximum in isolated condition followed by its value in no blockage condition.

#### 7.4.2.5 Fish Shape-1 building

1. Axial force in front column is maximum in isolated $180^0$ case.
2. Axial force in back edge column and back corner column are maximum at isolated $0^0$ condition.
3. Moment about X-axis is highly influenced by interference condition. Its values in different interference conditions are less than that in isolated condition in all three columns under consideration.
4. Moment about Y-axis is not affected by interference conditions much.
5. Horizontal displacements of all three columns in all four interference conditions are less than those in two isolated conditions. It is to say that there is beneficial effect of interference on horizontal deflection of Fish Shape-1 building.

#### 7.4.2.6 Fish Shape-2 building

1. Axial force in face column is maximum at isolated $180^0$ condition.
2. Axial forces in back edge column and back corner column are maximum at isolated $0^0$ condition.
3. Values of axial force in all three columns under consideration fall between the values for isolated $0^0$ and isolated $180^0$ condition.
4. Moment about X-axis is maximum in isolated $180^0$ condition in face column, in isolated $0^0$ condition in back edge column and back corner column.
5. There is not much influence of blockage on moment about Y-axis in face column and back corner column.
6. Moment about Y-axis in back edge column is highly affected by blockage condition.
7. Blockage reduces the horizontal displacements of all columns under consideration.
8. Maximum deflection occurs in isolated $180^0$ condition followed by isolated $0^0$ condition.

#### 7.4.2.7 Fish Shape-3 building

1. Whereas axial force in face column and back corner column are affected by blockage condition, axial force in central column is not affected.
2. Moment about X-axis in all columns get reduced due to blockage.
3. Blockage has not much of influence on moments about Y-axis.
4. Deflection values in interference conditions are very small as compared to corresponding values in isolated conditions, in all columns under consideration.
5. Deflection values in isolated $180^0$ condition are slightly more than corresponding values in isolated $0^0$ condition in all columns.

## 7.5 MAJOR CONTRIBUTIONS / ACHIEVEMENTS

Following are the major contributions / achievements of the present study.

1. Very large amount of experimental data about the wind pressure distribution on various surfaces of Square Shape, Plus Shape, I-Shape and Fish Shape building have been generated which can be used by the designers while designing such buildings for wind loads in both isolated as well as interference conditions.
2. Effect of sudden change in building stiffness, due to variation in cross sectional shape, on the response of the buildings have been obtained analytically.
3. Effect of interference of one building block to another building block of same shape have been quantified as a result of both experimental and analytical response study.

## 7.6 RECOMMENDATIONS FOR FUTURE RESEARCH

Based on the present study, it is recommended that further studies should be carried out in the following areas.

1. Study of interference effects on each building with couple of buildings of different plan shapes in near vicinity.
2. Effects of aerodynamics modifications like openings, corner cut etc. on the wind pressure distribution and response of all seven buildings.
3. Dynamic response analysis of the buildings using time varying wind data.

## REFERENCES


1. Ahuja, R., Dalui, S.K. and Gupta, V.K. (2006), "Unpleasant pedestrian wind conditions around buildings", Asian Journal of Civil Engineering (Building and Housing), 7, pp. 147-154.
2. Amin, J.A. (2008), "Effect of Plan Shape on Wind Induced Response of Tall Buildings", Ph.D. Thesis, Department of Civil Engineering, Indian Institute of Technology Roorkee, Roorkee, India.
3. Amin, J.A. and Ahuja, A.K. (2008), "Experimental study of wind pressures on irregular plan shape buildings", BBAA VI International Colloquium on: Bluff Bodies Aerodynamics and Application, pp. 2008.
4. Amin, J.A. and Ahuja, A.K. (2009), "Mean interference effects between two buildings: effects of close proximity", The Structural Design of Tall and Special Buildings, published online in Wiley Interscience.
5. Amin, J.A. and Ahuja, A.K. (2011), "Experimental study of wind-induced pressure on buildings of various geometries", International Journal of Engineering, Science and Technology, 3, pp. 1-19.
6. AS/NZS: 1170.2 (2002), "Structural Design Actions, Part-2 : Wind Action"
7. ASCE: 7-02 (2002), "Minimum Design Loads for Buildings and Other Structures"
8. Bailey, P.A. and Kwok, K.C.S. (1985), "Interference excitation of twin tall buildings", Journal of Wind Engineering and Industrial Aerodynamics, 21, pp. 323-338.
9. Bairagi, A.K. and Dalui, S.K. (2014), "Optimization of interference effects on high-rise buildings for different angle using CFD simulation", Electronics Journal of Structural Engineering, 14, pp. 39-49.
10. Balendra, T. and Nathan, G.K. (1987), "Longitudinal, lateral and torsional oscilation of a square section tower model in an atmospheric boundary layer", Engineering Structures, 9, pp. 218-224.
11. Balendra, T. and Nathan, G.K. (1988), "Dynamic response of a triangular building model in an atmospheric boundary layer", Journal of Wind Engineering and Industrial Aerodynamics, 31, pp. 29-39.
12. Balendra, T., Anwar, M.P. and Tey, K.L. (2005) "Direct measurement of wind-induced displacements in tall building models using laser positioning technique", Journal of Wind Engineering and Industrial Aerodynamics, 93, pp. 399-412.
13. Balendra, T., Ma, Z. and Tan, C.L. (2003), "Design of tall residential buildings in Singapore for wind effects", Wind and Structure, 6, pp. 221-248.

14. Balendra, T., Wang, C.M. and Rakesh, G. (1999), "Vibration control of various types of buildings using TLCD", Journal of Wind Engineering and Industrial Aerodynamics, 83, pp. 197-208.
15. Bazeos, N. and Beskos, D.E. (1996), "Torsional moments on buildings subjected to wind loads", Engineering analysis with boundary elements, 18, pp. 305-310.
16. Beneke, D.L. and Kwok, K.C.S. (1993), "Aerodynamics effect of wind induced torsion on tall buildings", Journal of Wind Engineering and Industrial Aerodynamics, 50, pp. 271-280.
17. Bhatnagar, N.K. (2011), "Effects of Geometrical Shapes on Wind Loads on Buildings", Ph.D. Thesis, Department of Civil Engineering, Indian Institute of Technology Roorkee, Roorkee, India.
18. Blessmann, J. (1992), "Neighboring wind effects on two tall buildings", Journal of Wind Engineering and Industrial Aerodynamics, 41-44, pp. 1041-1052.
19. Blessmann, J. and Riera, J.D. (1985), "Wind excitation of neighboring tall buildings", Journal of Wind Engineering and Industrial Aerodynamics, 18, pp. 91-103.
20. BS: 63699 (1995), "Loading for Buildings: Part 2 – Code of Practice for Wind Loads"
21. Chakraborty, S., Dalui, S.K. and Ahuja, A.K. (2014), "Wind Loads on irregular plan shaped tall building – a case study", Wind and Structures, 19, pp. 59-73.
22. Chaudhry, K.K. and Garg, R.K. (1993), "Wind Pressure distribution around the high-rise building curved in plan", Journal of Structural Engineering, Madras, Vol. 20, pp. 129-134.
23. Chaudhry, K.K. and Garg, R.K. (2006), "Wind Induced flow-field study for designing cruciform shaped buildings, Proc. of Third National Conference on Wind Engineering, Kolkata, India, 414-421,
24. Chaudhry, K.K., Seetharamulu, K. and Swami, B.L.P. (1990), "Wind tunnel investigation-typical cases", Proc. of International symposium on Wind loads on Structures, New Delhi, India, 151-163.
25. Chaudhry, K.K., Sharma, V.R. and Seetharamulu, K. (1995), "Response measurements of flexible structure", Proc. of Ninth International Conference on Wind Engineering, New Delhi, India, 2201-2211.
26. Cheong, H.F., Balendra, T., Chew, Y.T., Lee, T.S. and Lee, S.L. (1992), "An experimental technique for distribution of dynamic wind loads on tall buildings", Journal of Wind Engineering and Industrial Aerodynamics, 40, pp. 249-261.
27. Chetia, N. and Talukdar, S. (2006), "Tuned mass damper control of an asymmetric multistoried building under seismic excitation with inbuilt elevated reservoir", Proc.

of the Conference on High Rise Buildings: Materials and Construction practices, New Delhi, India, 335-343.

28. Cooper, K.R., Nakayama, M., Sasaki, Y., Fediw, A.A., Resende, S. and Zan, S.J. (1997), "Unsteady aerodynamic force measurement on a super-tall building with a tapered cross-section", Journal of Wind Engineering and Industrial Aerodynamics, 72, pp. 199-212.
29. Dalui, S.K. (2008), "Wind Effects on Tall Buildings With Peculiar Shapes", Ph. D. Thesis, Department of Civil Engineering, Indian Institute of Technology Roorkee, Roorkee, India.
30. Darla, A.R. and Talukdar, S. (2007), "Wind induced fatigue in lattice steel tower", Proc. of Fourth National Conference on Wind Engineering SERC, Chennai, India, 321-328.
31. EN 1991-1-4 (2005), "Euro code 1: Actions on Structures - Wind Actions"
32. Garg, R.K. and Chaudhry, K.K. (2007), "Wind induced flow-field around complex shaped buildings", Indian Concrete Institute Journal, 8, pp. 33-41.
33. Garg, R.K. and Goel, R. (2007), "Nonlinear study of towers in cyclonic wind region", Proc. IV National Conference on Wind Engineering, SERC, Chennai, 2007, pp. 367-372.
34. Goel, R., Ahuja, A.K. and Prasad, J. (2007), "Wind loads on building with attached canopies", Asian Journal of Civil Engineering, 8(3), 239-246.
35. Goel, R. and Ahuja, A.K. (2009), "Wind loads on attached projections to low rise building", Proc. of the 5$^{th}$ National Conference on Wind Engineering, Surat.
36. Gomes, M.G., Rodriques, A.M. and Mendis, P. (2005), "Experimental and numerical study of wind pressures on irregular-plan shapes", Journal of Wind Engineering and Industrial Aerodynamics, 93, pp. 741-756.
37. Gu. M. (2009), "Study on wind loads and responses of tall buildings and structures", the seventh Asia pacific conference on Wind Engineering, November 8-12.
38. Gu, M. and Xie, Z.N. (2011), "Interference effects of two and three super-tall buildings under wind action", The Chinese Society of Theoretical and applied mechanics, 27, pp. 687-696.
39. Gupta, R. and Krishna, P. (2002), "Zones of Critical interference around a TV tower", Proc. of National Conference on Wind Engineering (NCWE 02), Indian Institute of Technology Roorkee, Roorkee, India, pp. 255-265.

40. Gupta, R., Poddar, K. and Sheth, A. (2007-a), “Experimental study on tall residential towers at NWTF”, Proc. of Fourth National Conference on Wind Engineering, SERC, Chennai, India, 95-104.
41. Gupta, R., Poddar, K. and Sheth, A. (2007-b), “BLWT tests on tall residential towers”, Proc. of International conference on Wind Engineering (ECWE 12), Caims, Australia, 367-374.
42. Hayashida, H., and Iwasa, Y. (1990), “Aerodynamics shape effects of tall buildings for vortex induced vibration”, Journal of Wind Engineering and Industrial Aerodynamics, 33, pp. 237-242.
43. Hui, Y., Tamura, Y., Yoshida, A. and Kikuchi, H. (2013), “Pressure and flow field investigation of interference effects on external pressure between high-rise buildings”, Journal of Wind Engineering and Industrial Aerodynamics, 115, pp. 150-161.
44. IS:875-Part-3 (1987), “Code of Practice for Design Loads (other than Earthquake Loads) for Buildings and Structures- Wind Loads”
45. Isyumov, N., Fediw, A.A., Colaco, J. and Banavalkar, P.V. (1992), “Performance of a tall building under wind action”, Journal of Wind Engineering and Industrial Aerodynamics, 41-44, pp. 1053-1064.
46. Jaminson, N.J., Carpenter, P. and Cenek, P.D. (1992), “Wind induced external pressures on a tall building with various corner configurations”, Journal of Wind Engineering and Industrial Aerodynamics, 41-44, pp. 2401-2412.
47. Kareem, A. and Cermak, J.E. (1984), “Pressure fluctuation on a square building model in boundary-layer flows”, Journal of Wind Engineering and Industrial aerodynamics, 16, pp. 17-41.
48. Katagiri, J., Nakamura, O., Ohkuma, T., Marukawa, H., Tsujimoto, T. and Kondo, K. (1992), “Wind induced lateral-torsional motion of a tall building”, Journal of Wind Engineering and Industrial Aerodynamics, 41-44, pp. 1127-1137.
49. Kawai, H. (1993), “Bending and torsional vibration of tall buildings in strong wind”, Journal of Wind Engineering and Industrial Aerodynamics, 50, pp. 281-288.
50. Kawai, H. (1998), “Effect of corner modification on aeroelastic instabilities of tall buildings”, Journal of Wind Engineering and Industrial Aerodynamics, 74-76, pp. 719-729.
51. Kheyari, P. and Dalui, S.K. (2015), “Estimation of wind load on a tall building under interference effects – a case study”, Jordan Journal of Civil Engineering, 9, pp. 84-101.

52. Kim, W., Tamura, Y. and Yoshida, A. (2009), "Interference effects of local peak pressures acting on wall of tall buildings", 11th American Conference on Wind Engineering, June22-26.
53. Kim, Y.M., You, K.P. and Ko, N.H. (2008), "Across wind response of an aeroelastic tapered tall building", Journal of Wind Engineering and Industrial Aerodynamics, 96, pp. 1307-1319.
54. Kumar, S. (2013), "Effects of Steps on Wind Loads on Tall Buildings", M.Tech. Thesis, Department of Civil Engineering, Indian Institute of Technology Roorkee, Roorkee, India.
55. Kushal, T. (2013), "Effect of Plan Shapes on the Response of Tall Buildings Under Wind Loads", M.Tech. Thesis, Department of Civil Engineering, Indian Institute of Technology Roorkee, Roorkee, India.
56. Kwok, K.C.S., Wilheim, P.A. and Wilkie, B.G. (1987), "Effects of edge configuration on wind-induced response of tall buildings", Journal of Wind Engineering and Industrial Aerodynamics, 10, pp. 135-140.
57. Kwok, K.C.S. (1988), "Effect of building shape on wind-induced response of tall building", Journal of Wind Engineering and Industrial Aerodynamics, 28, pp. 381-390.
58. Lam, K.M., Leung, M.Y.H. and Zhao, J.G. (2008), "Interference effects on wind loading of a row of closely spaced tall buildings", Journal of Wind Engineering and Industrial Aerodynamics, 96, pp. 562-583.
59. Letchford, C. and Robertson, A.P. (1999), "Mean wind loading at the leading ends of free standing walls", Journal of wind engineering and industrial aerodynamics, 79, pp. 123-134.
60. Liang, S., Li, Q.S., Liu, S. Zhang, L. and Gu, M. (2004), "Torsional dynamic wind loads on rectangular tall buildings", Engineering Structures, 26, pp. 129-137.
61. Lin, N., Letchford, C., Tamujra, Y., Liang, B. and Nakamura, O. (2005), "Characteristics of wind forces acting on tall buildings", Journal of Wind Engineering and Industrial Aerodynamics, 93, pp. 217-242.
62. Lythe, G.R., and Surry, D. (1990), "Wind-induced torsional loads on tall buildings", Journal of Wind Engineering and Industrial Aerodynamics, 36, pp. 225-234.
63. Mendis, P. and Ngo, T. (2006), "9/11 Five years on-Change in tall building design?", Electronics Journal of Structural Engineering.
64. Mendis, P., Ngo, T., Haritos, N., Hira, A., Samali, B. and Cheung, J. (2007), "Wind loading on tall buildings", EJSE special issue: Loading on Structures, pp. 41-54.

65. Menicovich, D., Lander, D., Vollen, J., Amitay, M., Letchford, C. and Dyson, A. (2014), "Improving aerodynamics performance of tall buildings using fluid based aerodynamics modification", Journal of Wind Engineering and Industrial Aerodynamics, 133, pp. 263-273.
66. Merrick, R. and Bitsuamlak, G. (2009), "Shape effects on the wind-induced response of high-rise buildings", Journal of Wind Engineering and Industrial Aerodynamics, 6, pp. 1-18.
67. Miyashita, K., Katagiri, J and Nakamura, O. (1993), "Wind induced response of high rise buildings", Journal of Wind Engineering and Industrial Aerodynamics, 50, pp. 319-328.
68. Mohotti, D., Mendis, P. and Ngo, T.C. (2013), "Application of computational fluid dynamics (CFD) in wind analysis of tall buildings", 4th International Conference on Structural Engineering and Construction Management 2013, Kandy, Sri Lanka.
69. Mukherjee, S., Chakraborty, S., Dalui, S. K., and Ahuja, A.K. (2014), "Wind Induced Pressure on 'Y' Plan Shape Tall Building", Wind and Structures, An International Journal, Korea (Techno Press)- Vol. 19, No.5, 2014, pp-523-540.
70. Ngo, T. and Letchford, C. (2008), "A comparison of topographic effects on gust wind speed", Journal of Wind Engineering and Industrial Aerodynamics, 96, pp. 2273-2293.
71. Paterson, D.A. and Pepenfuss, A.T. (1993), "Computation of wind flows around two tall buildings", Journal of Wind Engineering and Industrial Aerodynamics, 50, pp. 69-74.
72. Rai, S.K. and Prasad, J. (2005), "Non-linear static analysis of shear wall in tall buildings", Proc. of International Structural Engineering Convention, Indian Institute of Science, Bangalore, India.
73. Rai, S.K., Prasad, J. and Ahuja, A.K. (2006-a), "Reducing drifts and damages in tall buildings by shear wall panels", Proc. of the Conference on High Rise Buildings: Materials and Construction Practices, New Delhi, India, 397-409.
74. Rai, S.K., Prasad, J. and Ahuja, A.K. (2006-b), "Importance of shear wall in tall buildings", Proc. of the Conference on High Rise Buildings: Materials and Construction Practices, New Delhi, India, 411-42.
75. Ramakant, M. (2012), "Wind Effects on Tall Building" , M.Tech. Thesis, Department of Civil Engineering, Indian Institute of Technology Roorkee, Roorkee, India.
76. Selvam, R.P. (1990), "Computer simulation on wind load on a house", Journal of Wind Engineering and Industrial Aerodynamics, 36, pp. 1029-1036.

77. Selvam R.P. and Konduru, P.B. (1993), “Computational and experimental roof corner pressures on the Texas Tech Building”, Journal of Wind Engineering and Industrial Aerodynamics, 46 & 47, pp. 449-454.
78. Selvam, R.P. (1997), “Computation of pressures on Texas Tech University building using large eddy simulation”, Journal of Wind Engineering and Industrial aerodynamics, 67 & 68, pp. 647-657.
79. Shankar, K. and Balendra, T. (2002), “Application of the energy flow method to vibration control of buildings with multiple tuned liquid dampers”, Journal of Wind Engineering and Industrial Aerodynamics, 90, pp. 1893-1906.
80. Shykes, D.M. (1983), “Interference effects on the response of a tall building model”, Journal of Wind Engineering and Industrial Aerodynamics, 11, pp. 365-380.
81. Srinivas, Talukdar, S. and Maity, D. (2005), “Along wind vibration of a tapered chimney”, Journal of Wind and Engineering, Indian Society for Wind Engineering, Vol. 2, pp. 40-44.
82. Stathopoulos, T. (1985), “Wind environmental condition around tall buildings with chamfered corners”, Journal of wind engineering and Industrial Aerodynamics, 21, pp. 71-87.
83. Stathopoulos, T. and Storms, R. (1986), “Wind environmental conditions in passage between buildings”, Journal of Wind Engineering and Industrial Aerodynamics, 24, pp. 19-31.
84. Stathopoulos, T., and Zhu, X., (1988), “Wind Prssures on buildings with appurtenances”, Journal of Wind Engineering and Industrial Aerodynamics, 31, pp. 265-281.
85. Stathopoulos. T. and Luchian, H.D. (1990), “Wind pressures on building with multi-level roofs”, Journal of Wind Engineering and Industrial Aerodynamics, 36, pp.1299-1306.
86. Surry, D. and Djakovich, D. (1995), “Fluctuating pressures on models of tall buildings”, Journal of Wind Engineering and Industrial Aerodynamics, 58, pp. 81-112.
87. Szalay, Z. (1989),”Drag on several polygon cylinders”, Journal of Wind Engineering and Industrial Aerodynamics, 32, pp. 135-143
88. Tanaka, H., and Lawen, N. (1986), “Test on the CAARC Standards Tall Building Model, with length scale of 1:1000”, Journal of Wind Engineering and Industrial Aerodynamics, 25, pp. 15-29.

89. Tanaka, H., Tamura, Y., Ohtake, K., Nakai, M. and Kim, Y.C. (2012), "Experimental investigation of aerodynamics forces and wind pressure acting on tall buildings with various unconventional configurations", Journal of Wind Engineering and Industrial Aerodynamics, 107-108, pp. 179-191.
90. Taniike, Y. (1992), "Interference mechanism for enhanced wind forces on neighboring tall buildings", Journal of Wind Engineering and Industrial Aerodynamics, 41-44, pp. 1073-1083.
91. Tamura, T. and Miyagi, T. (1999), "The effects of turbulence on aerodynamics forces on a square cylinder with various corner shapes", Journal of Wind Engineering and Industrial Aerodynamics, 83, pp. 135-145.
92. Thepmongkorn, S. and Kwok, K.C.S. (2002), "Wind-induced responses of tall buildings experiencing complex motion", Journal of Wind Engineering and Industrial Aerodynamics, 90, pp. 515-526.
93. Thepmongkorn, S., Wood, G.S. and Kwok, K.C.S. (2002), "Interference effects on wind-induced coupled motion of a tall building", Journal of Wind Engineering and Industrial Aerodynamics, 90, pp. 1807-1815.
94. Timothy, A.R. Tieleman, H.W. and Maher, F.J. (1977), "Interaction of Square prisms in two flow fields", Journal of Wind Engineering and Industrial Aerodynamics, 2, pp. 223-241.
95. Tsutsumi, T., Katayama, T. and Nishida, M. (1992), "Wind tunnel tests of wind pressure on regularly aligned buildings", Journal of Wind Engineering and Industrial Aerodynamics, 41-44, pp. 1799-1810.
96. Verma, S.K. (2009), "Wind Effects on Structurally Coupled Tall Buildings", Ph. D. Thesis, Department of Civil Engineering, Indian Institute of Technology Roorkee, Roorkee, India.
97. Verma, S.K. (2014), "Wind loads on structurally coupled through single bridge tall buildings", International Journal of Civil and Structural Engineering, 4, pp. 469-476.
98. Verma, S.K., Kumar, K. and Kaur, H. (2014), "Estimation of coefficients of pressure in high rise buildings using artificial neural network", International Journal of Engineering Research and applications, 4, pp. 105-110.
99. Verma, S.K., Roy, A.K. Lather, S. and Sood, M. (2015), "CFD simulation for wind load on octagonal tall buildings", International Journal of Engineering Trends and Technology, 24, pp. 211-216.

100. Vyavahare, A.Y., Godbole, P.N. and Nikose, T. (2012), “Analysis of tall building for across wind response”, International Journal of Civil and Structural Engineering, 2, pp. 979-986.
101. Wang, F., Tamura, Y. and Yoshida, A. (2014), “Interference effects of a neighboring building on wind loads on scaffolding”, Journal of Wind Engineering and Industrial Aerodynamics, 125, pp. 1-12.
102. Xie, Z.N. and Gu, M. (2004), “Mean interference effects among tall buildings”, Engineering Structures, 26, pp. 1173-1831.
103. Yahyai, M. (1990), “Aerodynamics Interference in Tall Buildings”, Ph.D. Thesis, Department of Civil Engineering, University of Roorkee, Roorkee, India.
104. Yahyai, M., Kumar, K., Krishna, P. and Pande, P.K. (1992), “Aerodynamics interference in tall rectangular buildings”, Journal of Wind Engineering and Industrial Aerodynamics, 41-44, pp. 859-866.
105. Yang, Z., Sarkar, P.P. and Hu, H. (2011), “An experimental study of a high rise building model in tornado like winds”, Journal of Fluids and Structures, 27, pp. 471-486.
106. Zhang, A. and Gu, M. (2008), “Wind tunnel tests and numerical simulations of wind pressures on building in staggered arrangement”, Journal of Wind Engineering and Industrial Aerodynamics, 96, pp. 2067-2079.
107. Zhang, W.L., Xu, Y.L. and Kwok, K.C.S. (1995), “Interference effects on aeroelastic response of structurally asymmetric tall buildings”, Journal of Wind Engineering and Industrial Aerodynamics, 57, 41-61.
108. Zhang, Y., Hu, H. and Sarkar, P.P. (2014-a), “Comparison of microburst-wind loads on low-rise structures of various geometric shapes”, Journal of Wind Engineering and Industrial Aerodynamics, 133, pp. 181-190.
109. Zhang, Y., Sarkar, P.P. and Hu, H. (2014-b), “An experimental study on wind loads acting on a high-rise building model induced by microburst-like winds”, Journal of Fluids and Structures, 50, pp. 547-564.

# LIST OF PUBLICATIONS

1. Raj, R., Ahuja, A.K. and Chakraborti, A. (2012), "Experimental Investigation of the Effect of Cross-Sectional Shape on Wind Loads on Tall Buildings", National Conference on Wind Engineering Organized by ISWE, 2012.
2. Raj, R. and Ahuja, A.K. (2012), "Influence of Cross-Sectional Shape on Wind Loads on Tall Buildings", REINFSRD Organized by Institute of Engineers (IE) Local Chapter, 2012.
3. Raj, R. and Ahuja, A.K. (2013), "Wind Loads on Tall Buildings with Varying Cross-Sectional Shapes", Internation Journal of Construction Materials and Structures, vol-2, pp. 29-38.
4. Raj, R. and Ahuja, A.K. (2013), "Effects of Wind incidence angle on Wind Pressure Distribution on Tall Buildings", International Journal of Management, IT and Engineering, vol.-3 issue 10, pp. 480-487.
5. Raj, R. and Ahuja, A.K. (2013), "Wind Loads on I-Shape Building", International Journal for Scientific Research & Development, vol.-1, issue-2, pp. 20-23.
6. Raj, R. and Ahuja, A.K. (2013), "Wind Loads on Cross-Shape Buildings", Journal of Academia and Industrial Research, vol.-2, issue-2, pp. 111-113.